A NEW SOIL STABILISATION TECHNIQUE

by

NICHOLAS HYTIRIS

BSc, MSc, AMICE, MICE (Greece)

A thesis submitted for the degree of

Doctor of Philosophy in the Department

of Civil Engineering, University of

Strathclyde, Glasgow, U.K.

October, 1986.

VOLUME II

LIST

OF

FIGURES

FIG. 1.1

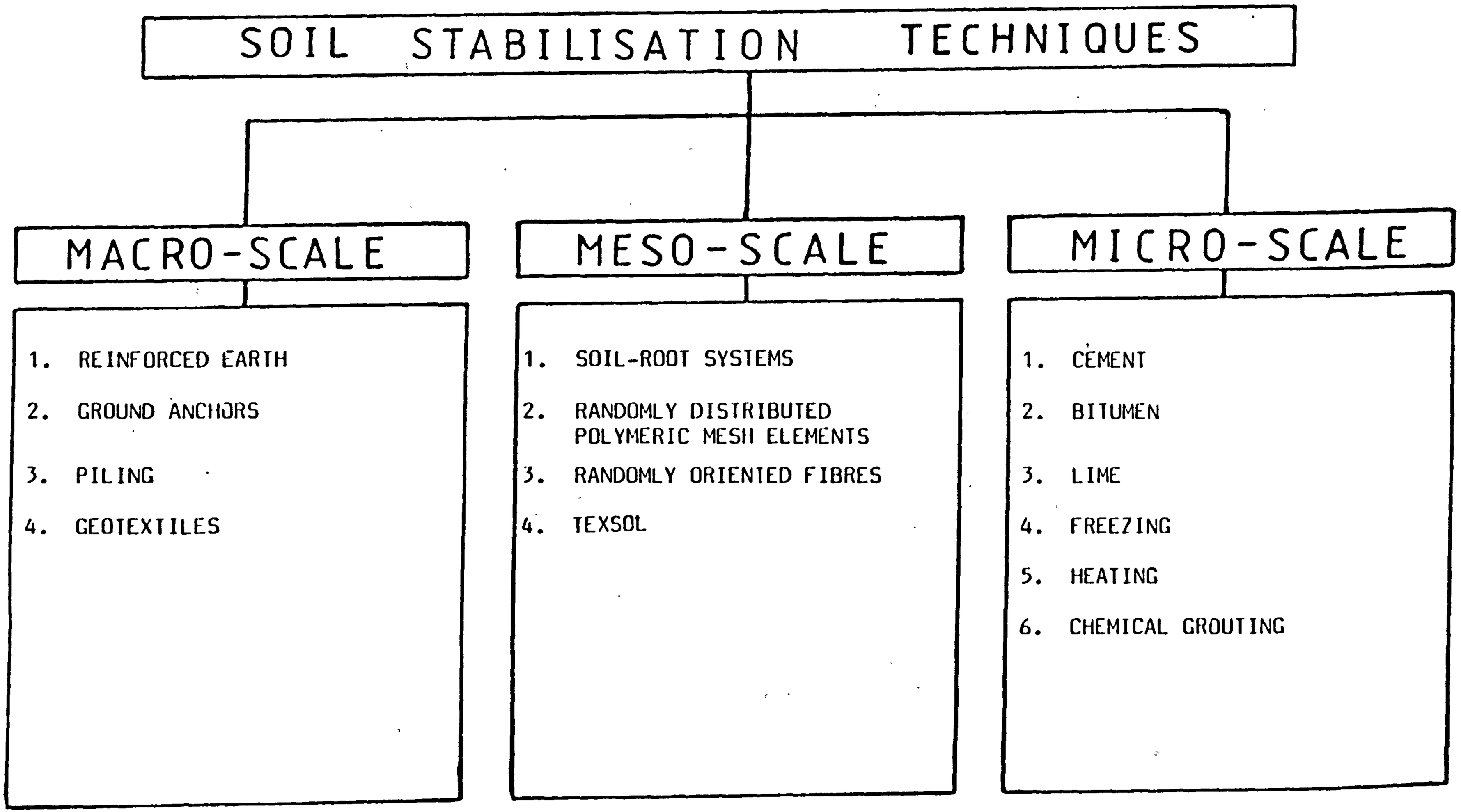
SOIL STABILISATION TECHNIQUES
MACRO-SCALE
1. REINFORCED EARTH
2. GROUND ANCHORS
3. PILING
4. GEOTEXTILES
MESO-SCALE
1. SOIL-ROOT SYSTEMS
2. RANDOMLY DISTRIBUTED POLYMERIC MESH ELEMENTS
3. RANDOMLY ORIENTED FIBRES
4. TEXSOL
MICRO-SCALE
1. CEMENT
2. BITUMEN
3. LIME
4. FREEZING
5. HEATING
6. CHEMICAL GROUTING

FIG. 1.2

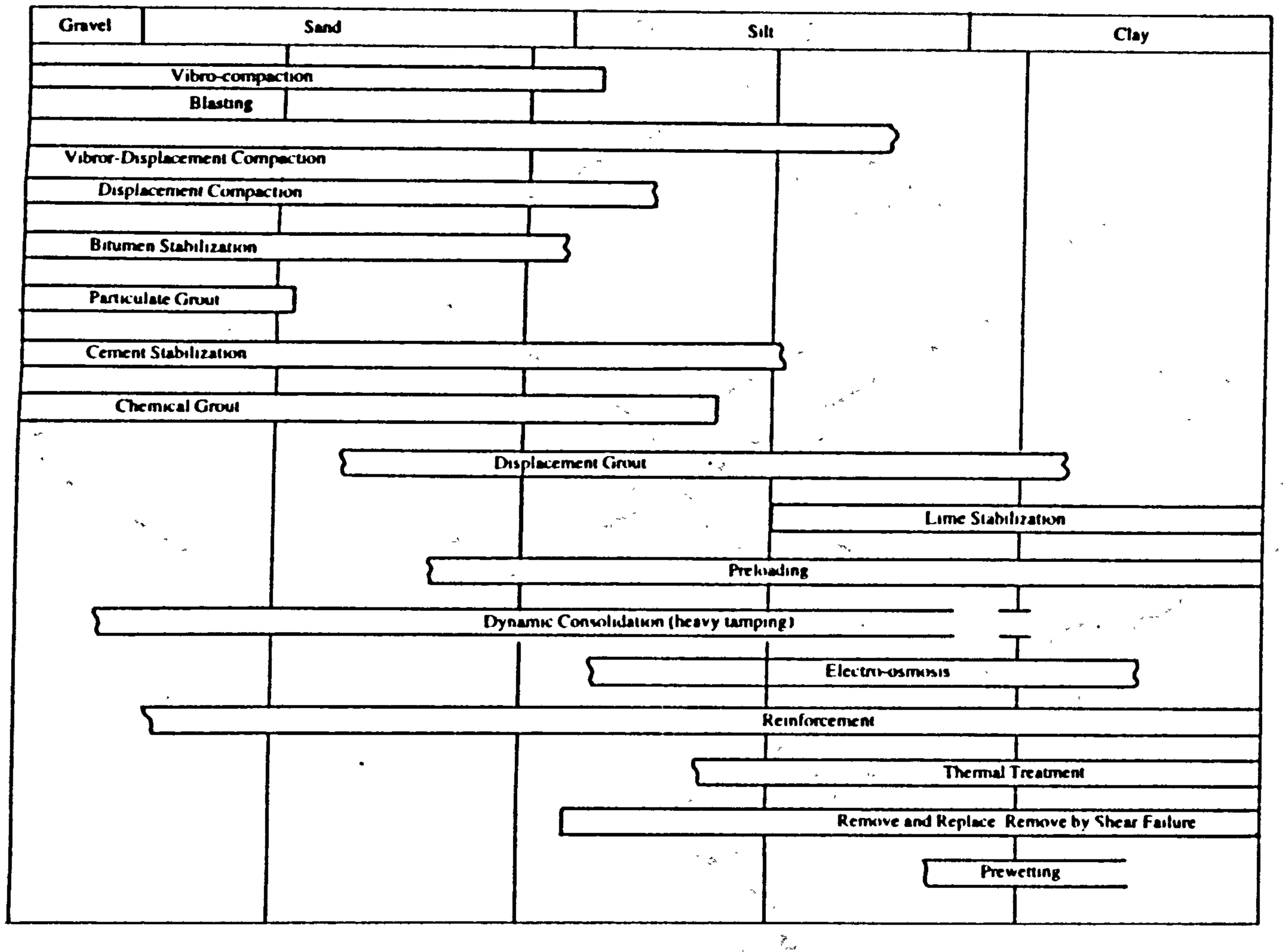

Feasibility of Stabilization Techniques (SOURCE: Based on Mitchell, 1976. Courtesy American Society of Civil Engineers.)

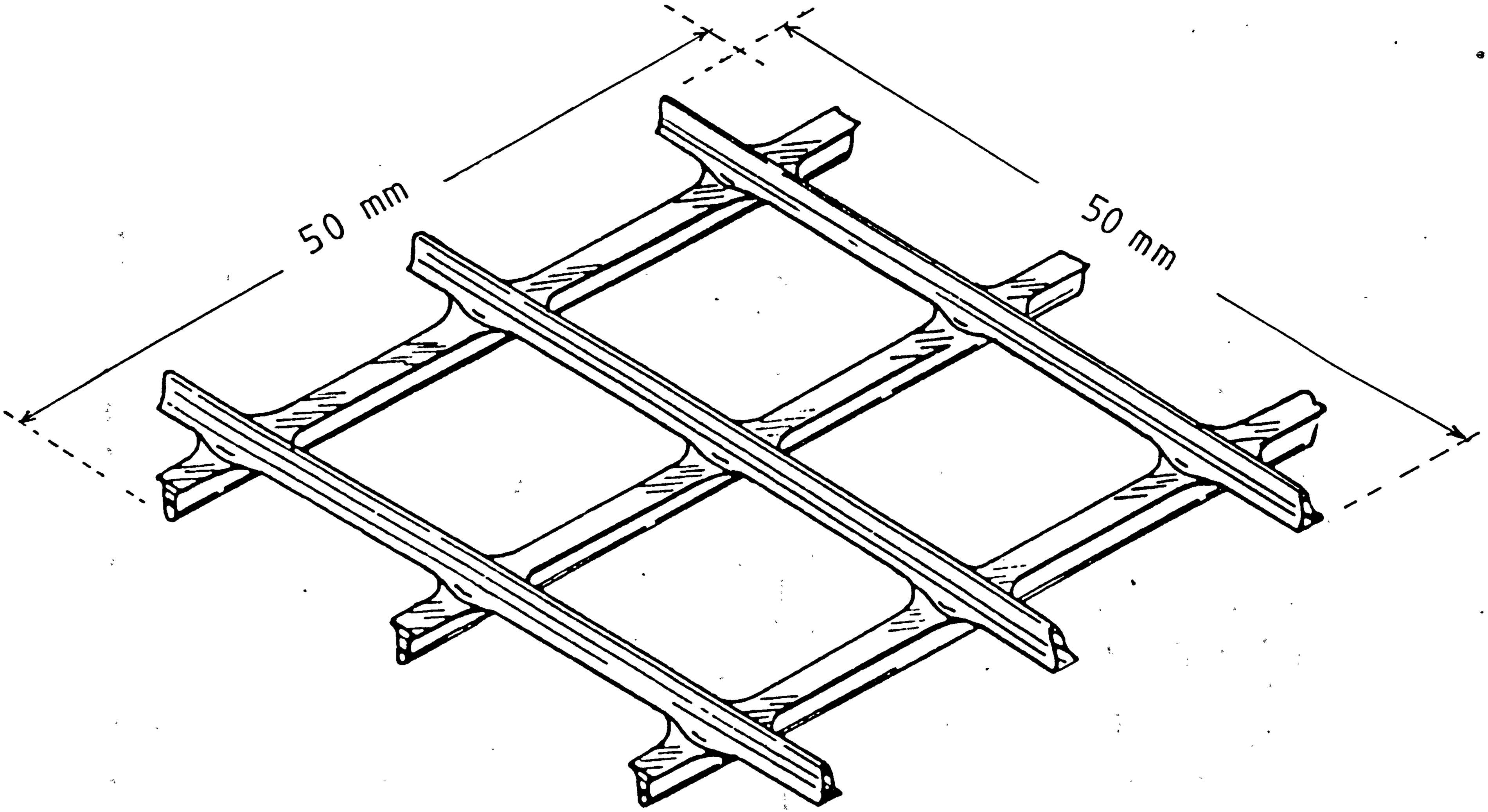

FIG. 1.3 EXAMPLE OF MESH STRUCTURE

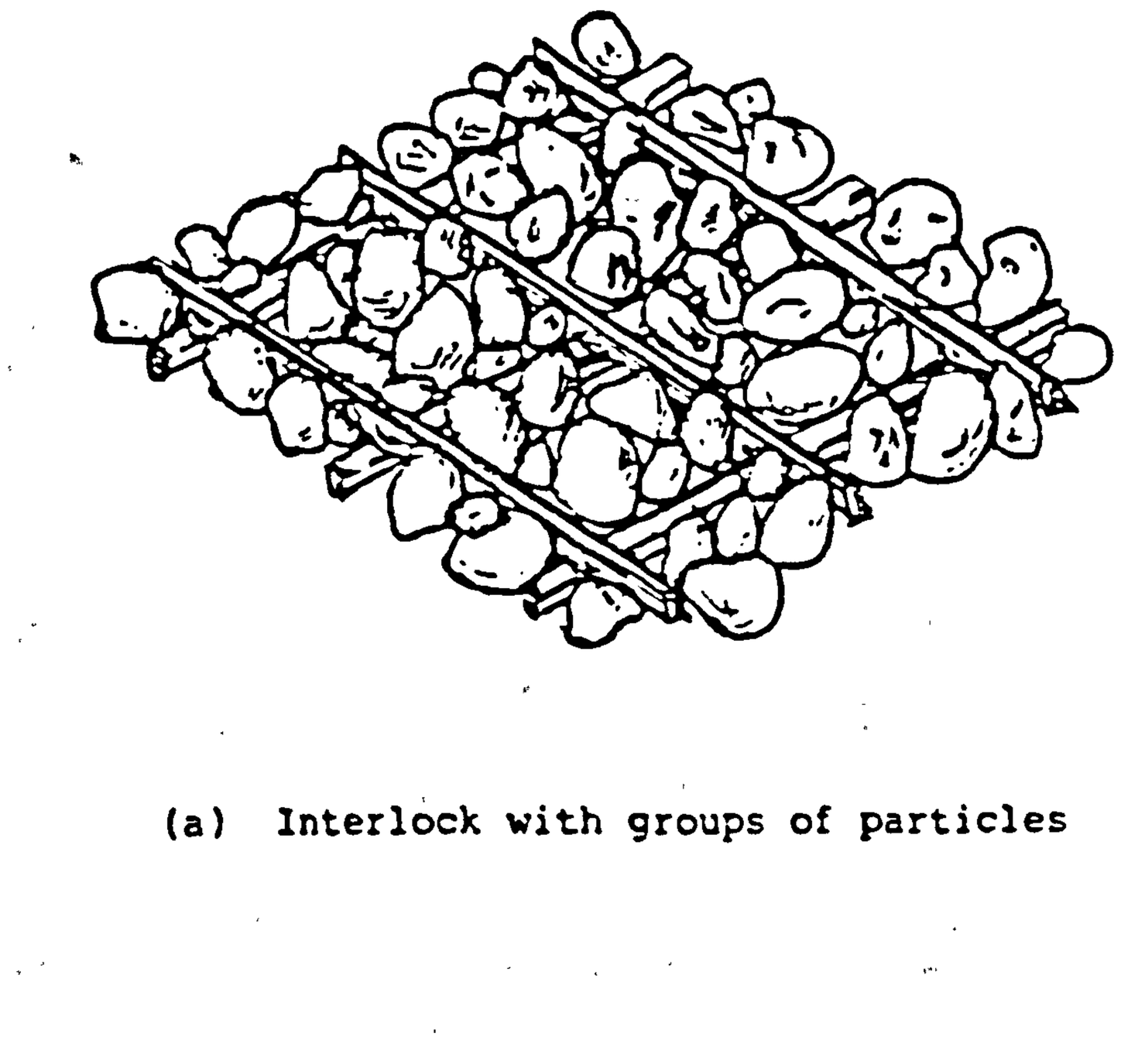

(a) Interlock with groups of particles

(b) Interlock of adjacent aggregations

FIG. 1.4 The interlock mechanism for mesh elements

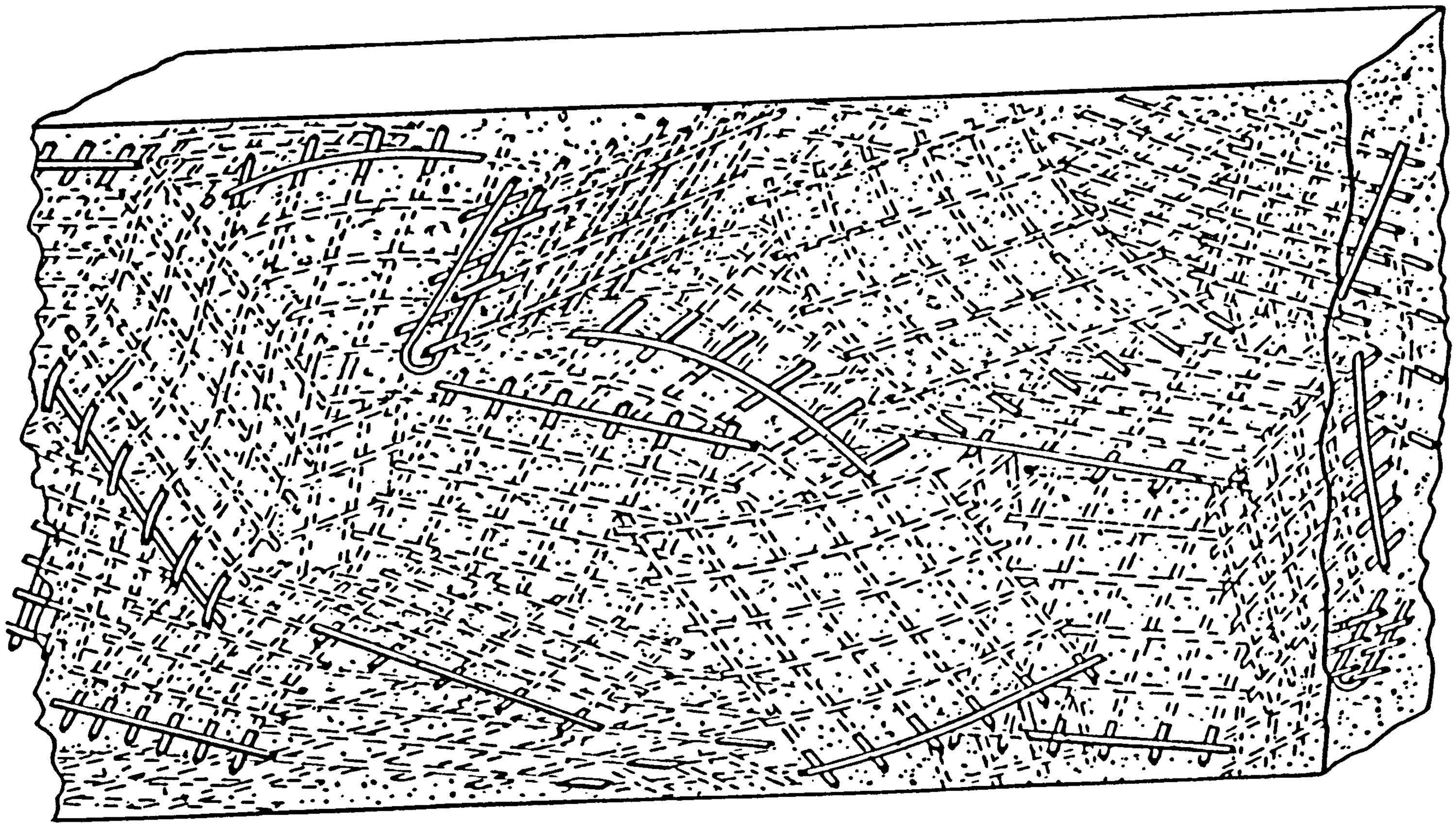

FIG. 1.5 FLEXIBLE MESHES AFTER MIXING

(After Kassiff & Kopelovitz, 1968)

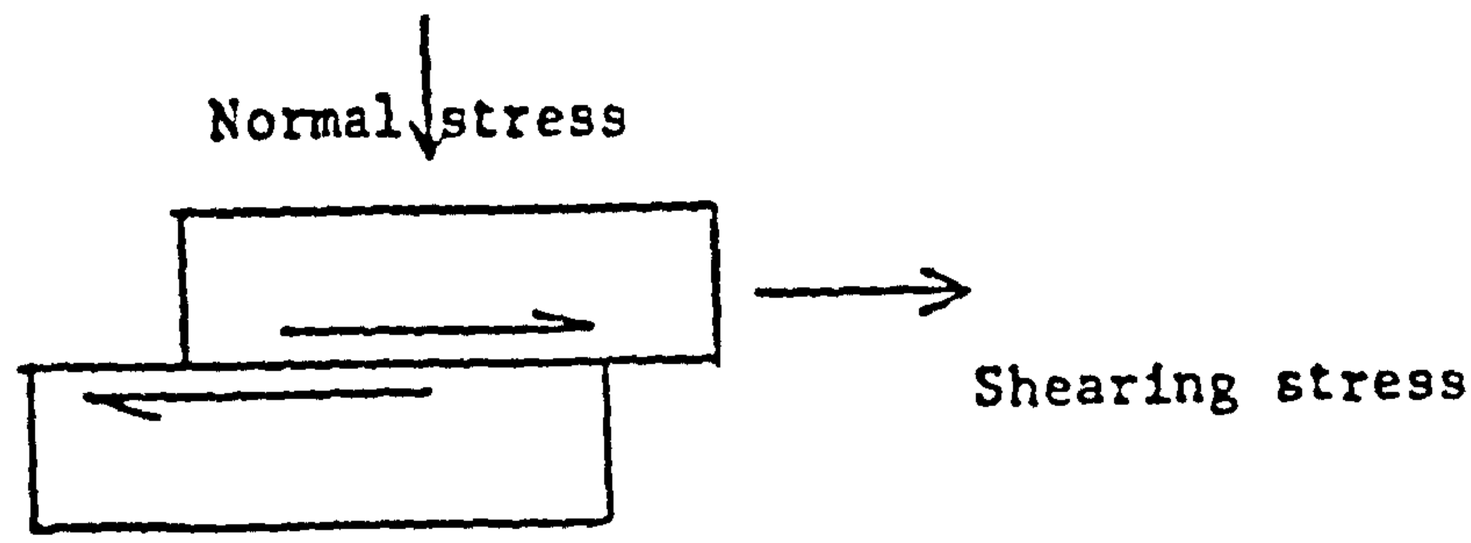

Fig. 2.1 Relative sliding of sheared parts.

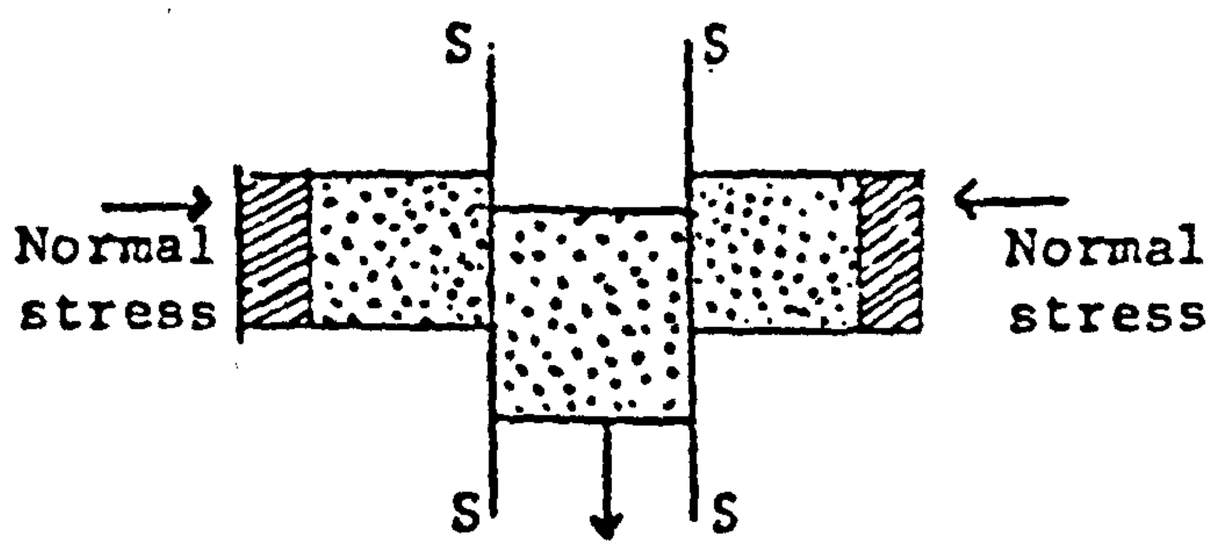

Fig. 2.2 Direct double shear apparatus.

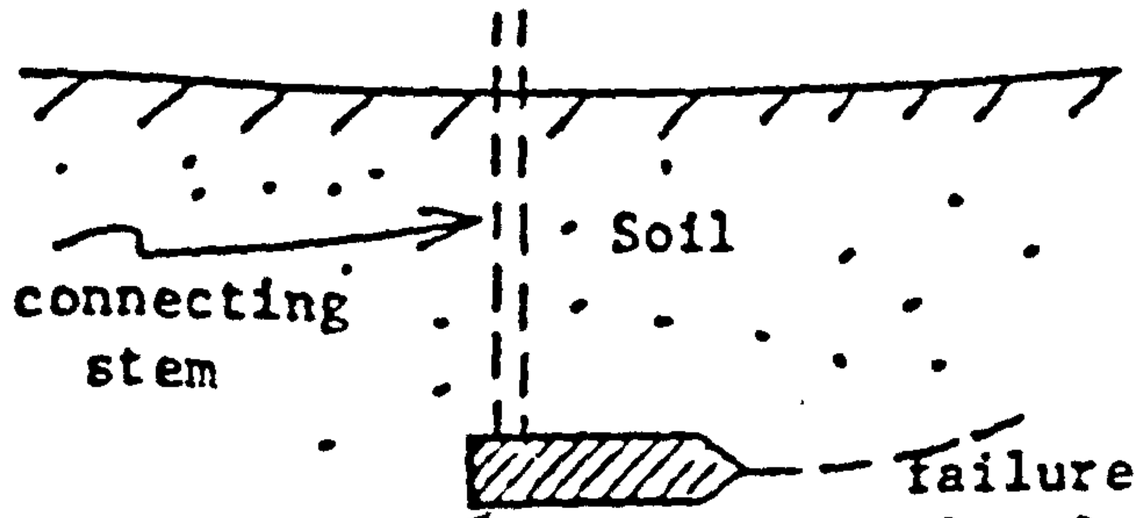

Fig. 2.3 Sketch showing cutting tool geometry in relation to the soil.

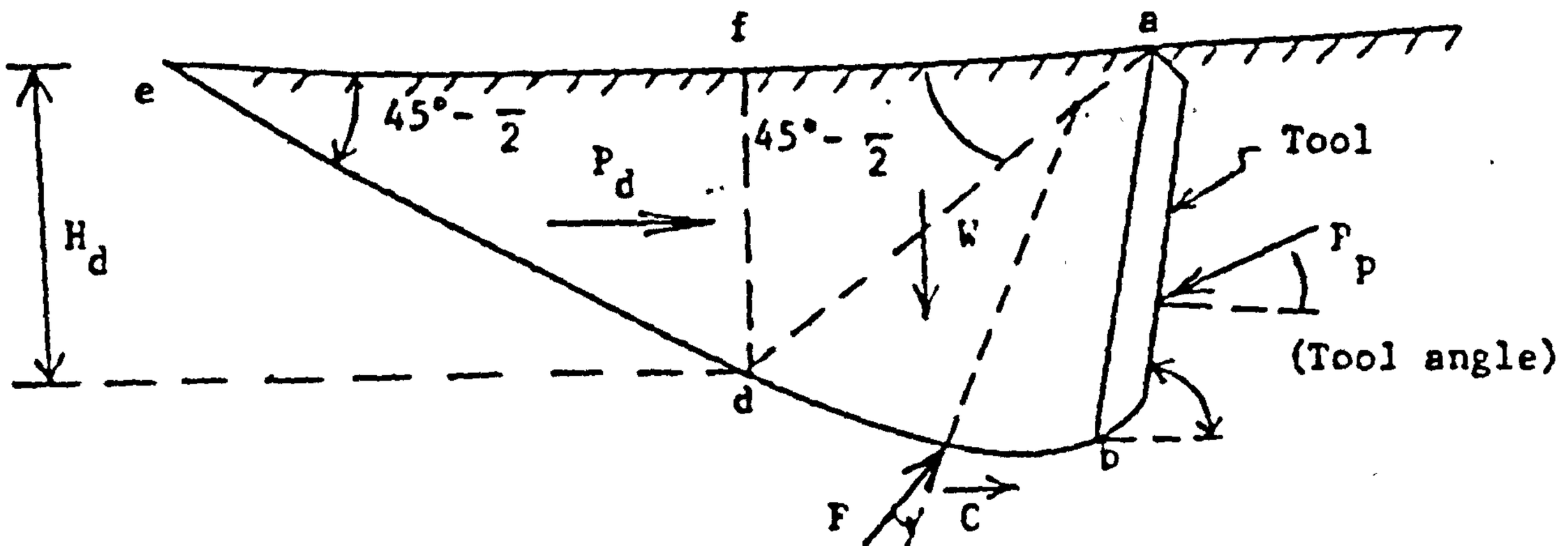

Fig. 2.4 Diagram of assumed forces acting on Soil Mass in front of tools near vertical.

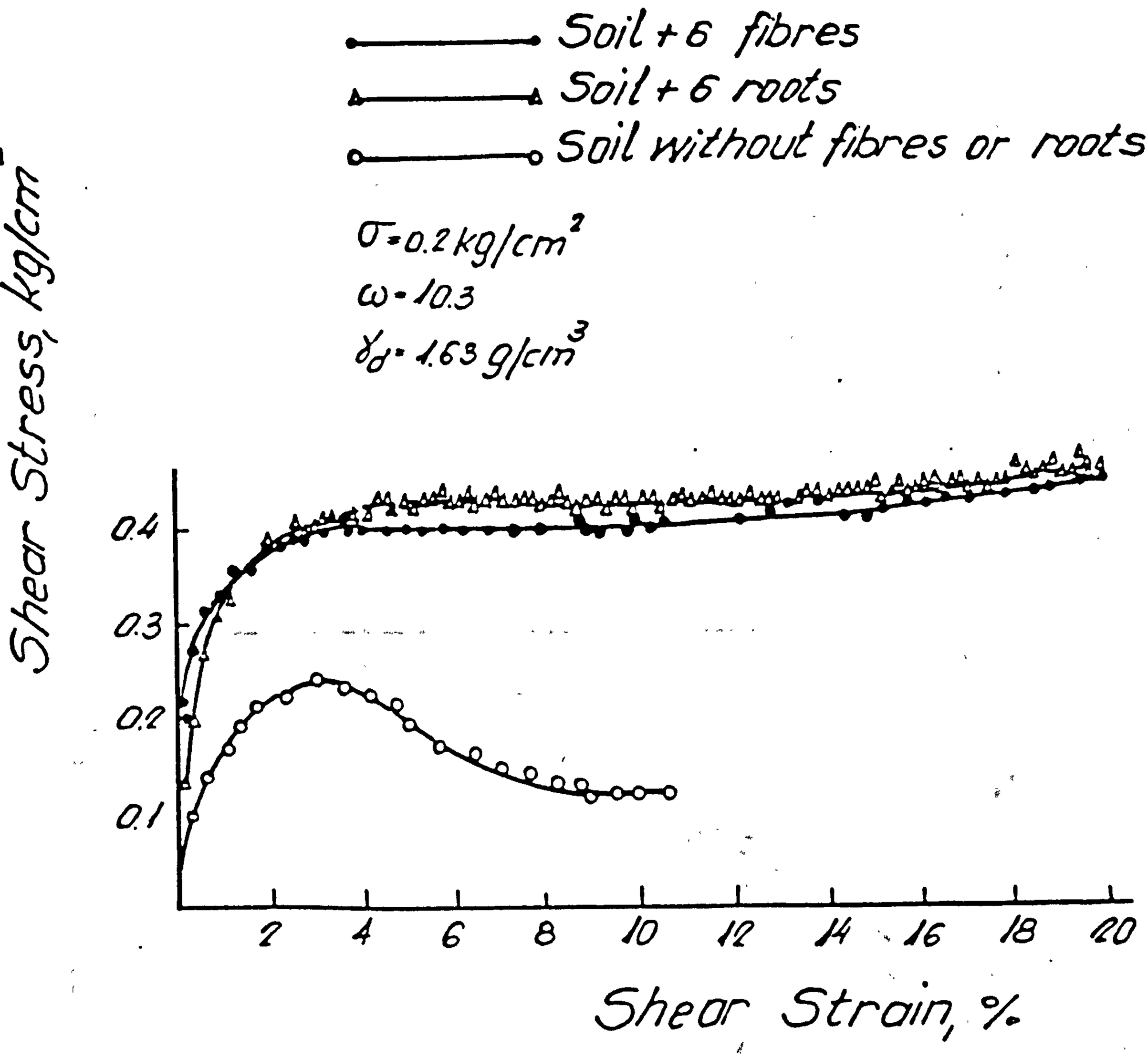

Fig. 2.5

Similarity of behavior under shear between soil-fibre and soil-root composites.

(After Kassiff & Kopelovitz, 1968)

(loess).

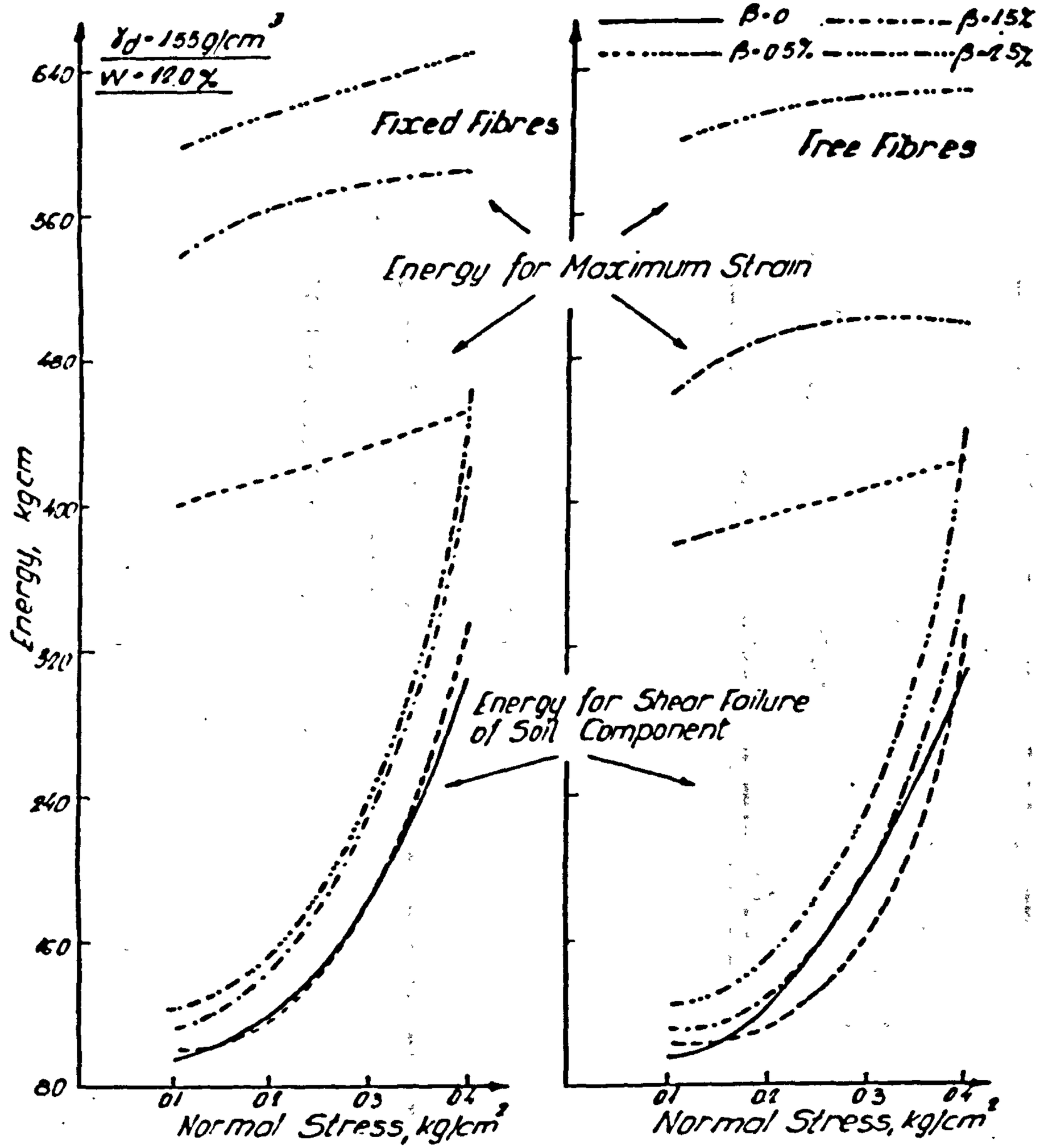

(clayey sand).

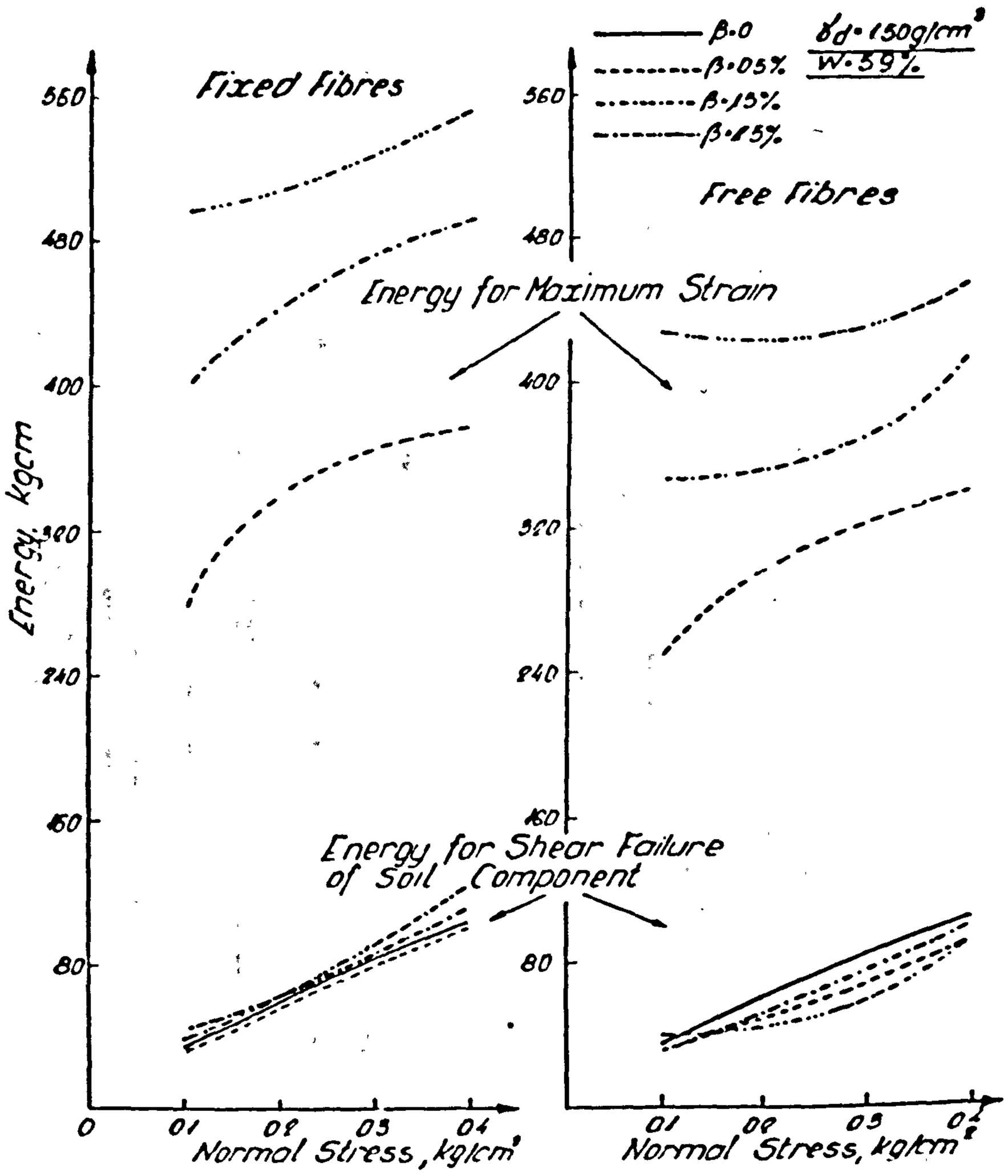

Fig. 2.6 Energies required for shear corresponding to strains causing failure to soil component and to soil composite

(After Kassiff & Kopelovitz, 1968)

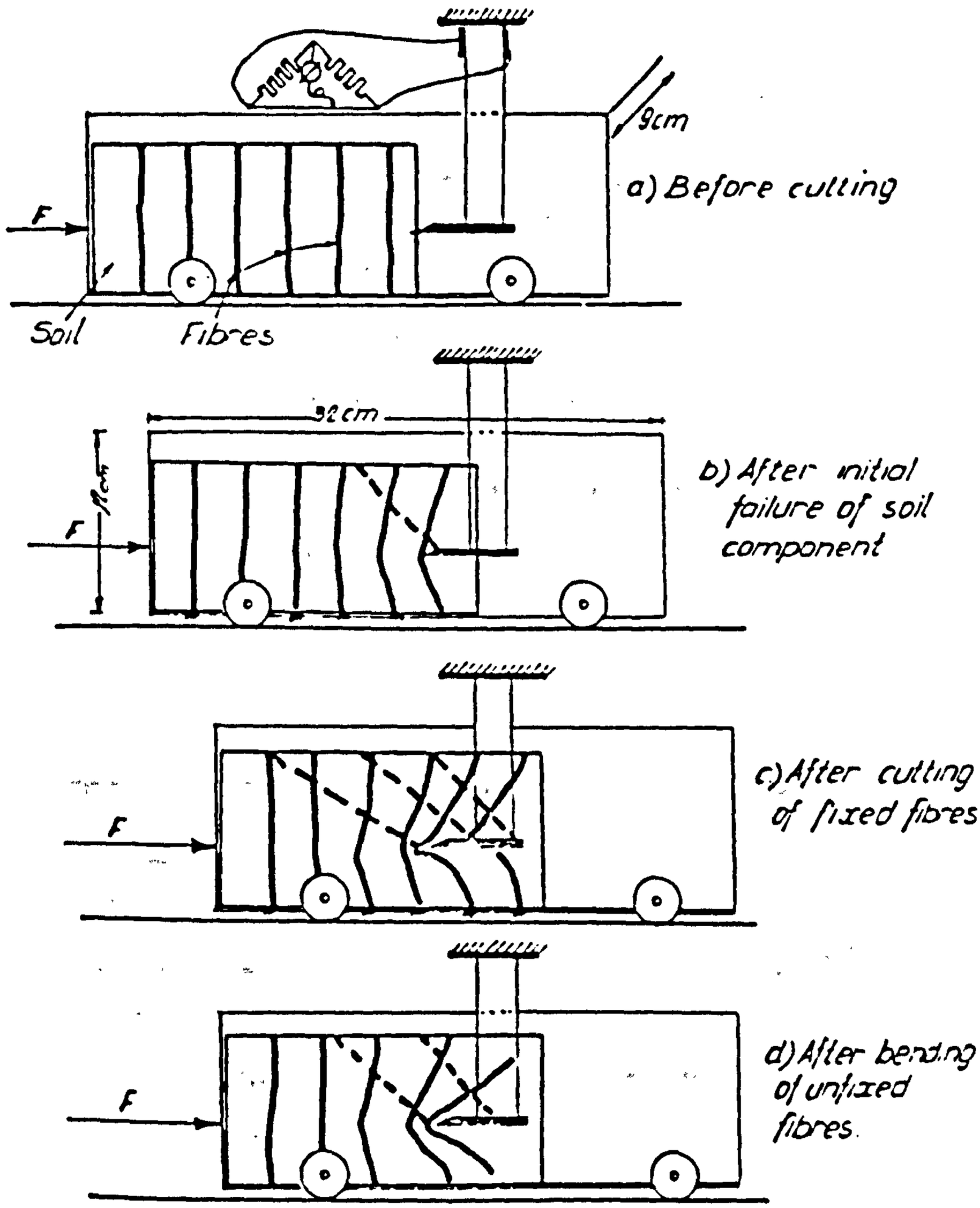

Fig. 2.7

Sketch showing the mode of failure of the composite material under different conditions of fibre fixity.

(After Kassiff & Kopelovitz, 1968)

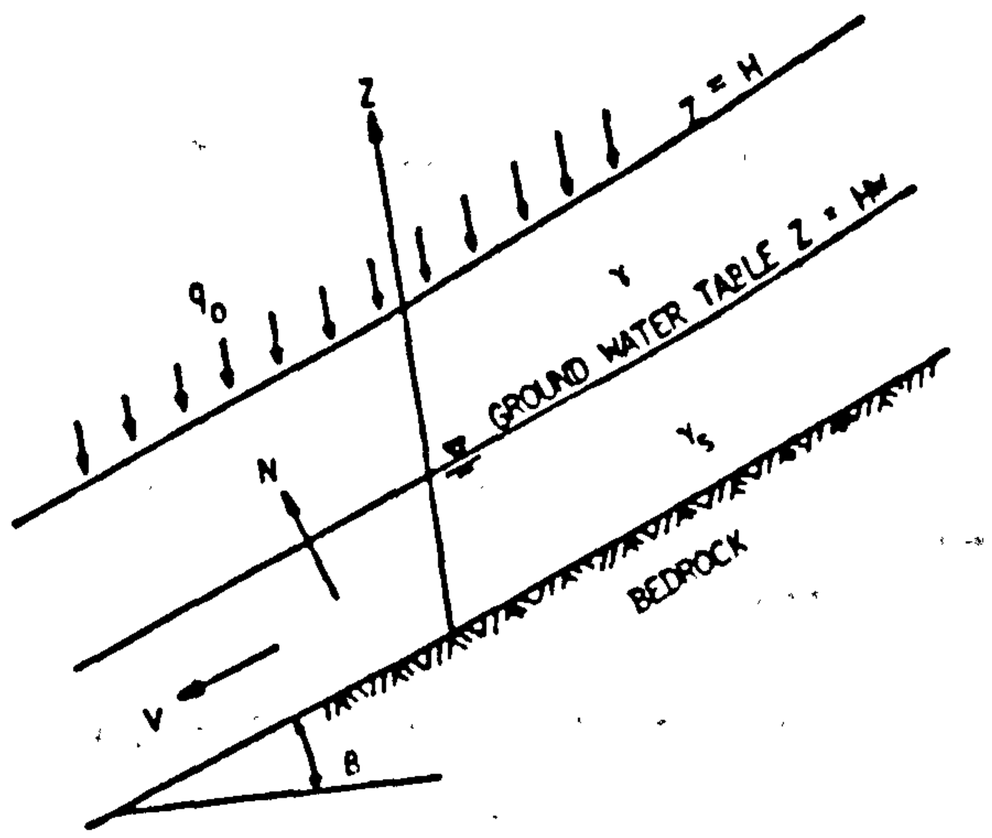

Fig. 2.8 Slope Idealization

(After Brown & Sheu, 1975)

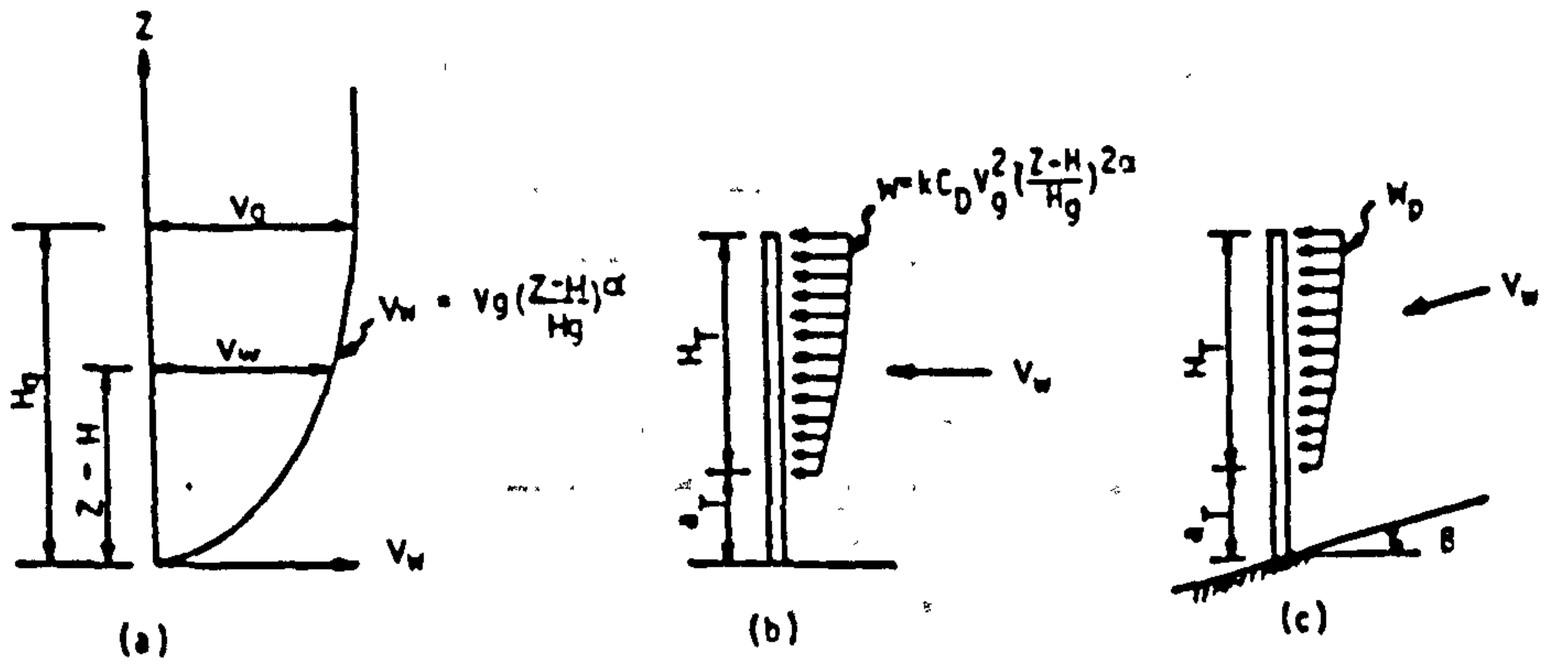

Fig. 2.9 Wind Gradient and Pressures

(After Brown & Sheu, 1975)

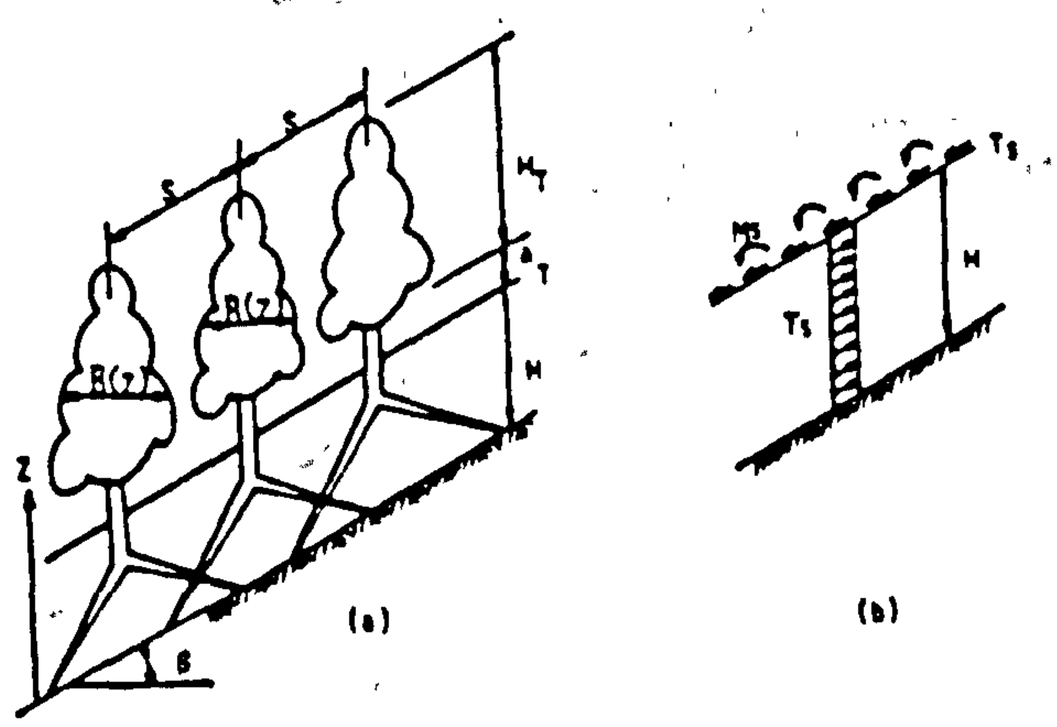

Fig. 2.10 Wind Effects on Trees and Mantle

(After Brown & Sheu, 1975)

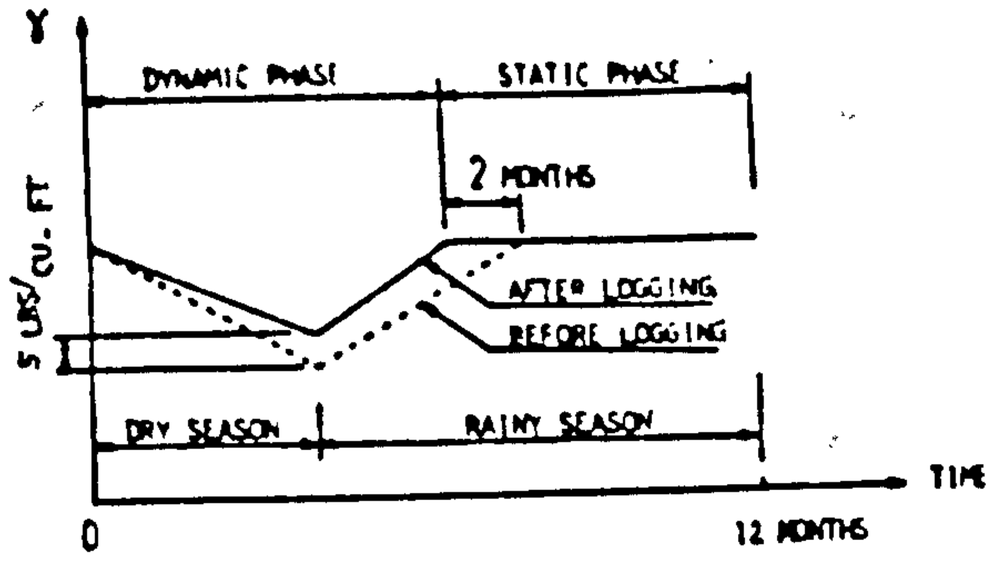

Fig. 2.11 Variation of γ with Time

(After Brown & Sheu, 1975)

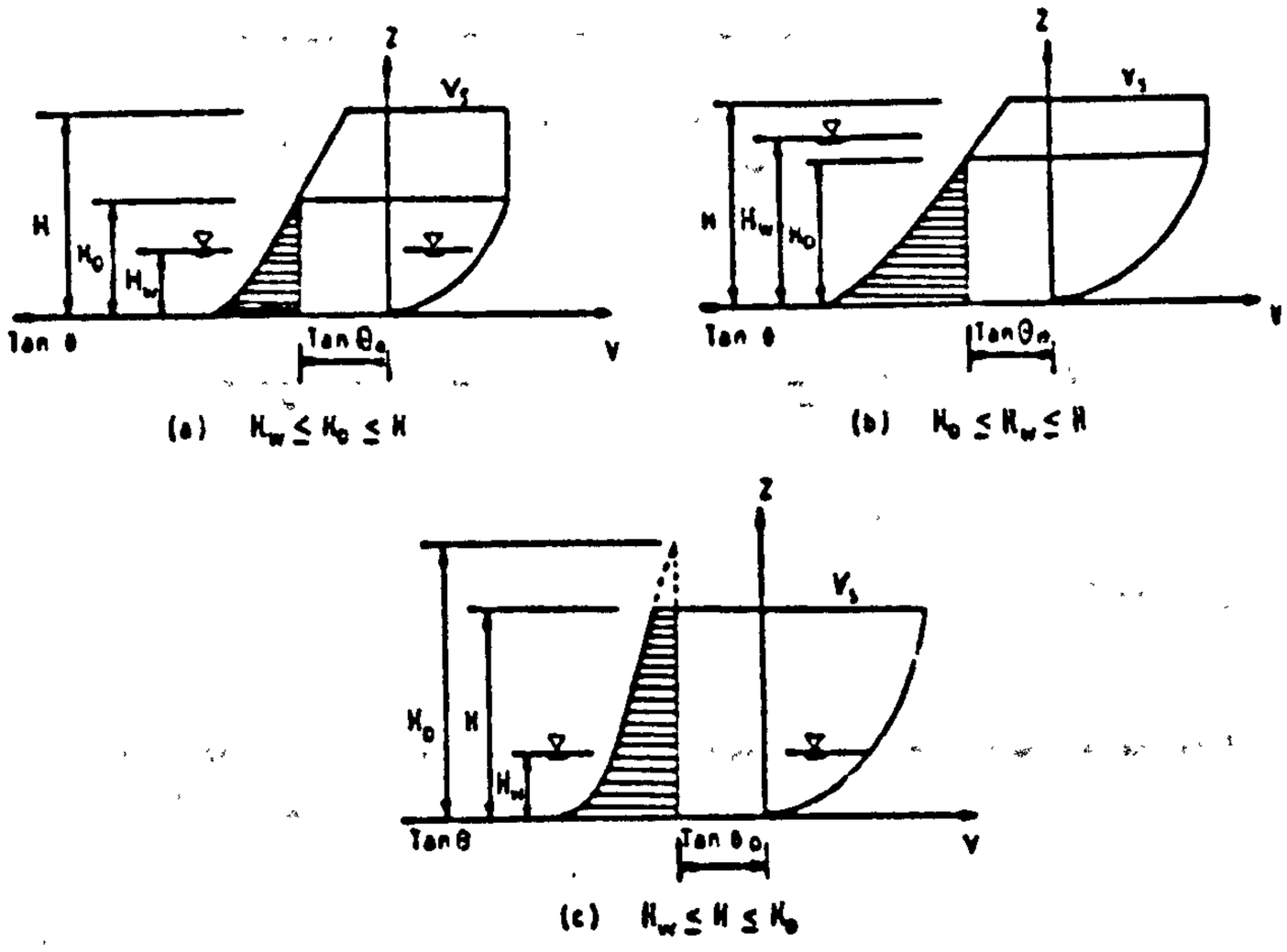

Fig. 2.12 Creep Speeds and tan θ as Function of Depth Z

(After Brown & Sheu, 1975)

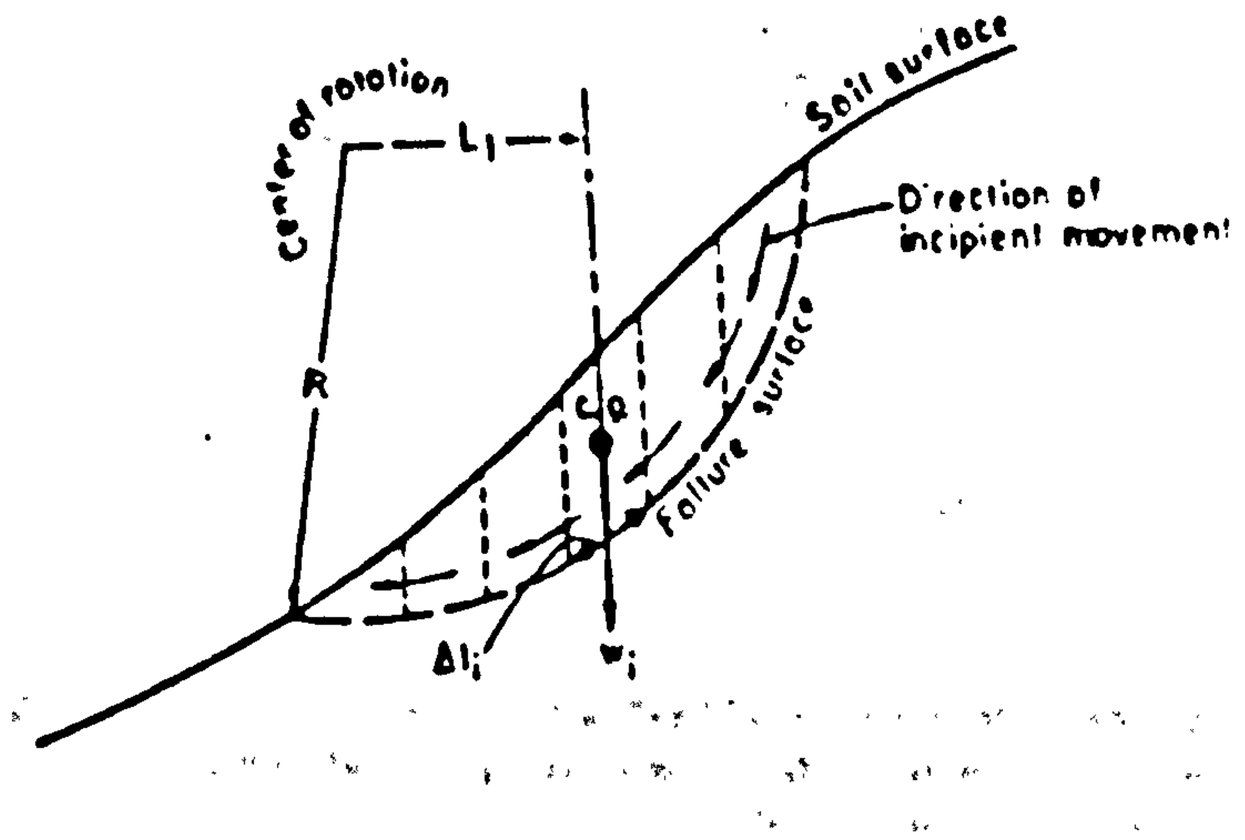

Fig. 2.13 Cross section of a slope illustrating the relationship of resisting and disturbing moments in a soil mass about to slide along an idealized circular failure surface. The mass has been arbitrarily divided into 6 slices indicated by the dashed vertical lines for analysis of moments.

(After Waldron, 1977)

1 Soil sample
2 Shear plane
3 Upper loading collar
4 Lower loading collar
5 Upper loading frame
6 Roller chain drive
7 Horizontal frame
8 Pallet
9 Steel plate
10 Reductor, 203 1 ratio
11 Reductor, 20:1 ratio
12 Motor
13 Motor speed control
14 Ball bearings
15 Proving ring
16 Ball bushing & ground steel shaft
17 Ball screw assembly
18 Sheaves
19 Counterweight
20 Winch

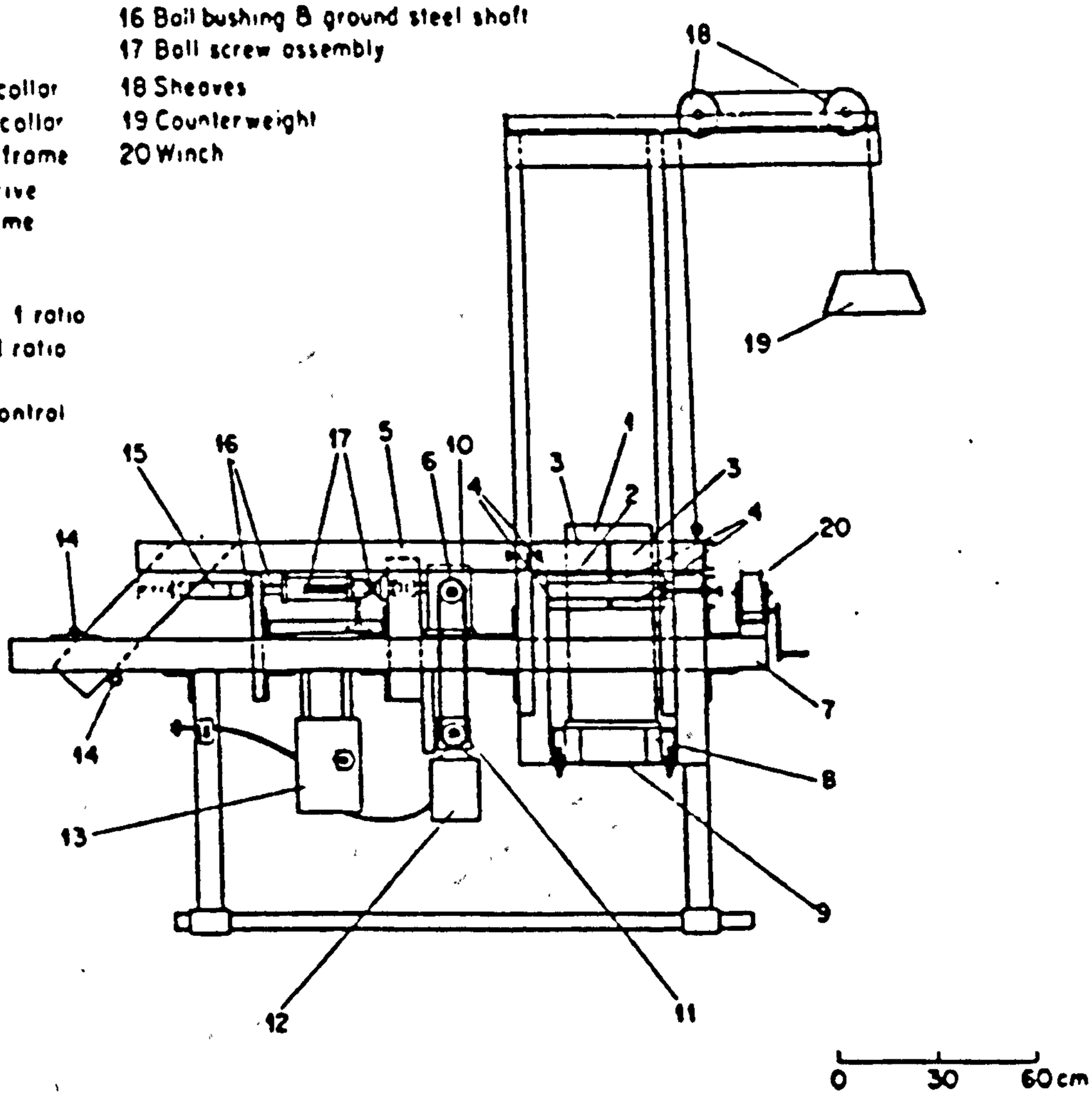

Fig. 2.14 Diagram of the large direct shear device with a soil sample mounted for testing at 15-cm depth. (After Waldron, 1977).

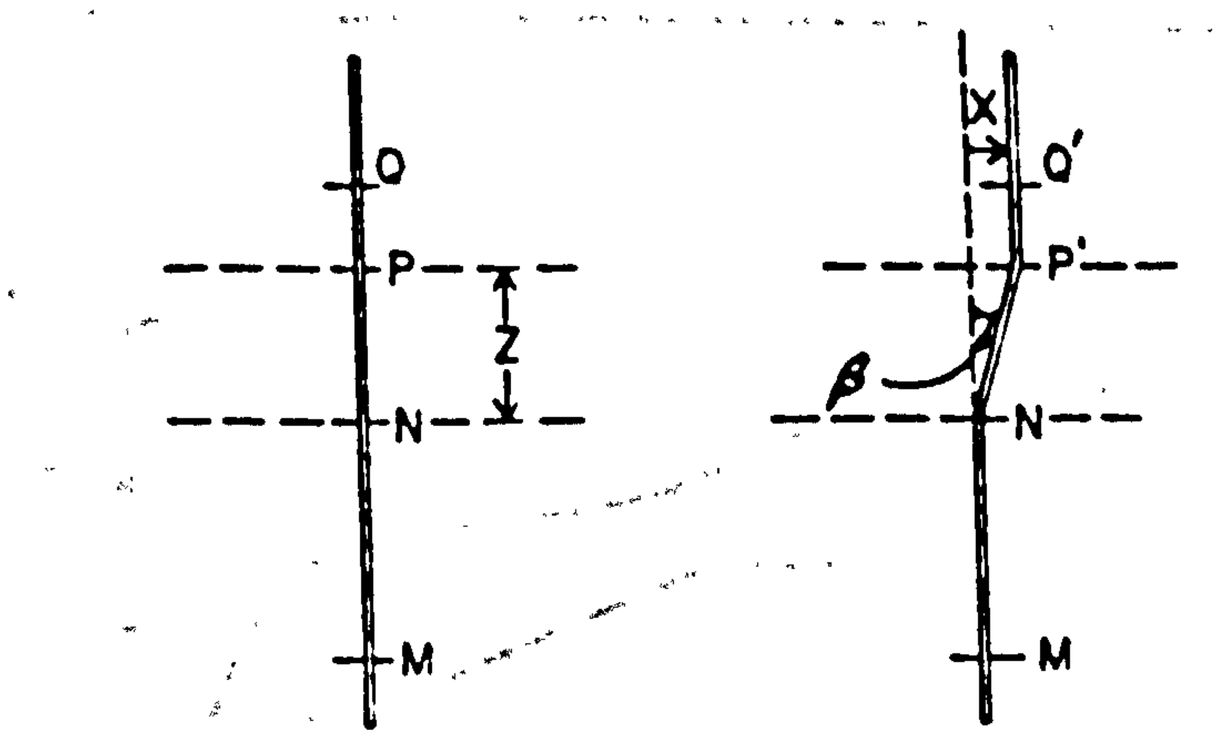

(a) (b)

Fig. 2.15 Model of a flexible, elastic root extending vertically through a horizontal shear zone of thickness *Z*. (a) Undisturbed soil. (b) Soil above *N* displaced horizontally a distance *x* with root segment *MNPQ* extended to length *MNP'Q'*.

(After Waldron, 1977)

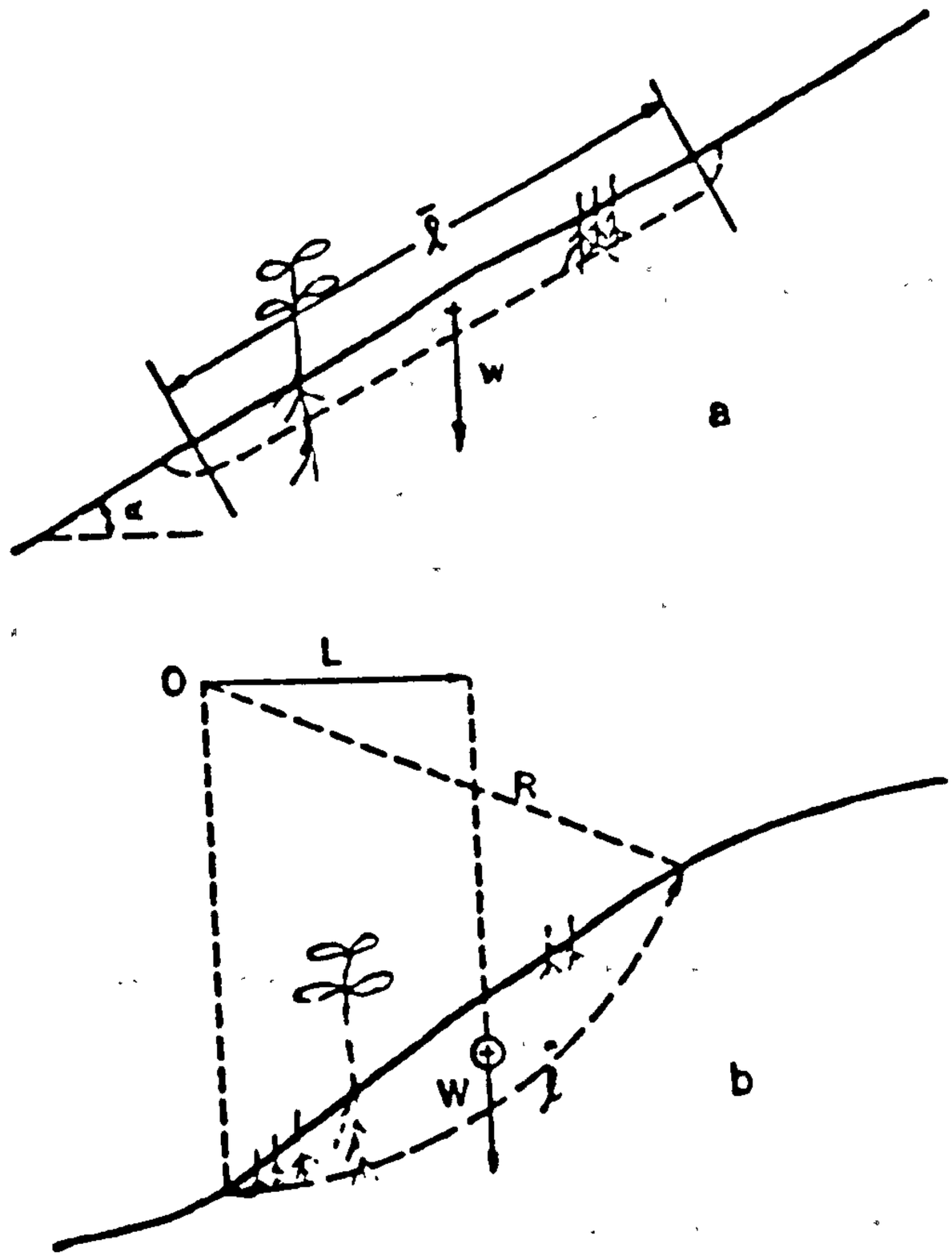

Fig. 2.16 Two modes of soil mass movement downslope: (*a*) planar slide; (*b*) rotary slide along circular failure surface.

(After Waldron & Dakessian, 1982)

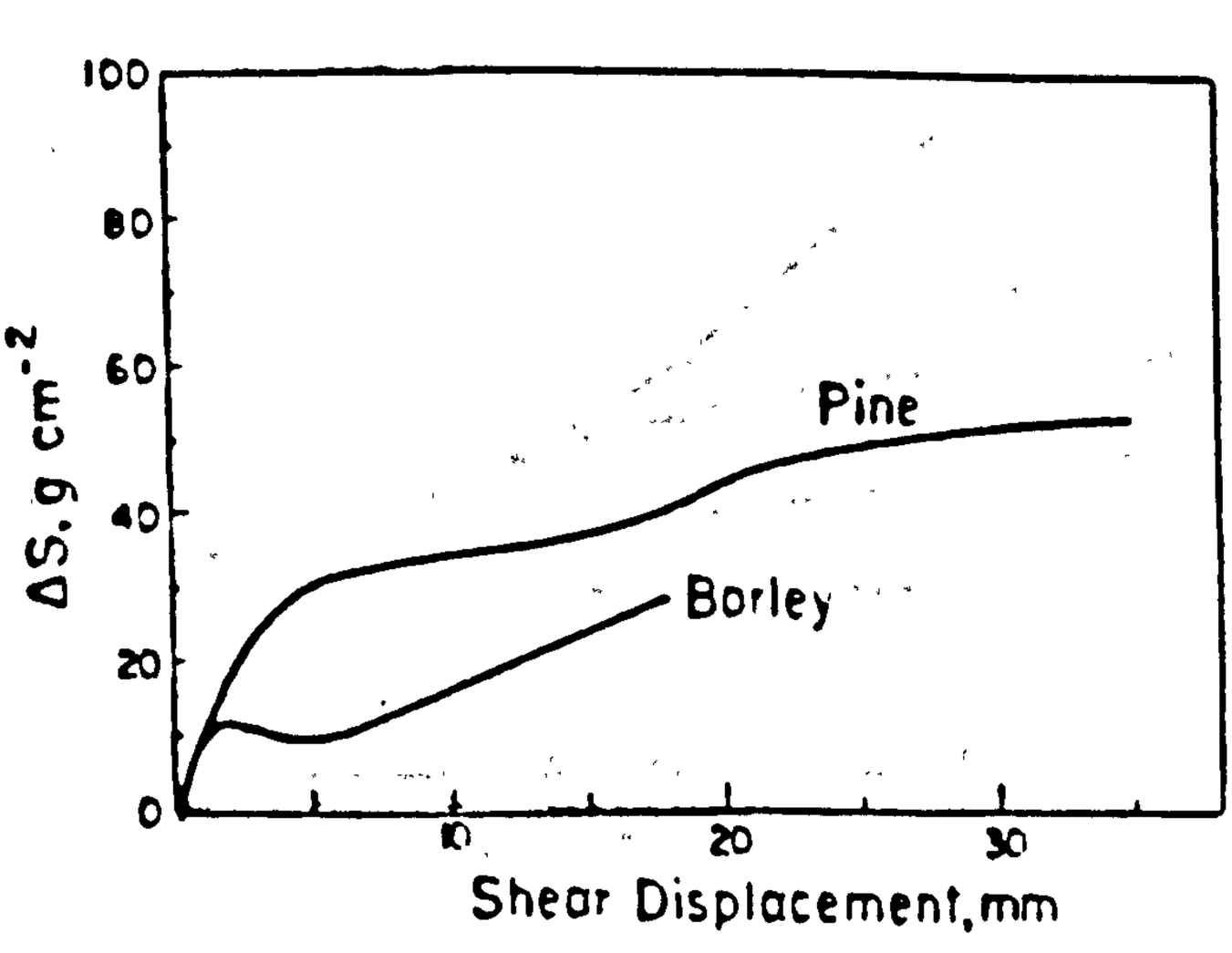

Fig. 2.17 Variation of Root Reinforcement with Shear Displacement

(Waldron & Dakessian, 1982)

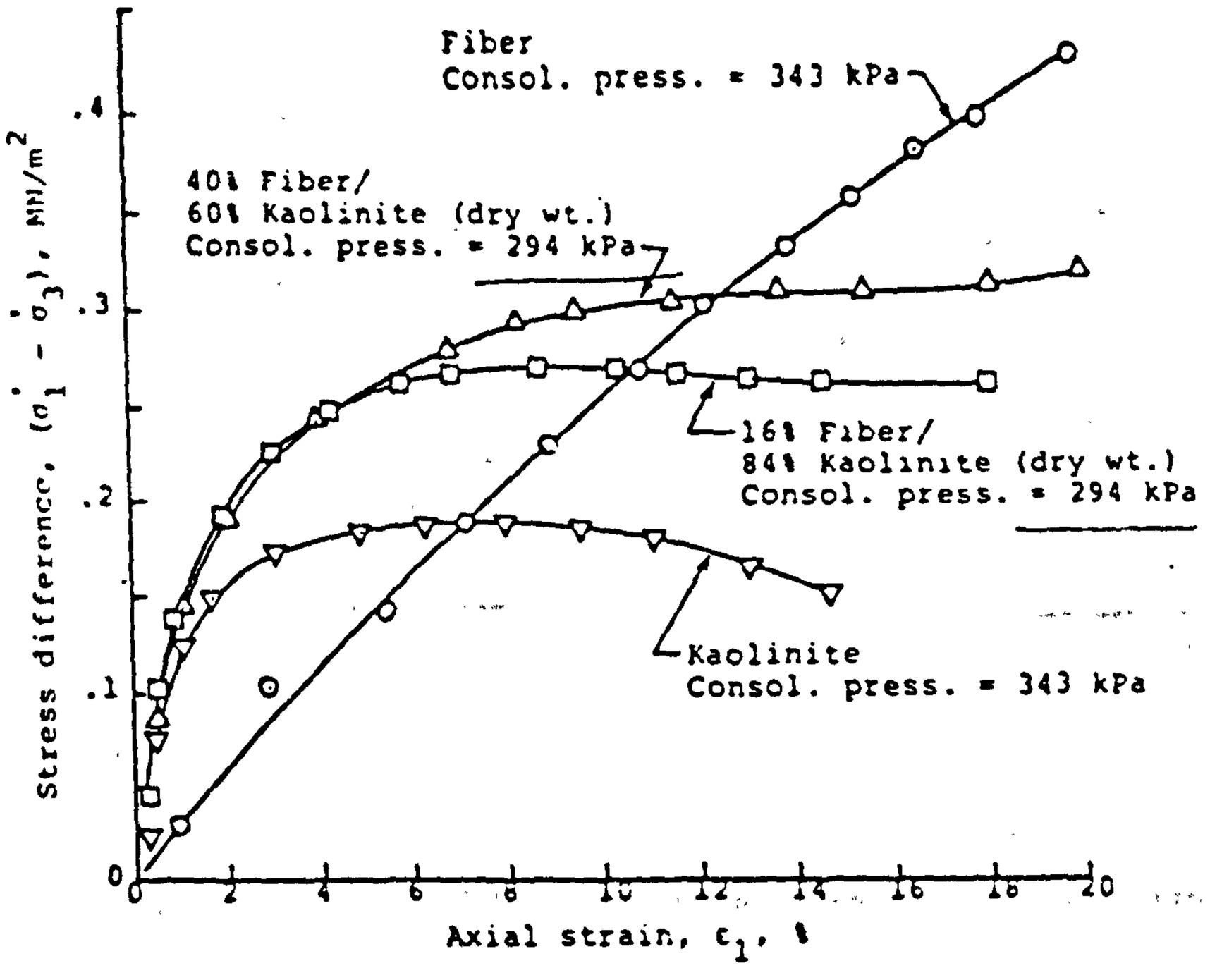

Fig. 2.18 Stress-strain curves for undrained conditions and samples with different kaolinite/fiber combinations.

(After Andersland & Khattak, 1979)

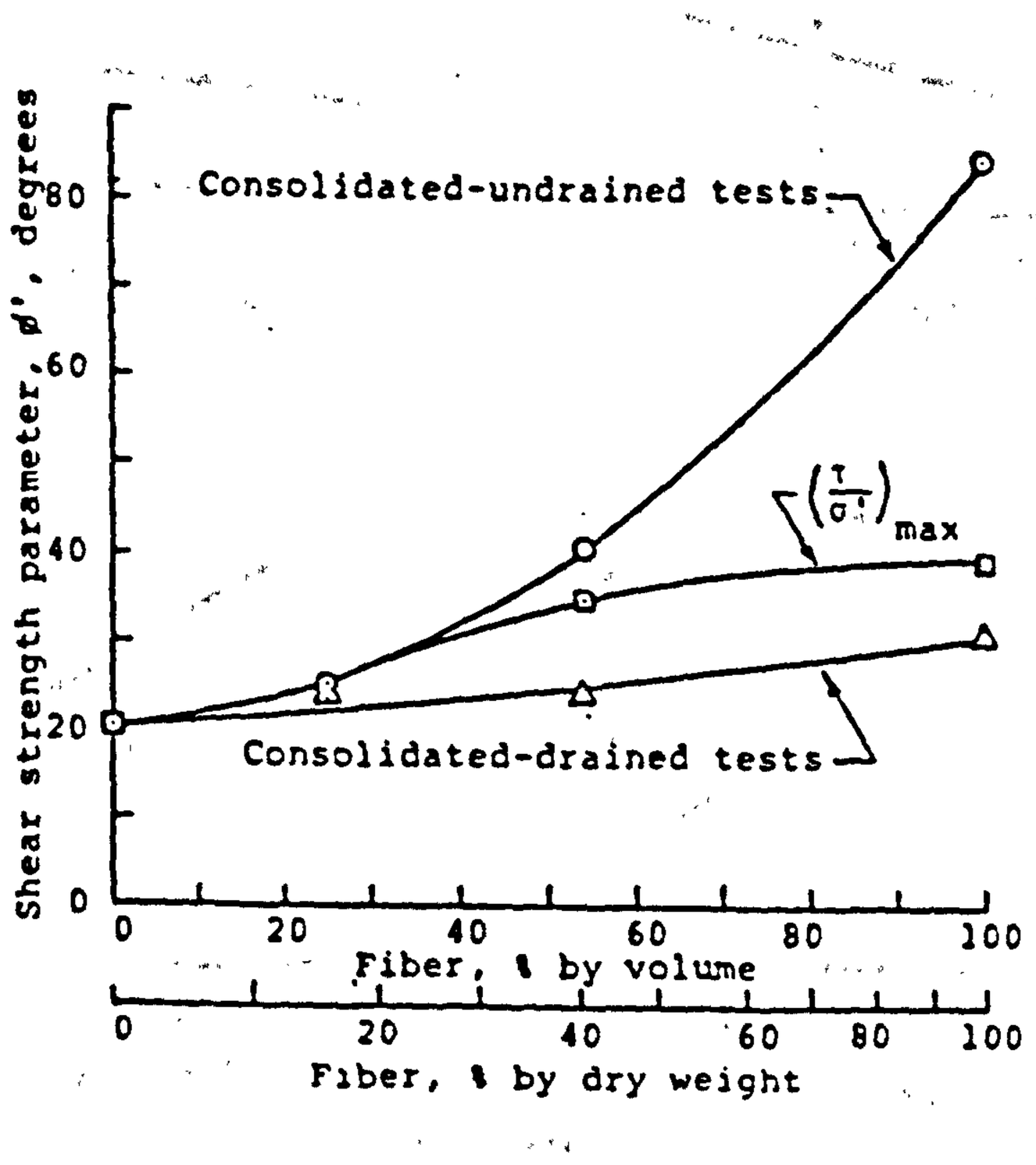

Fig. 2.19 Fiber content versus shear strength parameter ø' for kaolinite/fiber mixtures.

(After Andersland & Khattak, 1979)

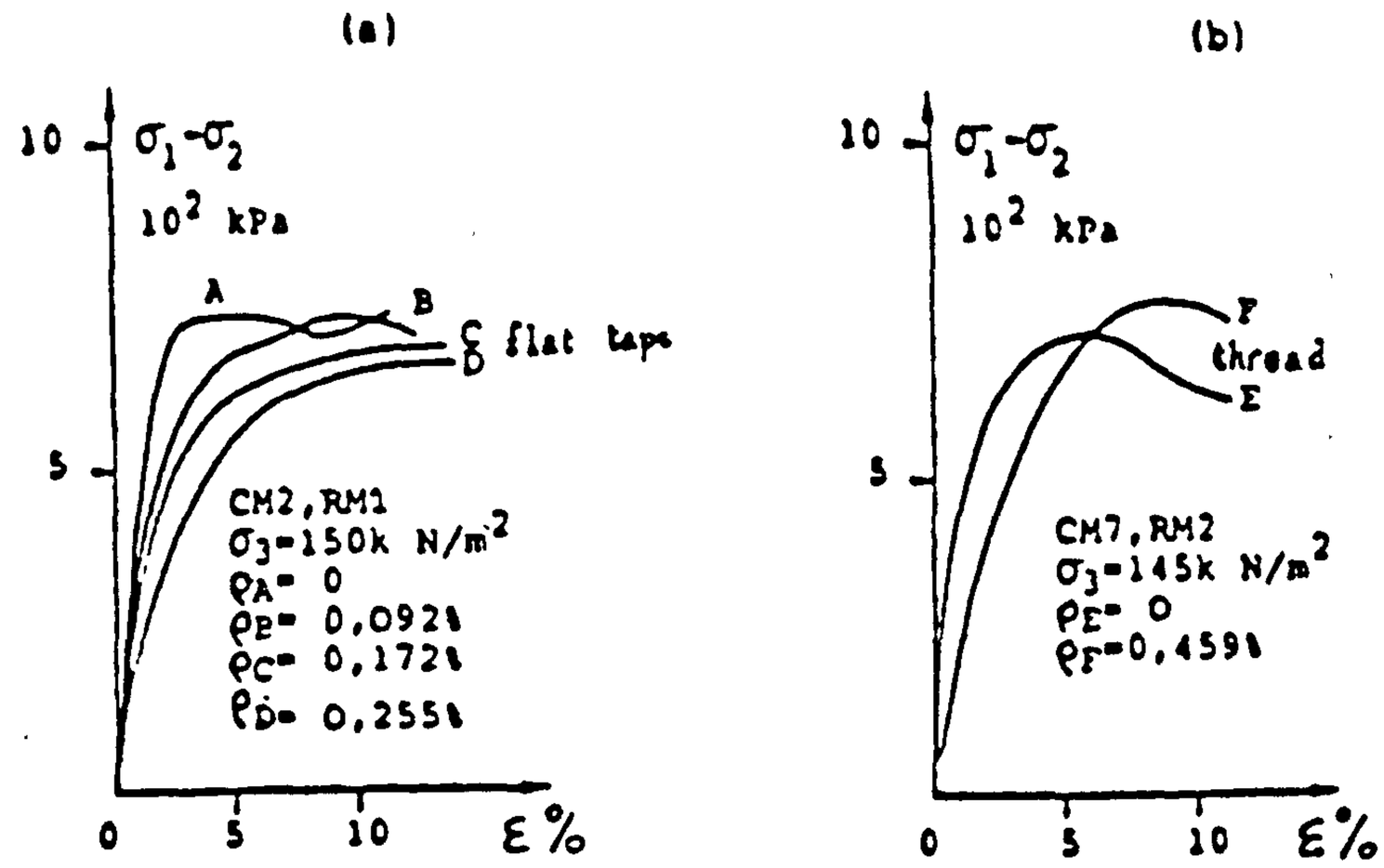

Fig. 2.20 **Results of triaxial tests** (Hoare, 1979)

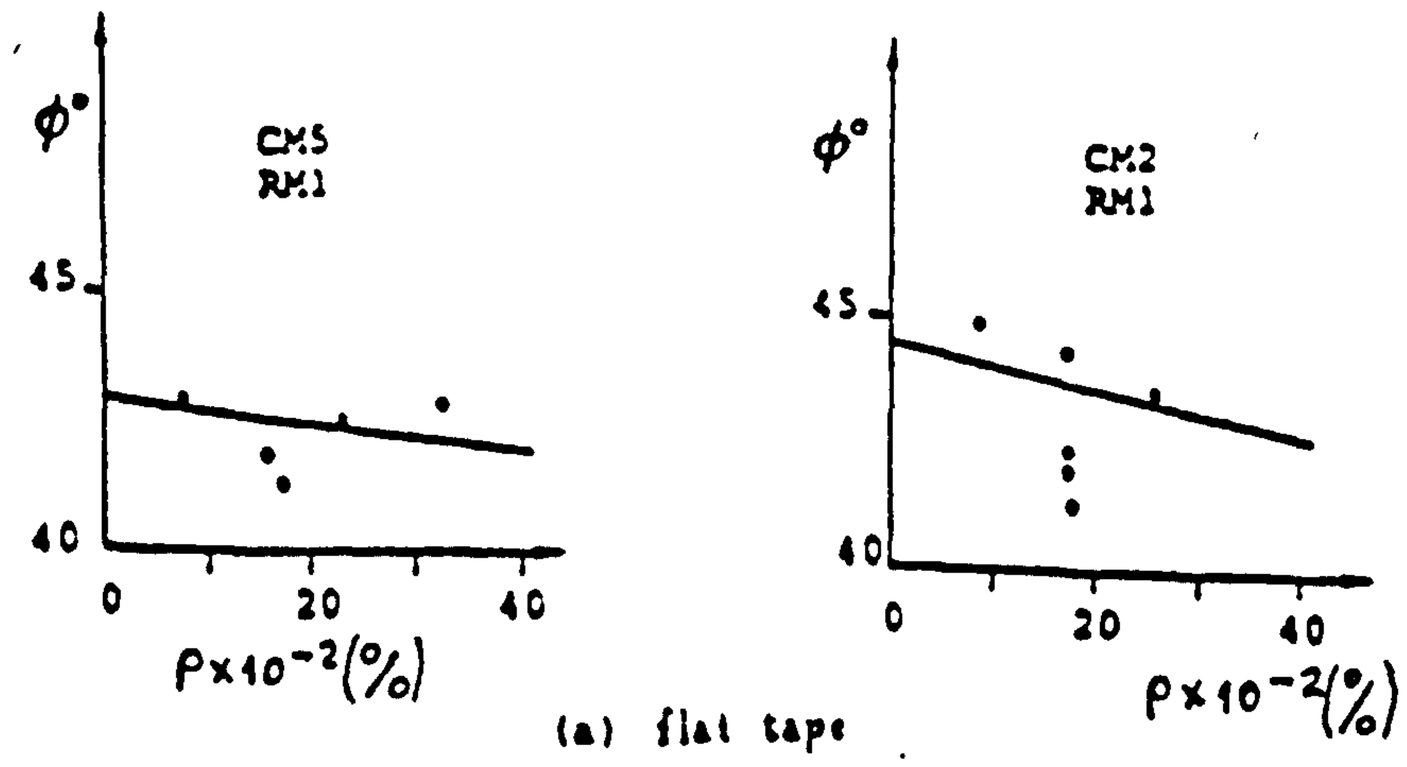

Fig. 2.21 **The angle of friction ϕ° as a function of the percentages of the mixture** (Hoare 1979)

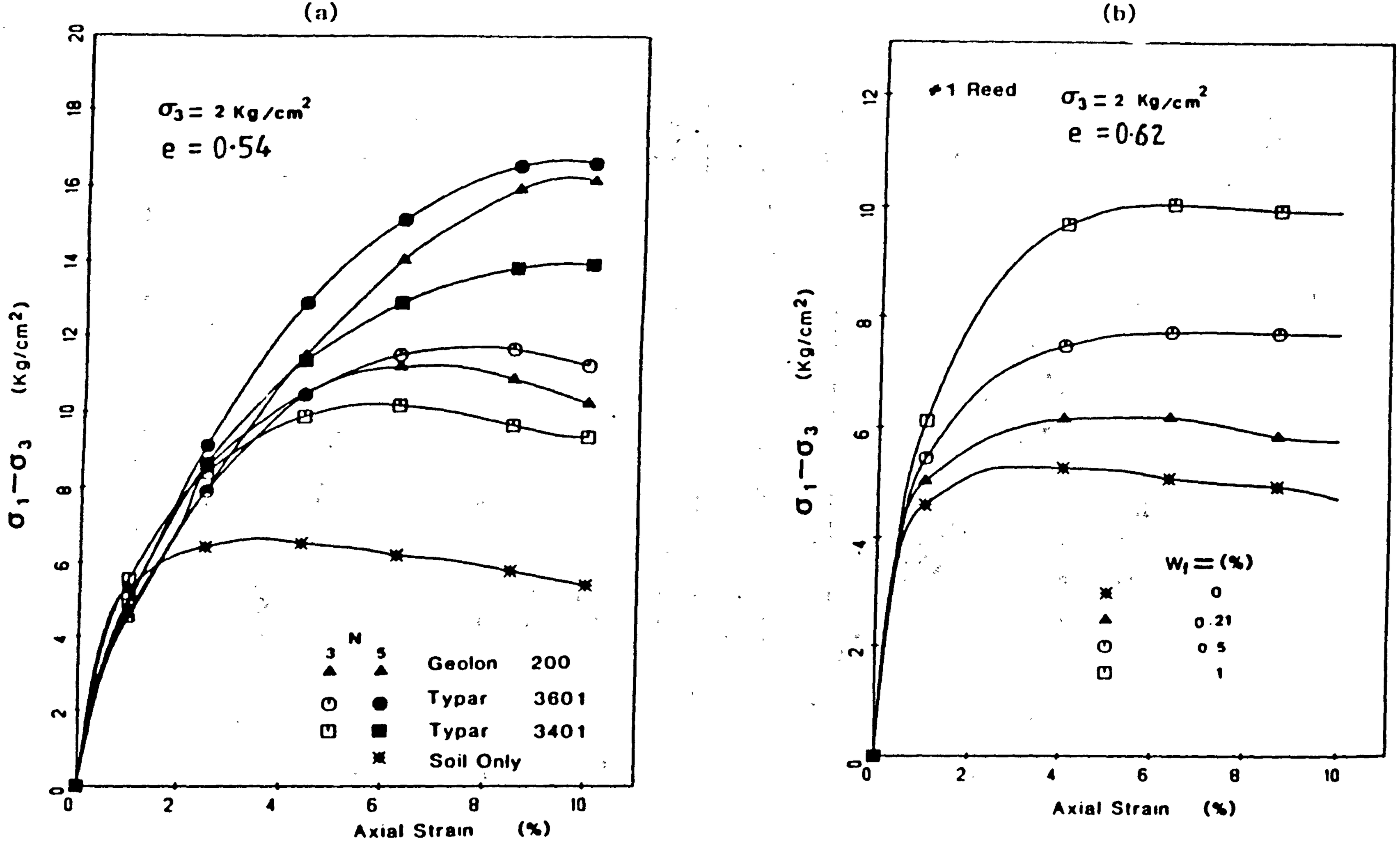

Fig. 2.22 Stress-strain relationships from triaxial compression tests on reinforced Muskegon dune sand. (a) Oriented, fabric layers, (b) Random discrete fibers. (After Gray & Al-Refeai, 1985)

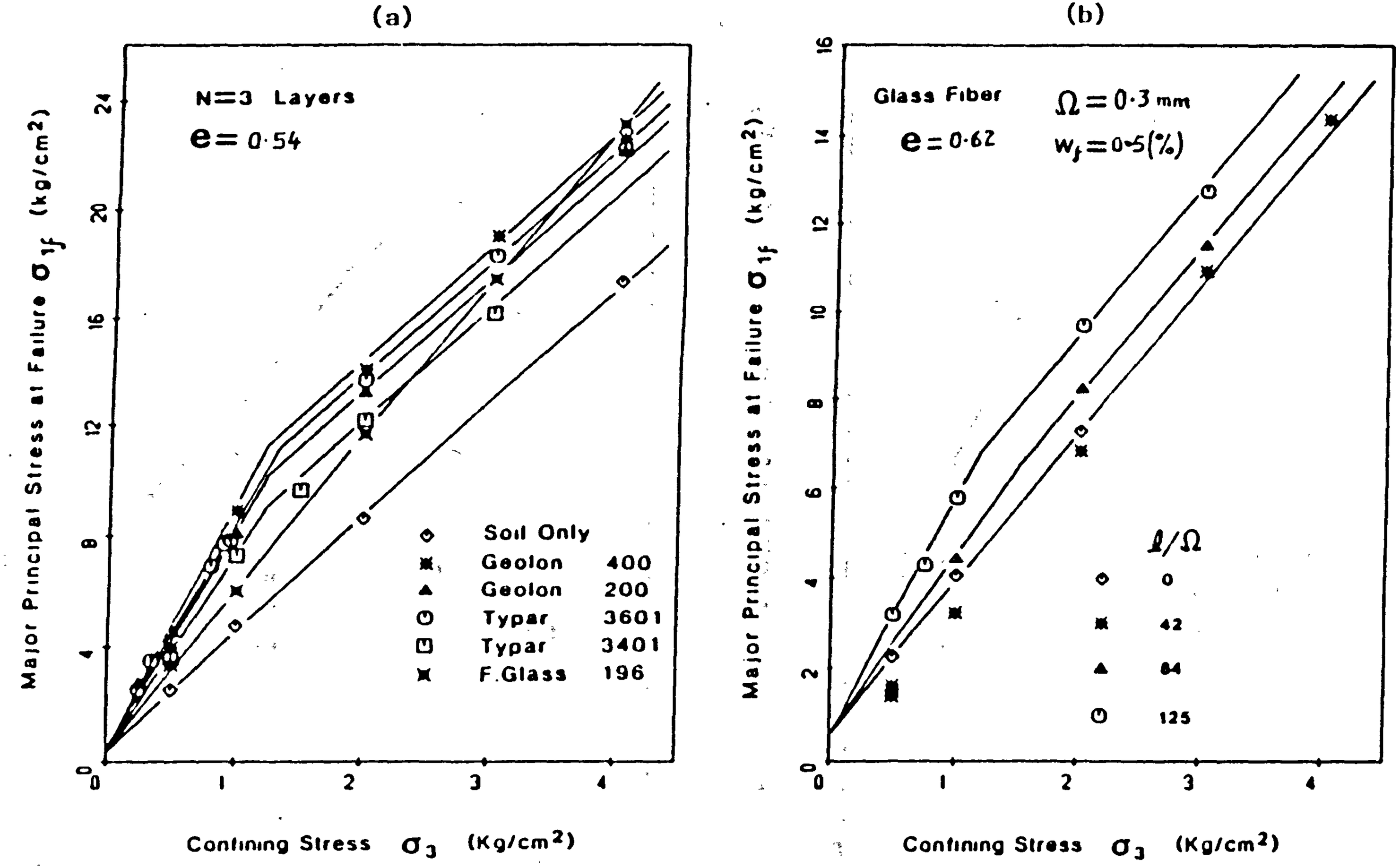

Fig. 2.23 Failure envelopes from triaxial compression tests on reinforced Muskegon dune sand. (a) Oriented, fabric layers, (b) Random, discrete fibers. (After Gray & Al-Refeai, 1985)

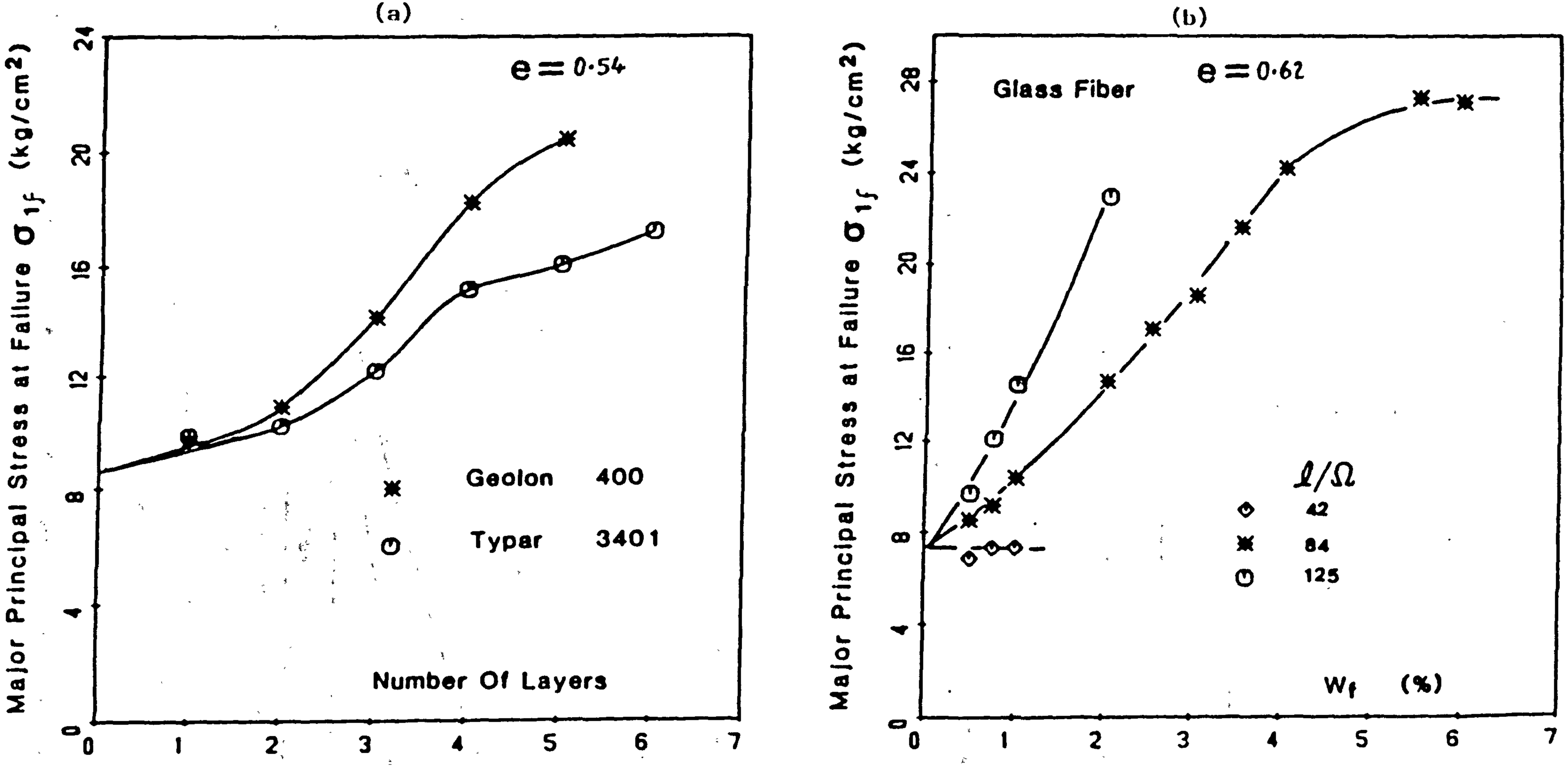

Fig. 2.24 Strength increase as a function of amount of internal reinforcement in triaxial compression tests on Muskegon dune sand. (a) Oriented, fabric layers, (b) Random, discrete fibers. (After Gray & Al-Refeai, 1985)

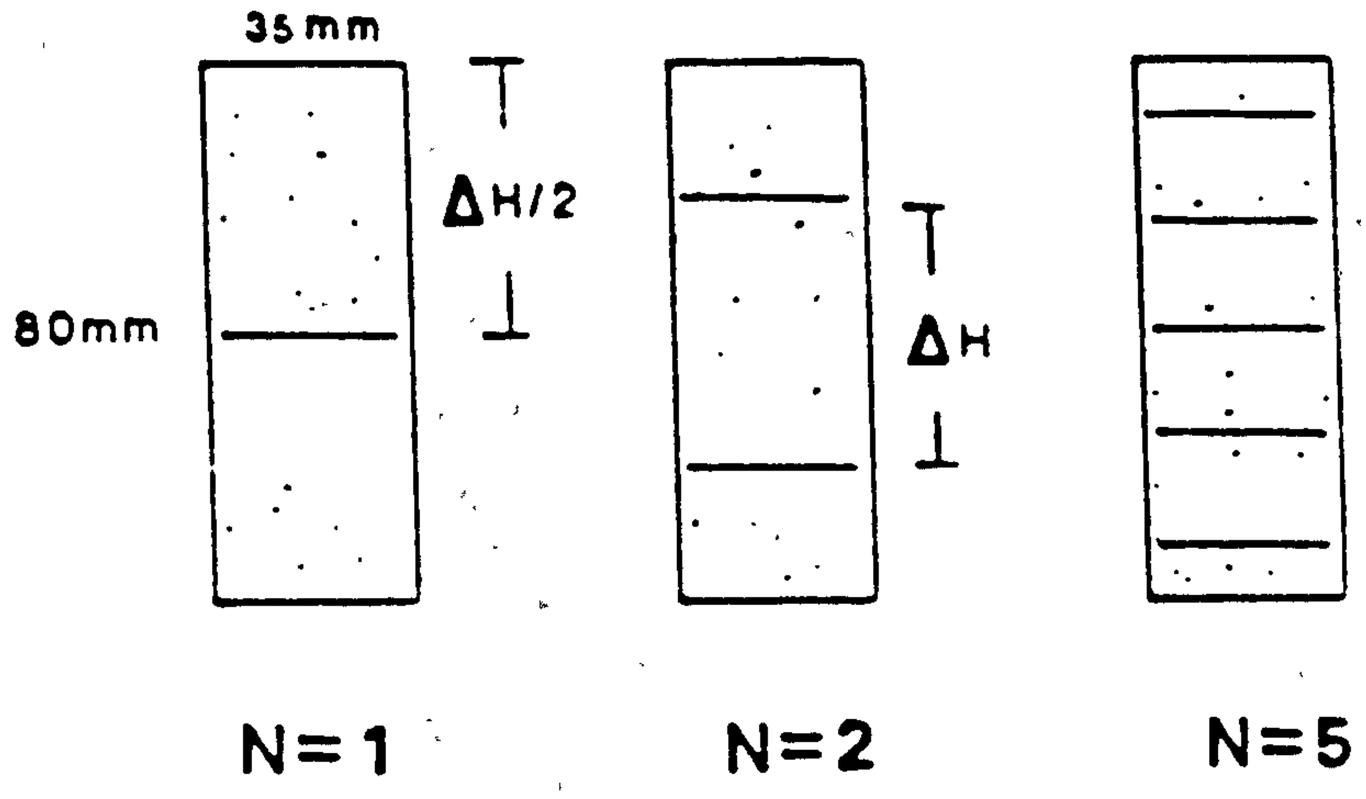

Fig. 2.25 Fabric layer positions in triaxial test specimens.
(After Gray & Al-Refeai, 1985)

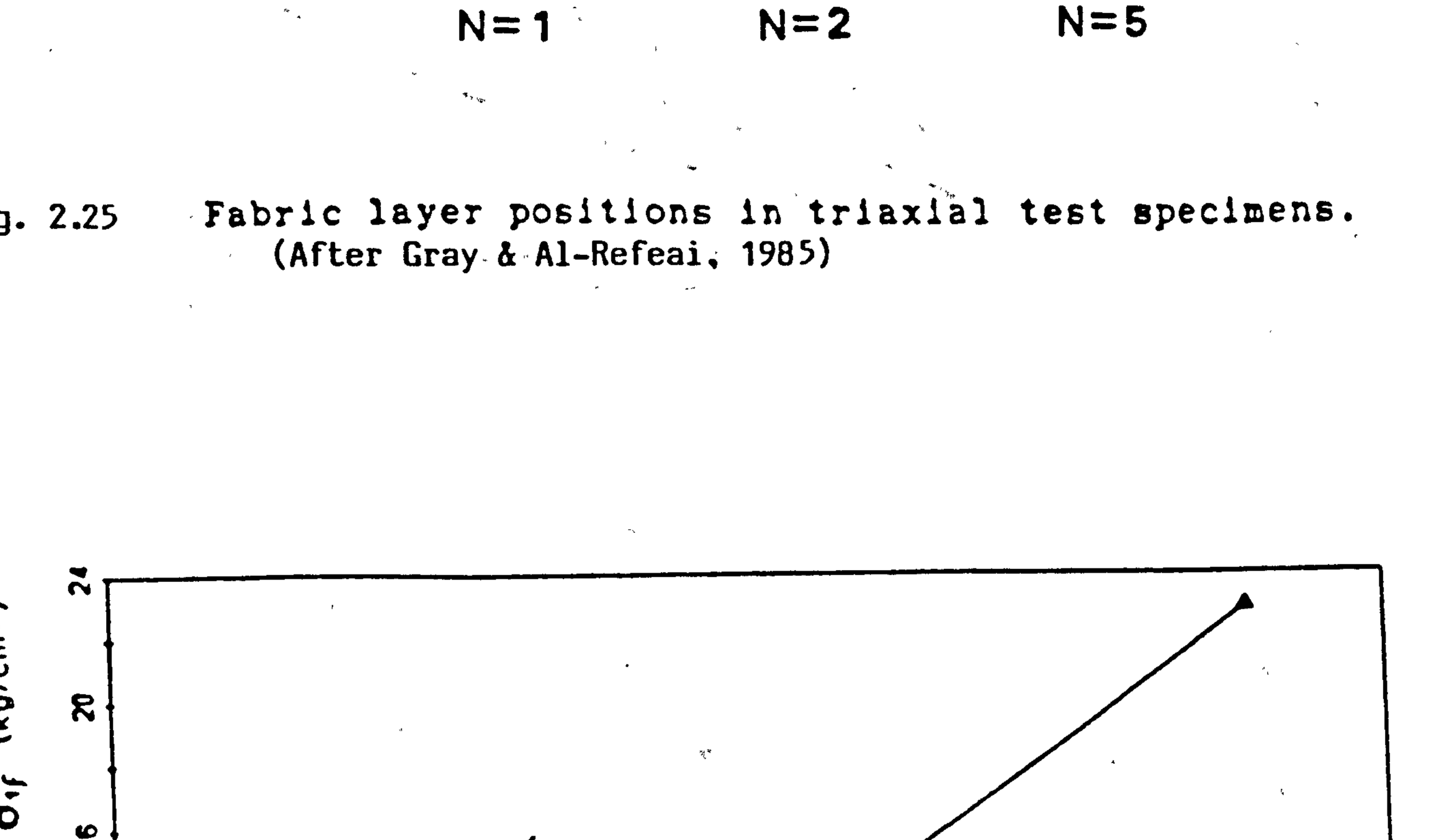

Fig. 2.26 Major principal stress at failure for fiber reinforced sand as a function of aspect ratio at different fiber weight concentrations.
(After Gray & Al-Refeai, 1985)

(After Leflaive & Long, 1983)

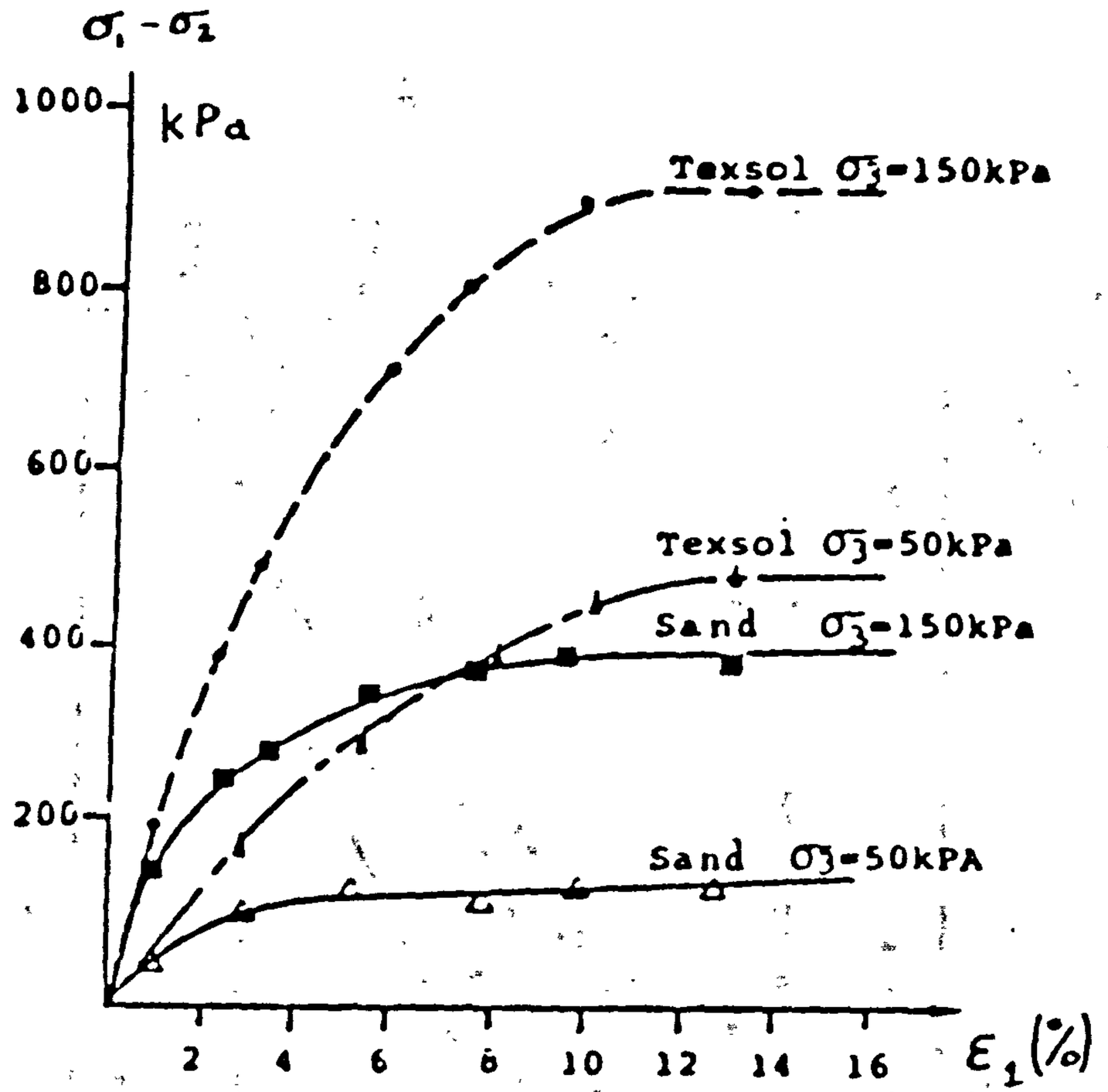

Fig. 2.27 Stress/deformation curves for loose texsol (Perche)

(After Leflaive & Long, 1983)

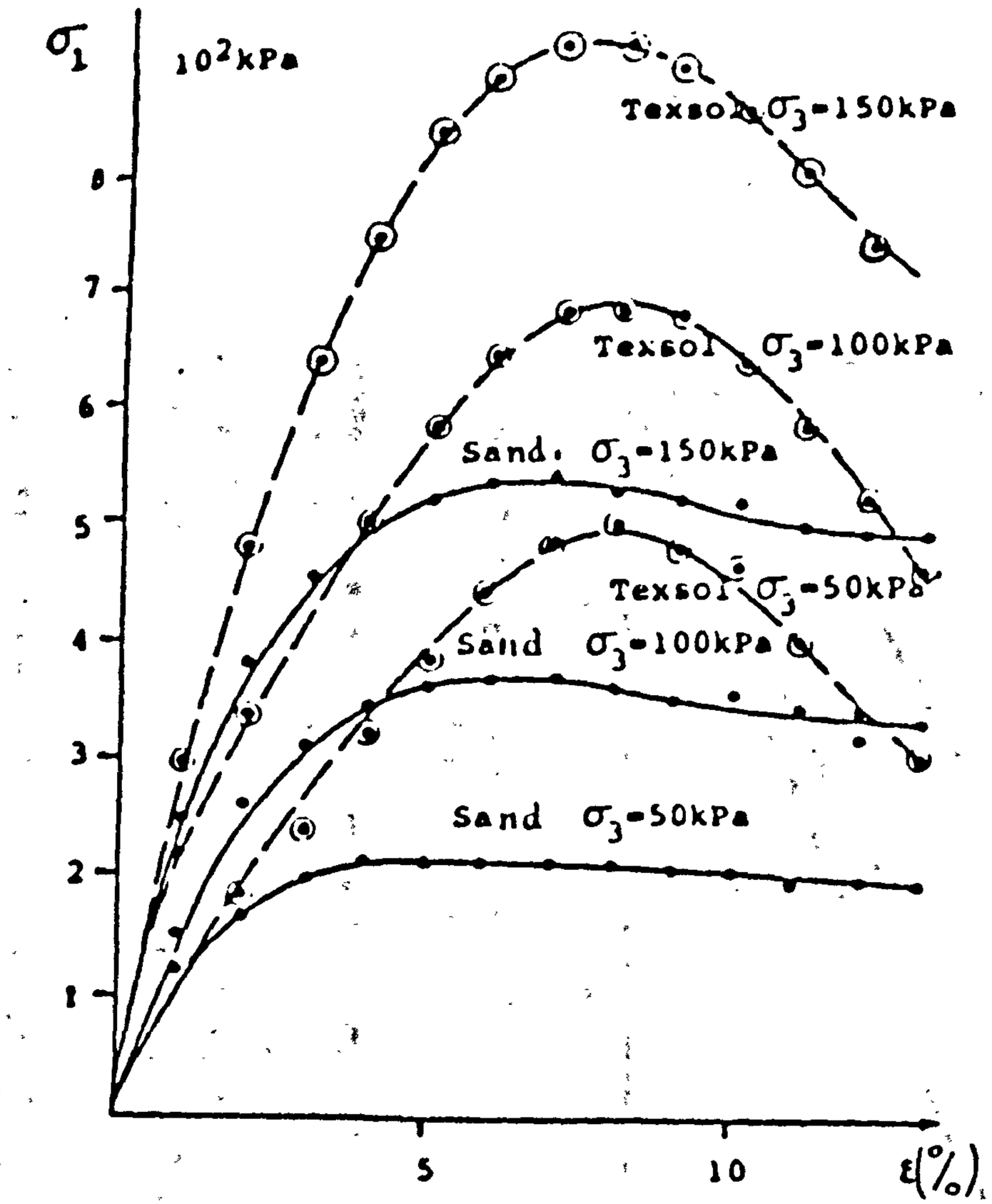

Fig. 2.28 Stress/deformation curves for compact texsol (Streff)

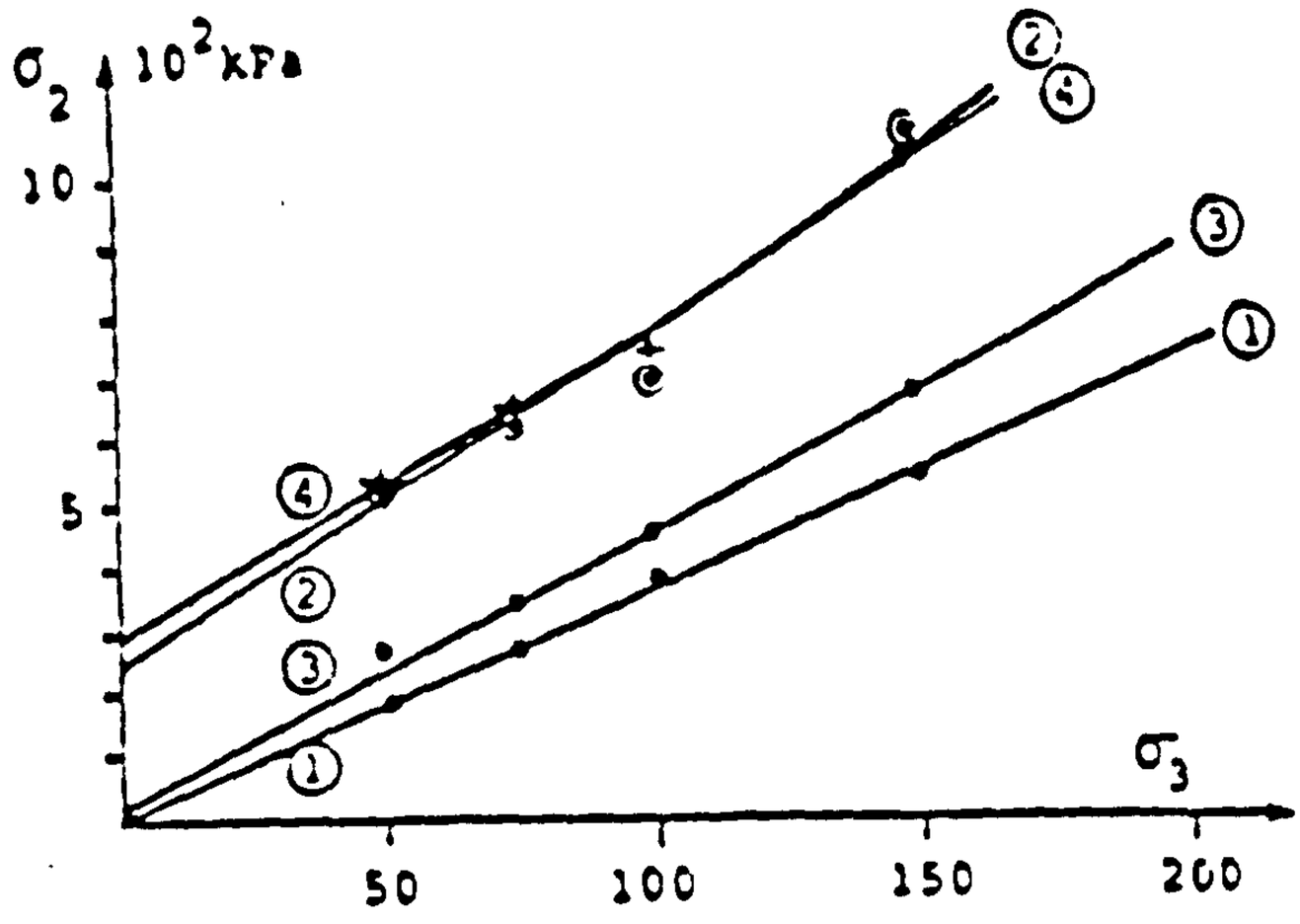

(After Leflaive & Long, 1983)

Fig. 2.29 Intrinsic properties of loose sand and texsol

Loose Perche alone $\sigma_1 = 3,71\ \sigma_3 + 2,55$ ①
Loose Perche + texsol $\sigma_1 = 5,24\ \sigma_3 + 244,71$ ②

Loose Streff alone $\sigma_1 = 4,44\ \sigma_3 + 18,85$ ③
Loose Streff + texsol $\sigma_1 = 4,85\ \sigma_3 + 293,3$ ④

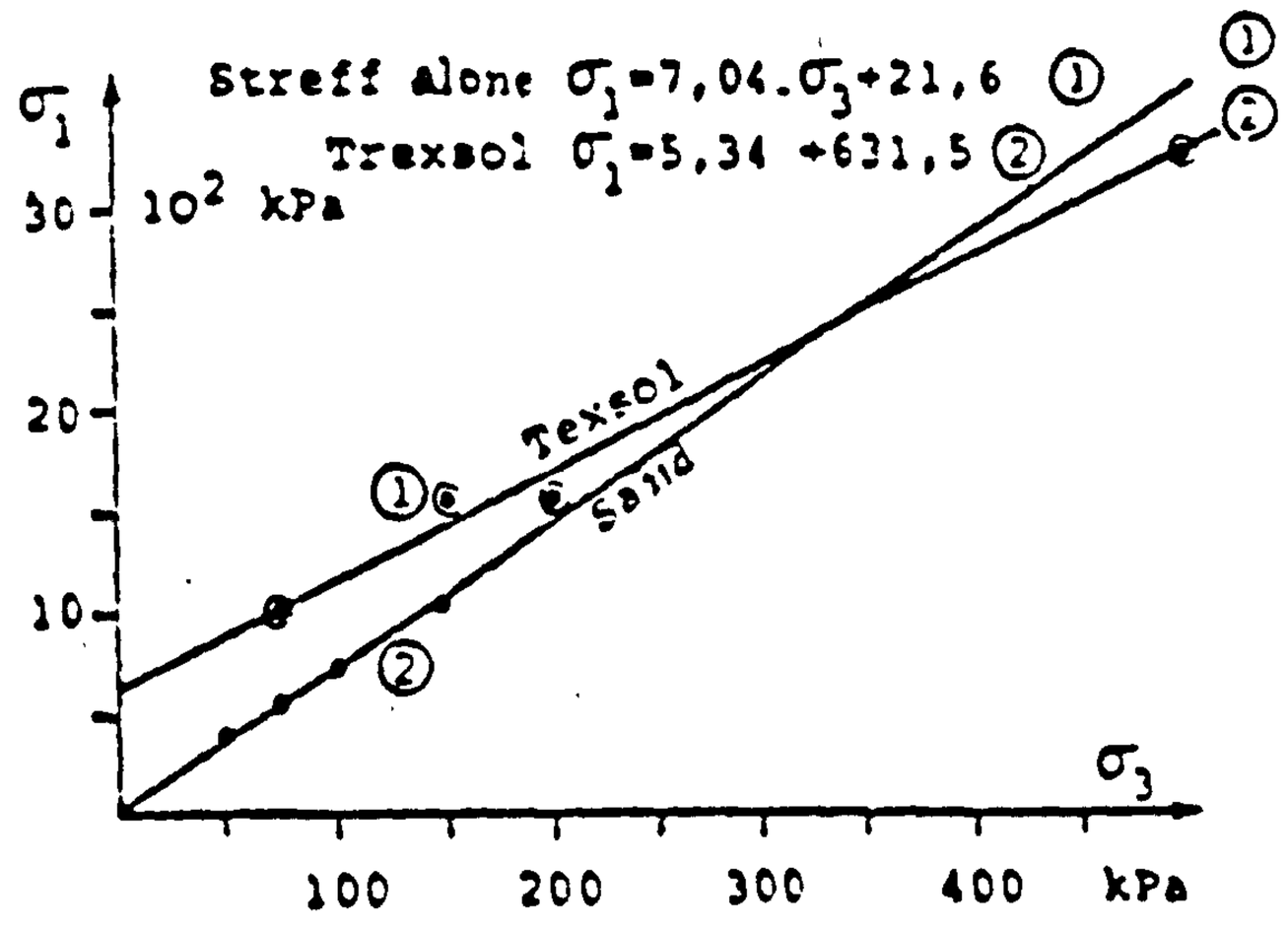

(After Leflaive & Long, 1983)

Fig. 2.30 Intrinsic properties of compact sand and texsol (Streff)

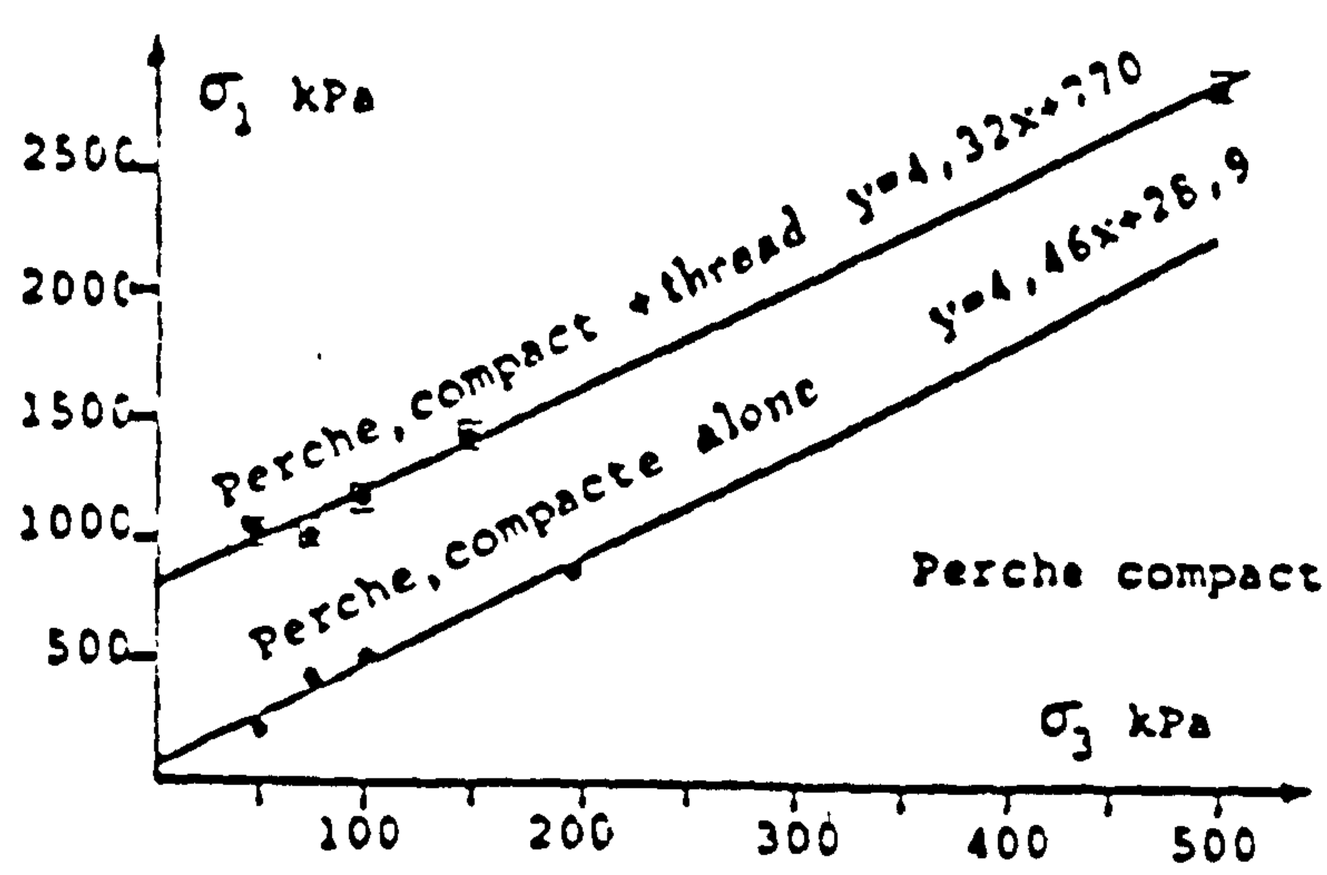

(After Leflaive & Long, 1983)

Fig. 2.31 Intrinsic properties of a compact sand with texsol

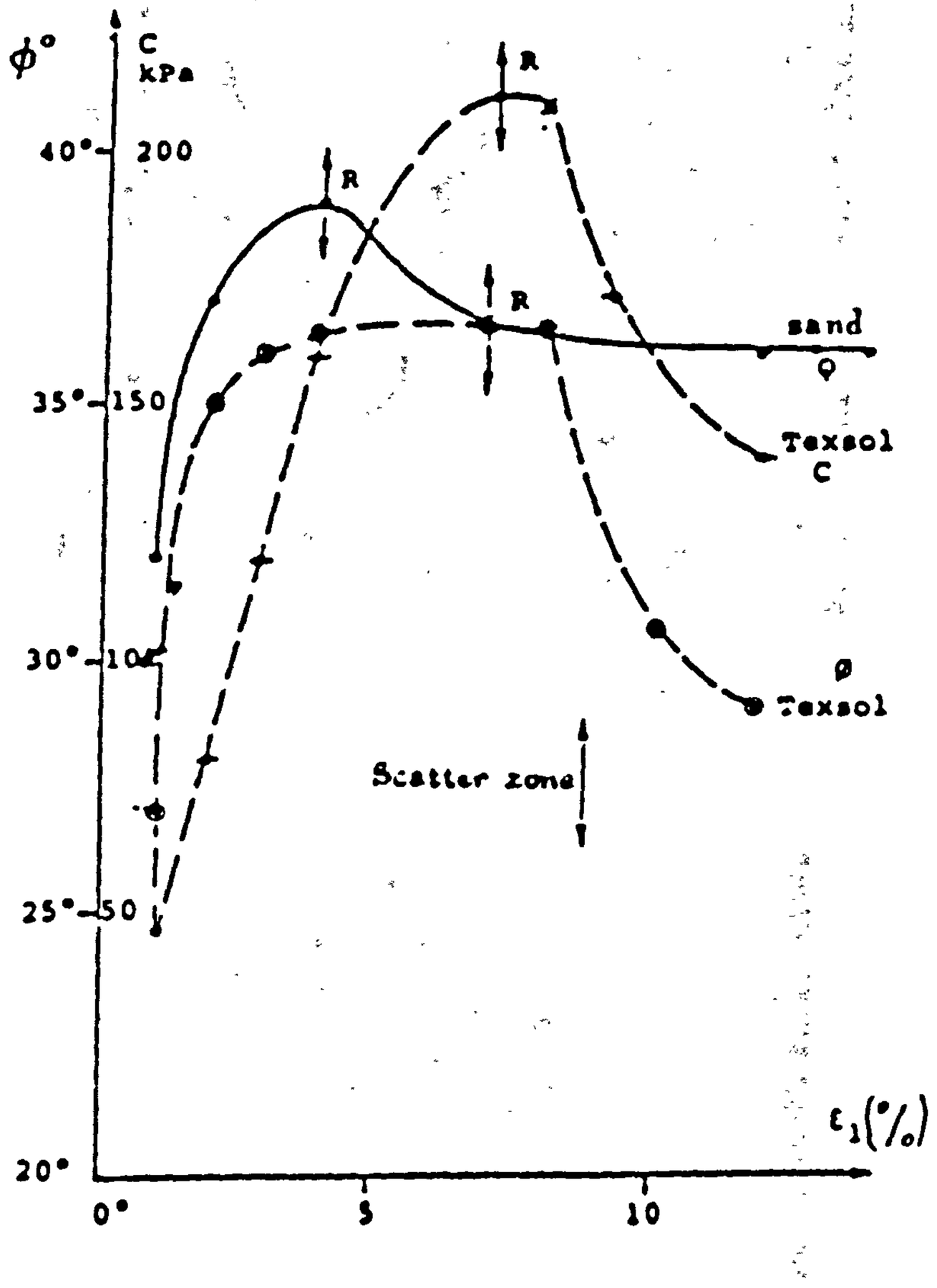

Fig. 2.32 Build-up of cohesion and the internal angle of friction in sand and loose Texsol (Perche)
(After Leflaive & Long, 1983)

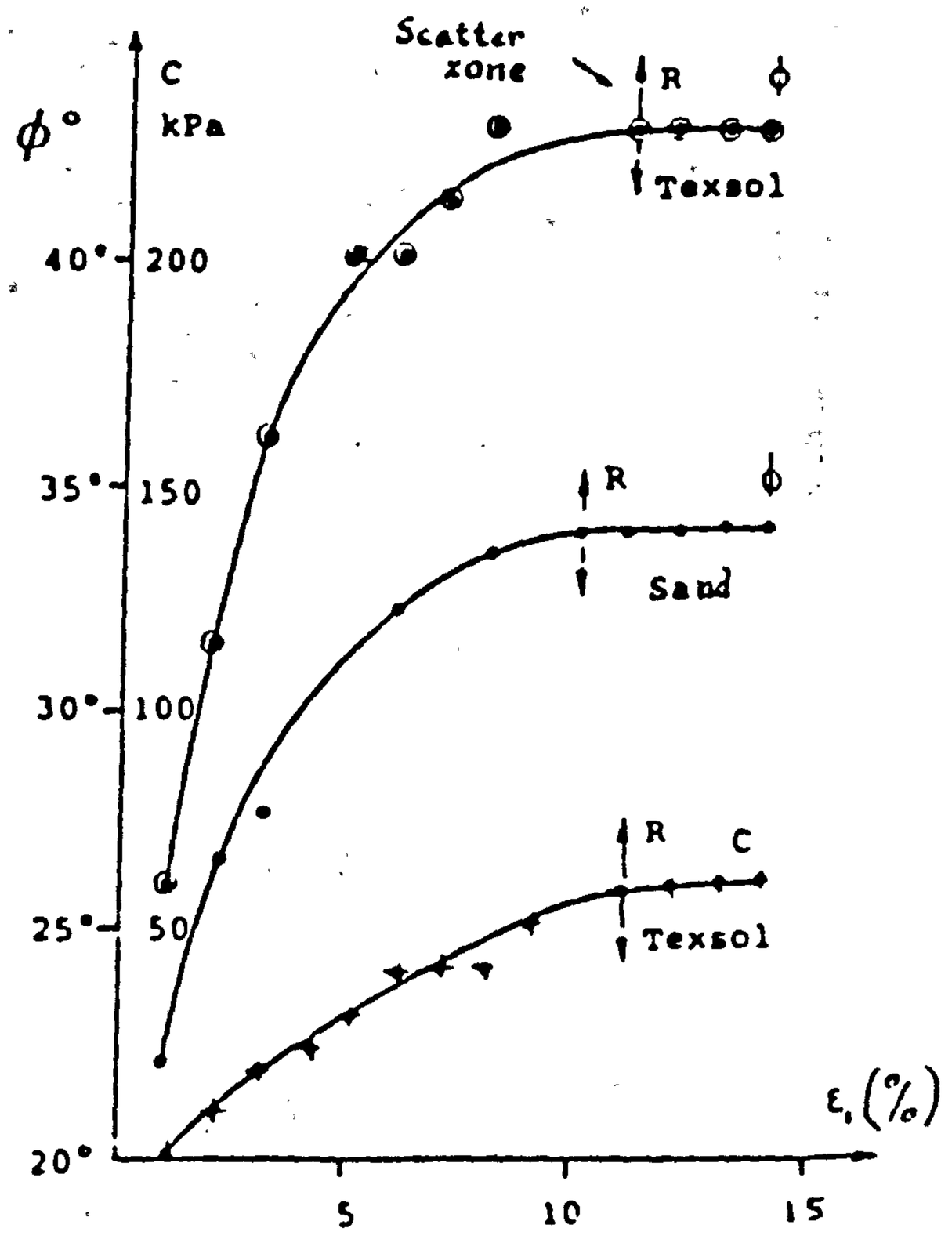

Fig. 2.33 Build-up of cohesion and the internal angle of friction in sand and compact Texsol(Perche)
(After Leflaive & Long, 1983)

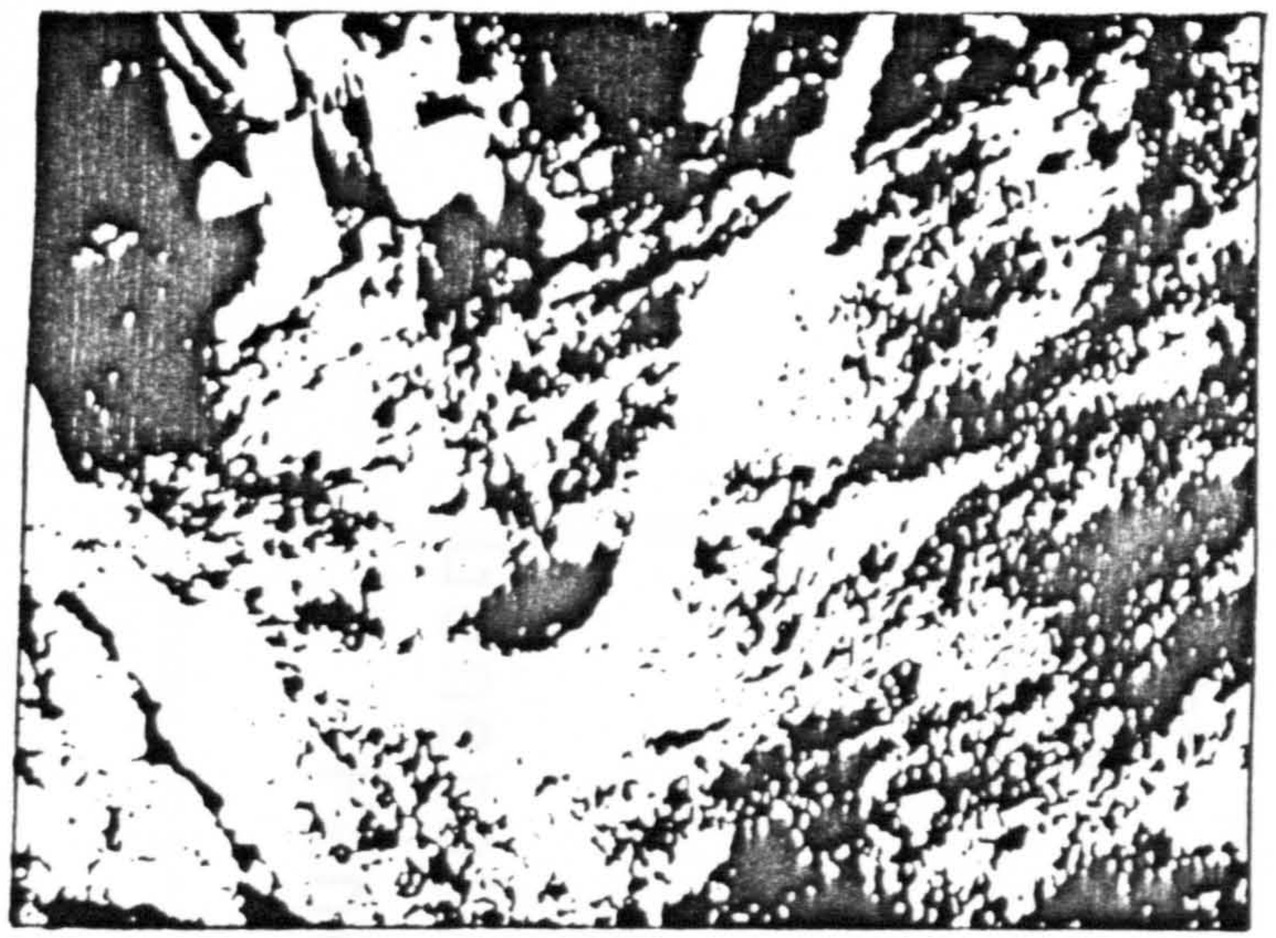

Fig. 2.34 A closed view of the actual mixing of simultaneous projection of sand and thread

(Leflaive, 1983)

Fig. 2.36 Mass of sand treated with a 20 min jet spray of water

(Leflaive, 1983)

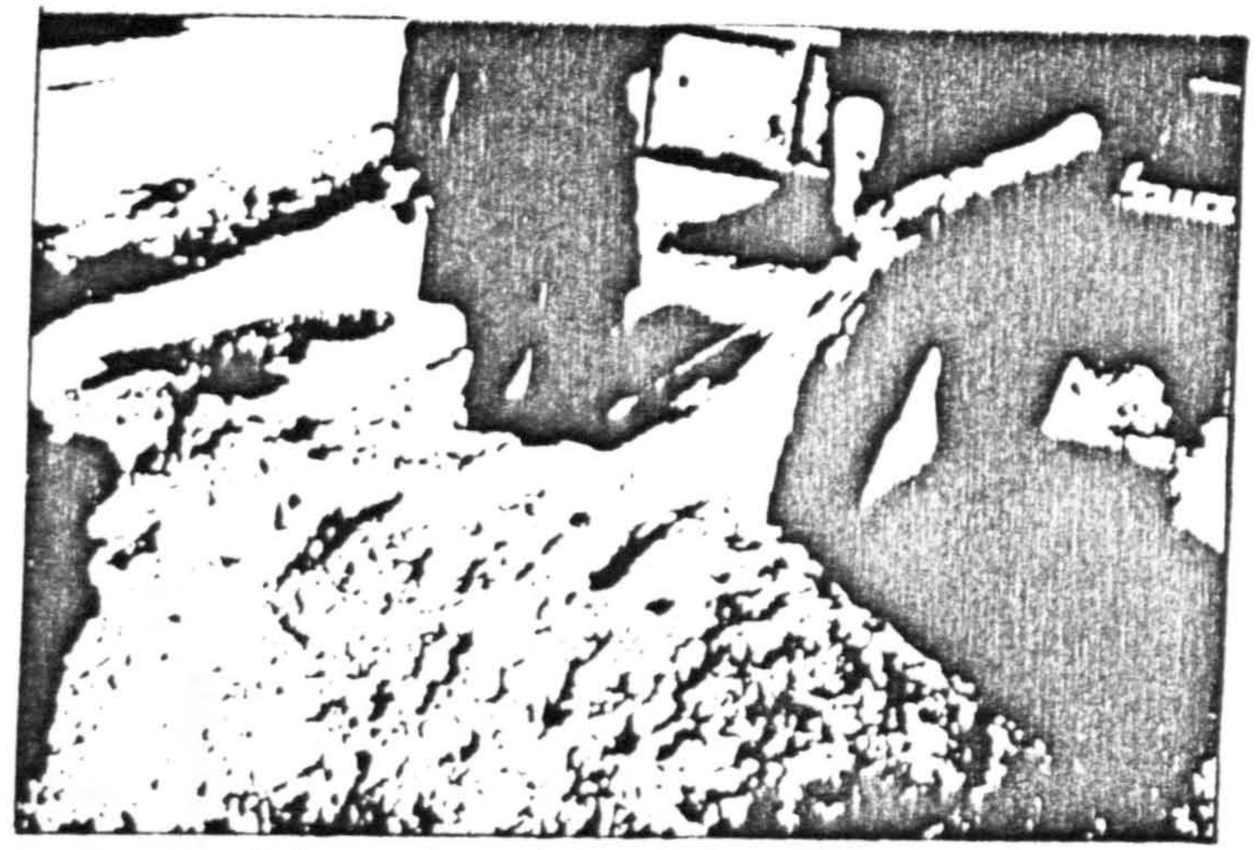

Fig. 2.35 Volume of sand treated with low dosage (around 0.5 per 1000) thread pulled from the mass

(Leflaive, 1983)

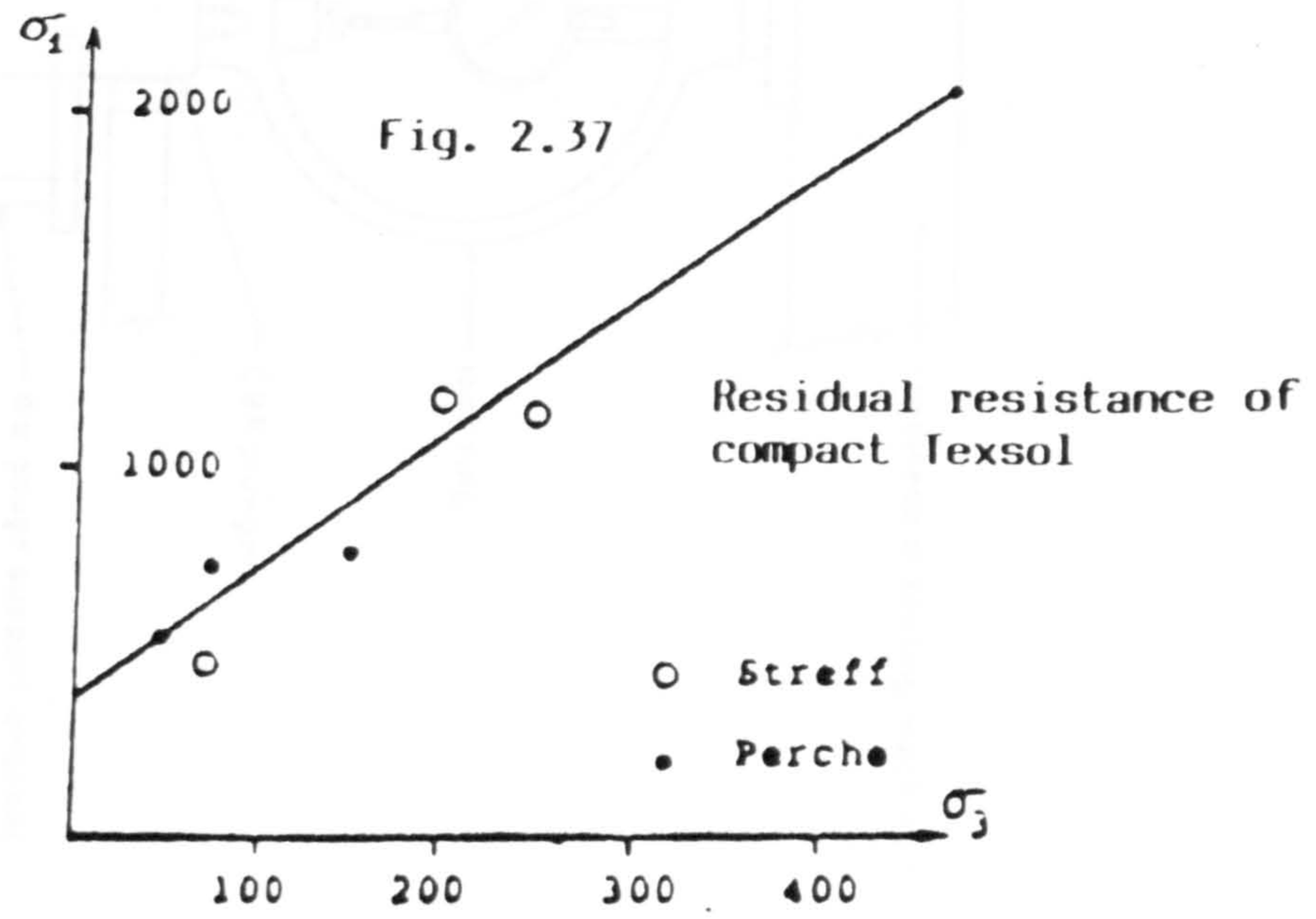

(Leflaive & Long, 1983)

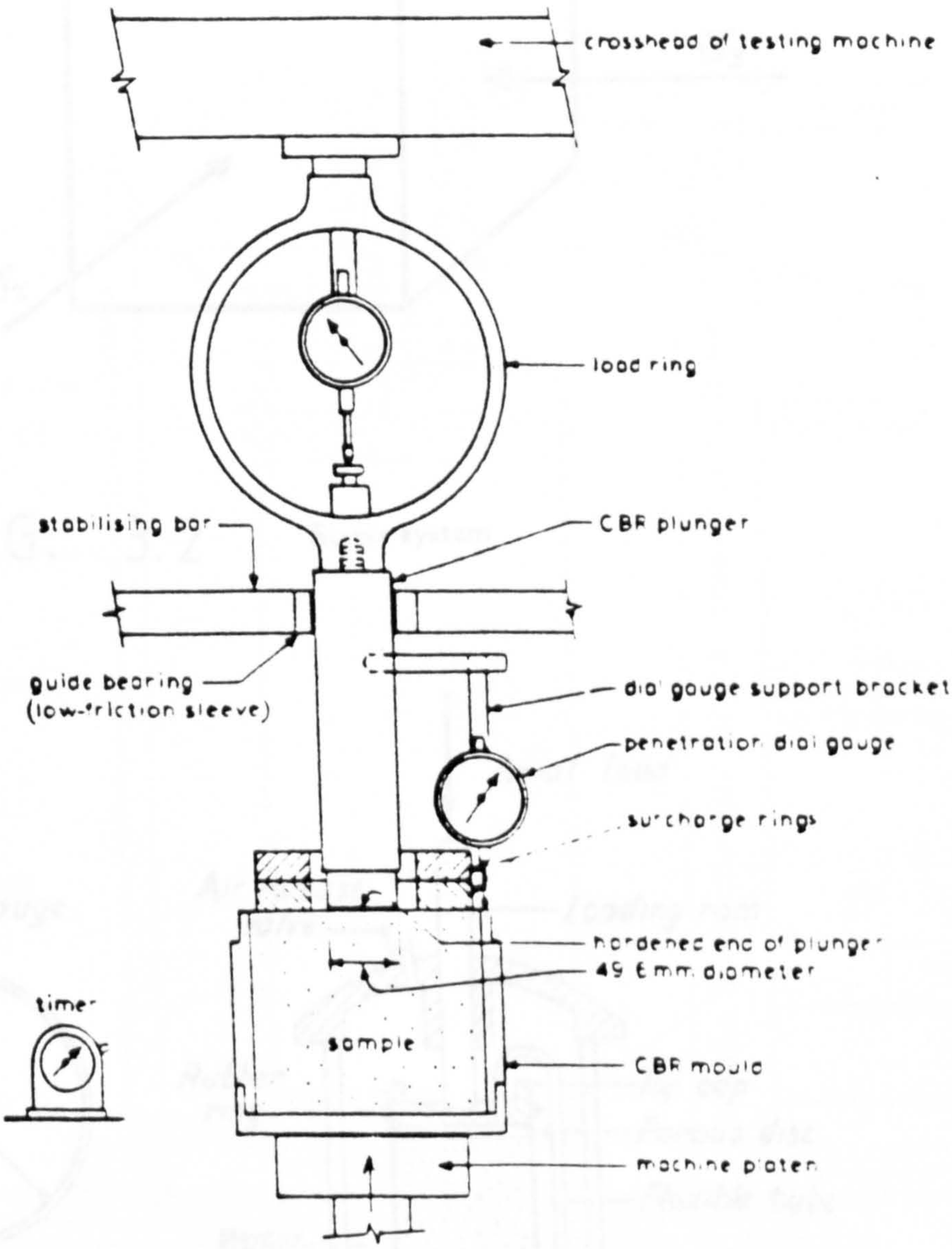

General arrangement for CBR Penetration test

FIG. 3.1

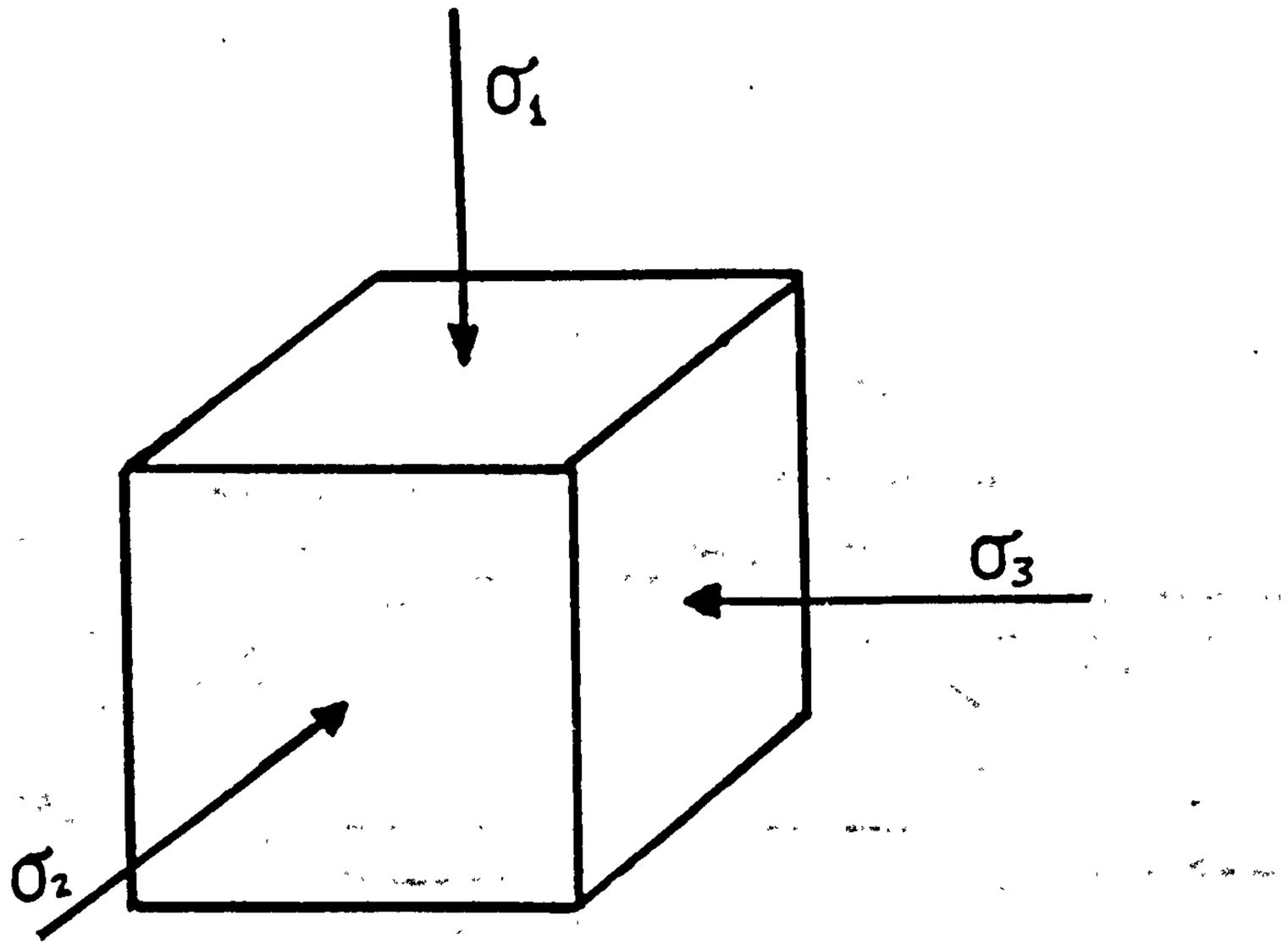

FIG. 3.2 Stress system

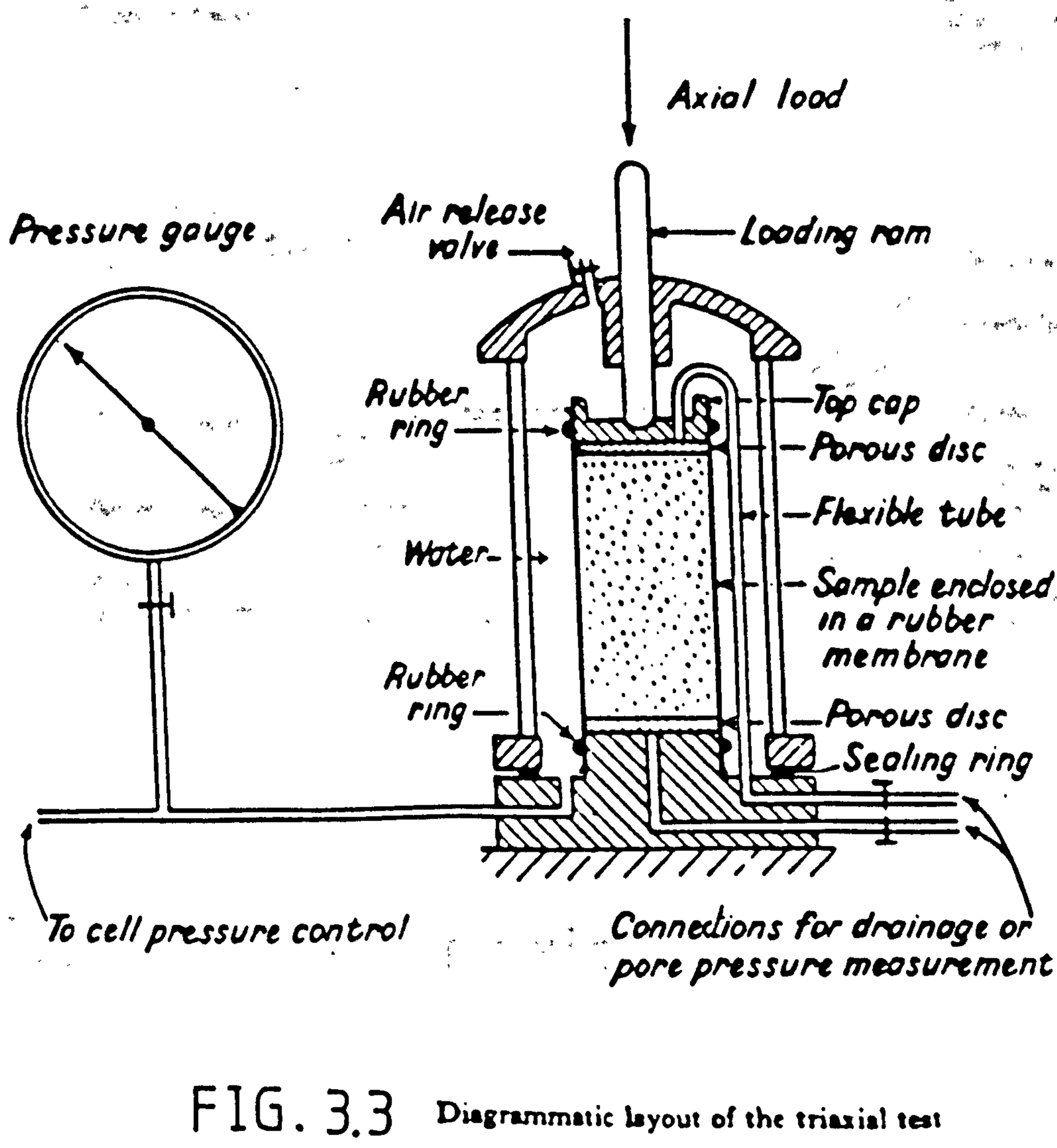

FIG. 3.3 Diagrammatic layout of the triaxial test

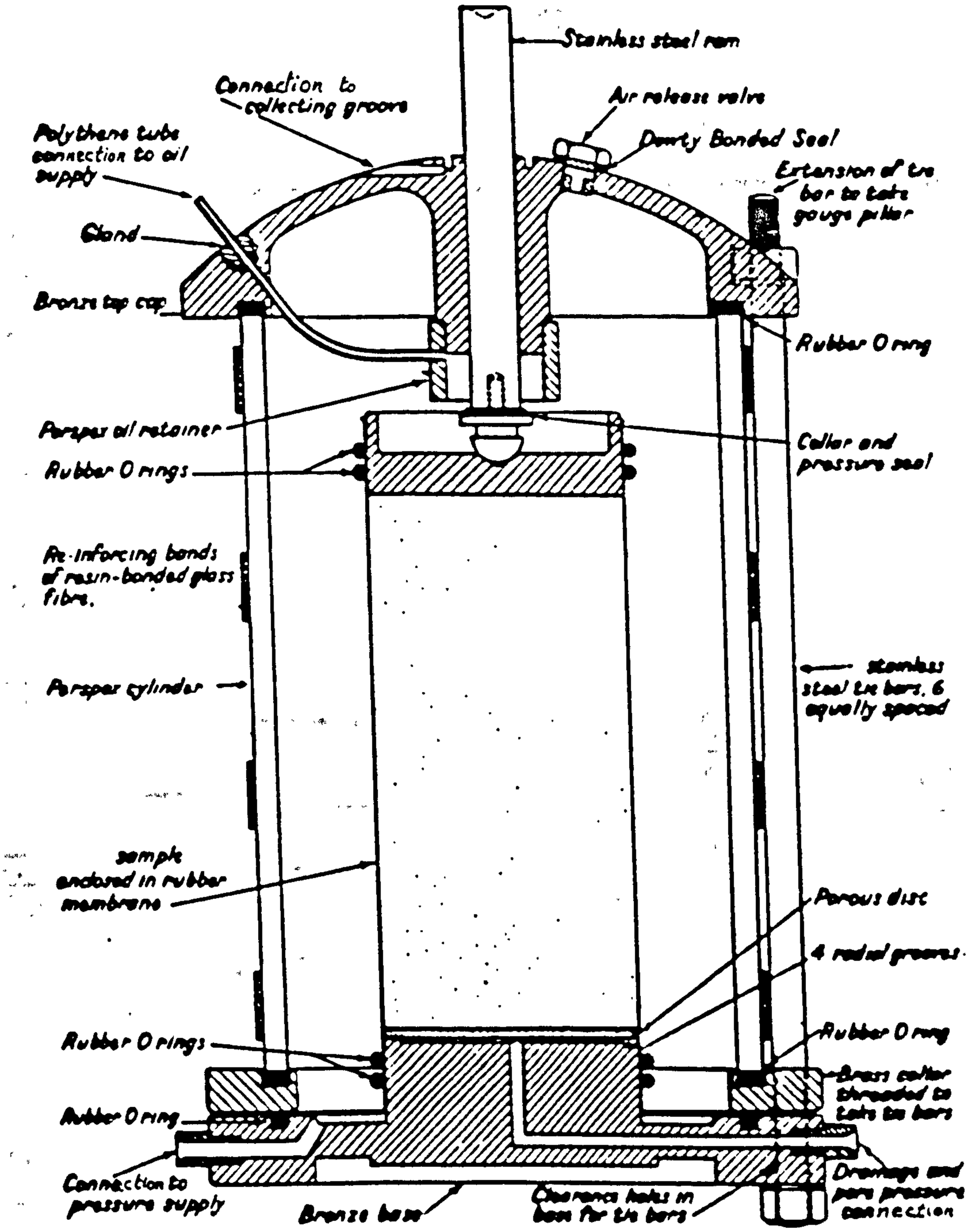

FIG. 3.4 The triaxial cell

FIG. 3.5 MODEL FOOTING APPARATUS

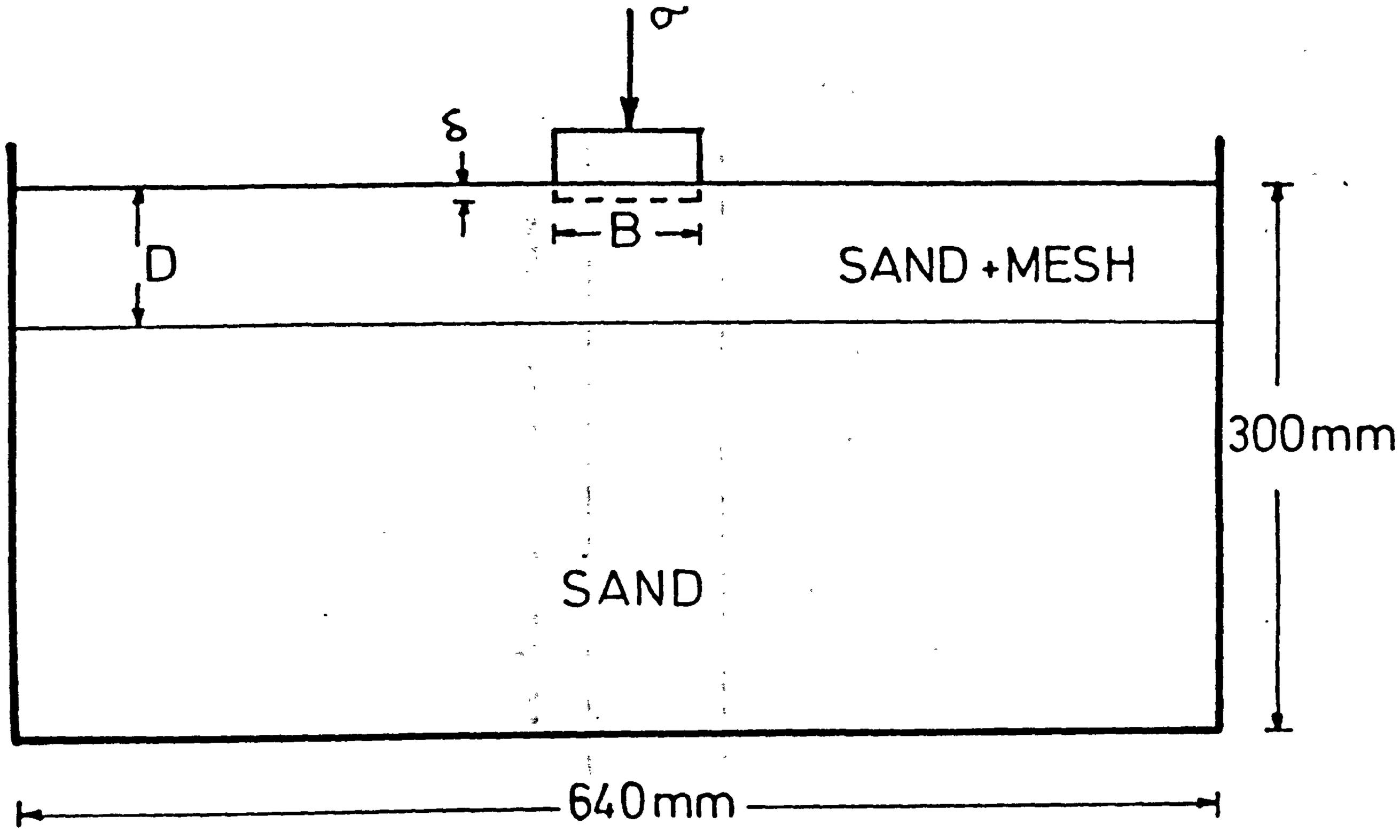

FIG 3.6

A TYPICAL STEREO PHOTOGRAMMETRIC PAIR

(NO MESH ELEMENTS USED)

INITIAL STAGE OF LOADING

δ/B = 0%

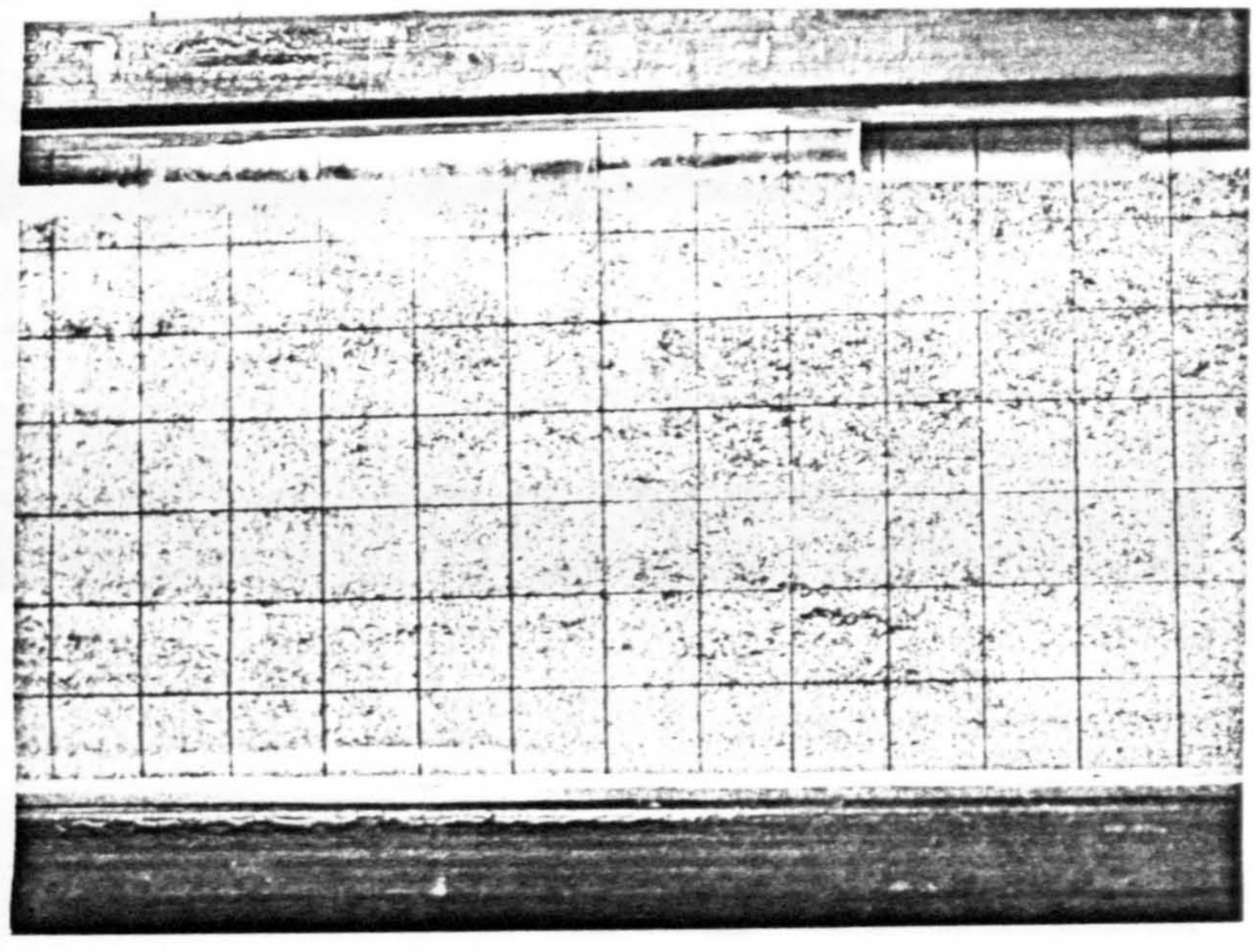

FINAL STAGE OF LOADING

δ/B = 20%

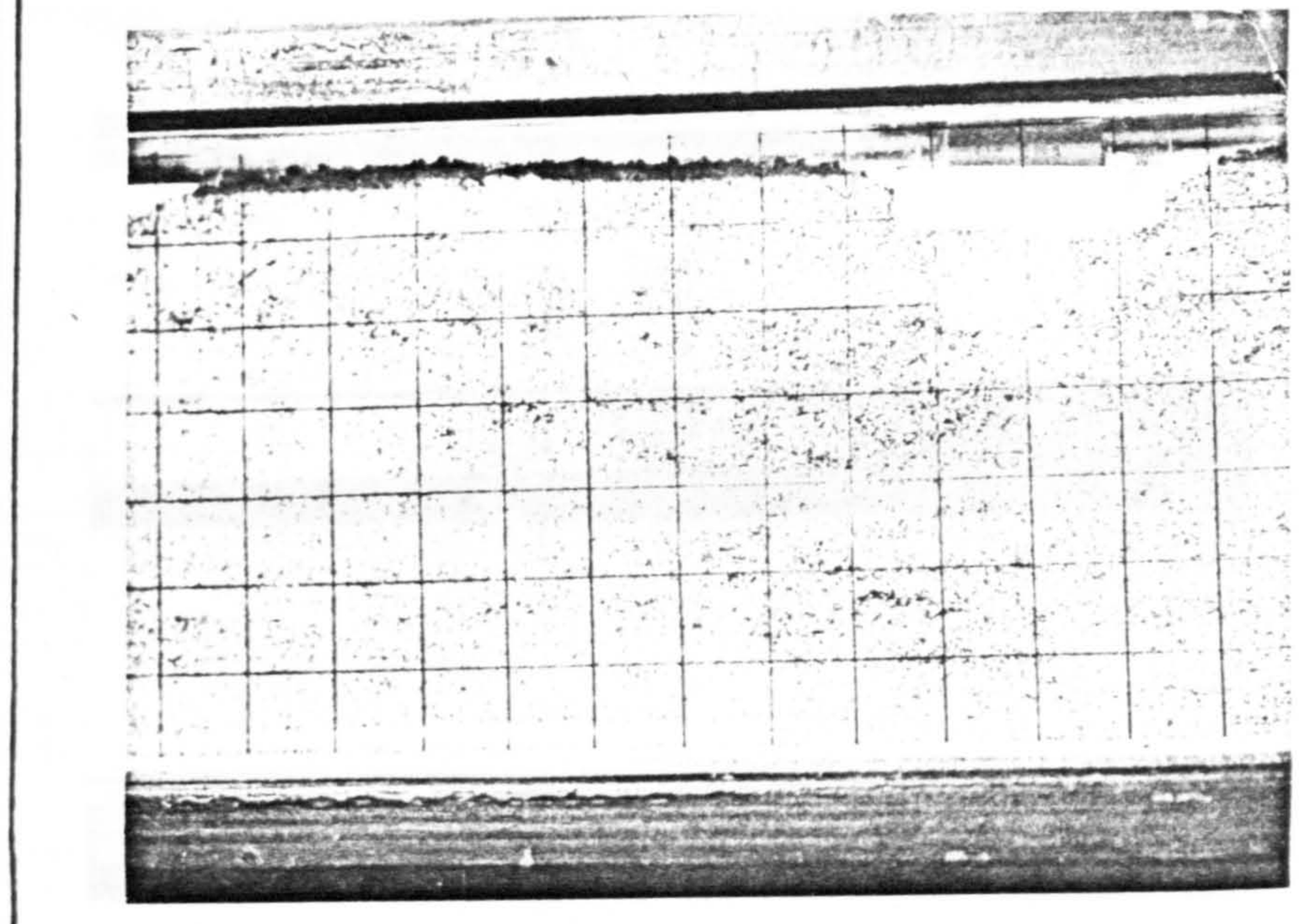

SOIL TYPE : MID-ROSS SAND.

FIG 3.7

A TYPICAL STEREO PHOTOGRAMMETRIC PAIR

(SOIL MIXED WITH MESH ELEMENTS)

SOIL TYPE : MID-ROSS SAND. MESH ELEMENT TYPE 7. MESH ELEMENT SIZE 50 x 50 mm

MESH CONTENT 66 m^2/m^3

INITIAL STAGE OF LOADING

δ/B = 0%

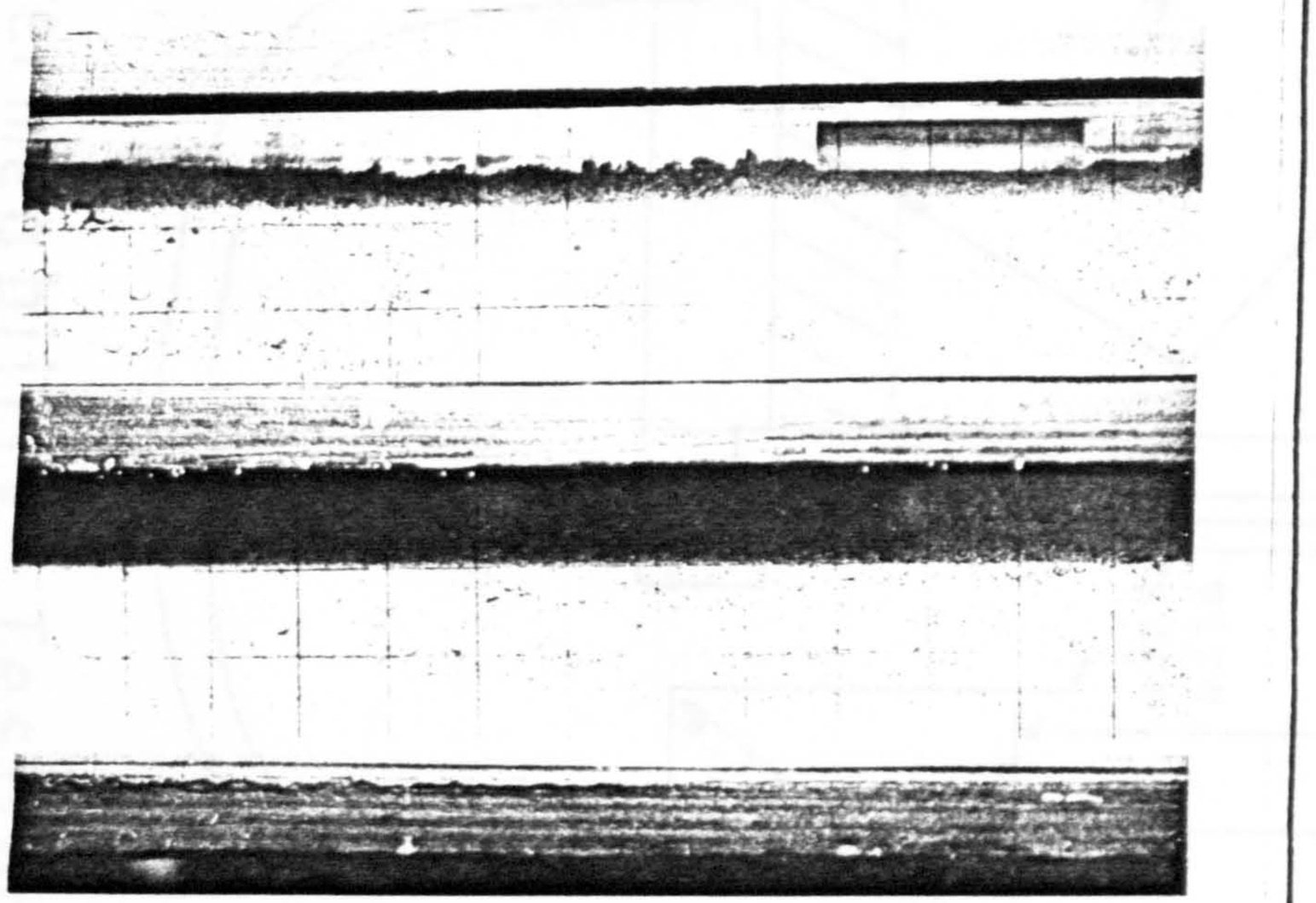

FINAL STAGE OF LOADING

δ/B = 20%

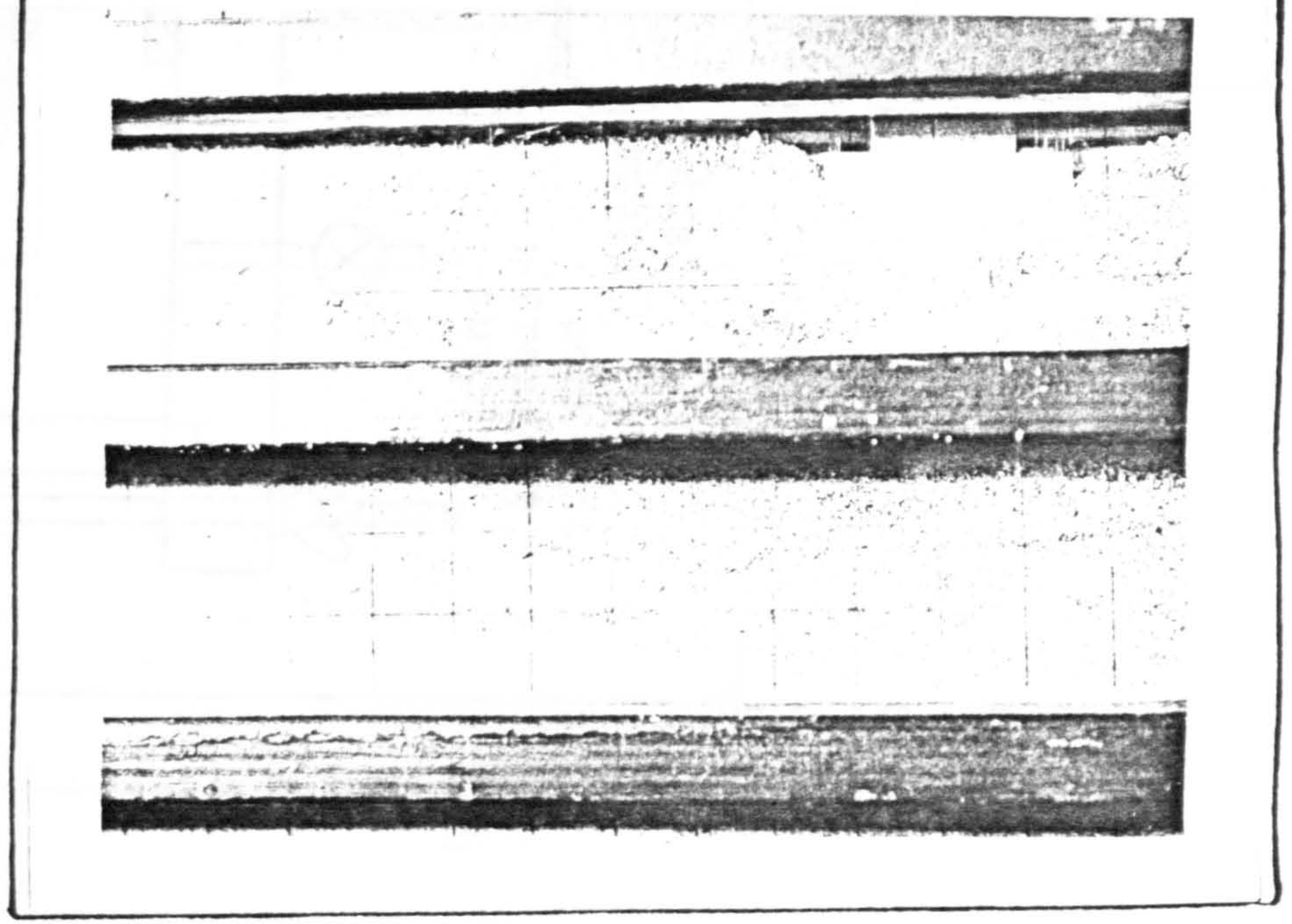

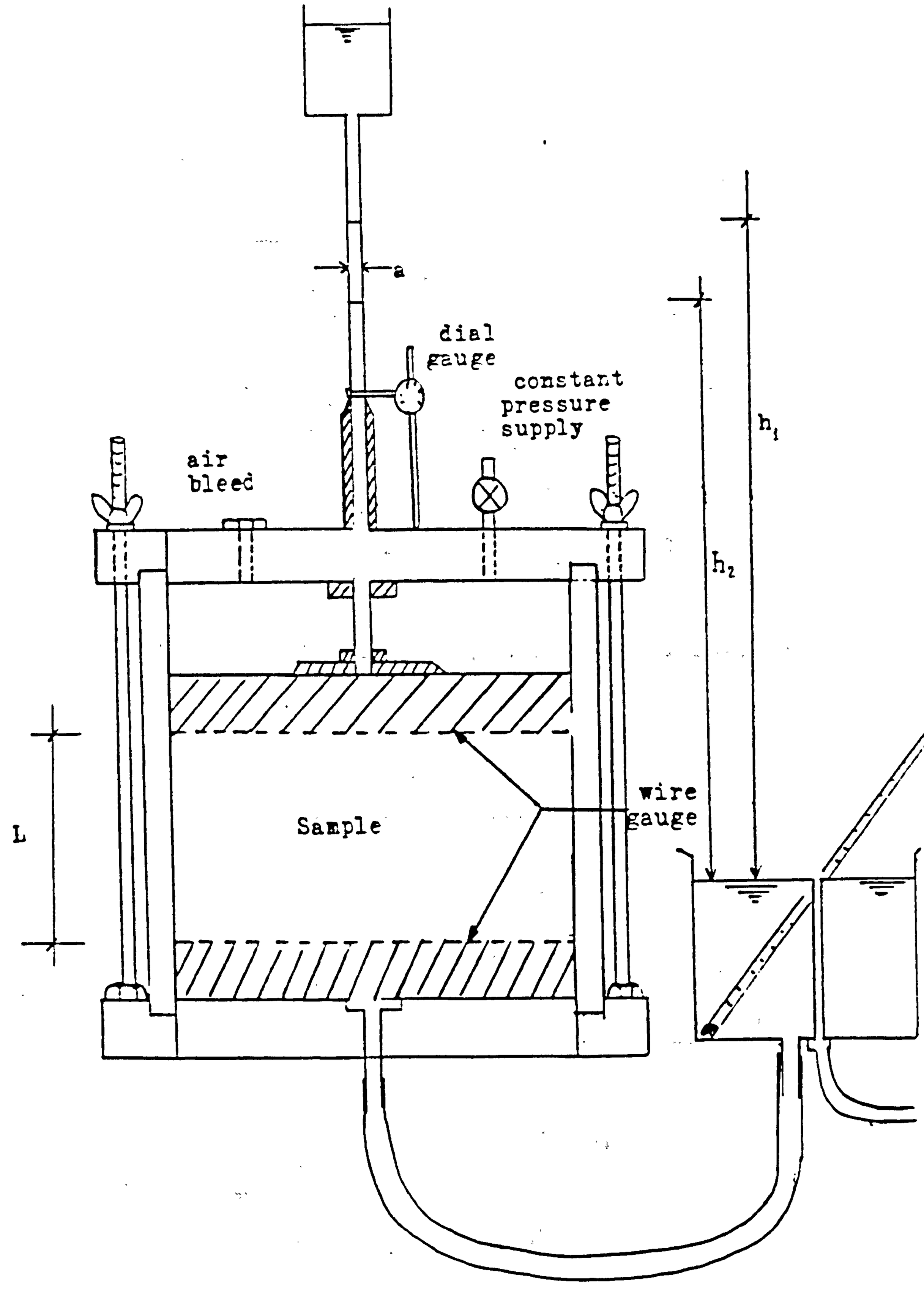

FIG 3.8 Permeability Testing Apparatus

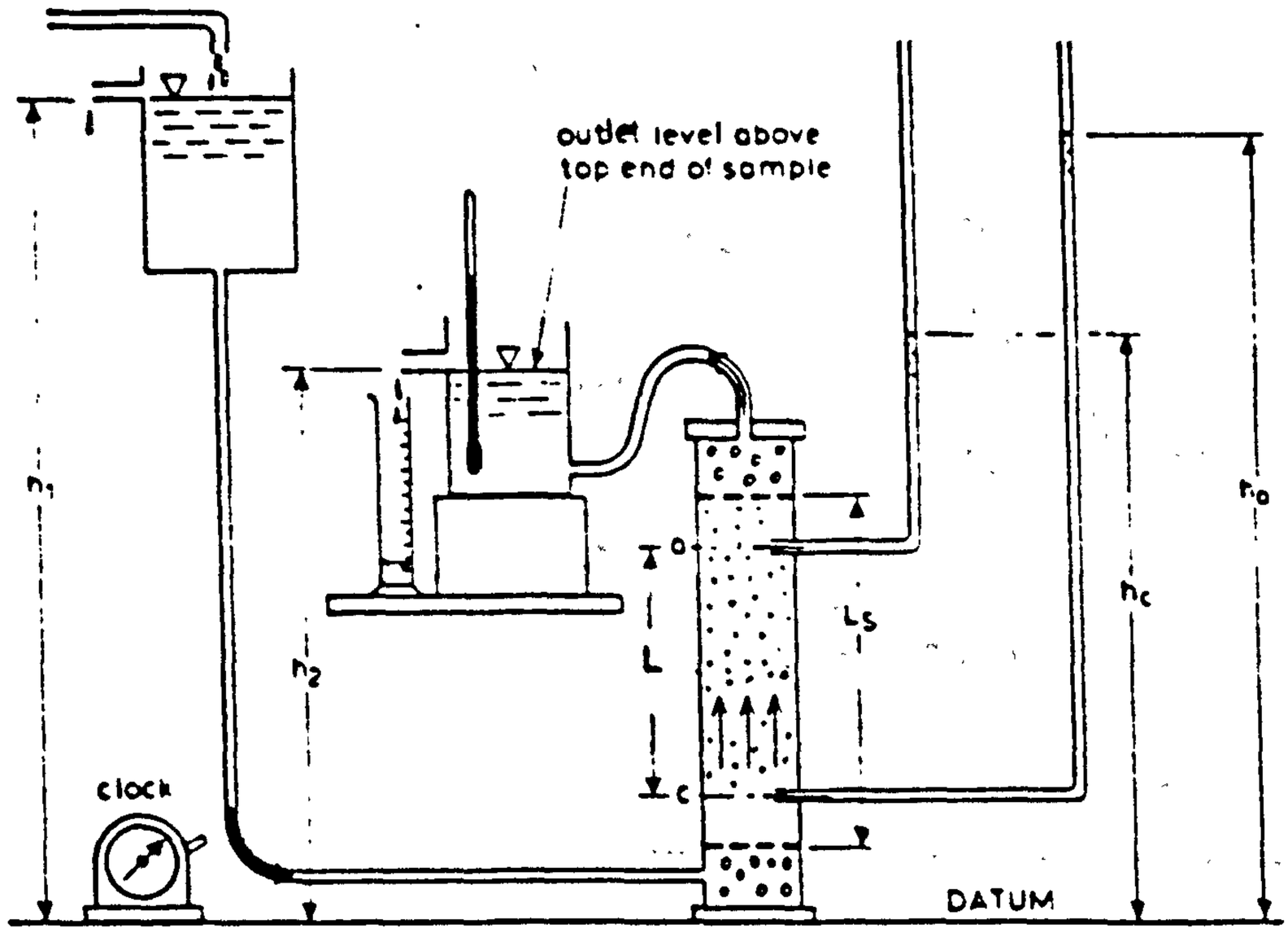

FIG. 3.9 *Principle of constant head permeability test — upward flow*

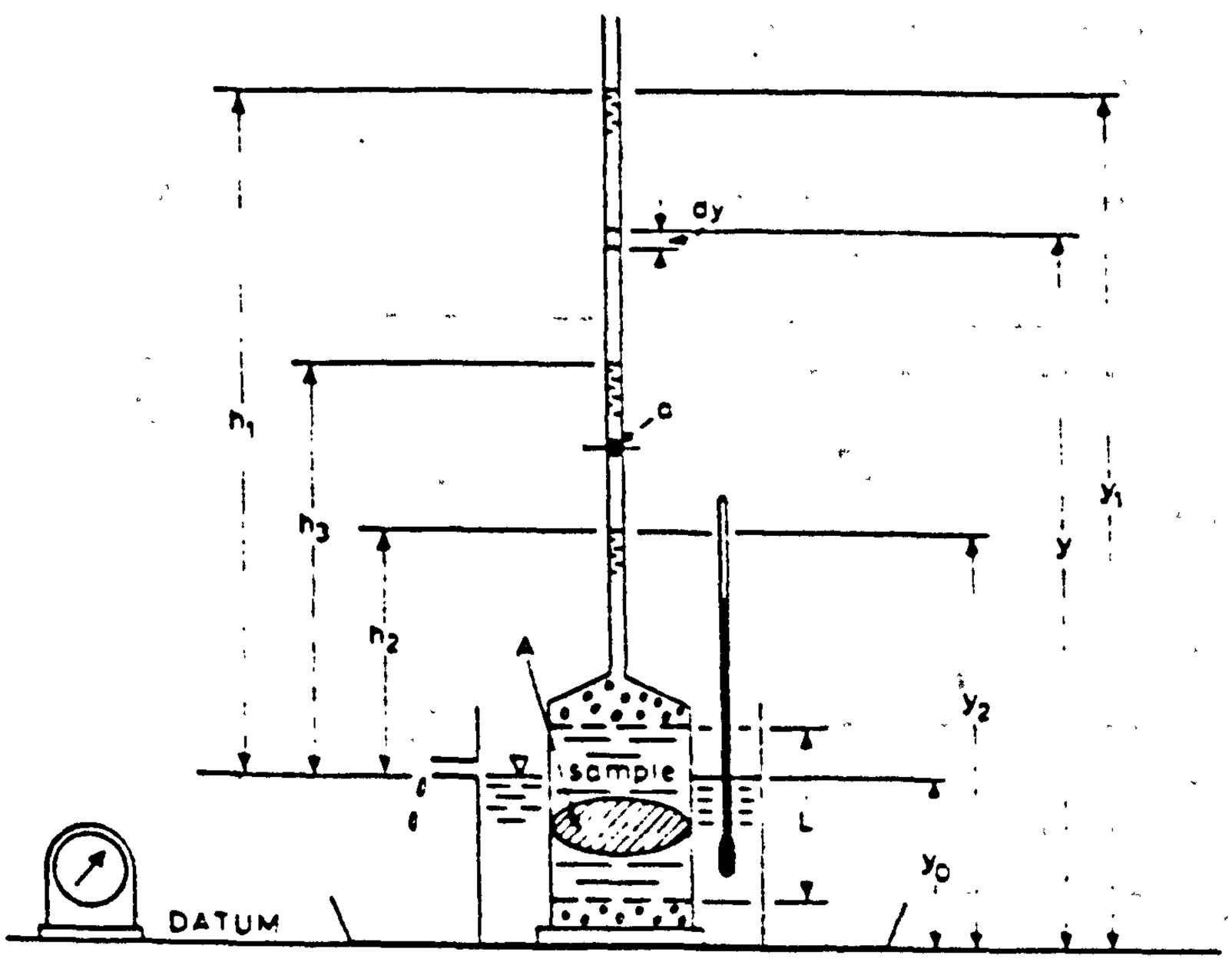

FIG. 3.10 *Principle of falling head permeability test*

FIG. 3.11

CURVE CORRECTIONS IN THE CBR TEST

1 CONVEX UPWARDS CURVES

CBR PENETRATION	UNCORRECTED 2.5mm	UNCORRECTED 5.0mm	CORRECTED 2.5mm	CORRECTED 5.0mm
Curve 11	14	11	Not Required	
Curve 12	5	7	Not Required	

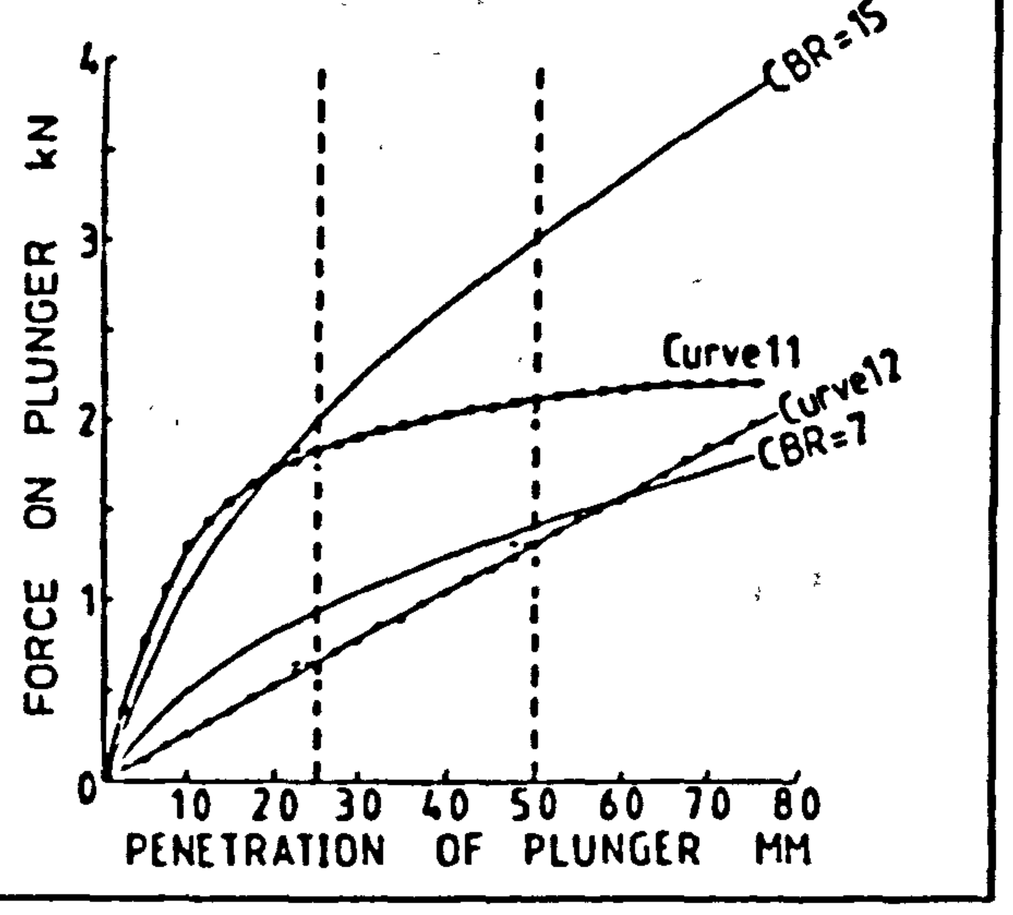

2 INITIALLY CONCAVE BECOMING CONVEX UPWARDS CURVES

CBR PENETRATION	UNCORRECTED 2.5mm	UNCORRECTED 5.0mm	CORRECTED 2.5mm	CORRECTED 5.0mm
Curve 21	18	18	21	19
Curve 22	6	10	9	12
Curve 23	3	8	15	13

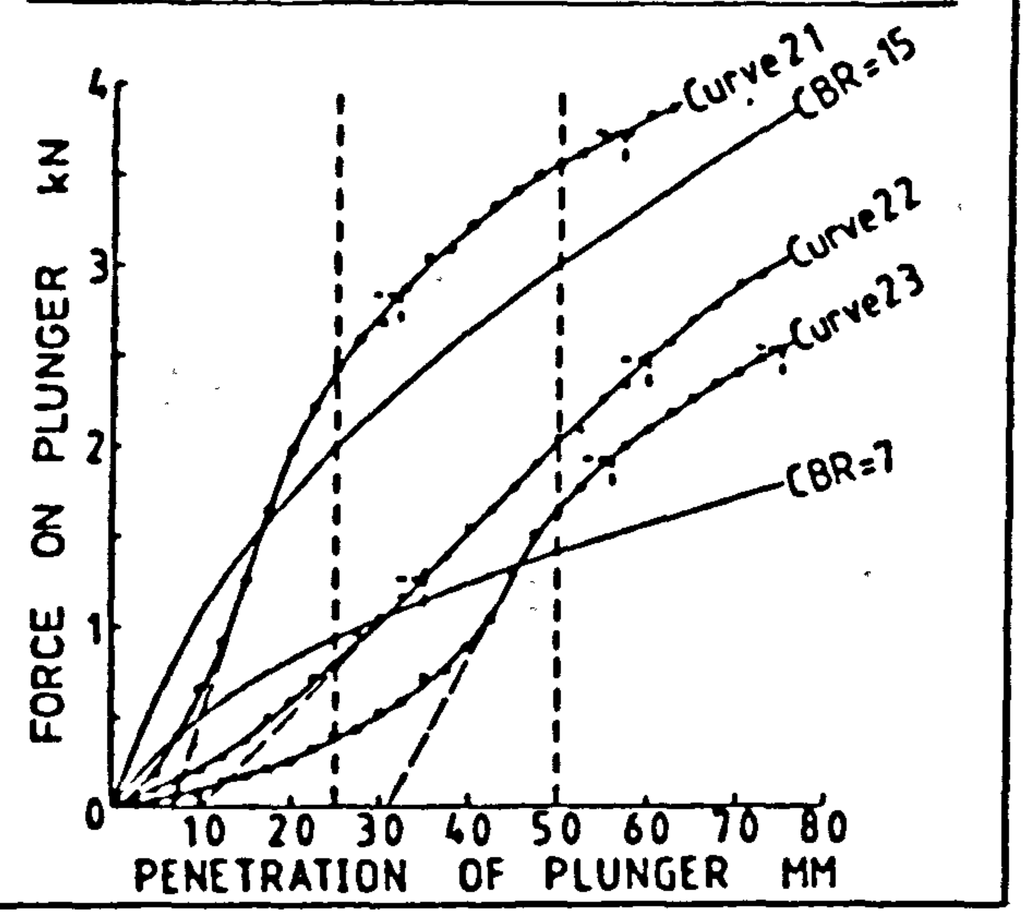

3 CONTINUOUSLY CONCAVE UPWARDS CURVES

CBR PENETRATION	UNCORRECTED 2.5mm	UNCORRECTED 5.0mm	CORRECTED 2.5mm	CORRECTED 5.0mm
Curve 31	8	16	16	21
Curve 32	6	10	12	16
Curve 33	3	7	11	14

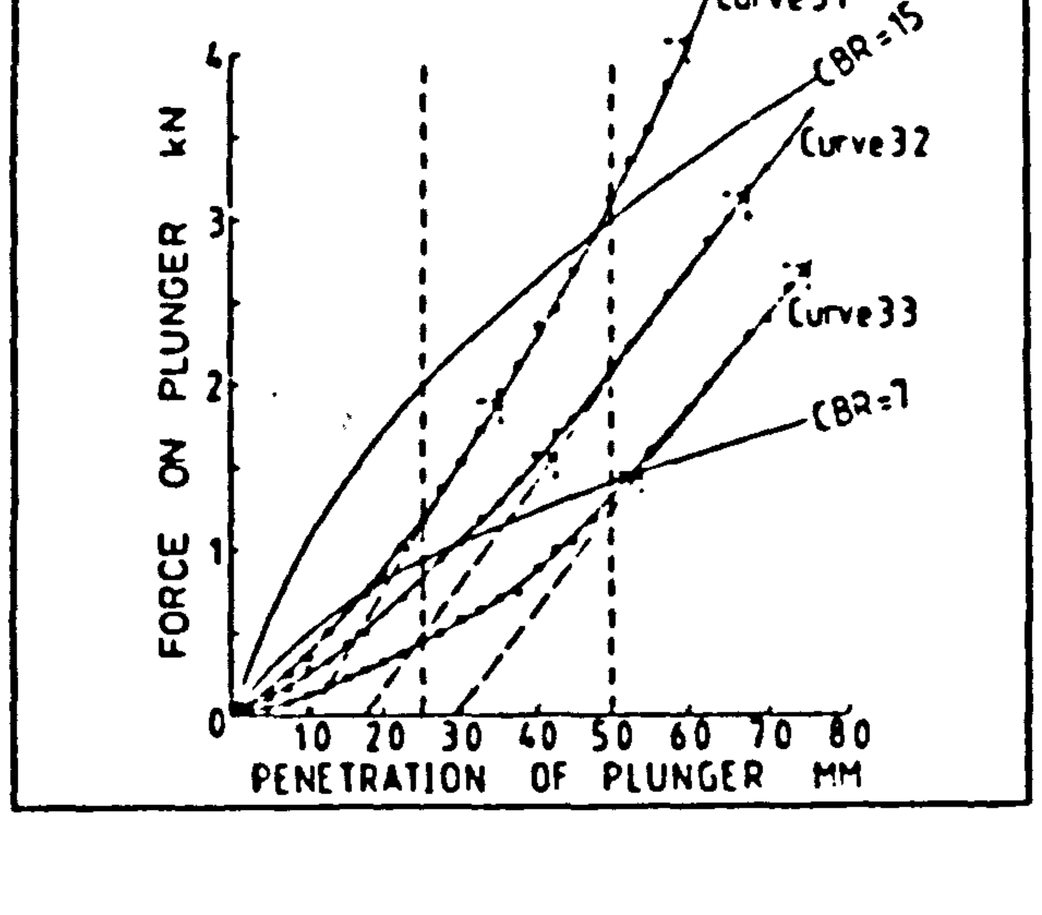

(After Marsh A.H.) The Highway Engineer (February 1983)

FIG. 3.11 (CONTINUED)

CURVE CORRECTIONS IN THE CBR TEST

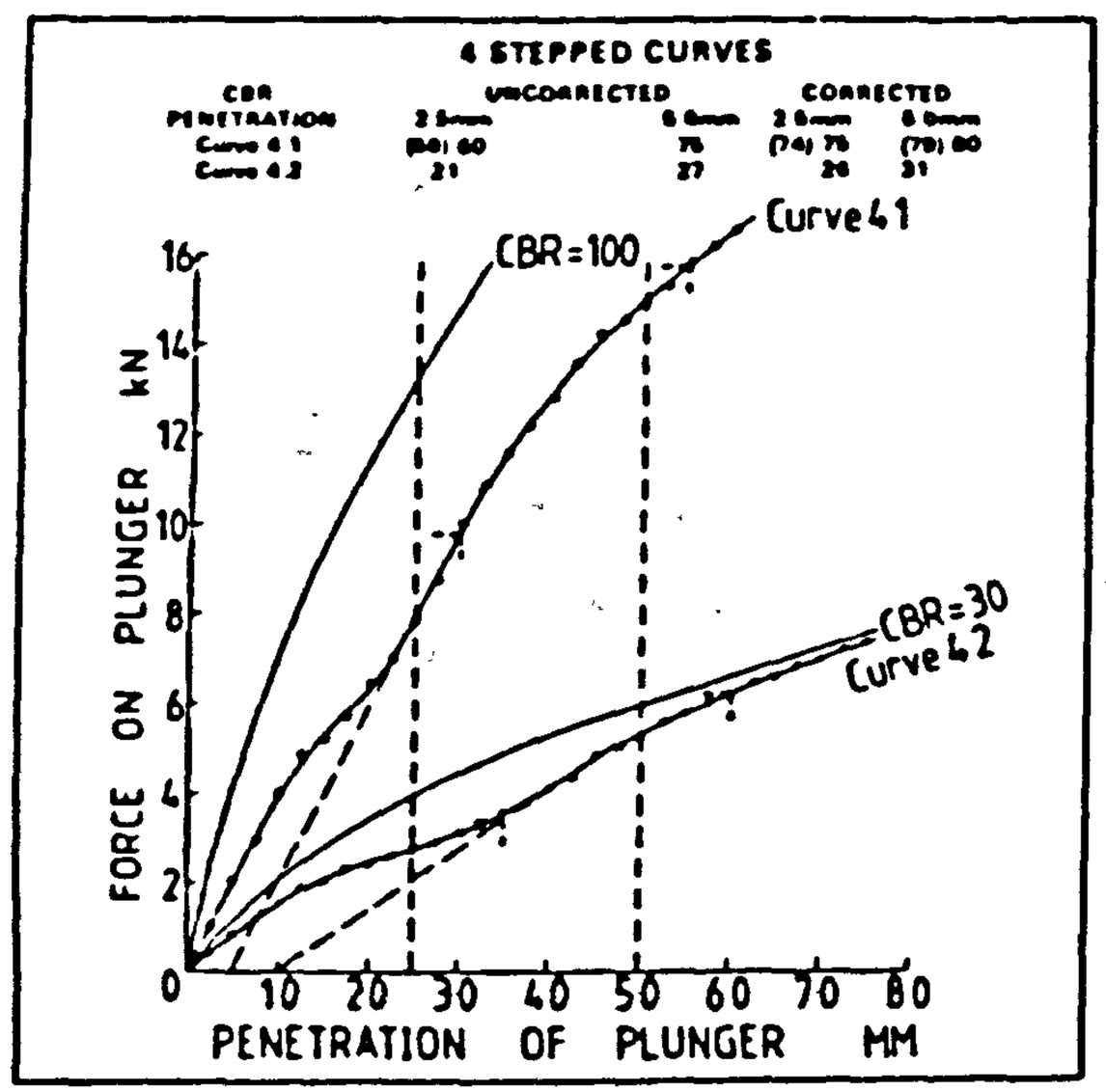

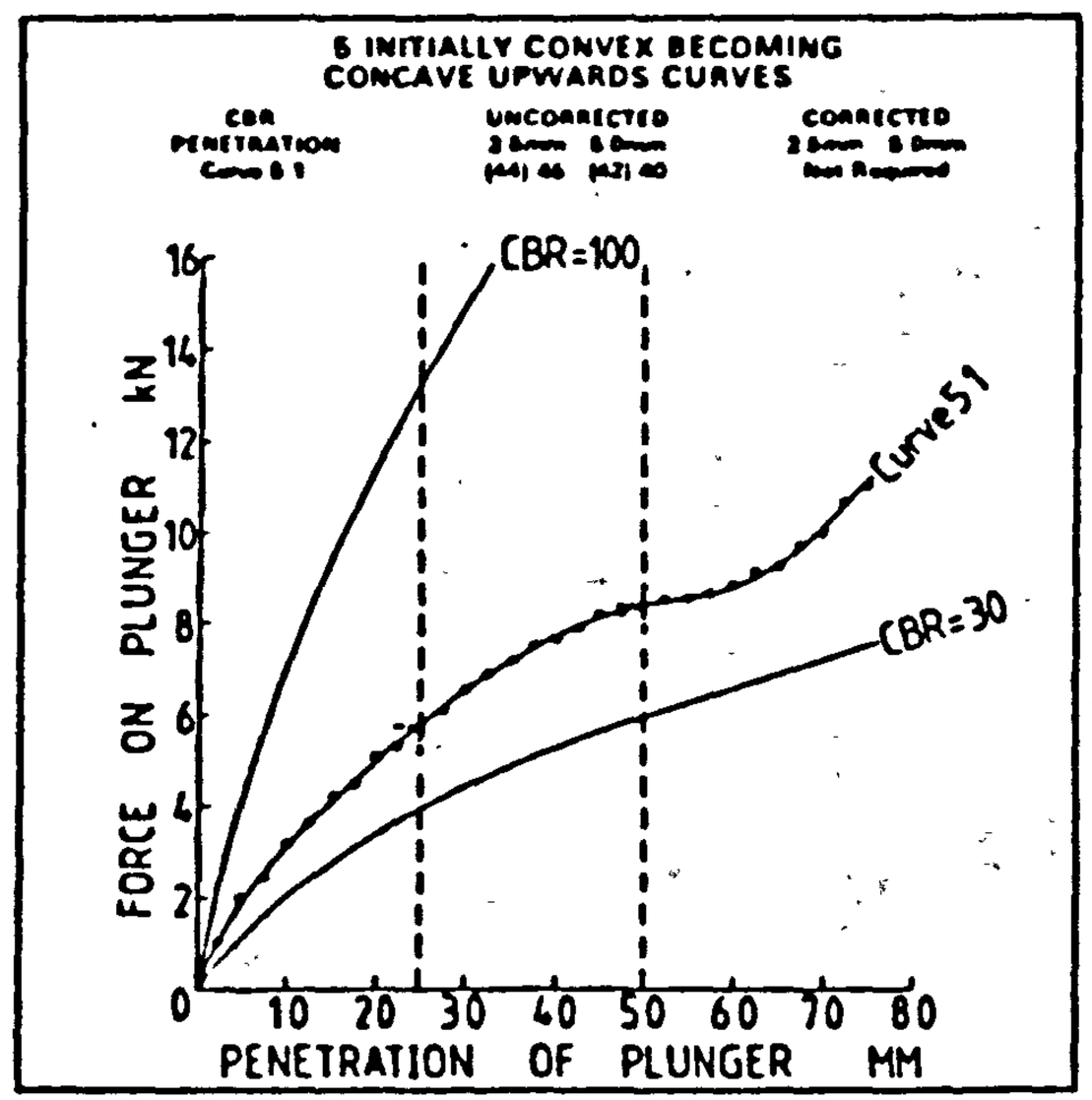

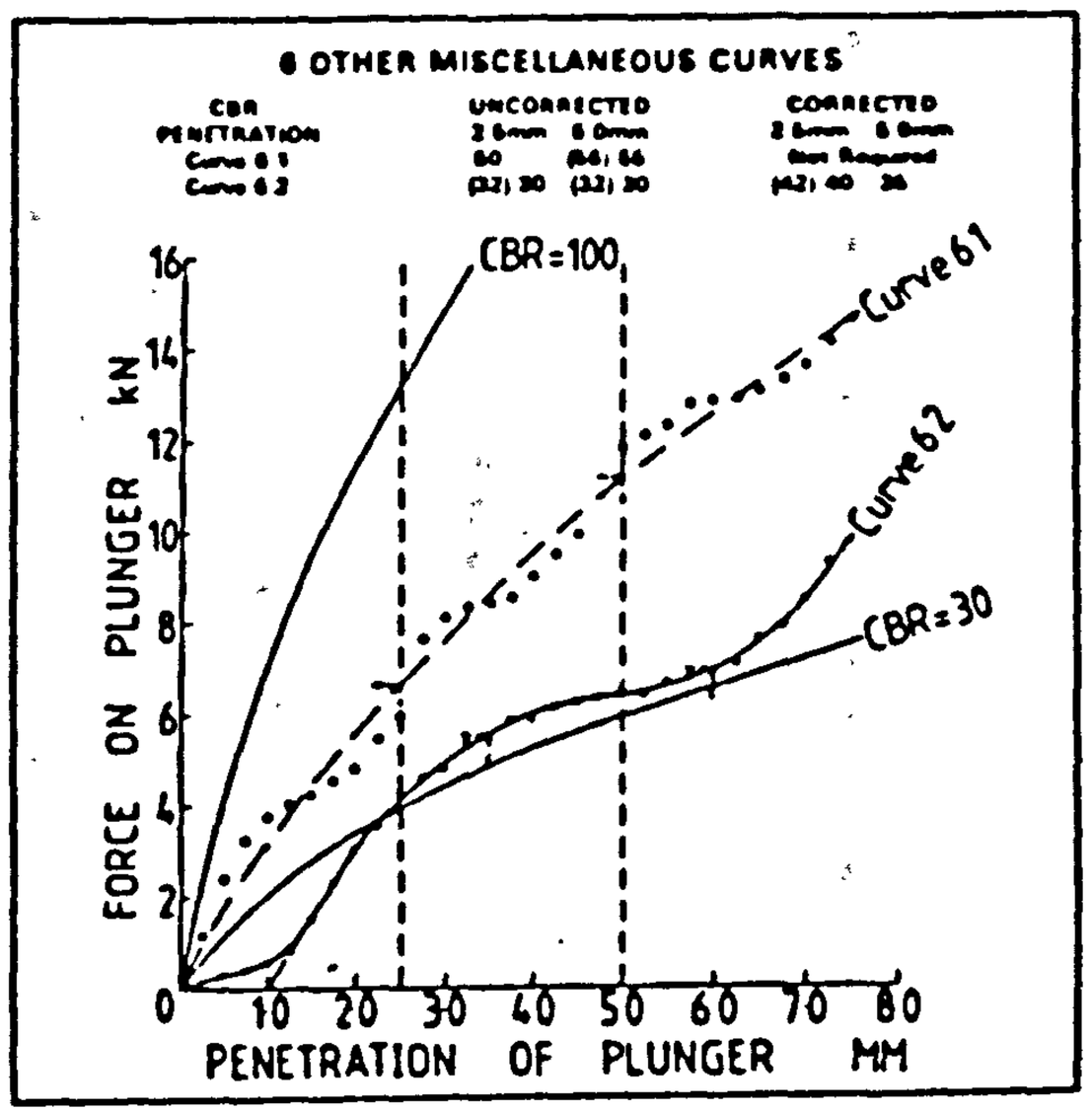

(After Marsh A.H.) The Highway Engineer (February 1983)

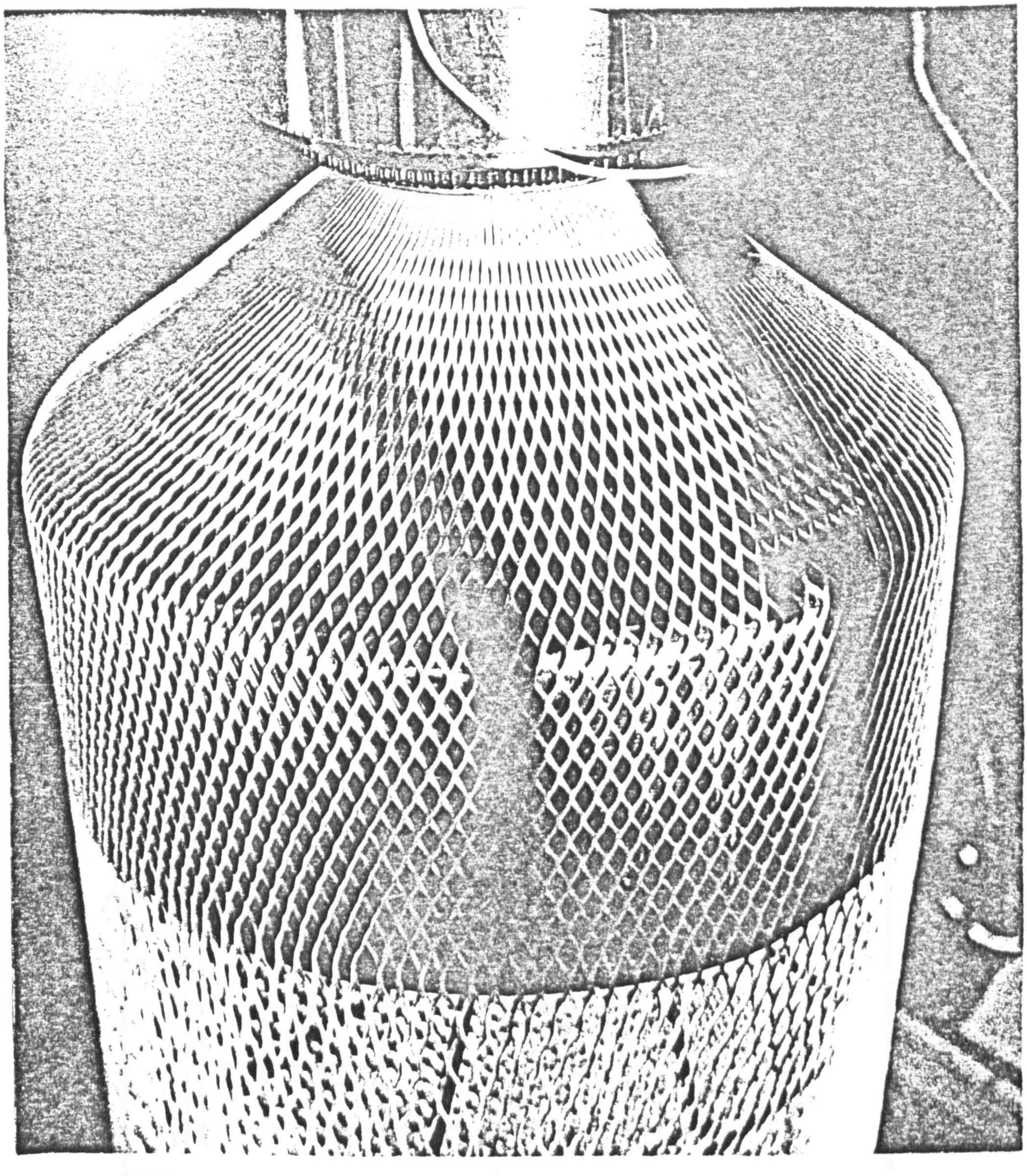

FIG 3.12 MESH POLYMER MANUFACTURING PROCESS

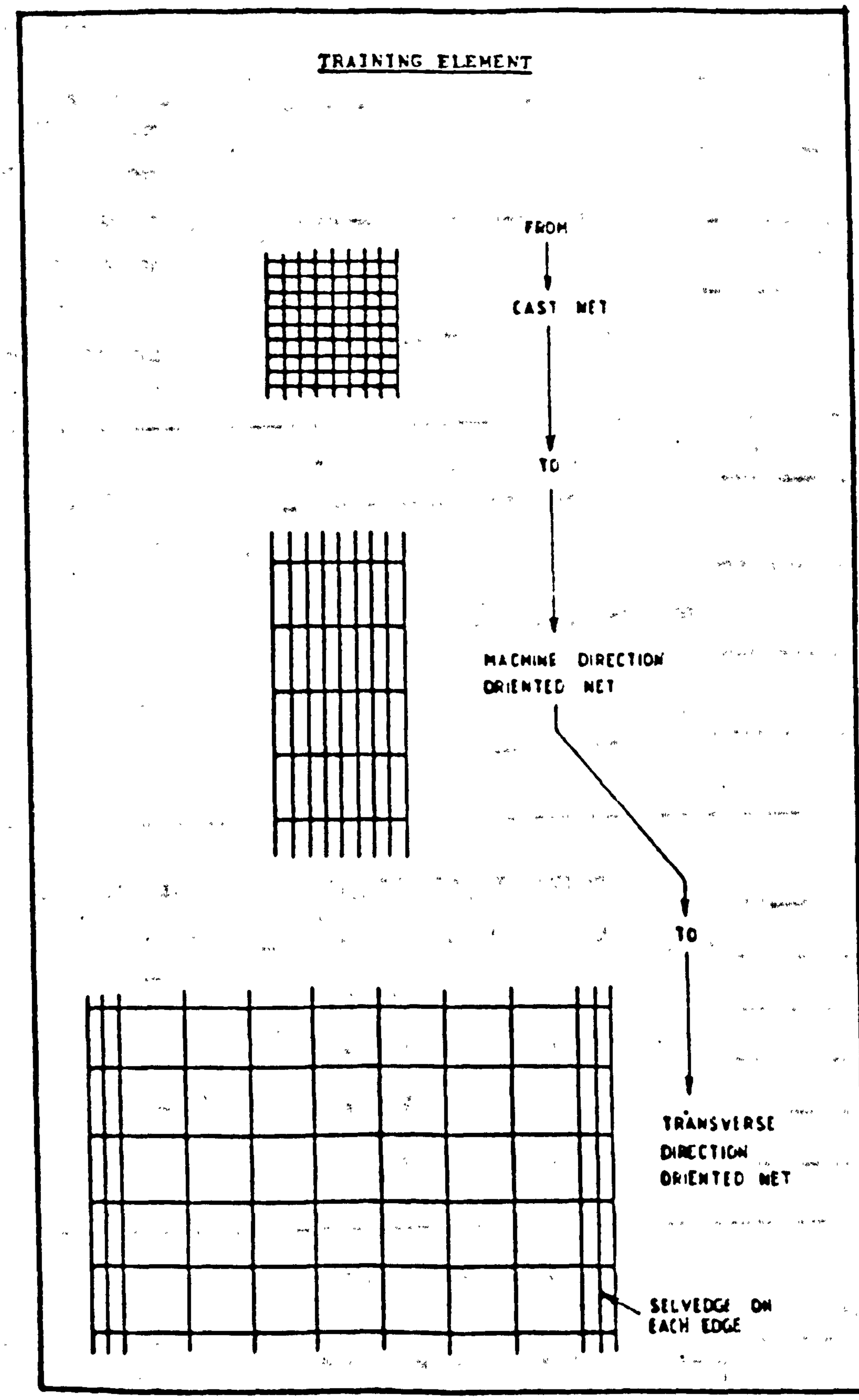

FIG. 3.13 PROGRESSION OF BI-AXIALLY ORIENTED NET.

TYPES OF MESH ELEMENTS

TYPE 1

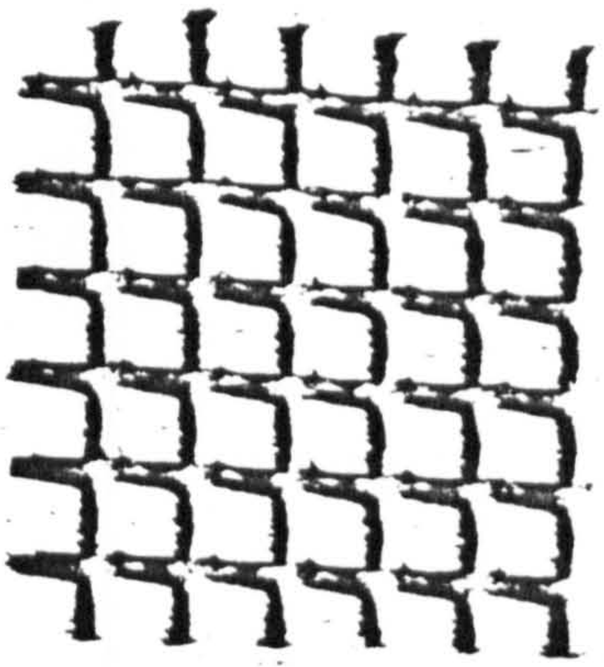

TYPE 5

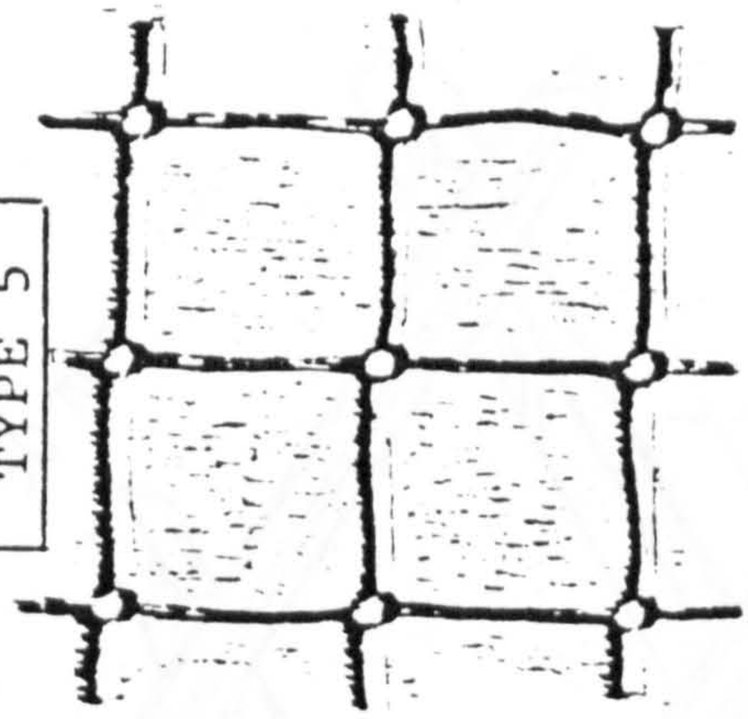

TYPE 10

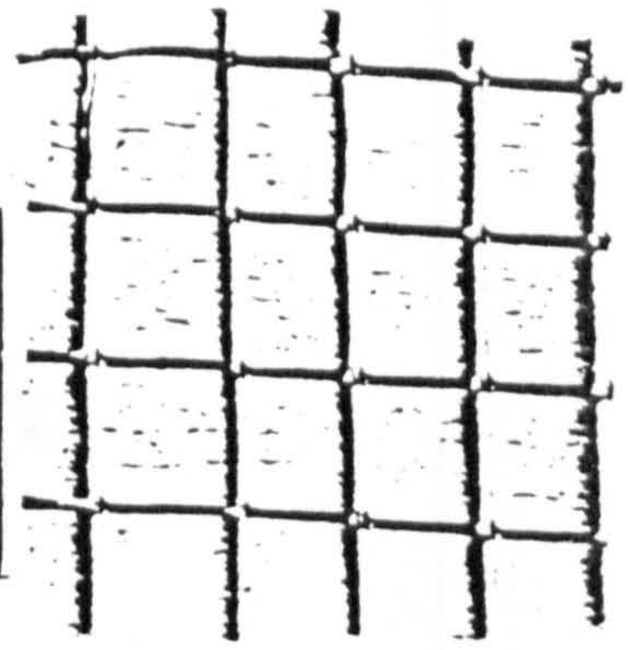

TYPE 8630

TYPE 4

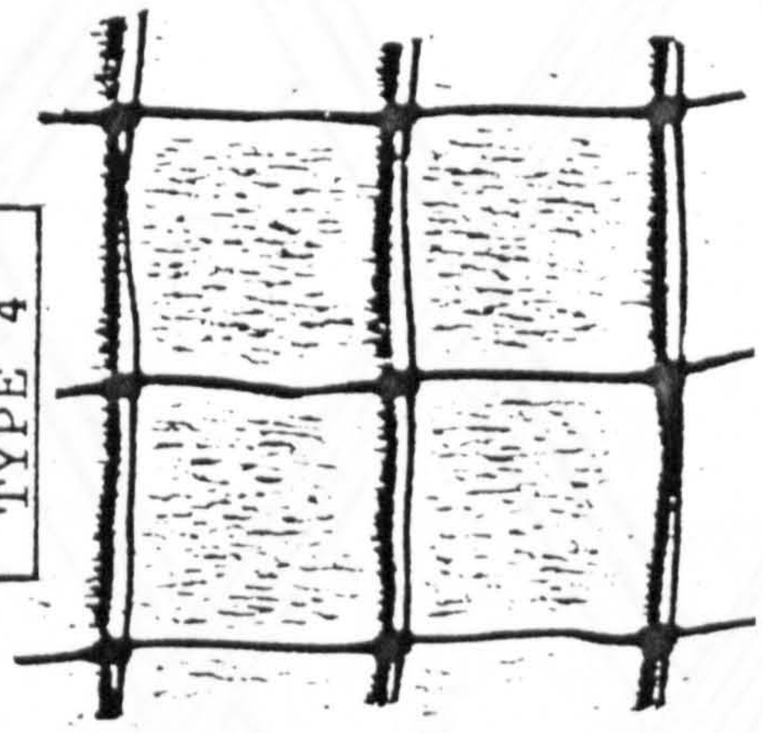

TYPE 12

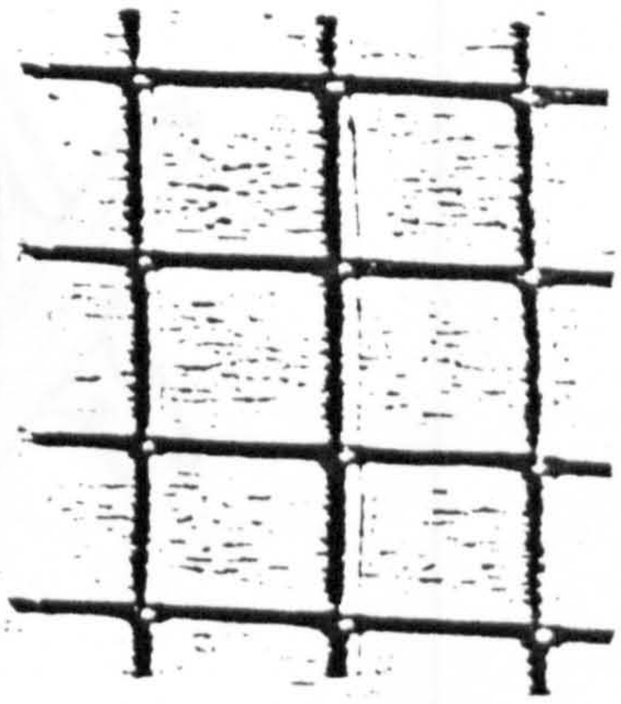

TYPE 5340

TYPE 3

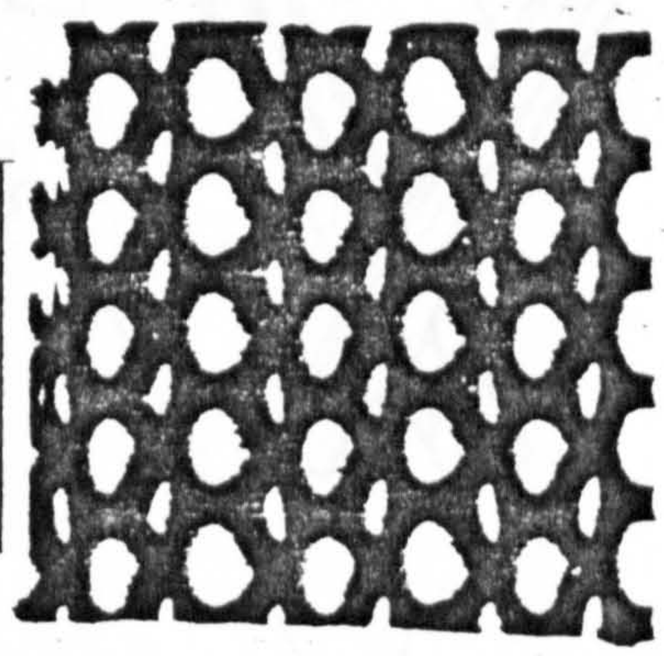

TYPE 7

TYPE 5345

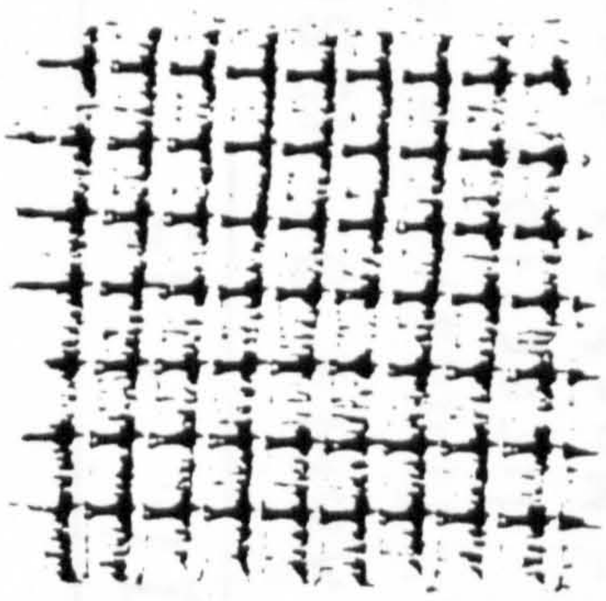

TYPE 2

TYPE 9

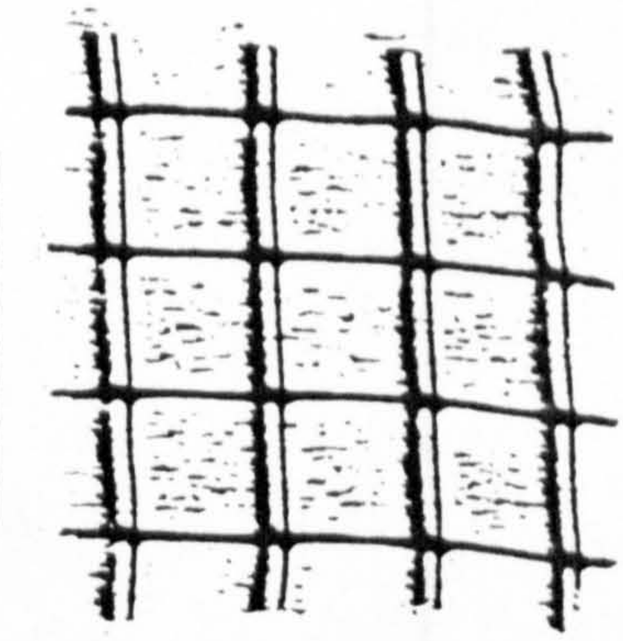

FIG. 3.14

FIG 3.15

EXAMPLE OF MESH ELEMENT STRUCTURE

D_1 : Transverse machine direction

D_2 : Machine direction

w : Filament width

h : Filament height

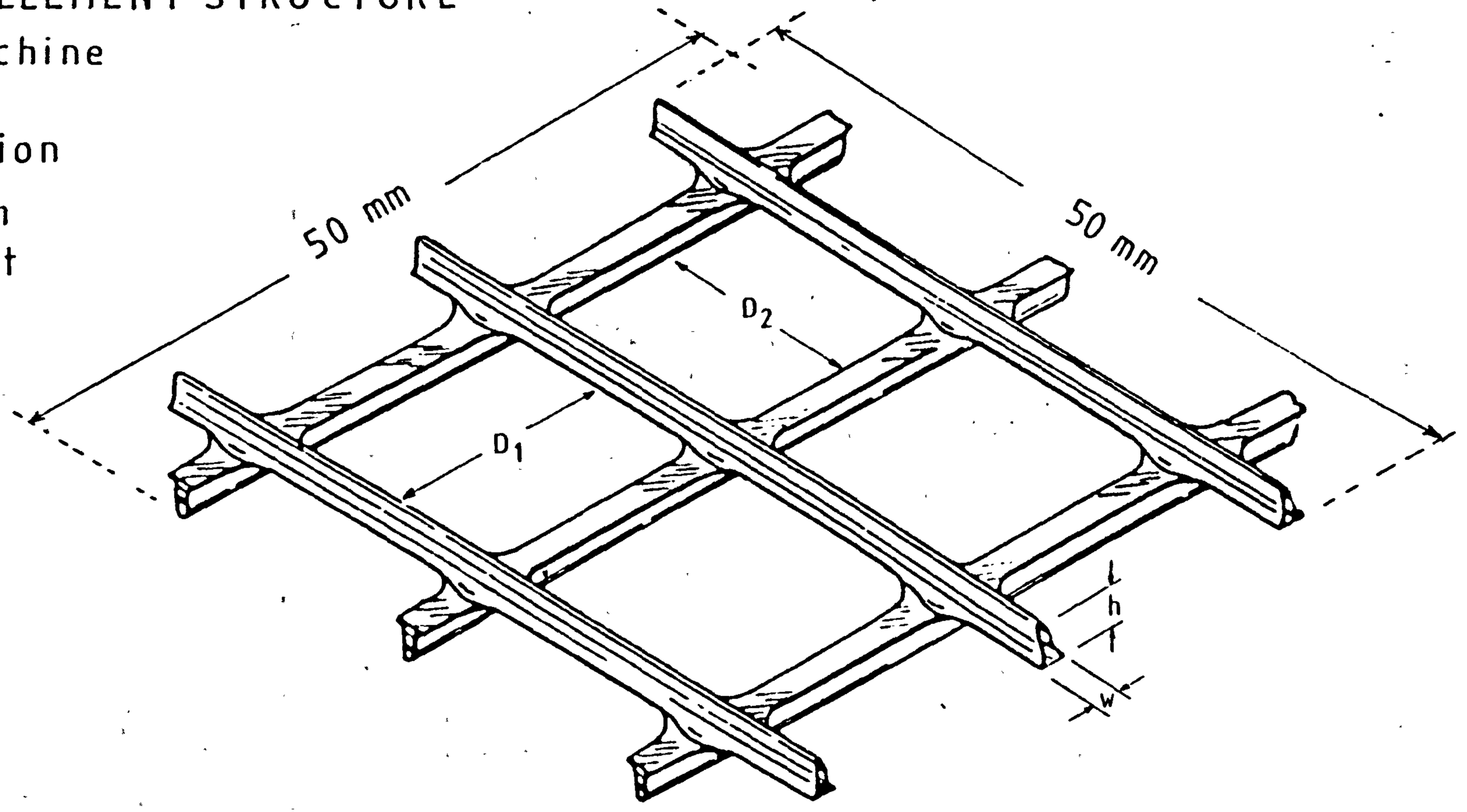

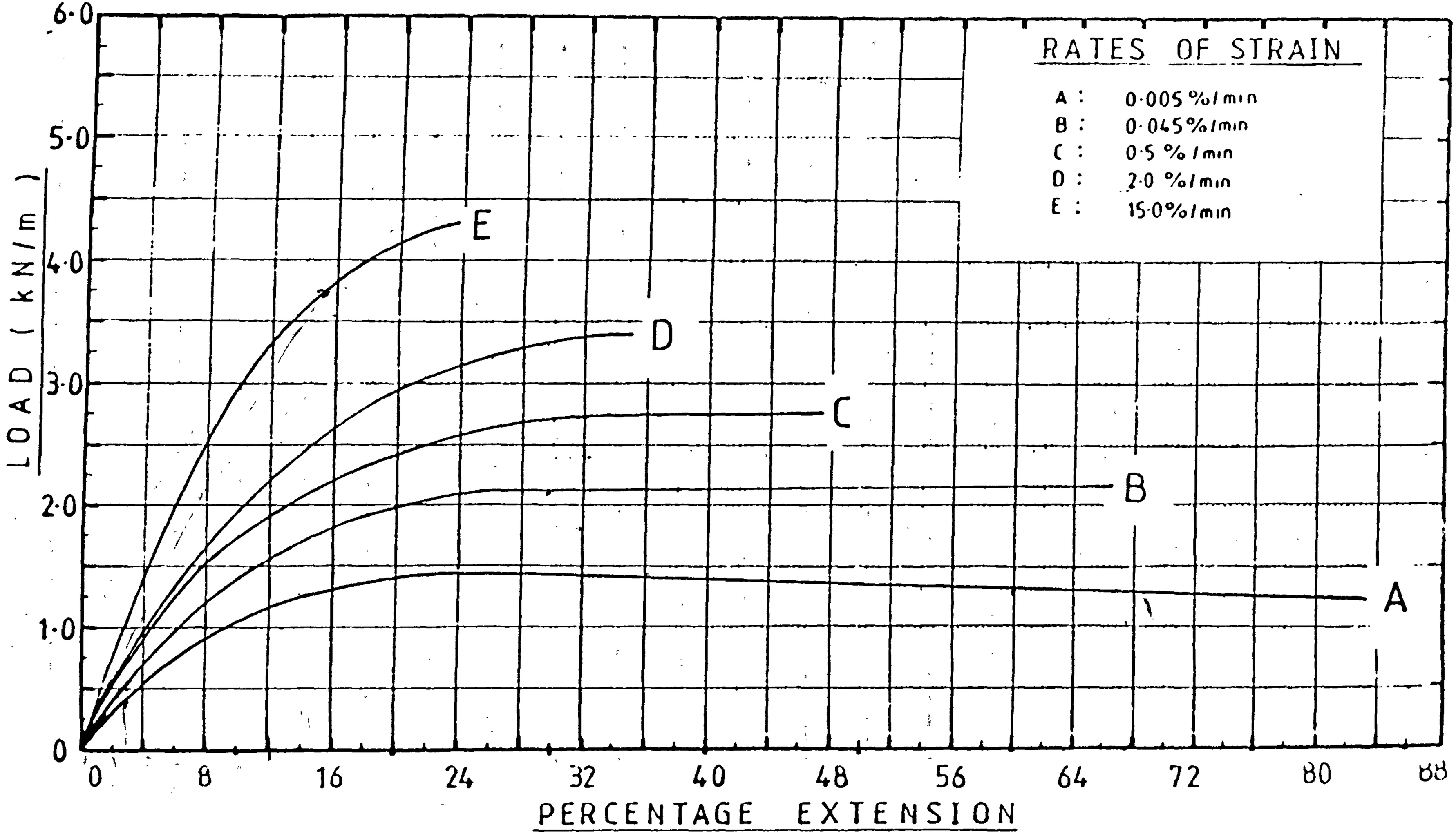

FIG. 3.16 LOAD-EXTENSION BEHAVIOUR OF MESH POLYMER AT VARIOUS RATES OF STRAIN AND CONSTANT TEMPERATURE

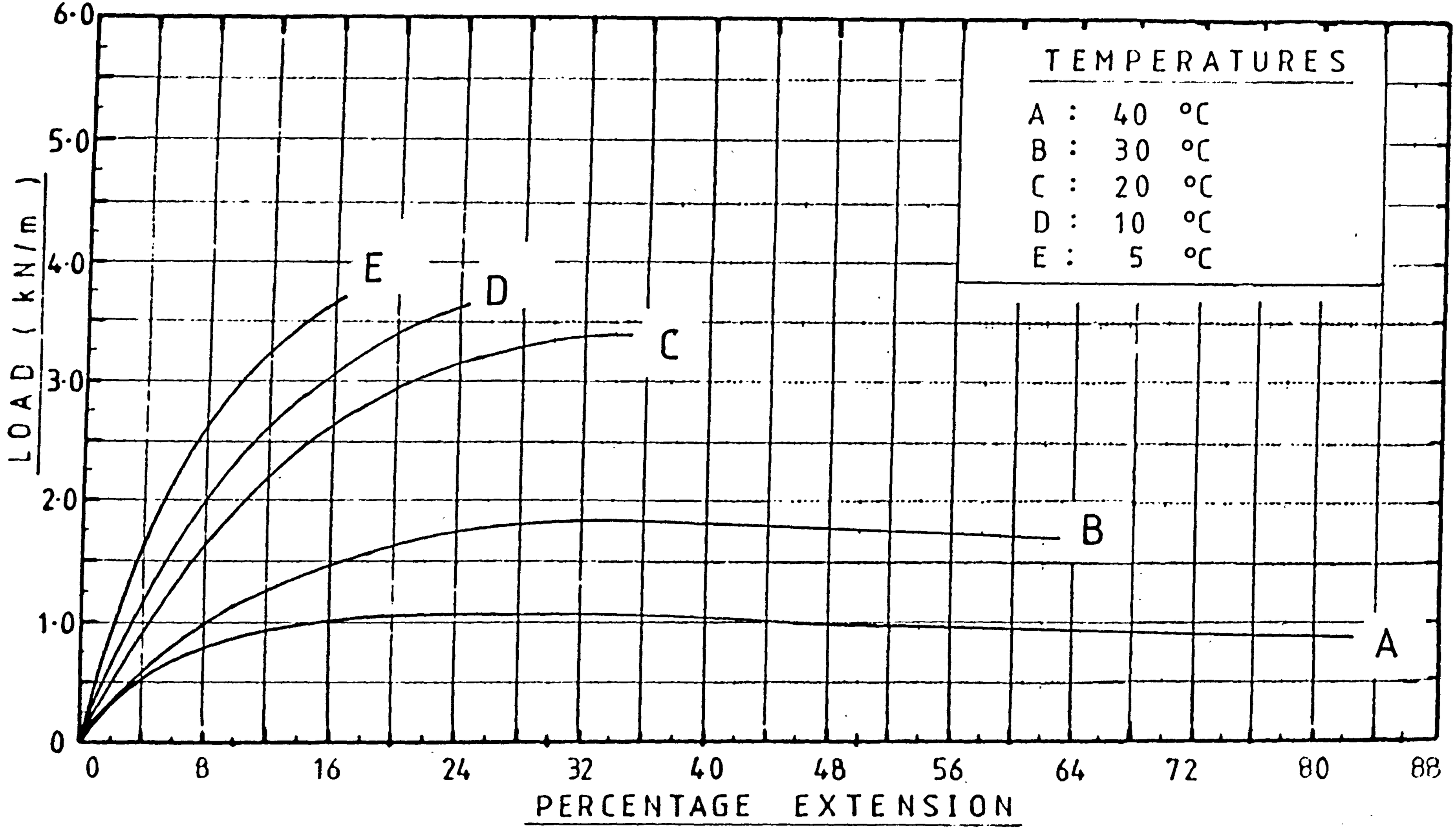

FIG. 3.17 LOAD-EXTENSION BEHAVIOUR OF MESH POLYMER AT VARIOUS TEMPERATURES AND CONSTANT RATE OF STRAIN

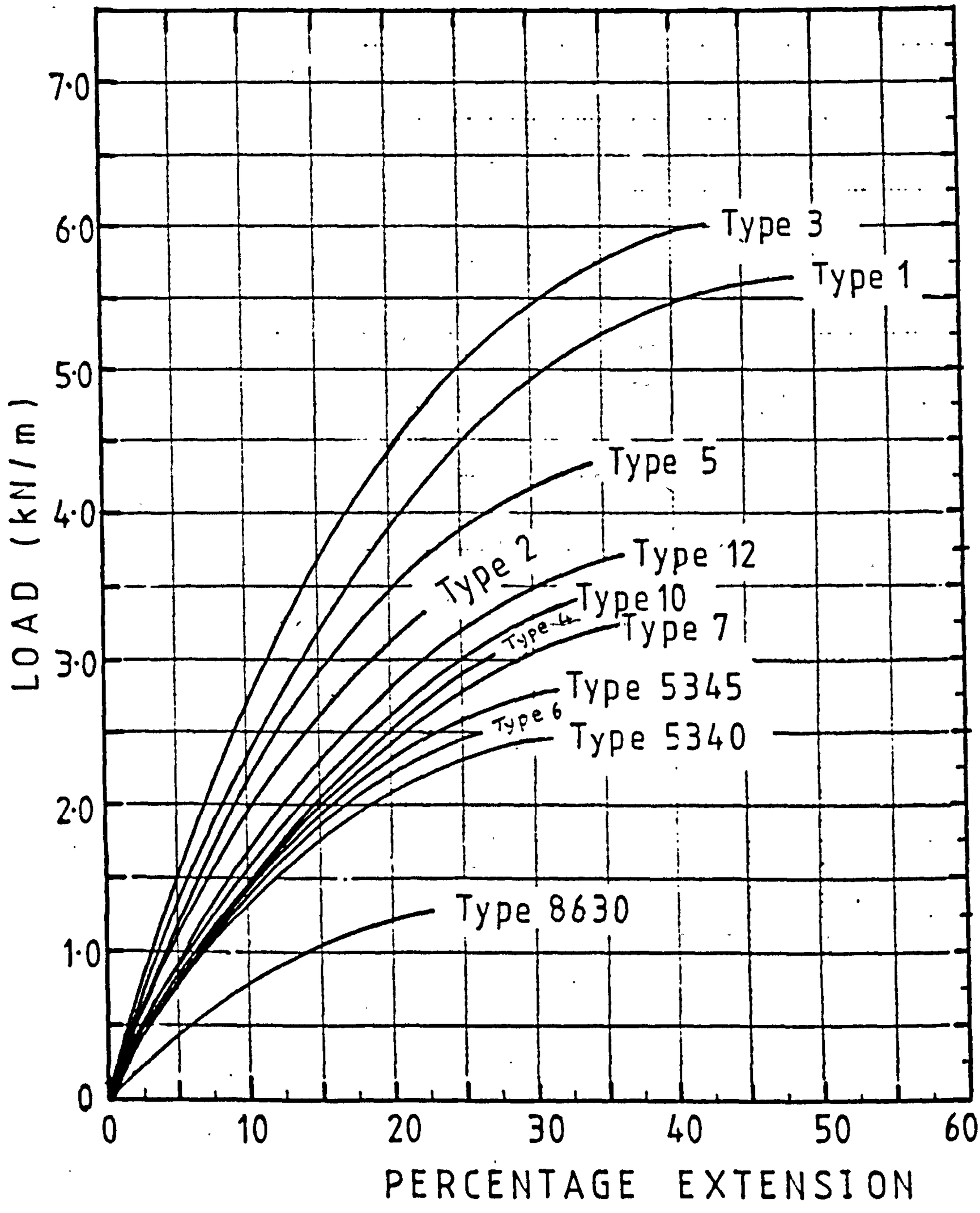

FIG. 3.18 LOAD-EXTENSION BEHAVIOUR OF MESH-ELEMENTS AT CONSTANT RATE OF STRAIN (2% / min) AND AT CONSTANT TEMPERATURE (20°C)

LOAD-EXTENSION CURVES FOR TYPE 10 MESH ELEMENTS MD FOR SEVERAL RATES OF EXTENSION (Nelton 1985)

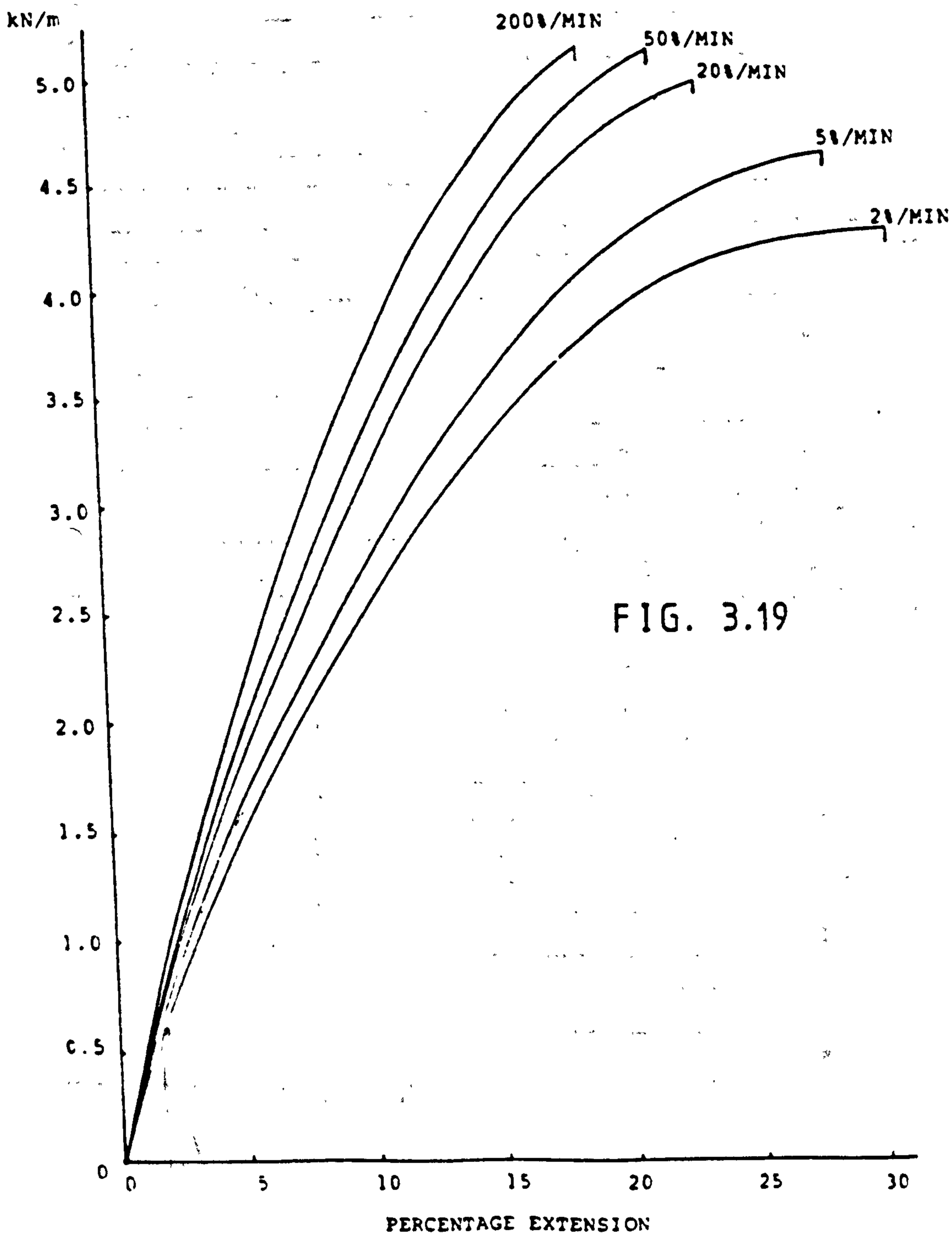

FIG. 3.19

MID-ROSS SAND

FIG. 3.20

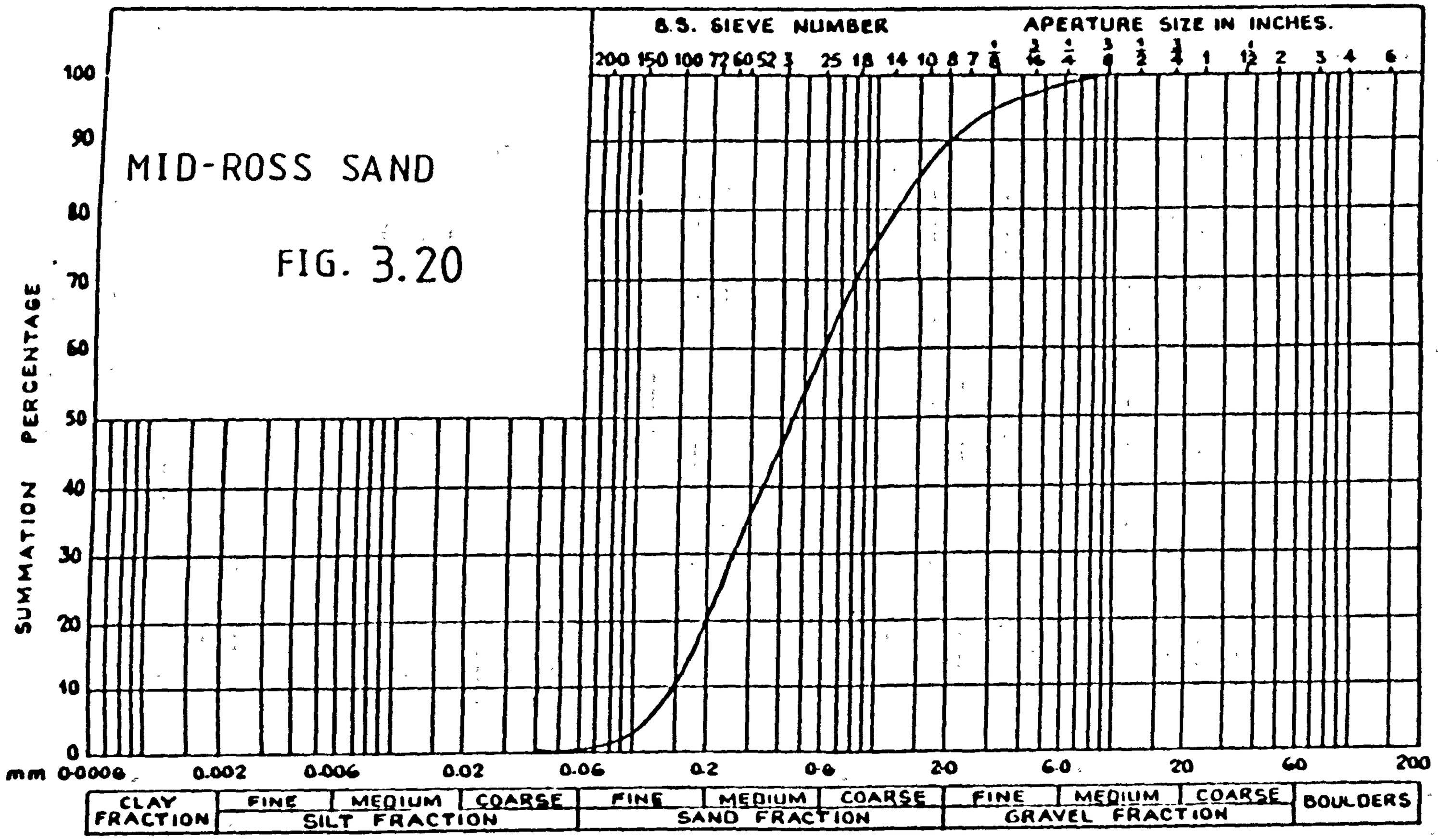

PARTICLE SIZE DISTRIBUTION

LEIGHTON BUZZARD SAND

FIG. 3.21

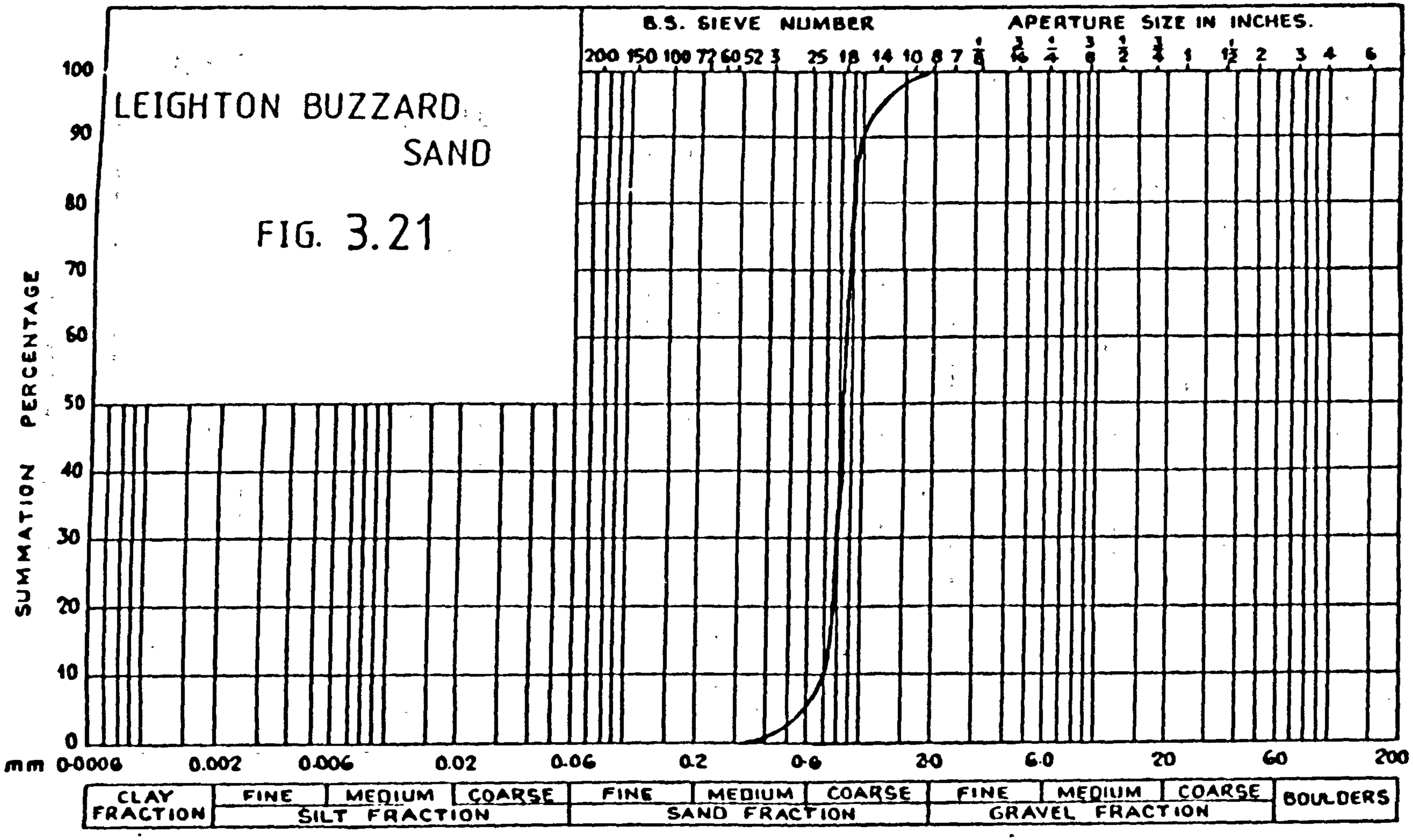

PARTICLE SIZE DISTRIBUTION

WEST HIGHLAND
MORAINE

FIG. 3.22

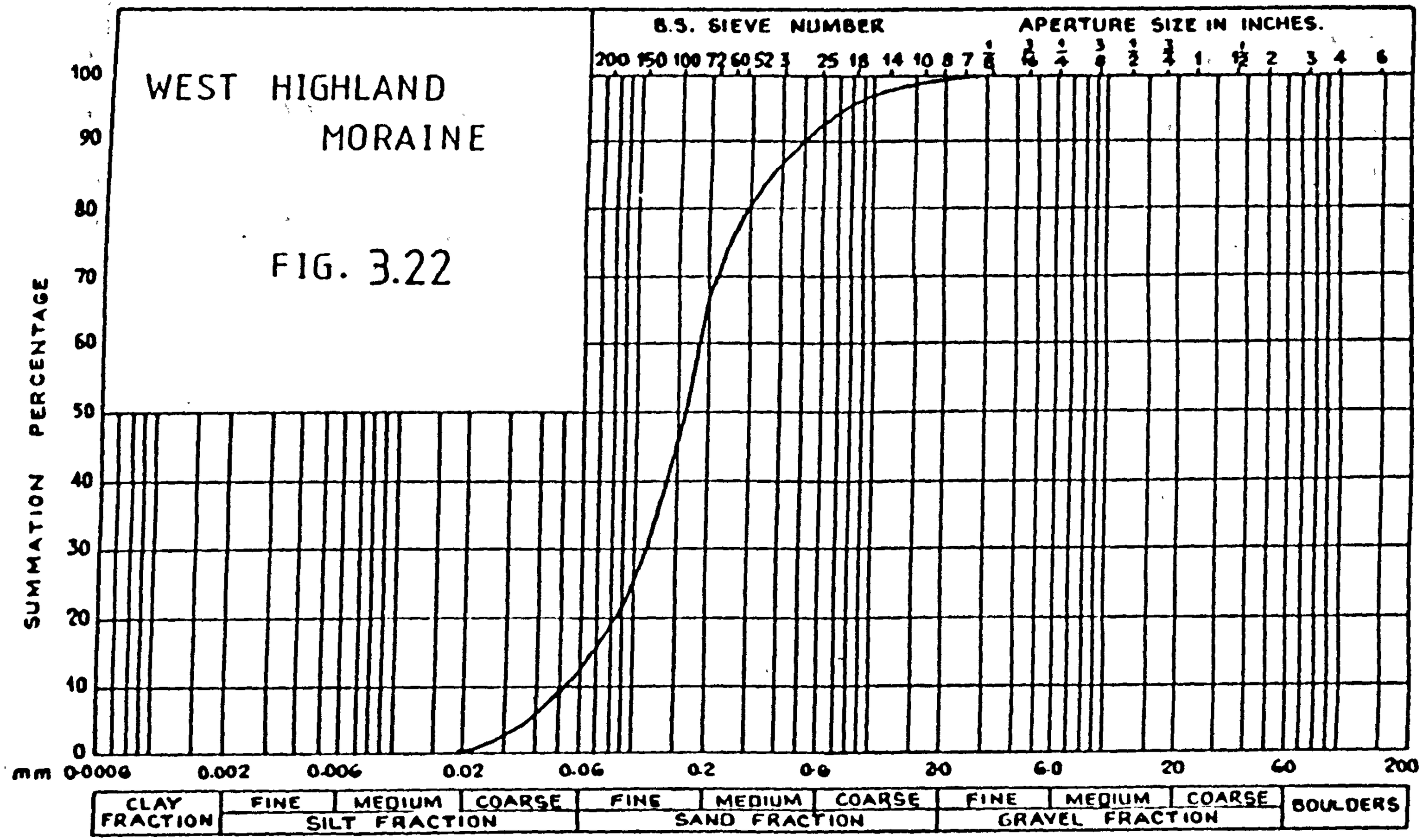

PARTICLE SIZE DISTRIBUTION

COLLIERY SPOIL

FIG. 3.23

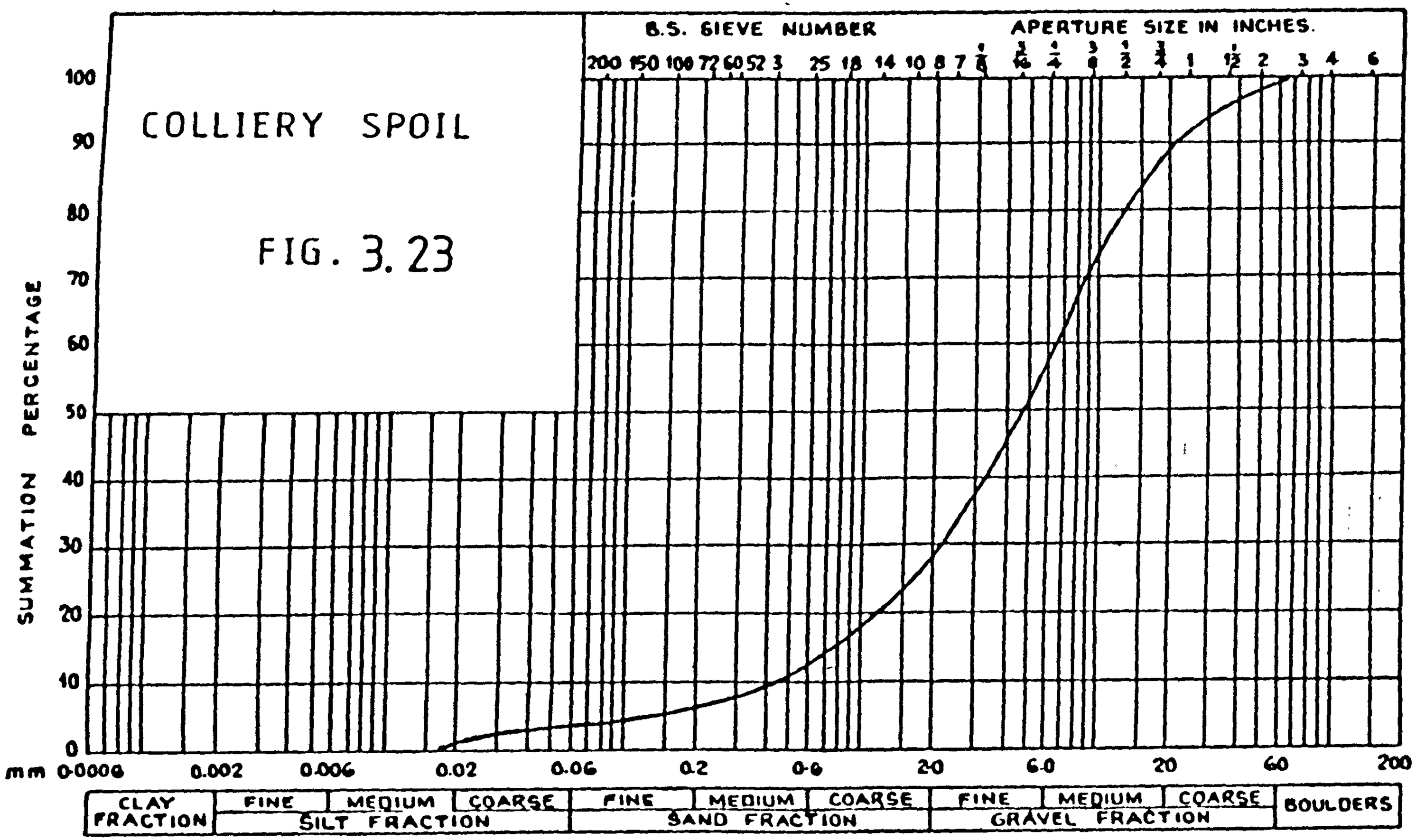

PARTICLE SIZE DISTRIBUTION

PULVERISED FUEL ASH

FIG. 3.24

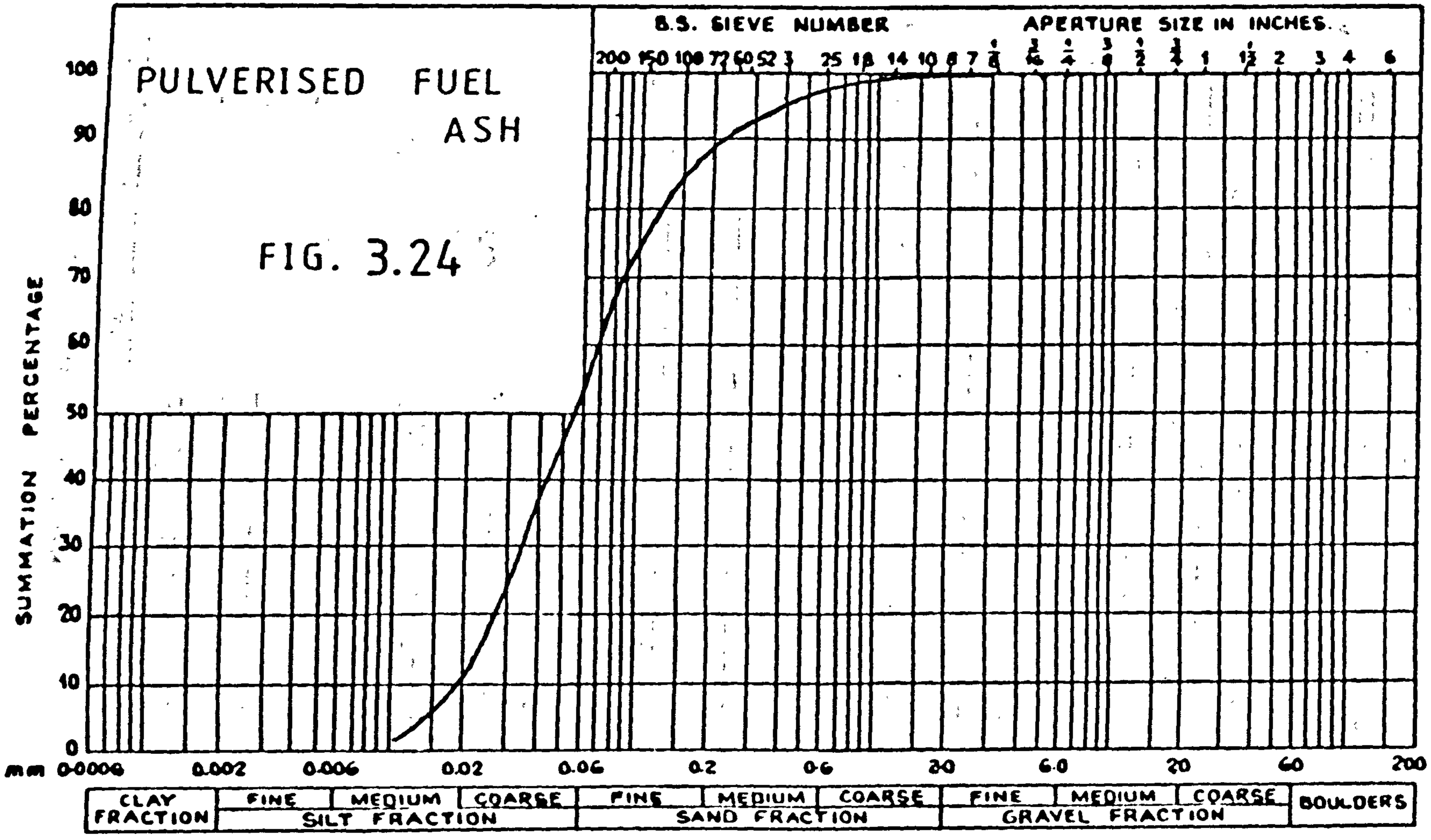

PARTICLE SIZE DISTRIBUTION

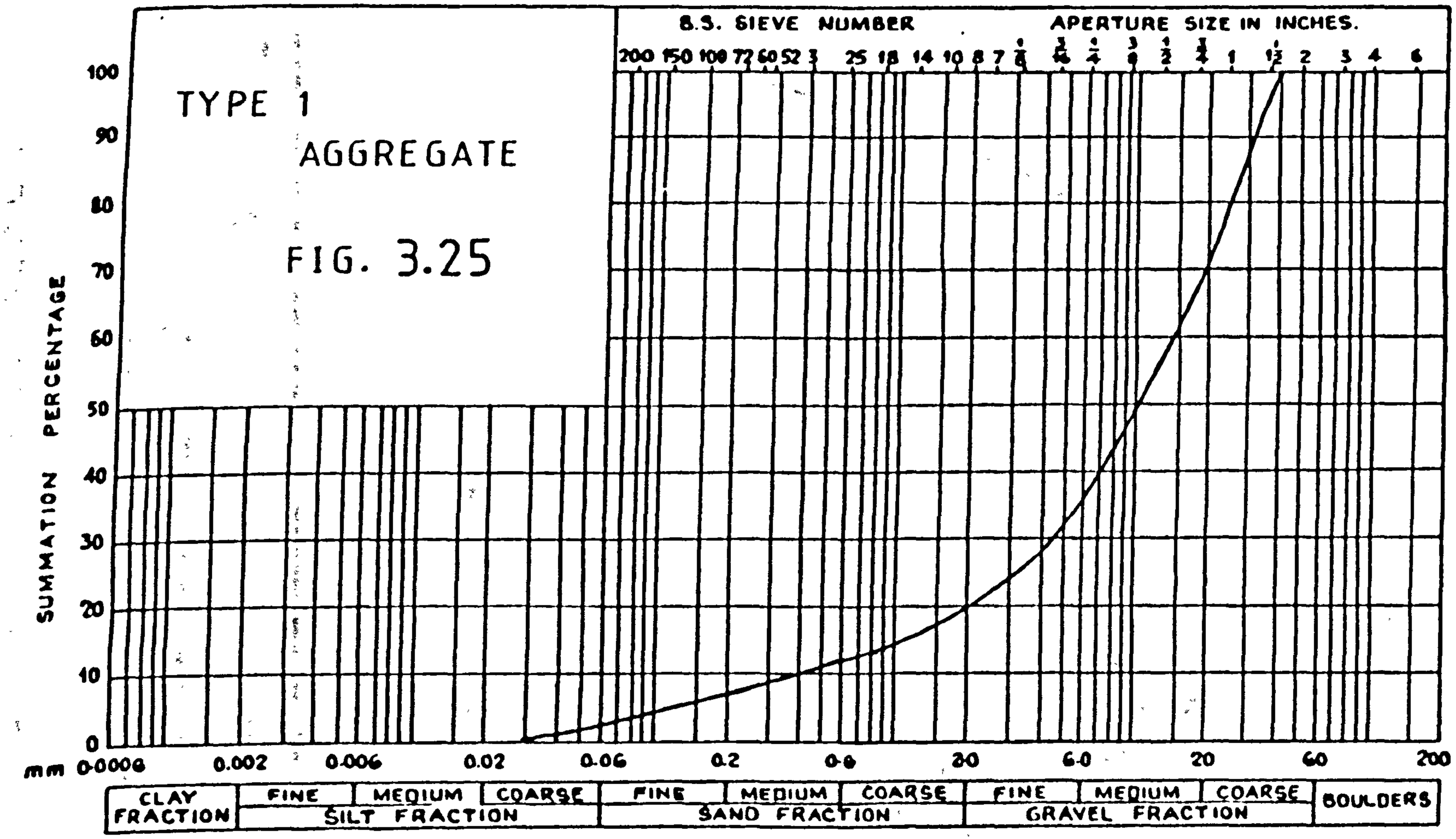

PARTICLE SIZE DISTRIBUTION

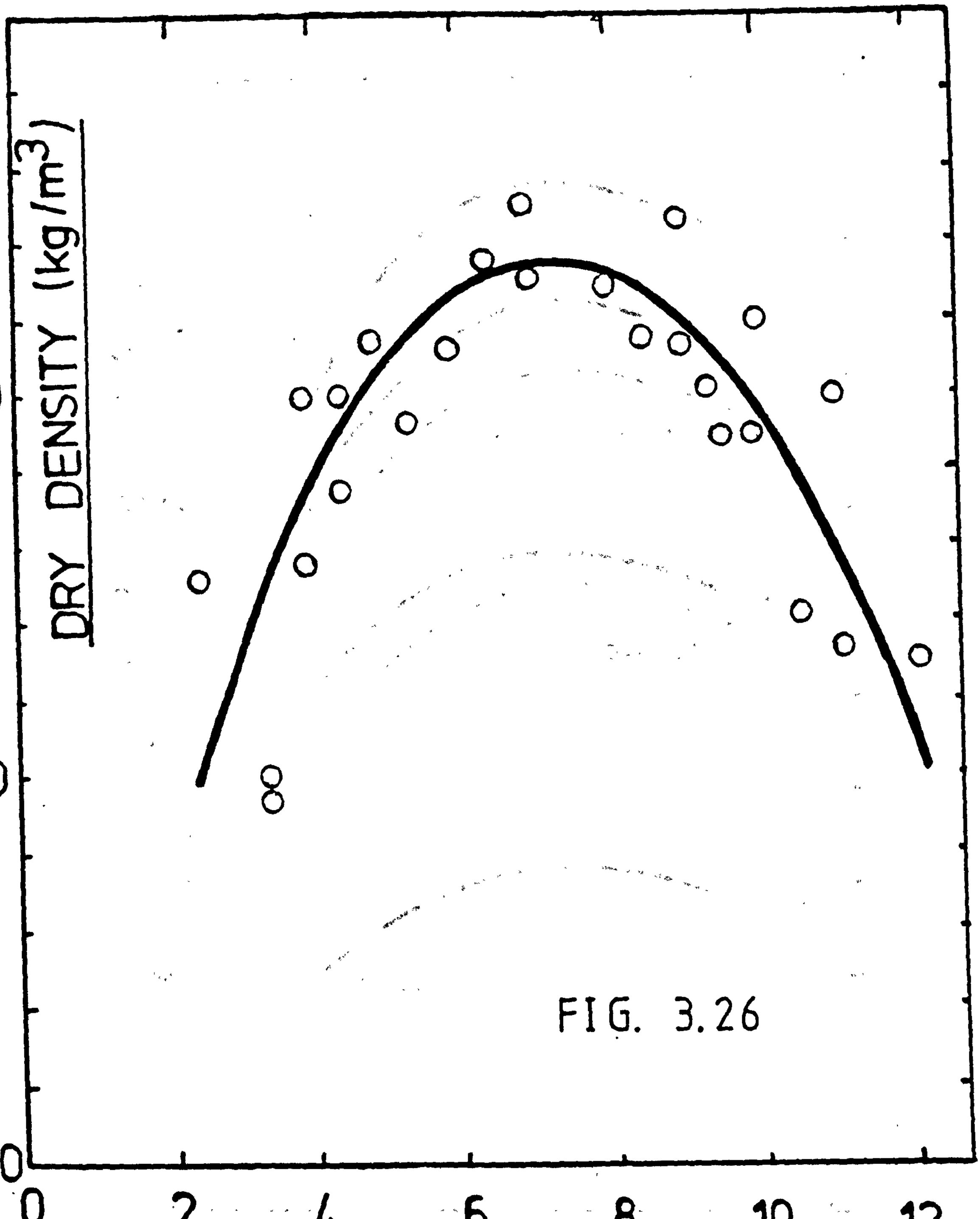

FIG. 3.26

COMPACTION CURVE
OF
MID-ROSS SAND

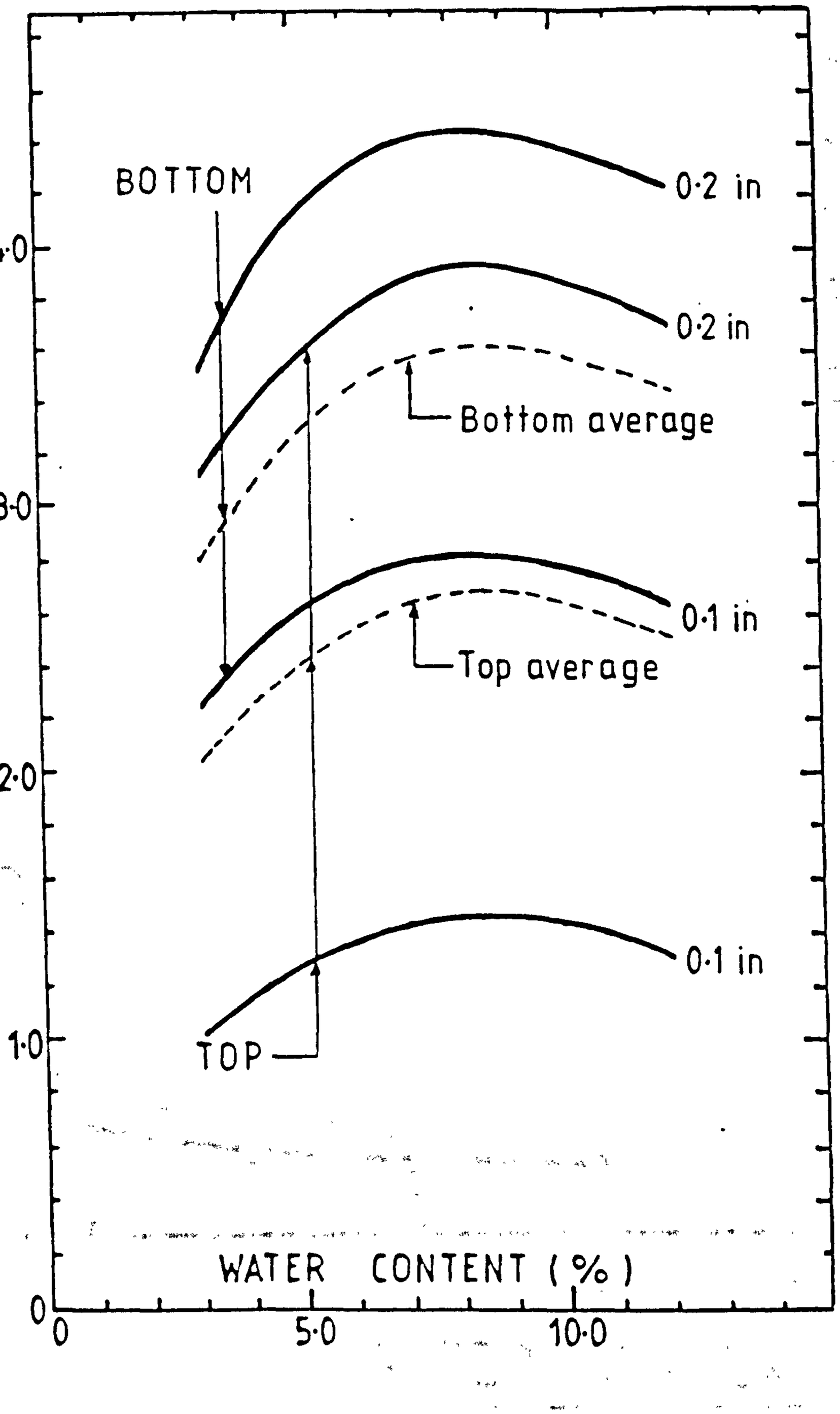

FIG. 3.27 Variation of C.B.R. values with water content for Mid-Ross sand

FIG. 3.28

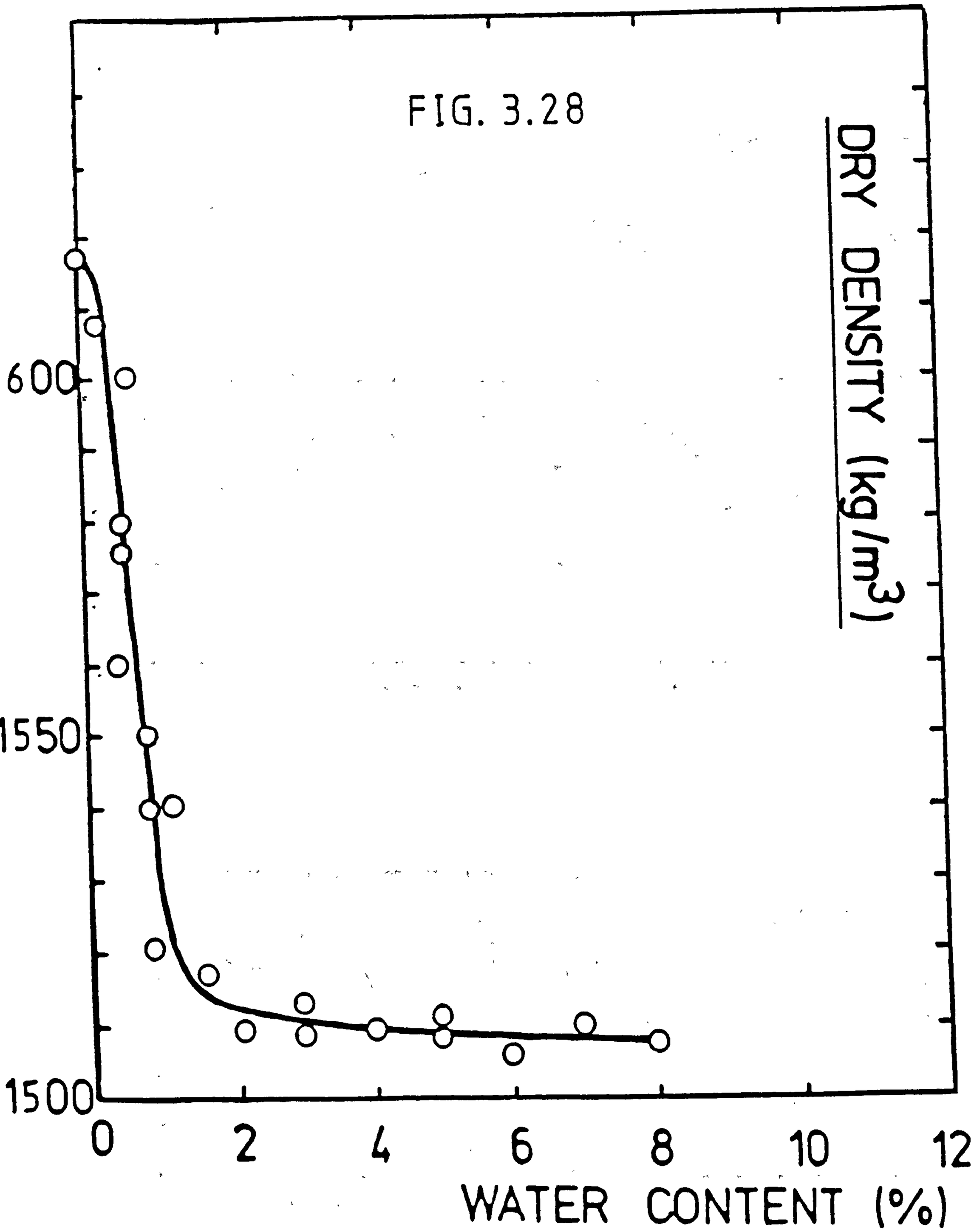

COMPACTION CURVE
OF
LEIGHTON BUZZARD SAND

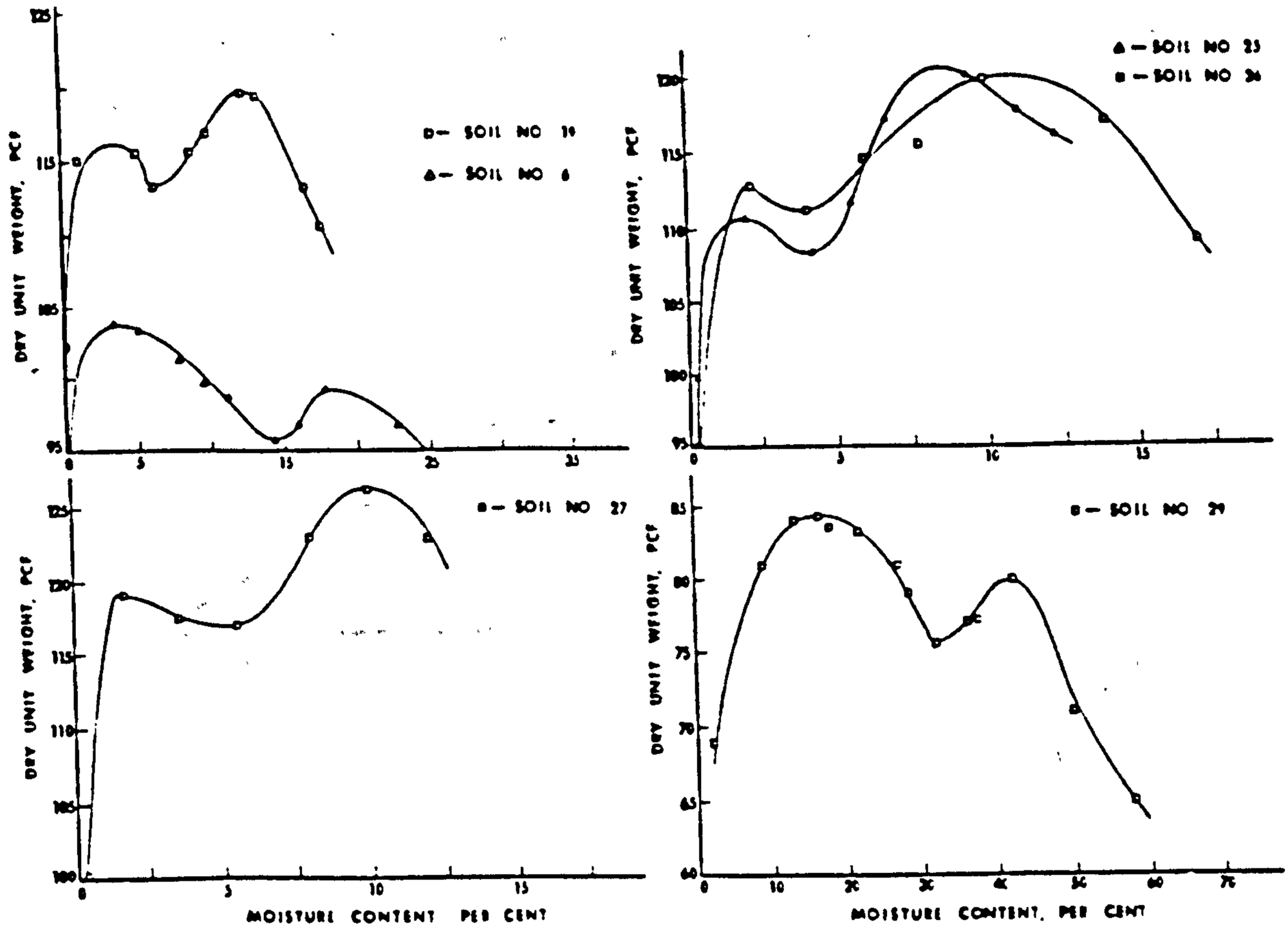

FIG. 3.29 Various forms of compaction curves. Lee & Suedkamp (1972) Transportation research record No 381

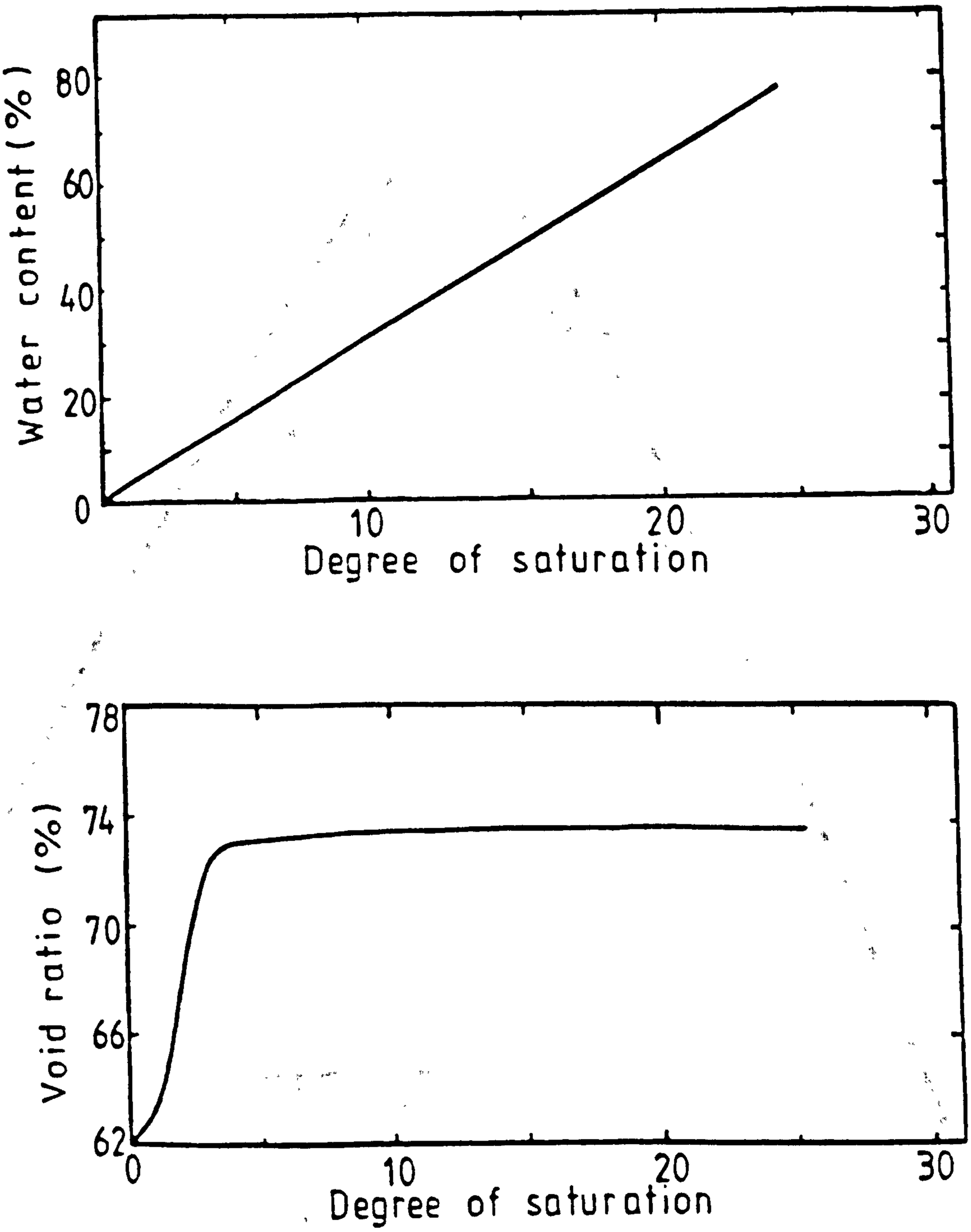

FIG. 3.30

Water content, Void ratio & Degree of Saturation relationship of Leighton Buzzard sand

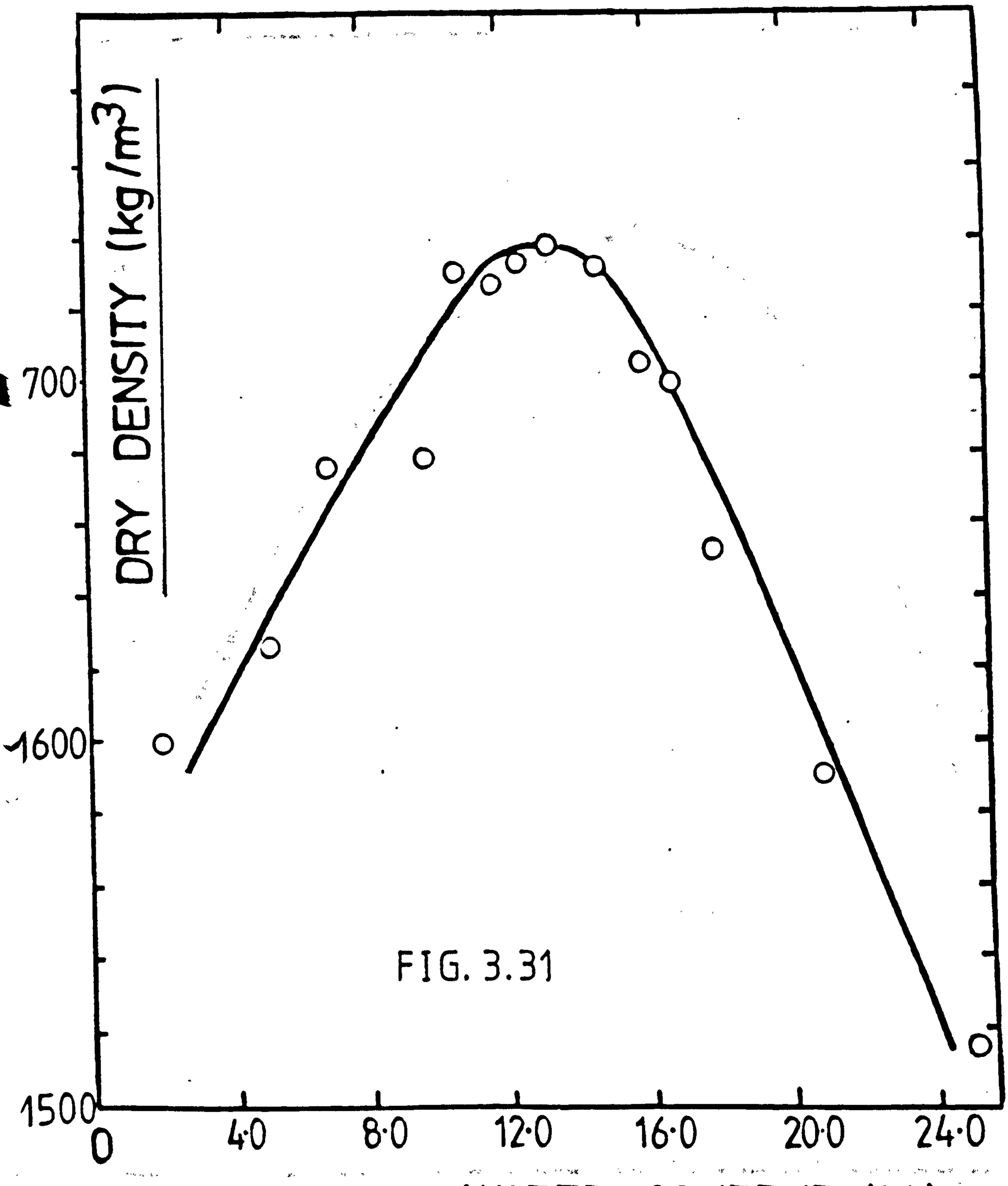

FIG. 3.31

COMPACTION CURVE OF WEST HIGHLAND MORAINE

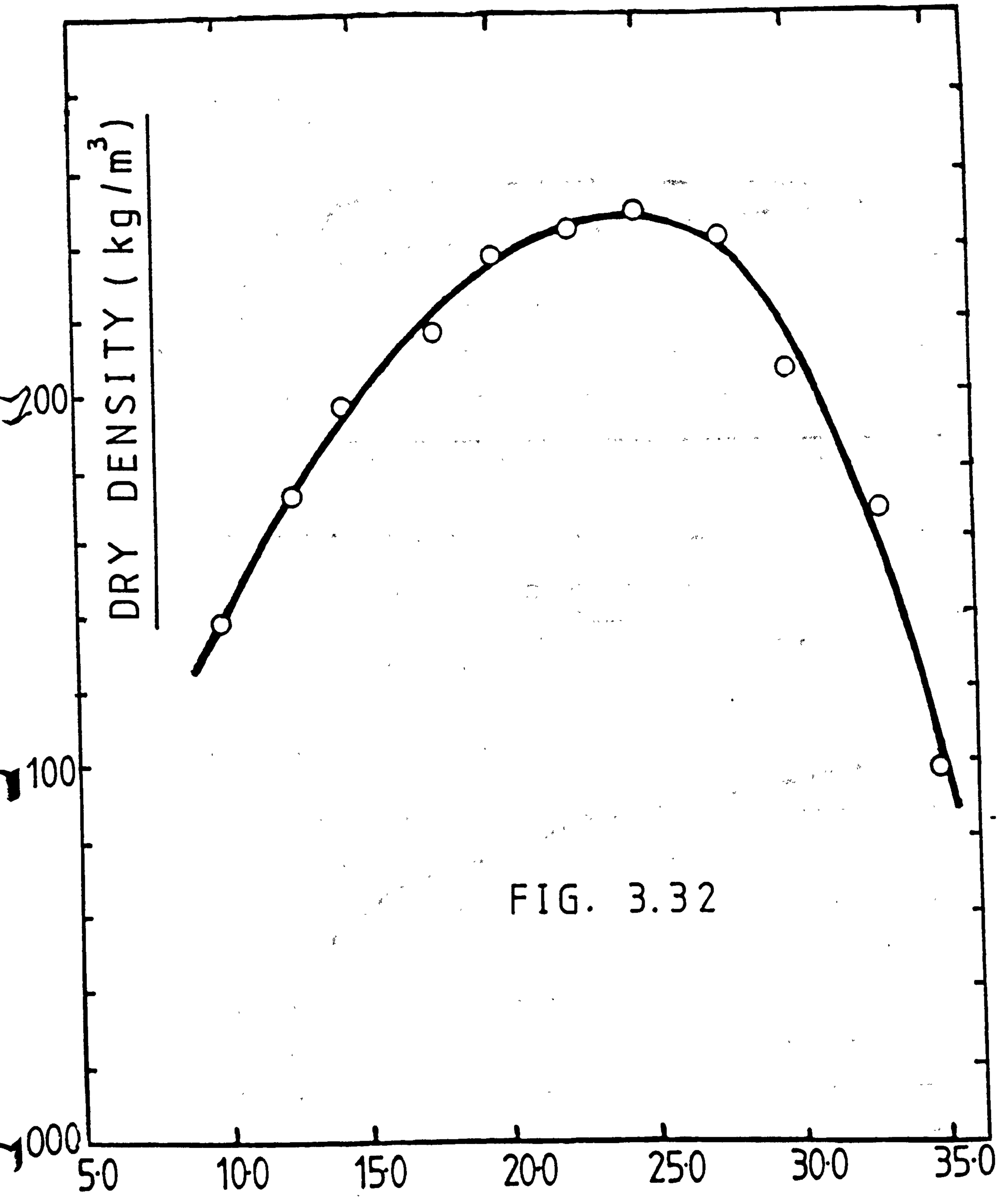

FIG. 3.32

COMPACTION CURVE
OF
PULVERISED FUEL ASH

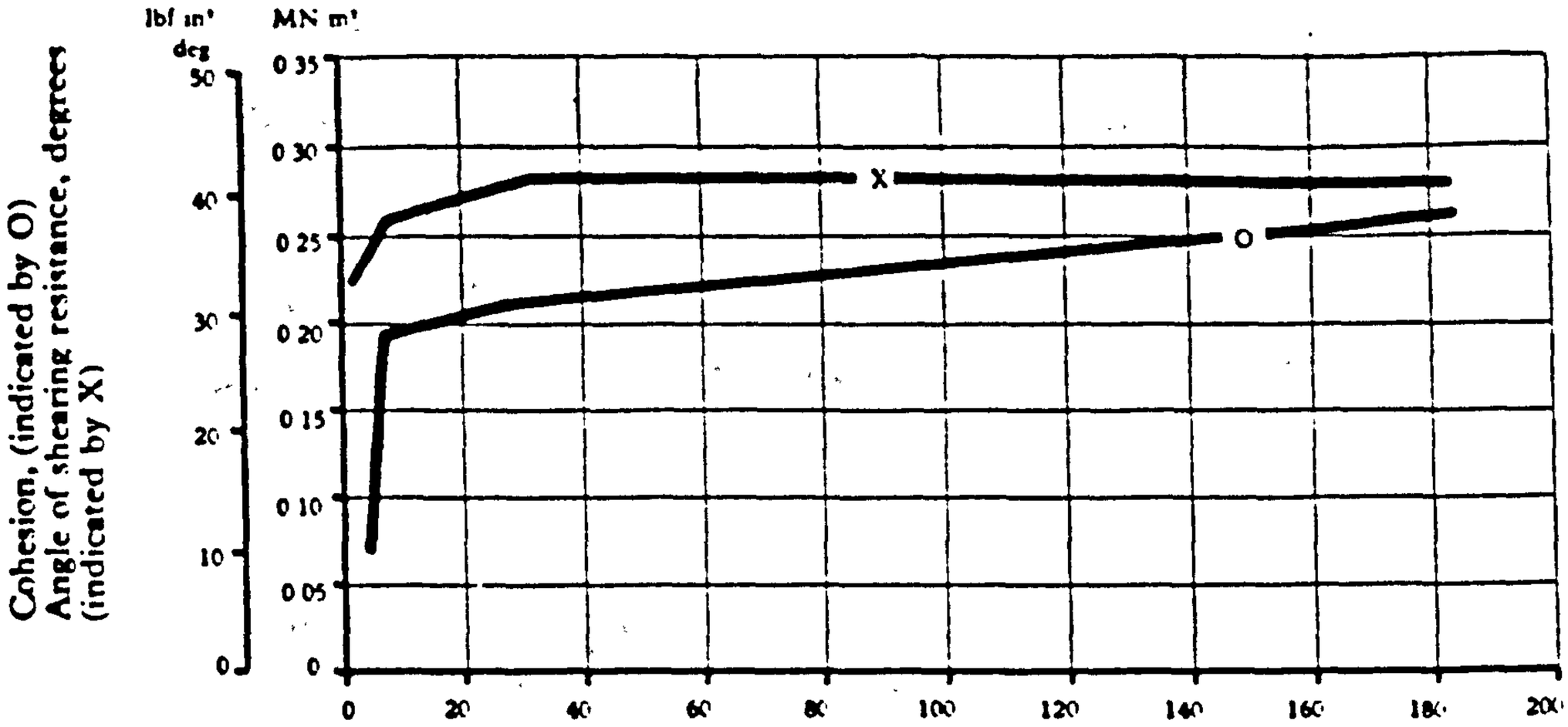

Increase of cohesion and angle of shearing resistance with age (for a typical conditioned PFA)

FIG. 3.33

(After S.G.E.B. 1981)

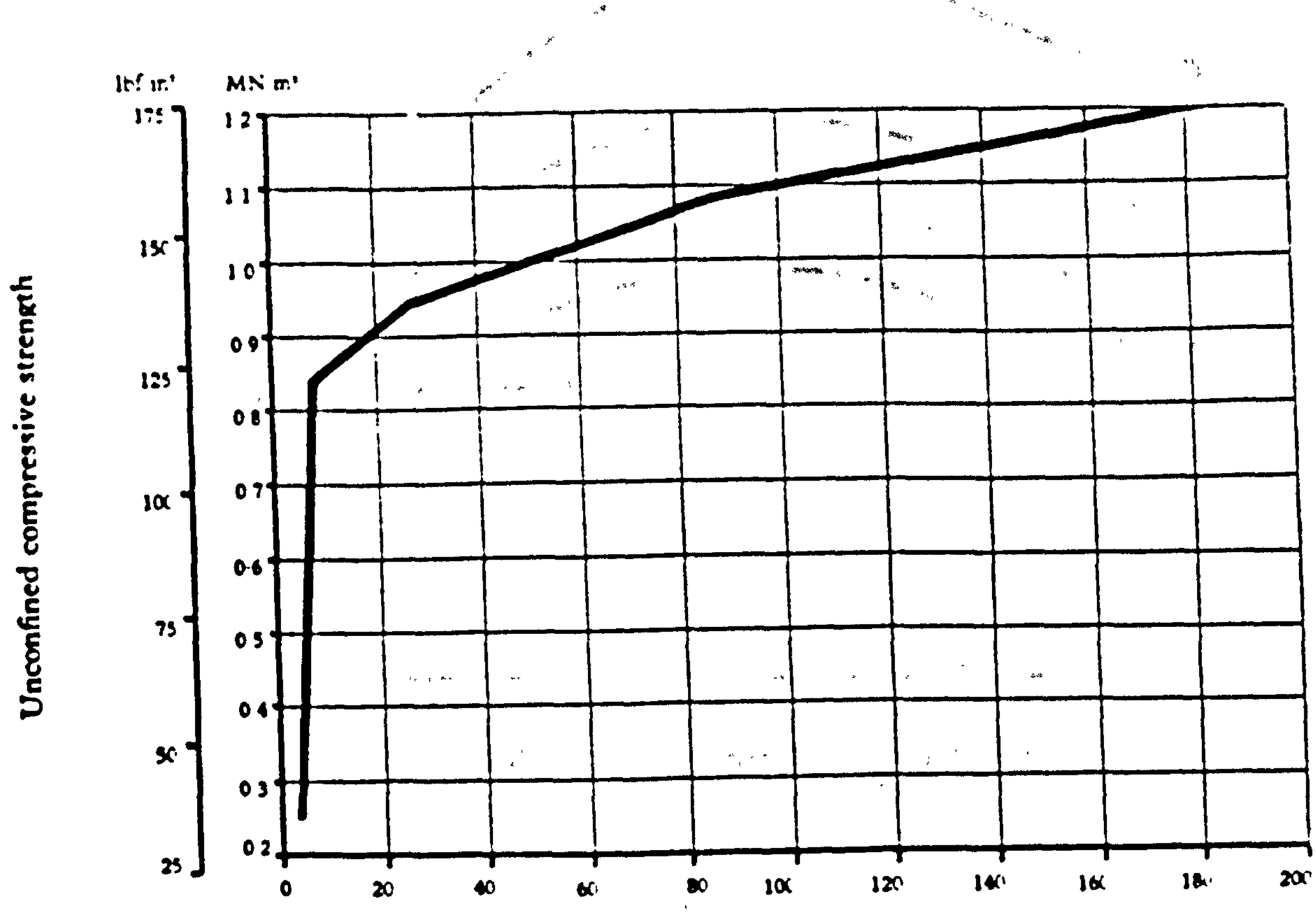

Increase of unconfined compressive strength with age (for a typical conditioned PFA)

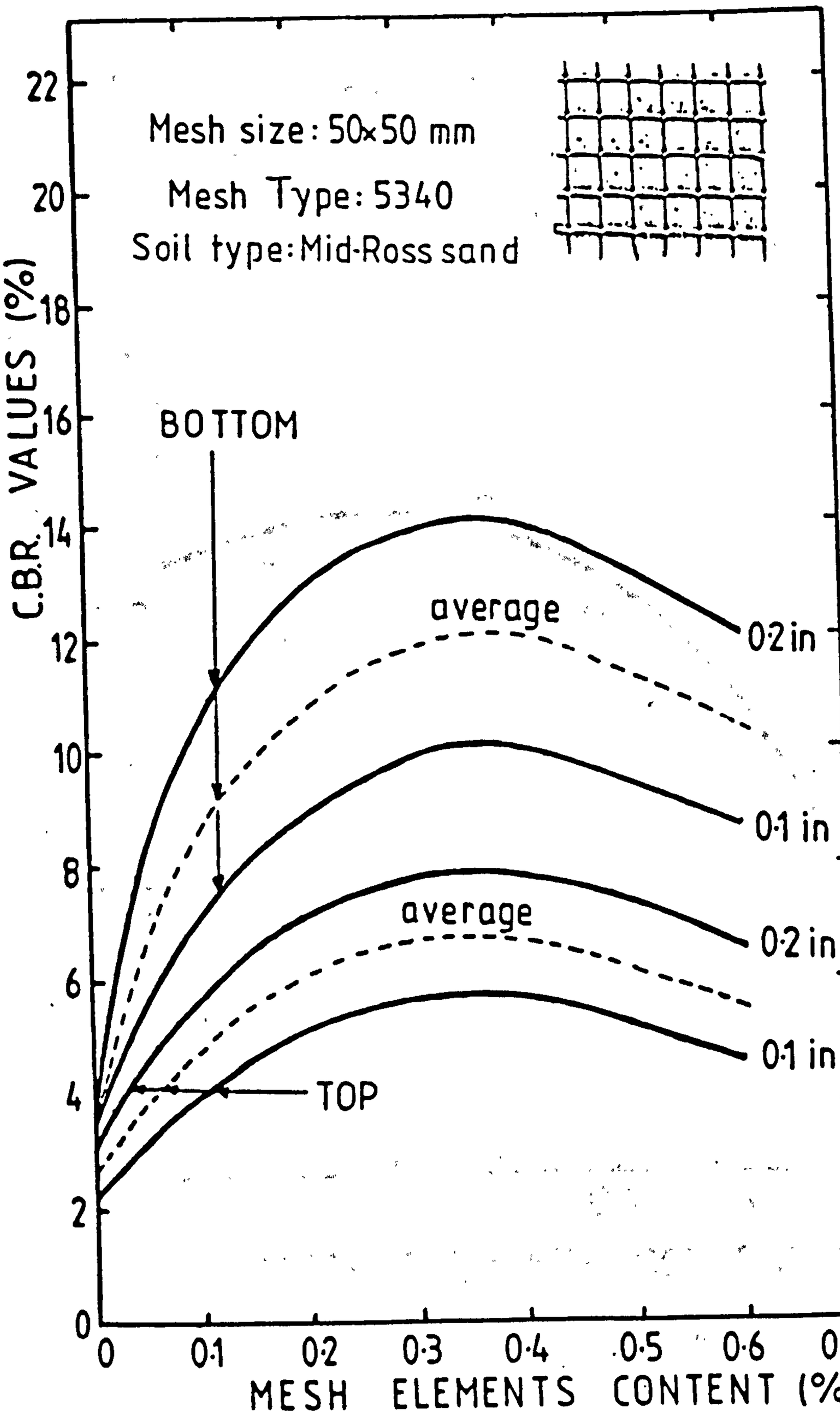

FIG. 4.1 Effect of mesh element content on C.B.R. values.

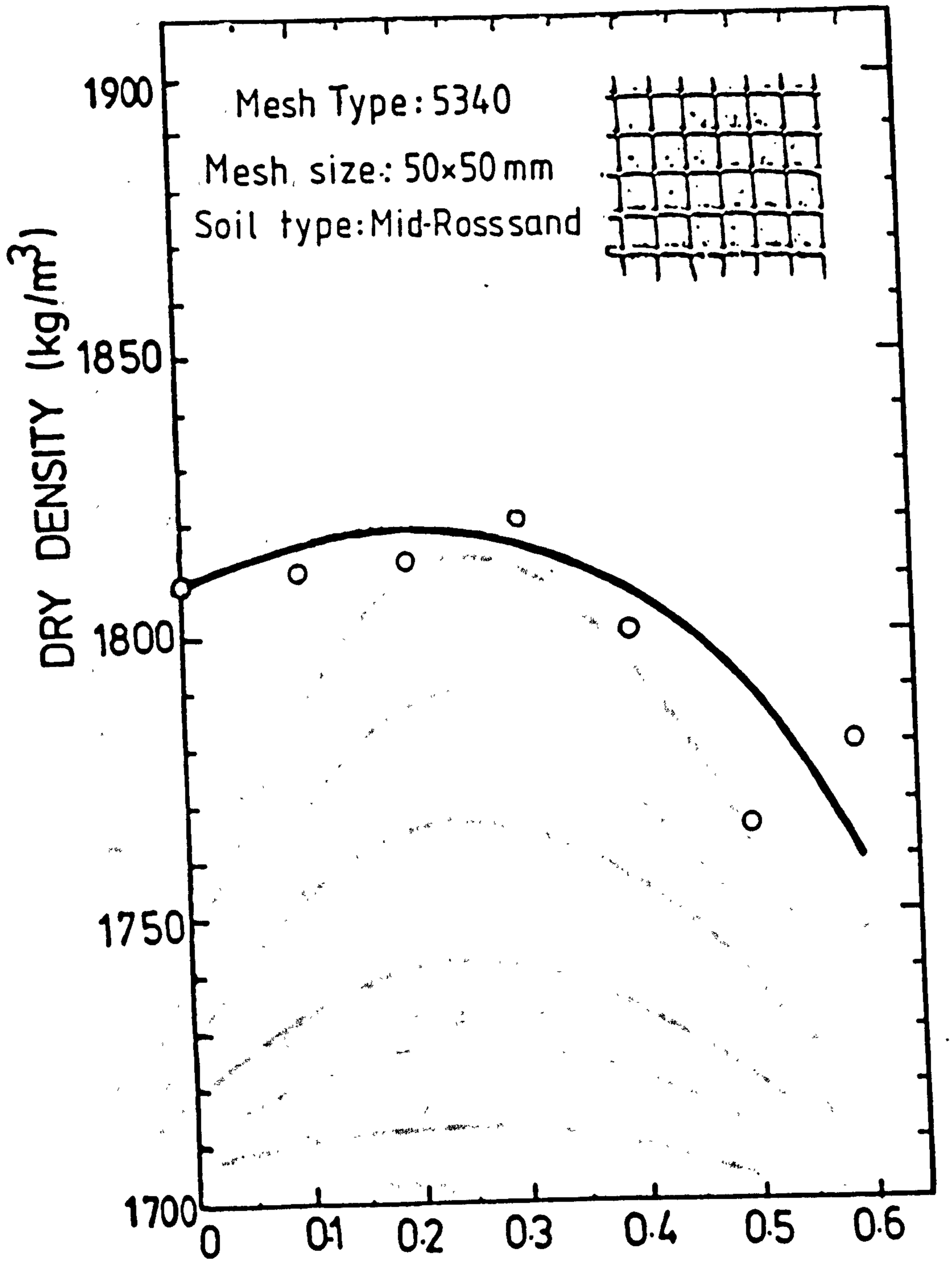

FIG. 4.2 Effect of mesh element content on the dry density of compacted samples

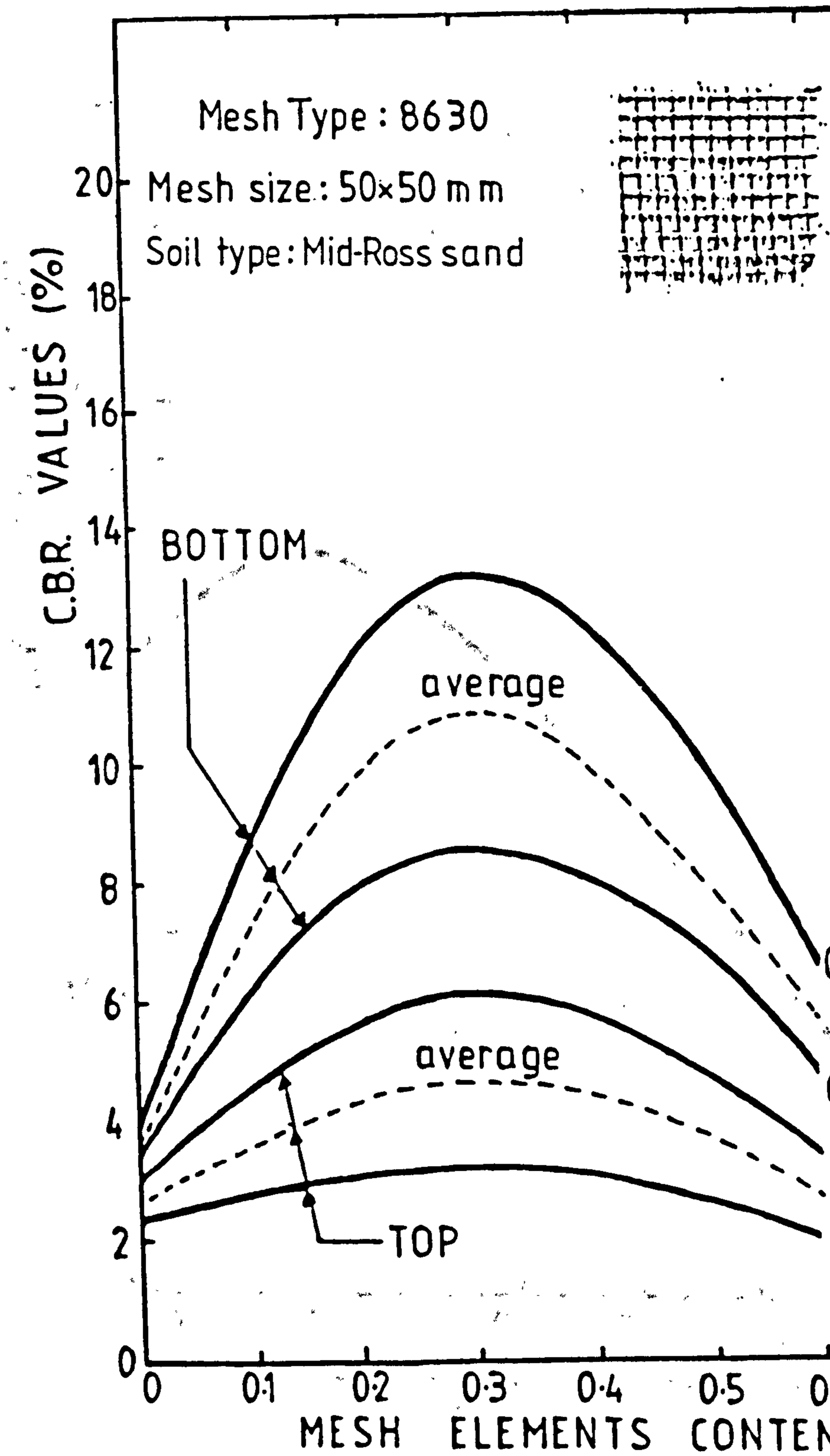

FIG. 4.3 Effect of mesh element content on C.B.R. values.

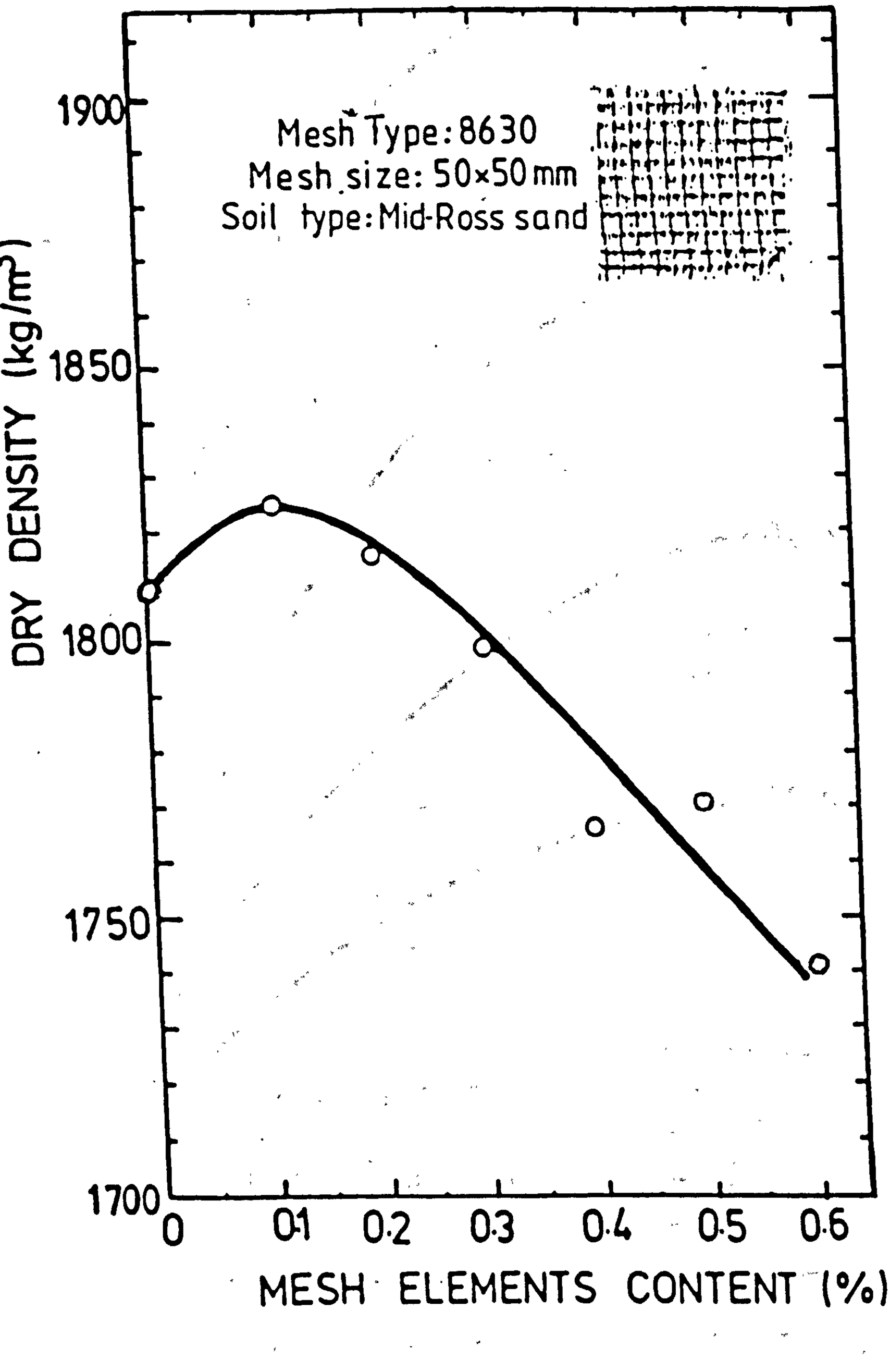

FIG. 4.4 Effect of mesh element content on the dry density of compacted samples

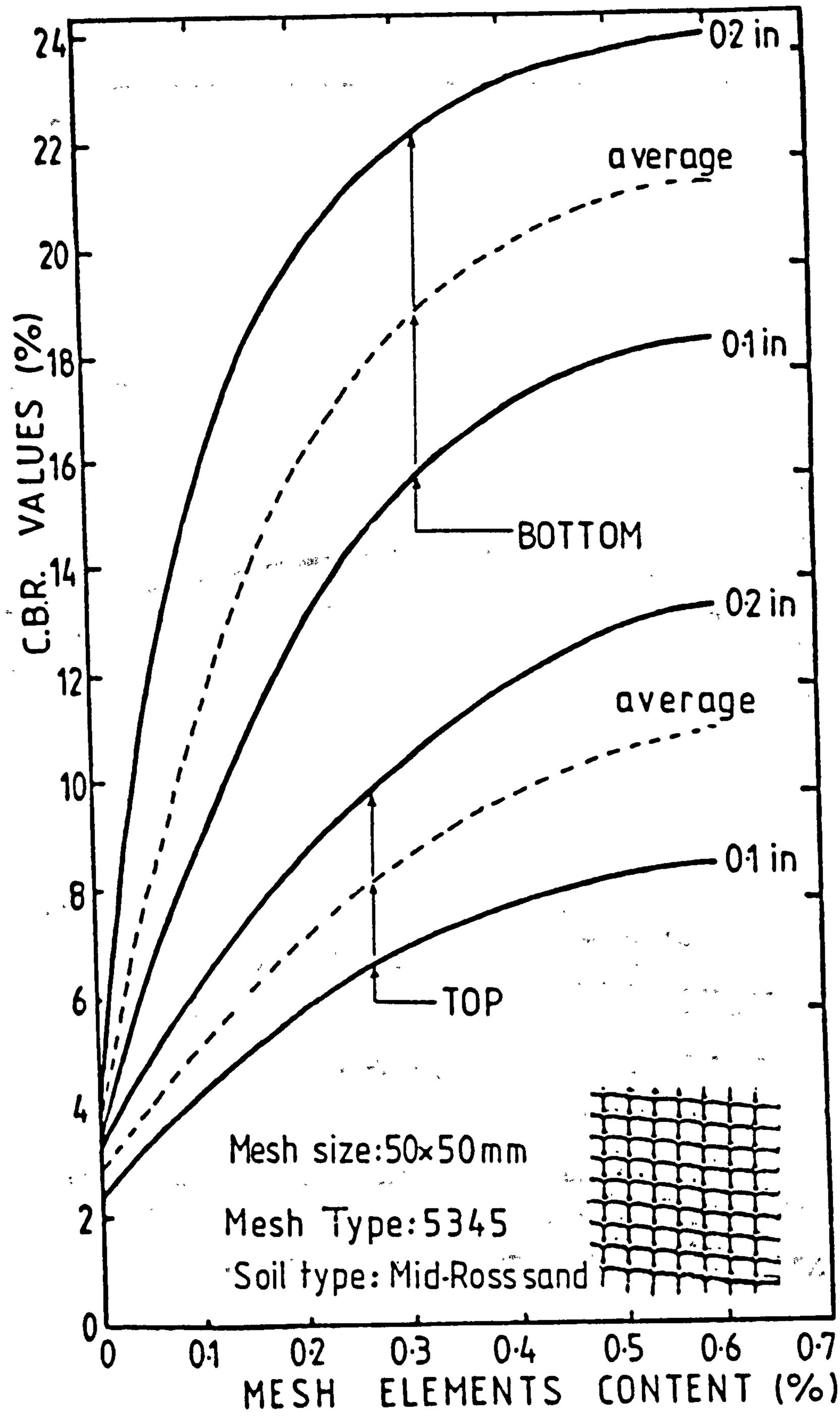

FIG. 4.5 Effect of mesh element content on C.B.R. values.

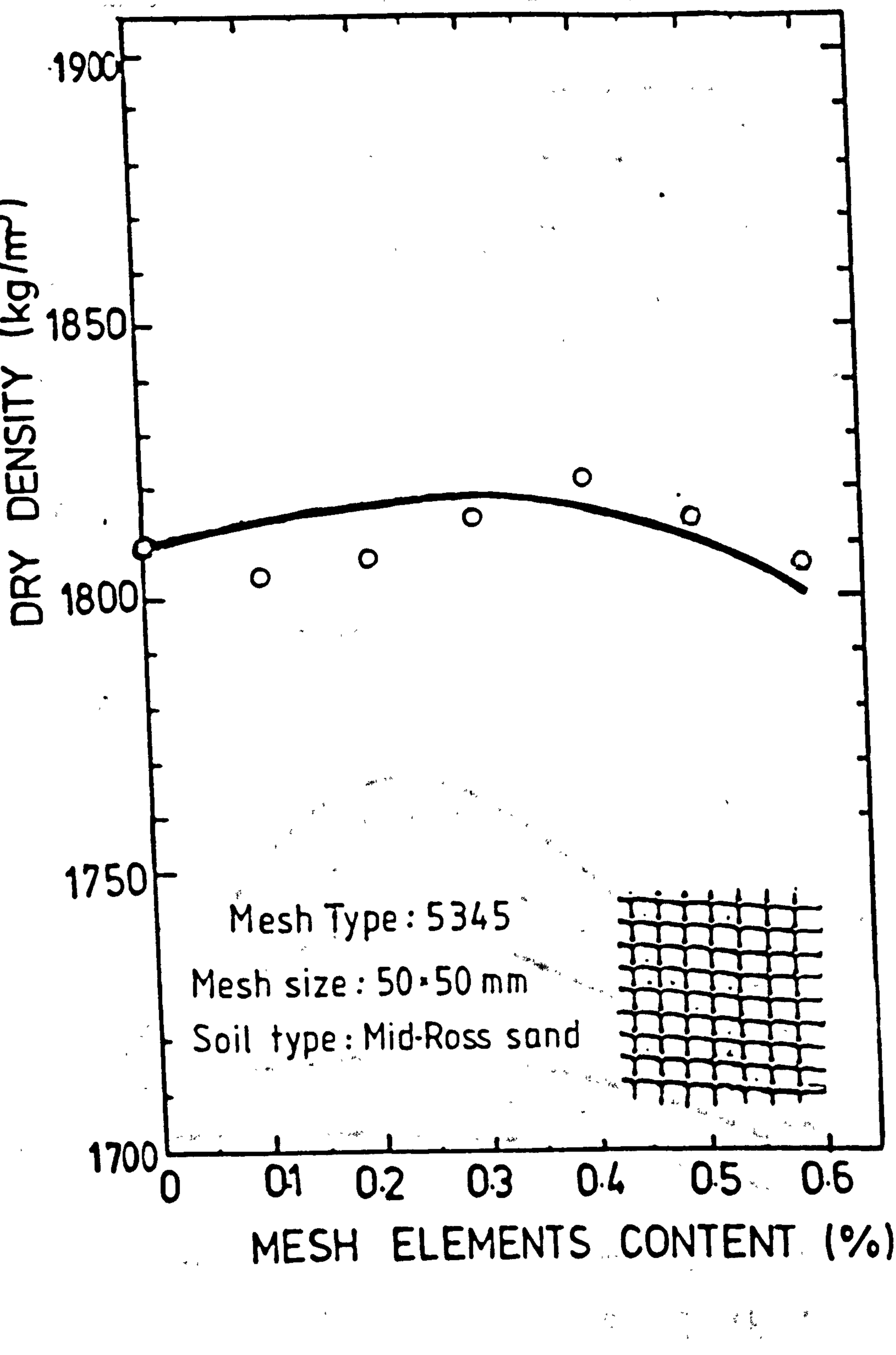

FIG. 4.6 Effect of mesh element content on the dry density of compacted samples

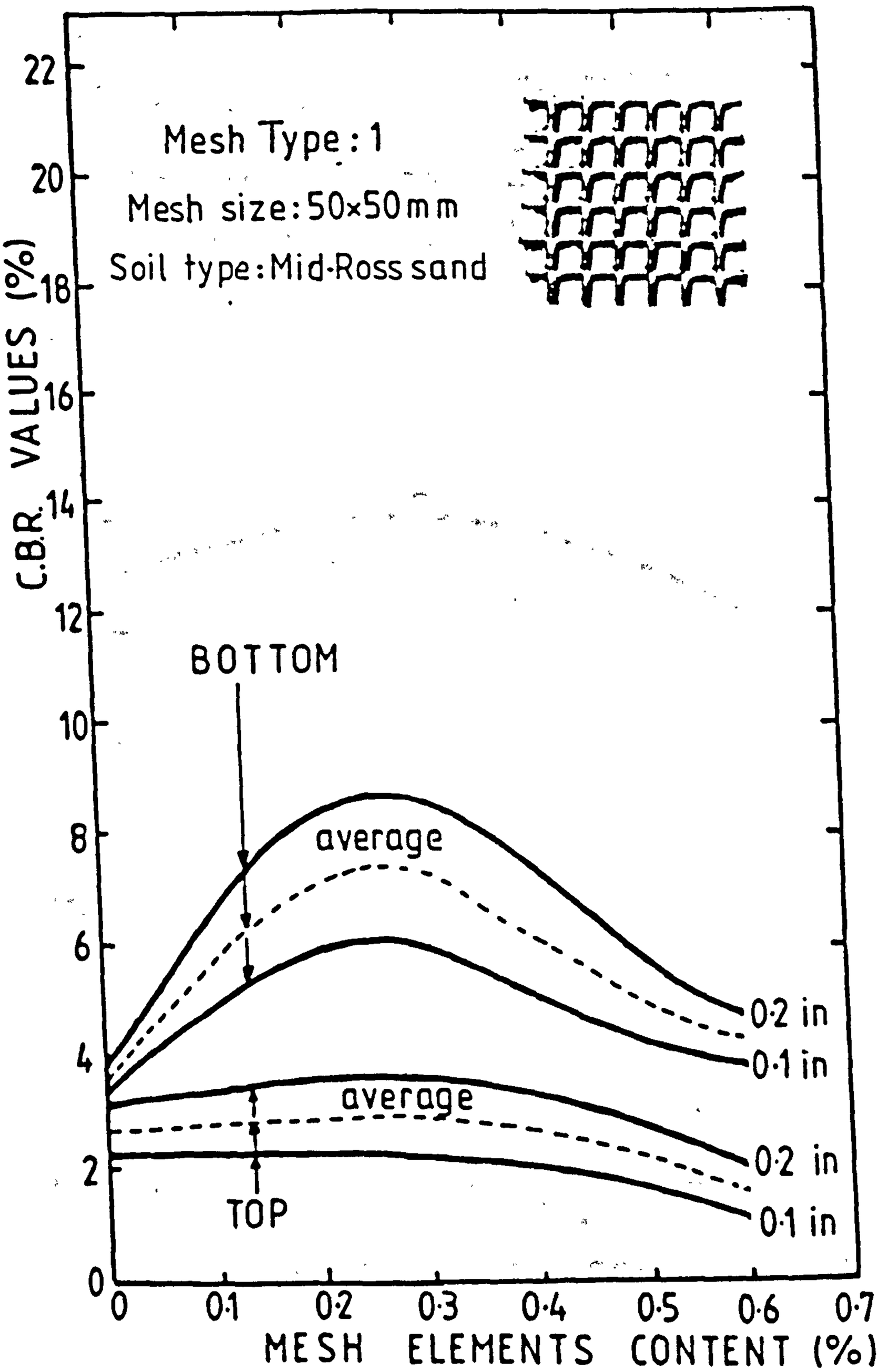

FIG 4.7 Effect of mesh element content on C.B.R. values.

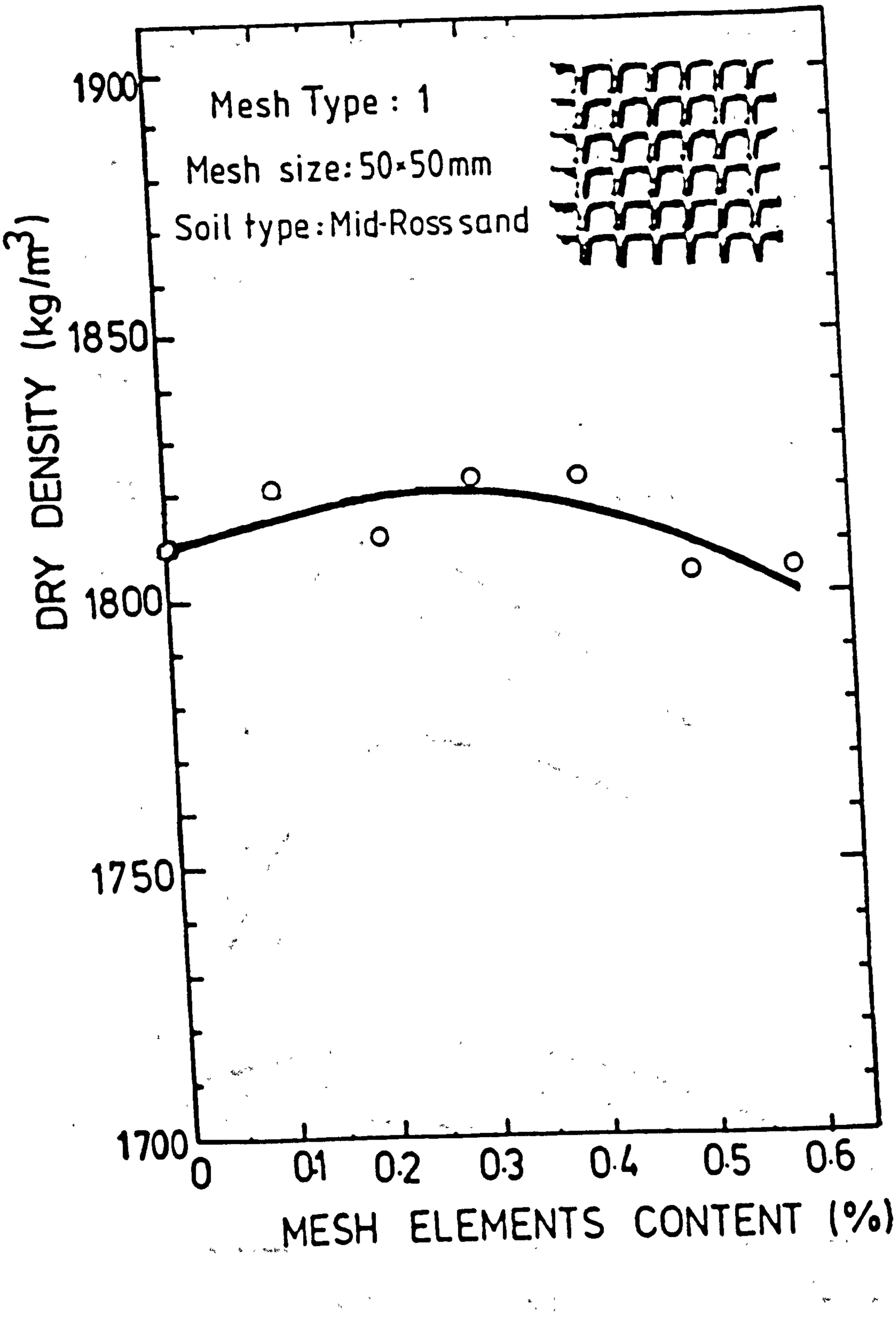

FIG. 4.8 Effect of mesh element content on the dry density of compacted samples

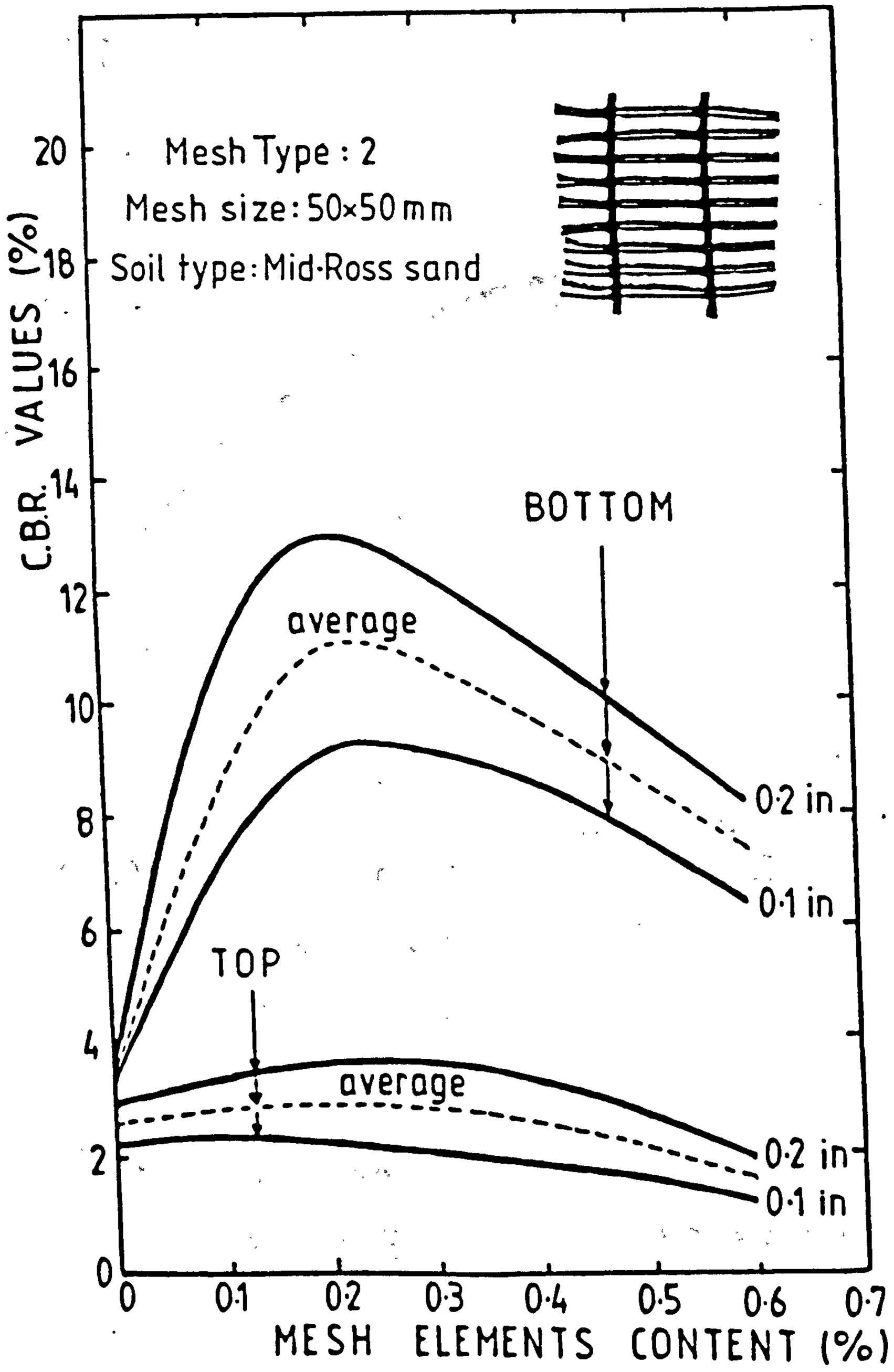

FIG. 4.9 Effect of mesh element content on C.B.R. values.

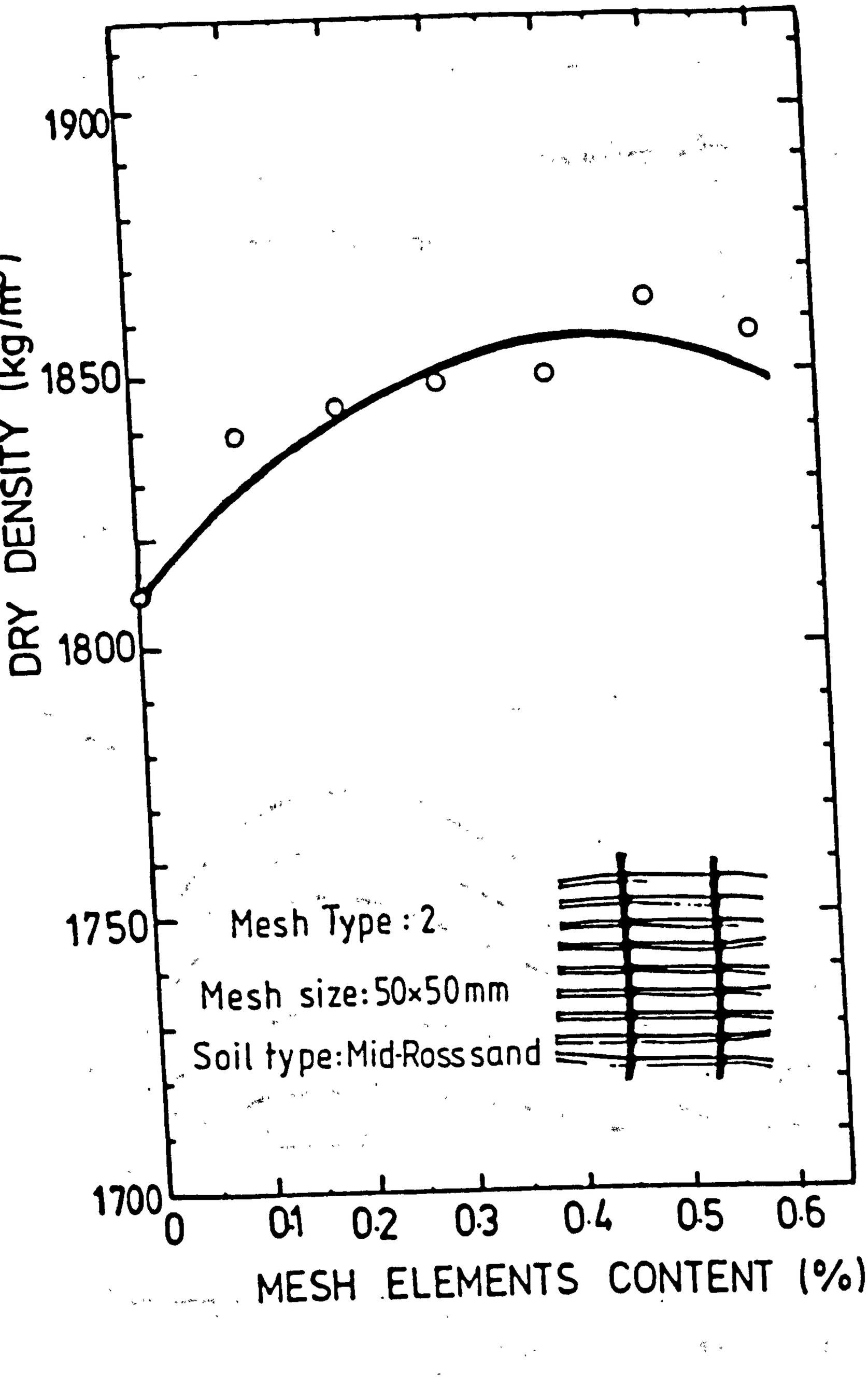

FIG. 4.10 Effect of mesh element content on the dry density of compacted samples

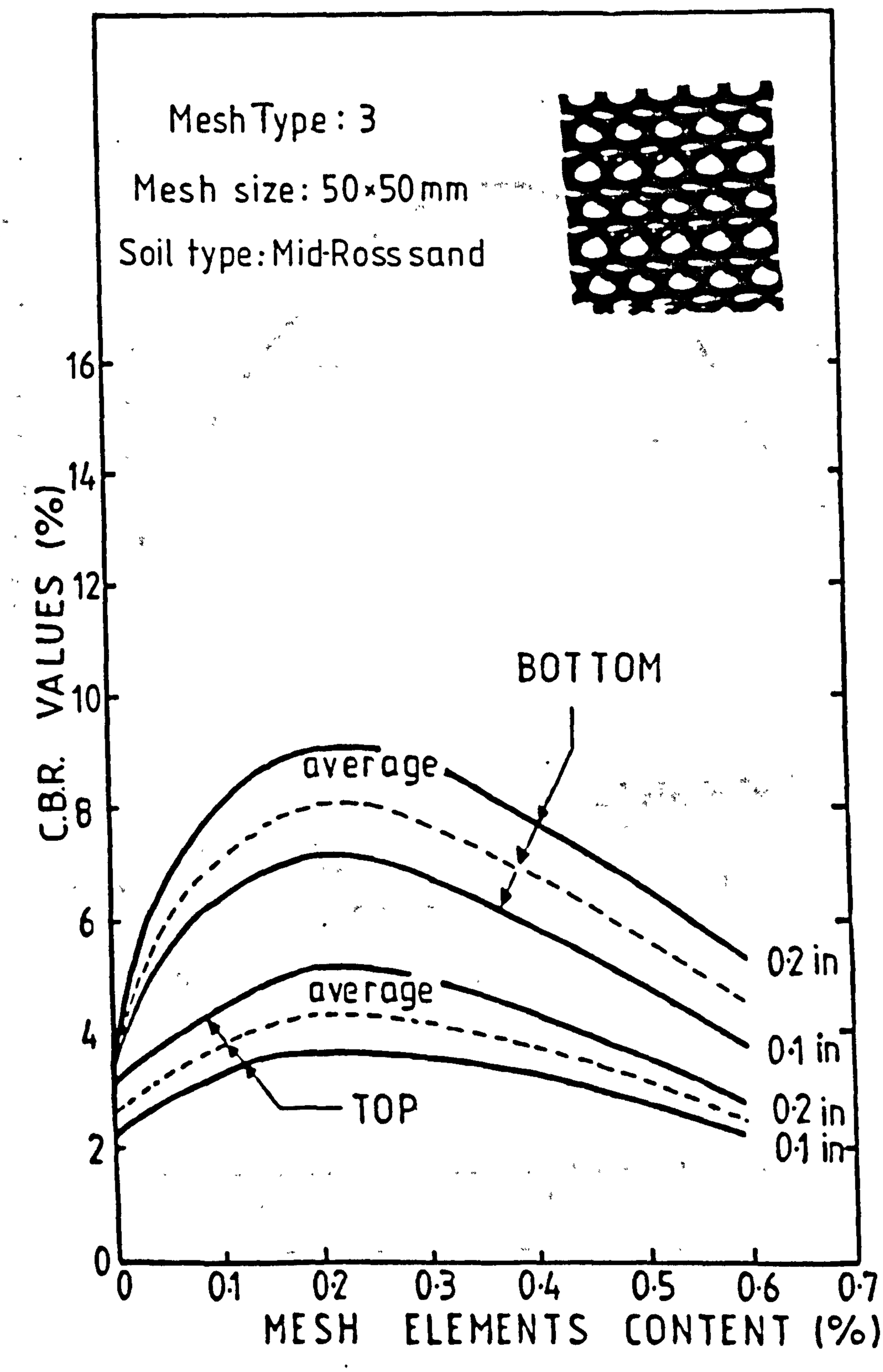

FIG. 4.11 Effect of mesh element content on C.B.R. values.

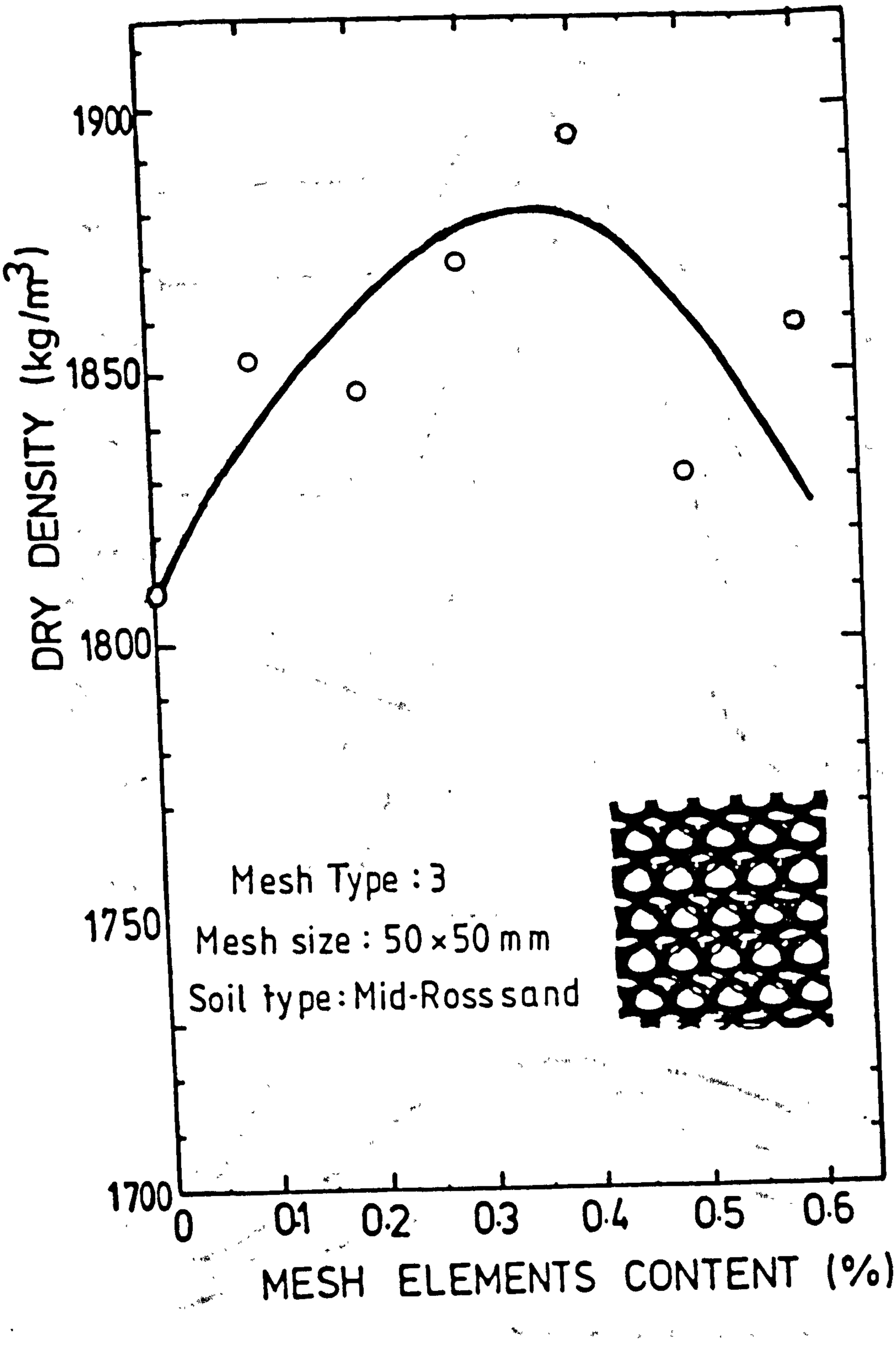

FIG. 4.12 Effect of mesh element content on the dry density of compacted samples

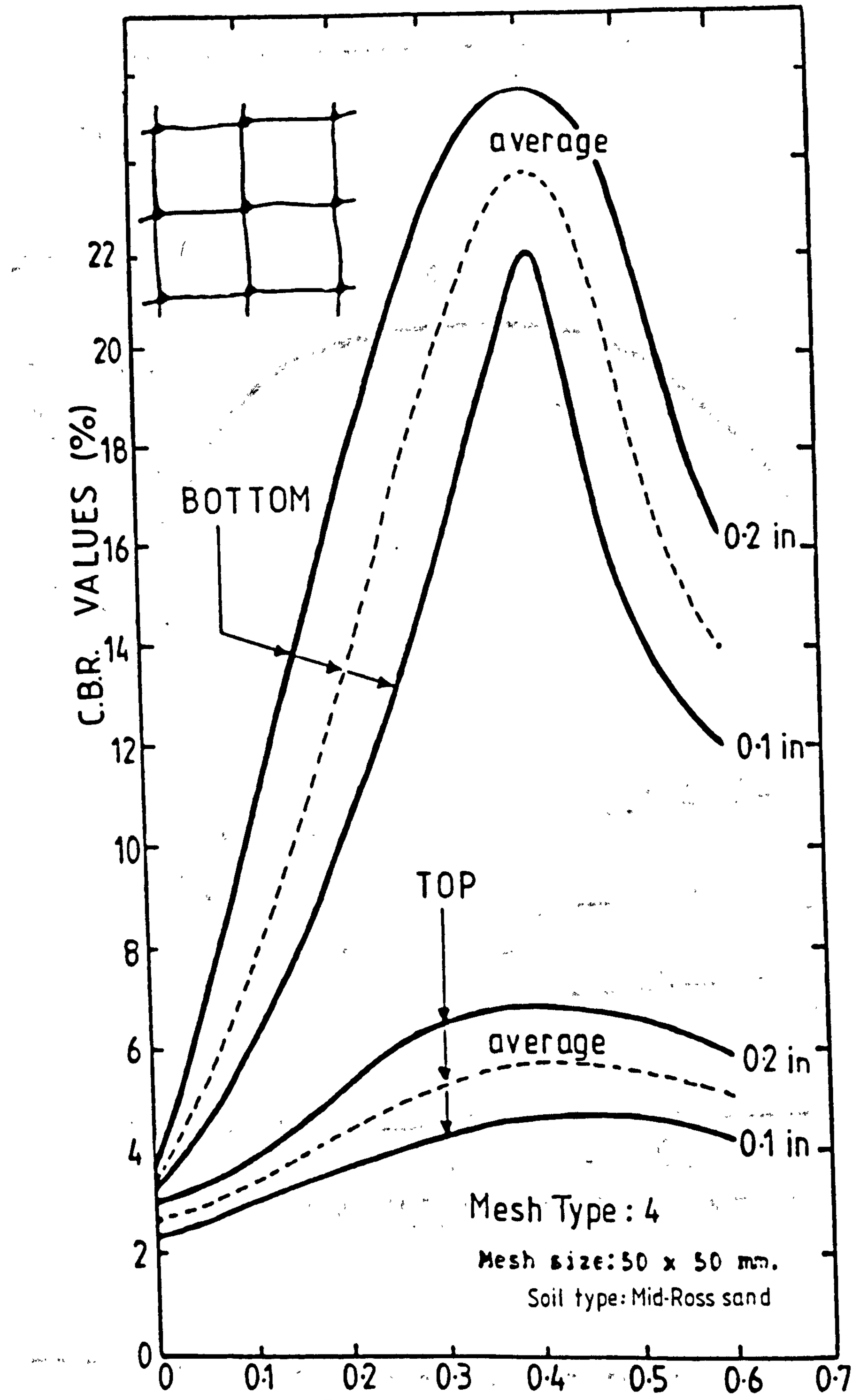

FIG. 4.13 Effect of mesh element content on C.B.R. values.

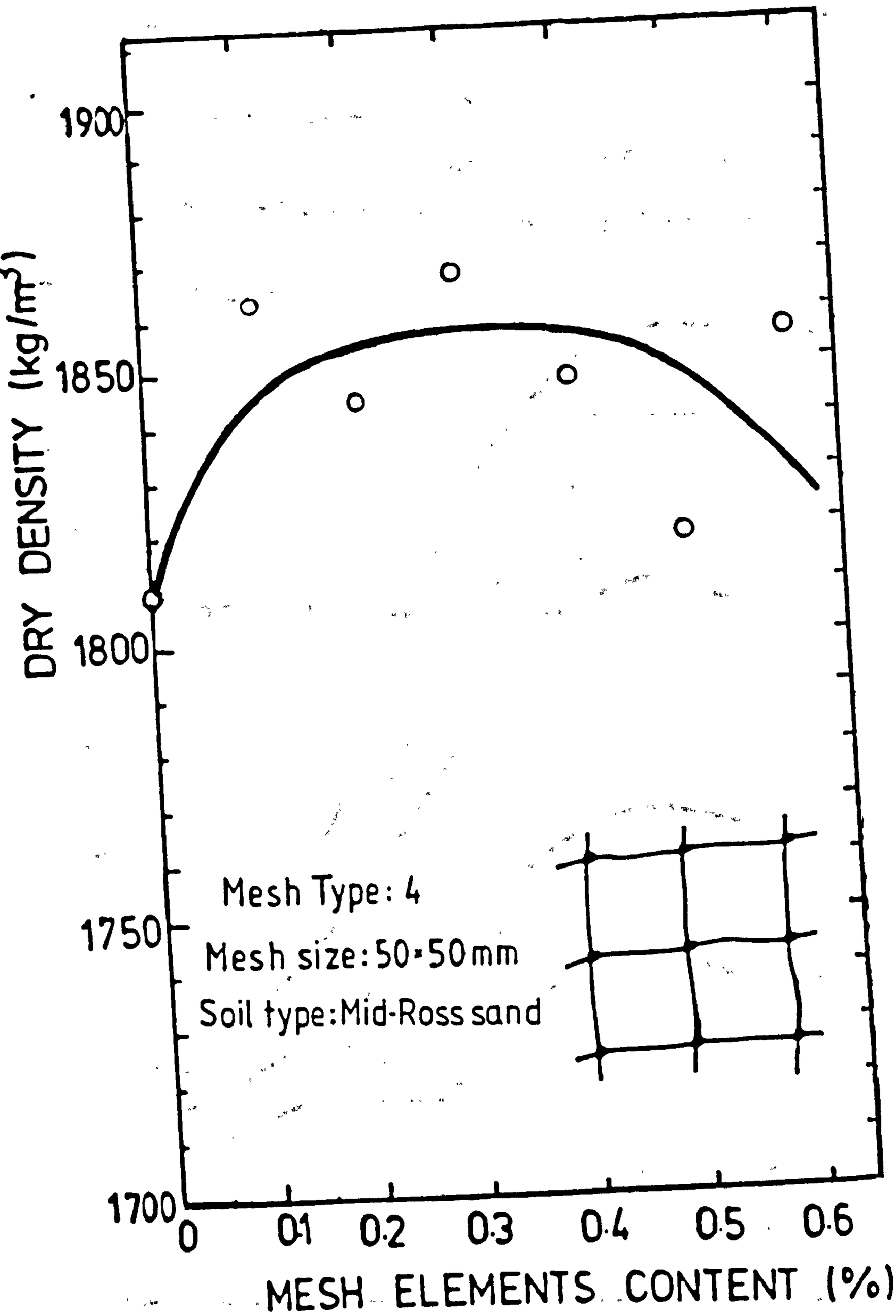

FIG. 4.14 Effect of mesh element content on the dry density of compacted samples

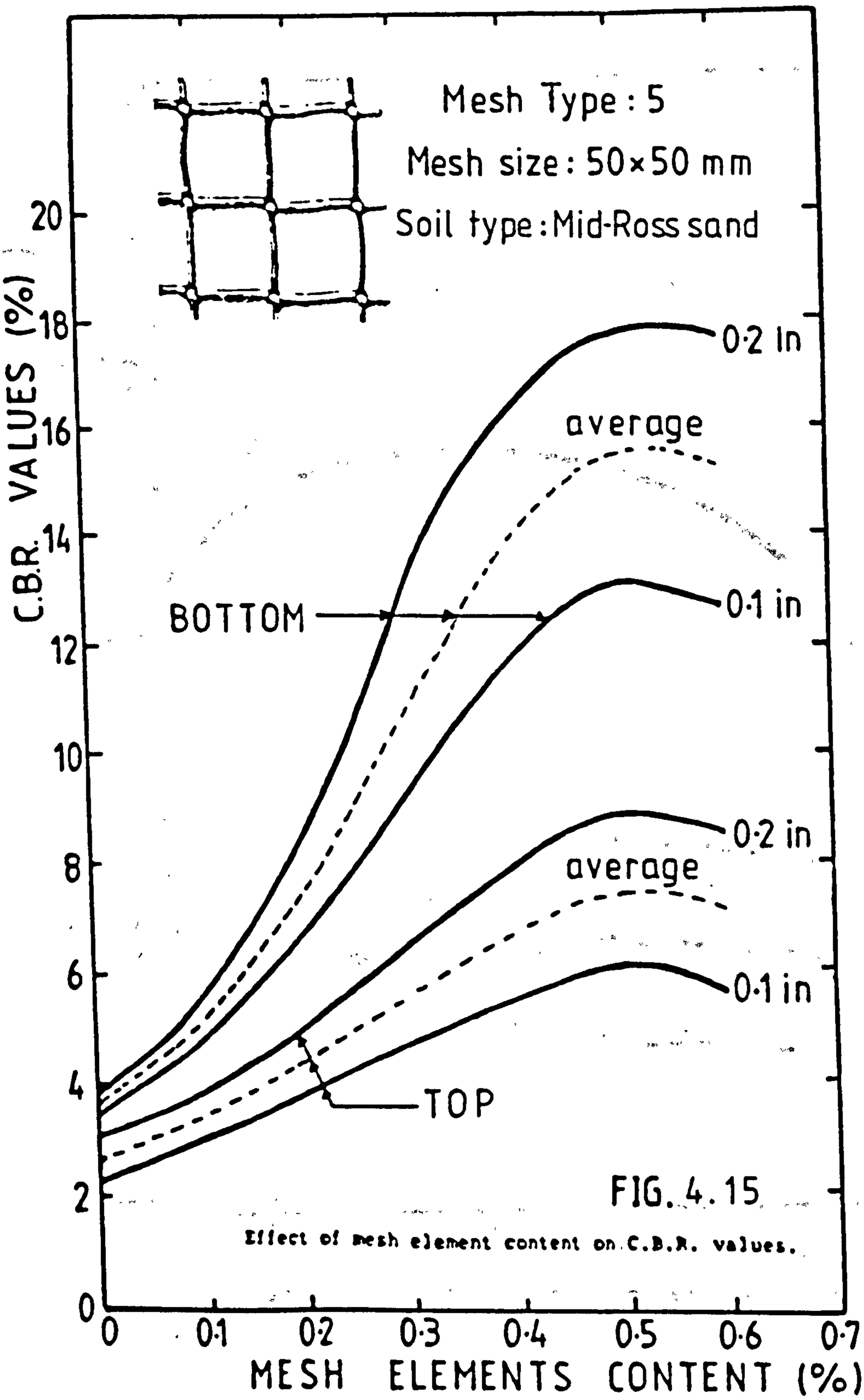

FIG. 4.15 Effect of mesh element content on C.B.R. values.

FIG. 4.15 Effect of mesh element content on C.B.R. values.

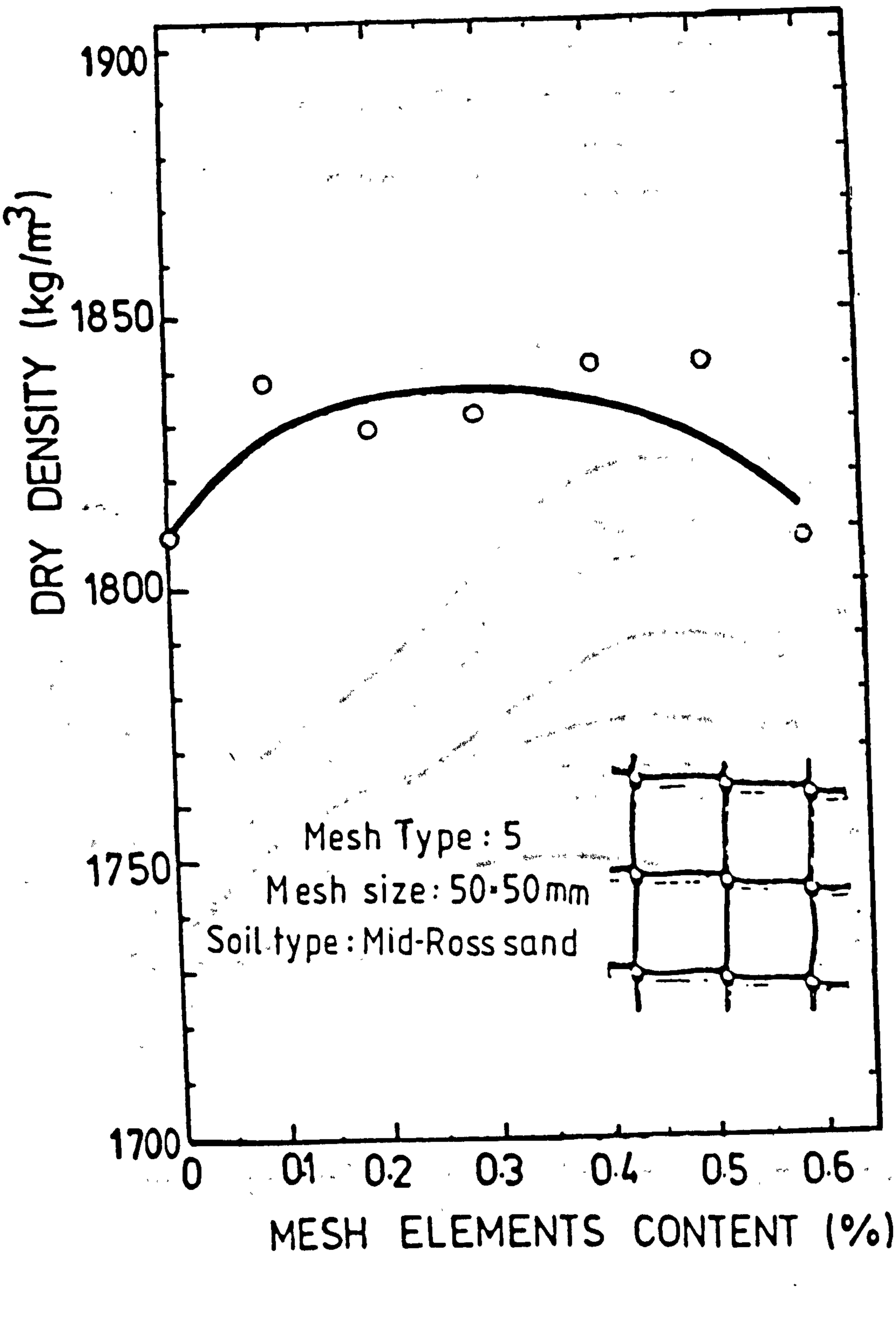

FIG. 4.16 Effect of mesh element content on the dry density of compacted samples

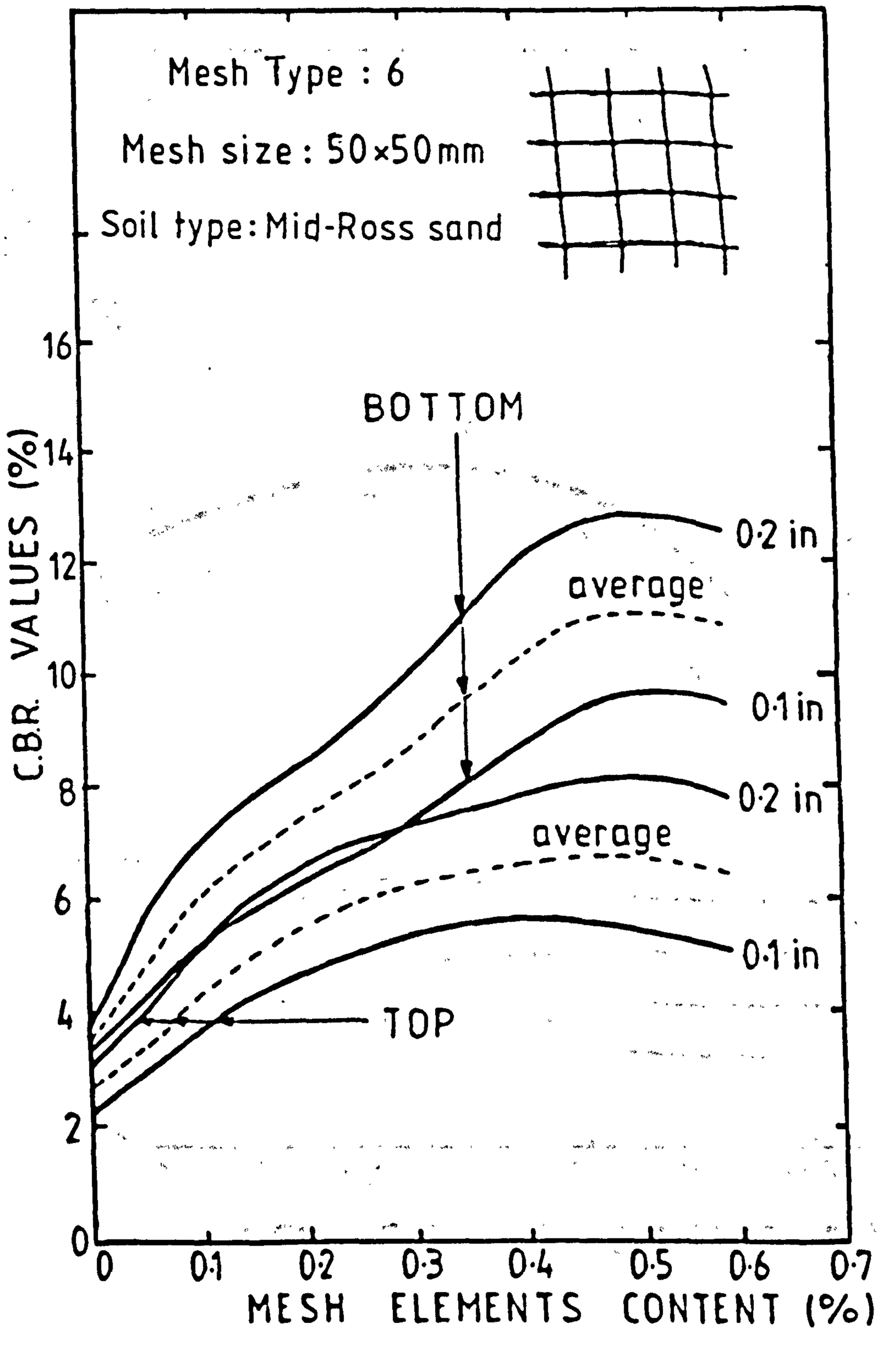

FIG. 4.17 Effect of mesh element content on C.B.R. values.

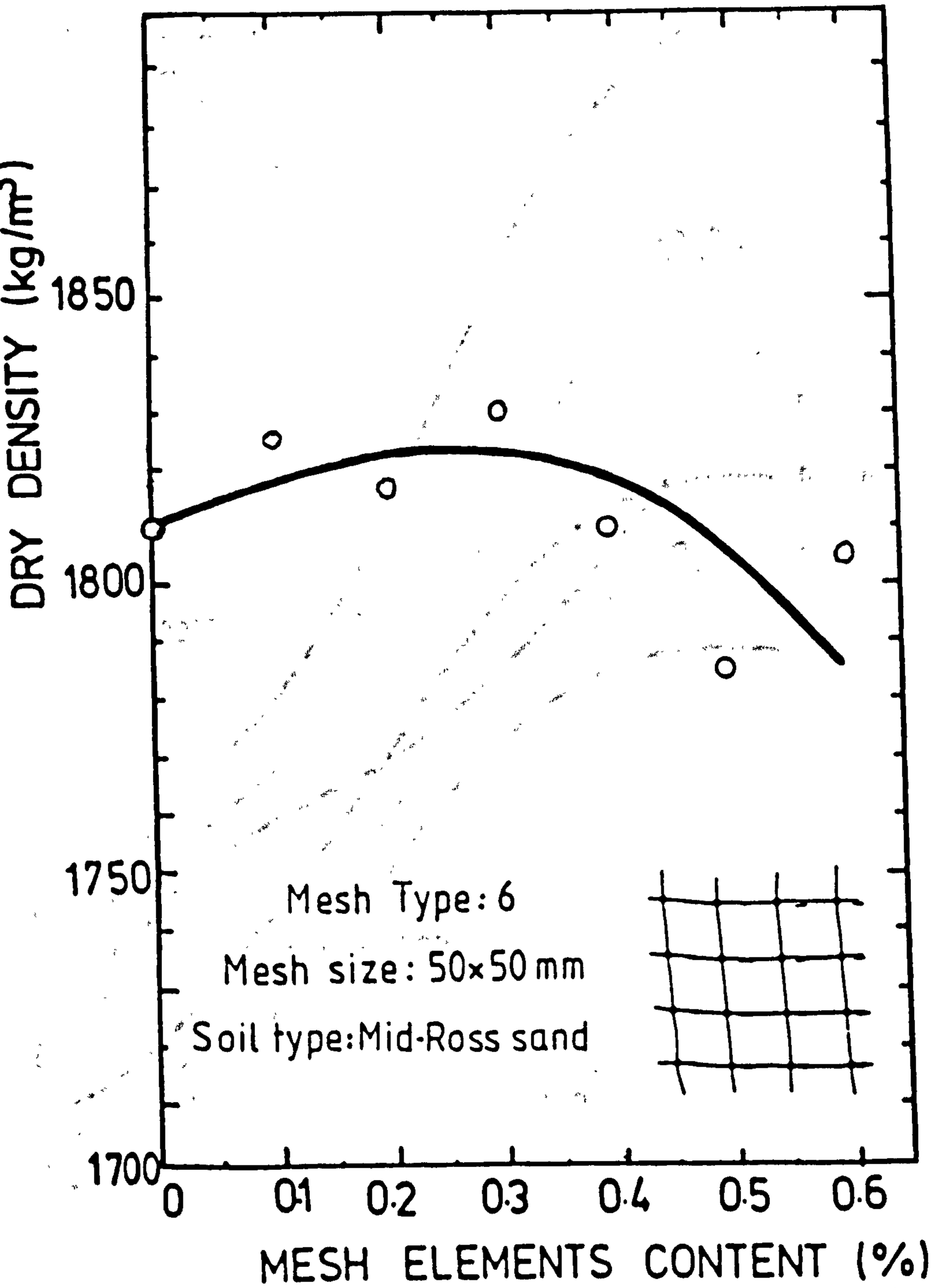

FIG. 4.18 Effect of mesh element content on the dry density of compacted samples

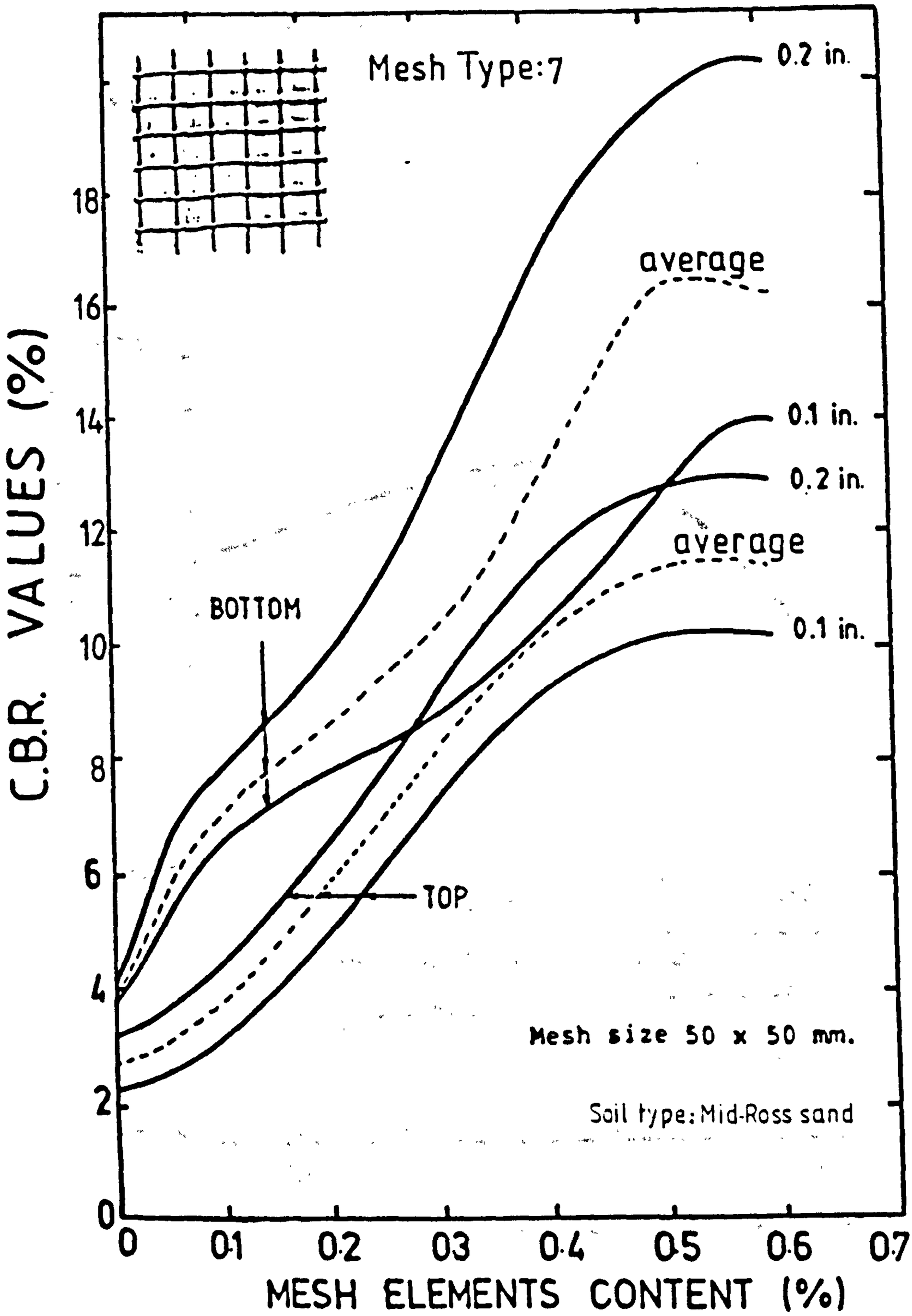

FIG. 4.19 Effect of mesh element content on C.B.R. values.

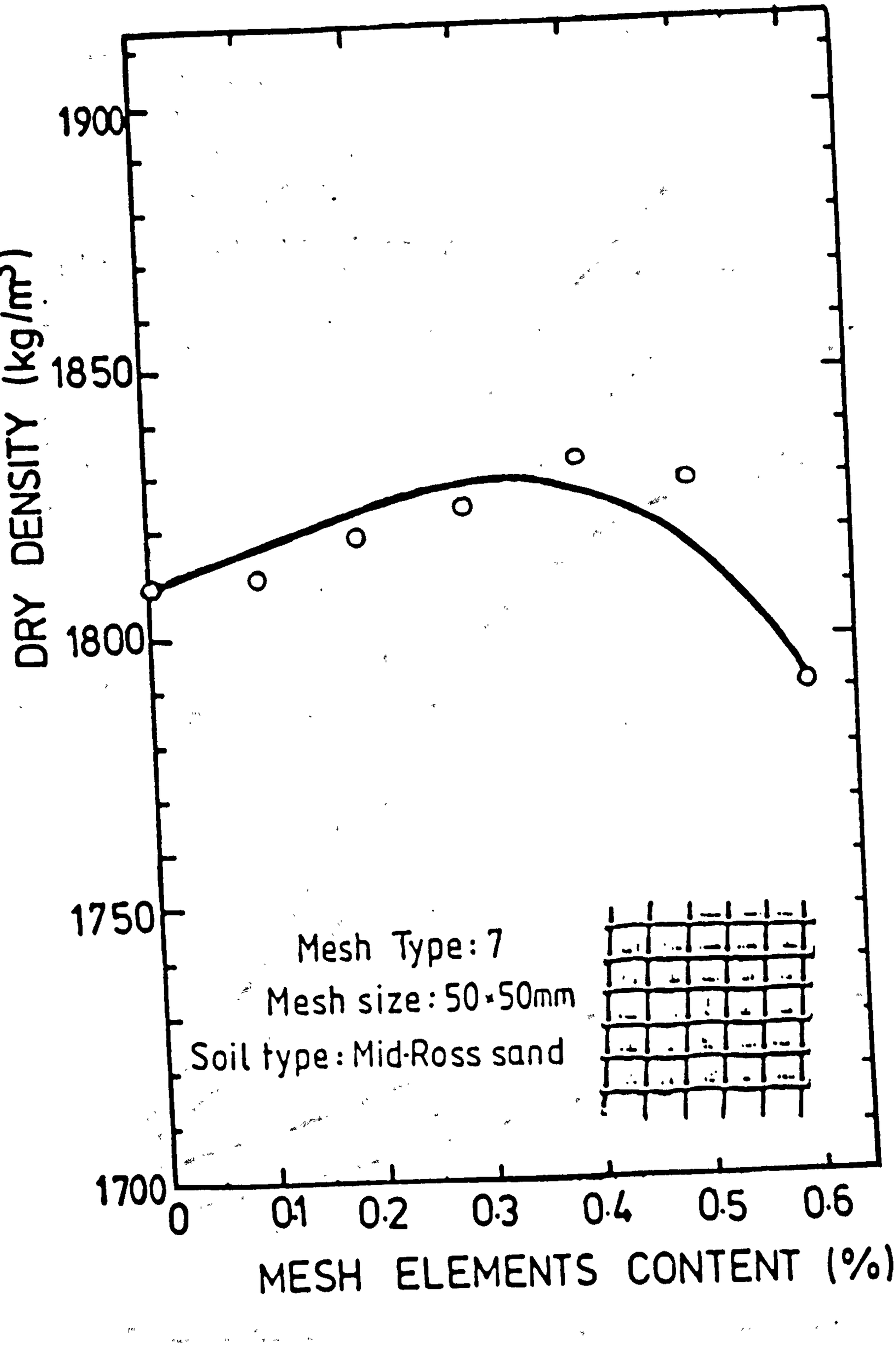

FIG. 4.20 Effect of mesh element content on the dry density of compacted samples

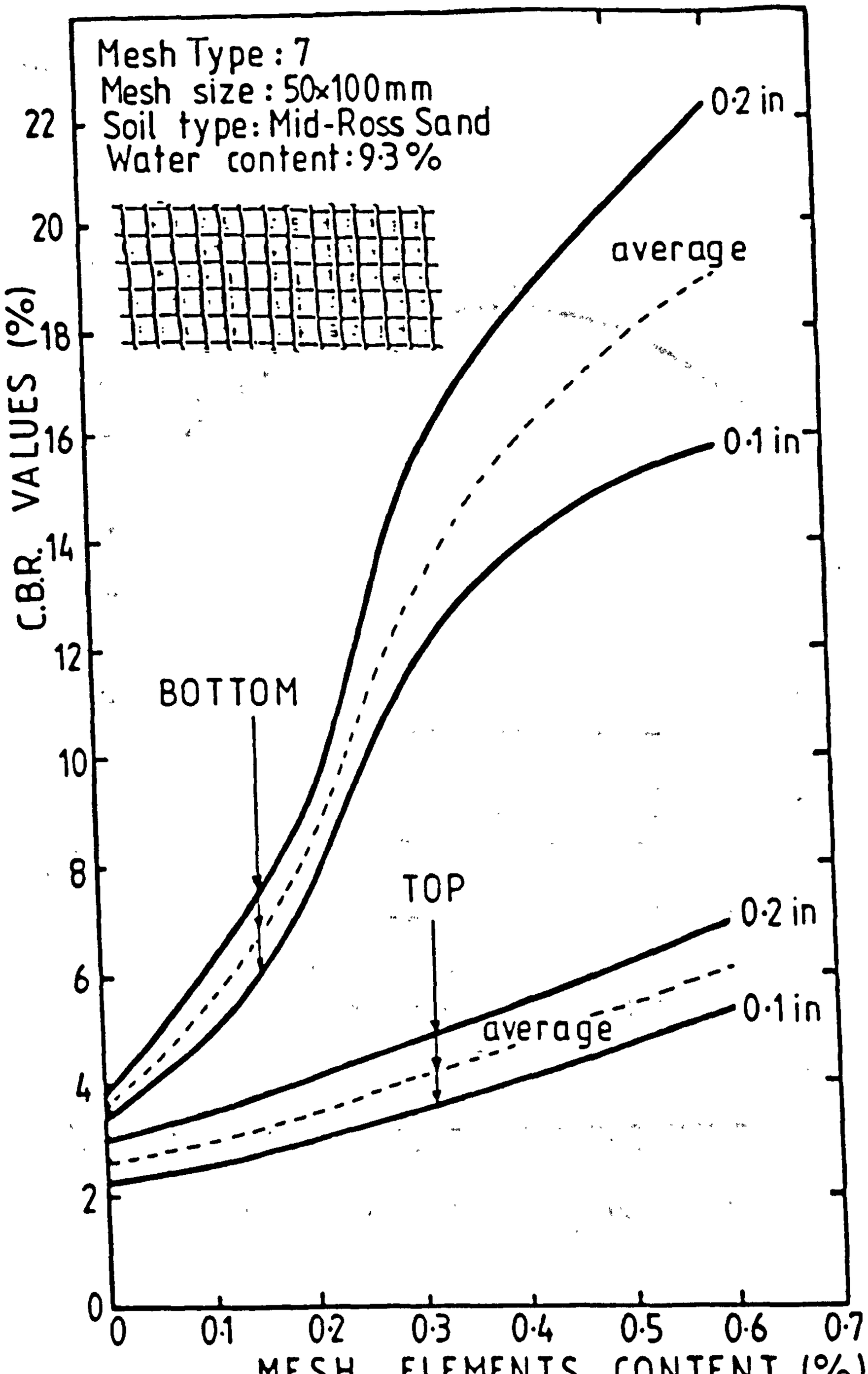

FIG. 4.21 Effect of mesh element content on C.B.R. values.

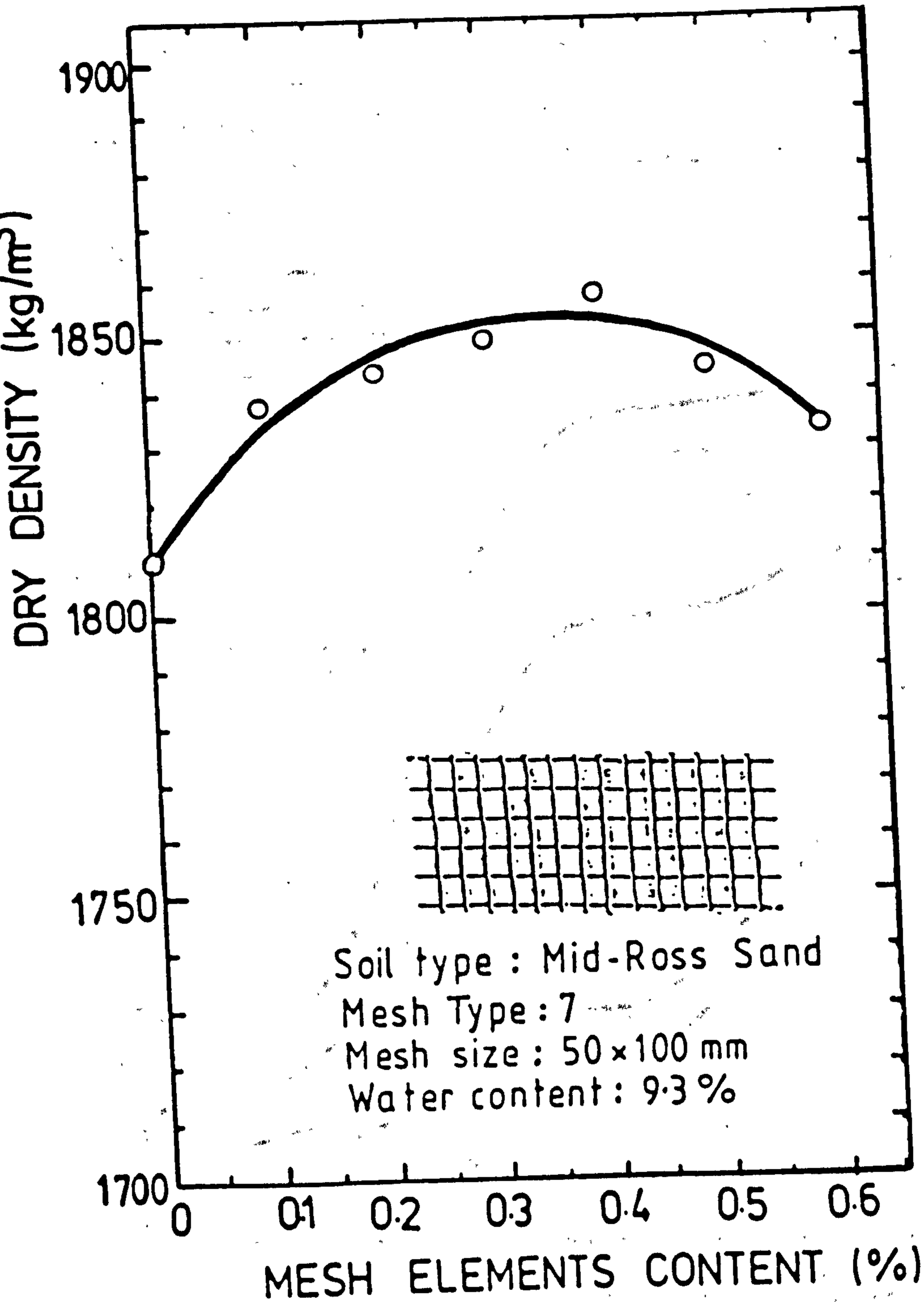

FIG. 4.22 Effect of mesh element content on the dry density of compacted samples

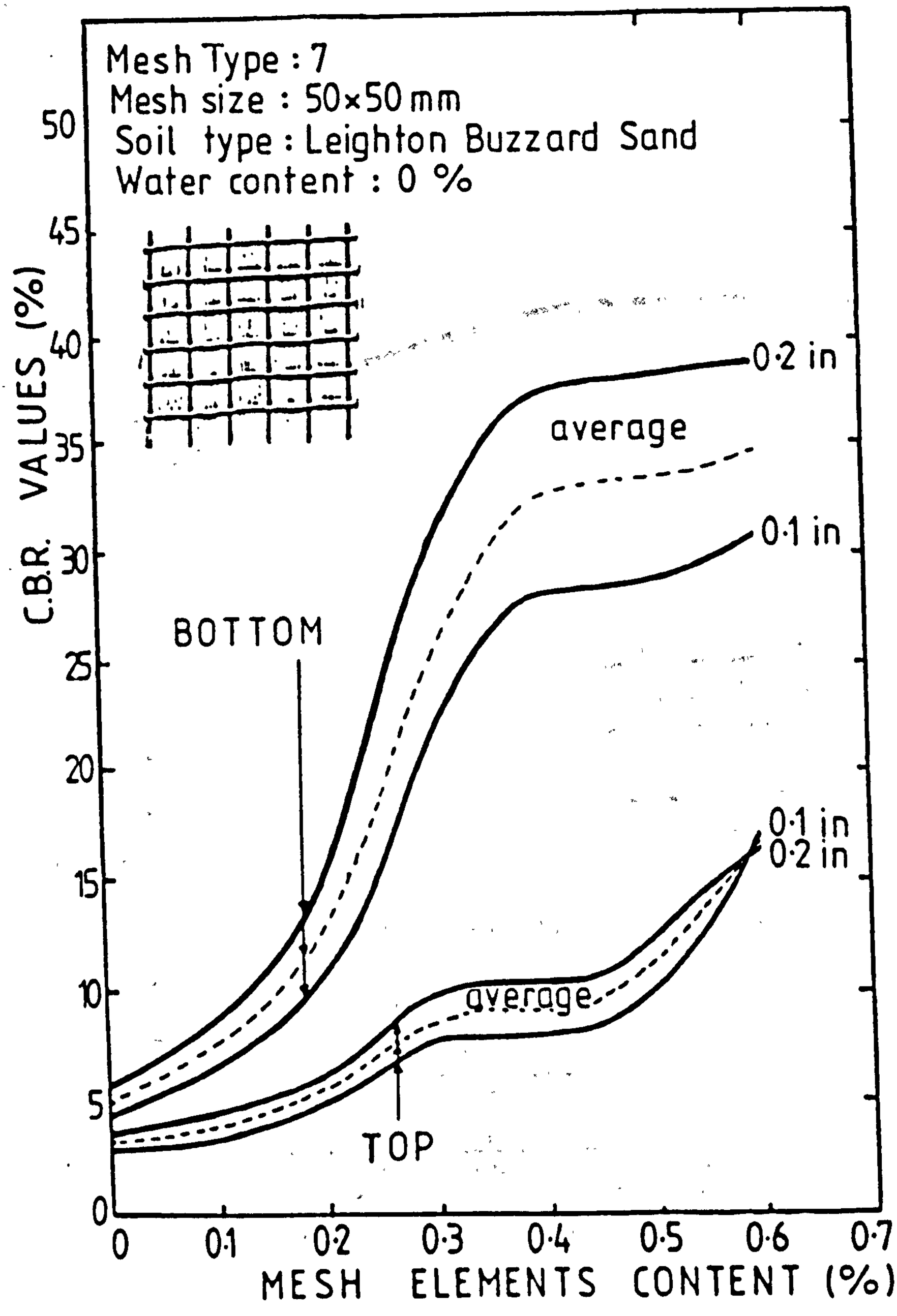

FIG. 4.23 Effect of mesh element content on C.B.R. values.

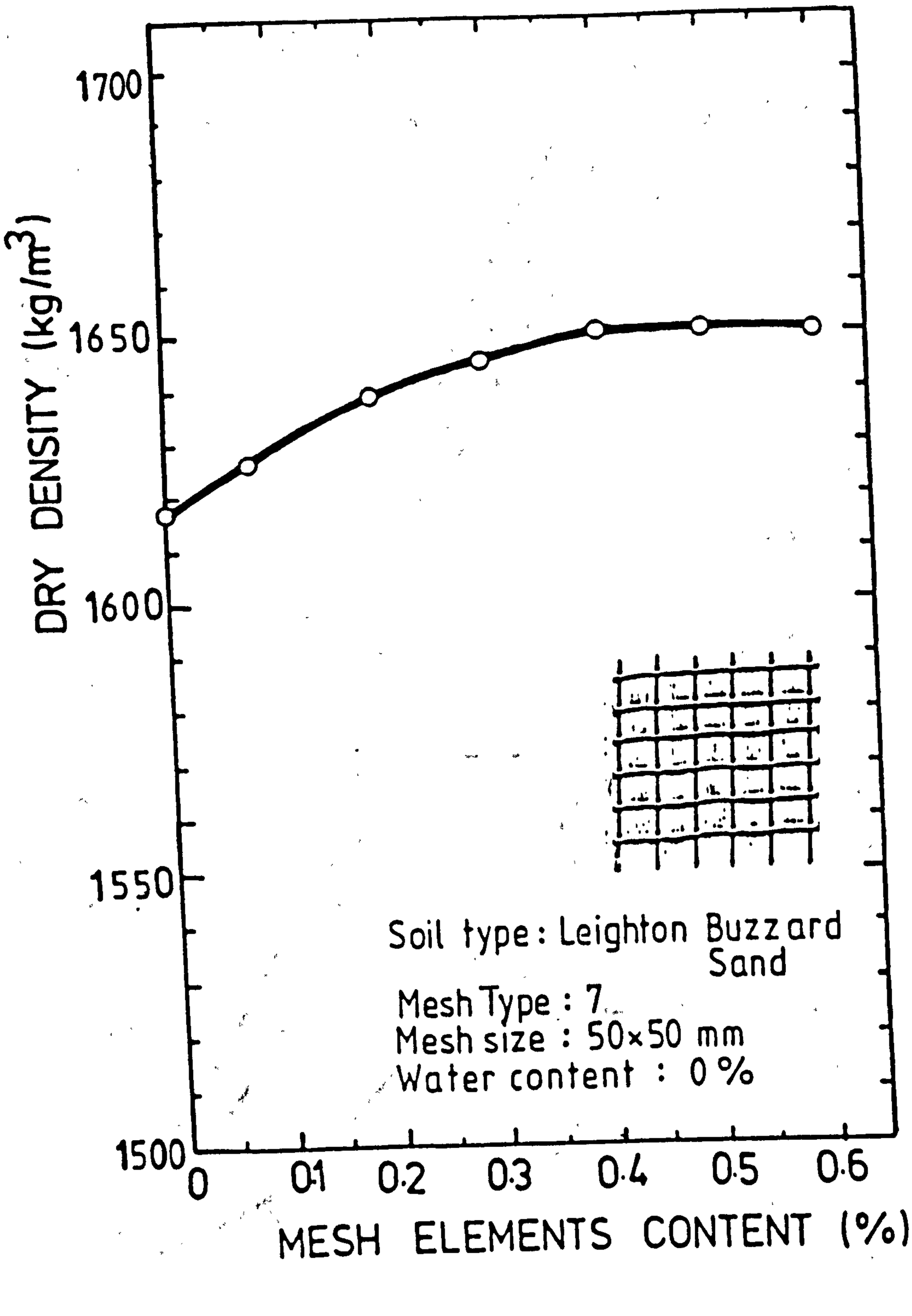

FIG. 4.24 Effect of mesh element content on the dry density of compacted samples

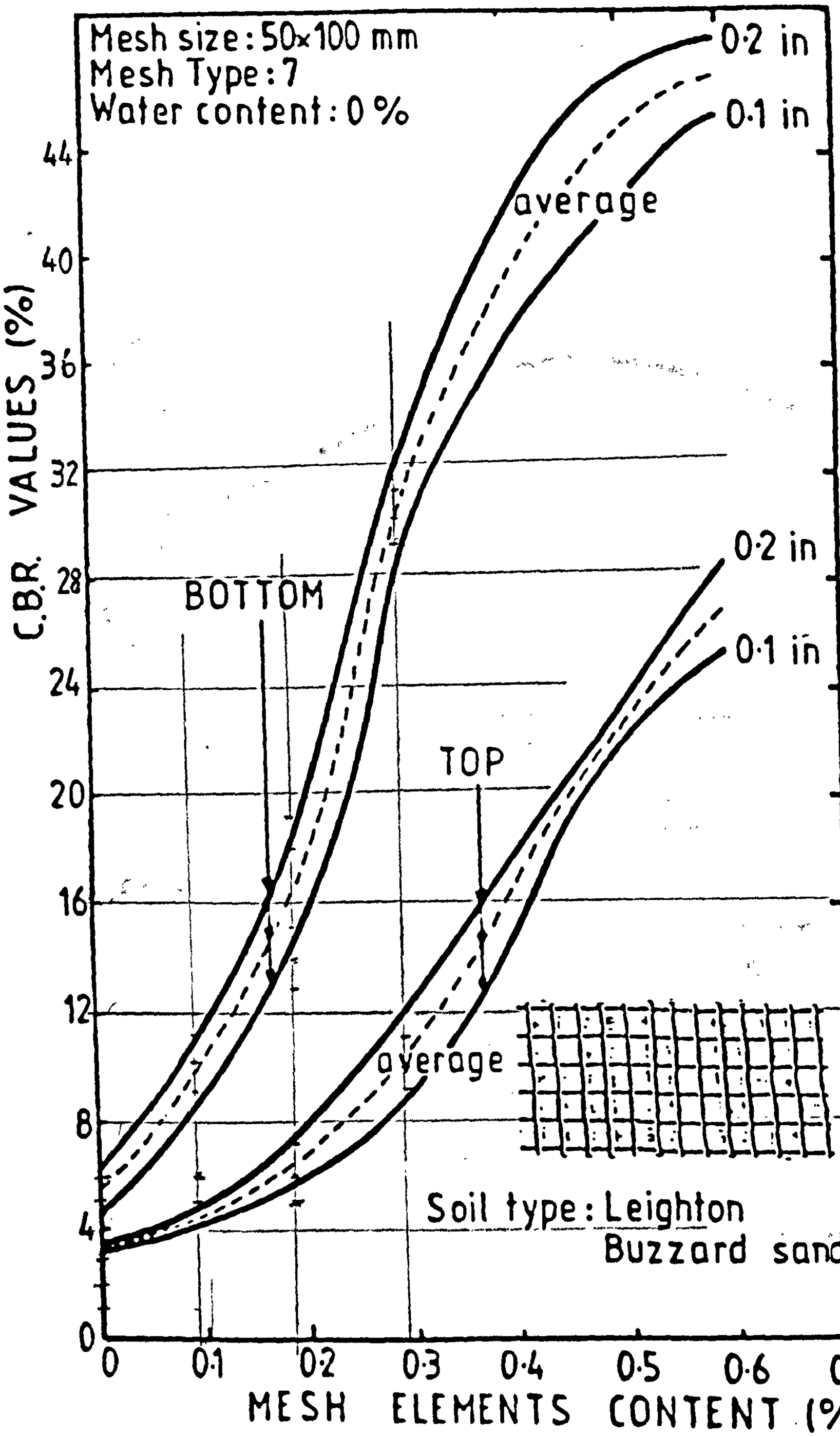

FIG. 4.25 Effect of mesh element content on C.B.R. values.

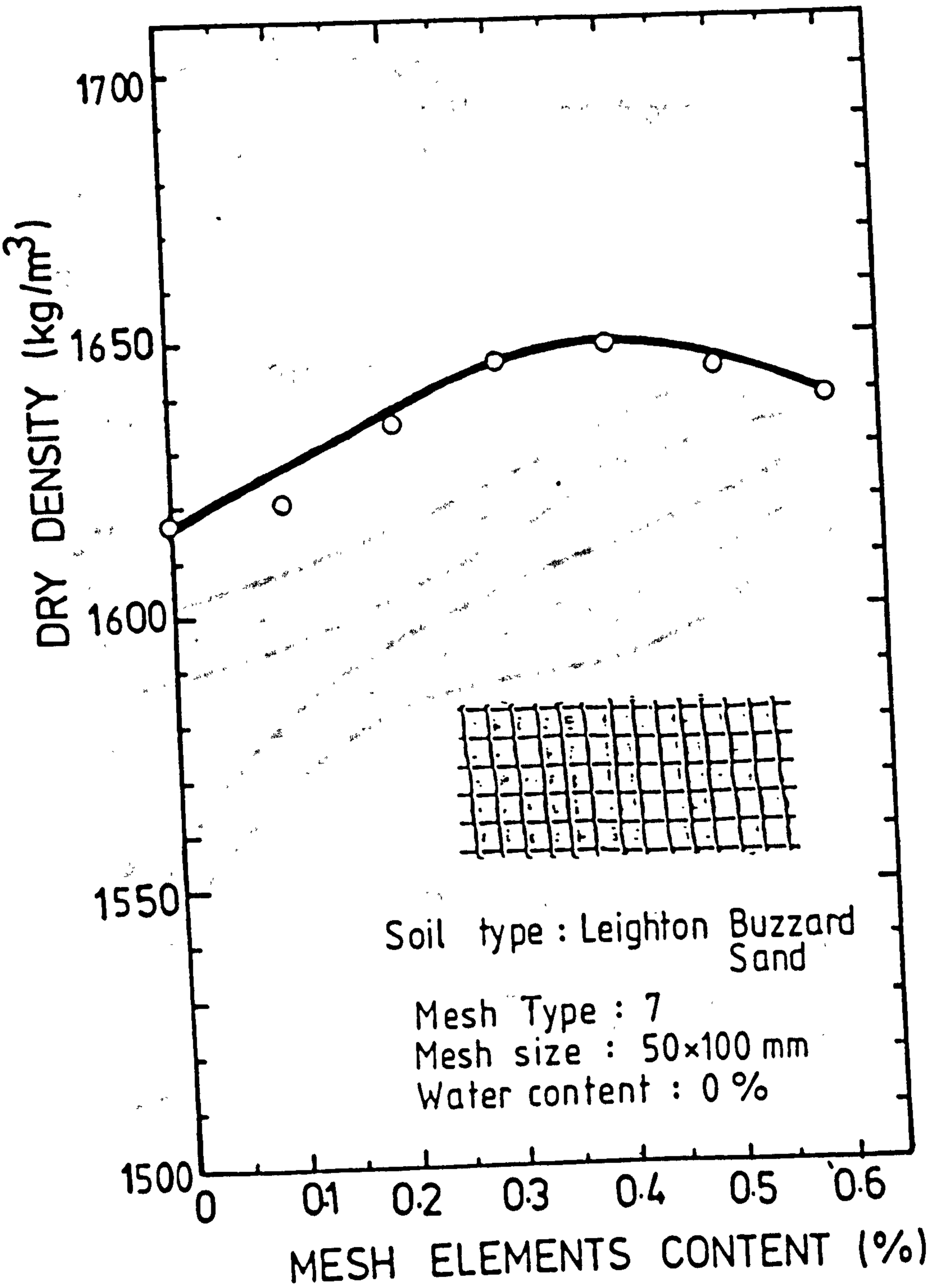

FIG. 4.26 Effect of mesh element content on the dry density of compacted samples

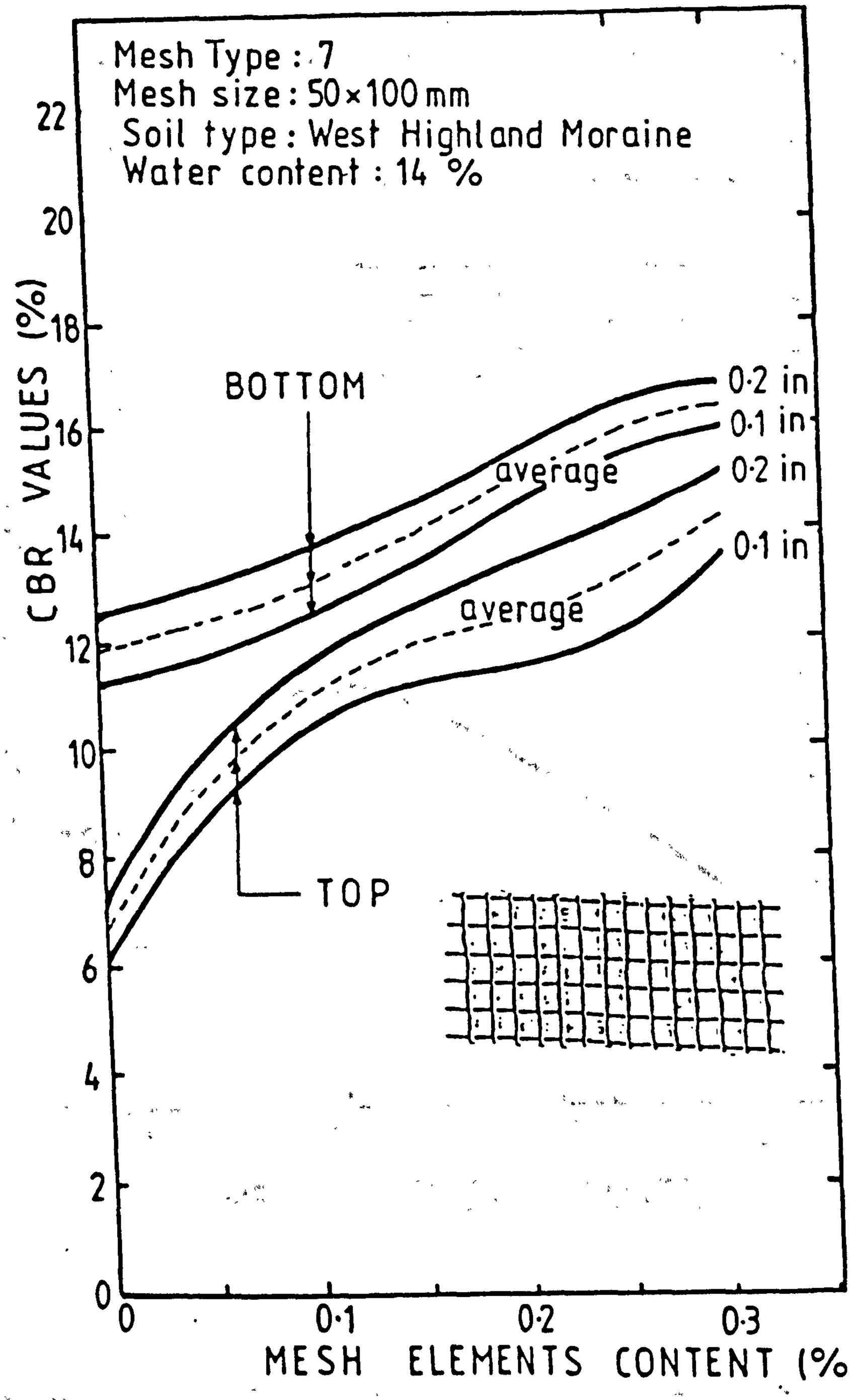

FIG. 4.27 Effect of mesh element content on C.B.R. values.

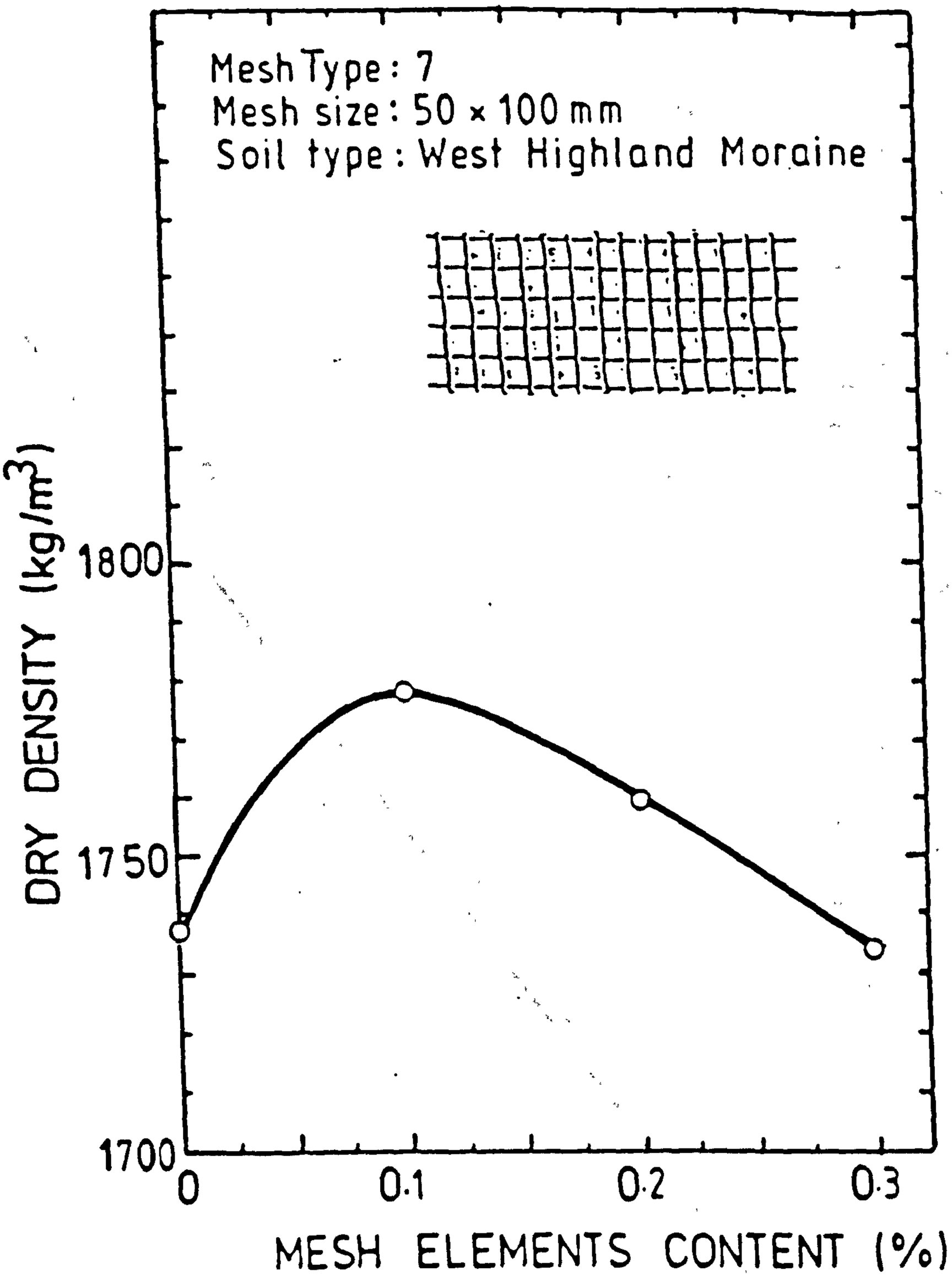

FIG. 4.28 Effect of mesh element content on the dry density of compacted samples

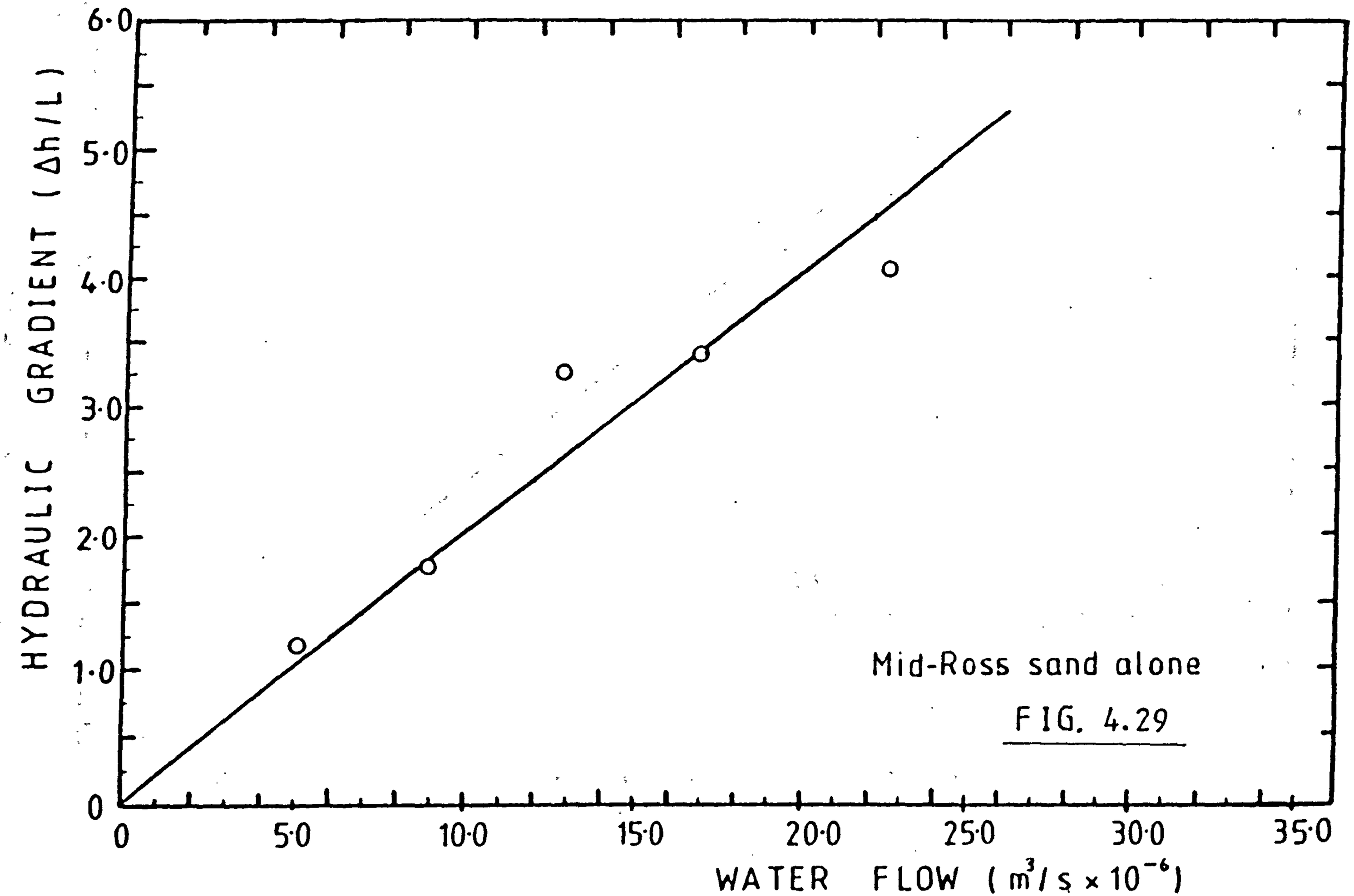
HYDRAULIC GRADIENT (Δh/L)
6·0
5·0
4·0
3·0
2·0
1·0
0
0
5·0
10·0
15·0
20·0
25·0
30·0
35·0
WATER FLOW (m³/s × 10⁻⁶)
Mid-Ross sand alone

FIG. 4.29

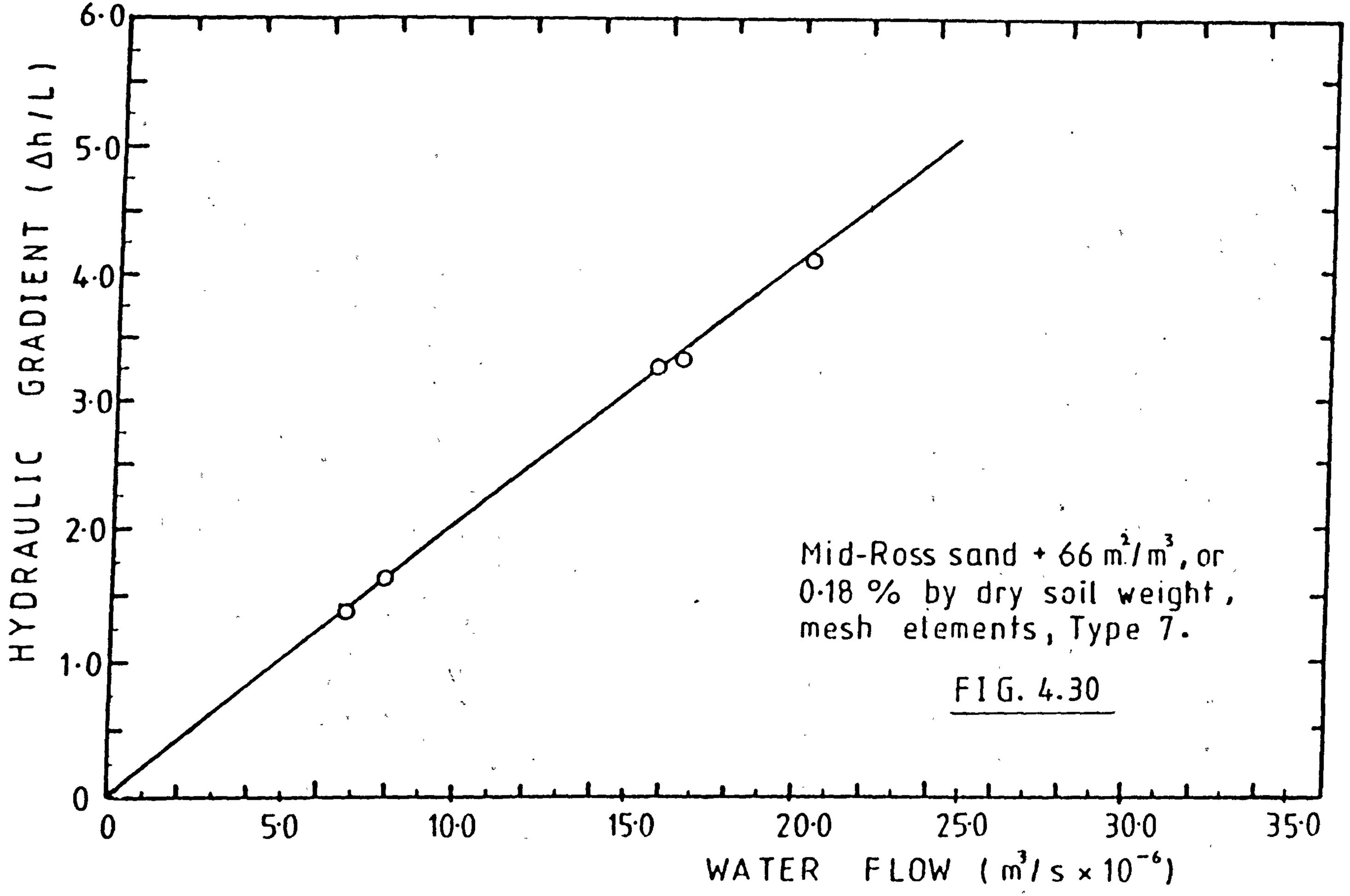
HYDRAULIC GRADIENT (Δh / L)
6·0
5·0
4·0
3·0
2·0
1·0
0
0
5·0
10·0
15·0
20·0
25·0
30·0
35·0
WATER FLOW (m³/s × 10⁻⁶)
Mid-Ross sand + 66 m²/m³, or
0·18 % by dry soil weight,
mesh elements, Type 7.

FIG. 4.30

coefficient of permeability m/s

	$k = 1$	10^{-1}	10^{-2}	10^{-3}	10^{-4}	10^{-5}	10^{-6}	10^{-7}	10^{-8}	10^{-9}	10^{-10}	10^{-11}	10^{-12}
Drainage characteristics	GOOD						POOR		PRACTICALLY IMPERVIOUS				
Permeability classification	HIGH			MEDIUM		LOW		VERY LOW		PRACTICALLY IMPERMEABLE			
General soil type	GRAVELS		CLEAN SANDS			FISSURED & WEATHERED CLAYS / VERY FINE OR SILTY SANDS			INTACT CLAYS				
Test methods: direct	large CH cell		standard CH cell			FH cell			FH in oedometer				
indirect	computation from PSD								from consolidation data				

CH = constant head
FH = falling head
PSD = particle size distribution analysis

Fig. 4.31 *Permeability and drainage characteristics of main soil types*

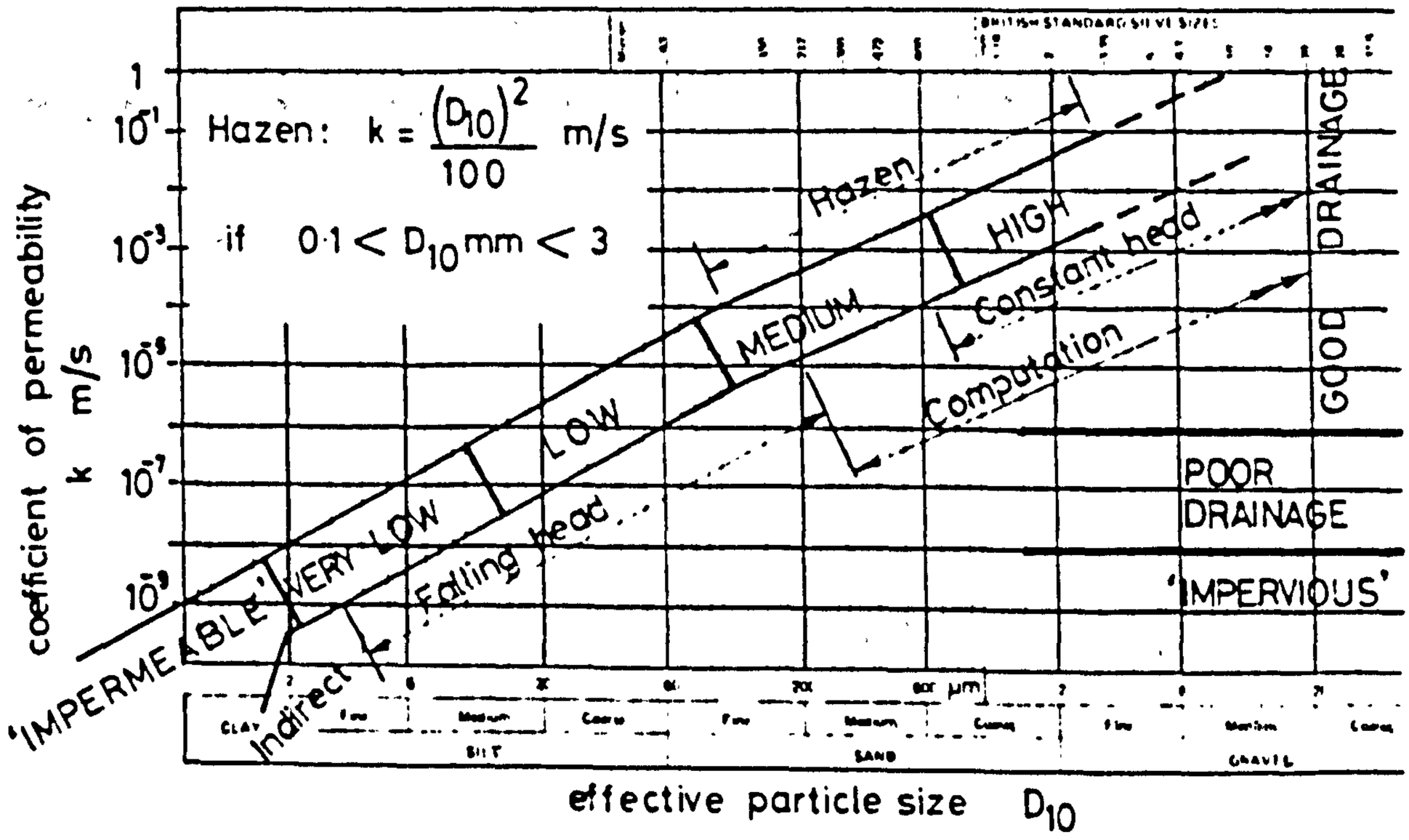

Fig. 4.32 *Permeability classification related to effective particle size*

HIGH STRESS TRIAXIAL DATA

of

MID-ROSS SAND
&
LEIGHTON BUZZARD SAND

mixed

with

TYPE 7, MESH-ELEMENTS

of

50×50 mm SIZE

at

various percentages

FIG. 5.1

SOIL TYPE	MID - ROSS SAND ALONE

200 mm × 155 mm diam. TRIAXIAL TEST DATA

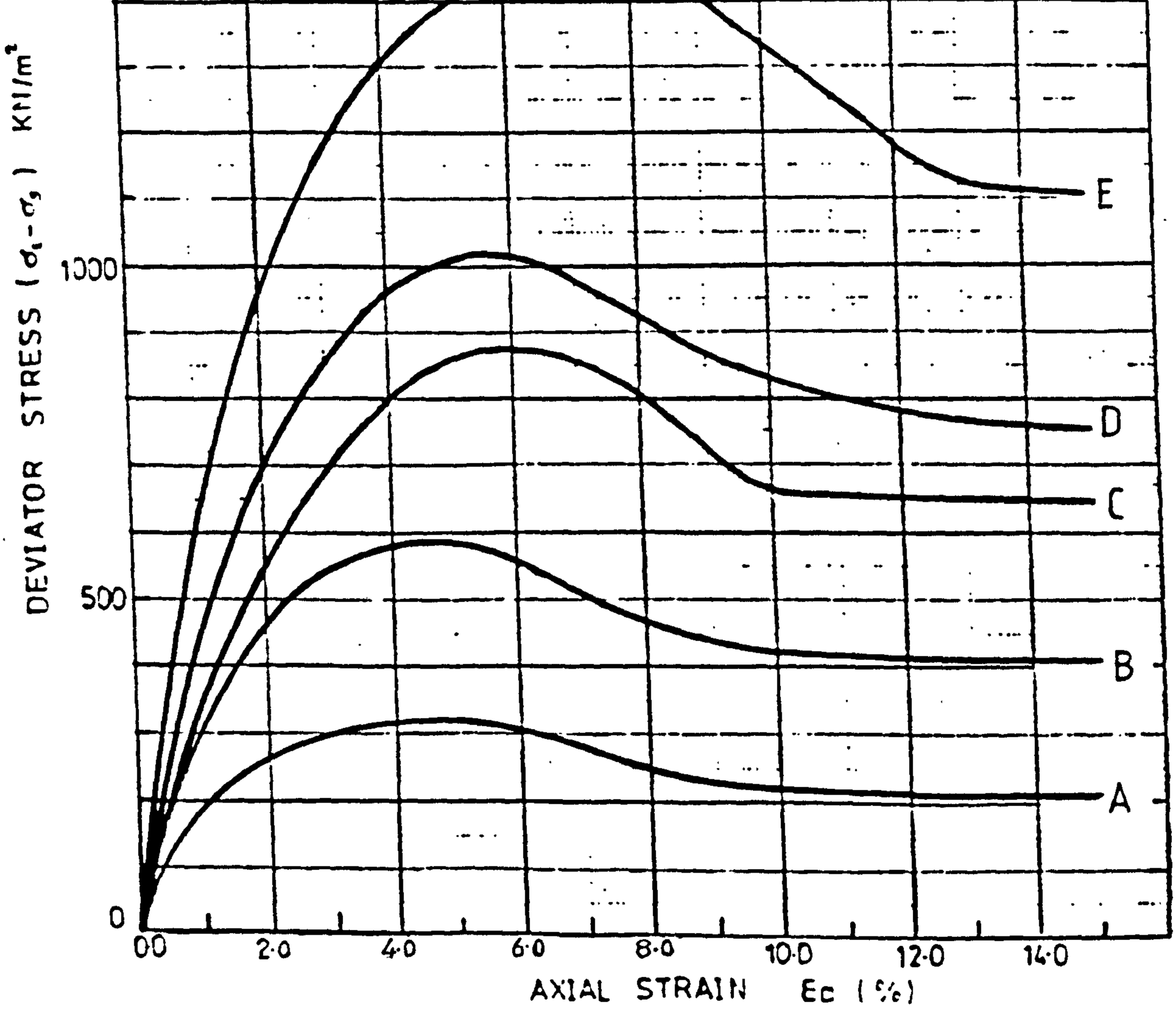

FIG. 5.2

SOIL TYPE	MID-ROSS SAND
MESH TYPE : 7	SIZE : 50×50 mm
MESH CONTENT	33 (m^2/m^3), or 0·09 (%) by dry weight

200 mm × 155 mm diam. TRIAXIAL TEST DATA

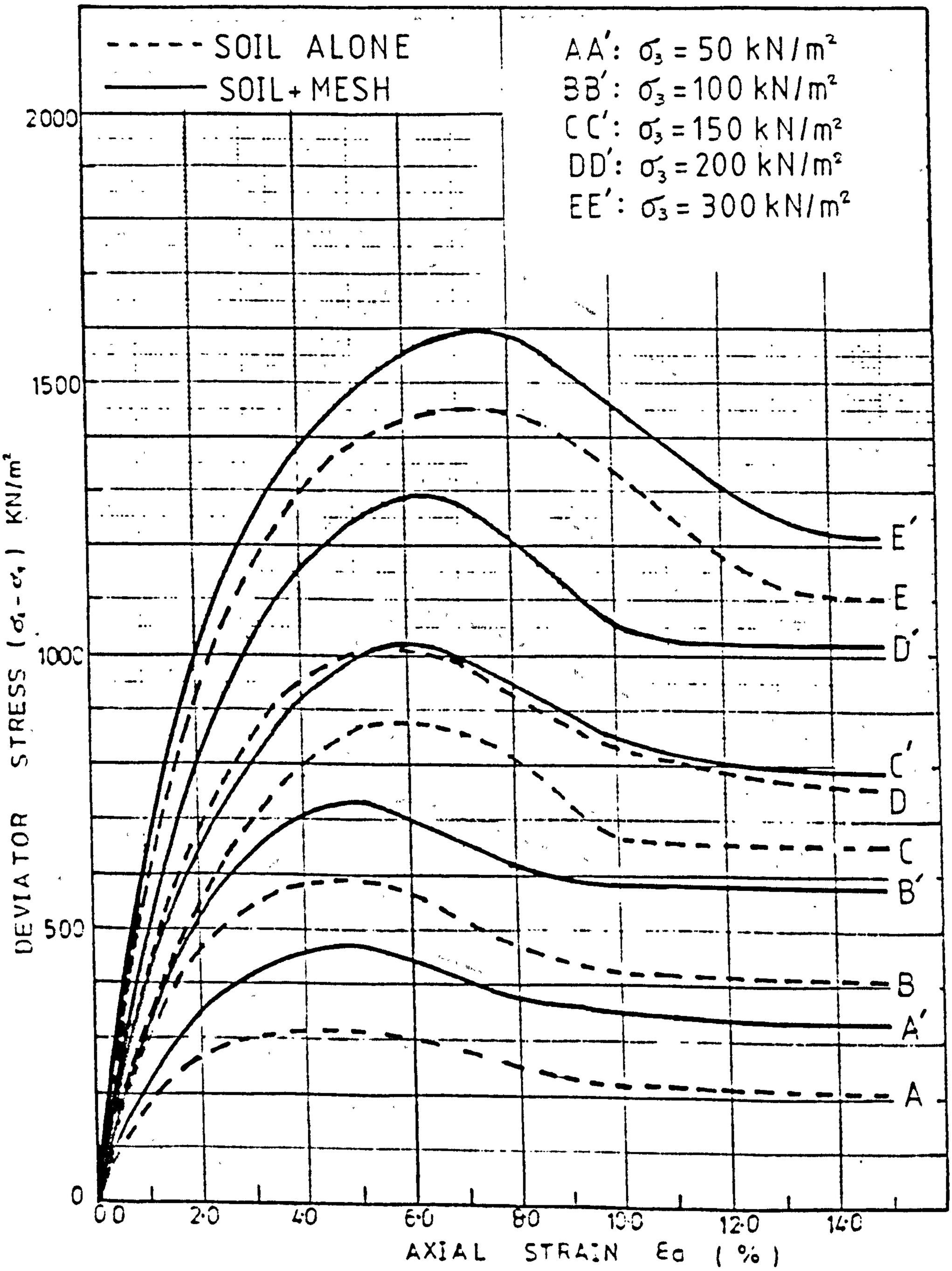

FIG. 5.3

SOIL TYPE	MID-ROSS SAND
MESH TYPE 7	MESH SIZE: 50×50 mm
MESH CONTENT	66 (m^2/m^3), or 0·18 (%) by dry weight

200 mm × 155 mm diam. TRIAXIAL TEST DATA

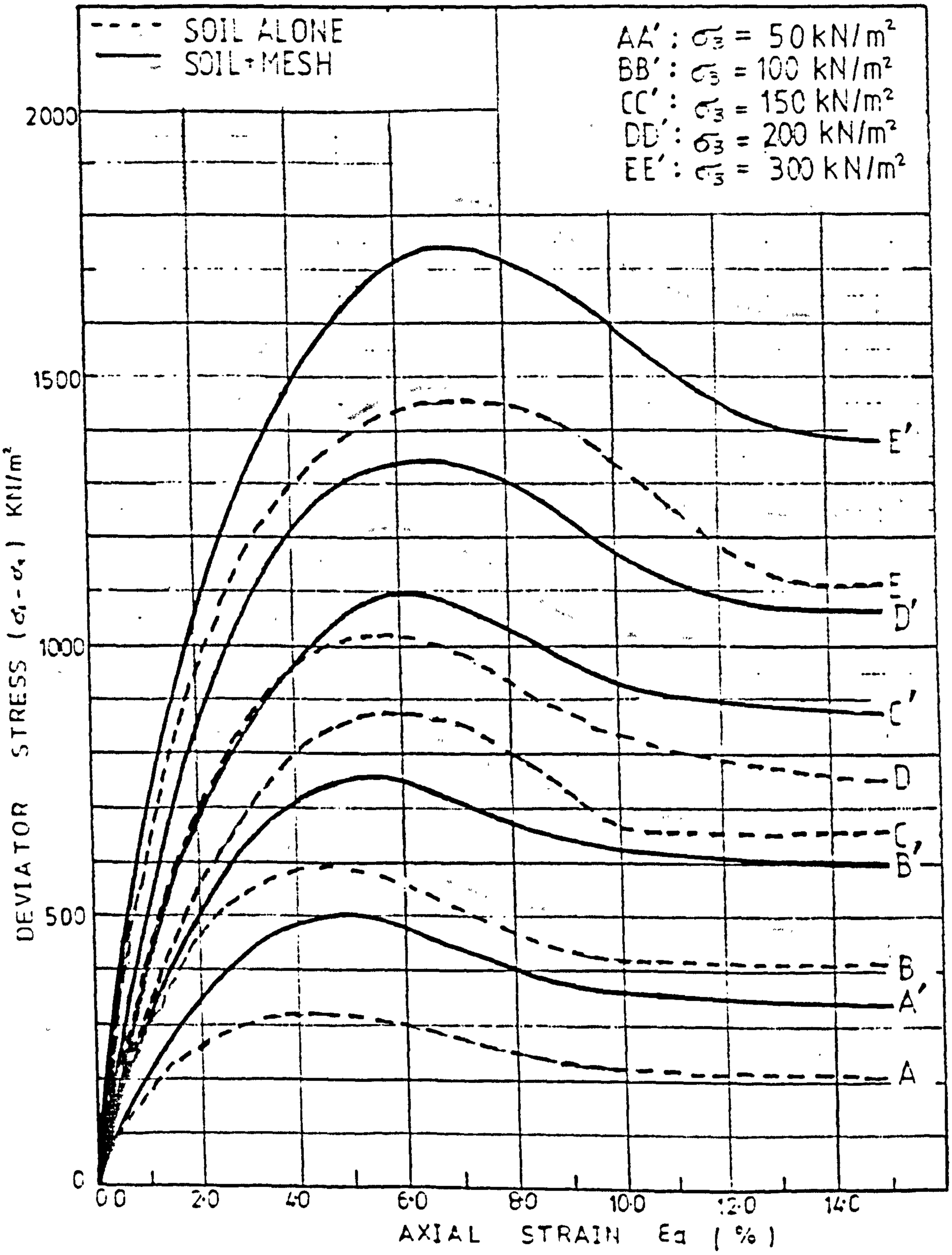

FIG. 5.4

SOIL TYPE	MID-ROSS SAND
MESH TYPE : 7	MESH SIZE : 50×50 mm
MESH CONTENT	90 (m^2/m^3), or 0·24 (%) by dry weight

200 mm × 155 mm diam. TRIAXIAL TEST DATA

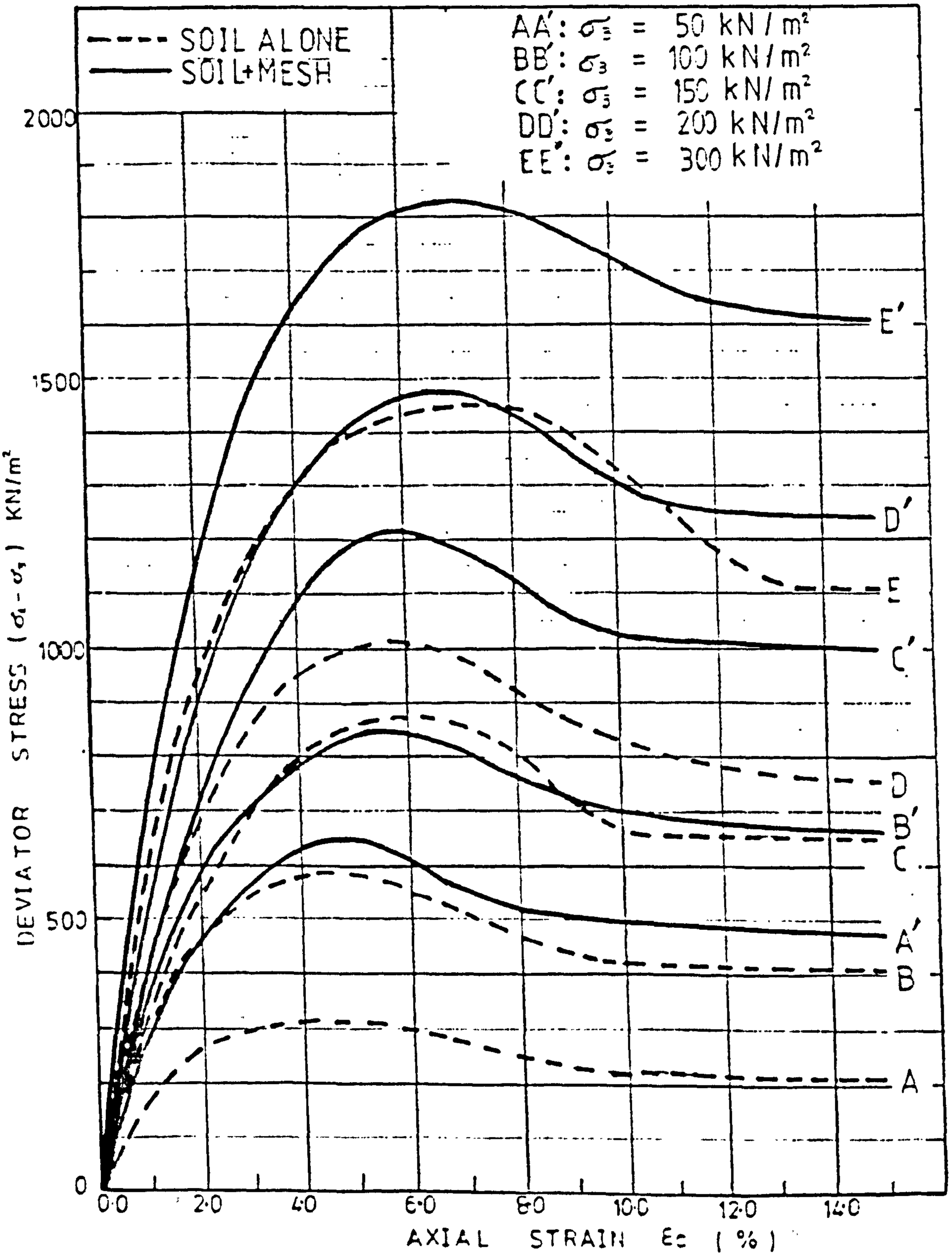

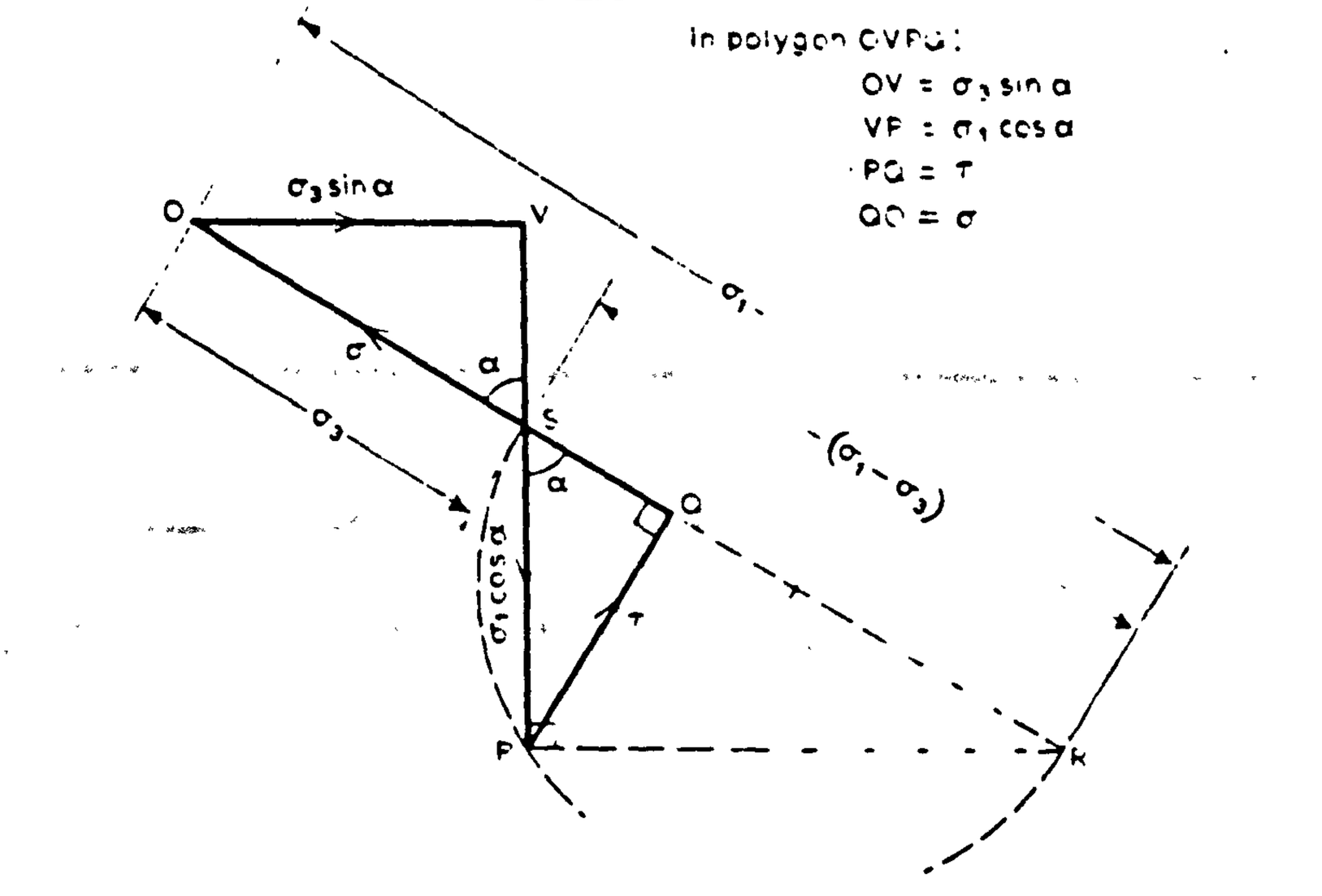

Polygon of forces for triaxial compression

FIG. 5.5

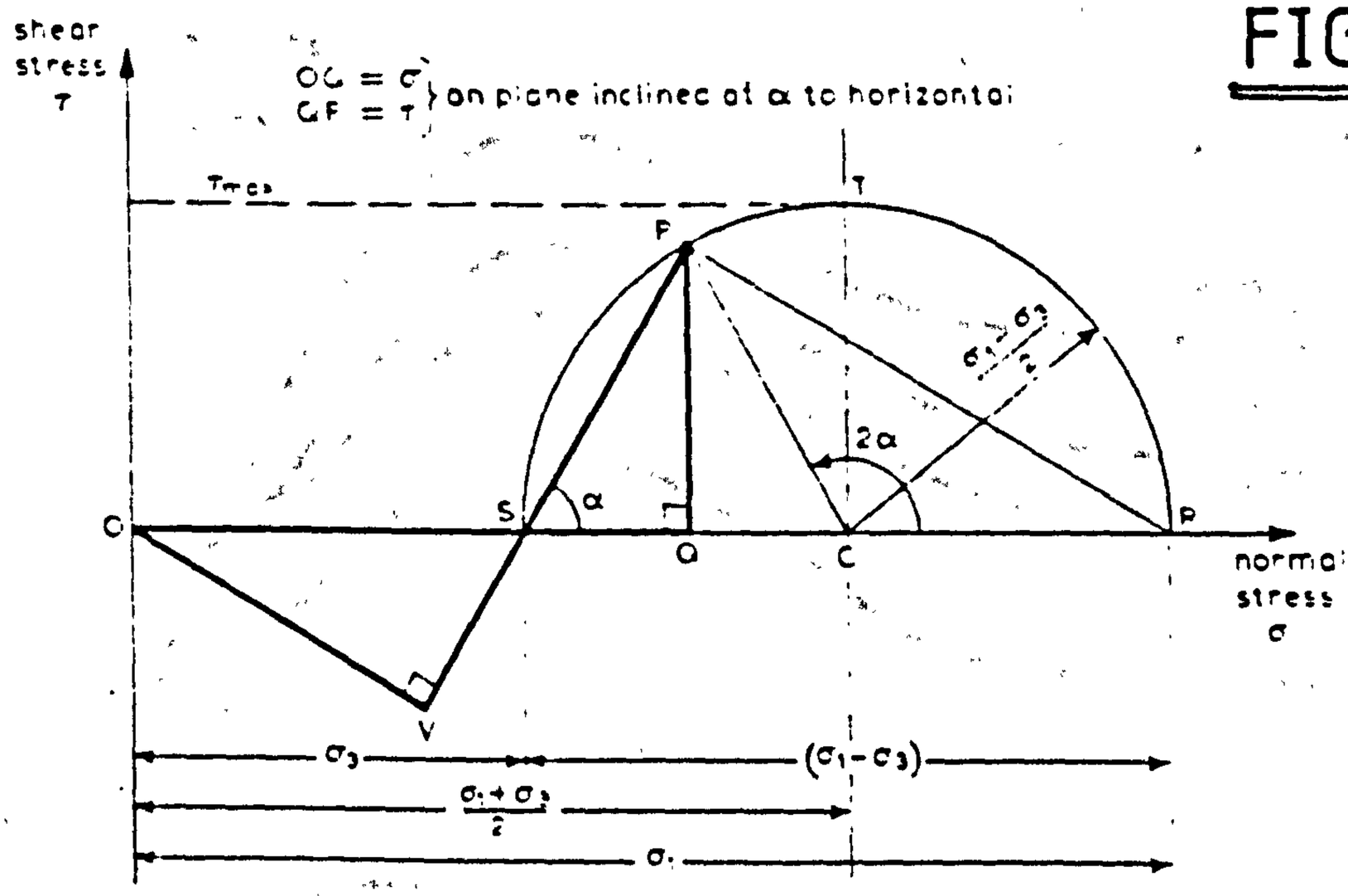

Mohr diagram for triaxial compression

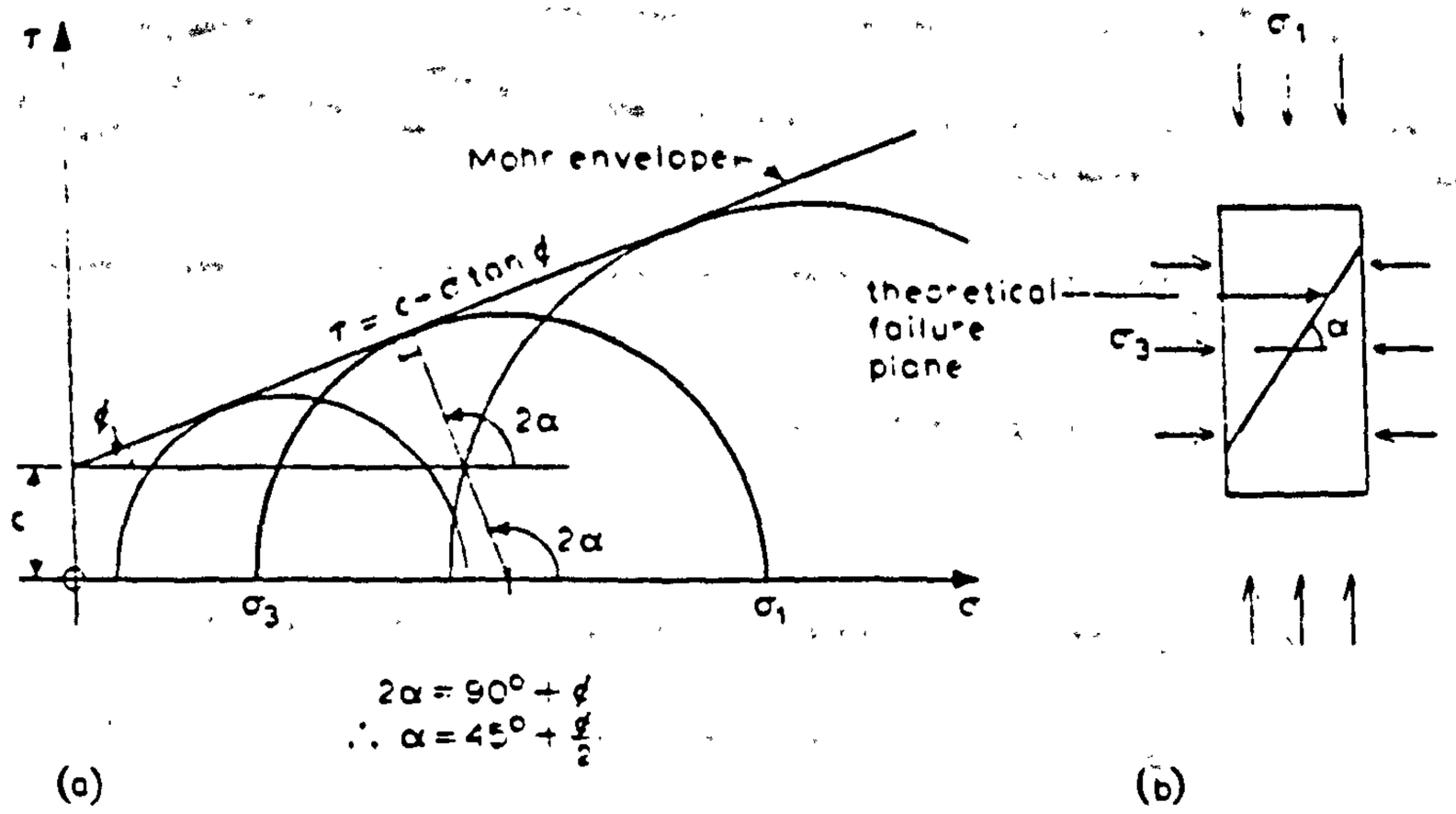

Mohr-Coulomb failure criterion: (a) Mohr envelope, (b) theoretical failure plane

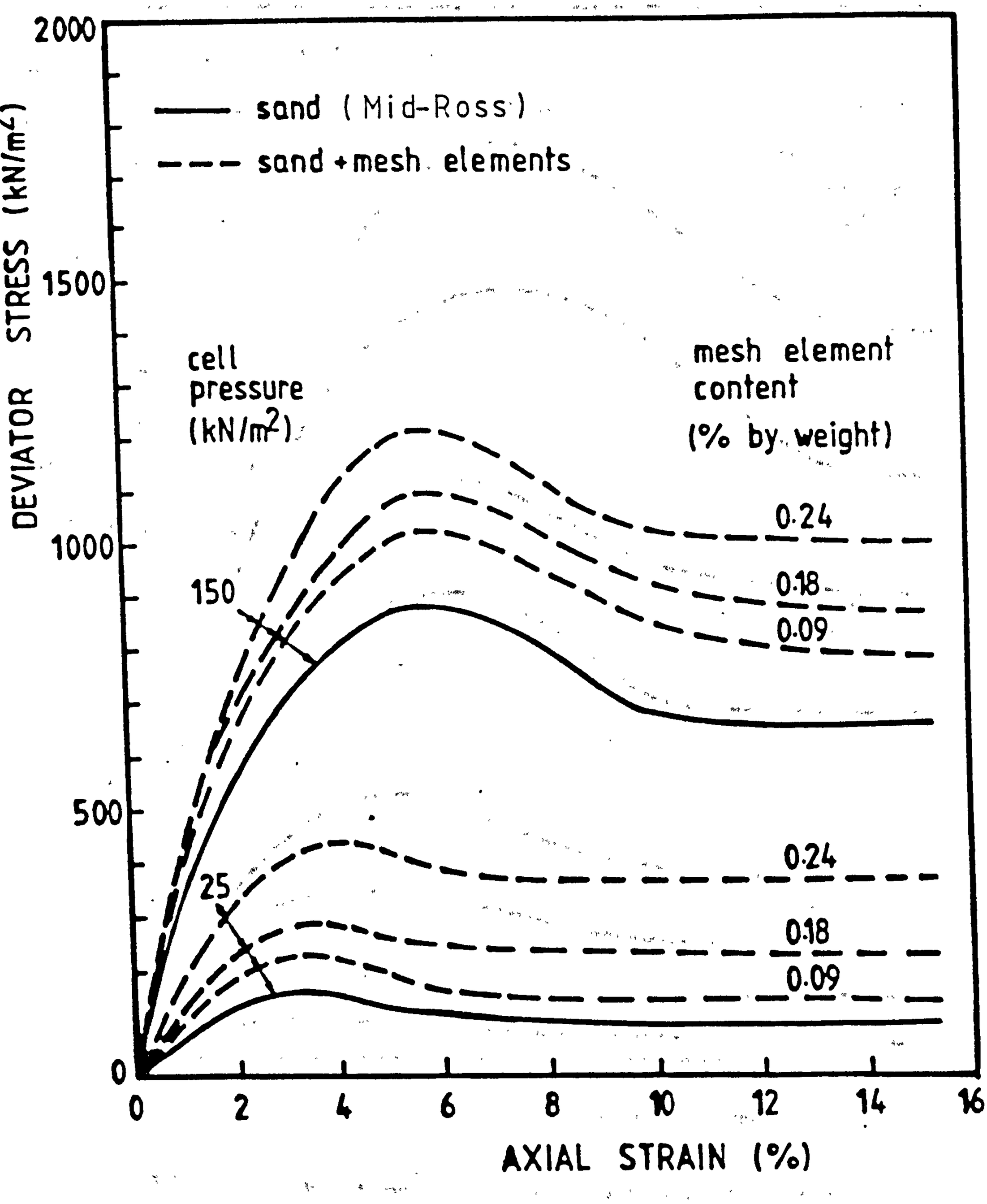

FIG. 5.6 Relationships between deviator stress and axial strain for different proportions of mesh elements. Mesh size 50 x 50 mm.

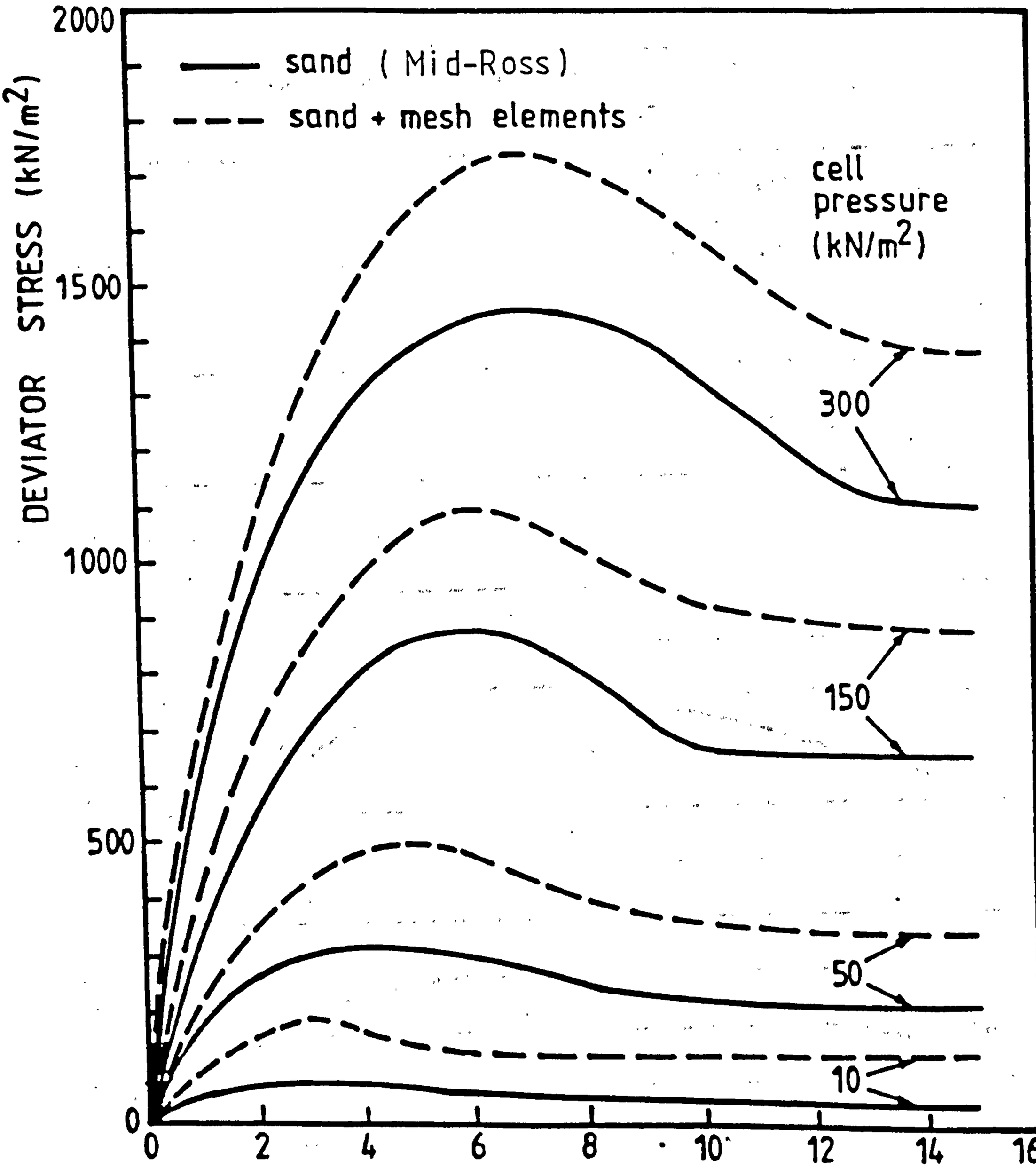

FIG. 5.7 Relationships between deviator stress and axial strain from drained triaxial tests.

Mesh size 50 x 50 mm. Mesh element content 0.18% by weight.

FIG. 5.8

SOIL TYPE	LEIGHTON BUZZARD SAND

200 mm × 155 mm diam. TRIAXIAL TEST DATA

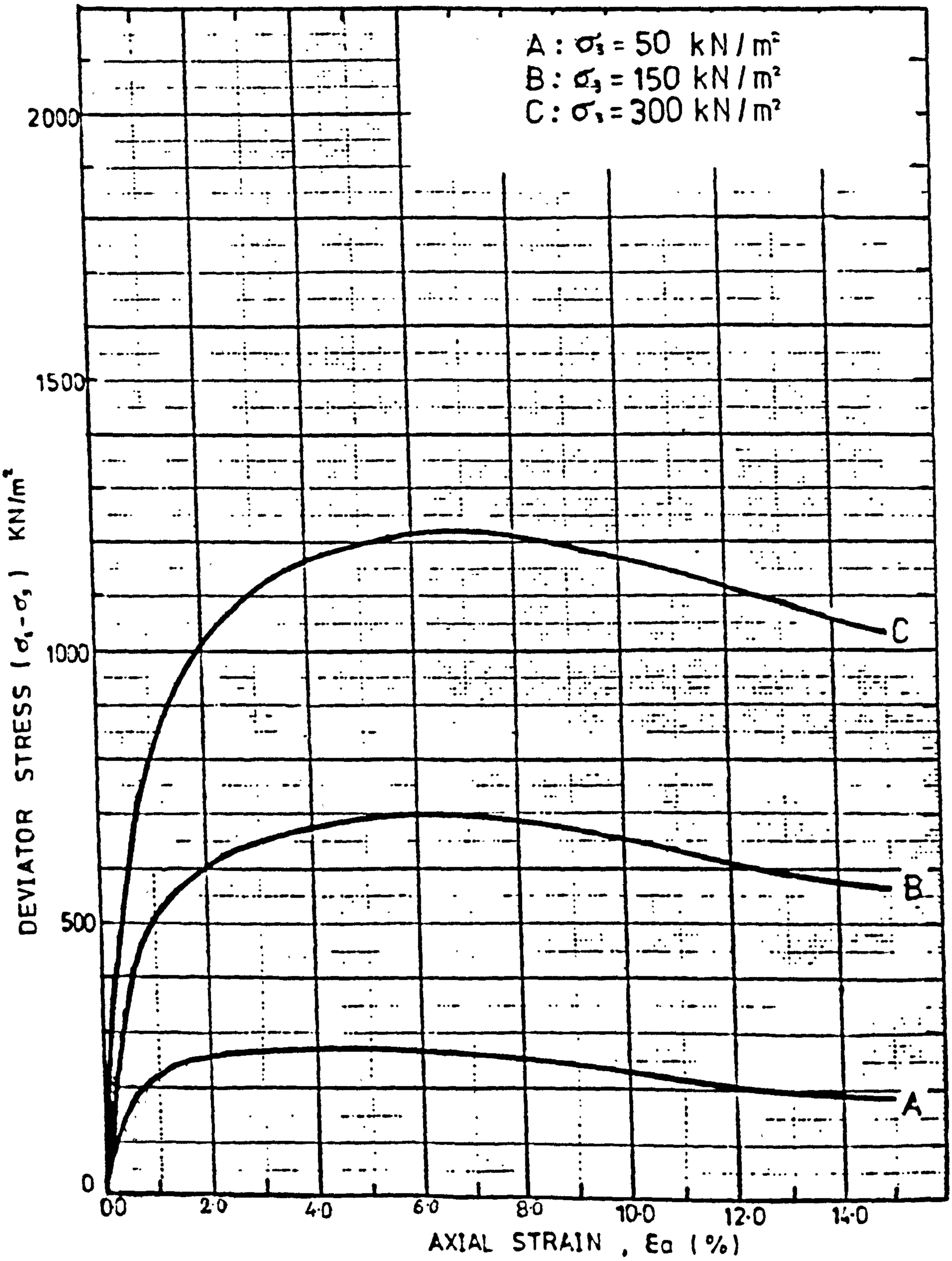

FIG. 5.9

SOIL TYPE	LEIGHTON BUZZARD SAND
MESH TYPE : 7	SIZE : 50 × 50 mm
MESH CONTENT	33 (m^2/m^3), or 0·10 (%) by dry weight

200 mm × 155 mm diam. TRIAXIAL TEST DATA

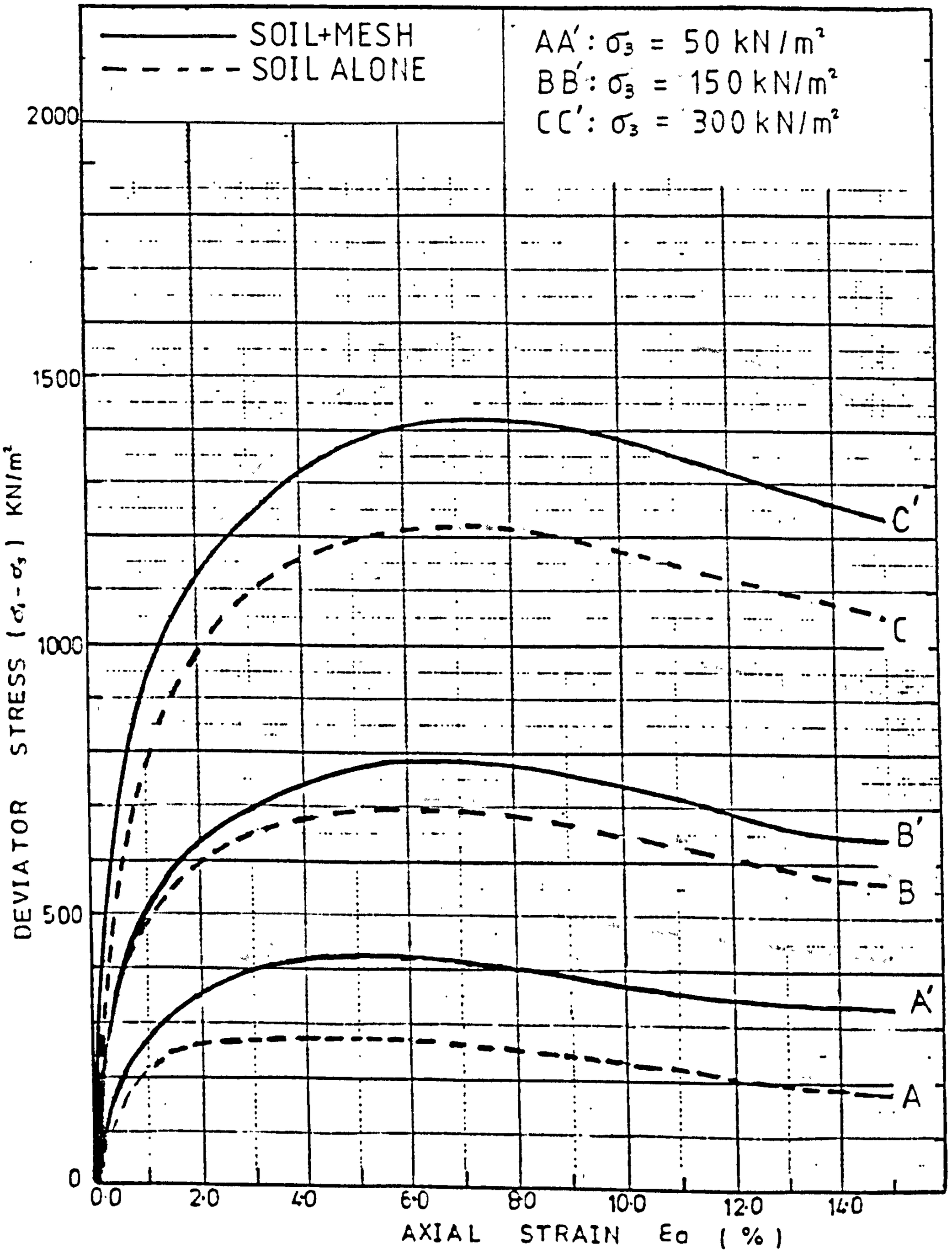

FIG. 5.10

SOIL TYPE	LEIGHTON BUZZARD SAND
MESH TYPE : 7	SIZE : 50×50 mm
MESH CONTENT	66 (m^2/m^3), or 0·20 (%) by dry weight

200 mm × 155 mm diam. TRIAXIAL TEST DATA

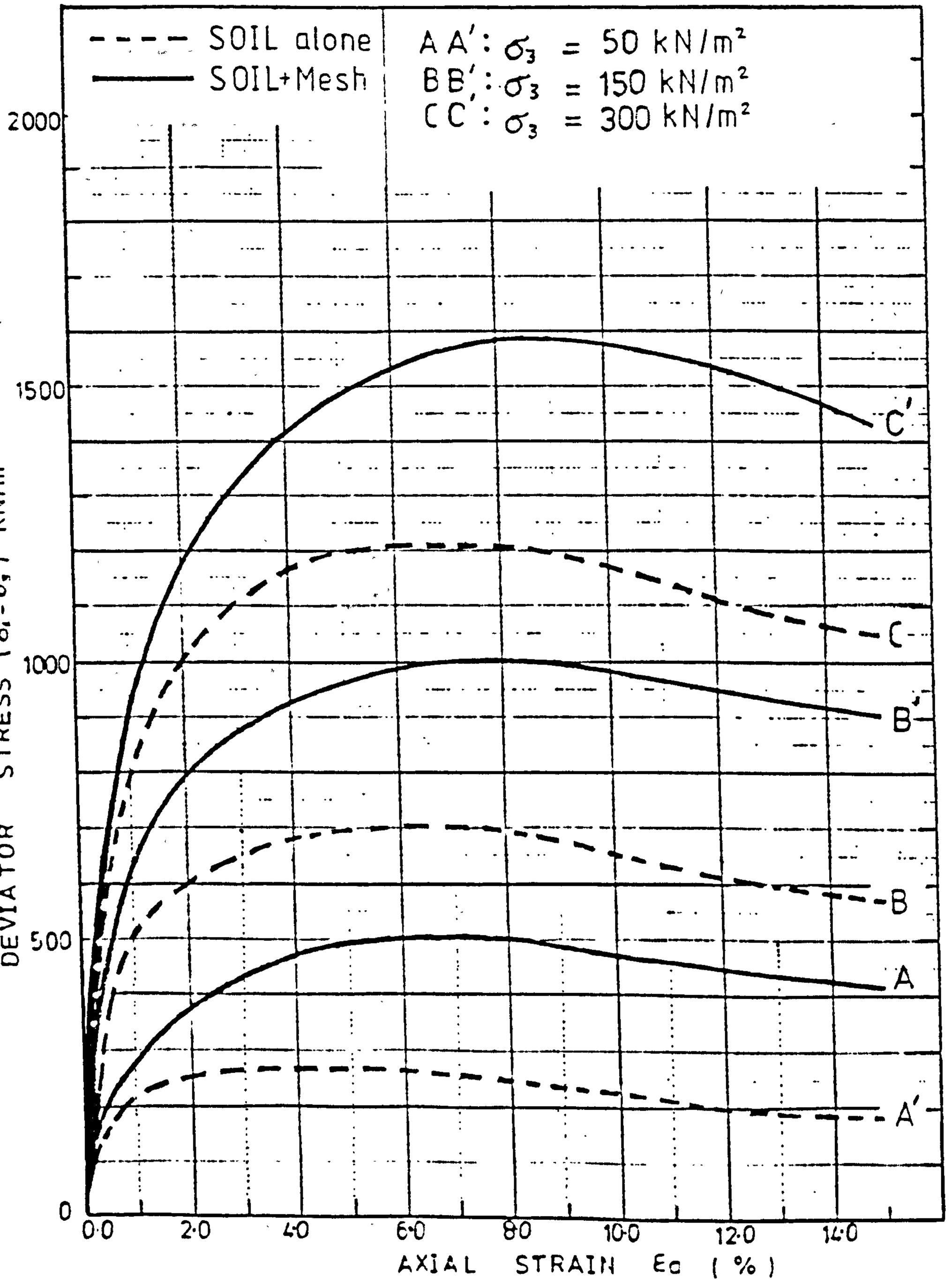

FIG. 5.11

SOIL TYPE	LEIGHTON BUZZARD SAND
MESH TYPE : 7	SIZE : 50 × 50 mm
MESH CONTENT	90 (m^2/m^3), or 0·27 (%) by dry weight

200 mm × 155 mm diam. TRIAXIAL TEST DATA

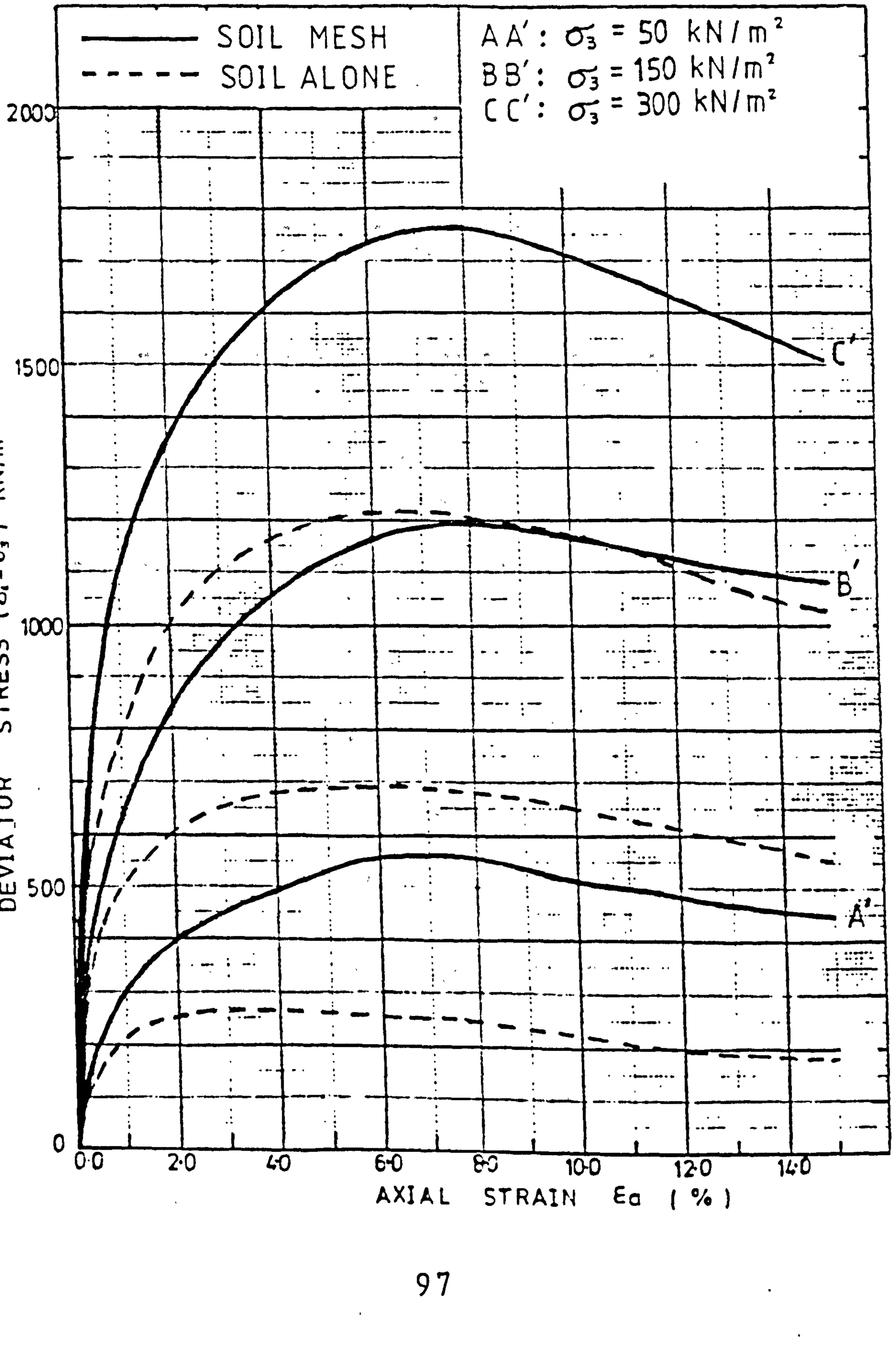

LOW STRESS TRIAXIAL DATA

of

MID-ROSS SAND
&
LEIGHTON BUZZARD SAND
mixed

with

TYPE 7, MESH-ELEMENTS

of

50×50 mm and 50×100 mm
SIZES

at

various percentages

FIG. 5.12

SOIL TYPE	MID-ROSS SAND
MESH TYPE	7
MESH CONTENT	33 (m^2/m^3), or 0·09 (%) by dry weight

$\sigma_3 = 0\ KN/m^2$

200mm × 155mm diam. TRIAXIAL TEST DATA

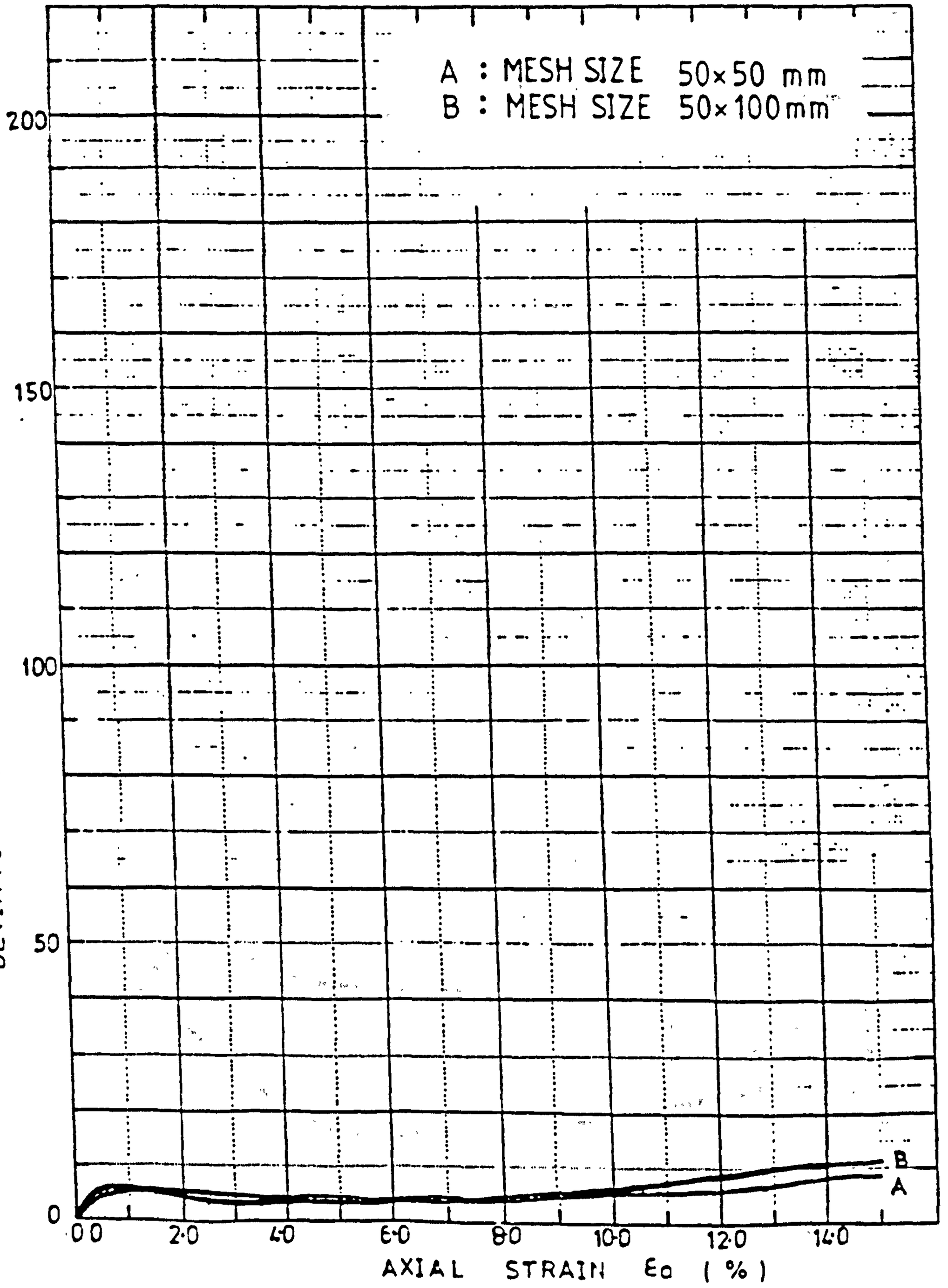

FIG. 5.13

SOIL TYPE	MID - ROSS SAND
MESH TYPE	7
MESH CONTENT	66 (m^2/m^3), or 0·18 (%) by dry weight

$\sigma_3 = 0\ KN/m^2$

200 mm × 155 mm diam. TRIAXIAL TEST DATA

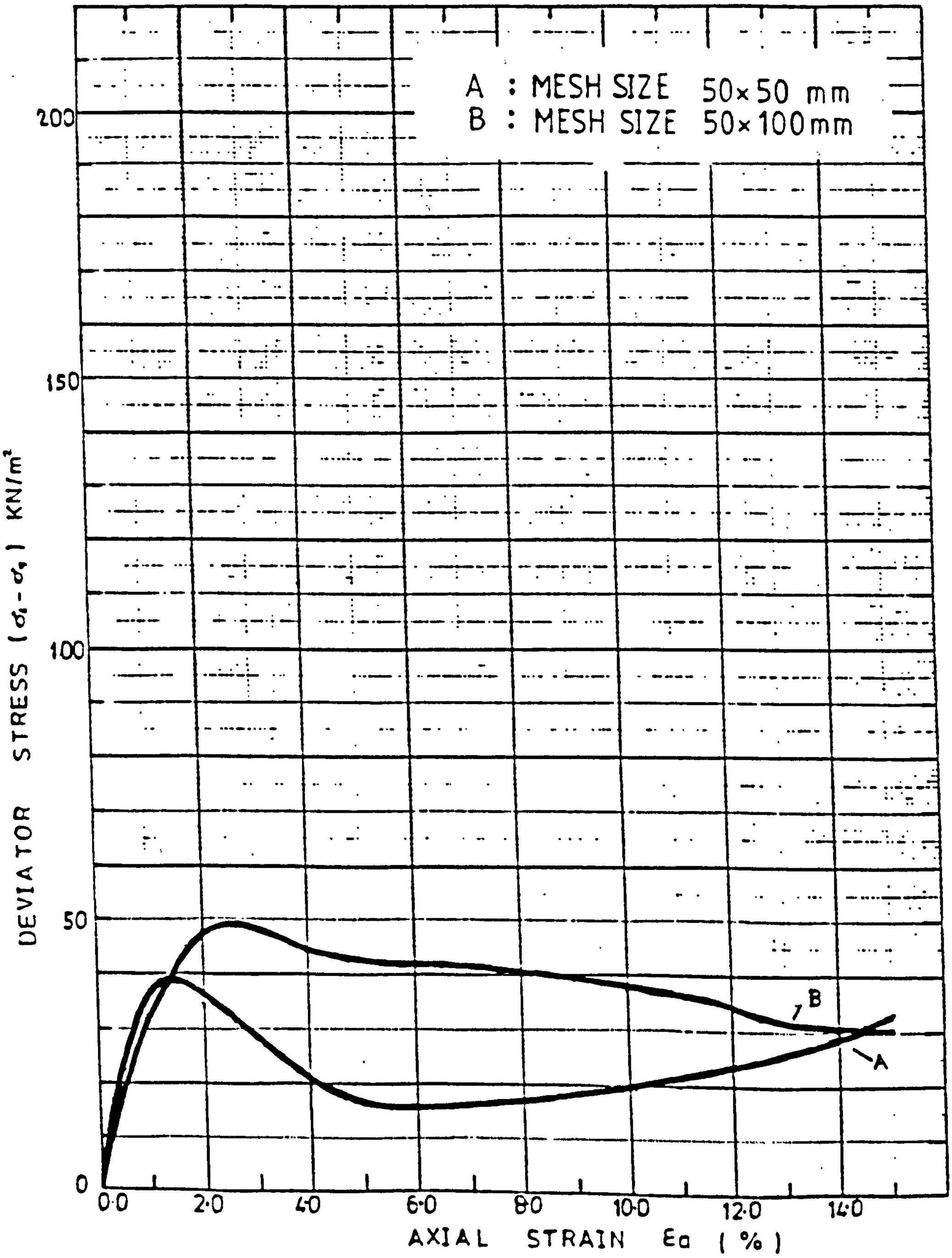

FIG. 5.14

SOIL TYPE	MID-ROSS SAND
MESH TYPE	7
MESH CONTENT	90 (m^2/m^3), or 0·24 (%) by dry weight

$\sigma_3 = 0\ KN/m^2$

200mm × 155mm diam. TRIAXIAL TEST DATA

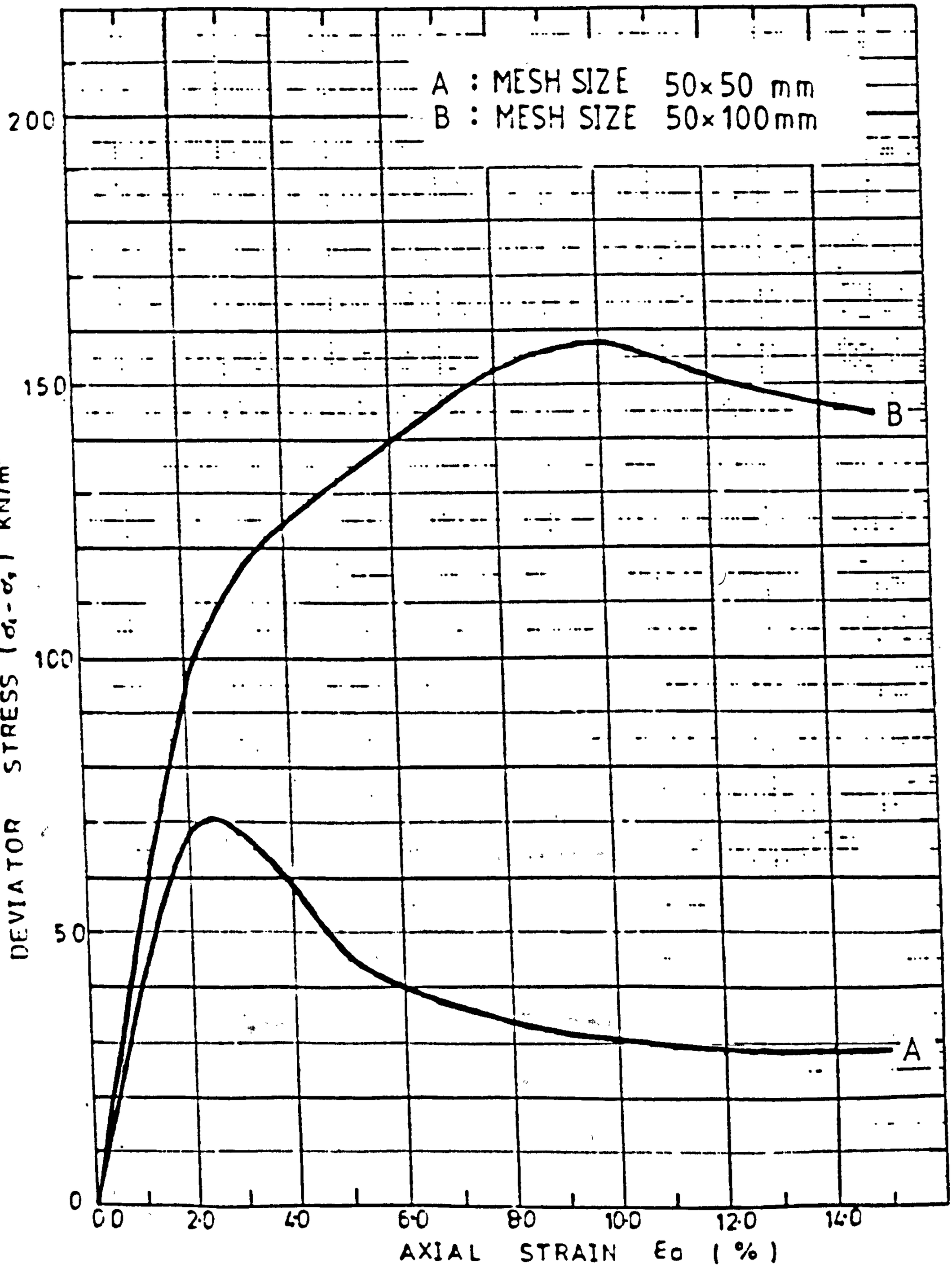

FIG. 5.15

SOIL TYPE	MID-ROSS SAND
MESH TYPE	7
MESH CONTENT	33 (m^2/m^2), or 0·09 (%) by dry weight

$\sigma_3 = 10\ kN/m^2$

200mm × 155mm diam. TRIAXIAL TEST DATA

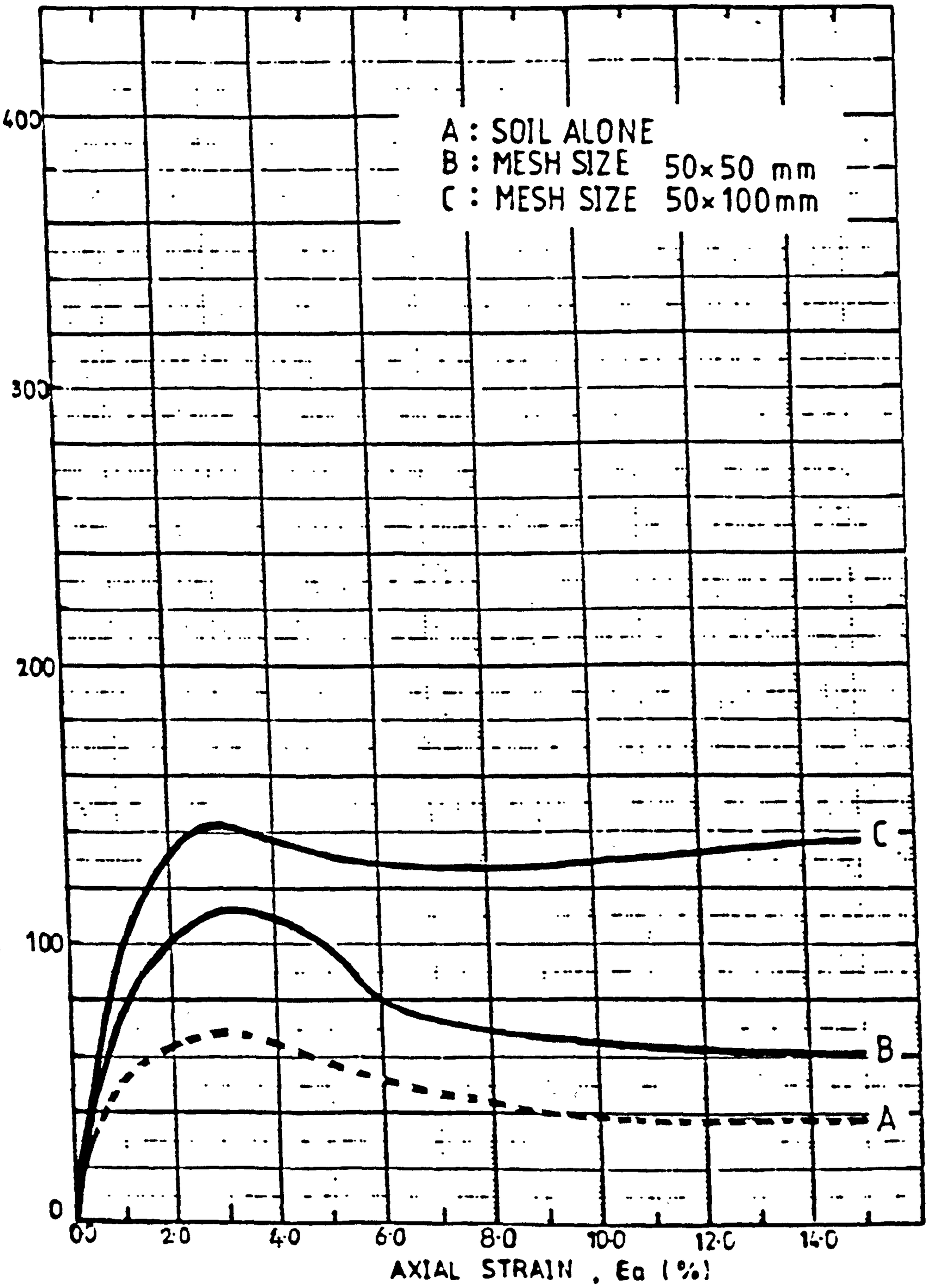

FIG. 5.16

SOIL TYPE	MID-ROSS SAND
MESH TYPE	7
MESH CONTENT	66 (m^2/m^3), or 0.18 (%) by dry weight

$\sigma_3 = 10\ kN/m^2$

200mm × 155mm diam. TRIAXIAL TEST DATA

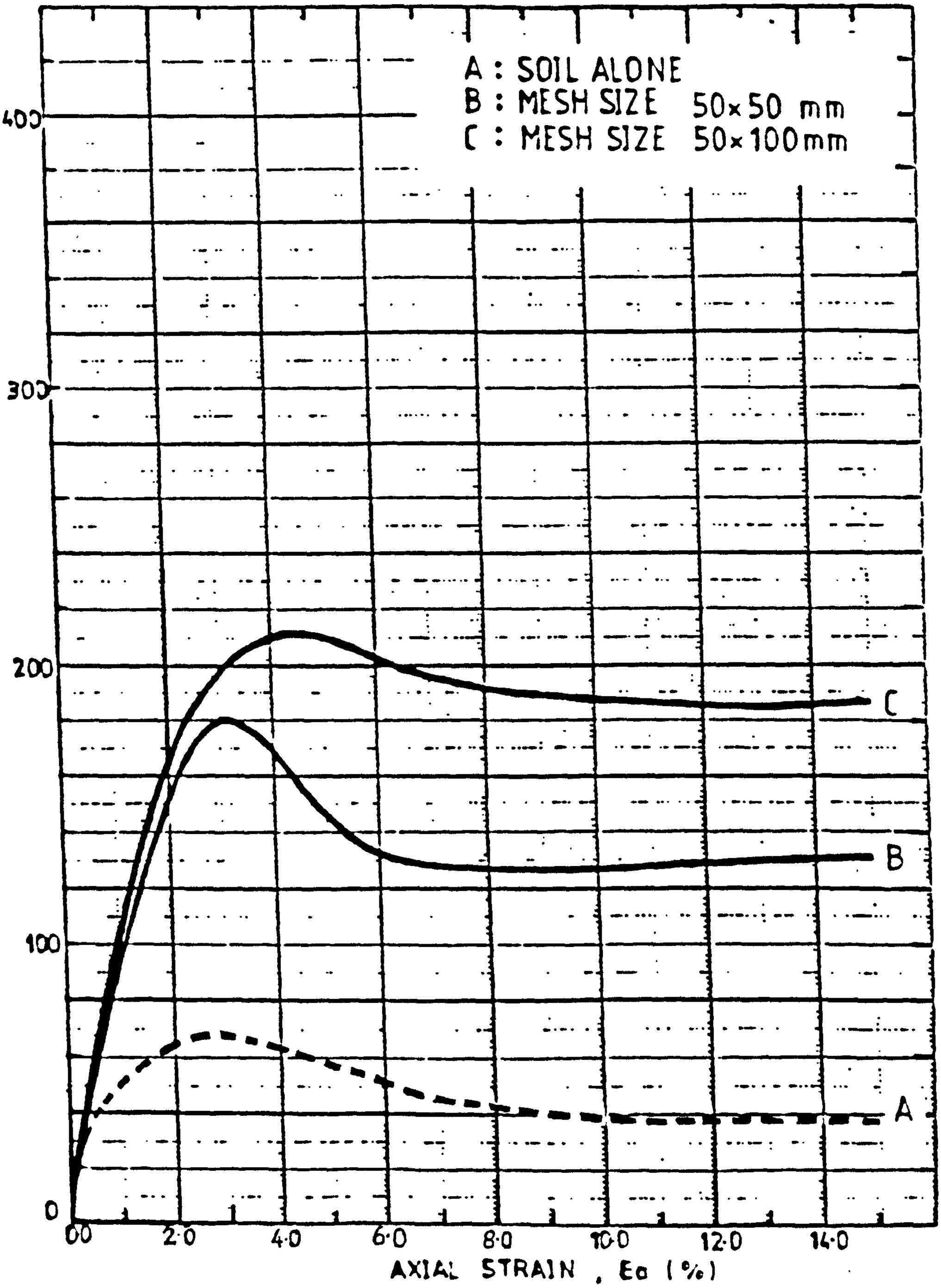

FIG. 5.17

SOIL TYPE	MID-ROSS SAND
MESH TYPE	7
MESH CONTENT	90 (m^2/m^3), or 0·24 (%) by dry weight

$\sigma_3 = 10\ kN/m^2$

200 mm × 155 mm diam. TRIAXIAL TEST DATA

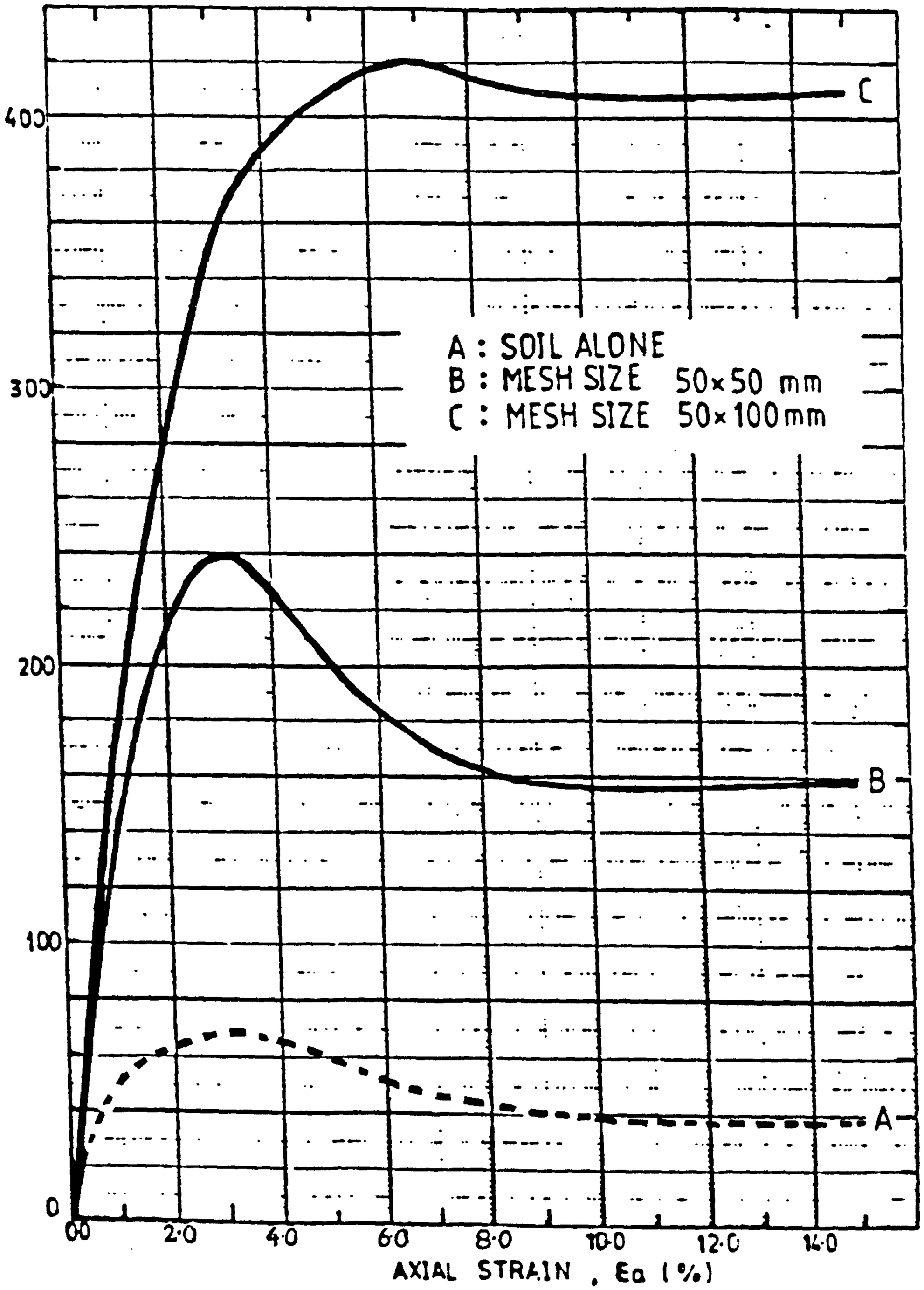

FIG. 5.18

SOIL TYPE	MID-ROSS SAND
MESH TYPE	7
MESH CONTENT	33 (m^2/m^3), or 0·09 (%) by dry weight

$\sigma_3 = 25\ kN/m^2$

200 mm × 155 mm diam. TRIAXIAL TEST DATA

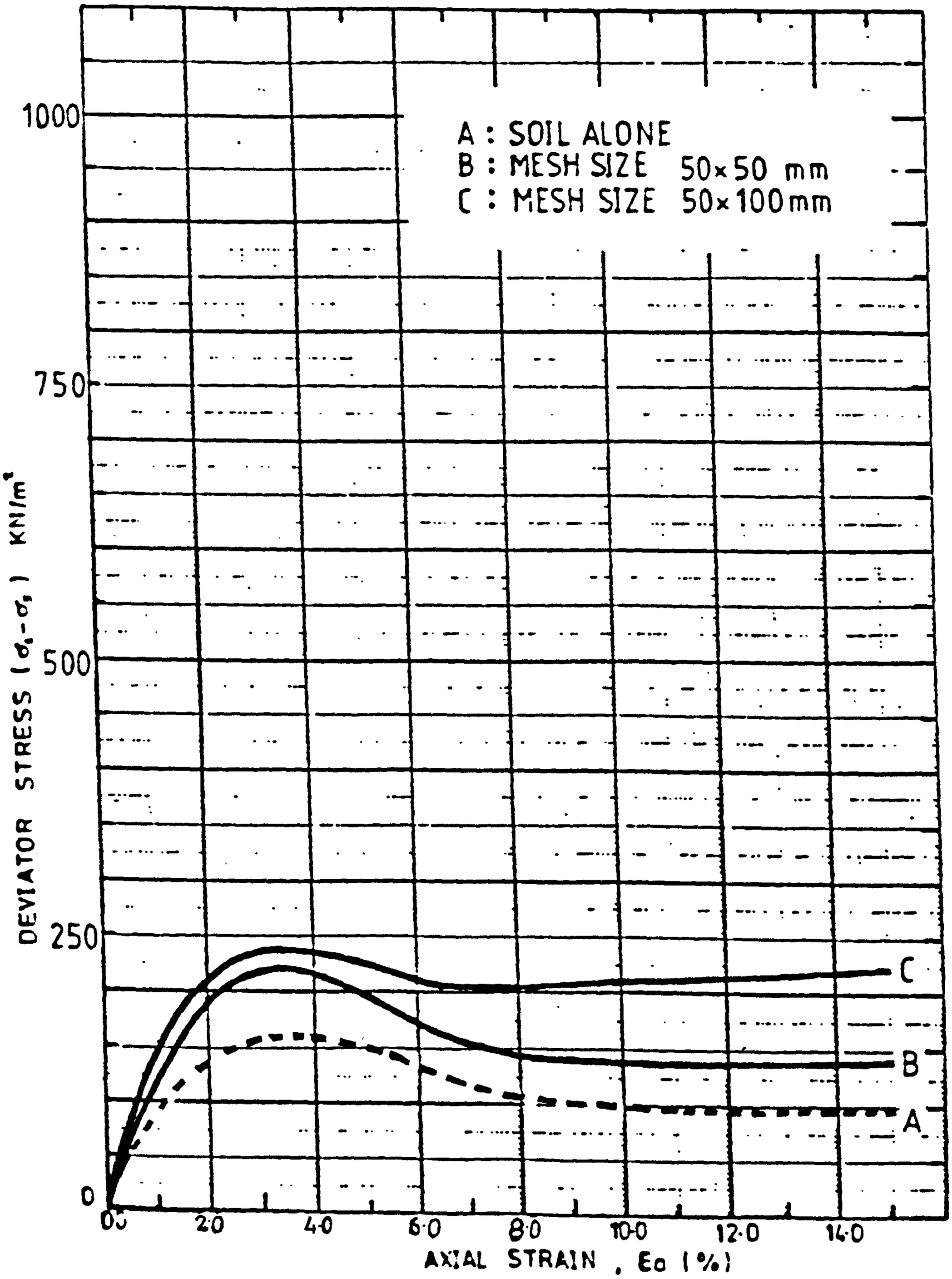

FIG. 5.19

SOIL TYPE	MID-ROSS SAND
MESH TYPE	7
MESH CONTENT	66 (m^2/m^2), or 0.18 (%) by dry weight

$\sigma_3 = 25\ kN/m^2$

200 mm × 155 mm diam. TRIAXIAL TEST DATA

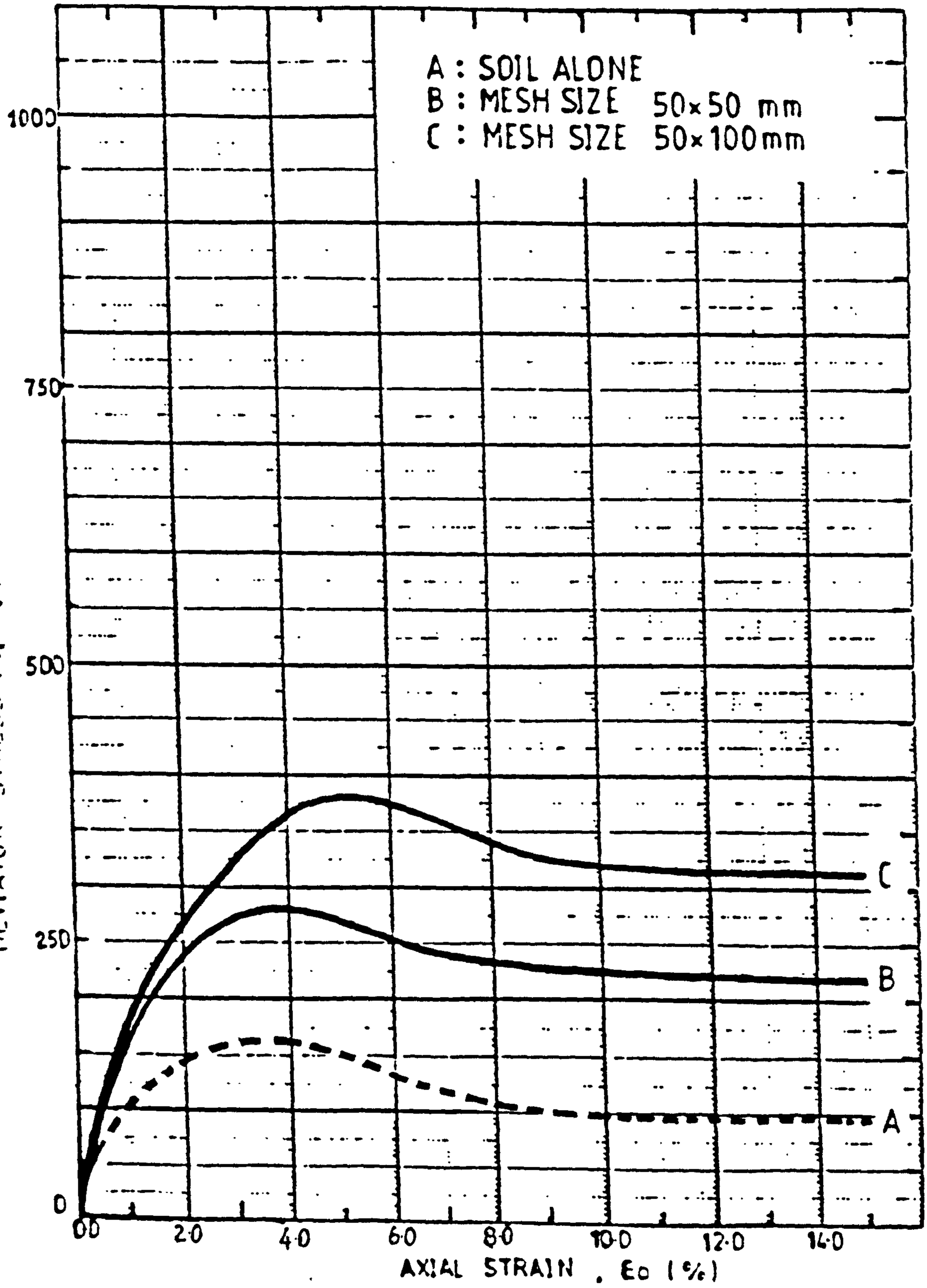

FIG. 5.20

SOIL TYPE	MID-ROSS SAND
MESH TYPE	7
MESH CONTENT	90 (m^2/m^2), or 0·24 (%) by dry weight

$\sigma_3 = 25\ kN/m^2$

200mm × 155mm diam. TRIAXIAL TEST DATA

FIG. 5.21

SOIL TYPE	LEIGHTON BUZZARD SAND
MESH TYPE	7
MESH CONTENT	33 (m^2/m^3), or 0·10 (%) by dry weight

$\sigma_3 = 0\ kN/m^2$

200mm × 155mm diam. TRIAXIAL TEST DATA

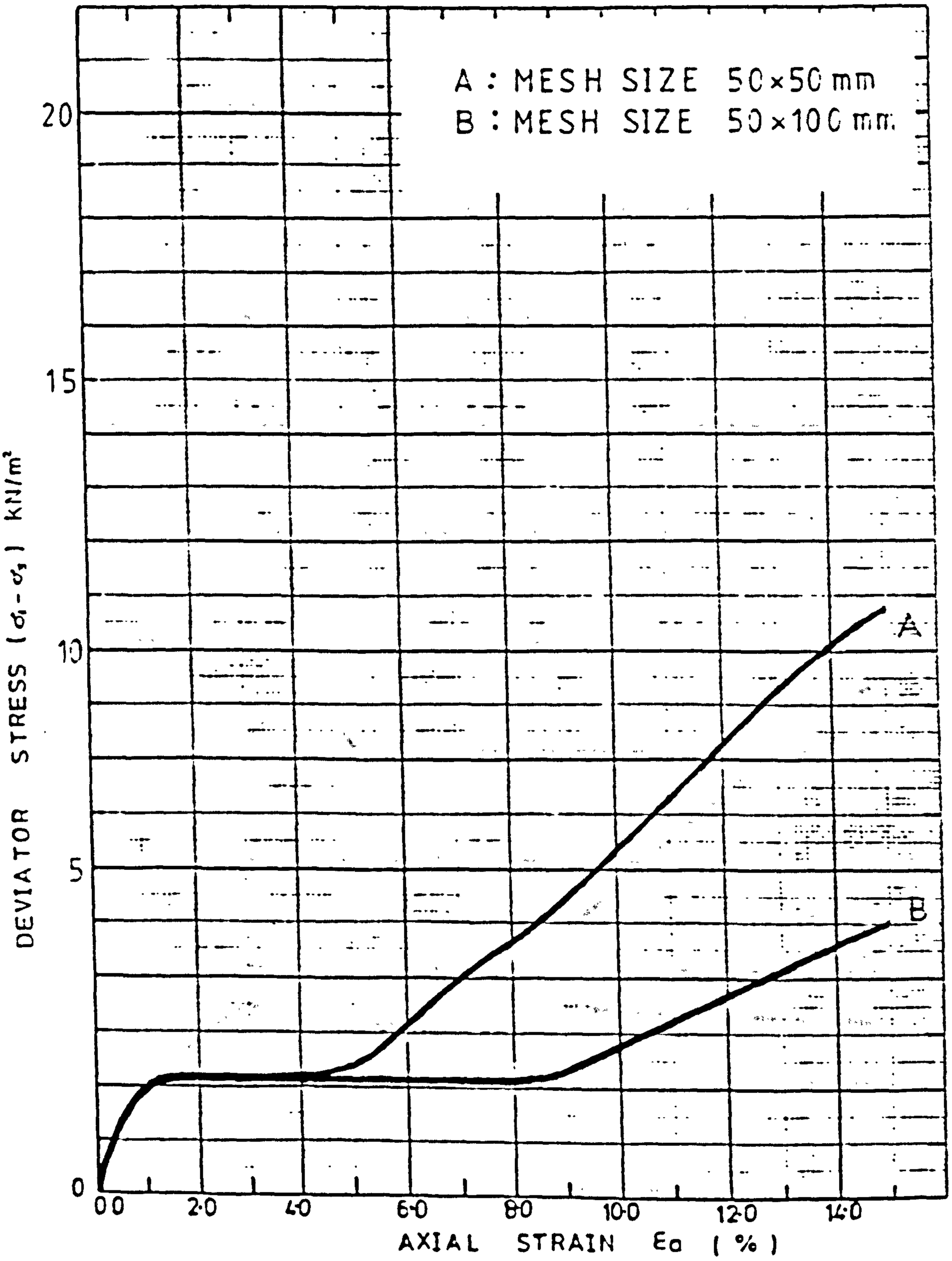

FIG. 5.22

SOIL TYPE	LEIGHTON BUZZARD SAND
MESH TYPE	7
MESH CONTENT	66 (m^2/m^3), or 0·20 (%) by dry weight

$\sigma_3 = 0\ kN/m^2$

200mm × 155mm diam. TRIAXIAL TEST DATA

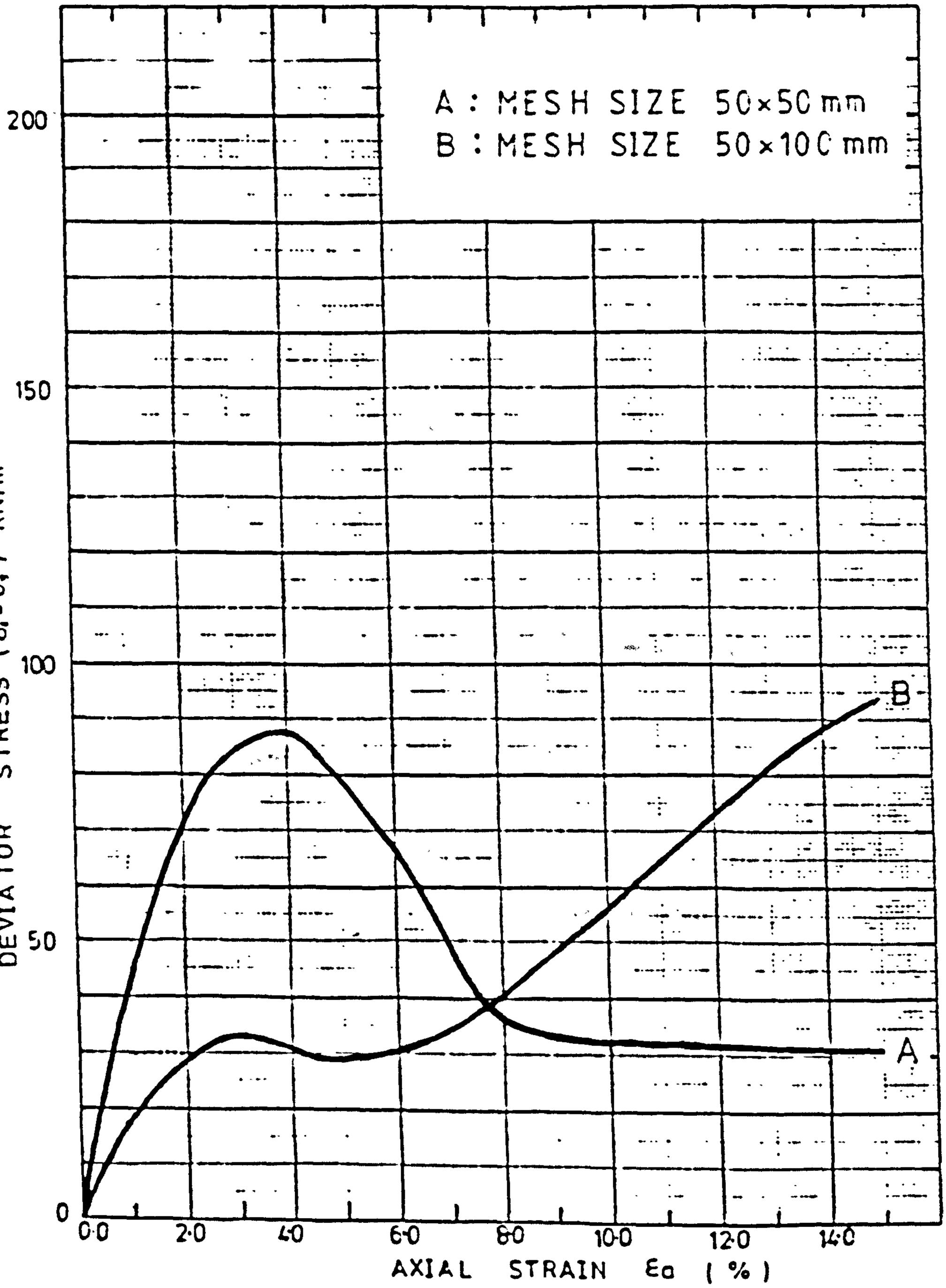

FIG. 5.23

SOIL TYPE	LEIGHTON BUZZARD SAND
MESH TYPE	7
MESH CONTENT	90 (m^2/m^3), or 0·27 (%) by dry weight

$\sigma_3 = 0\ kN/m^2$

200 mm × 155 mm diam. TRIAXIAL TEST DATA

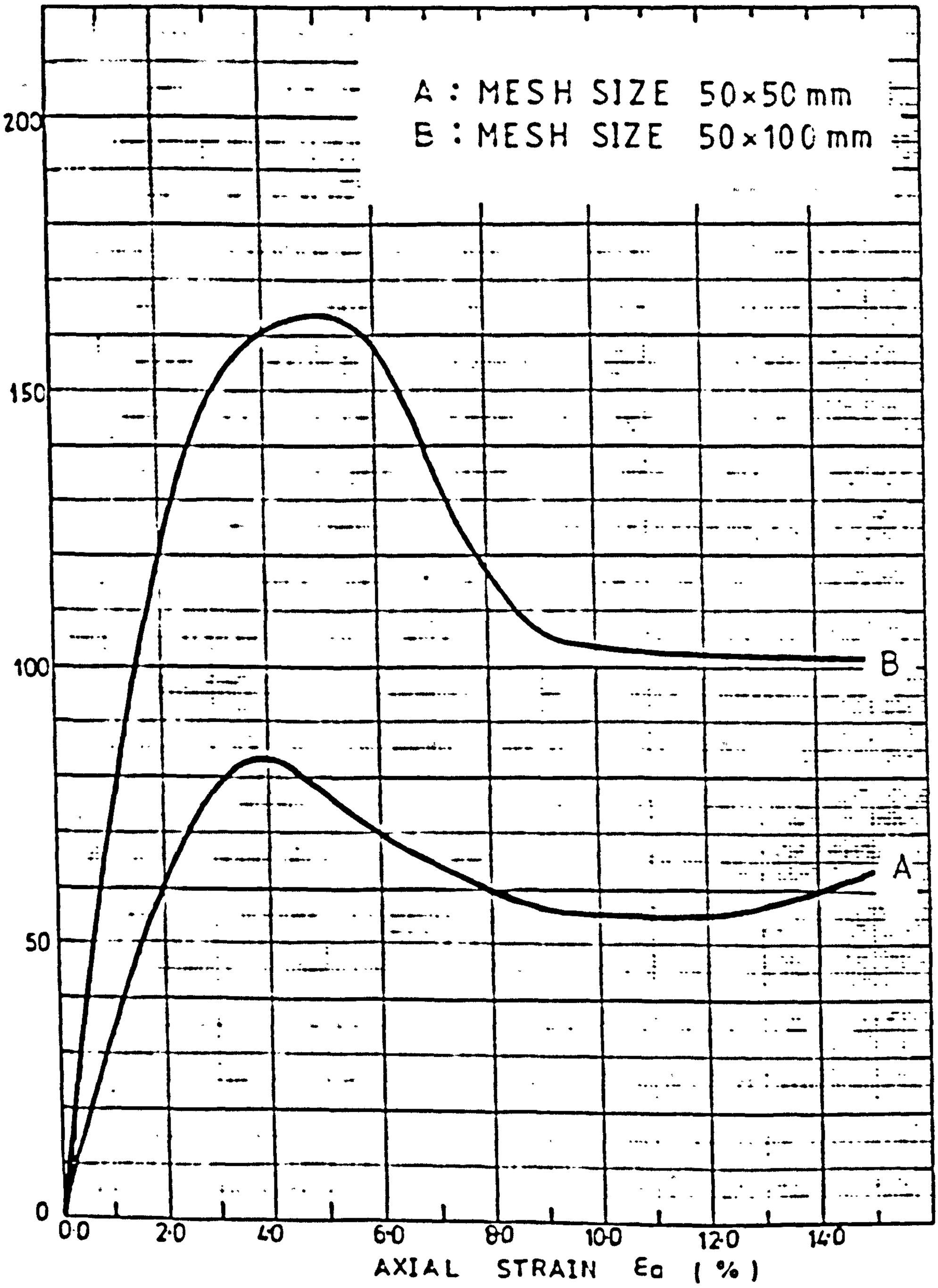

FIG. 5.24

SOIL TYPE	LEIGHTON BUZZARD SAND

200 mm×155 mm diam. TRIAXIAL TEST DATA

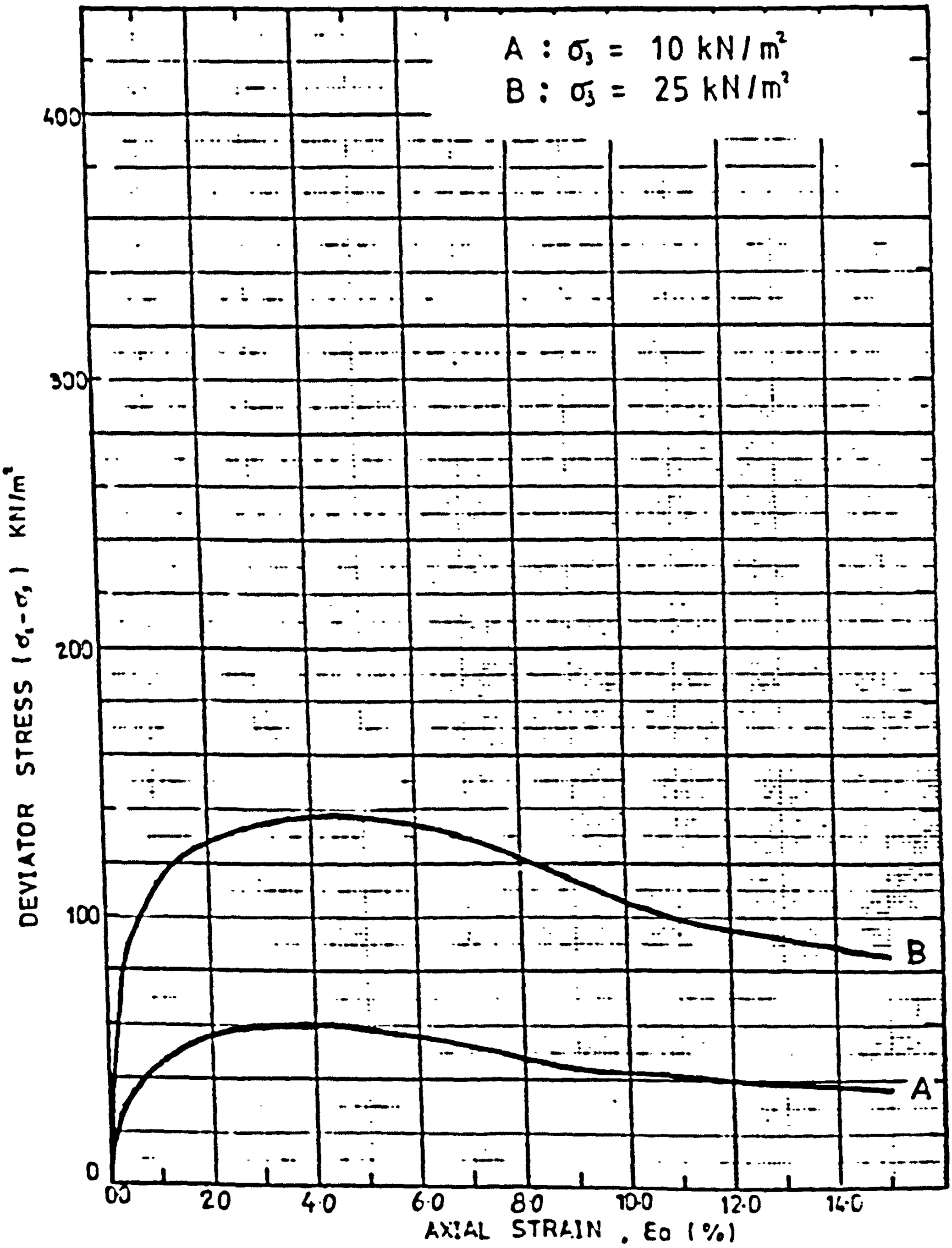

FIG. 5.25

SOIL TYPE	LEIGHTON BUZZARD SAND
MESH TYPE	7
MESH CONTENT	33 (m^2/m^3), or 0·10 (%) by dry weight

$\sigma_3 = 10\ kN/m^2$

200mm × 155mm diam. TRIAXIAL TEST DATA

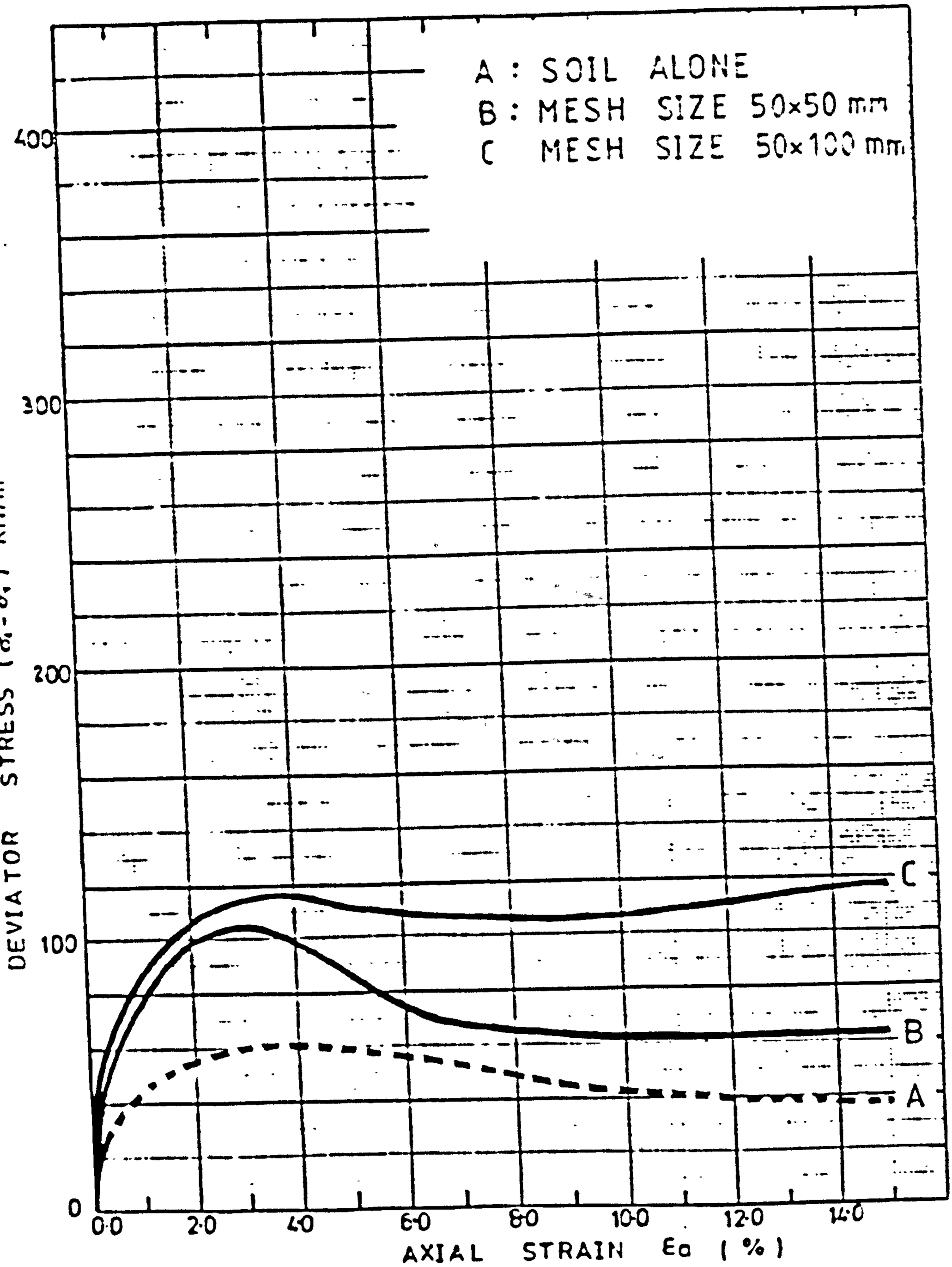

FIG. 5.26

SOIL TYPE	LEIGHTON BUZZARD SAND
MESH TYPE	7
MESH CONTENT	66 (m^2/m^3), or 0·20 (%) by dry weight

$\sigma_3 = 10\ kN/m^2$

200mm × 155mm diam. TRIAXIAL TEST DATA

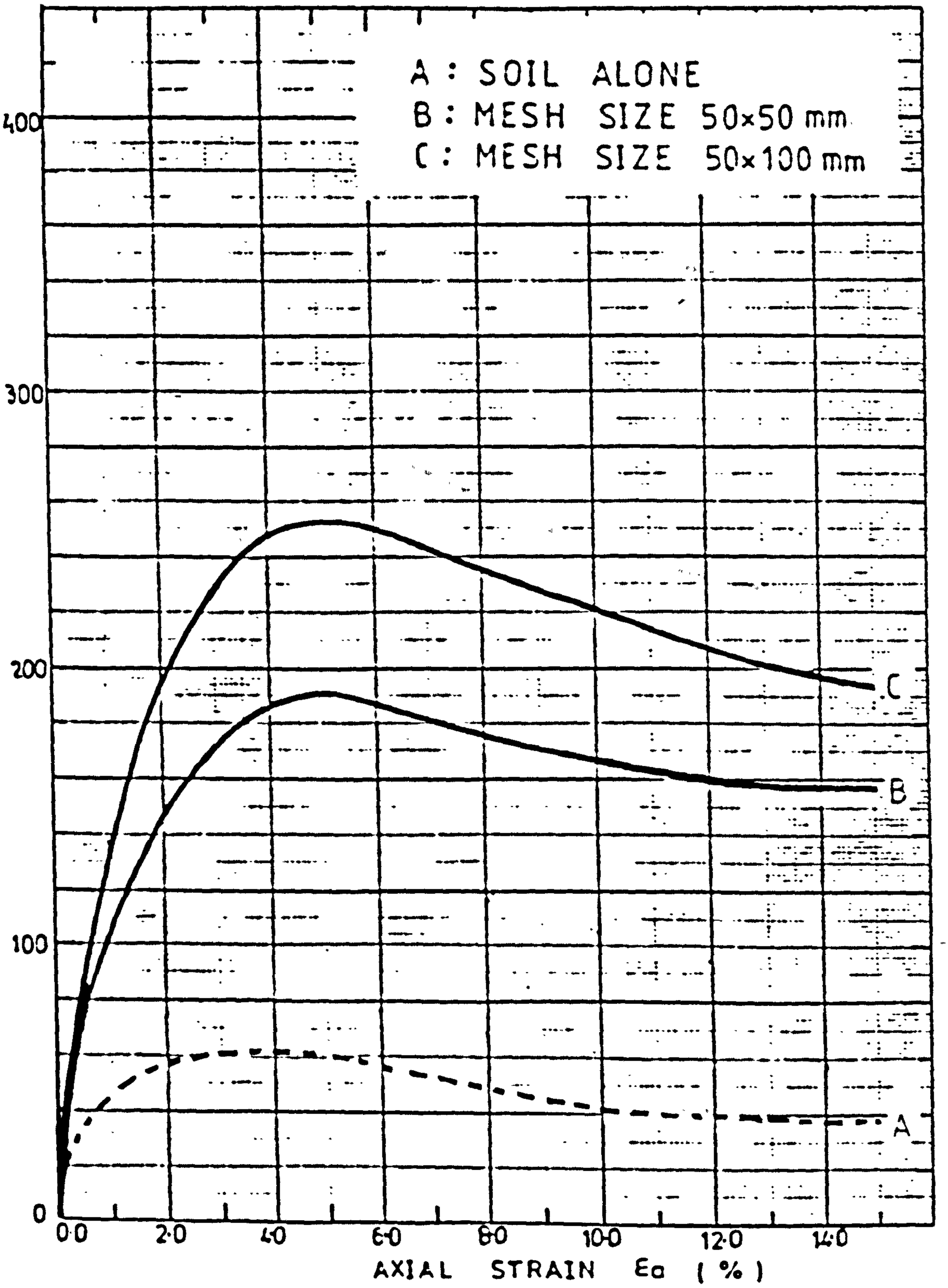

FIG. 5.27

SOIL TYPE	LEIGHTON BUZZARD SAND
MESH TYPE	7
MESH CONTENT	90 (m^2/m^3), or 0·27 (%) by dry weight

$\sigma_3' = 10\ kN/m^2$

200mm × 155mm diam. TRIAXIAL TEST DATA

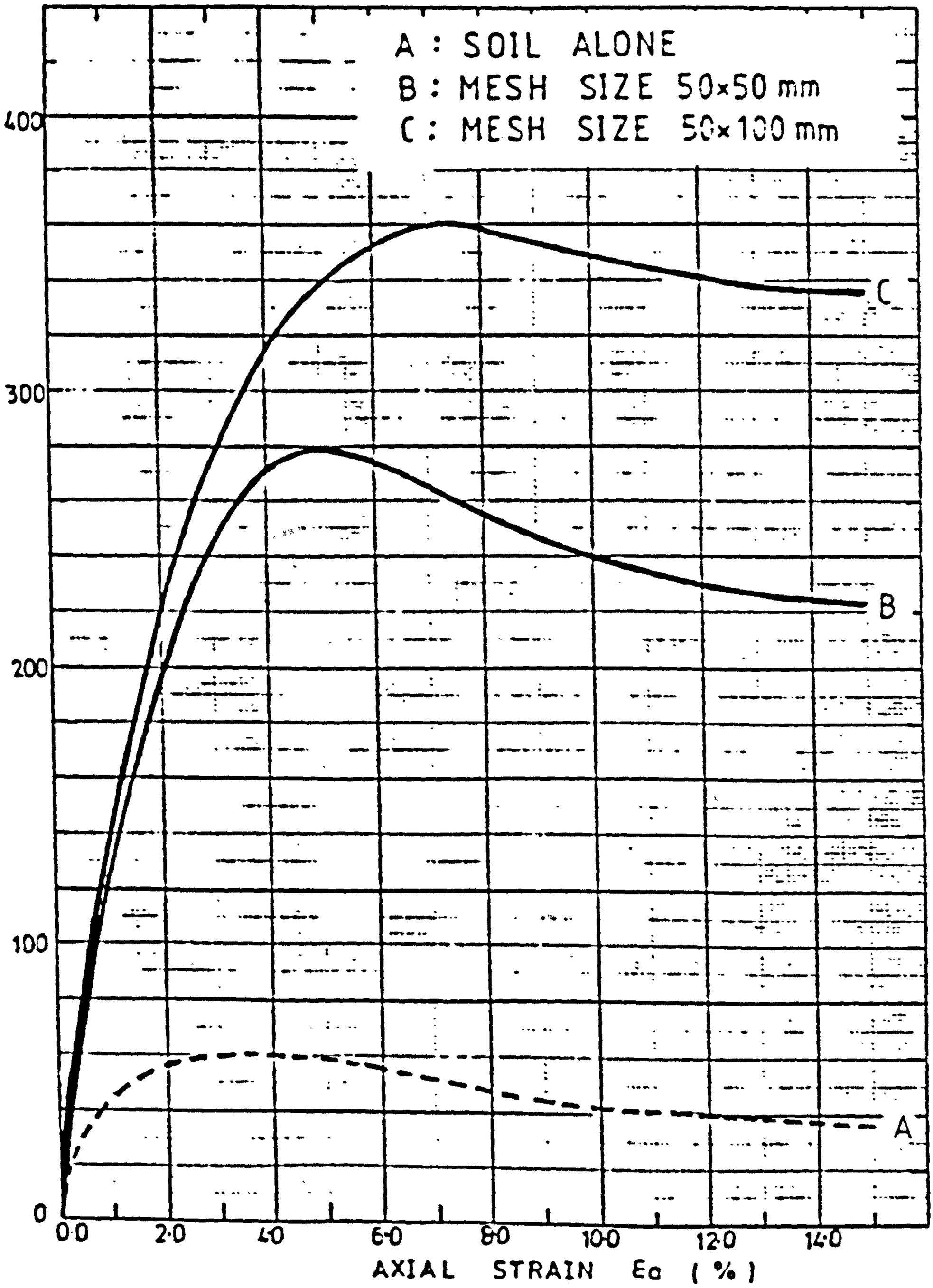

FIG. 5.28

SOIL TYPE	LEIGHTON BUZZARD SAND
MESH TYPE	7
MESH CONTENT	33 (m^2/m^3), or 0·10 (%) by dry weight

$\sigma_3 = 25\ kN/m^2$

200mm × 155mm diam. TRIAXIAL TEST DATA

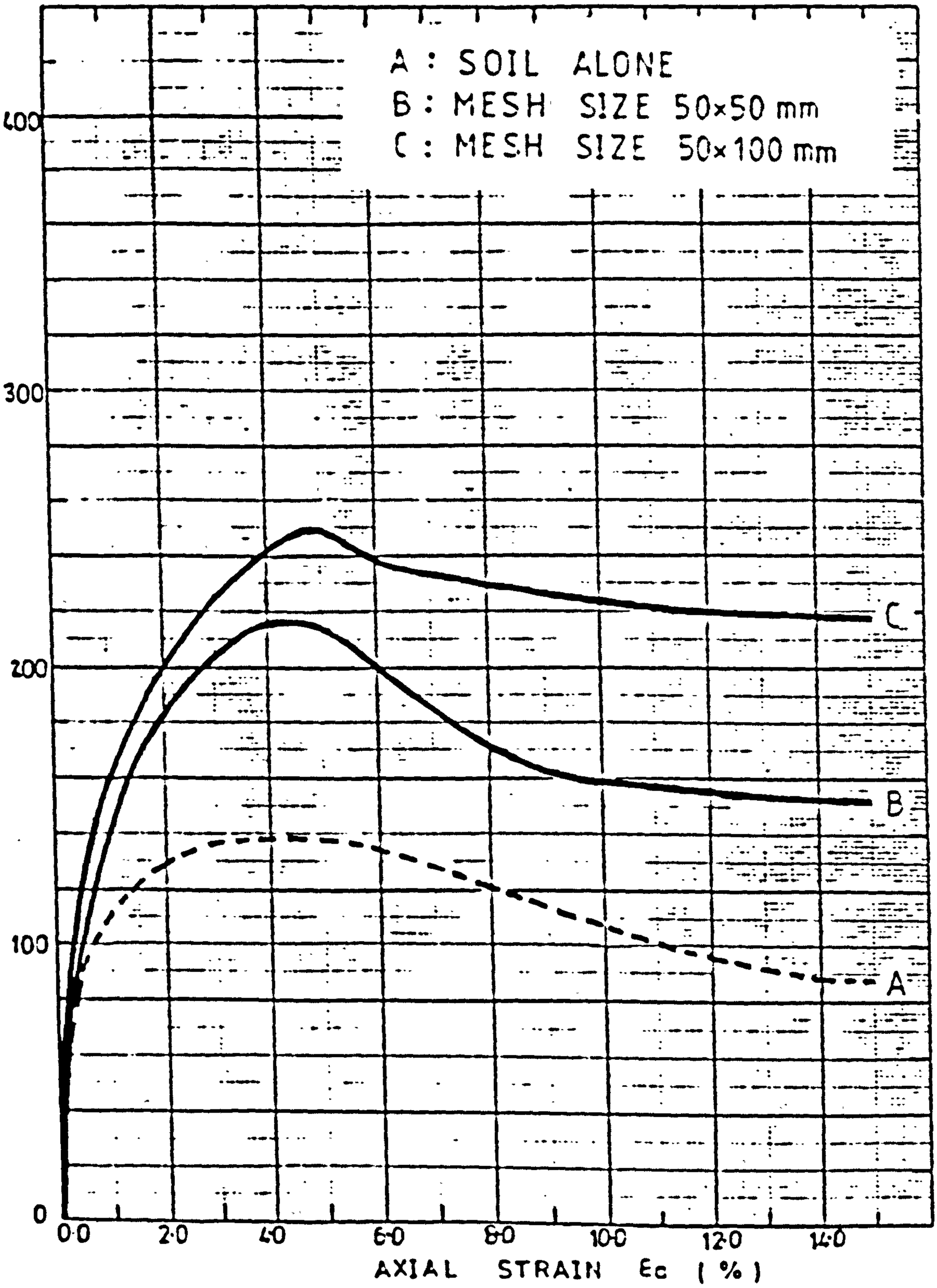

FIG. 5.29

SOIL TYPE	LEIGHTON BUZZARD SAND
MESH TYPE	7
MESH CONTENT	66 (m^2/m^3), or 0.20 (%) by dry weight

$\sigma_3 = 25\ kN/m^2$

200 mm × 155 mm diam. TRIAXIAL TEST DATA

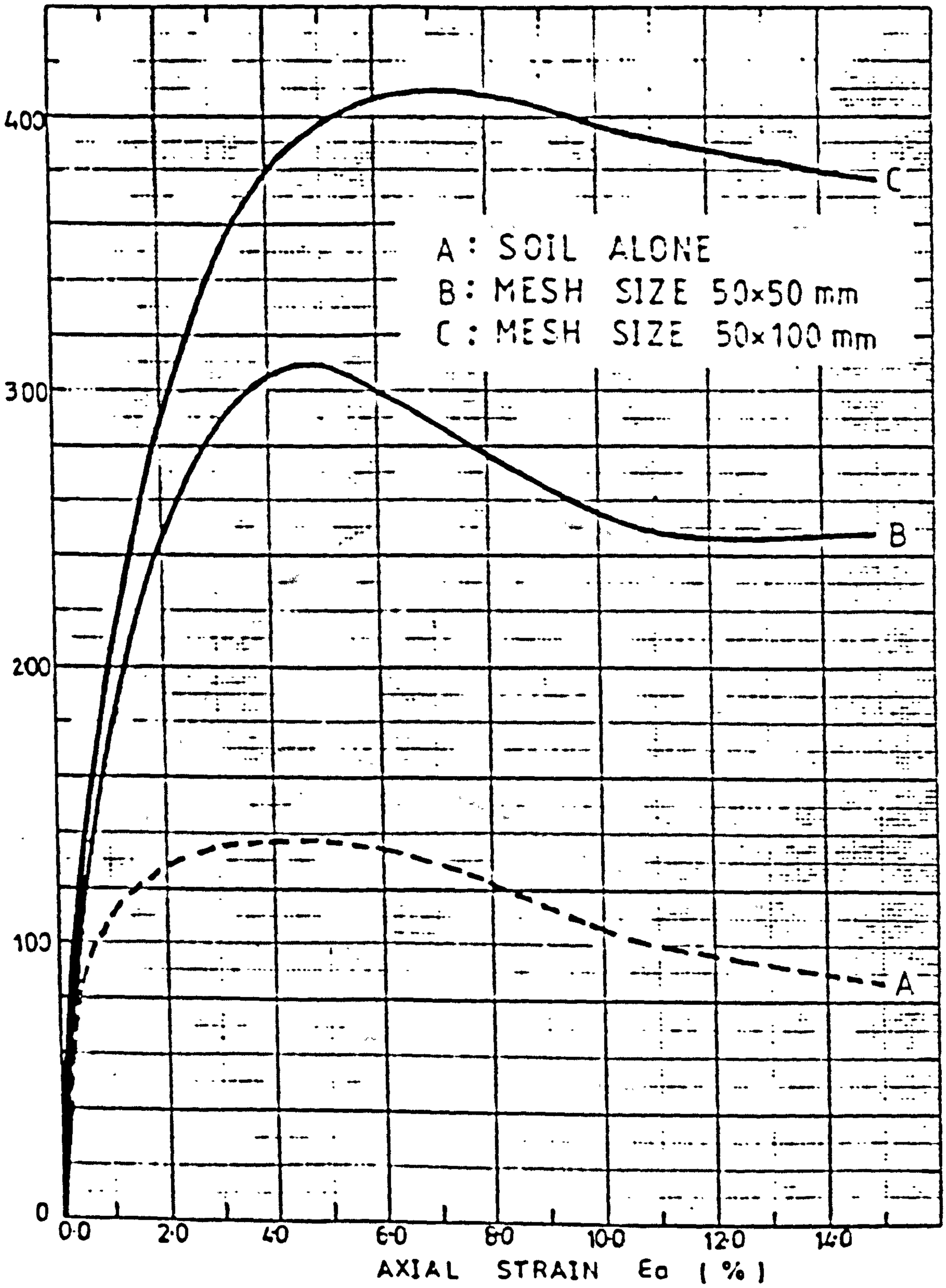

FIG. 5.30

SOIL TYPE	LEIGHTON BUZZARD SAND
MESH TYPE	7
MESH CONTENT	90 (m^2/m^3), or 0.27 (%) by dry weight

$\sigma_3 = 25\ kN/m^2$

200mm × 155mm diam. TRIAXIAL TEST DATA

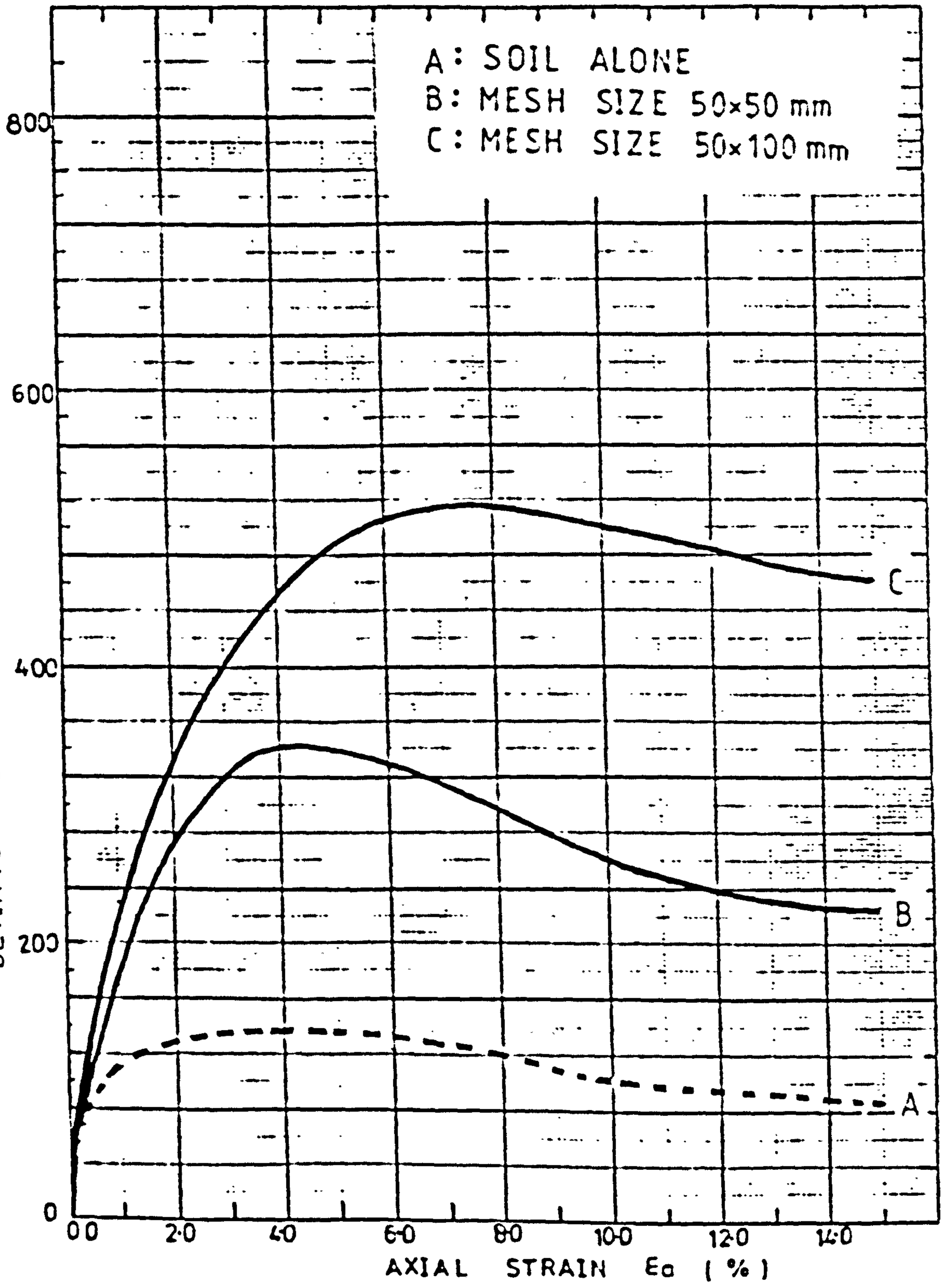

HIGH STRESS TRIAXIAL DATA

of

MID-ROSS SAND
&
LEIGHTON BUZZARD SAND

mixed

with

TYPE 7, MESH-ELEMENTS

of

50×50 mm and 50×100 mm
SIZES

at

various percentages

FIG. 5.31

SOIL TYPE	LEIGHTON BUZZARD SAND
MESH TYPE	7
MESH CONTENT	33 (m^2/m^3), or 0·10 (%) by dry weight

$\sigma_3 = 50\ kN/m^2$

200 mm × 155 mm diam. TRIAXIAL TEST DATA

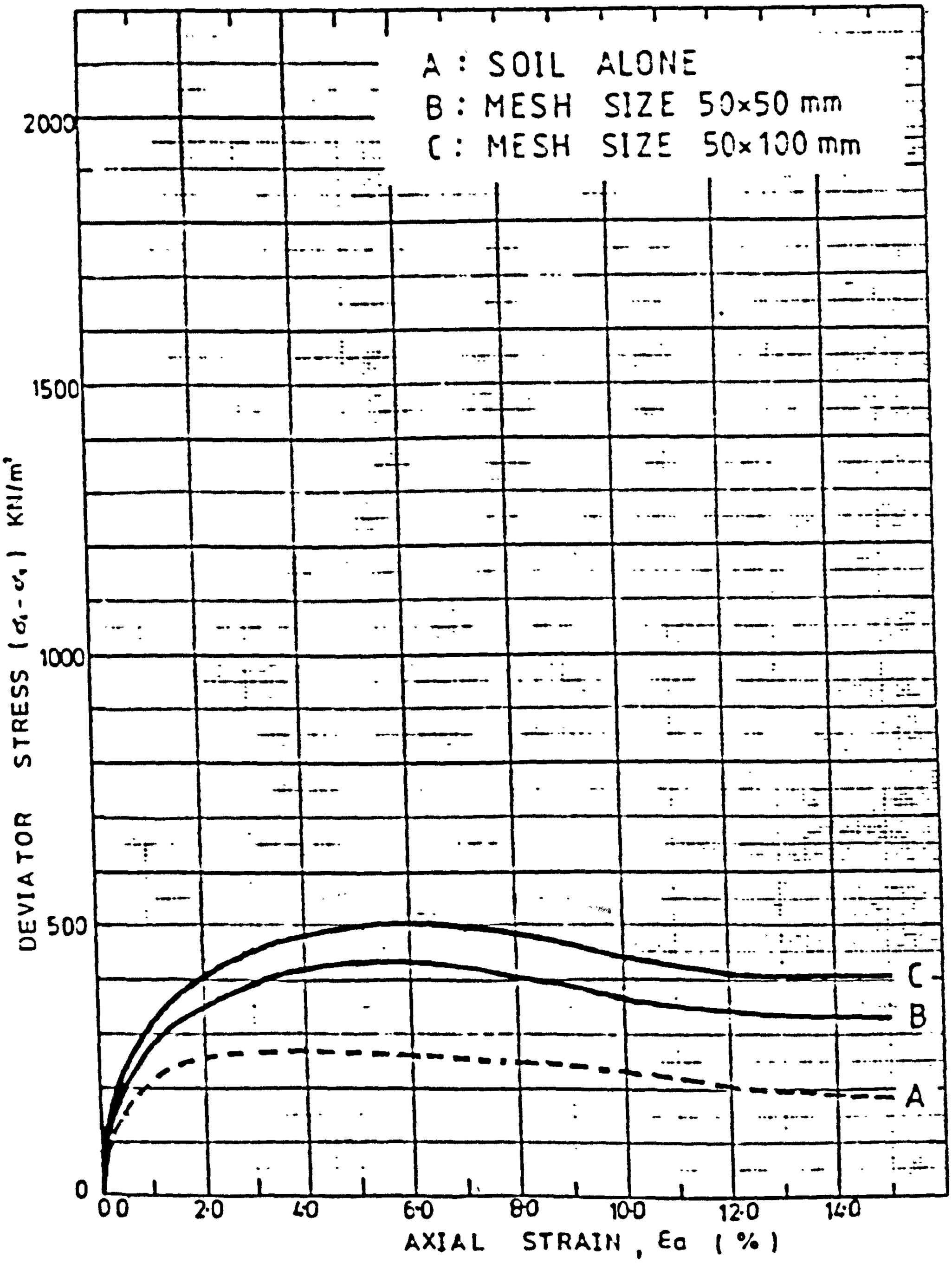

FIG. 5.32

SOIL TYPE	LEIGHTON BUZZARD SAND
MESH TYPE	7
MESH CONTENT	66 (m^2/m^3), or 0·20 (%) by dry weight

$\sigma_3 = 50\ kN/m^2$

200 mm × 155 mm diam. TRIAXIAL TEST DATA

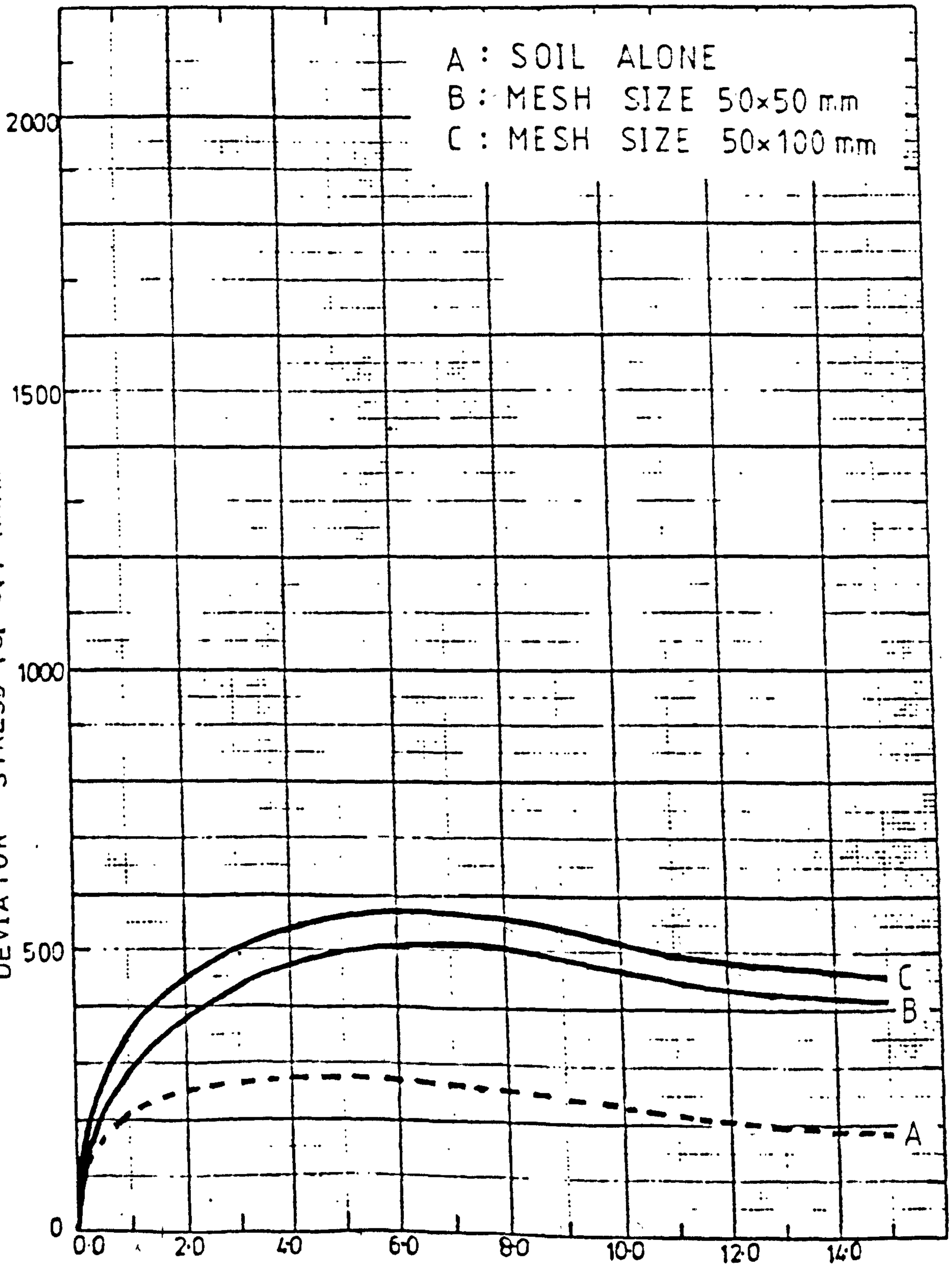

FIG. 5.33

SOIL TYPE	LEIGHTON BUZZARD SAND
MESH TYPE	7
MESH CONTENT	90 (m^2/m^3), or 0·27 (%) by dry weight

$\sigma_3 = 50\ kN/m^2$

200mm × 155mm diam. TRIAXIAL TEST DATA

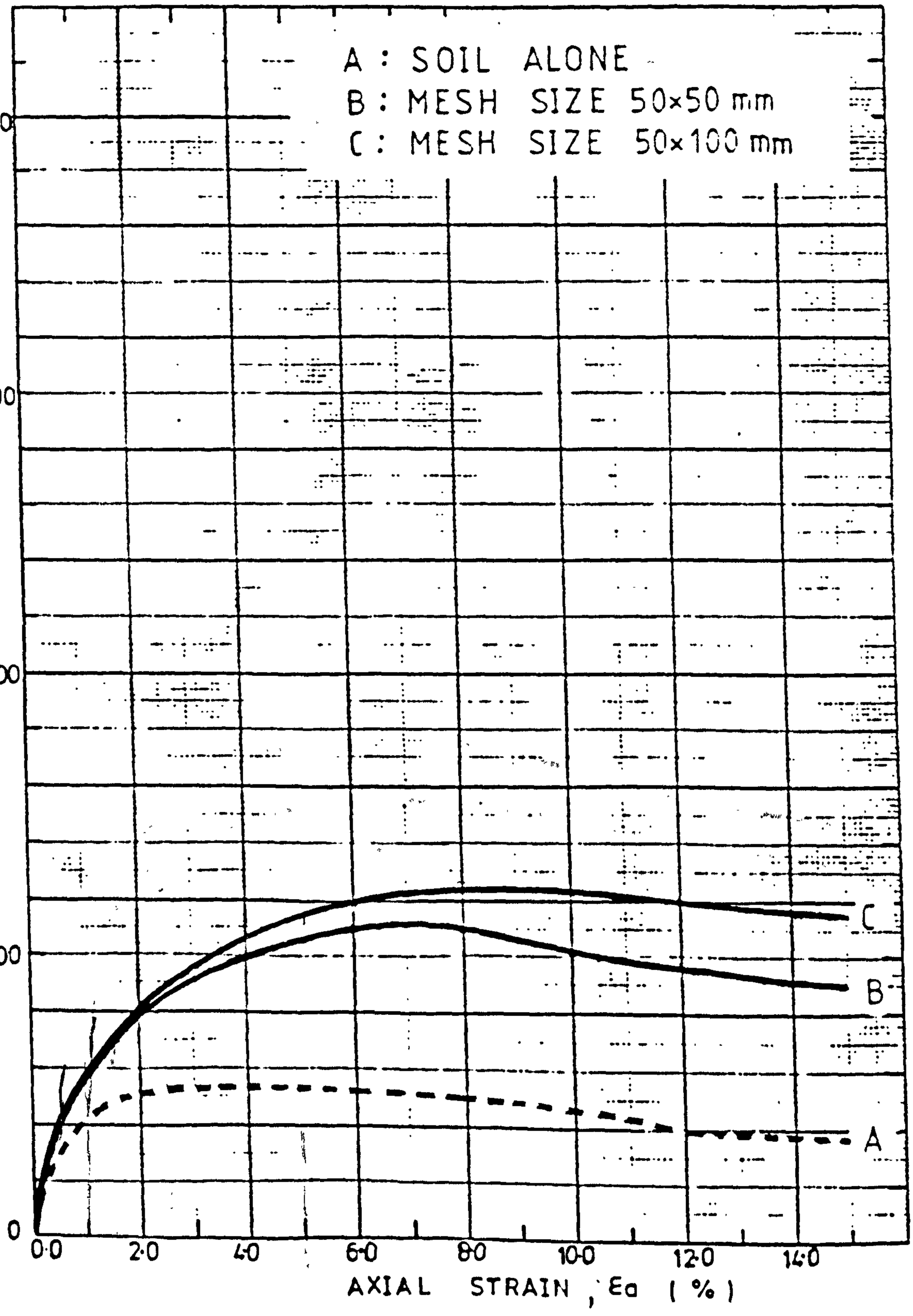

FIG. 5.34

SOIL TYPE	LEIGHTON BUZZARD SAND
MESH TYPE	7
MESH CONTENT	33 (m^2/m^3), or 0·10 (%) by dry weight

$\sigma_3 = 150\ kN/m^2$

200 mm × 155 mm diam. TRIAXIAL TEST DATA

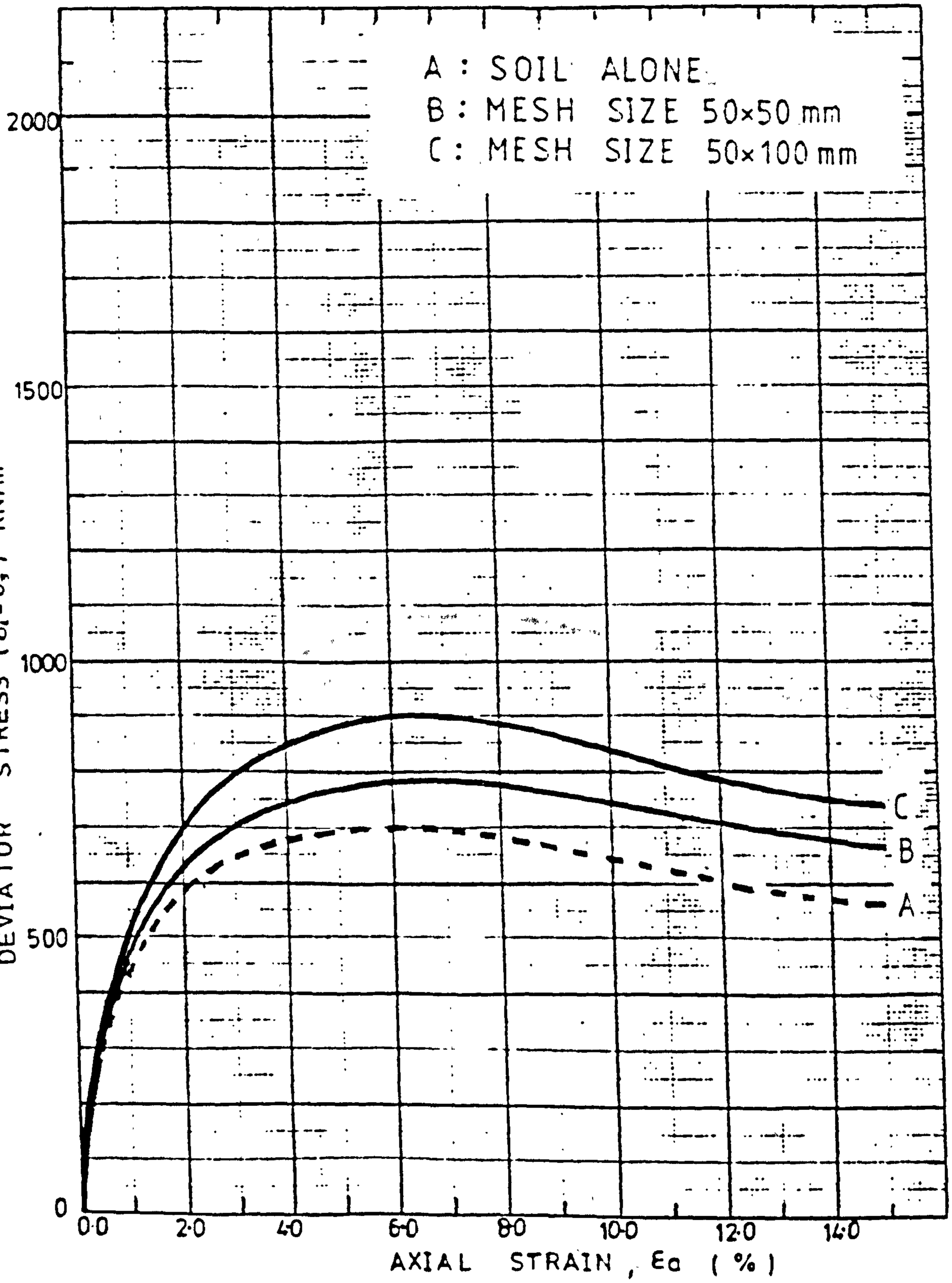

FIG. 5.35

SOIL TYPE	LEIGHTON BUZZARD SAND
MESH TYPE	7
MESH CONTENT	66 (m^2/m^3), or 0·20 (%) by dry weight

$\sigma_3 = 150\ kN/m^2$

200 mm × 155 mm diam. TRIAXIAL TEST DATA

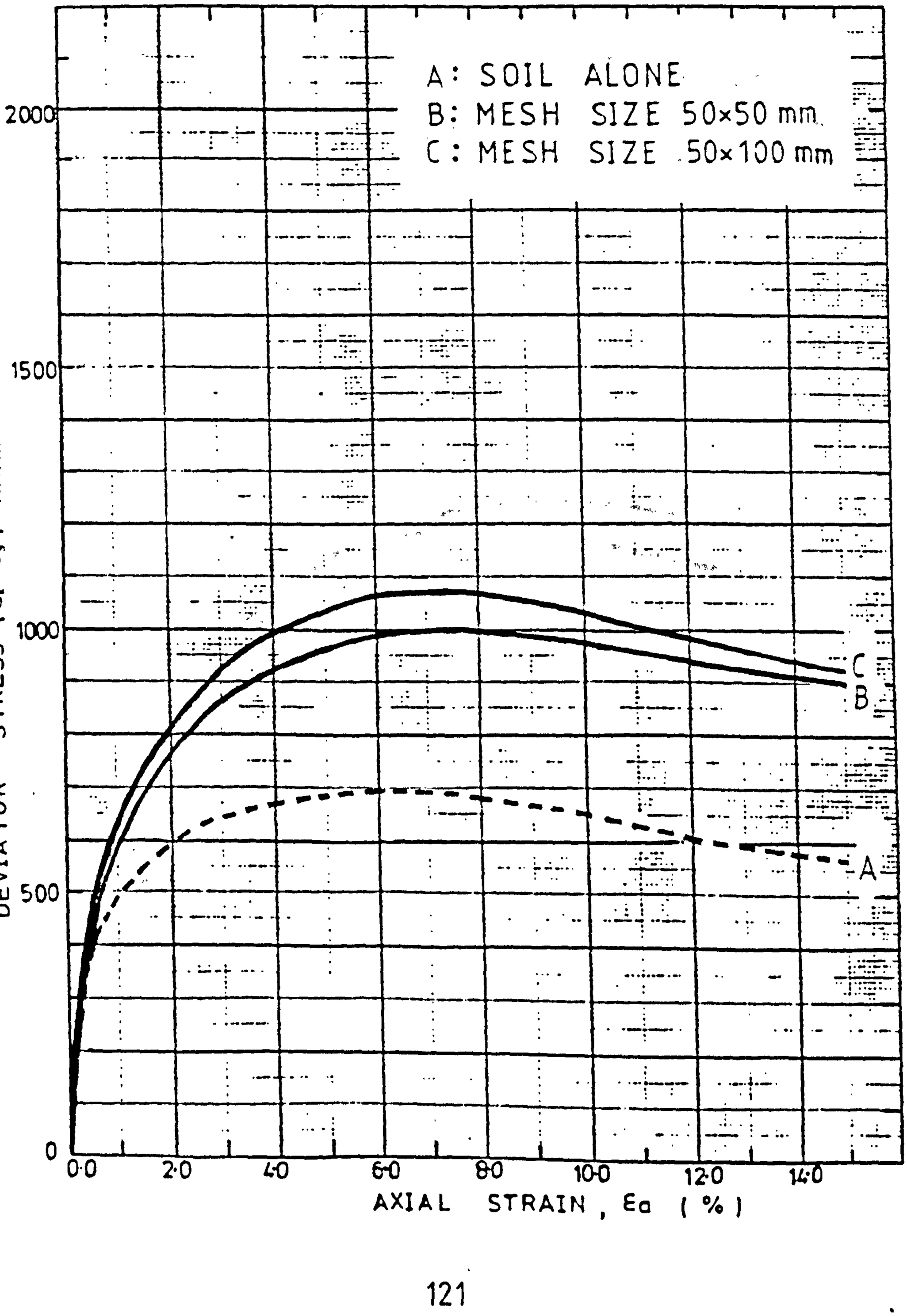

FIG. 5.36

SOIL TYPE	LEIGHTON BUZZARD SAND
MESH TYPE	7
MESH CONTENT	90 (m^2/m^3), or 0·27 (%) by dry weight

$\sigma_3 = 150\ kN/m^2$

200 mm × 155 mm diam. TRIAXIAL TEST DATA

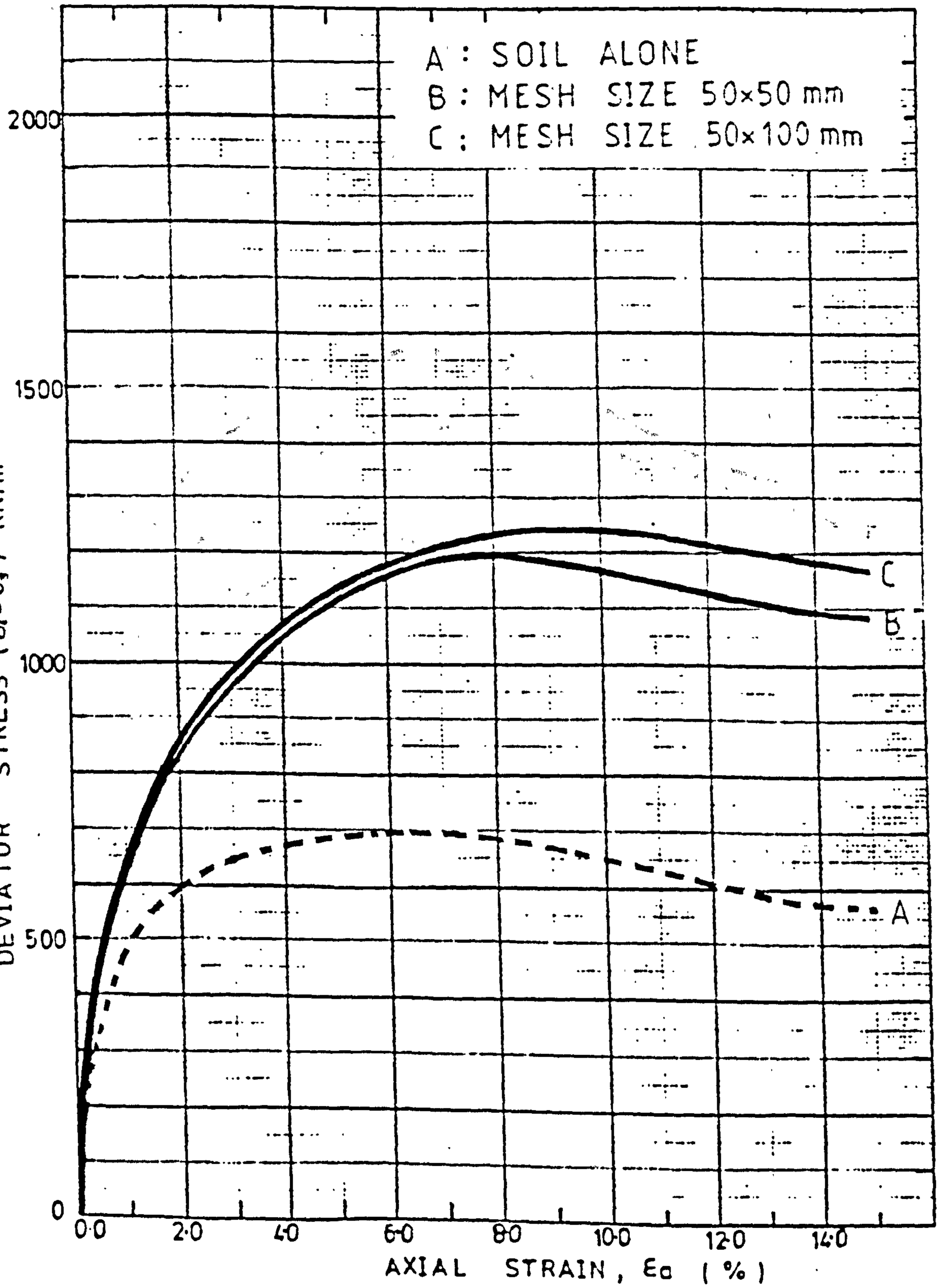

FIG. 5.37

SOIL TYPE	LEIGHTON BUZZARD SAND
MESH TYPE	7
MESH CONTENT	33 (m^2/m^3), or 0·10 (%) by dry weight

$\sigma_3 = 300\ kN/m^2$

200 mm × 155 mm diam. TRIAXIAL TEST DATA

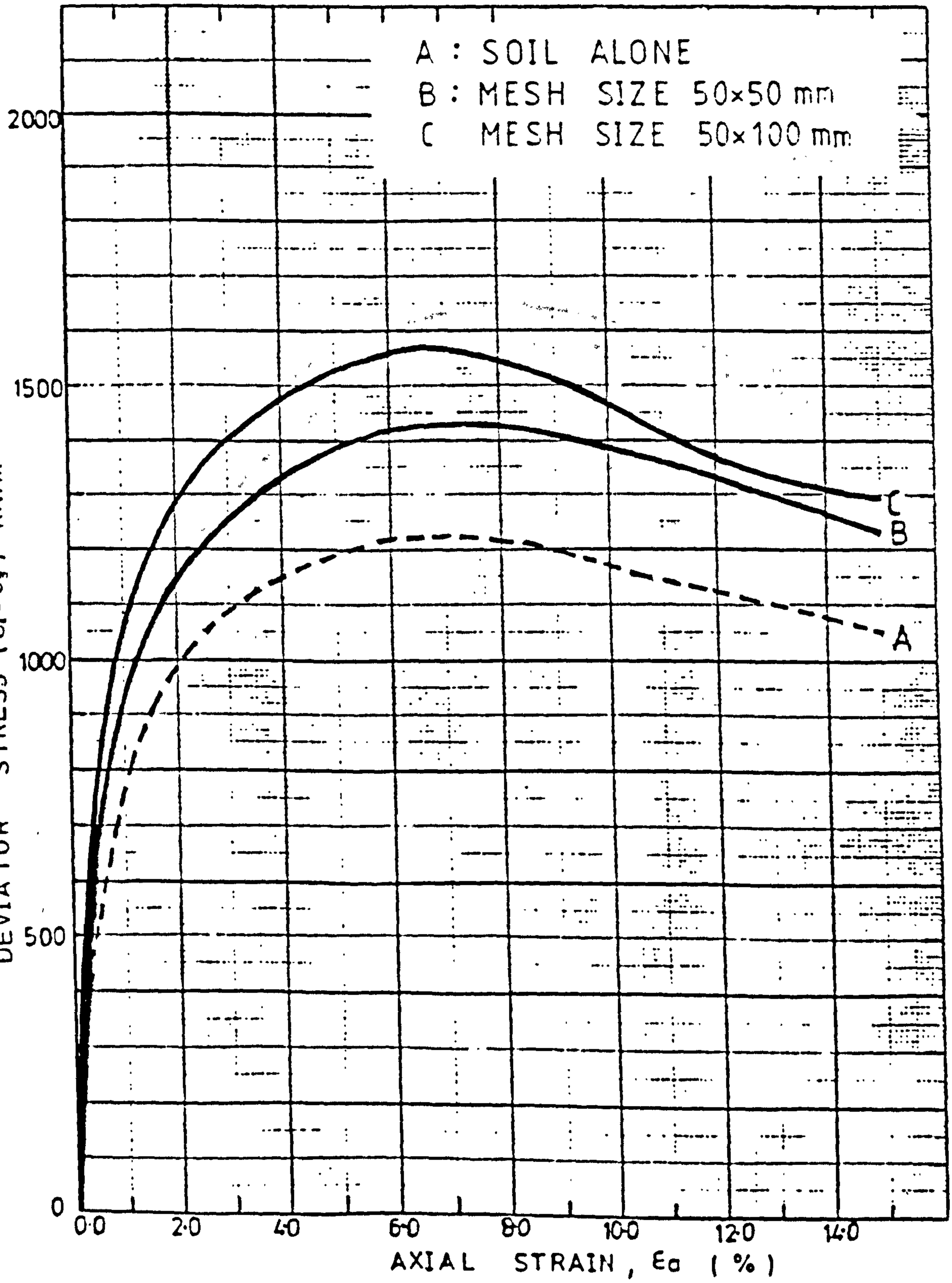

FIG. 5.38

SOIL TYPE	LEIGHTON BUZZARD SAND
MESH TYPE	7
MESH CONTENT	66 (m^2/m^3), or 0·20 (%) by dry weight

$\sigma_3 = 300\ kN/m^2$

200 mm × 155 mm diam. TRIAXIAL TEST DATA

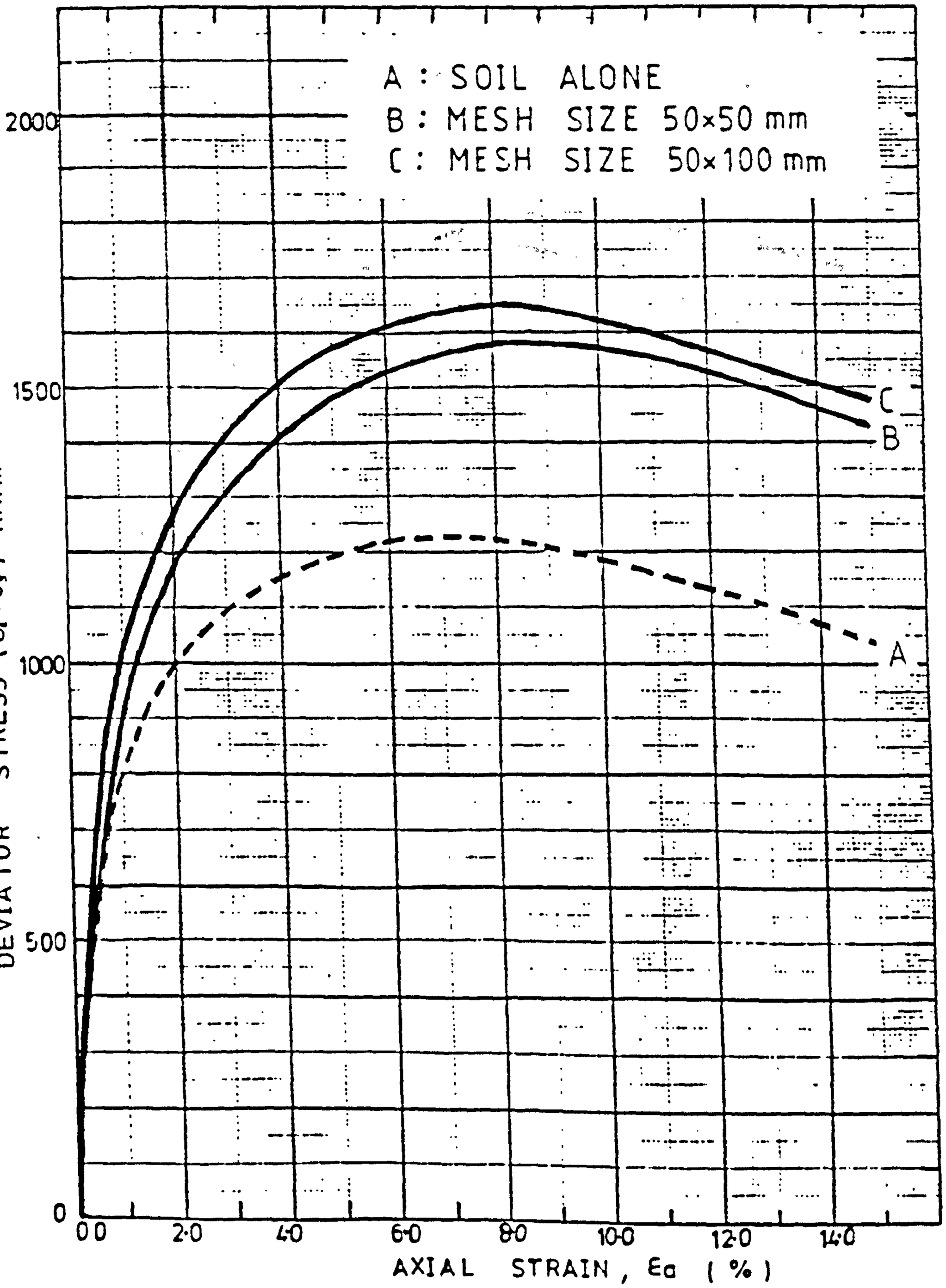

FIG. 5.39

SOIL TYPE	LEIGHTON BUZZARD SAND
MESH TYPE	7
MESH CONTENT	90 (m^2/m^3), or 0·27 (%) by dry weight

$\sigma_3 = 300\ kN/m^2$

200 mm × 155 mm diam. TRIAXIAL TEST DATA

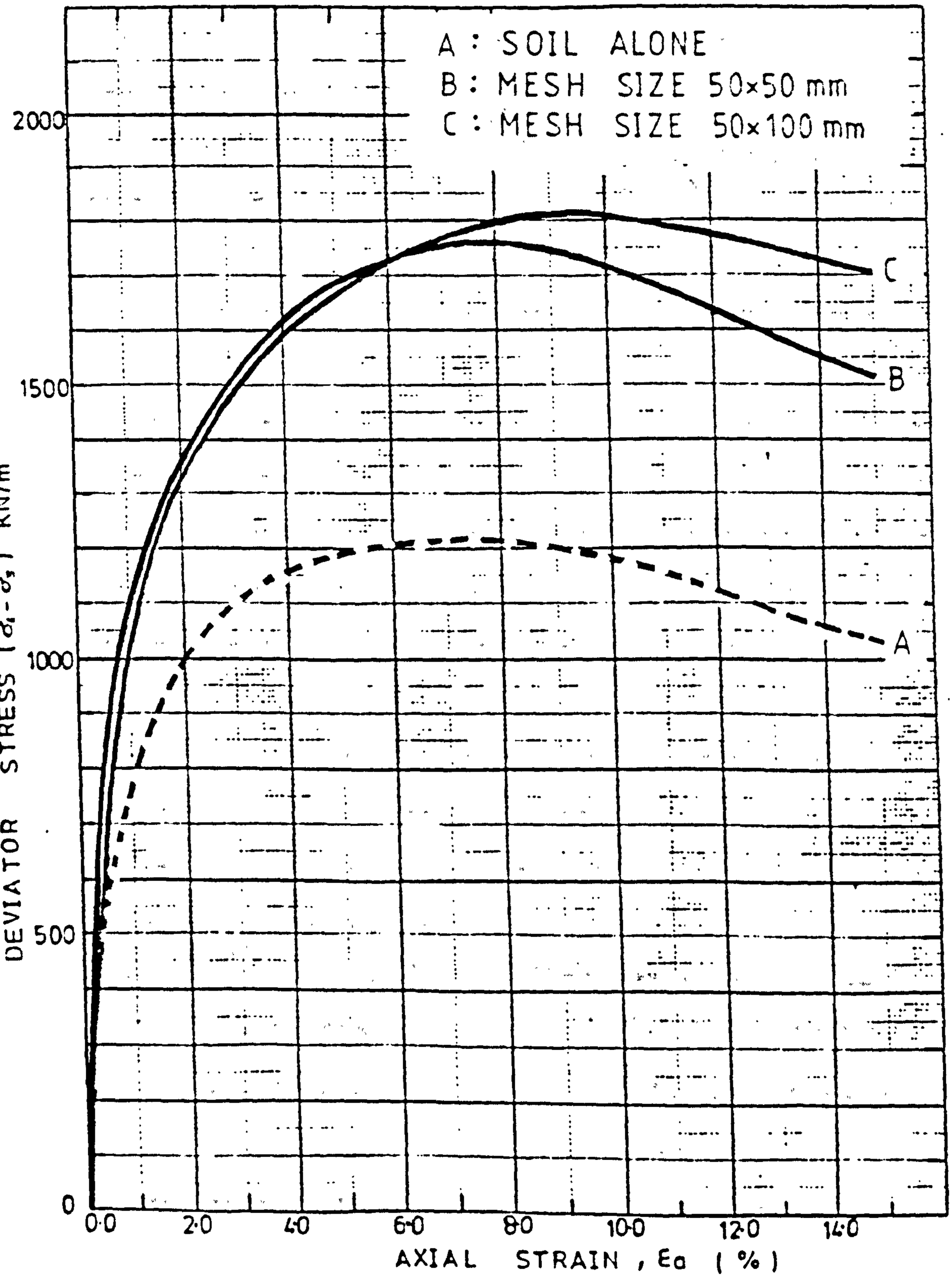

FIG. 5.40

SOIL TYPE	MID-ROSS SAND
MESH TYPE	7
MESH CONTENT	33 (m^2/m^2)% or 0·09 (%) by dry weight

$\sigma_3 = 50\ kN/m^2$

200 mm × 155 mm diam. TRIAXIAL TEST DATA

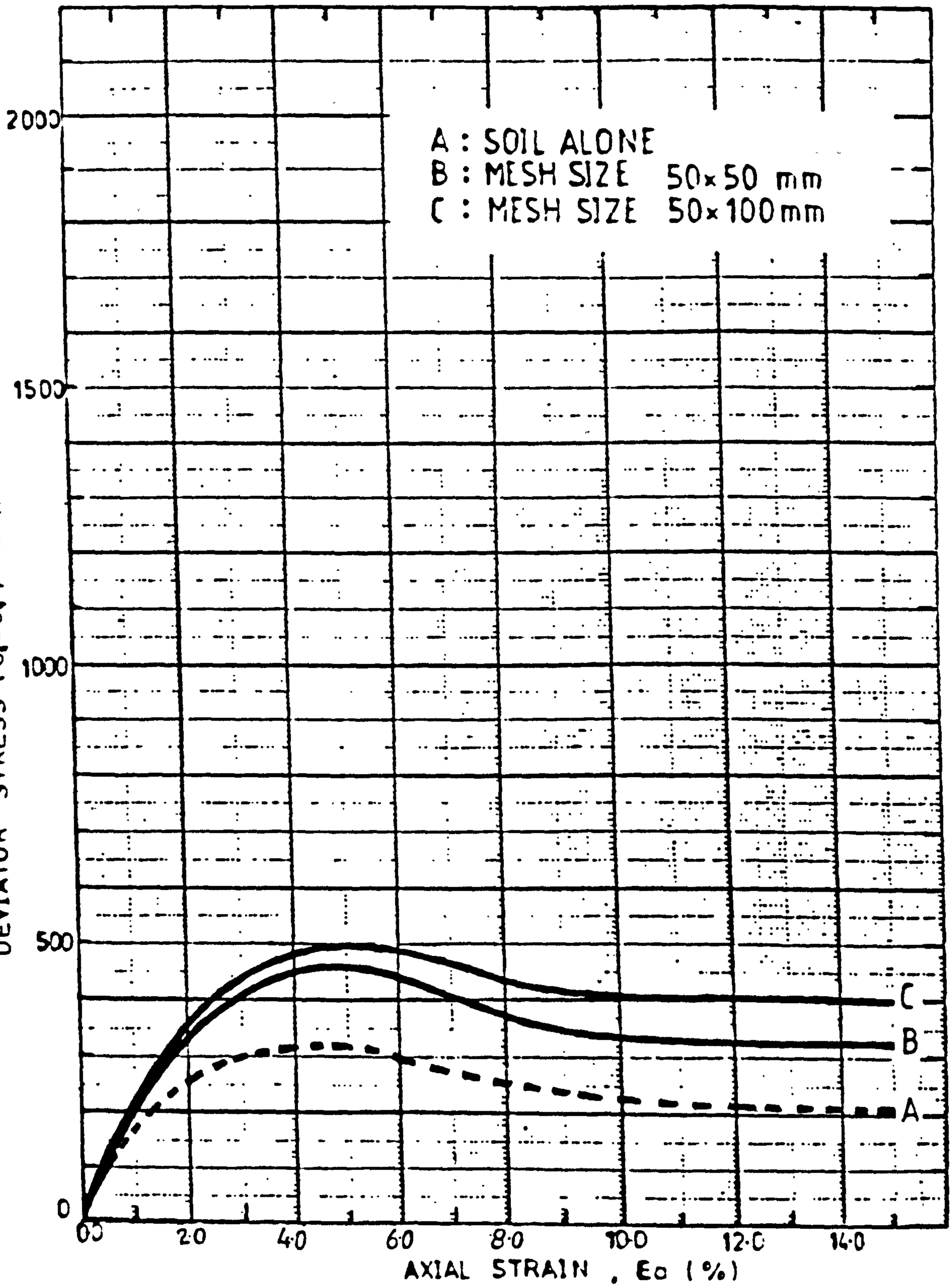

FIG. 5.41

SOIL TYPE	MID-ROSS SAND
MESH TYPE	7
MESH CONTENT	66 (m^2/m^2), or 0.18 (%) by dry weight

$\sigma_c = 50\ kN/m^2$

200mm × 155mm diom. TRIAXIAL TEST DATA

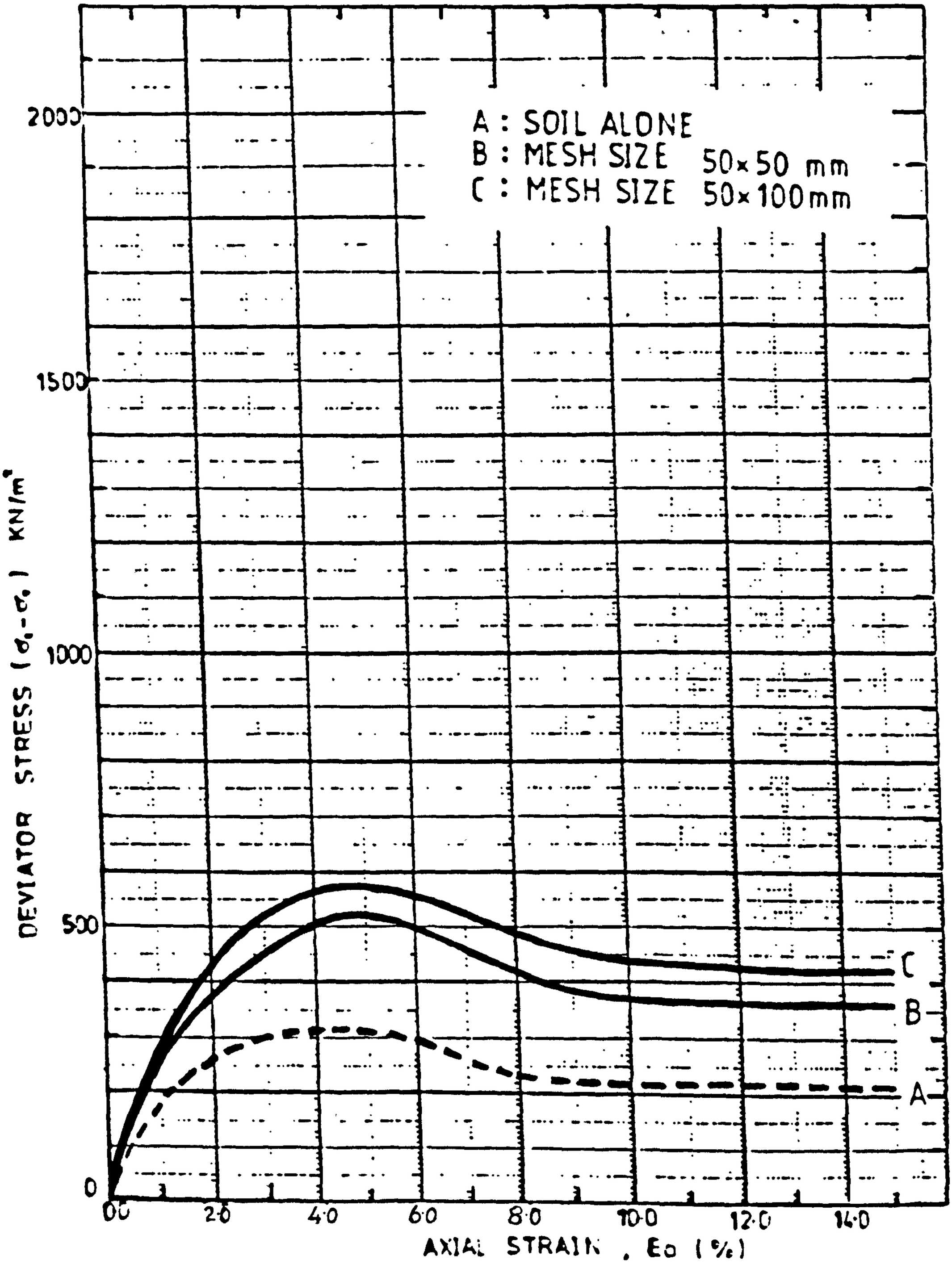

FIG. 5.42

SOIL TYPE	MID-ROSS SAND
MESH TYPE	7
MESH CONTENT	90 (m^2/m^2)% or 0·24 (%) by dry weight

$\sigma_3 = 50\ kN/m^2$

200mm × 155mm diam. TRIAXIAL TEST DATA

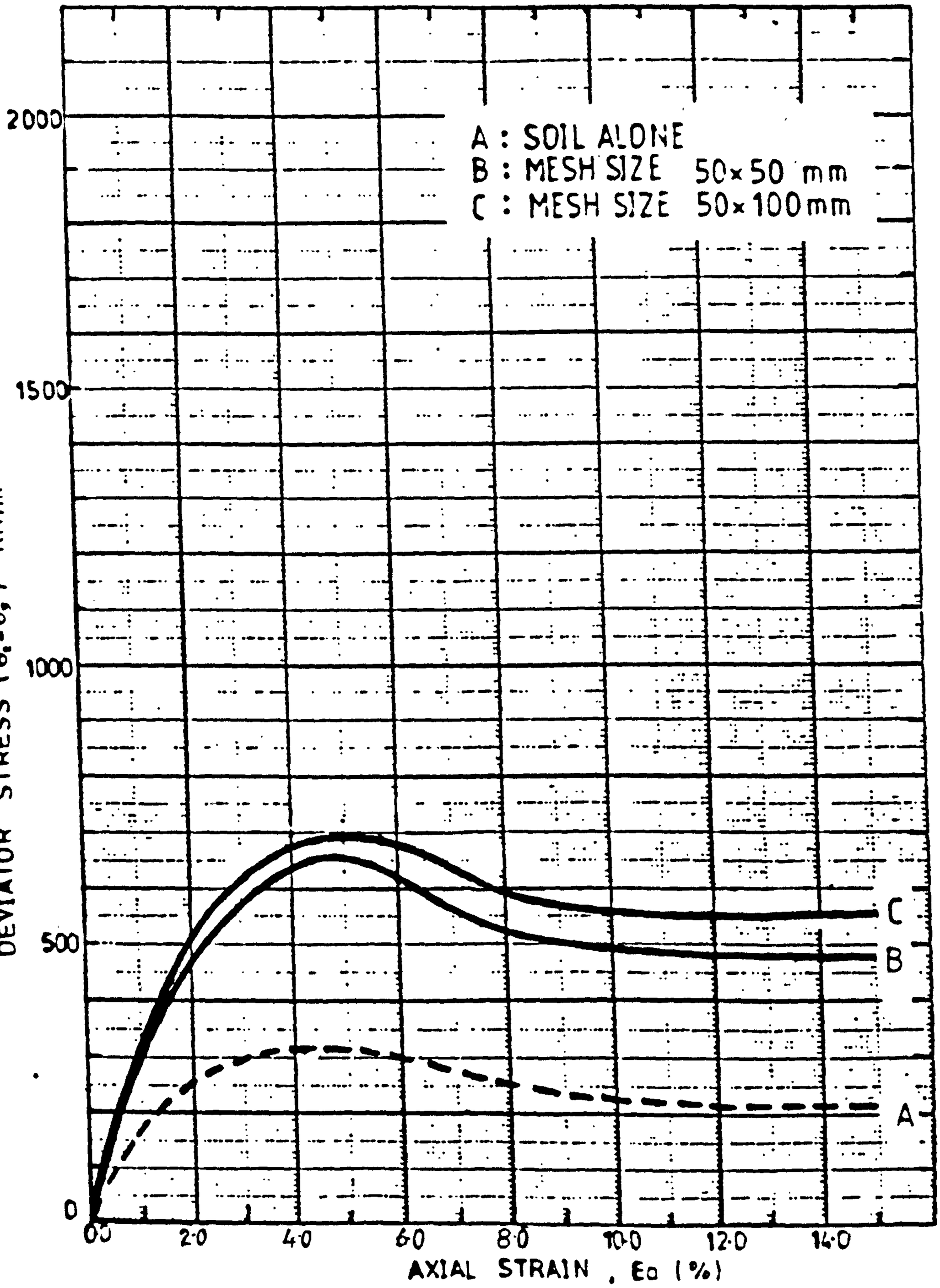

FIG. 5.43

SOIL TYPE	MID-ROSS SAND
MESH TYPE	7
MESH CONTENT	33 (m^2/m^3), or 0·09 (%) by dry weight

σ_3 = 150 KN/m²

200 mm × 155 mm diam. TRIAXIAL TEST DATA

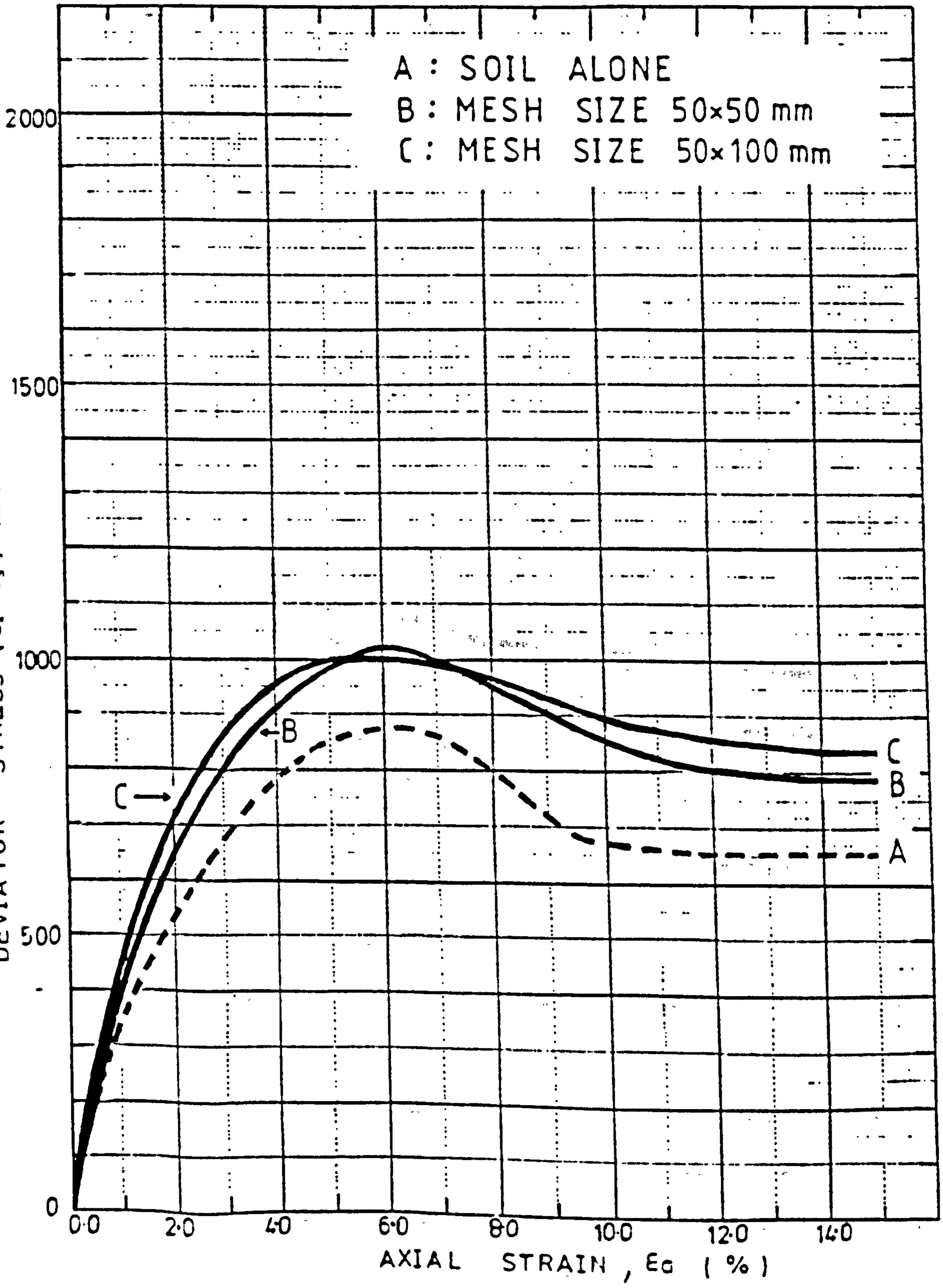

FIG. 5.44

SOIL TYPE	MID-ROSS SAND
MESH TYPE	7
MESH CONTENT	66 (m^2/m^3), or 0·18 (%) by dry weight

$\sigma_3 = 150\ kN/m^2$

200 mm × 155 mm diam. TRIAXIAL TEST DATA

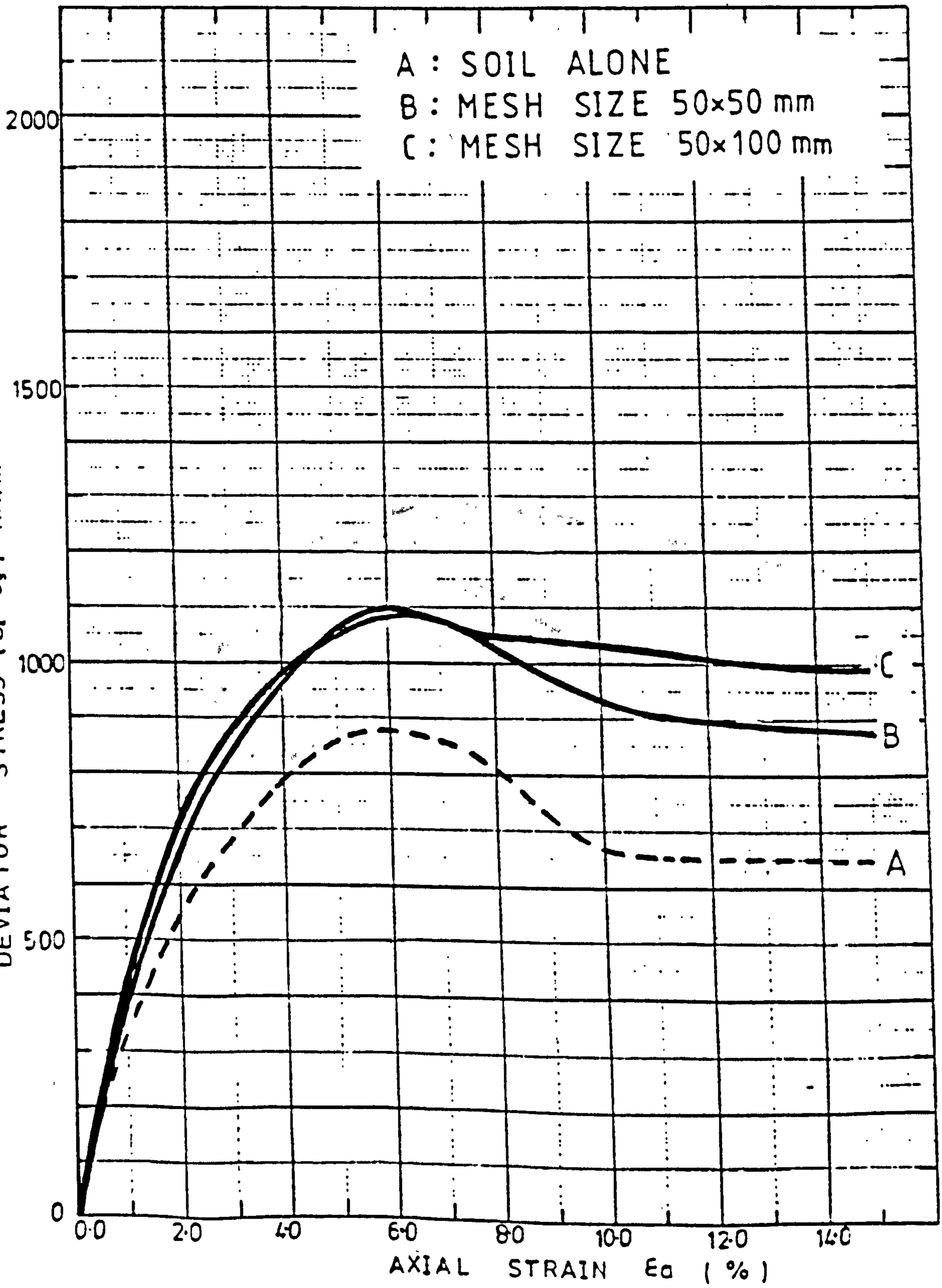

FIG. 5.45

SOIL TYPE	MID-ROSS SAND
MESH TYPE	7
MESH CONTENT	90 (m^2/m^3), or 0·24 (%) by dry weight

$\sigma_3 = 150\ kN/m^2$

200 mm × 155 mm diam. TRIAXIAL TEST DATA

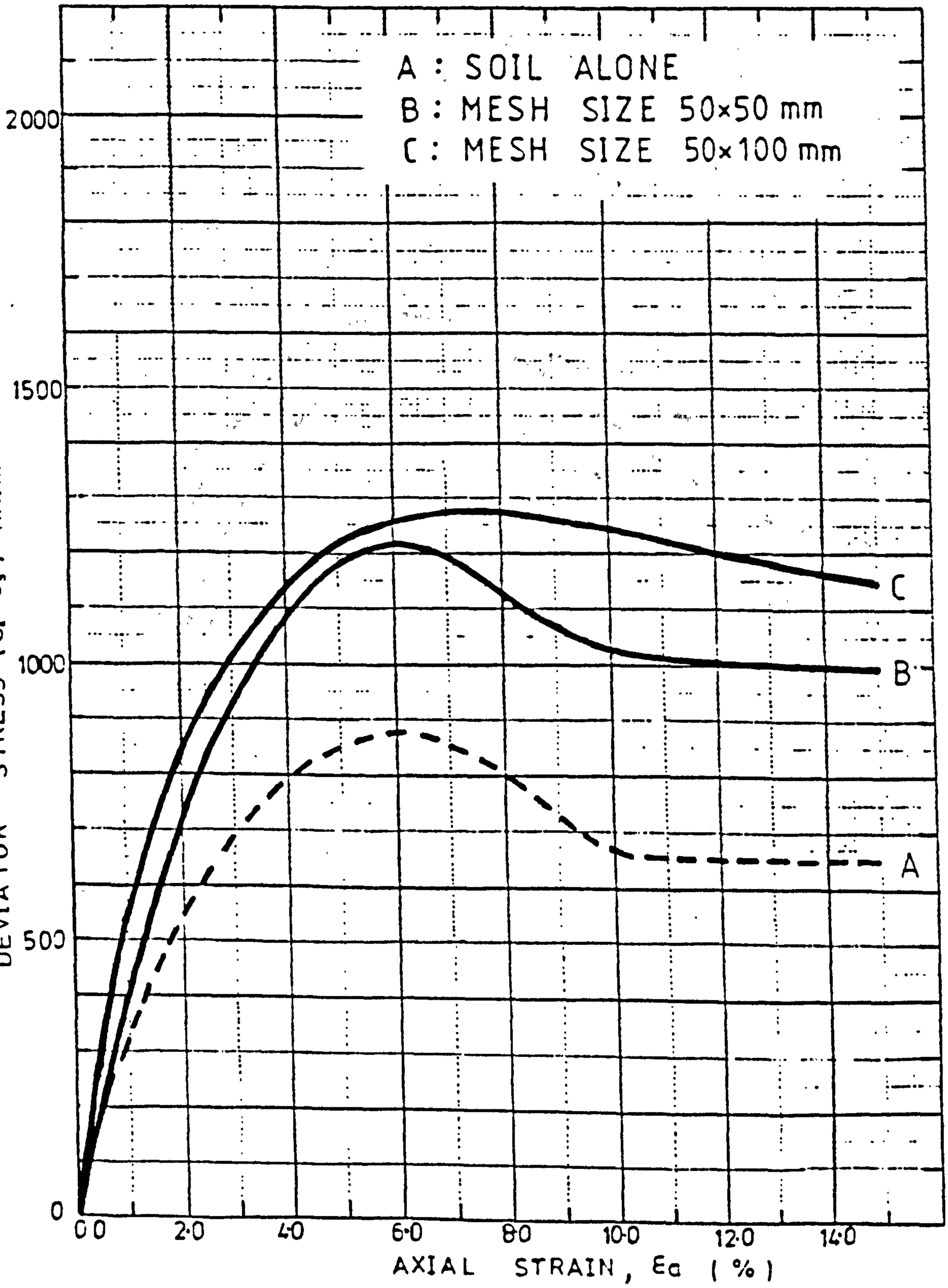

FIG. 5.46

SOIL TYPE	MID-ROSS SAND
MESH TYPE	7
MESH CONTENT	33 (m^2/m^3), or 0·09 (%) by dry weight

$\sigma_3 = 300\ kN/m^2$

200 mm × 155 mm diam. TRIAXIAL TEST DATA

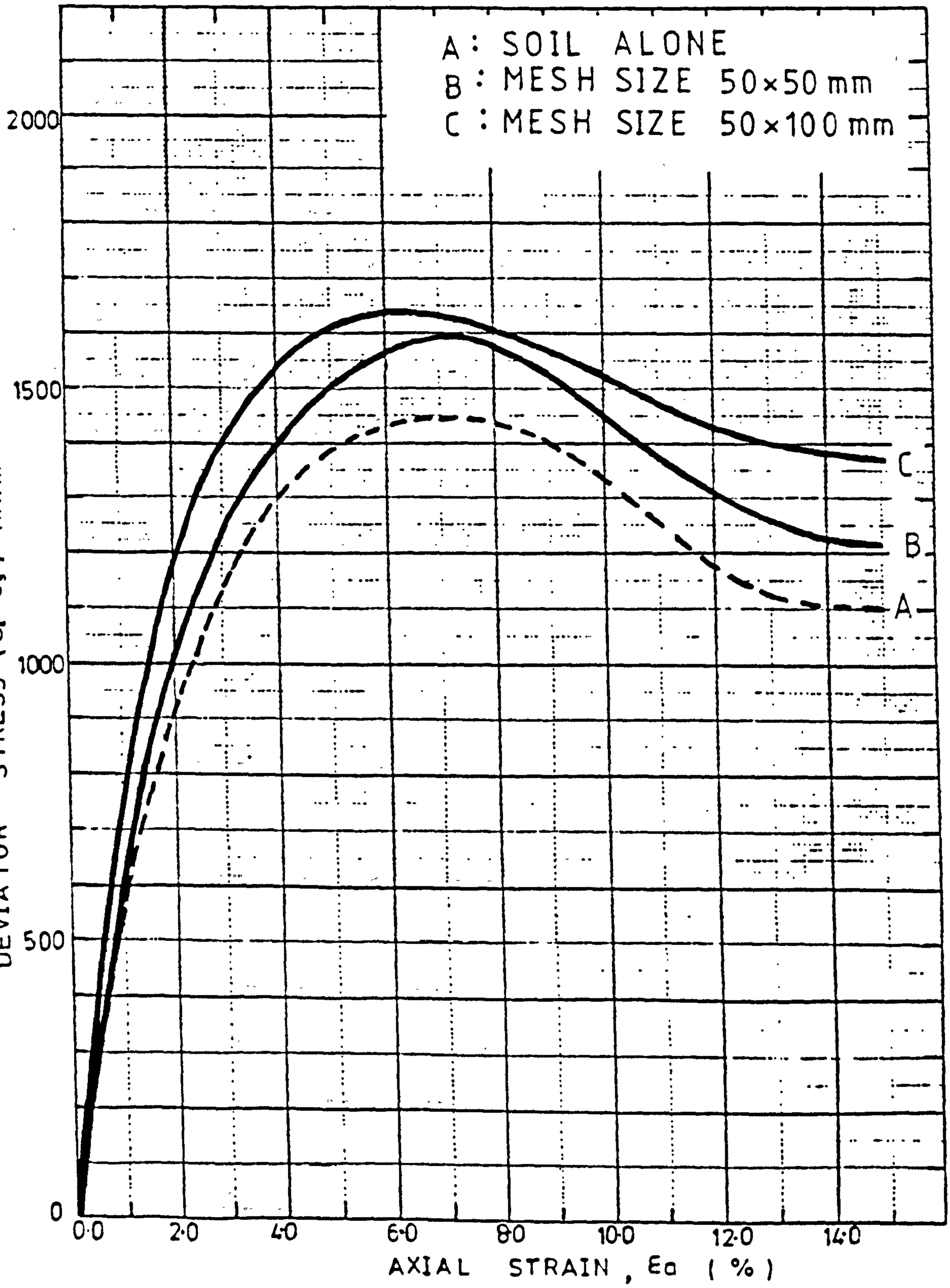

FIG. 5.47

SOIL TYPE	MID-ROSS SAND
MESH TYPE	7
MESH CONTENT	66 (m^2/m^3), or 0·18 (%) by dry weight

$\sigma_3 = 300\ kN/m^2$

200 mm × 155 mm diam. TRIAXIAL TEST DATA

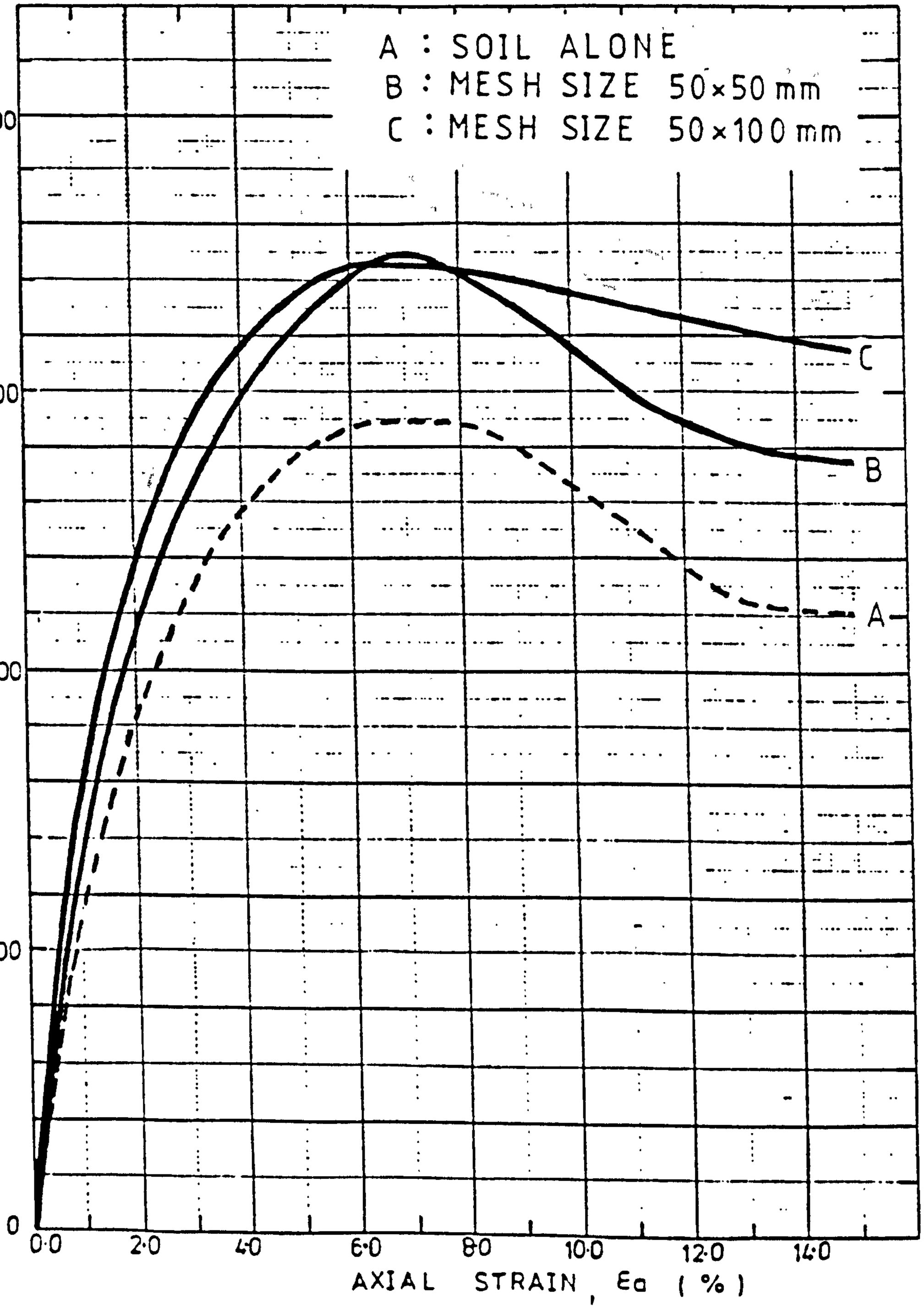

FIG. 5.48

SOIL TYPE	MID-ROSS SAND
MESH TYPE	7
MESH CONTENT	90 (m^2/m^3), or 0·24 (%) by dry weight

$\sigma_3 = 300\ kN/m^2$

200 mm × 155 mm diam. TRIAXIAL TEST DATA

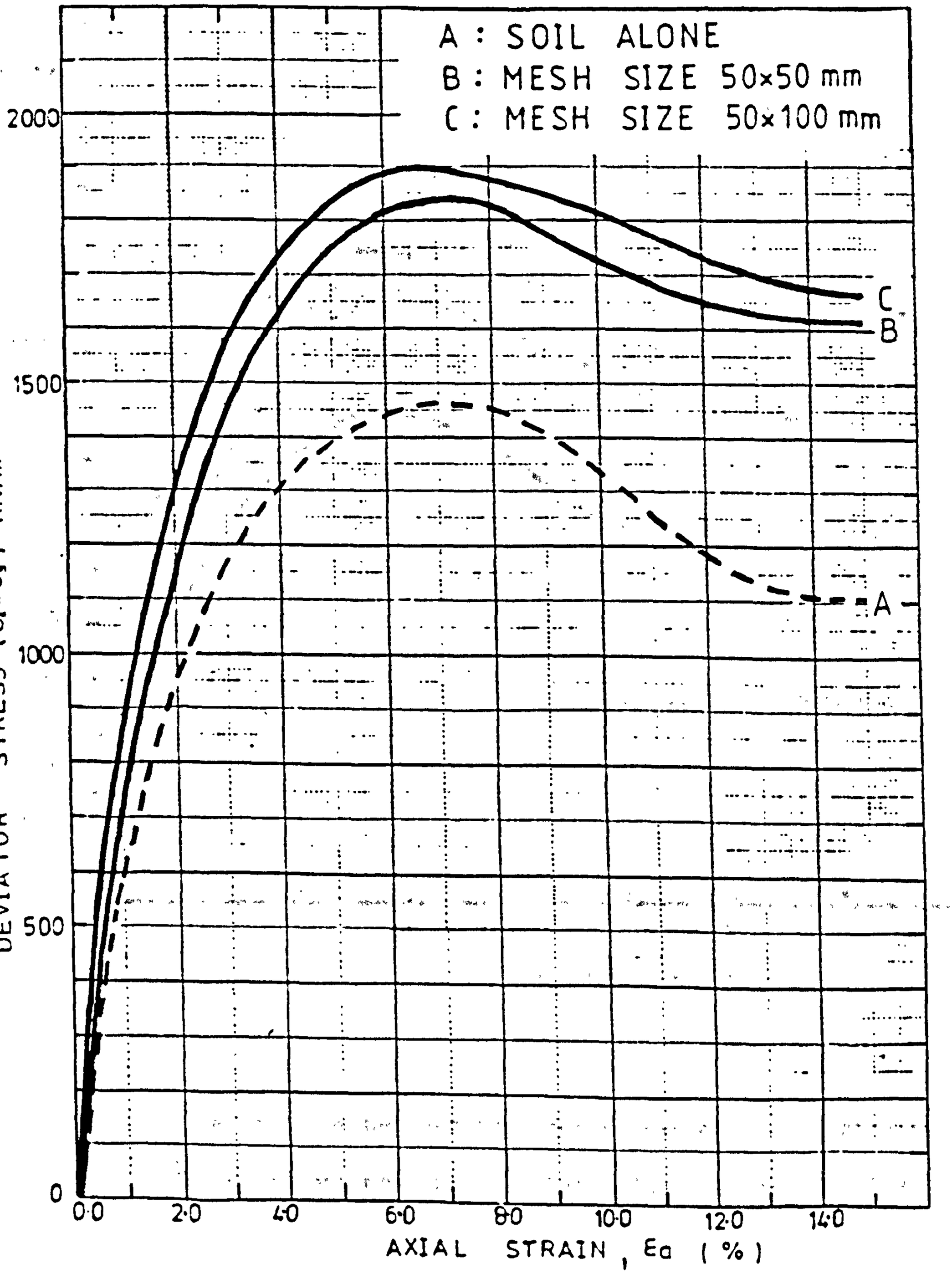

FIG. 5.49

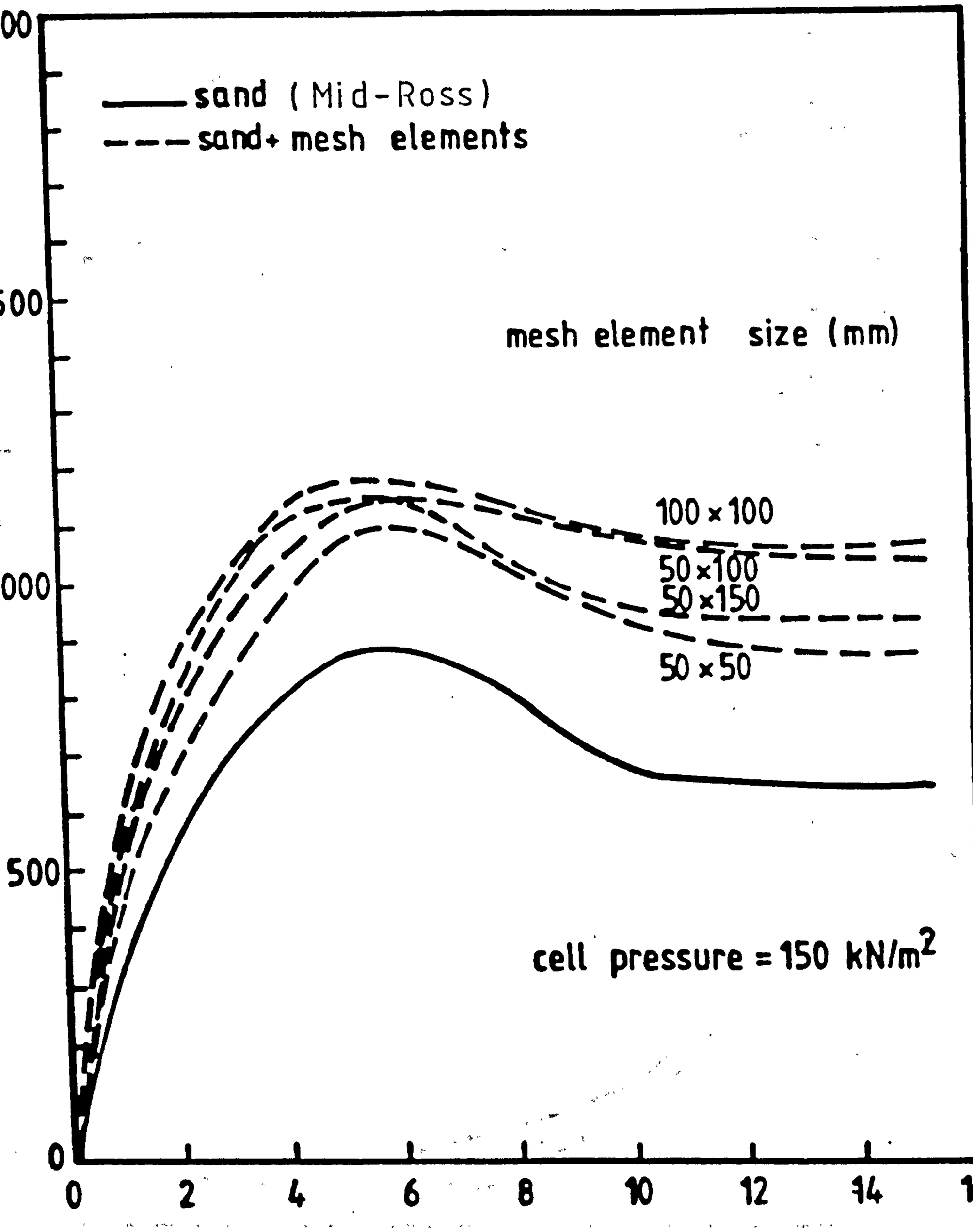

Relationships between deviator stress and axial strain for different mesh sizes. Mesh element content 0.18% by weight.

FIG. 5.50

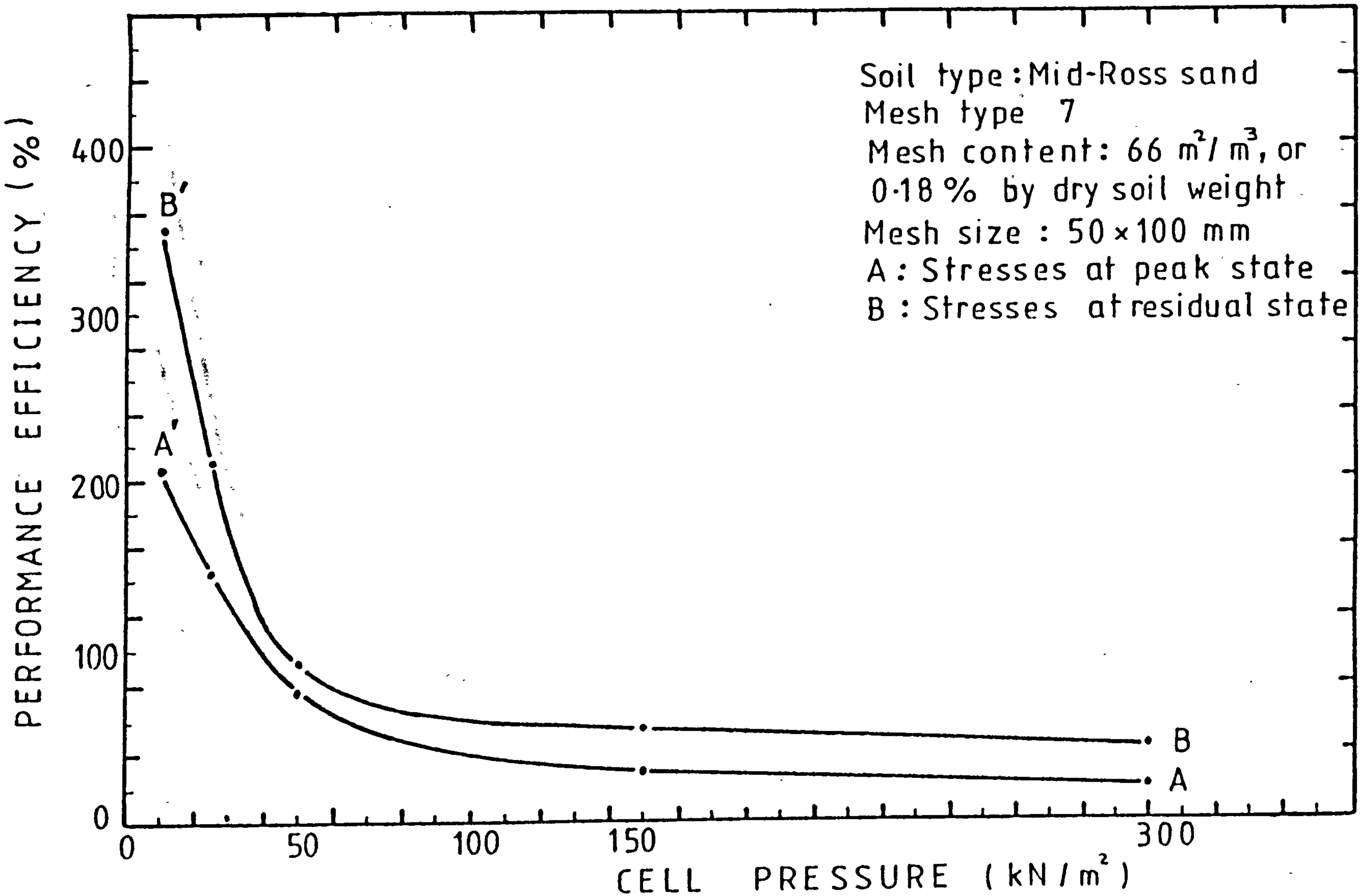
Soil type : Mid-Ross sand
Mesh type 7
Mesh content : 66 m²/m³, or
0·18 % by dry soil weight
Mesh size : 50 × 100 mm
A : Stresses at peak state
B : Stresses at residual state
PERFORMANCE EFFICIENCY (%)
400
300
200
100
0
B'
A'
B
A
0
50
100
150
300
CELL PRESSURE (kN/m²)

FIG. 5.51

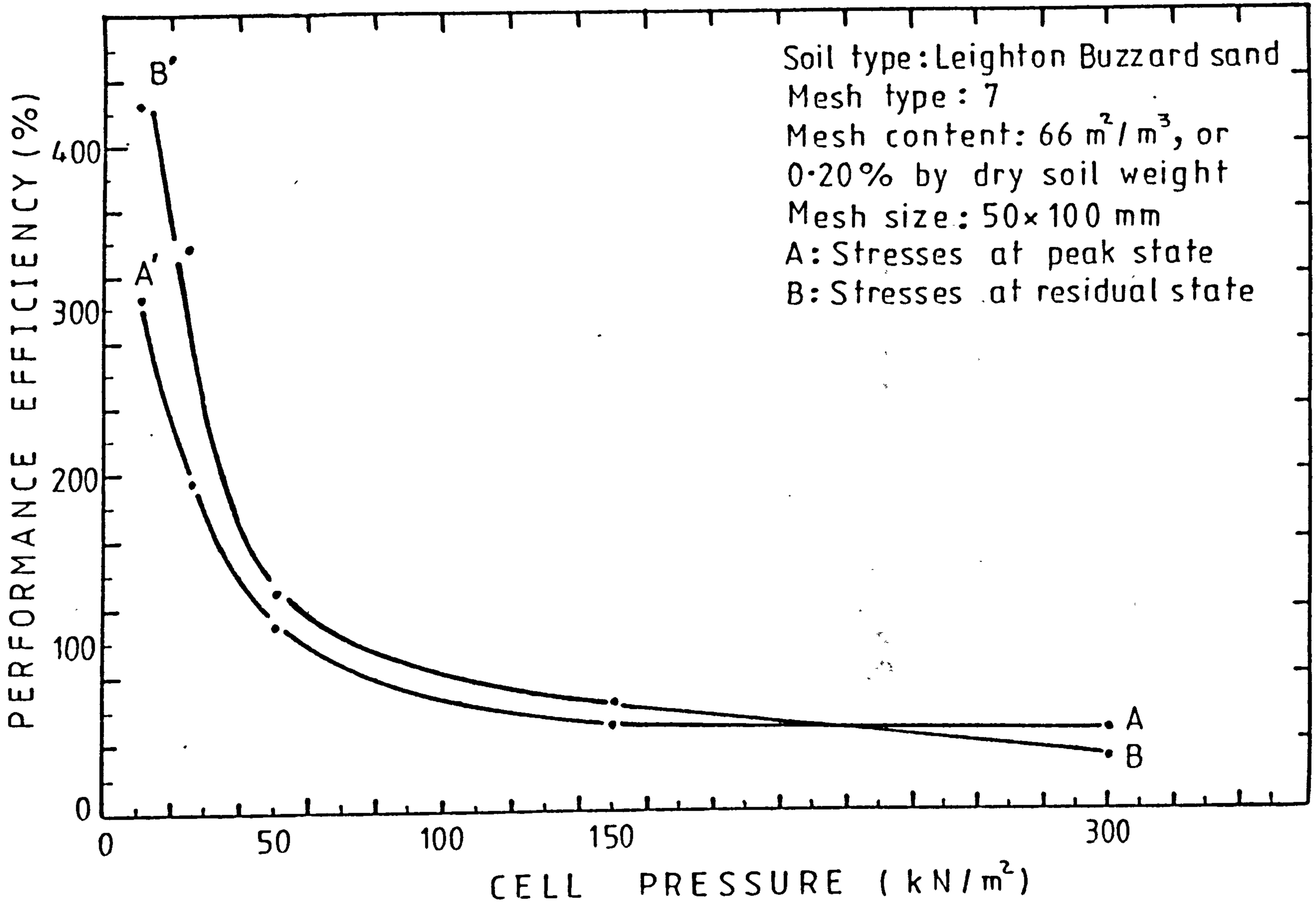
Soil type: Leighton Buzzard sand
Mesh type: 7
Mesh content: 66 m²/m³, or
0·20% by dry soil weight
Mesh size: 50×100 mm
A: Stresses at peak state
B: Stresses at residual state
PERFORMANCE EFFICIENCY (%)
400
300
200
100
0
B'
A'
A
B
0
50
100
150
300
CELL PRESSURE (kN/m²)

MOHR CIRCLES

&

BI-LINEAR FAILURE

ENVELOPE ANALYSIS

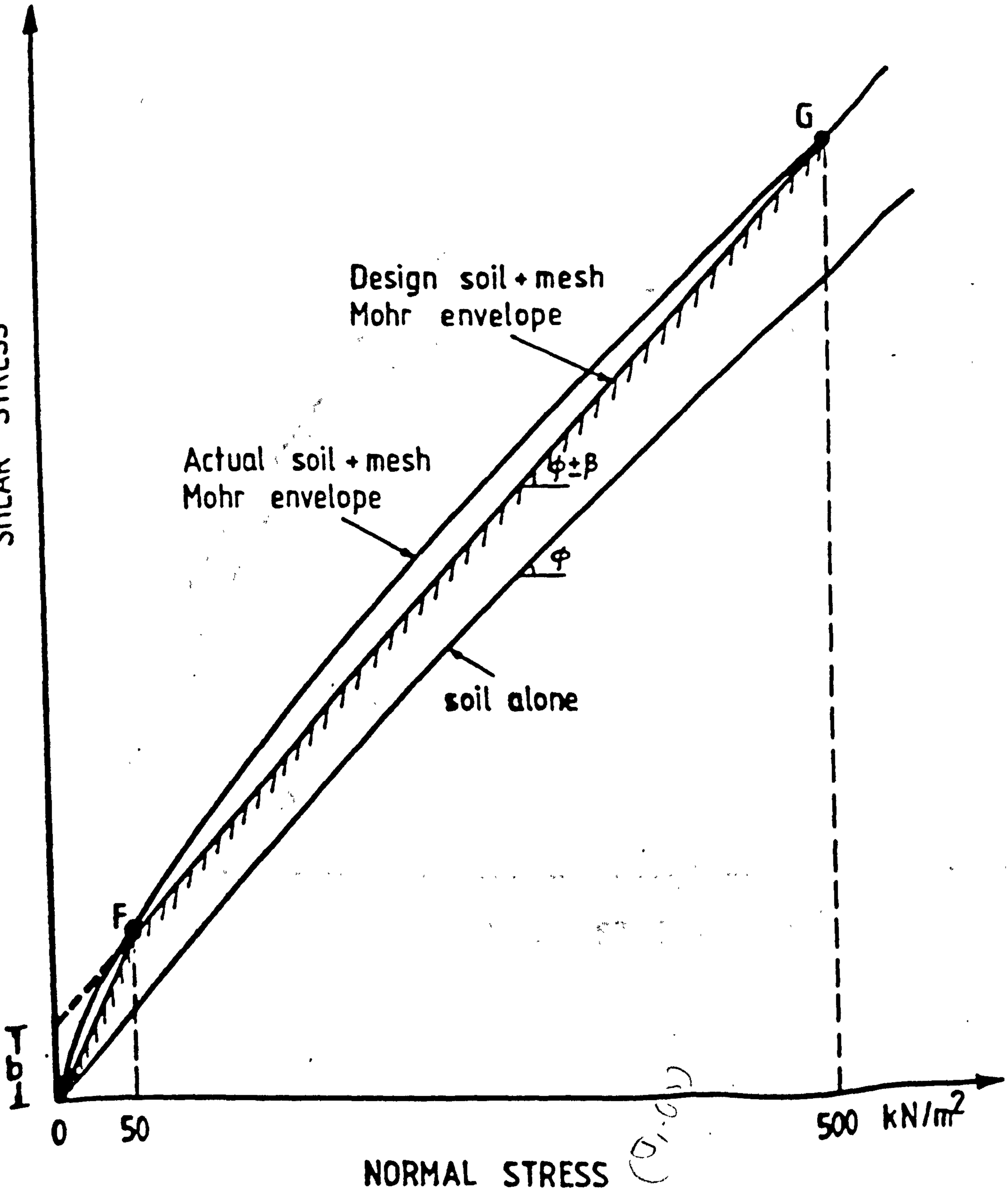

FIG. 5.52 Bi-linear failure envelope

FIG. 5.53

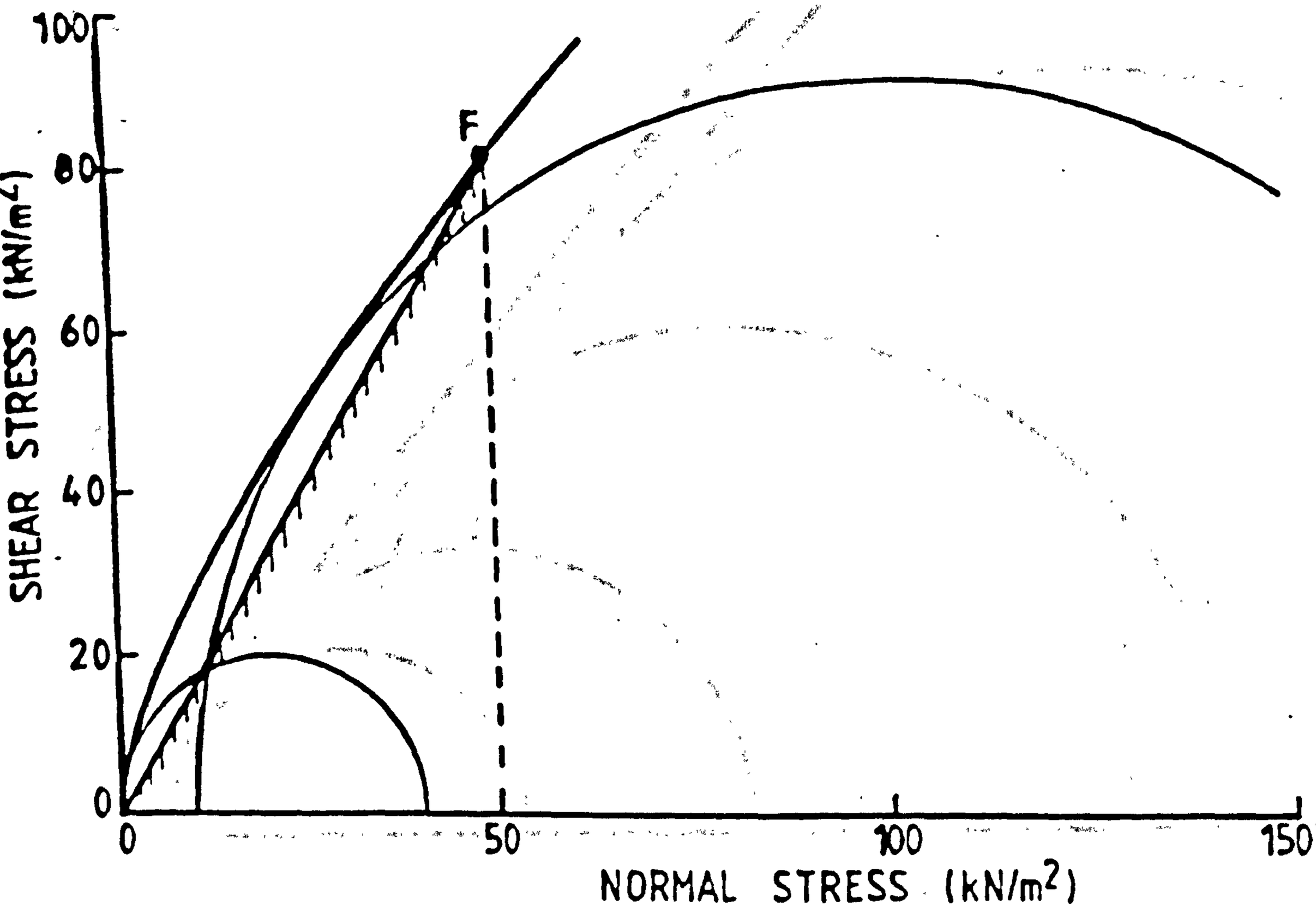

LOW STRESS BEHAVIOUR

(50 × 50 mm elements)

FIG. 5.54

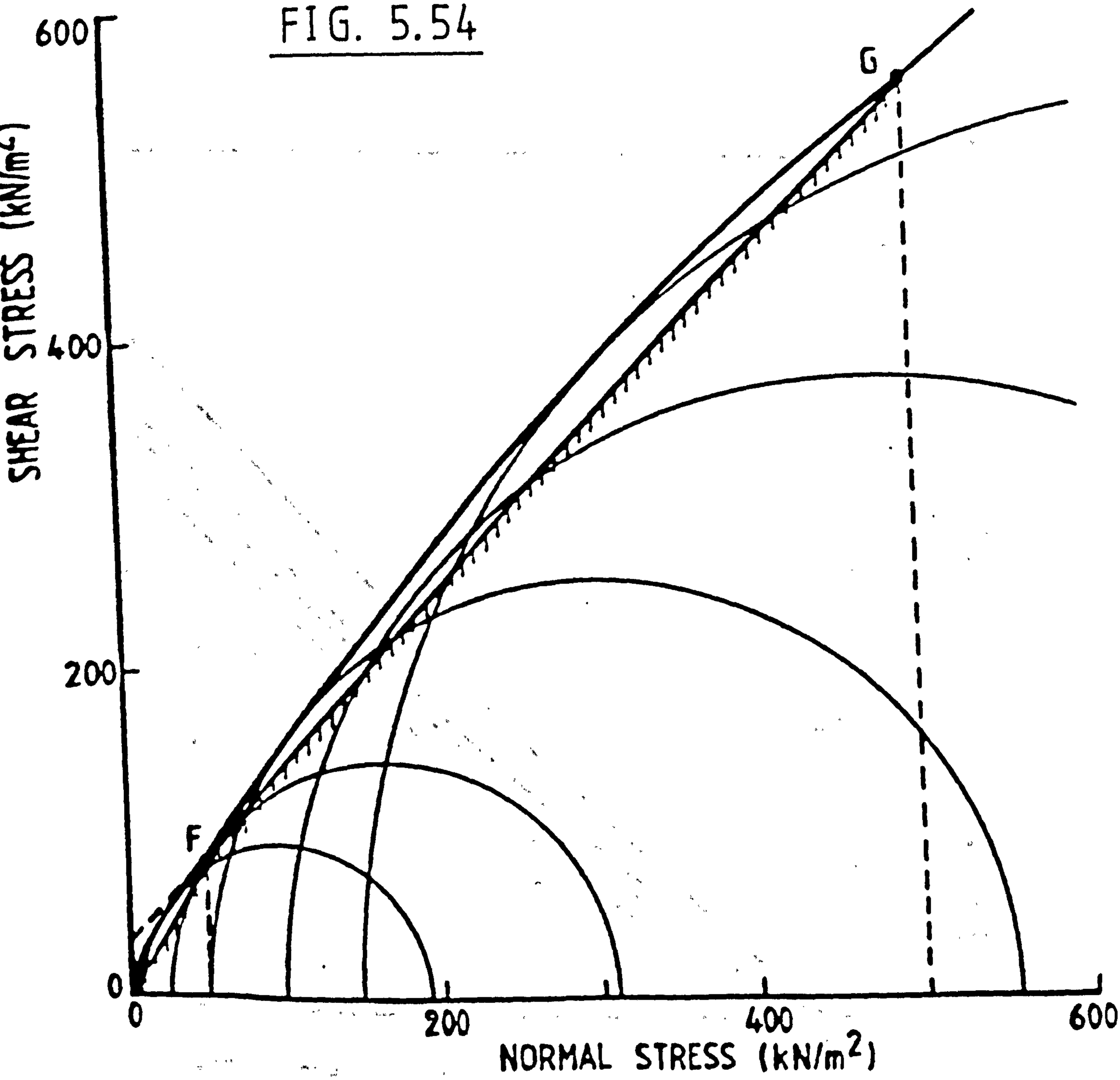

OVERALL STRESS BEHAVIOUR

(50×50 mm elements)

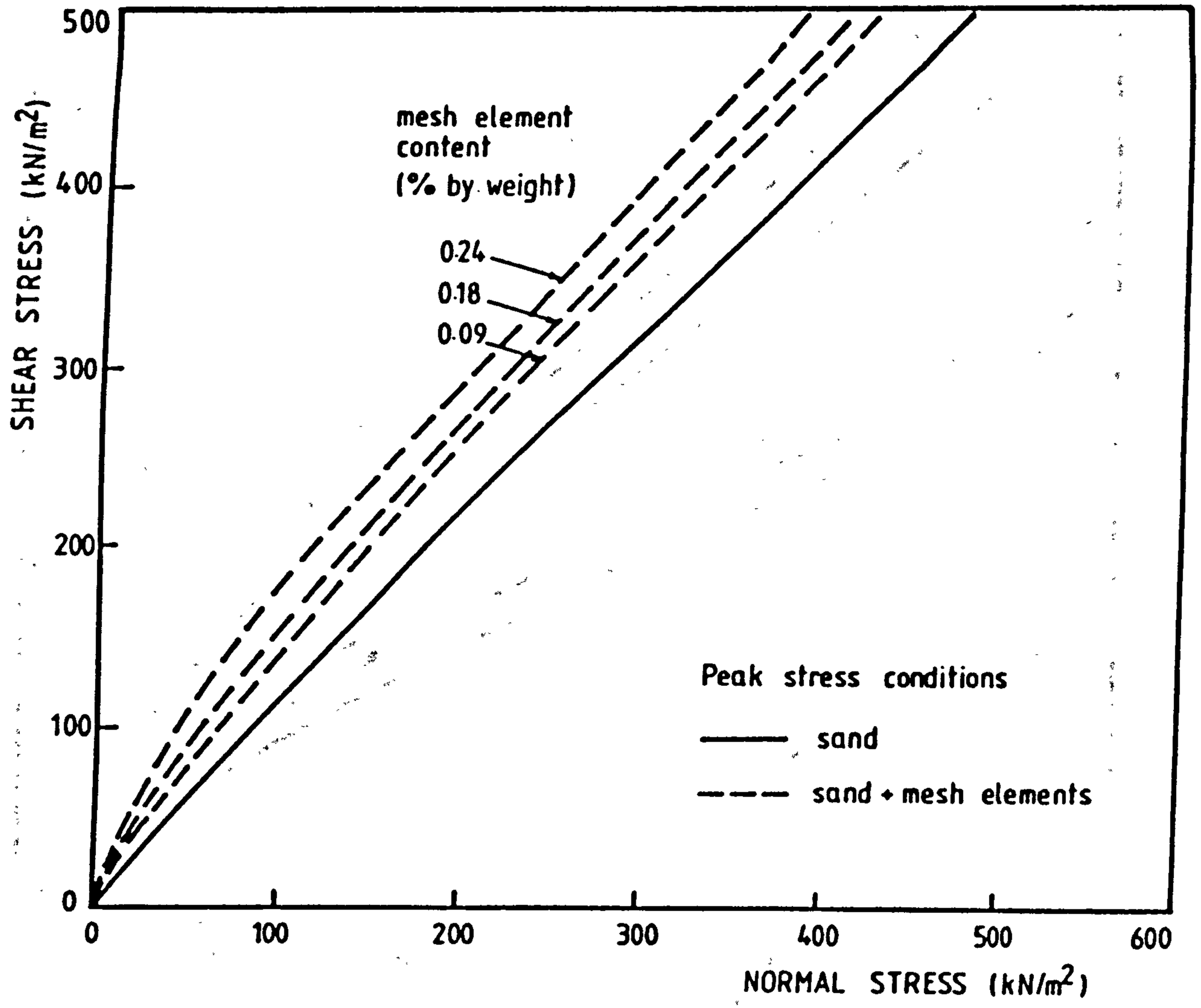

FIG. 5.55 Mohr envelopes at peak stress conditions

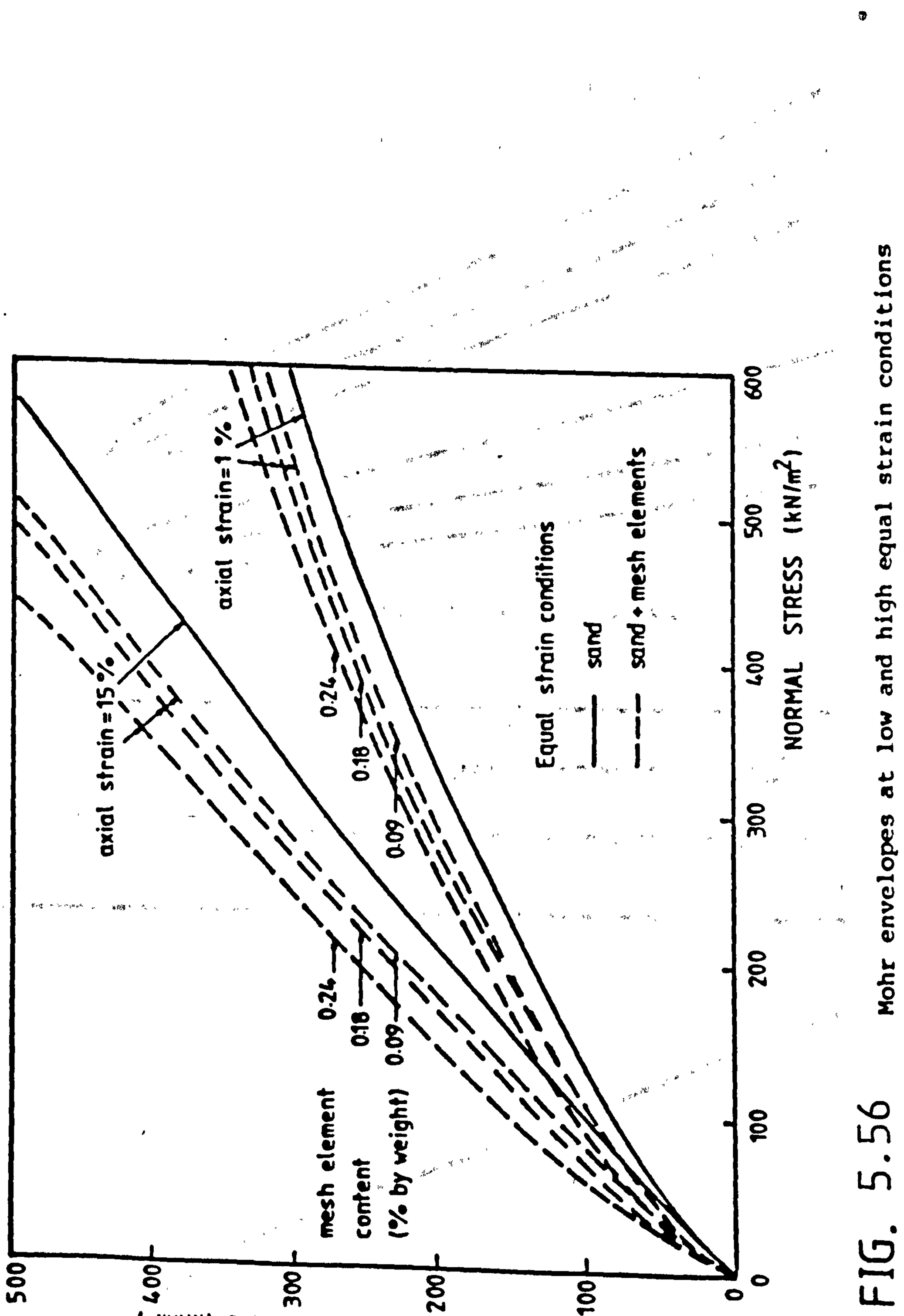
Mohr envelopes at low and high equal strain conditions
SHEAR STRESS (kN/m²)
NORMAL STRESS (kN/m²)
Equal strain conditions
sand
sand + mesh elements
axial strain=1%
axial strain=15%
mesh element content (% by weight)
0.0
0.09
0.18
0.24
0
100
200
300
400
500
600

FIG. 5.56

TEXT CUT OFF IN ORIGINAL

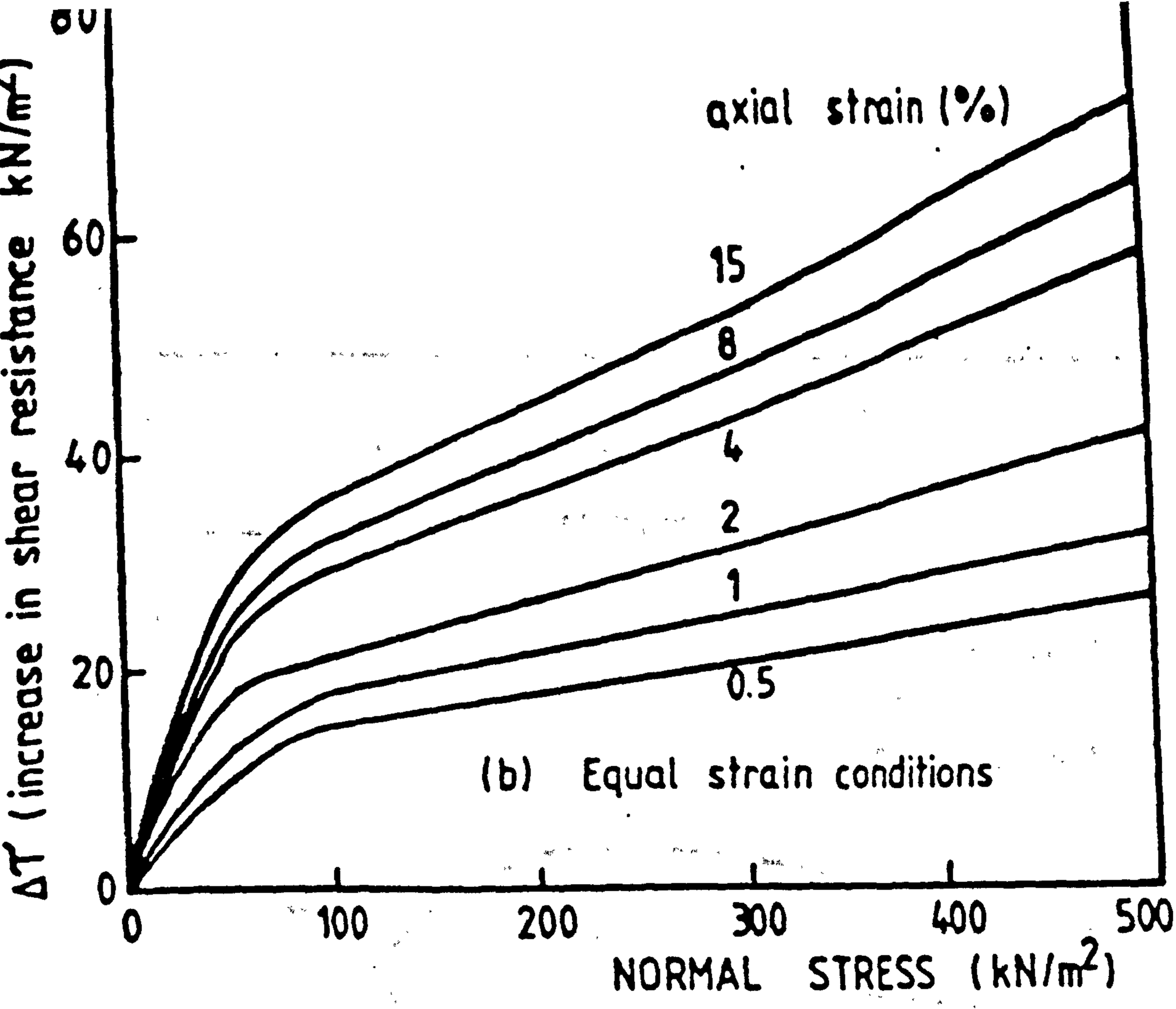

FIG. 5.57 Increase in shear resistance with normal stress

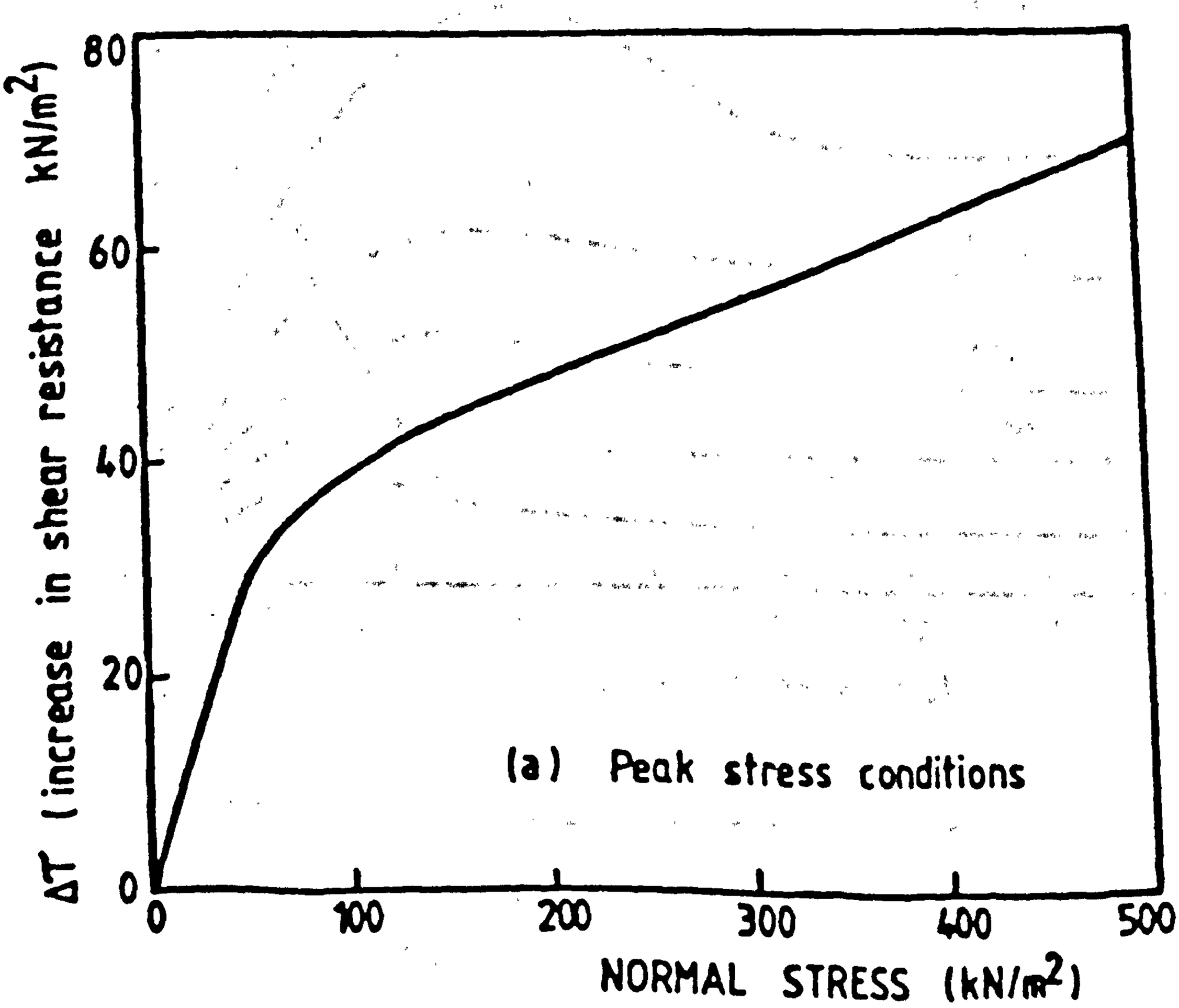

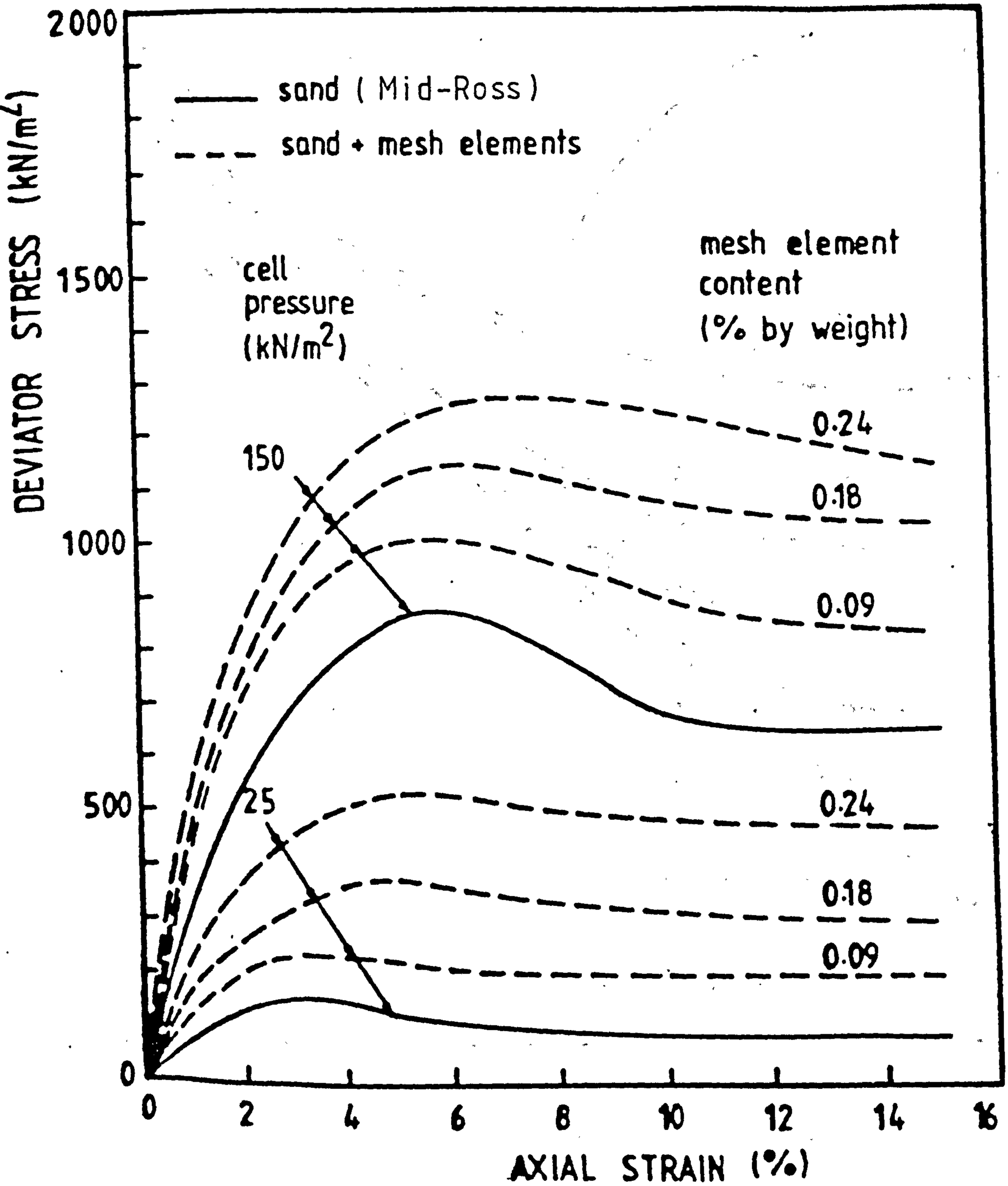

FIG. 5.58 Relationships between deviator stress and axial strain for different proportions of mesh elements. Mesh size 50 x 100 mm.

FIG. 5.59

OVERALL STRESS BEHAVIOUR

Soil type :
Mid-Ross sand
Mesh type : 7
Mesh content :
33 m^2/m^3
or 0·09 % by soil weight.

STRESS STATE :
PEAK

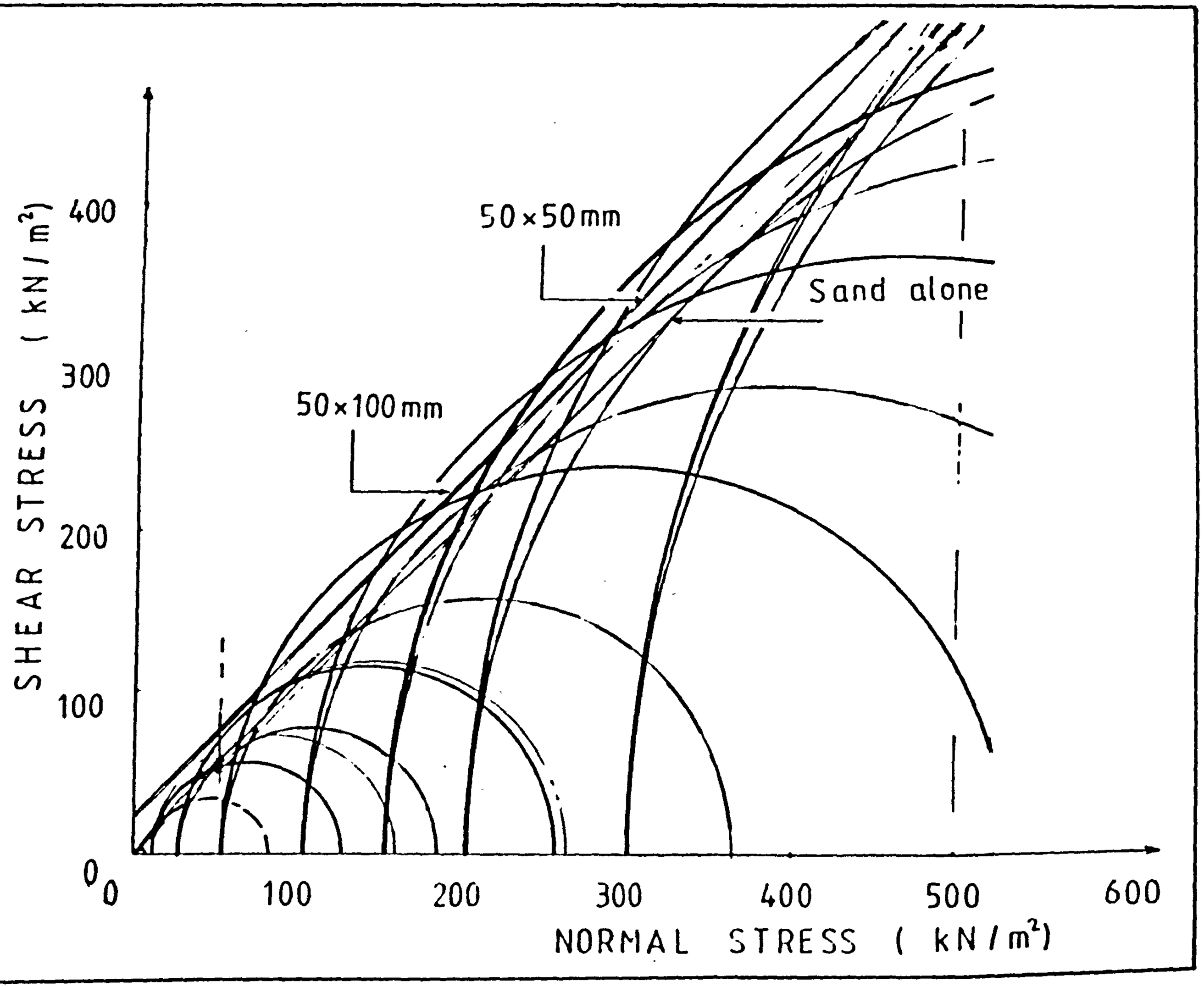

FIG. 5.60

OVERALL STRESS BEHAVIOUR

Soil type :
Mid-Ross sand
Mesh type : 7
Mesh content :
33 m^2/m^3
or 0.09 % by soil weight.

STRESS STATE:

RESIDUAL

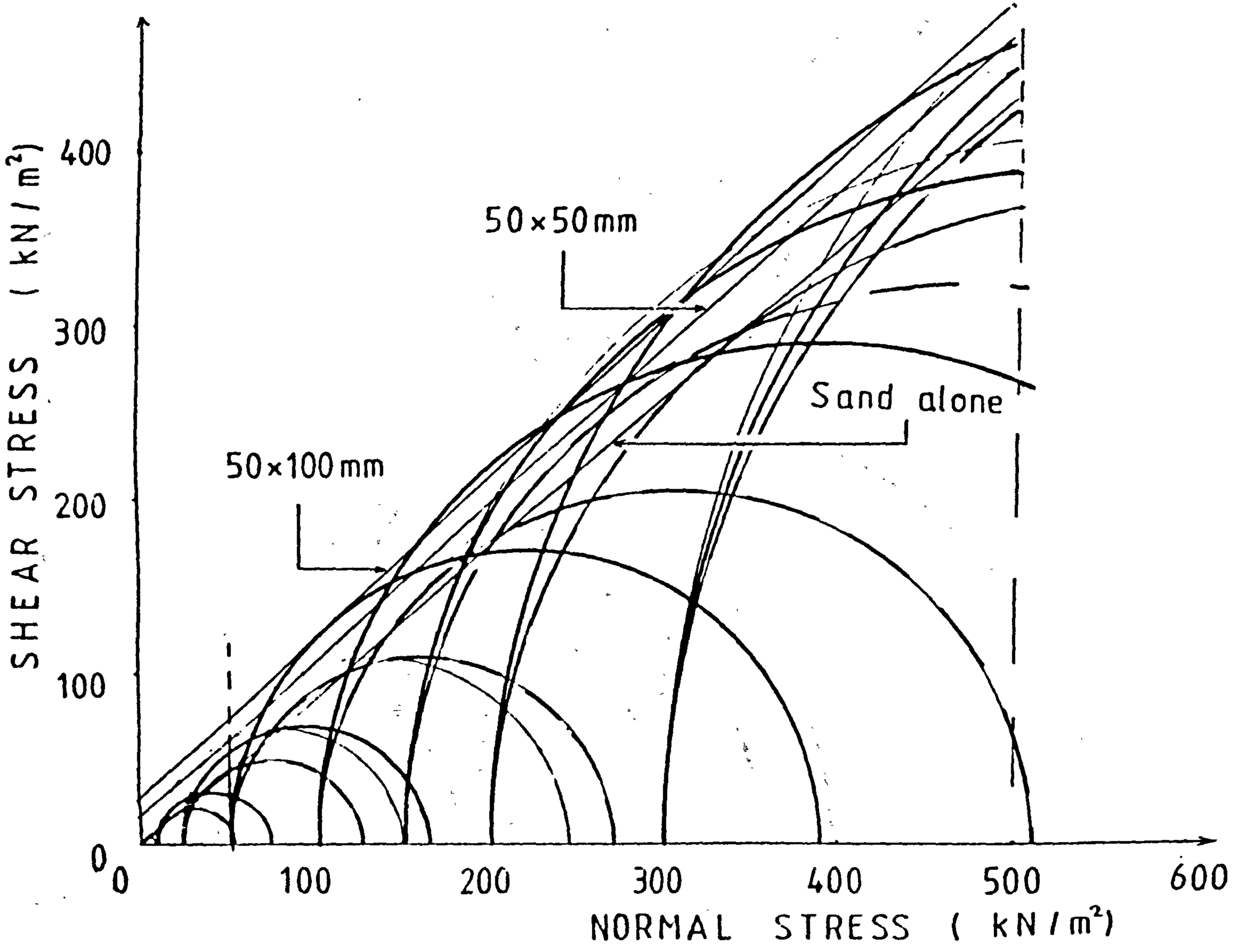

FIG. 5.61

OVERALL STRESS BEHAVIOUR

Soil type :
Mid-Ross sand
Mesh type : 7
Mesh content :
66 m^2/m^3
or 0·18 % by soil weight.

STRESS STATE :

PEAK

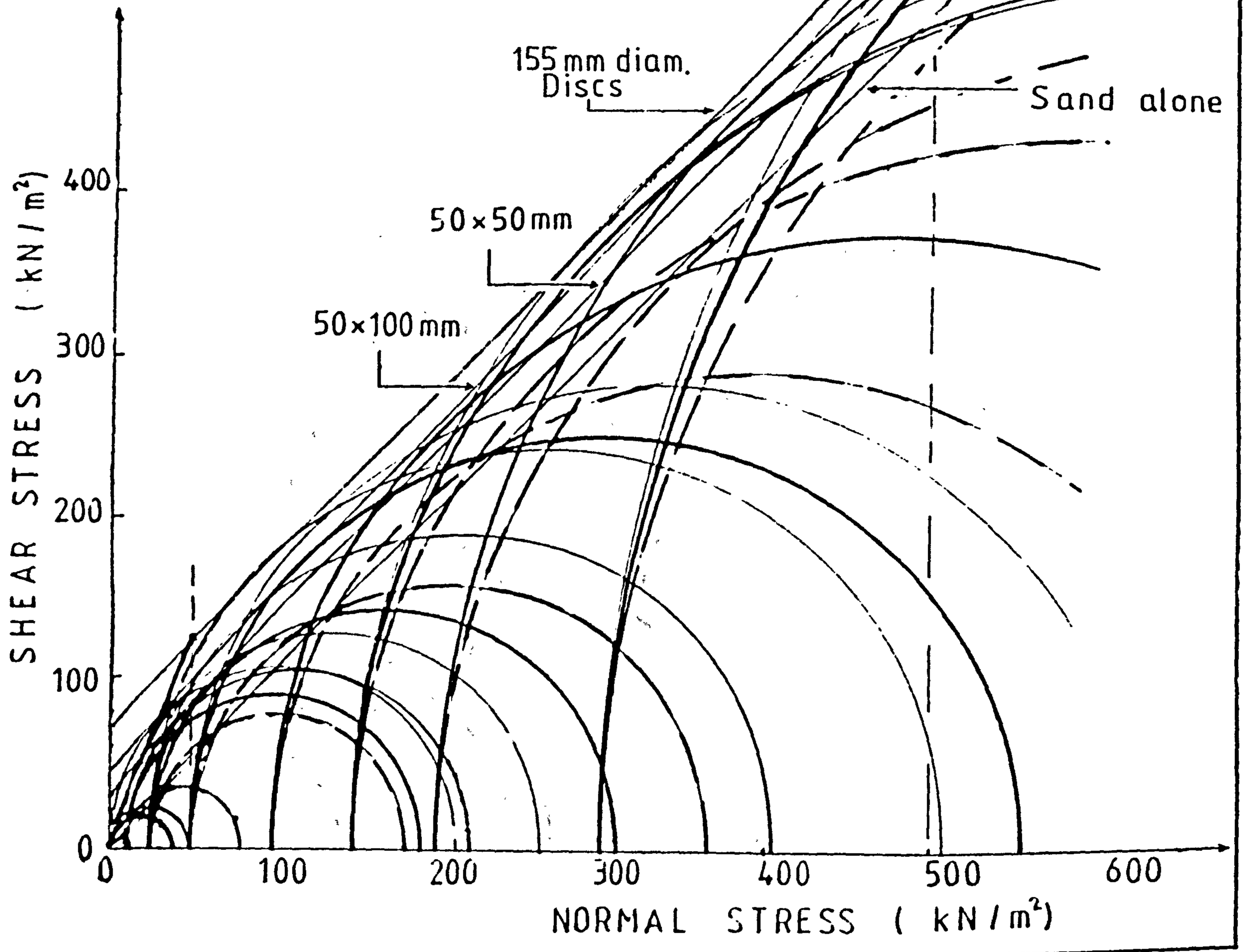

FIG. 5.62

OVERALL STRESS BEHAVIOUR

Soil type:
Mid-Ross sand
Mesh type : 7
Mesh content:
66 m^2/m^3
or 0·18 % by soil weight.

STRESS STATE:

RESIDUAL

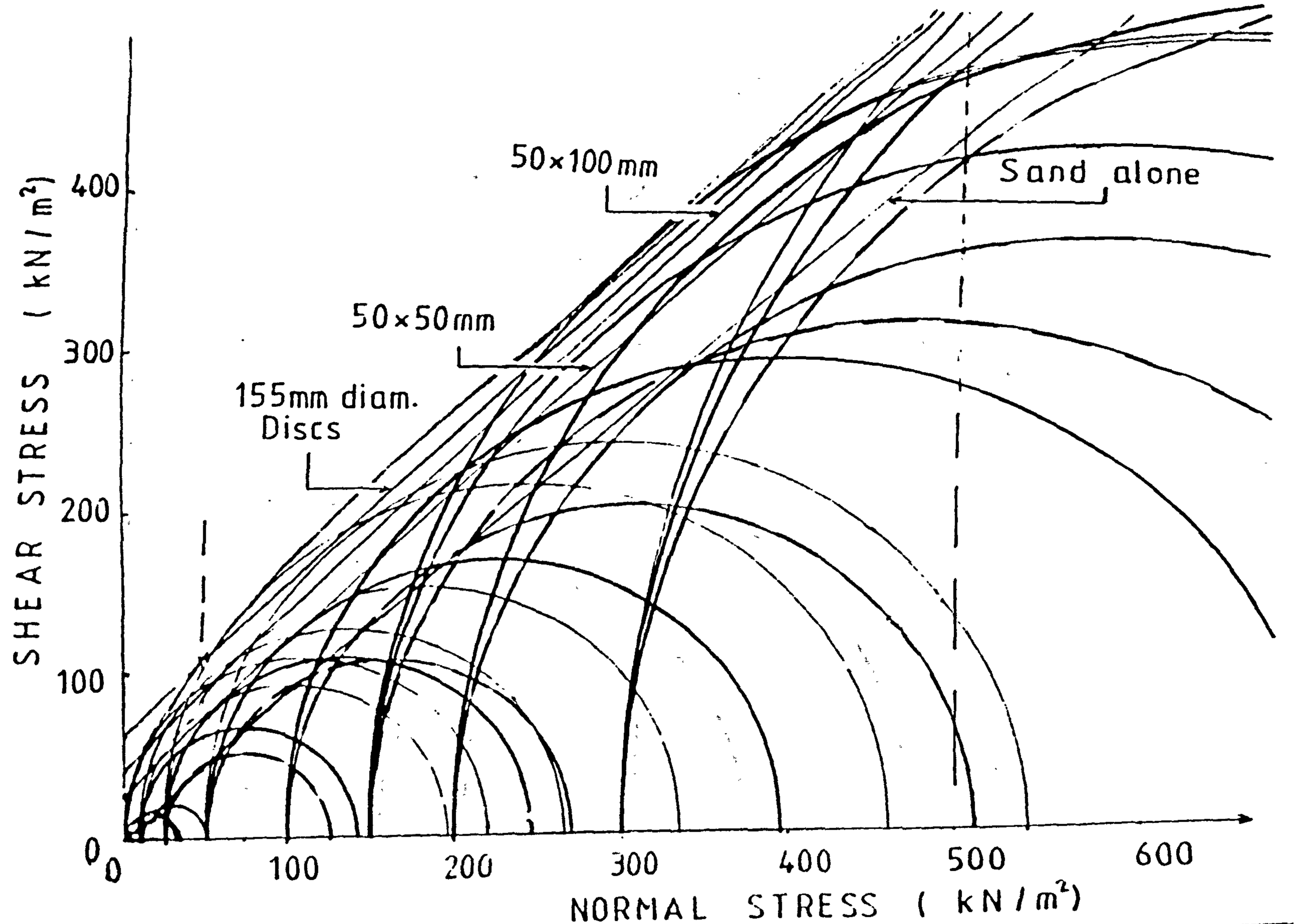

FIG. 5.63

OVERALL STRESS BEHAVIOUR

Soil type:
Mid-Ross sand
Mesh type : 7
Mesh content:
90 m^2/m^3
or 0·24 % by soil weight.

STRESS STATE:
PEAK

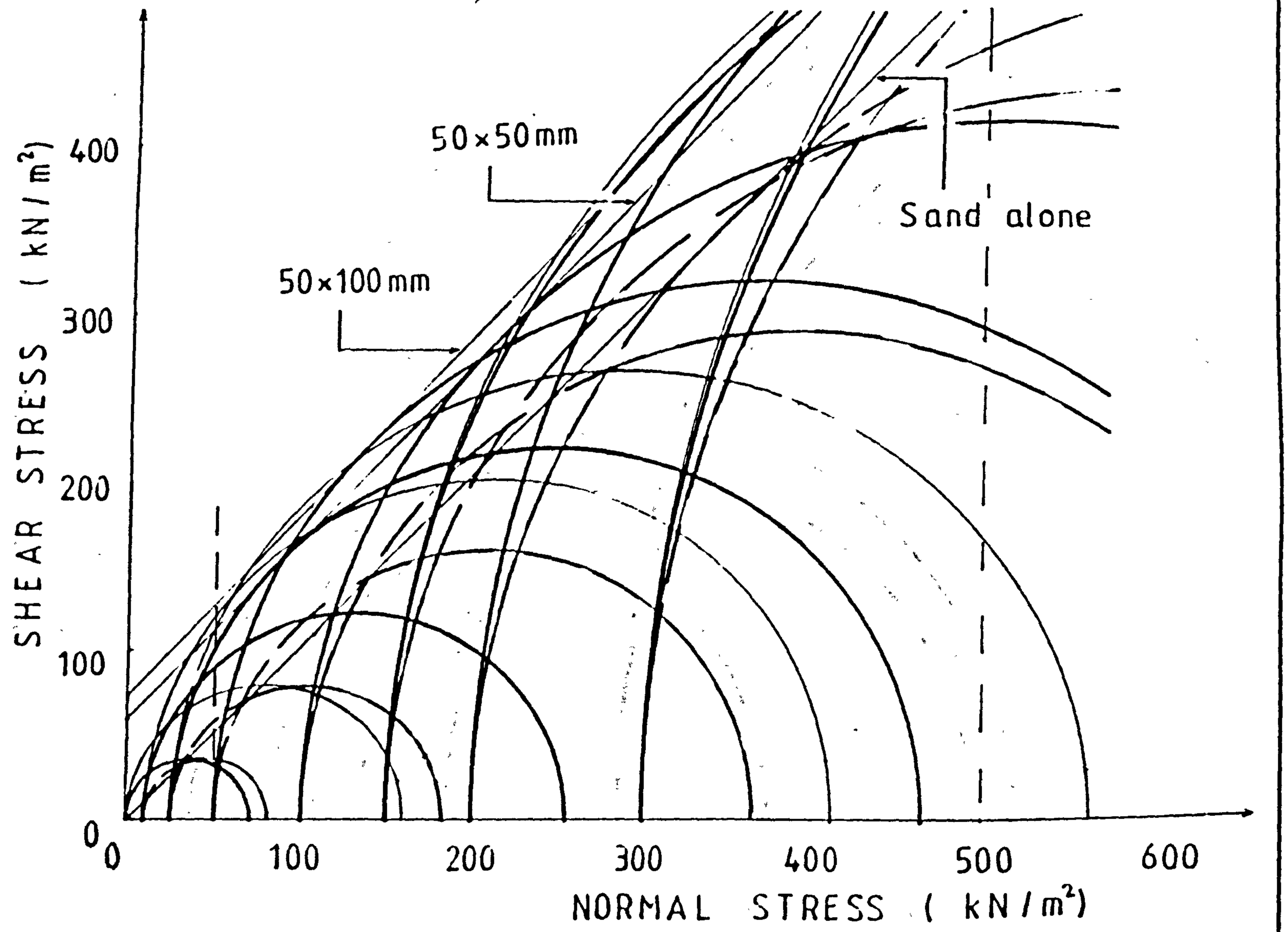

FIG. 5.64

OVERALL STRESS BEHAVIOUR

Soil type :
Mid-Ross sand
Mesh type : 7
Mesh content :
90 m^2/m^3
or 0·24 % by soil weight.

STRESS STATE :

RESIDUAL

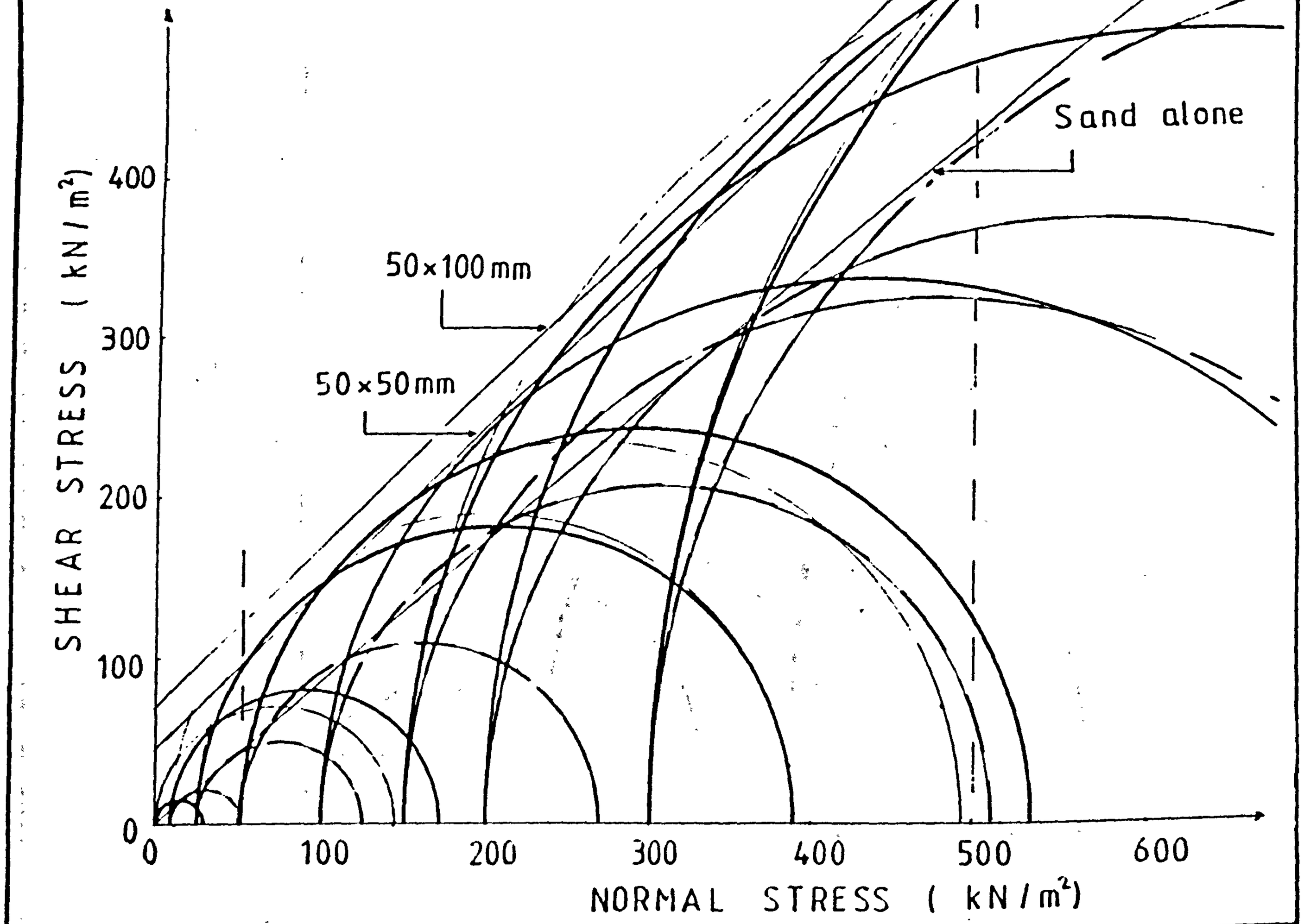

150

FIG. 5.65

OVERALL STRESS BEHAVIOUR

Soil type :
Leighton Buzzard sand
Mesh type : 7
Mesh content :
33 m^2/m^3
or 0·1 % by soil weight.

STRESS STATE :
PEAK

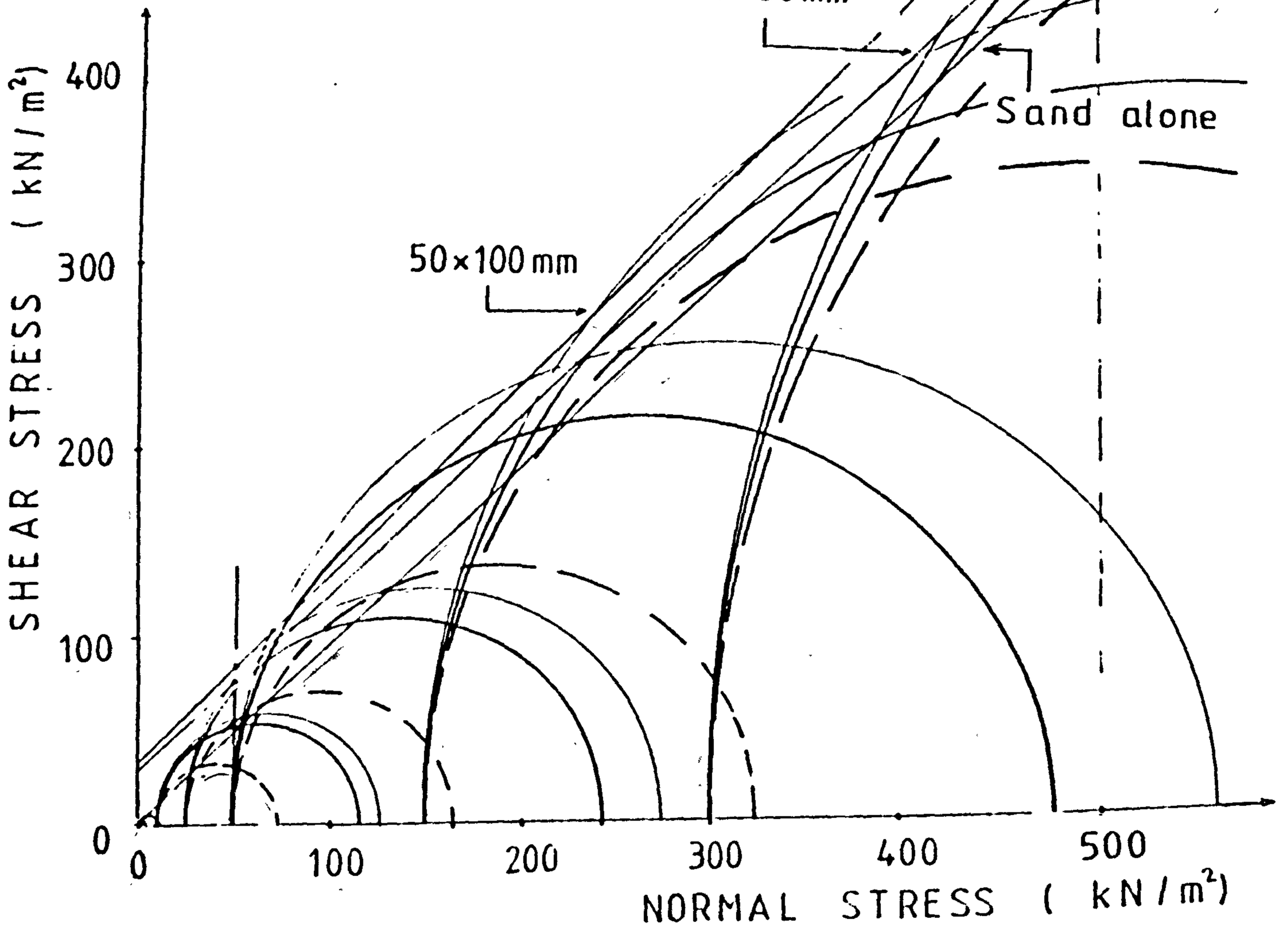

FIG. 5.66

OVERALL STRESS BEHAVIOUR

Soil type :
Leighton Buzzard sand
Mesh type : 7
Mesh content :
33 m^2/m^3
or 0·1 % by soil weight.

STRESS STATE :

RESIDUAL

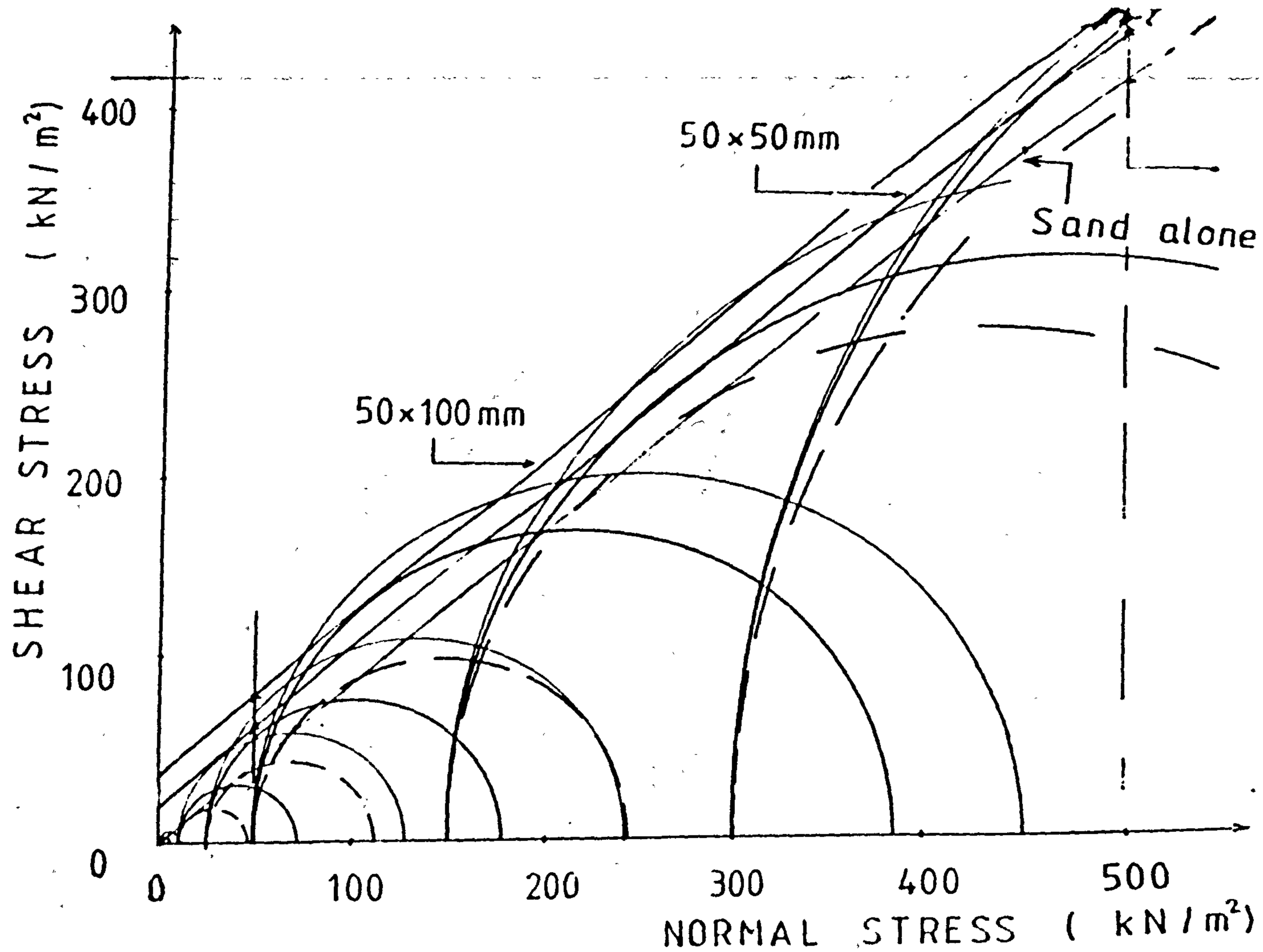

FIG. 5.67

OVERALL STRESS BEHAVIOUR

Soil type :
Leighton Buzzard sand
Mesh type : 7
Mesh content :
66 m^2/m^3
or 0·2 % by soil weight.

STRESS STATE :
PEAK

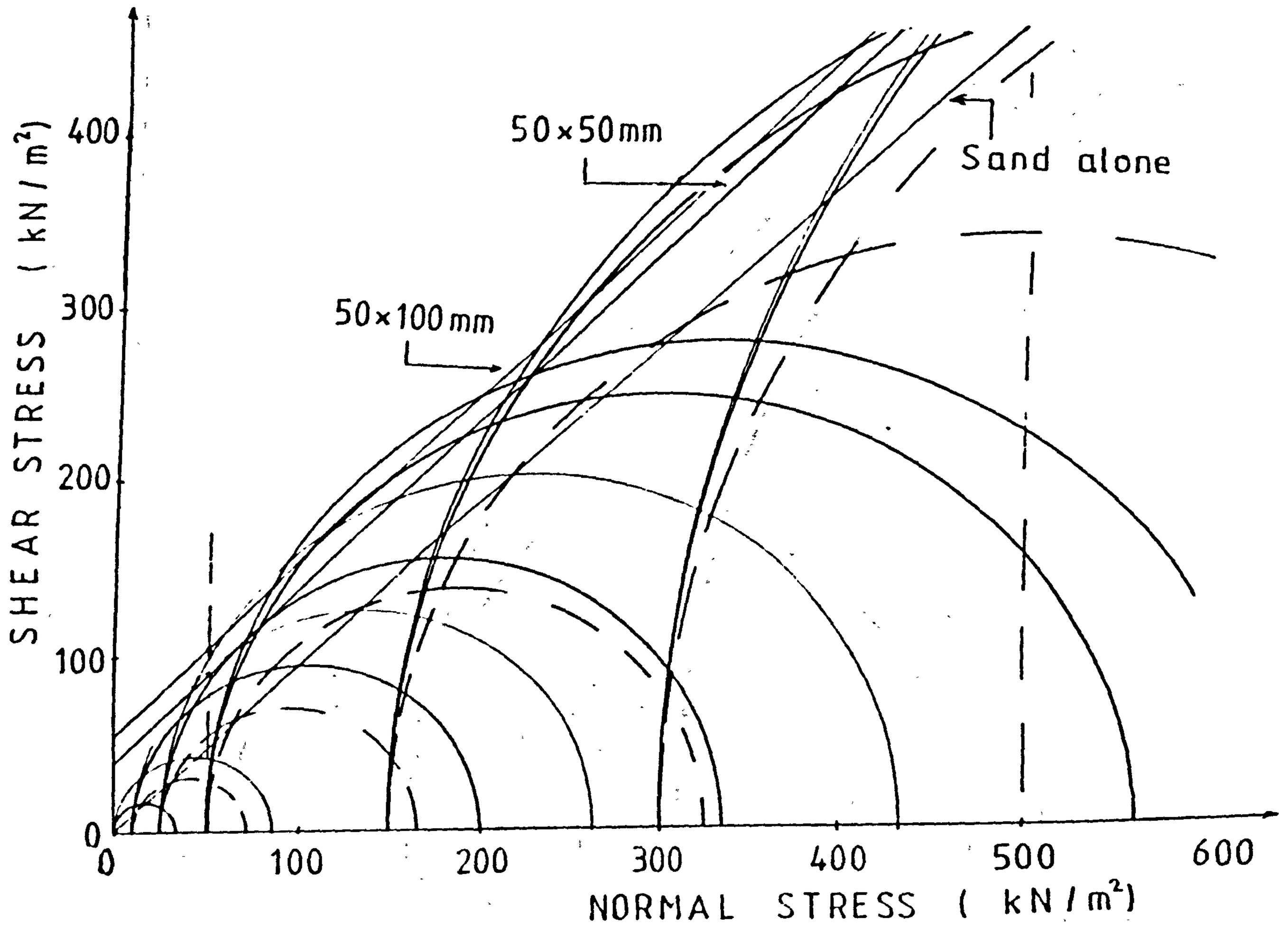

FIG. 5.68

OVERALL STRESS BEHAVIOUR

Soil type :
Leighton Buzzard sand
Mesh type : 7
Mesh content :
66 m^2/m^3
or 0·2 % by soil weight.

STRESS STATE:

RESIDUAL

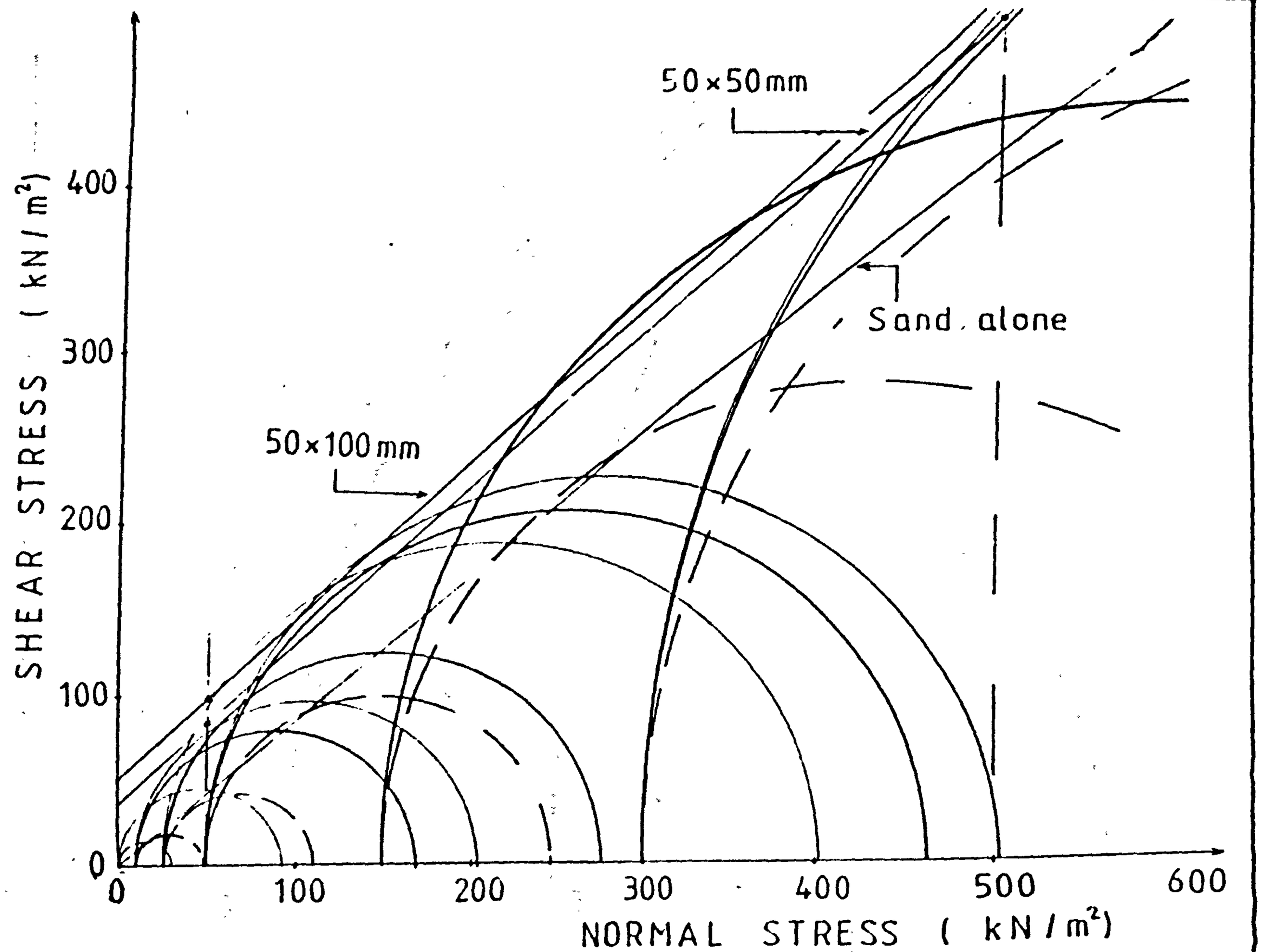

FIG. 5.69

OVERALL STRESS BEHAVIOUR

Soil type :
Leighton Buzzard sand
Mesh type : 7
Mesh content :
90 m^2/m^3
or 0·27 % by soil weight.

STRESS STATE:
PEAK

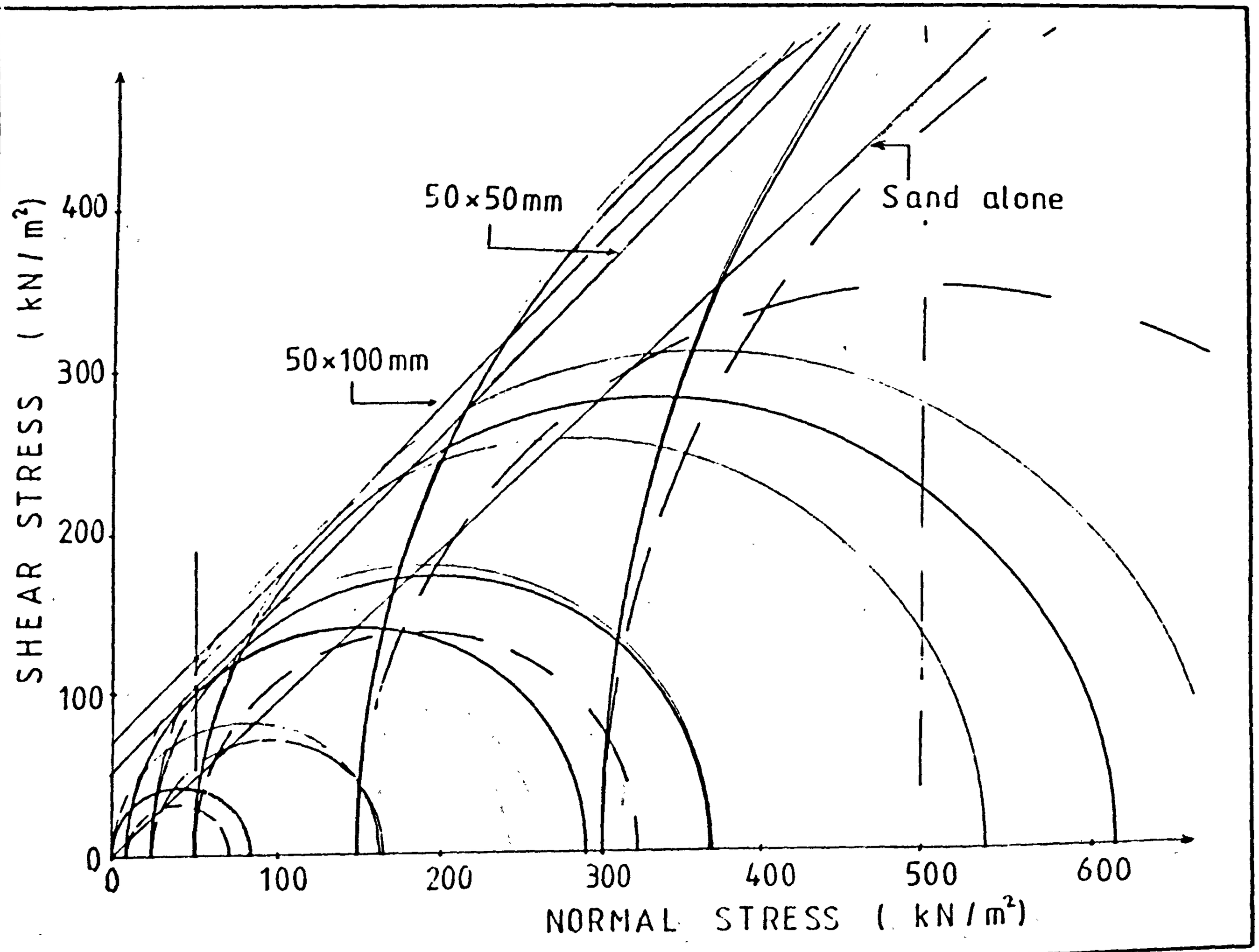

FIG. 5.70

OVERALL STRESS BEHAVIOUR

Soil type :

Leighton Buzzard sand
Mesh type : 7
Mesh content :
90 m^2/m^3
or 0·27% by soil weight.

STRESS STATE :

RESIDUAL

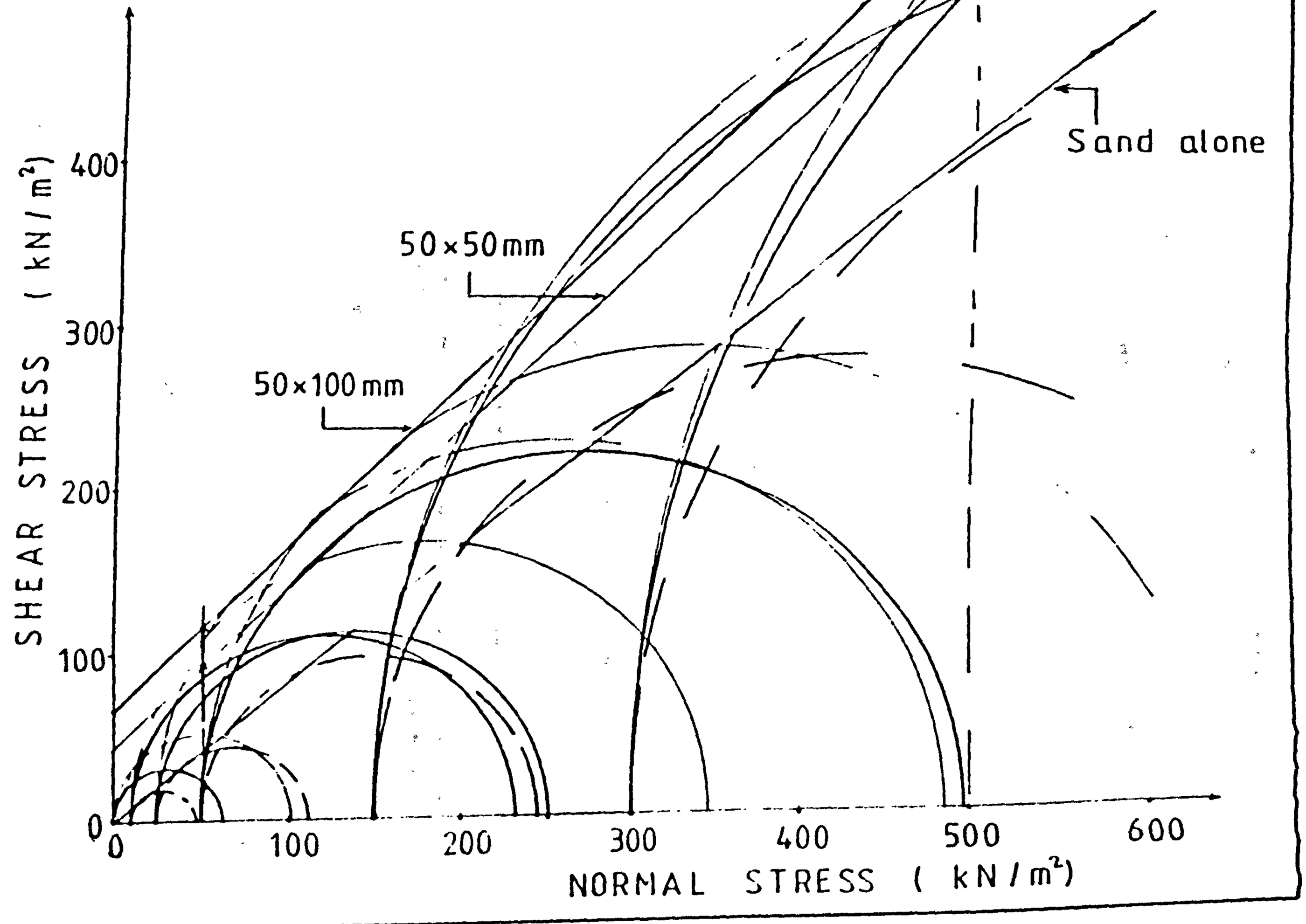

(a)

sand alone

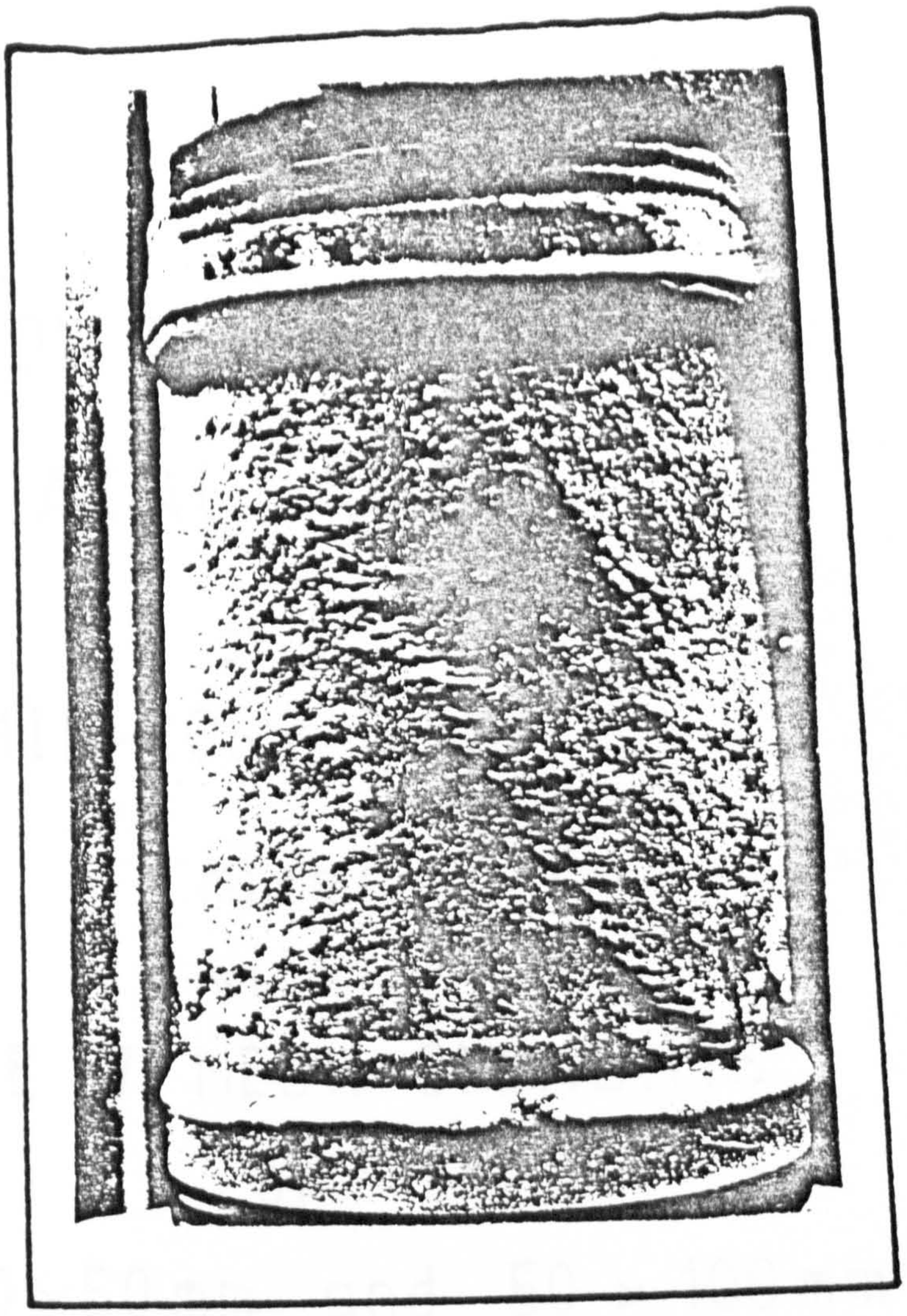

(b)

sand +

mesh elements

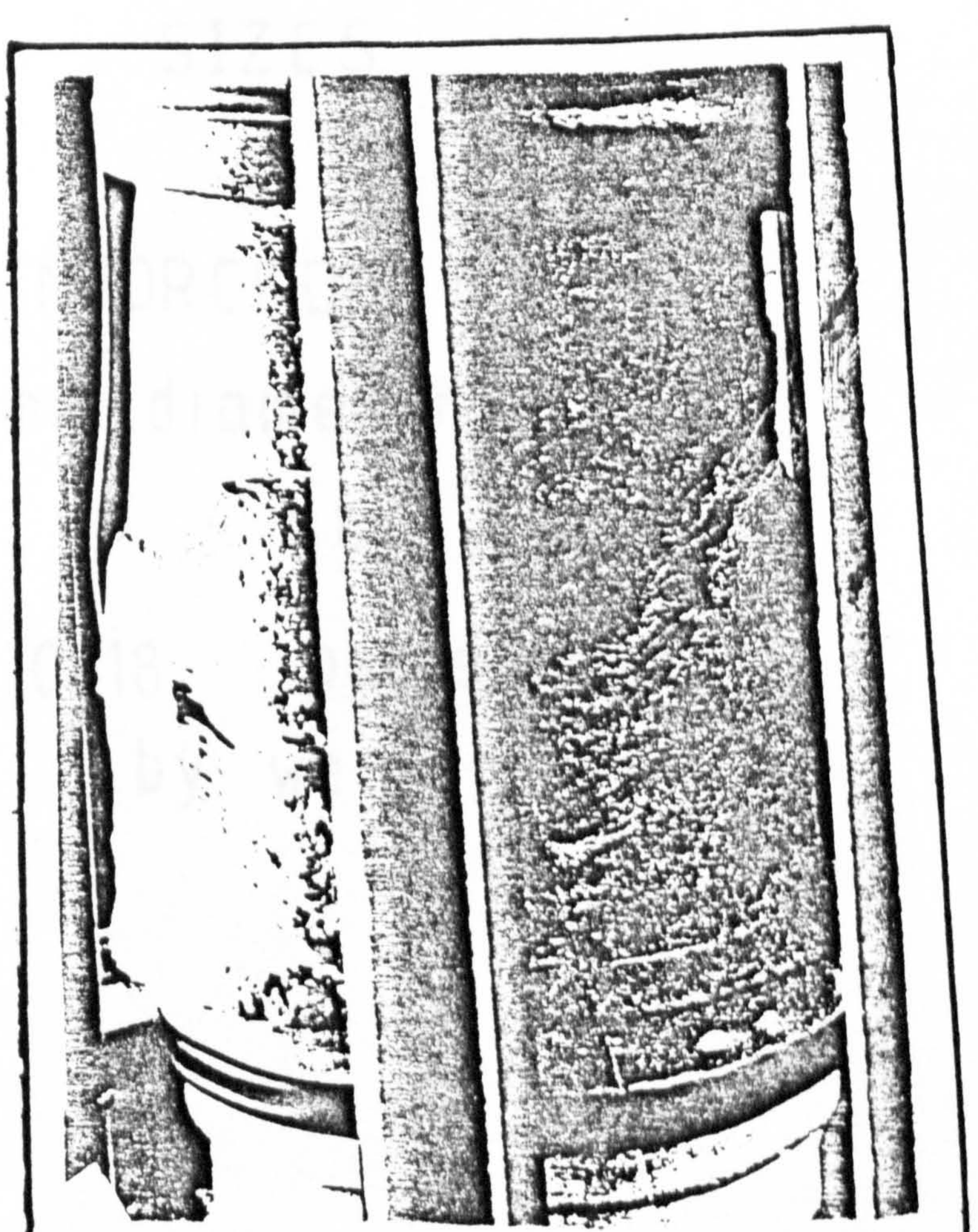

FIG. 5.71 The deformed triaxial samples at large strains

LOW & HIGH STRESS
TRIAXIAL DATA
of
MID-ROSS SAND
mixed
with
TYPE 7, MESH ELEMENTS
of
50 × 50 mm and 50 × 100 mm
SIZES
&
REINFORCED BY
155 mm diameter DISCS
at
0·18 percentage
by weight

FIG. 5.72

SOIL TYPE	MID-ROSS SAND
MESH TYPE	7
MESH CONTENT	66 (m^2/m^2), or 0.18 (%) by dry weight

$\sigma_3 = 0$ kN/m^2

200mm × 155mm diam. TRIAXIAL TEST DATA

RATE OF appl. STRAIN: 0·05 % /min

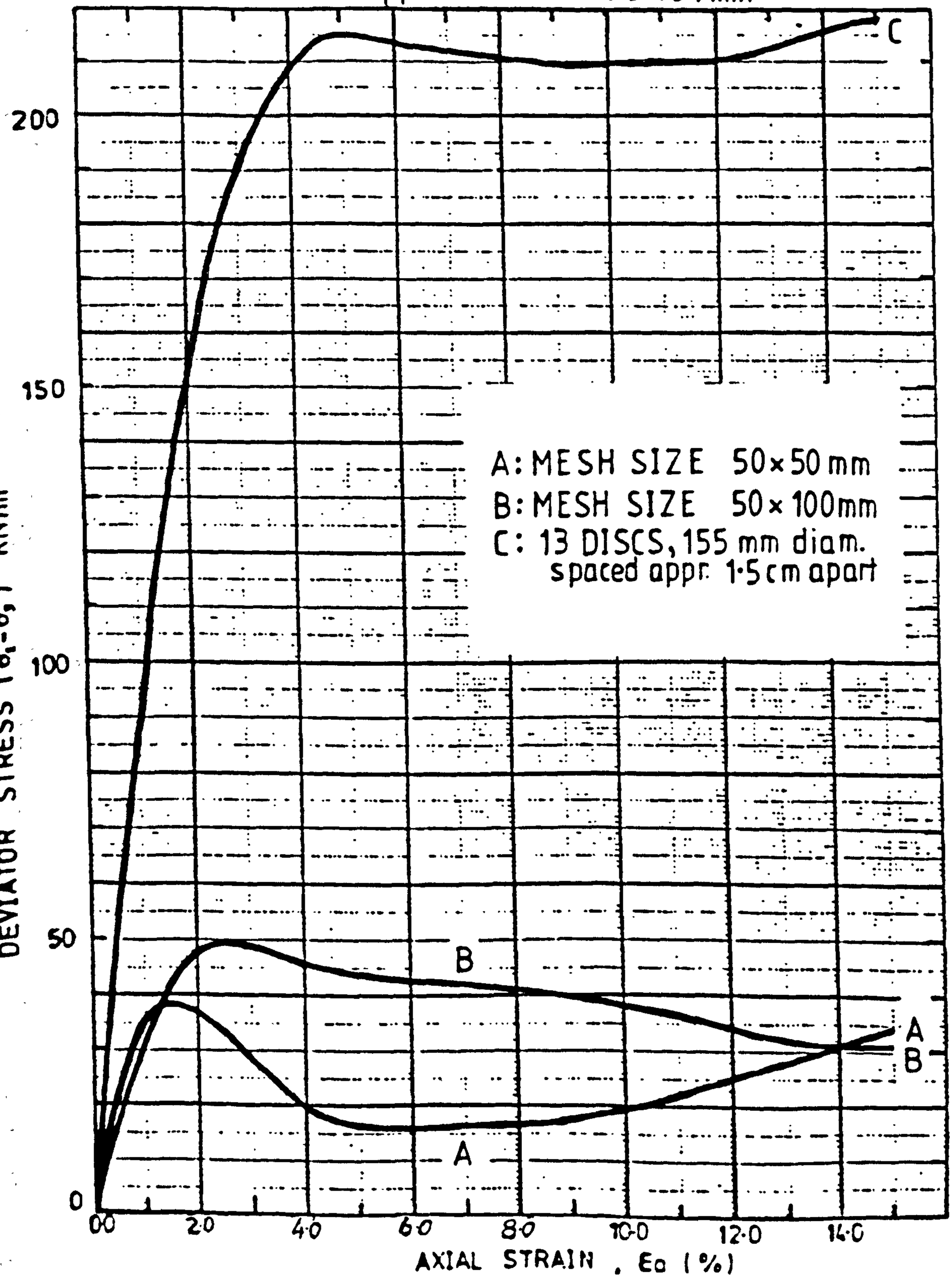

FIG. 5.73

SOIL TYPE	MID-ROSS SAND
MESH TYPE	7
MESH CONTENT	66 (m^2/m^3), or 0·18(%) by dry weight

$\sigma_3 = 10\ kN/m^2$

200mm × 155mm diam. TRIAXIAL TEST DATA

RATE OF app. STRAIN : 0·05 % /min

FIG. 5.74

SOIL TYPE	MID-ROSS SAND
MESH TYPE	7
MESH CONTENT	66 (m^2/m^3), or 0·18 (%) by dry weight

$\sigma_3 = 25\ kN/m^2$

200mm × 155mm diam. TRIAXIAL TEST DATA

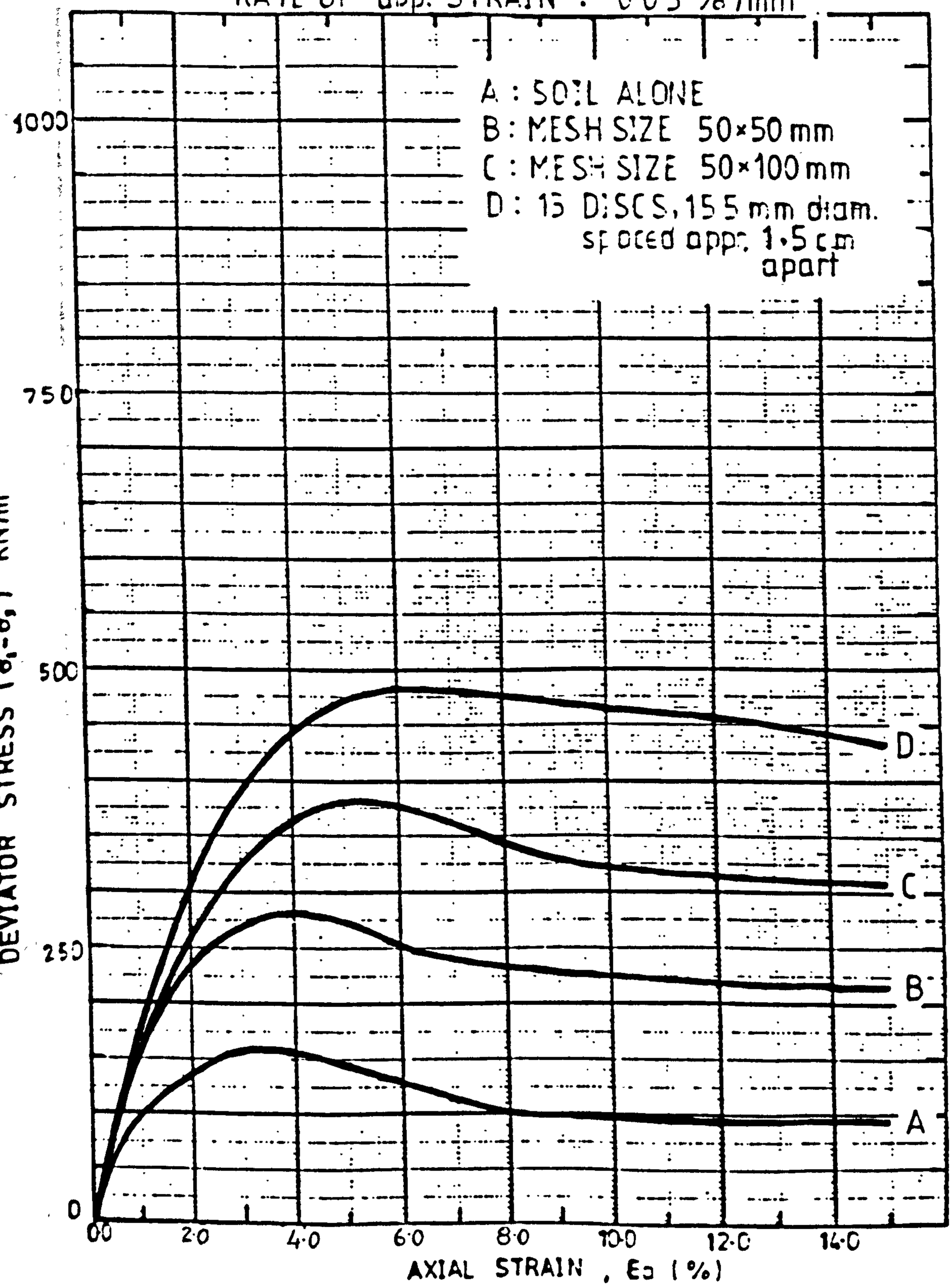

FIG. 5.75

SOIL TYPE	MID-ROSS SAND
MESH TYPE	7
MESH CONTENT	66 (m^2/m^3), or 0·18 (%) by dry weight

σ_3 = 50 kN/m^2

200mm × 155mm diam. TRIAXIAL TEST DATA

RATE OF appl. STRAIN 0·05 % / min

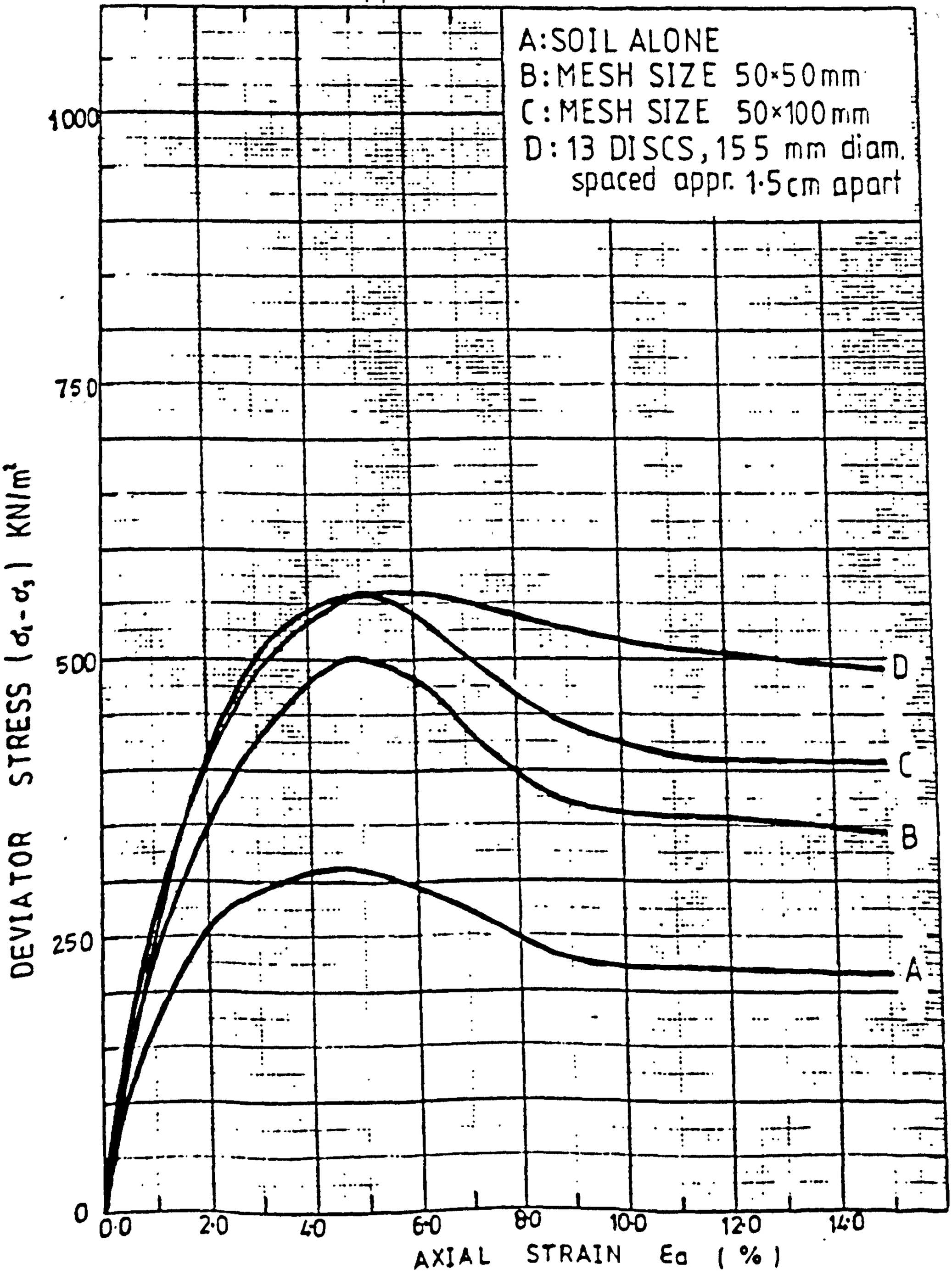

FIG. 5.76

SOIL TYPE	MID ROSS SAND
MESH TYPE	7
MESH CONTENT	66 (m^2/m^3), or 0·18 (%) by dry weight

$\sigma_3 = 150\ kN/m^2$

200 mm × 155 mm diam. TRIAXIAL TEST DATA

RATE OF appl. STRAIN : 0·05%/min

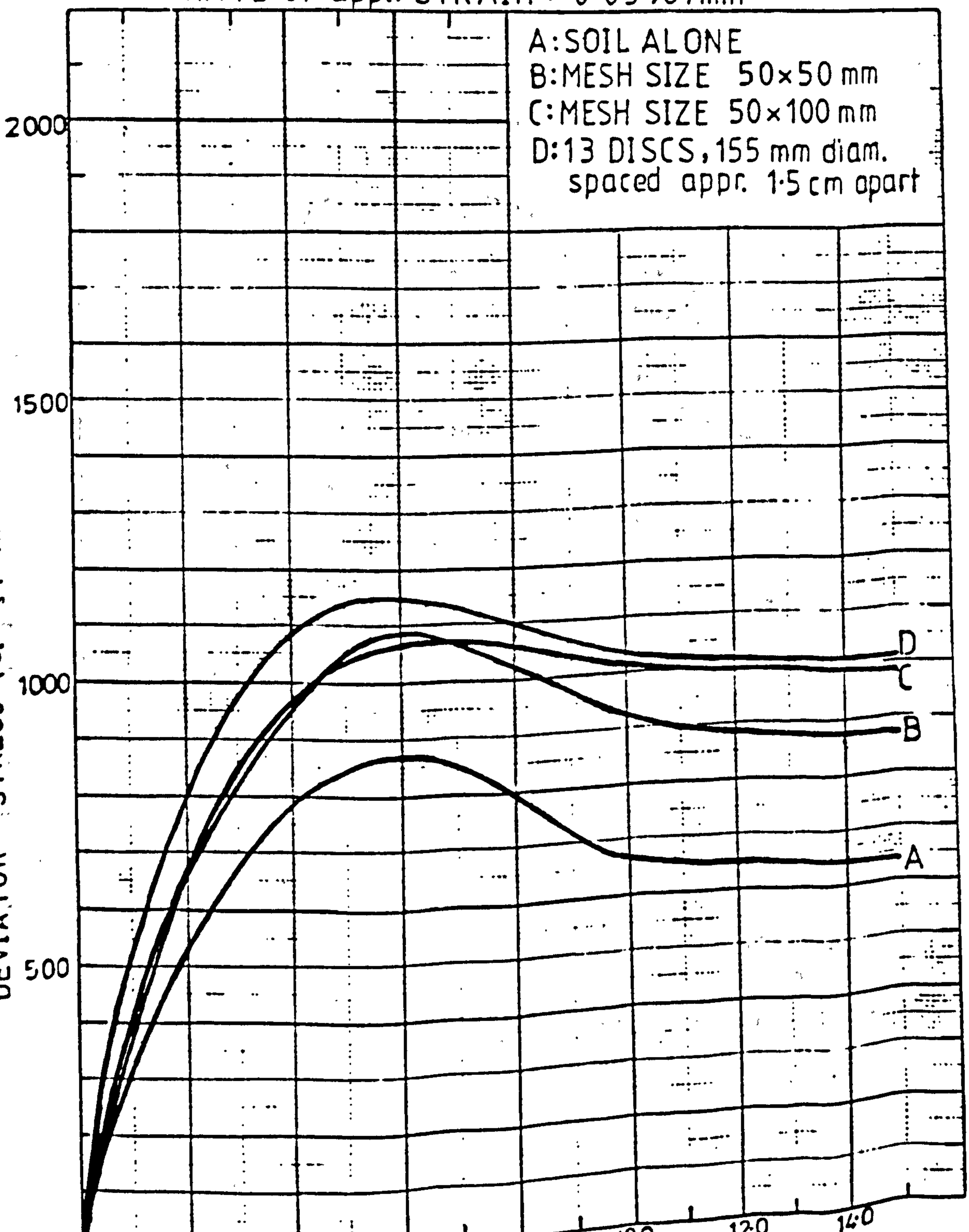

FIG. 5.77

SOIL TYPE	MID-ROSS SAND
MESH TYPE	7
MESH CONTENT	66 (m^2/m^2), or 0.18 (%) by dry weight

$\sigma_3 = 300\ kN/m^2$

200 mm × 155 mm diam. TRIAXIAL TEST DATA

RATE OF appl. STRAIN : 0·05 % / min

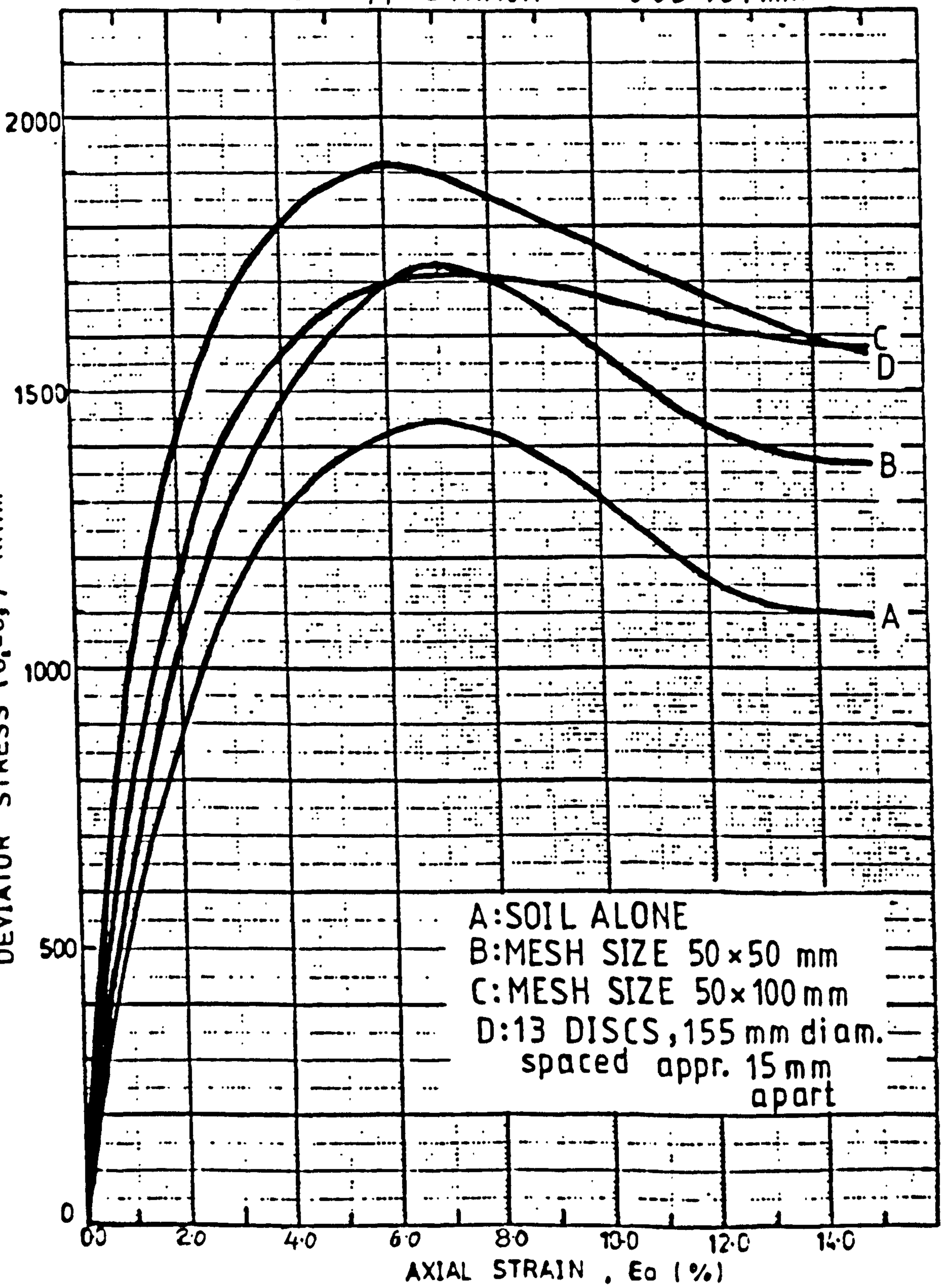

EFFECT

OF

RATE OF STRAIN

ON

SOIL-MESH

MIXTURE SAMPLES

FIG. 5.78

SOIL TYPE	MID-ROSS SAND

200mm×155 mm diam..TRIAXIAL TEST DATA

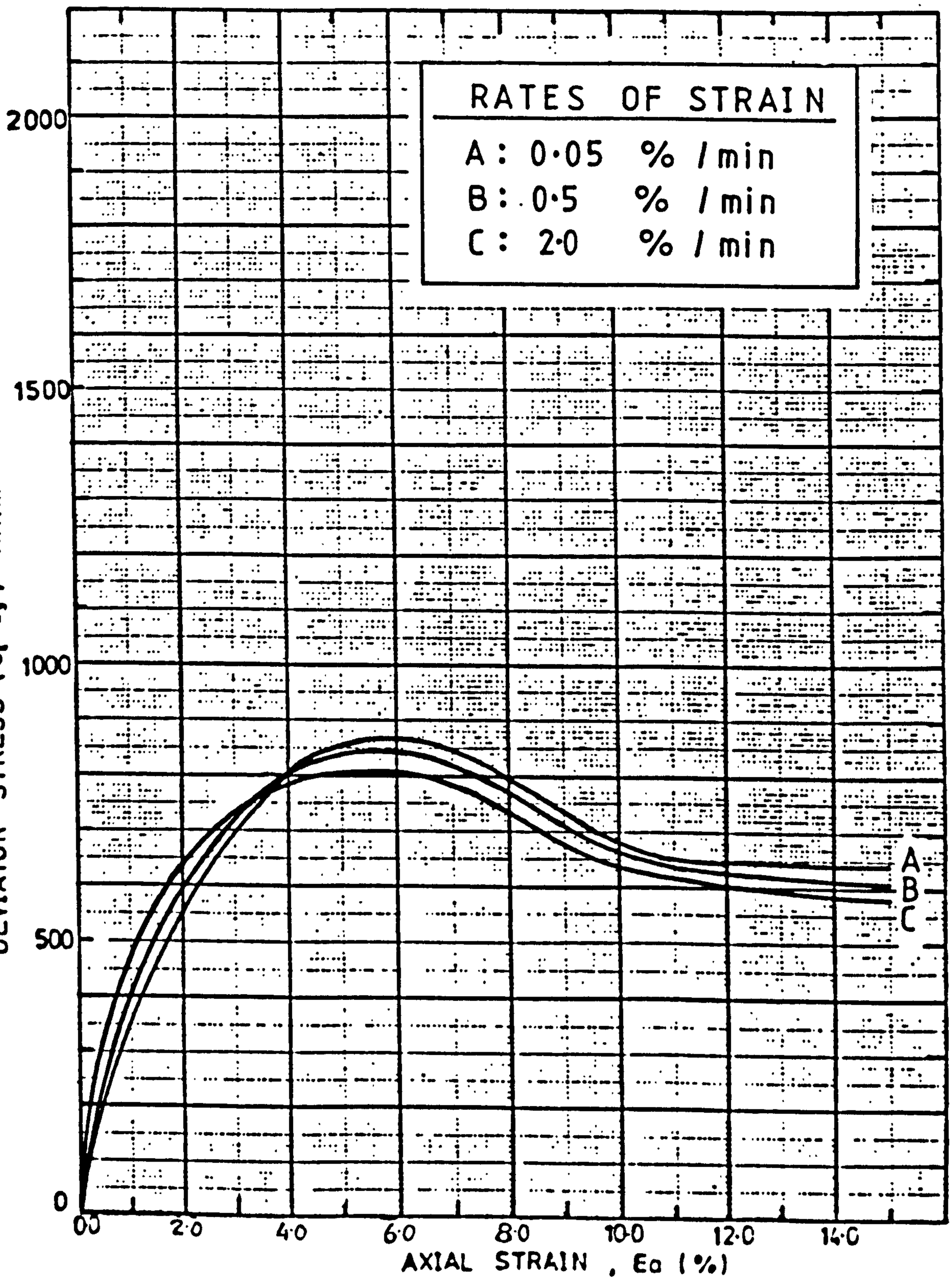

FIG. 5.79

SOIL TYPE	LEIGHTON BUZZARD SAND

200mm×155 mm diam. TRIAXIAL TEST DATA

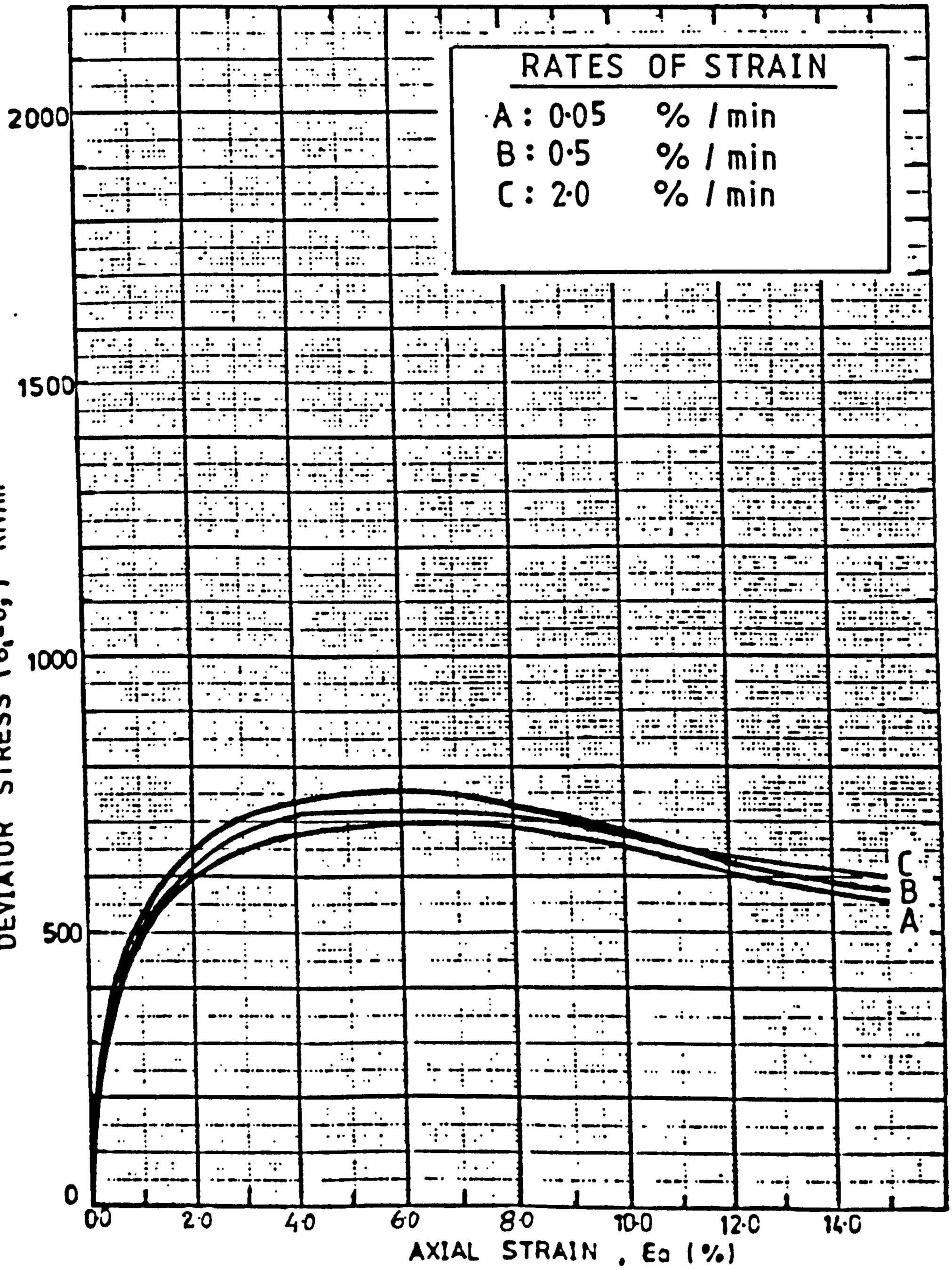

FIG. 5.80

SOIL TYPE	MID ROSS SAND
MESH TYPE : 7	MESH SIZE : 13 DISCS, 155 mm diam.
MESH CONTENT	66 (m^2/m^3), or 0·18 (%) by dry weight

σ_3 = 150 kN/m^2

200 mm × 155 mm diam. TRIAXIAL TEST DATA

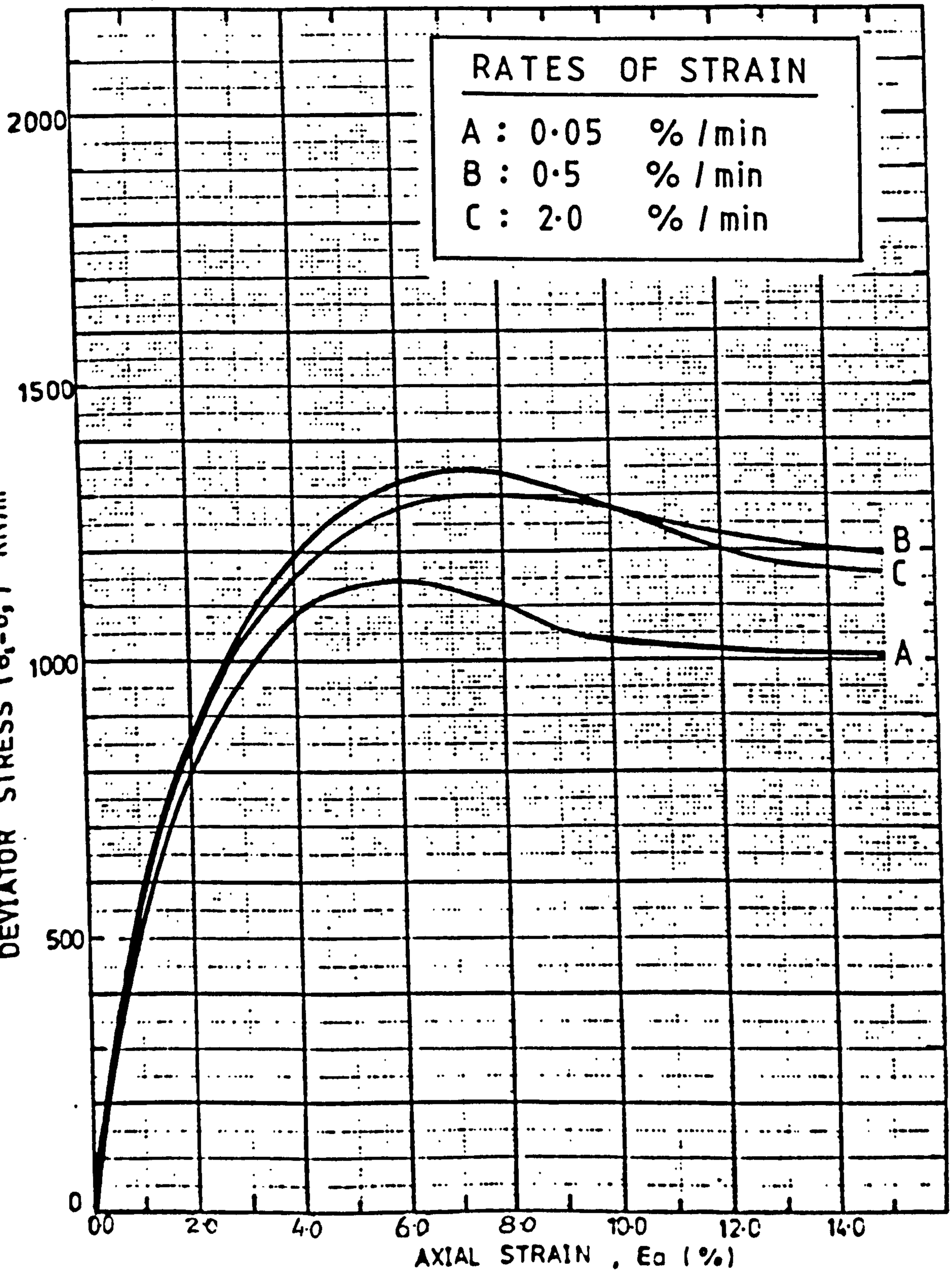

FIG. 5.81

SOIL TYPE	MID-ROSS SAND
MESH TYPE : 7	MESH SIZE: 50×100 mm
MESH CONTENT	66 (m^2/m^3), or 0 18 (%) by dry weight

$\sigma_3 = 150\ kN/m^2$

200 mm × 155 mm diam. TRIAXIAL TEST DATA

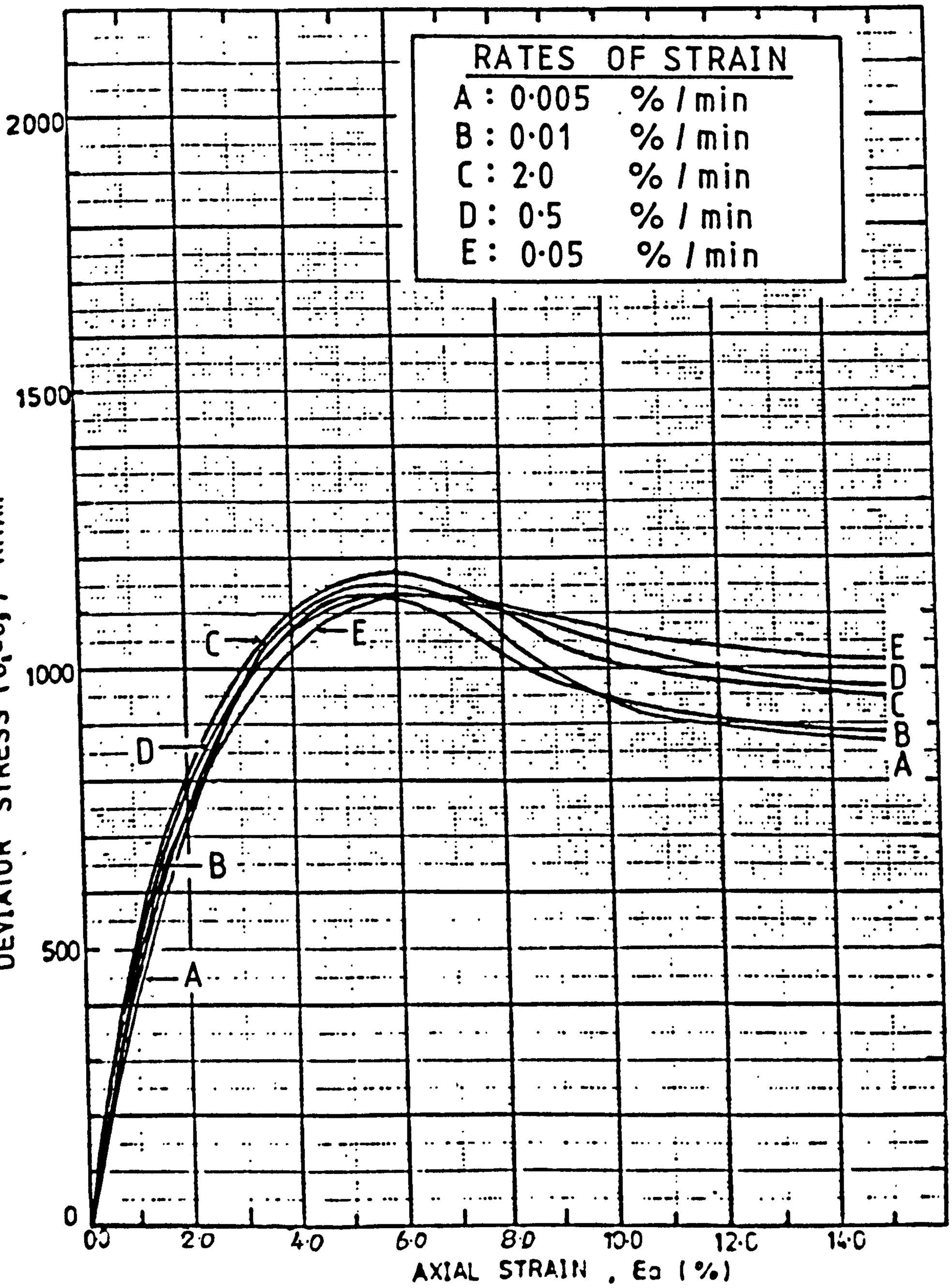

FIG. 5.82

SOIL TYPE	LEIGHTON BUZZARD SAND
MESH TYPE : 7	MESH SIZE : 50 × 100 mm
MESH CONTENT	66 (m^2/m^3), or 0·20 (%) by dry weight

$\sigma_3 = 150\ kN/m^2$

200 mm × 155 mm diam. TRIAXIAL TEST DATA

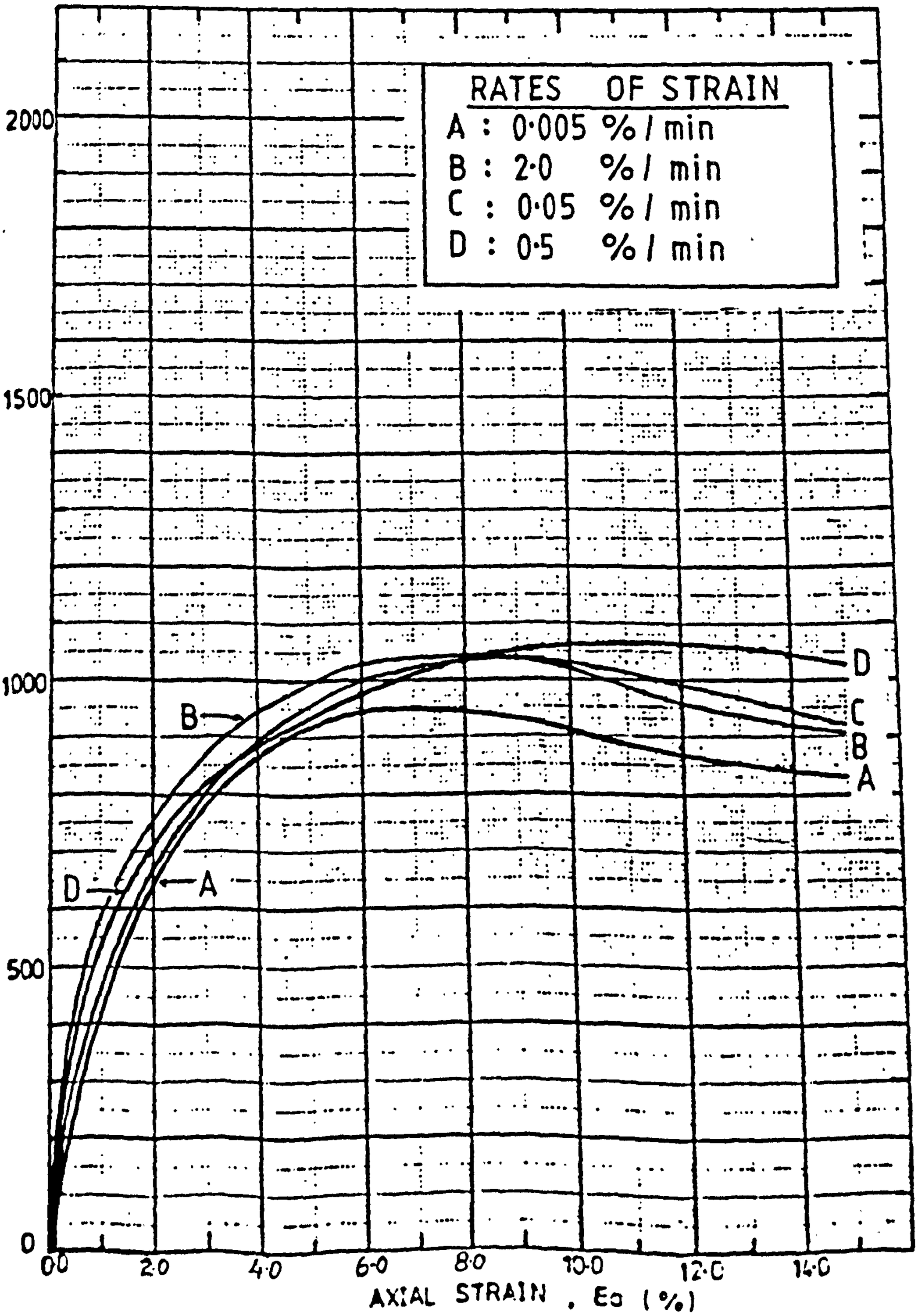

FIG. 5.83

SOIL TYPE	COLLIERY SPOIL

$\sigma_3 = 150\ kN/m^2$

200mm × 155mm diam. TRIAXIAL TEST DATA

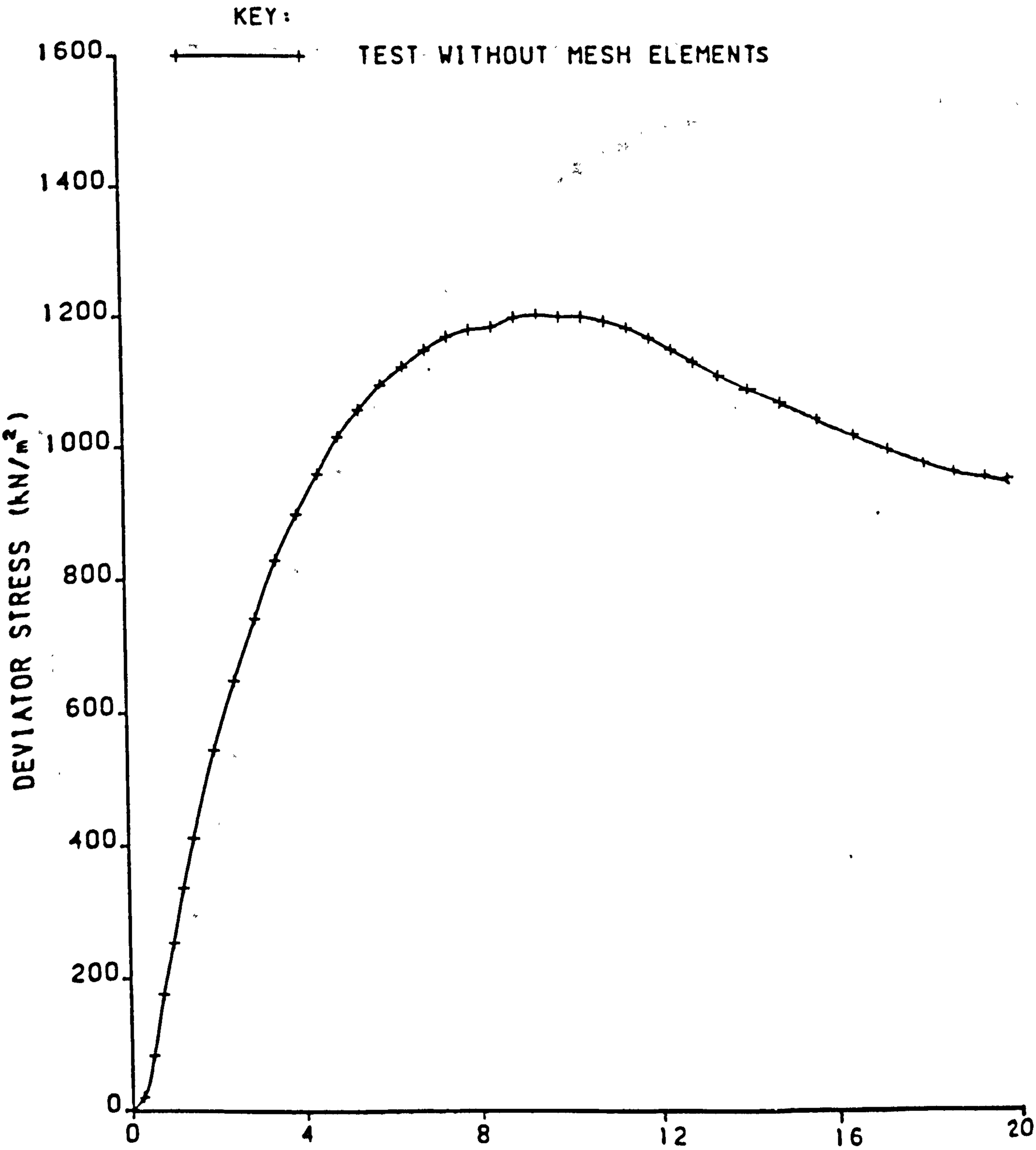

FIG. 5.84

SOIL TYPE	COLLIERY SPOIL
MESH TYPE : 7	MESH SIZE : 50×100 mm
MESH CONTENT	66 (m^3/m^3), or 0·20 (%) by dry weight

$\sigma_3 = 150\ kN/m^2$

200 mm × 155 mm diam. TRIAXIAL TEST DATA

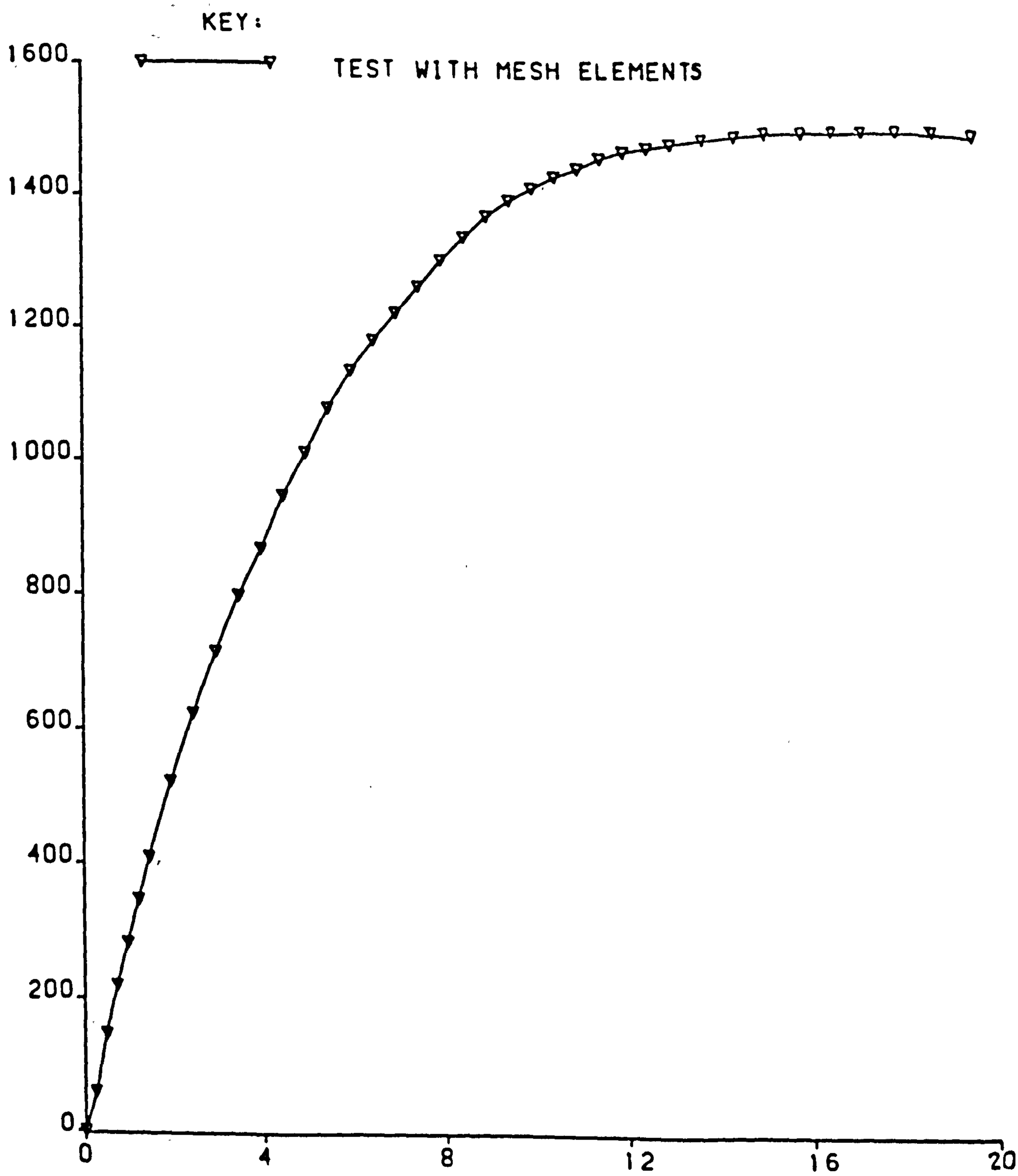

FIG. 5.85

SOIL TYPE	COLLIERY SPOIL
MESH TYPE : 7	MESH SIZE : 50×100 mm
MESH CONTENT	66 (m^2/m^3), or 0·20 (%) by dry weight

$\sigma_3 = 150\ kN/m^2$

200 mm × 155 mm diam. TRIAXIAL TEST DATA

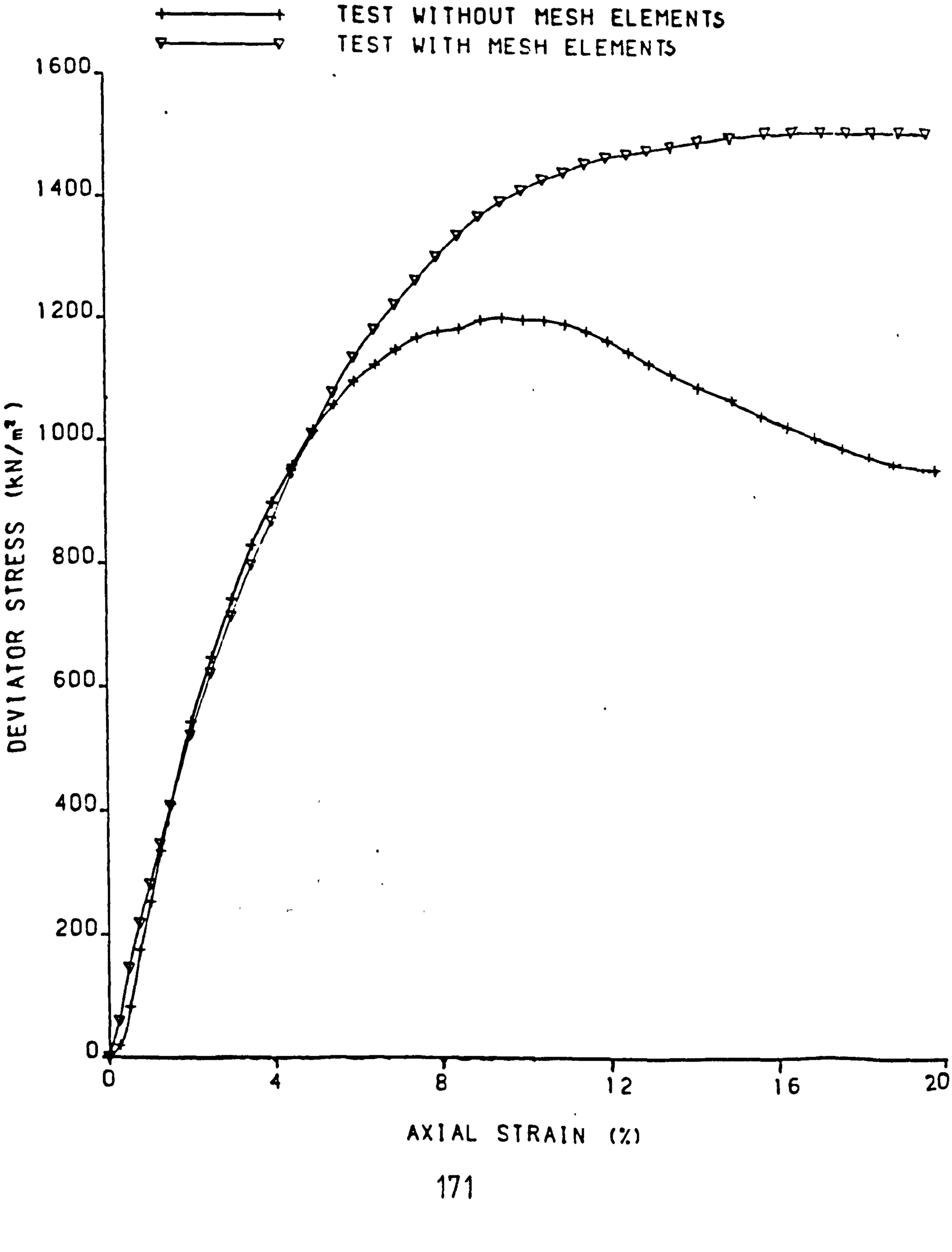

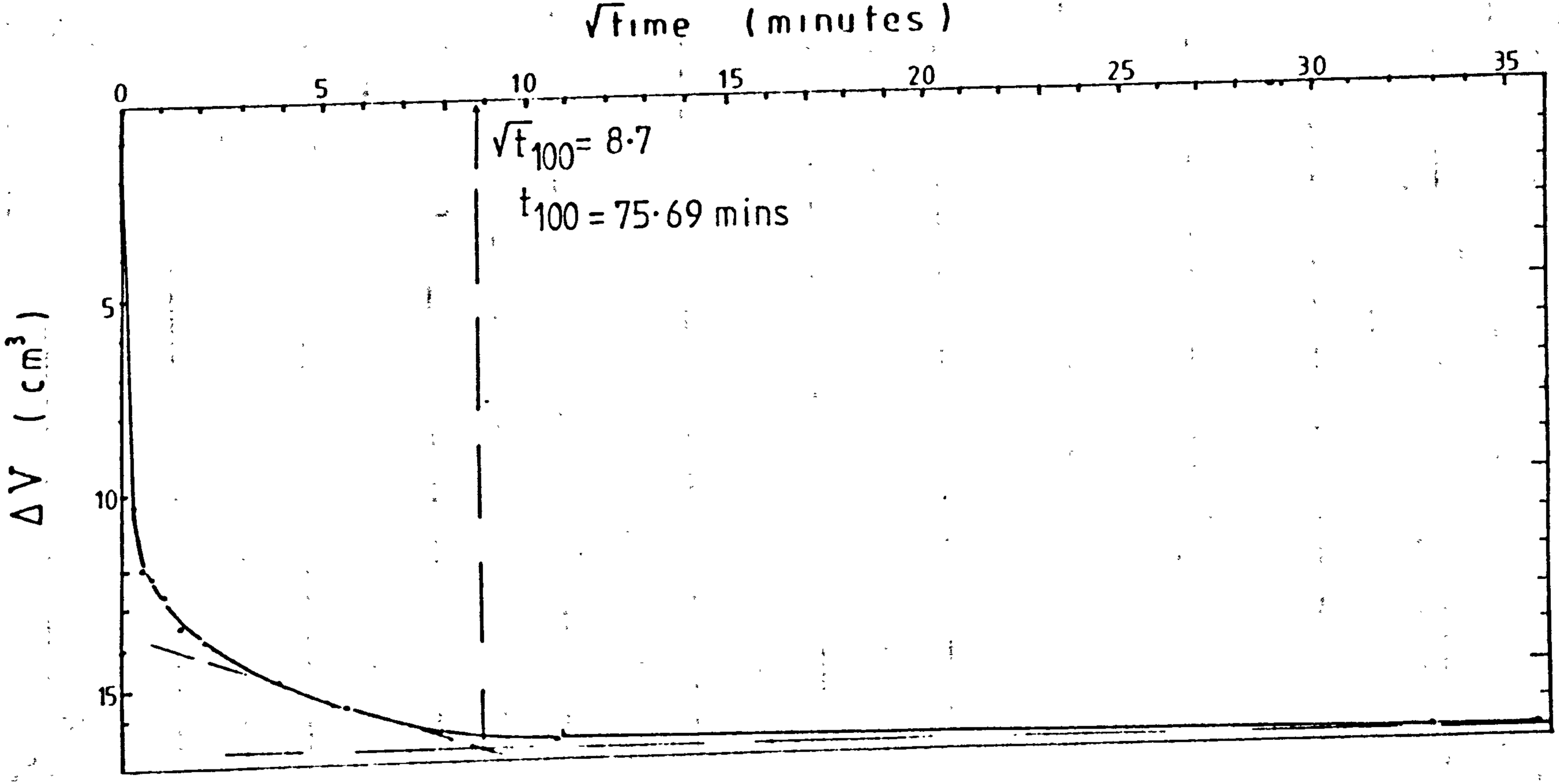

FIG. 5.86 CONSOLIDATION OF WEST HIGHLAND MORAINE

FIG. 5.87

SOIL TYPE	WEST HIGHLAND MORAINE
MESH TYPE : 7	MESH SIZE : 50 × 100 mm
MESH CONTENT	66 (m^2/m^3), or 0·20 (%) by dry weight

$\sigma_3 = 150\ kN/m^2$

200 mm × 155 mm diam. TRIAXIAL TEST DATA

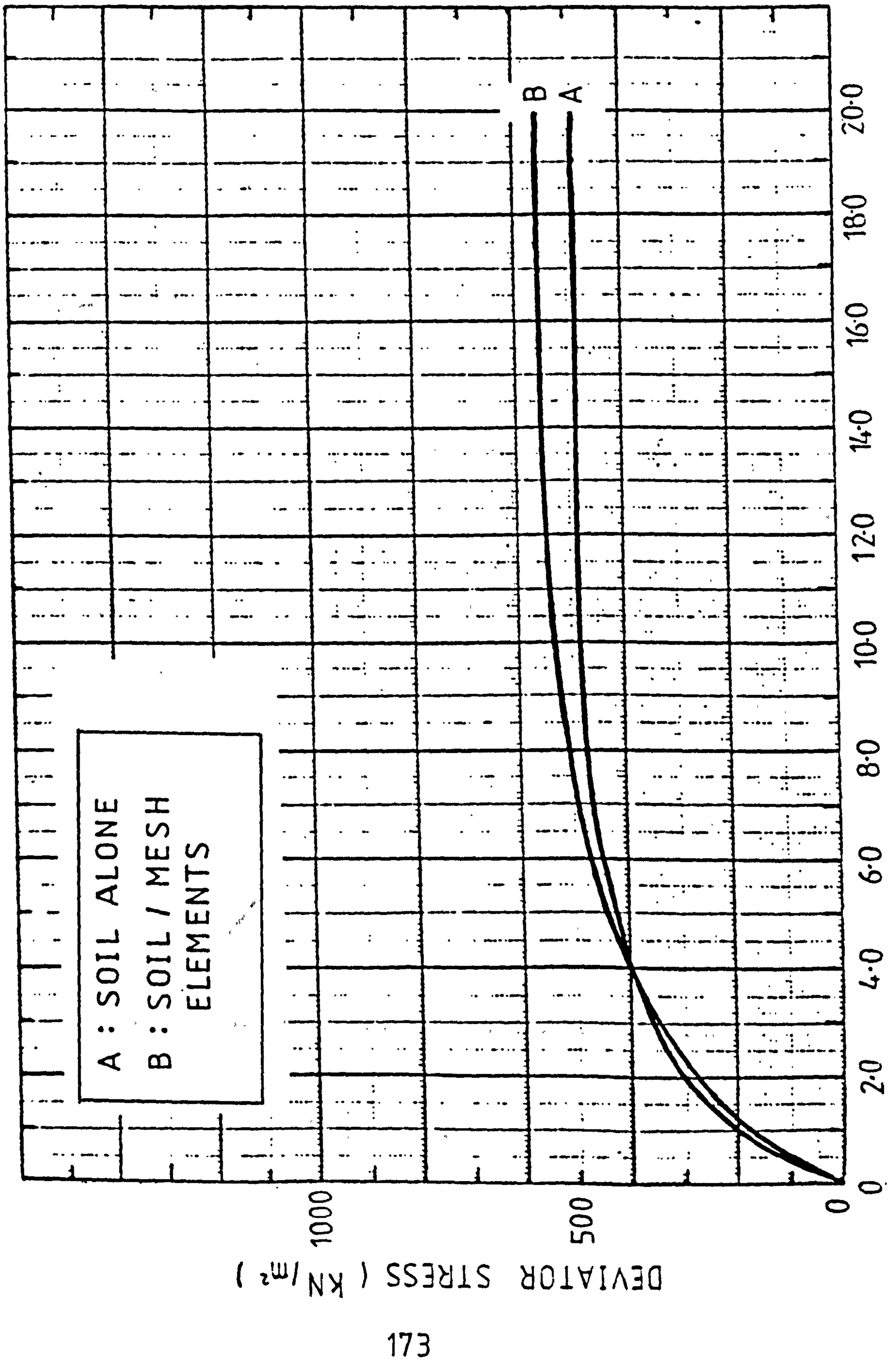

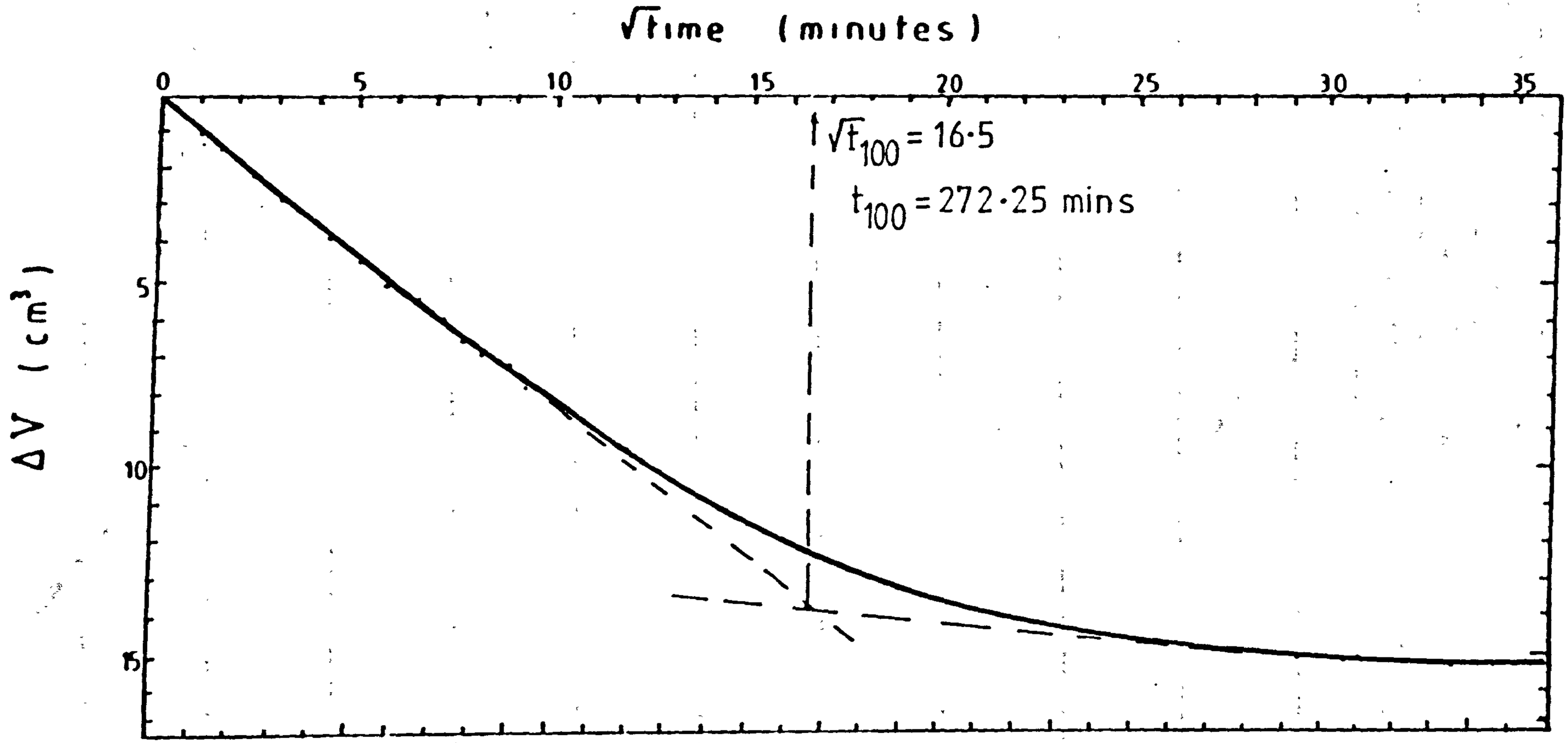

FIG. 5.88 CONSOLIDATION OF PULVERISED FUEL ASH

FIG. 5.89

SOIL TYPE	PULVERISED FUEL ASH
MESH TYPE : 7	MESH SIZE : 50 × 100 mm
MESH CONTENT	66 (m^2/m^3), or 0·27 (%) by dry weight

$\sigma_3 = 150\ kN/m^2$

200 mm × 155 mm diam. TRIAXIAL TEST DATA

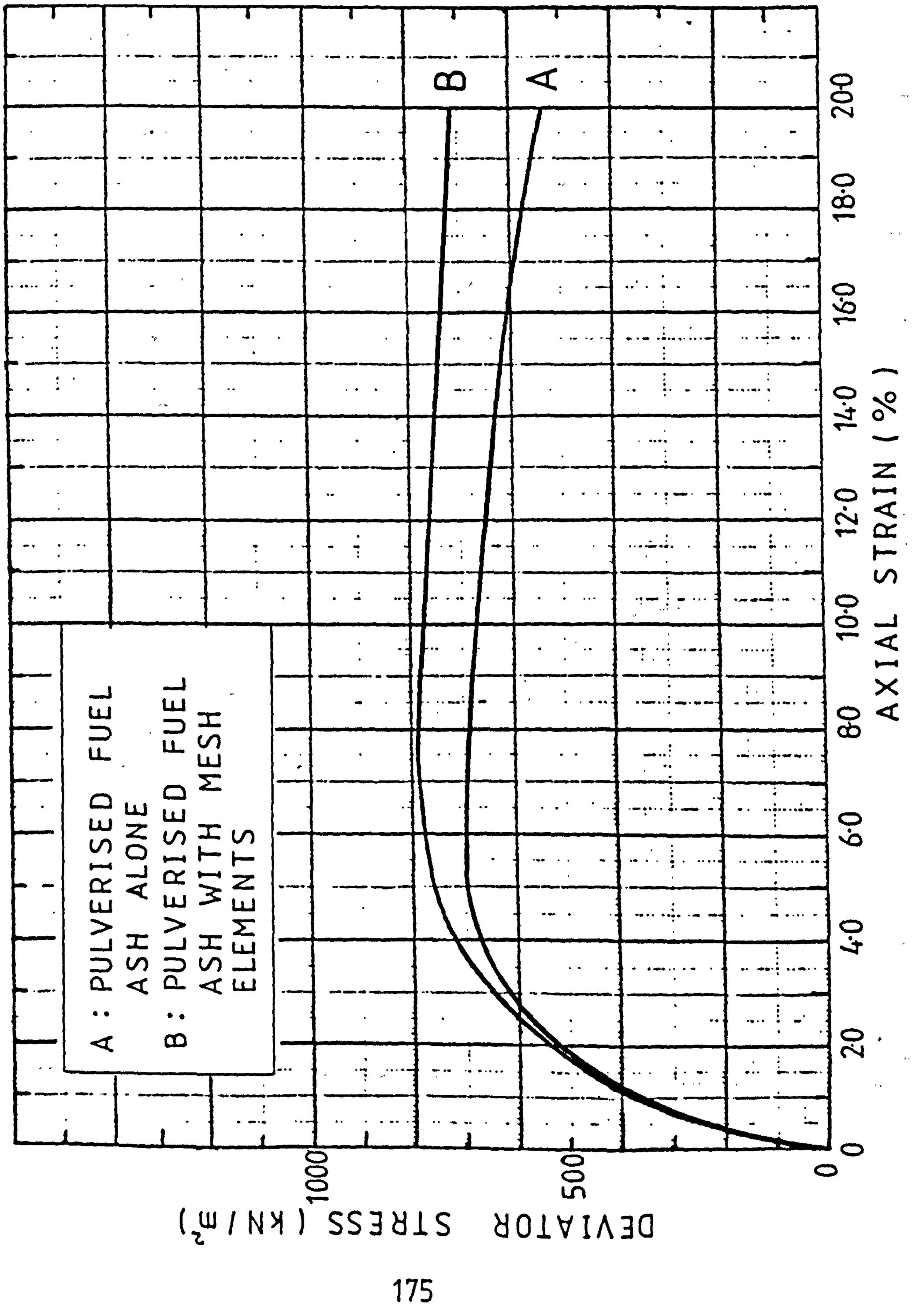

FIG. 5.90

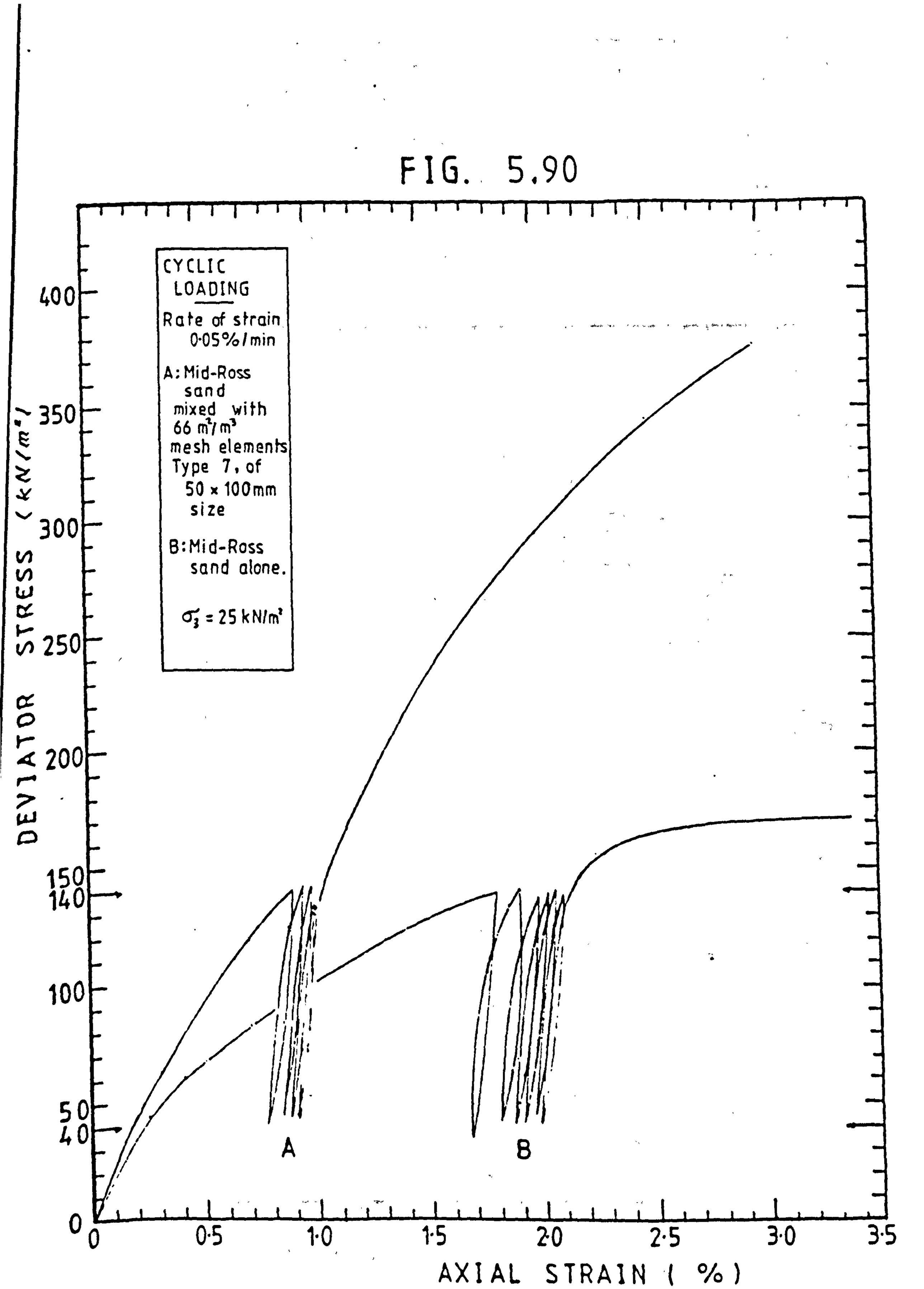
CYCLIC LOADING
Rate of strain 0·05%/min
A: Mid-Ross sand mixed with 66 m²/m³ mesh elements Type 7, of 50 × 100mm size
B: Mid-Ross sand alone.
σ₃ = 25 kN/m²
DEVIATOR STRESS (kN/m²)
AXIAL STRAIN (%)
A
B
0
40
50
100
140
150
200
250
300
350
400
0·5
1·0
1·5
2·0
2·5
3·0
3·5

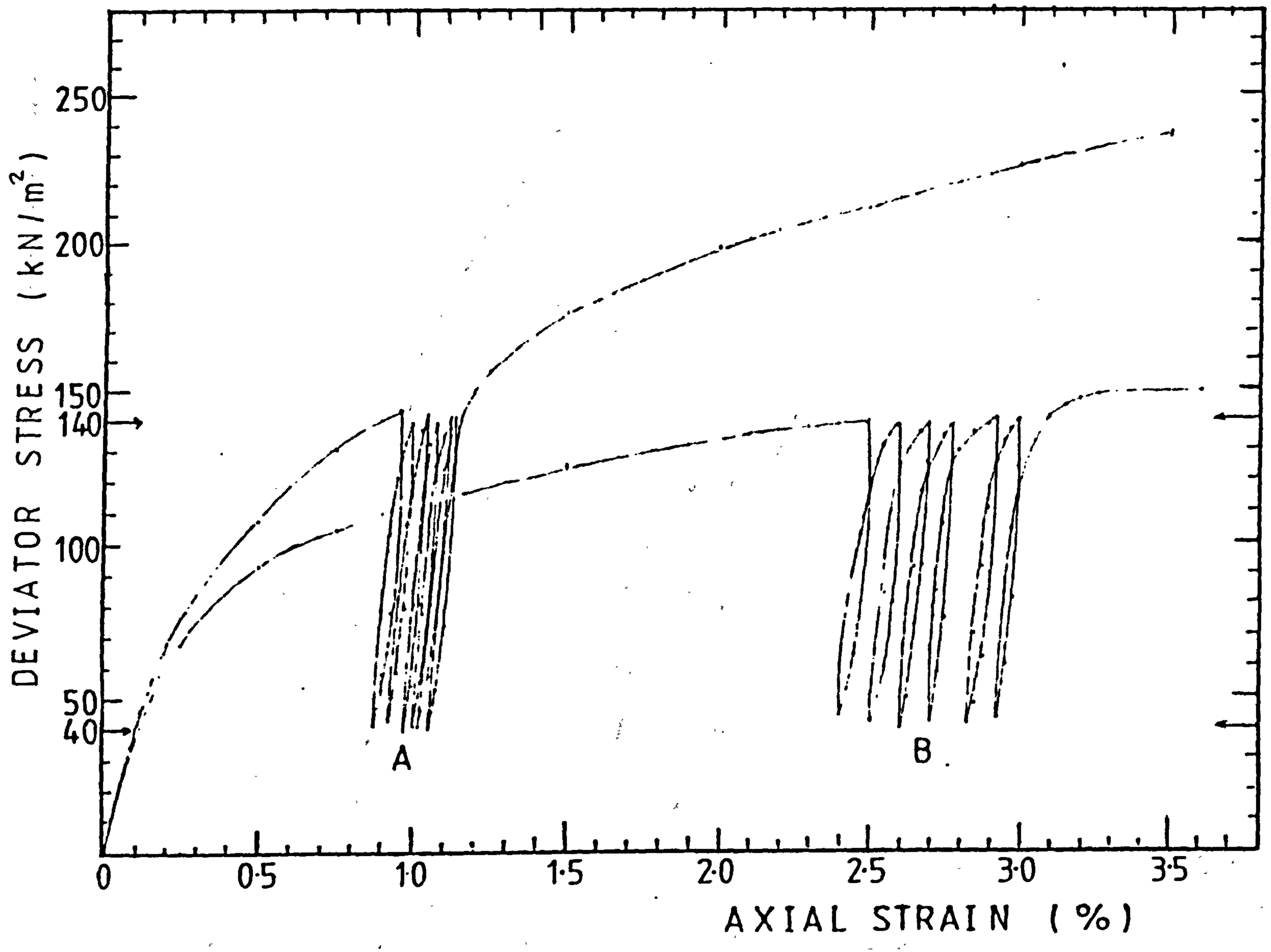

CYCLIC LOADING

Rate of strain 0·05 %/min

A: Leighton Buzzard sand containing 66 m²/m³ mesh type 7 of 50 × 100 mm size

B: Leighton Buzzard sand alone.

$\sigma_2 = 25$ kN/m²

FIG. 5.91

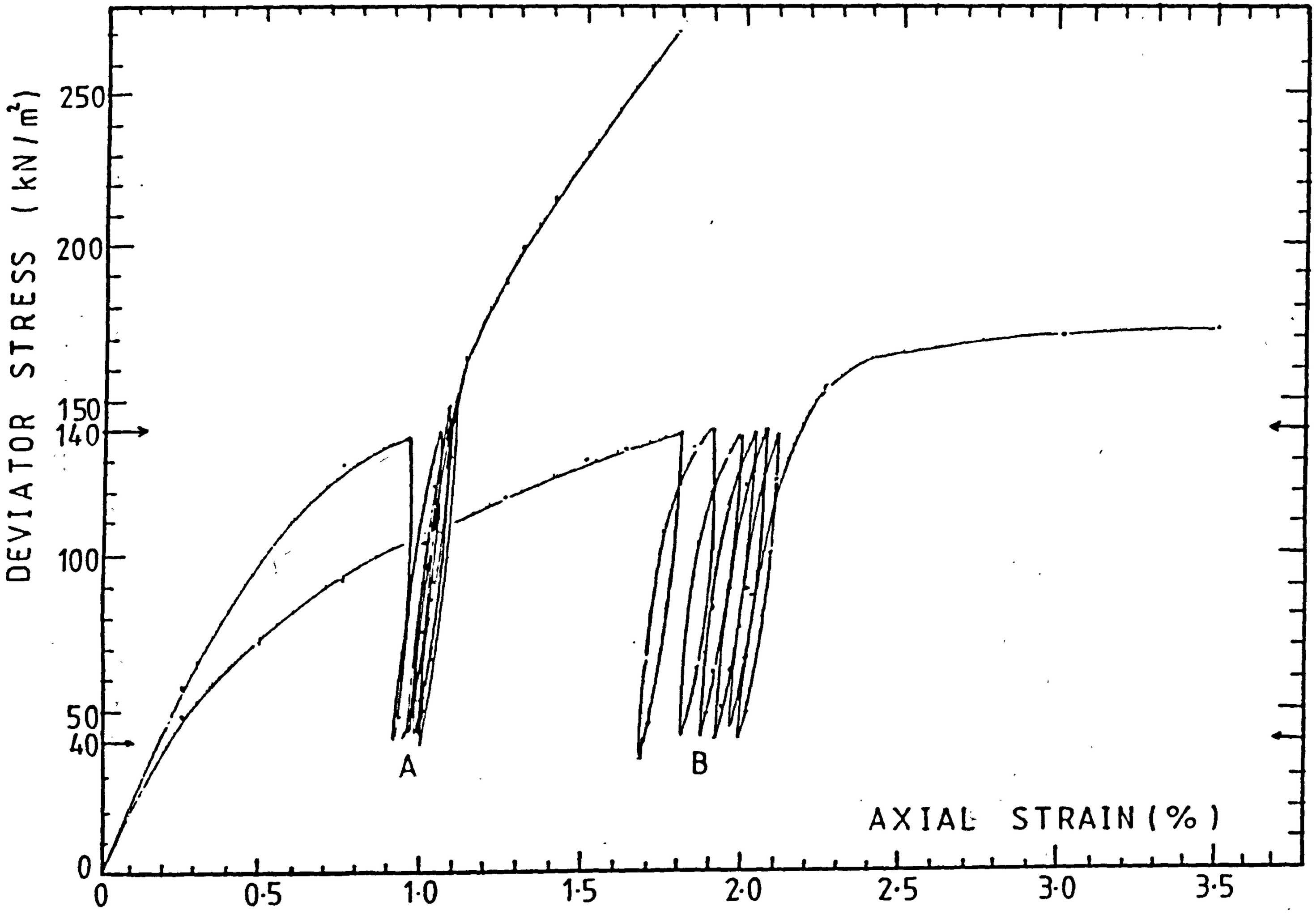

CYCLIC LOADING

Rate of strain 0·05%/min

A: Mid-Ross sand reinforced by 13, Type 7, horizontal, 155 mm diameter, 66 m^2/m^3, DISCS.

B: Mid-Ross sand alone.

$\sigma_2 = 25\ kN/m^2$

FIG. 5.92

SOIL TYPE : MID-ROSS SAND	MESH TYPE : 7	MESH SIZE: 50×100 mm
MESH CONT. 66 m^2/m^3, or 0·18 % by dry weight	Cell pressure : 10 kPa	Applied stress: 73 kN/m^2

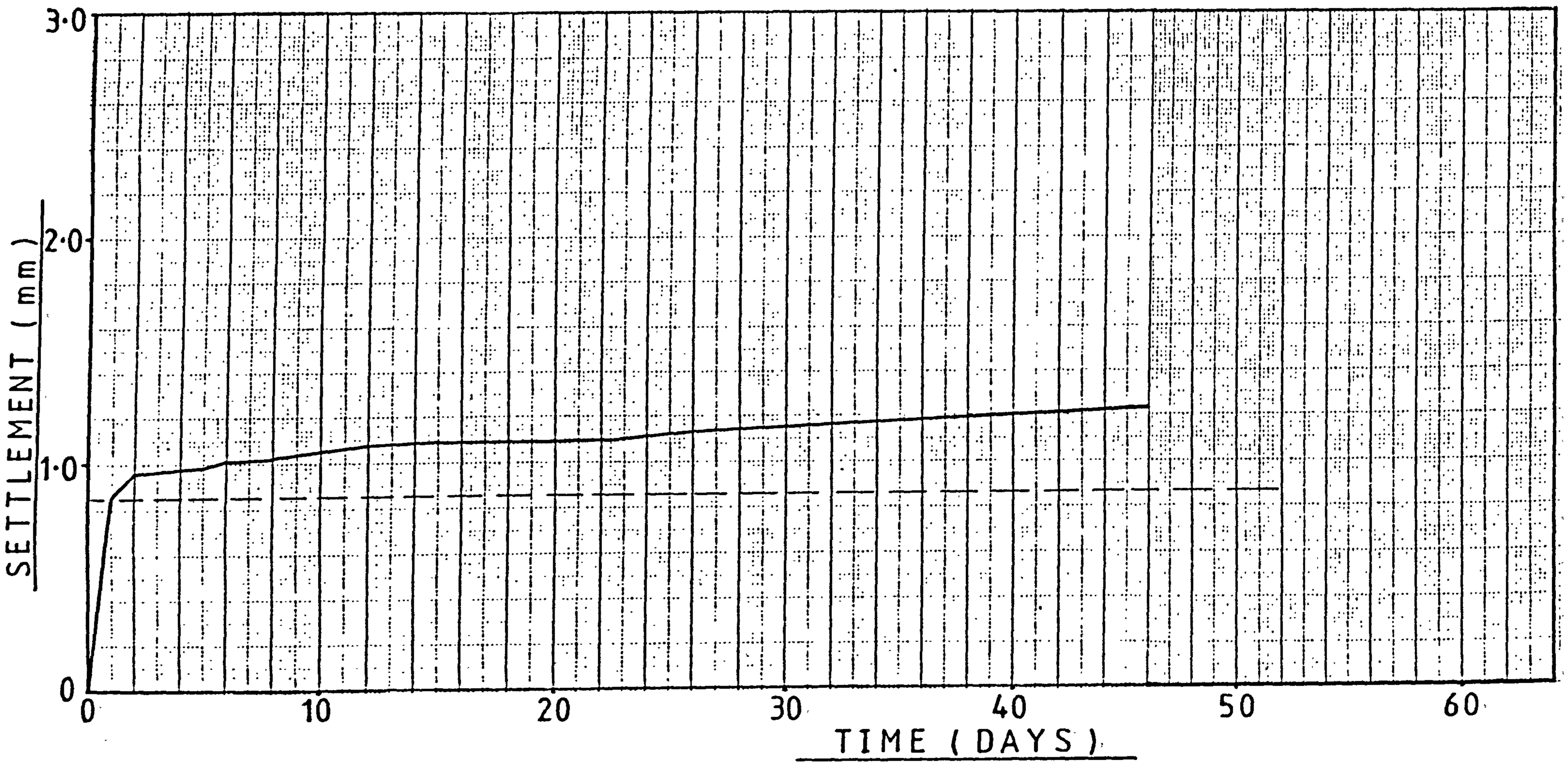

FIG. 5.93 CREEP ANALYSIS OF SOIL/MESH MIXTURE

SOIL TYPE : MID-ROSS SAND	MESH TYPE : 7	MESH SIZE: 50×100 mm
MESH CONT. 66 m^2/m^3, or 0·18 % by dry weight	Cell pressure : 25 kPa	Applied stress : 127 kN/m^2

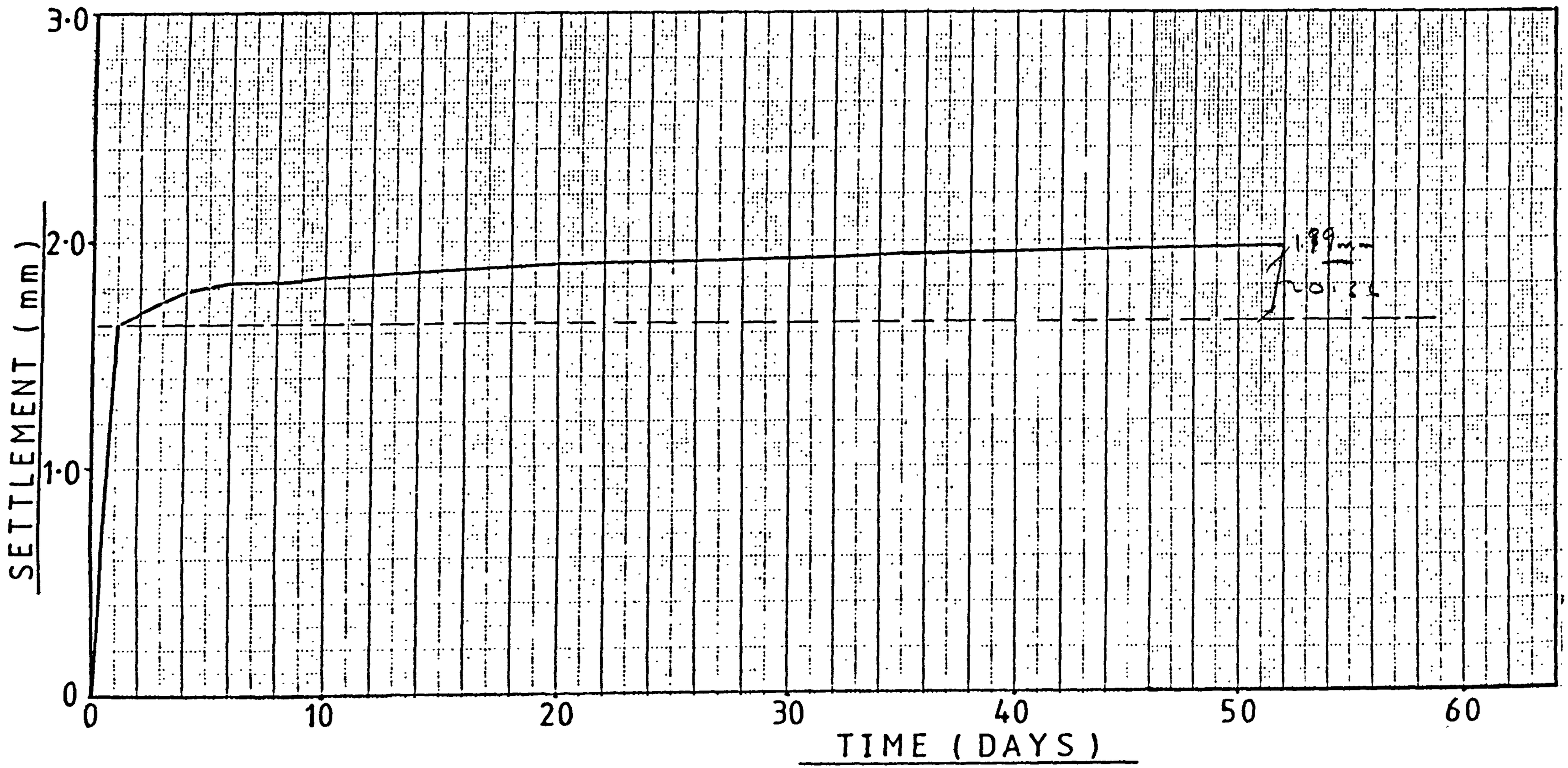

FIG. 5.94 CREEP ANALYSIS OF SOIL/MESH MIXTURE

SOIL TYPE : MID-ROSS SAND	MESH TYPE : 7	MESH SIZE: 50×100 mm
MESH CONT. 66 m^2/m^3, or 0·18 % by dry weight	Cell pressure : 50 kPa	Applied stress: 186 kN/m^2

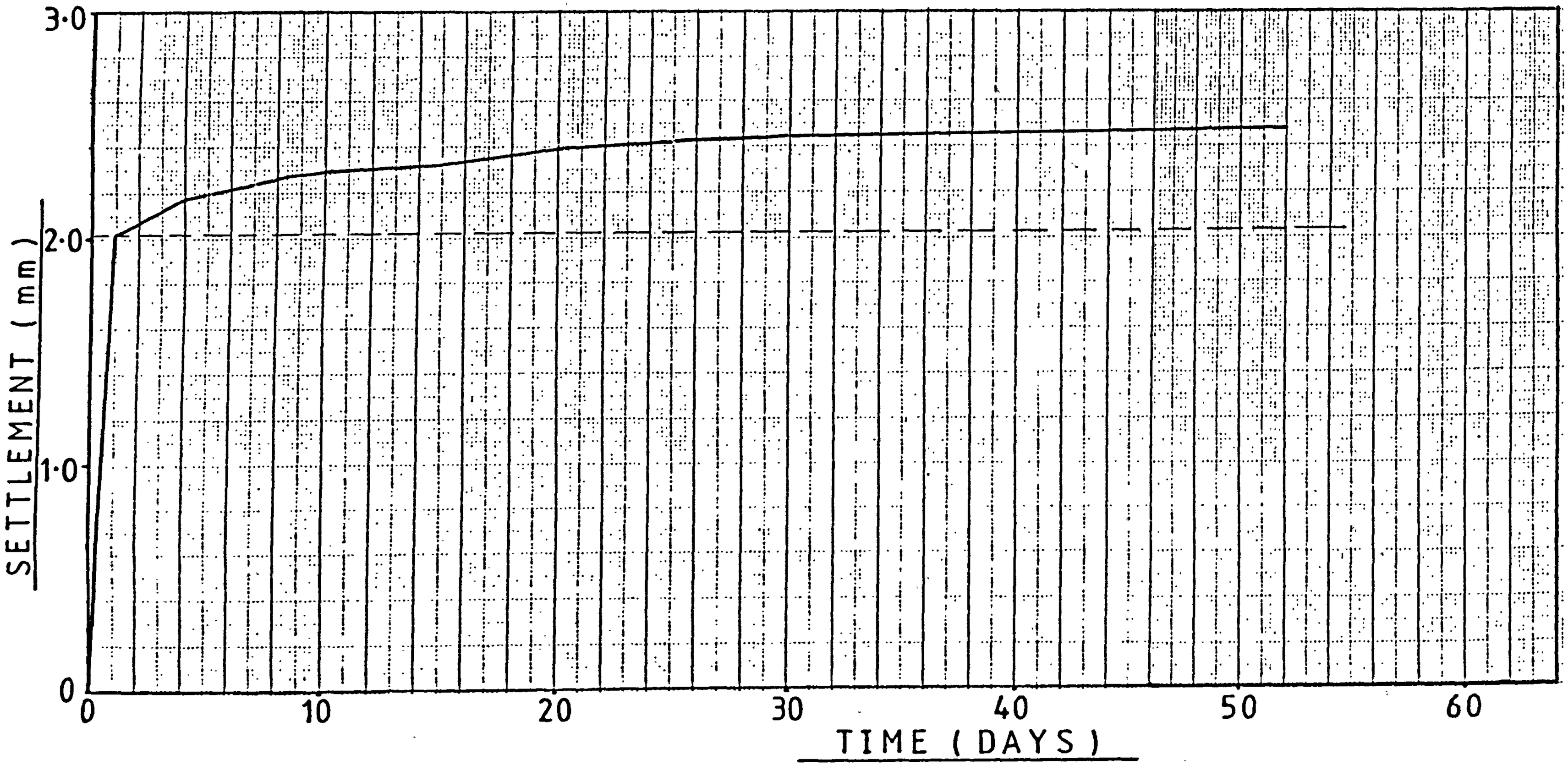

FIG. 5.95 CREEP ANALYSIS OF SOIL/MESH MIXTURE

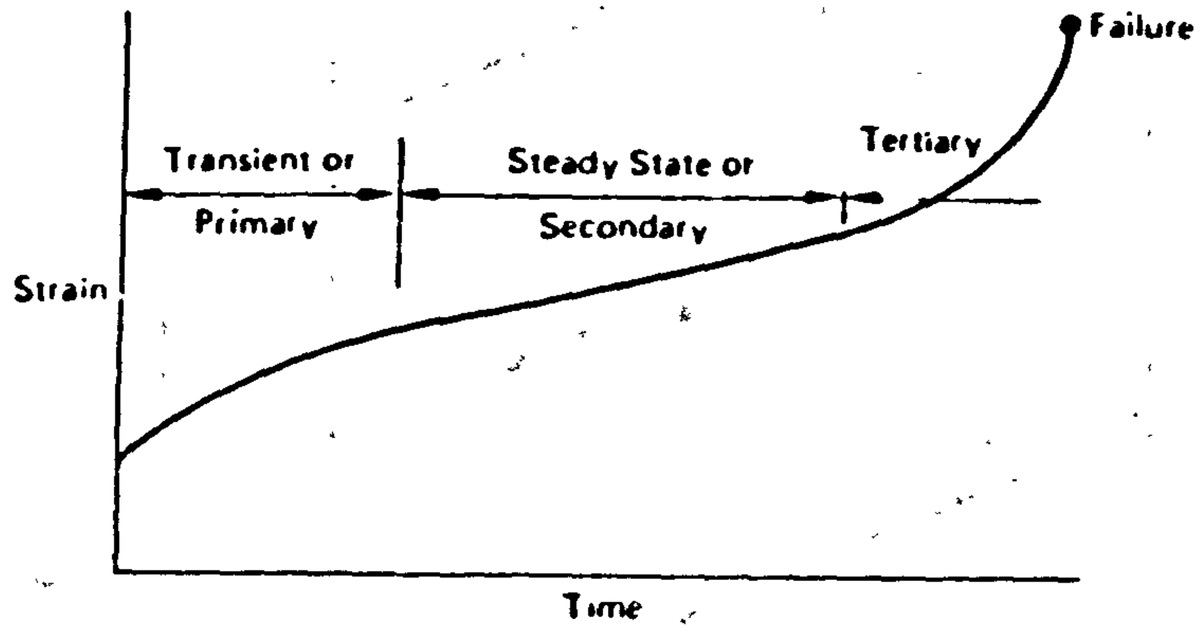

Fig. 5.96 Stages of creep. (after Mitchell)

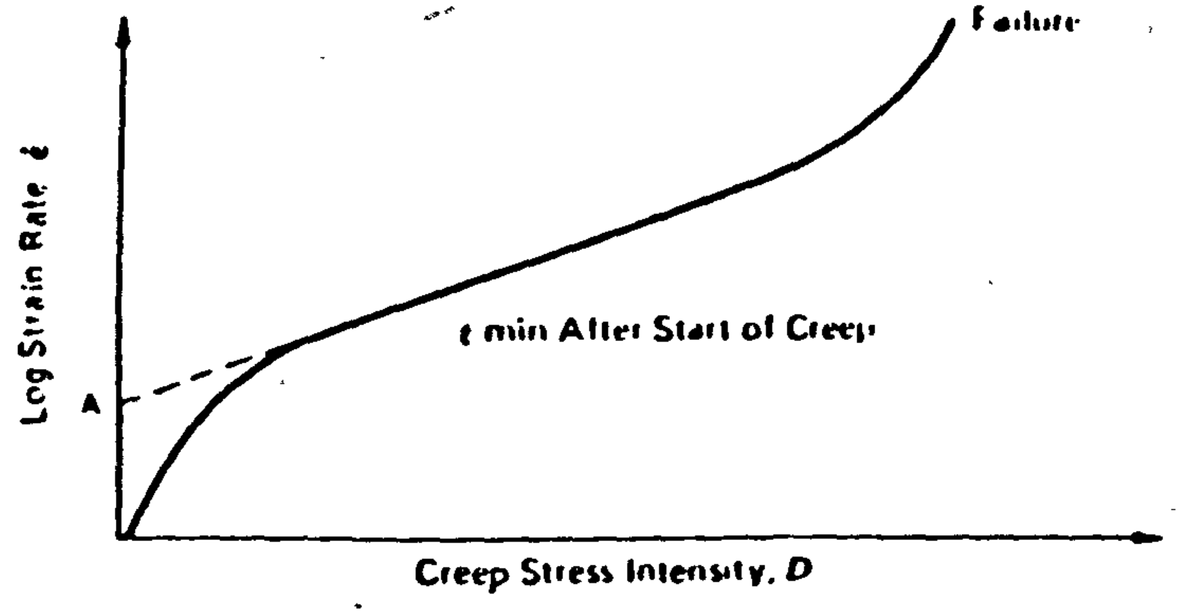

Fig. 5.97 Influence of creep stress intensity on creep rate. (after Mitchell)

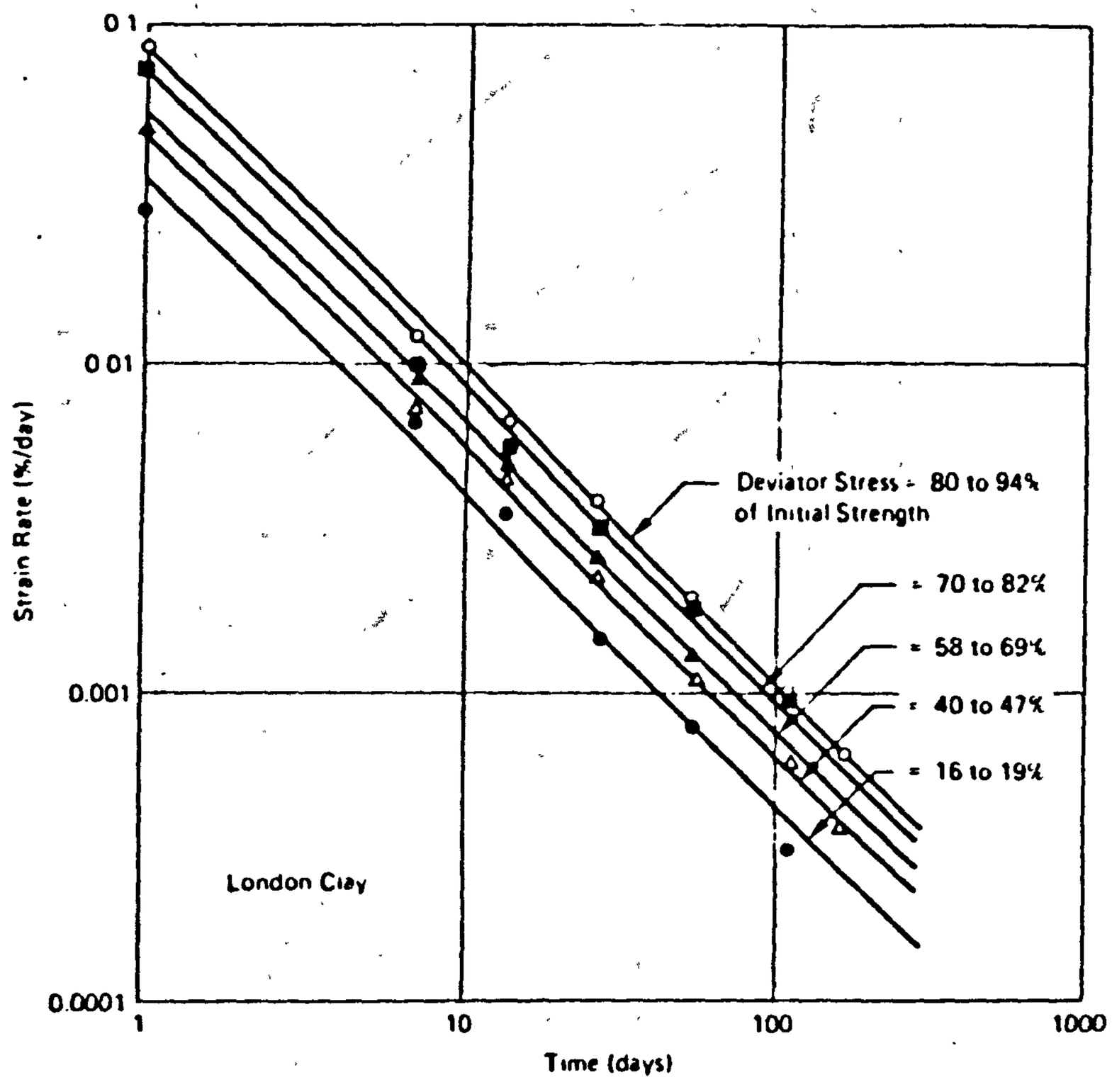

Fig. 5.98 Strain rate vs. time relationships during drained creep of London clay (Data from Bishop, 1966). (after Mitchell).

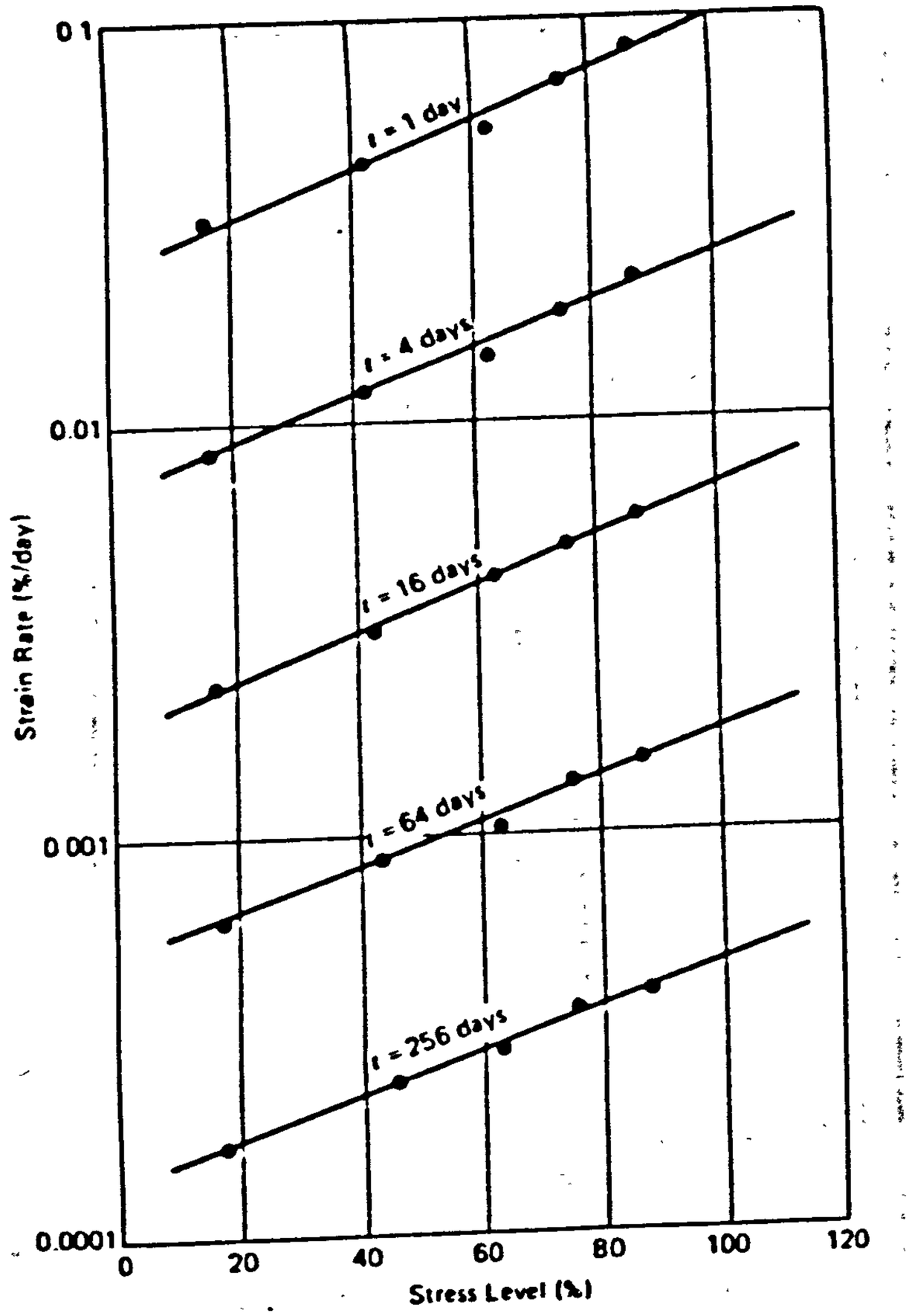

Fig. 5.99 Variation of strain rate with deviator stress for drained creep of London clay (Bishop, 1966). (after Mitchell)

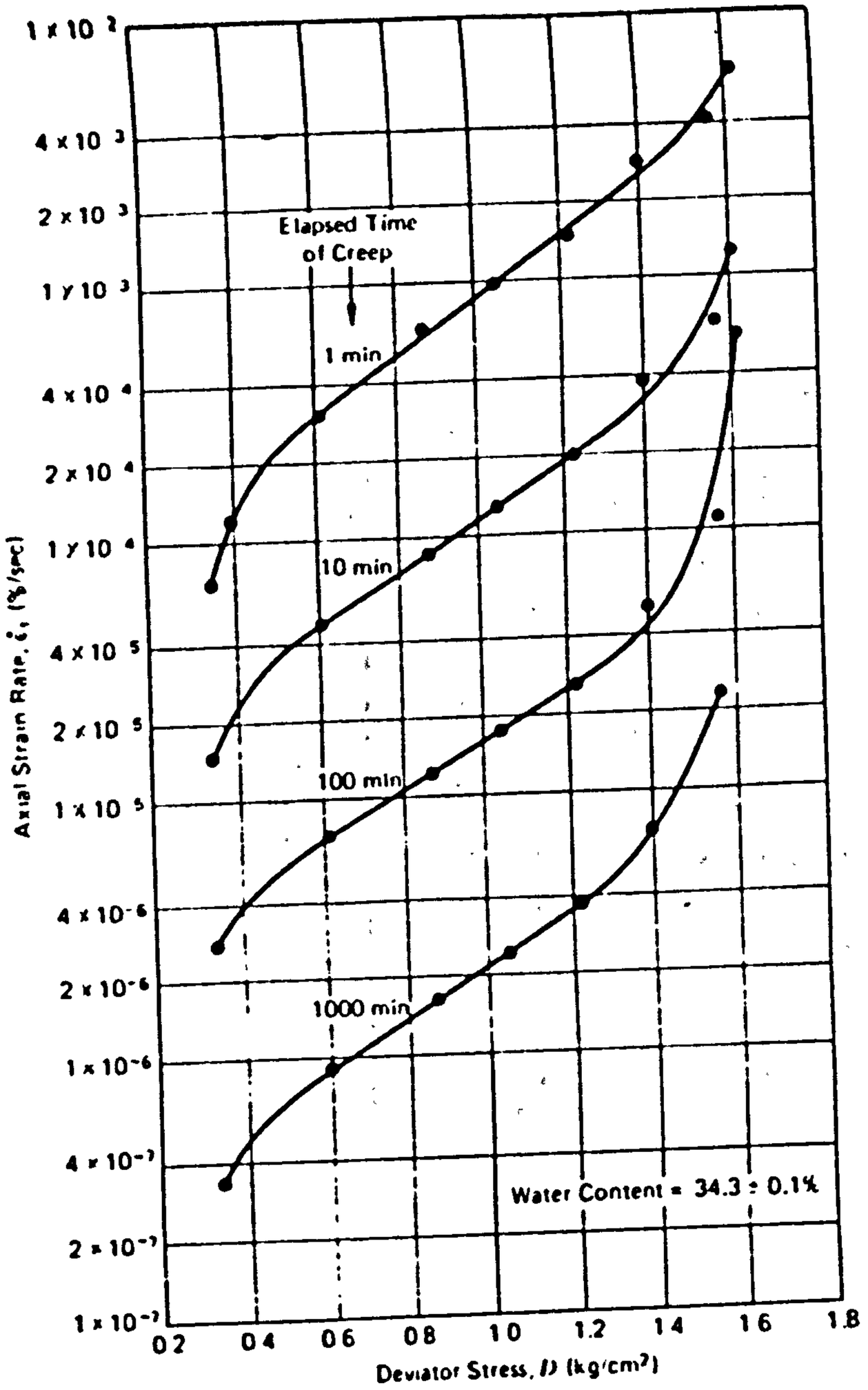

Fig. 5.100 Variation of strain rate with deviator stress for undrained creep of remolded illite. (after Mitchell)

Fig. 5.101 Creep Analysis of Mid-Ross Sand Mixed With Mesh Elements
(Determination of m)

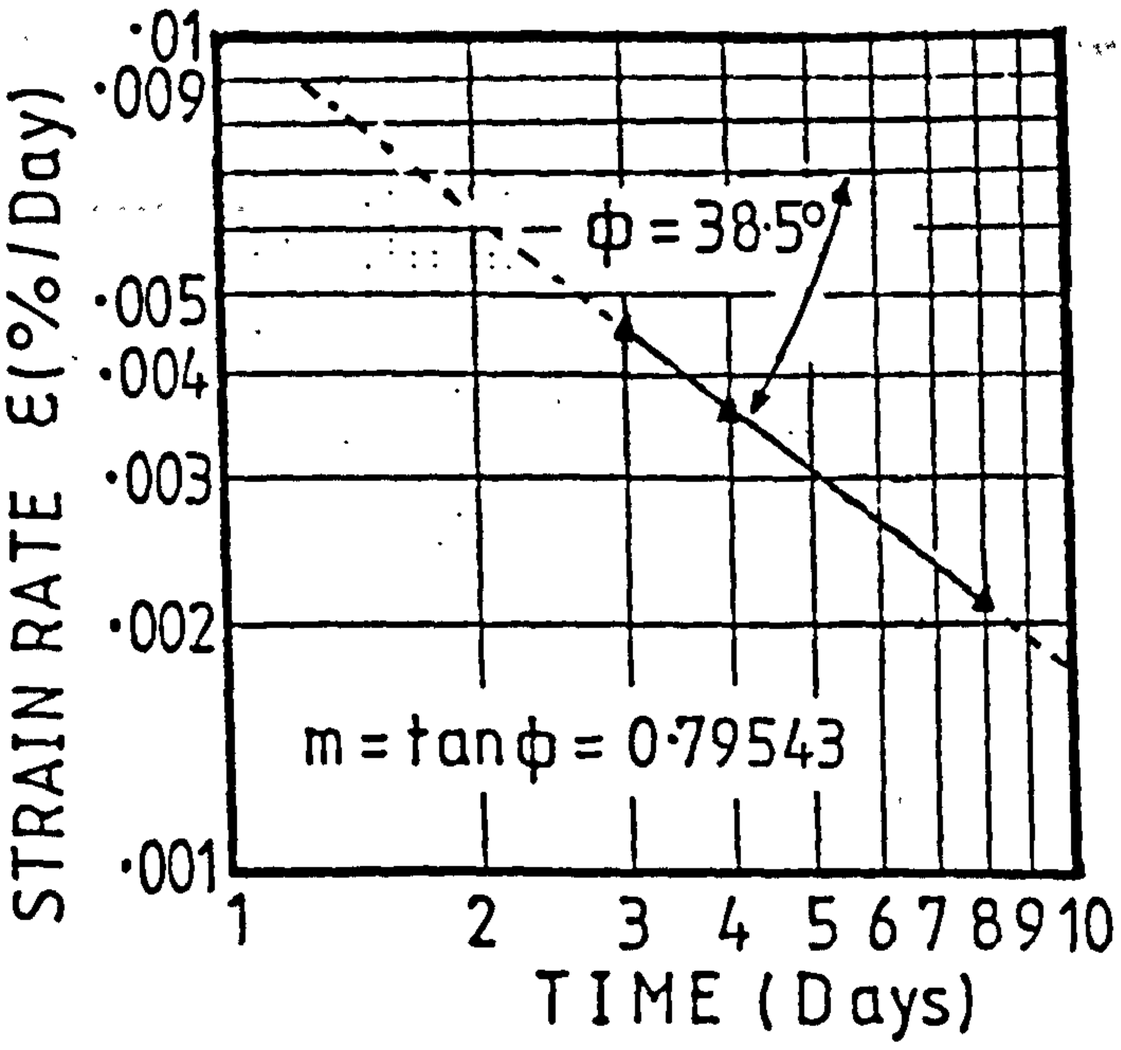

Fig. 5.102 Creep Analysis of Mid-Ross Sand Mixed With Mesh Elements
(Determination of A and a)

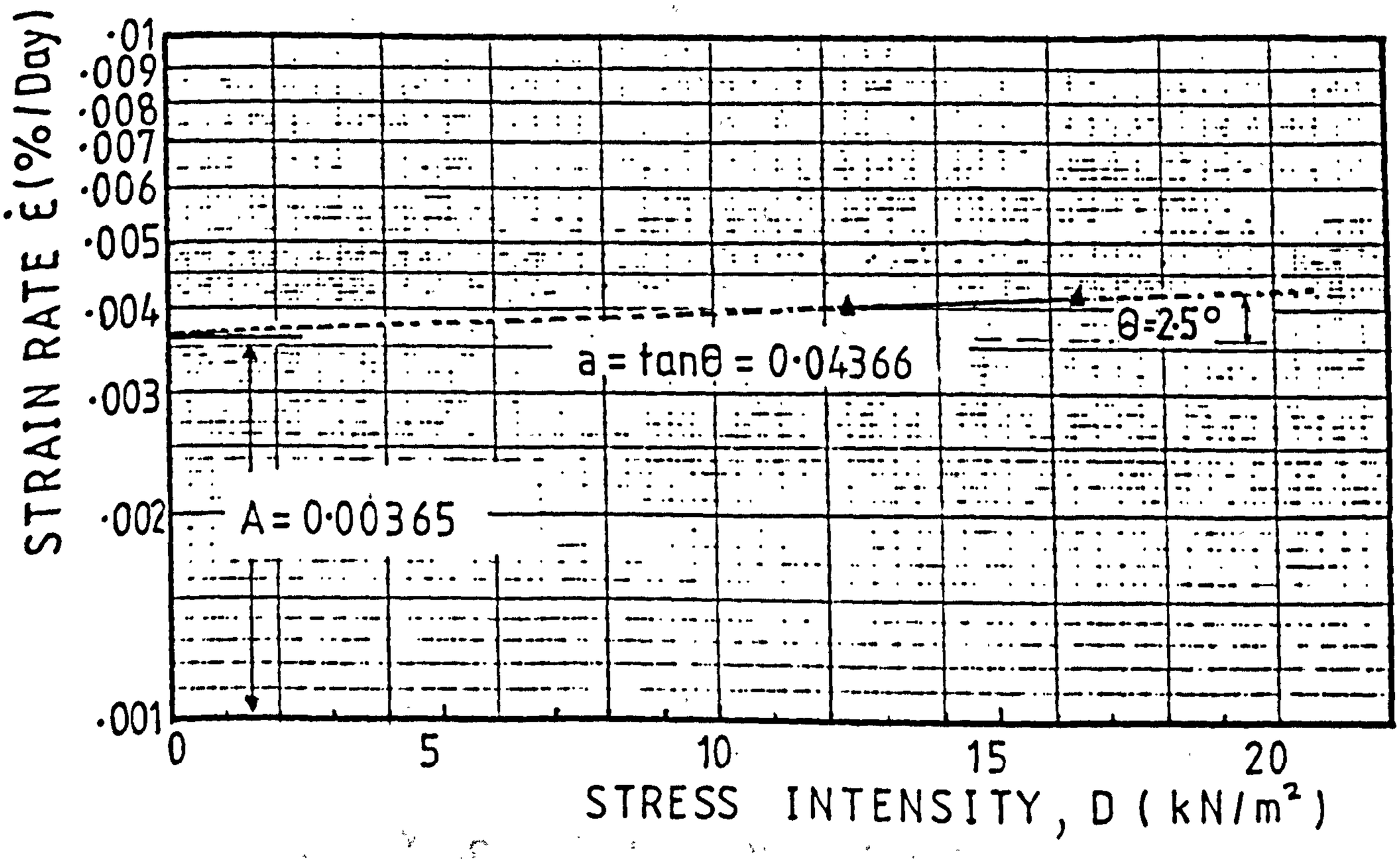

FOOTING TEST DATA

Leighton Buzzard sand alone

FIG. 6.1

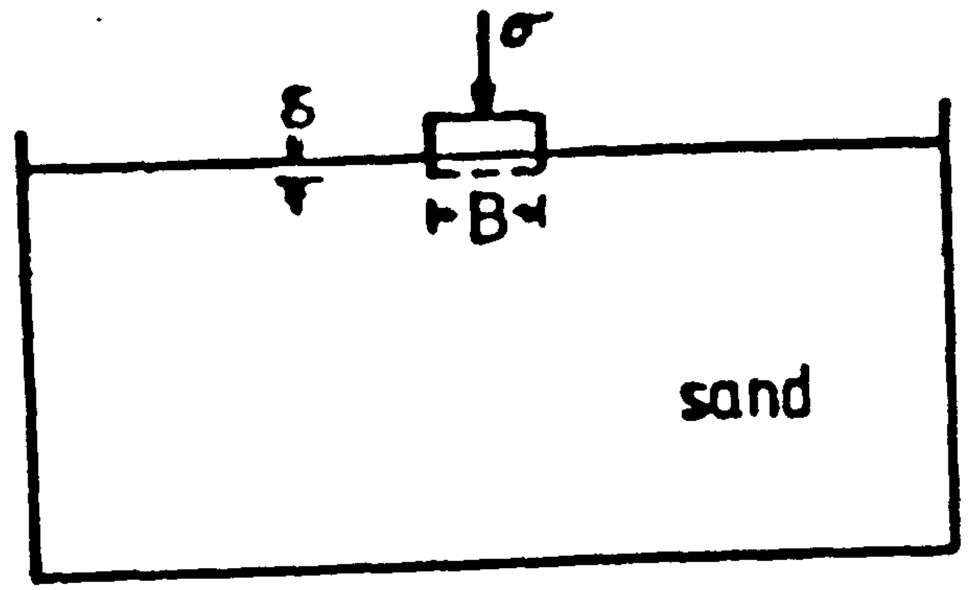

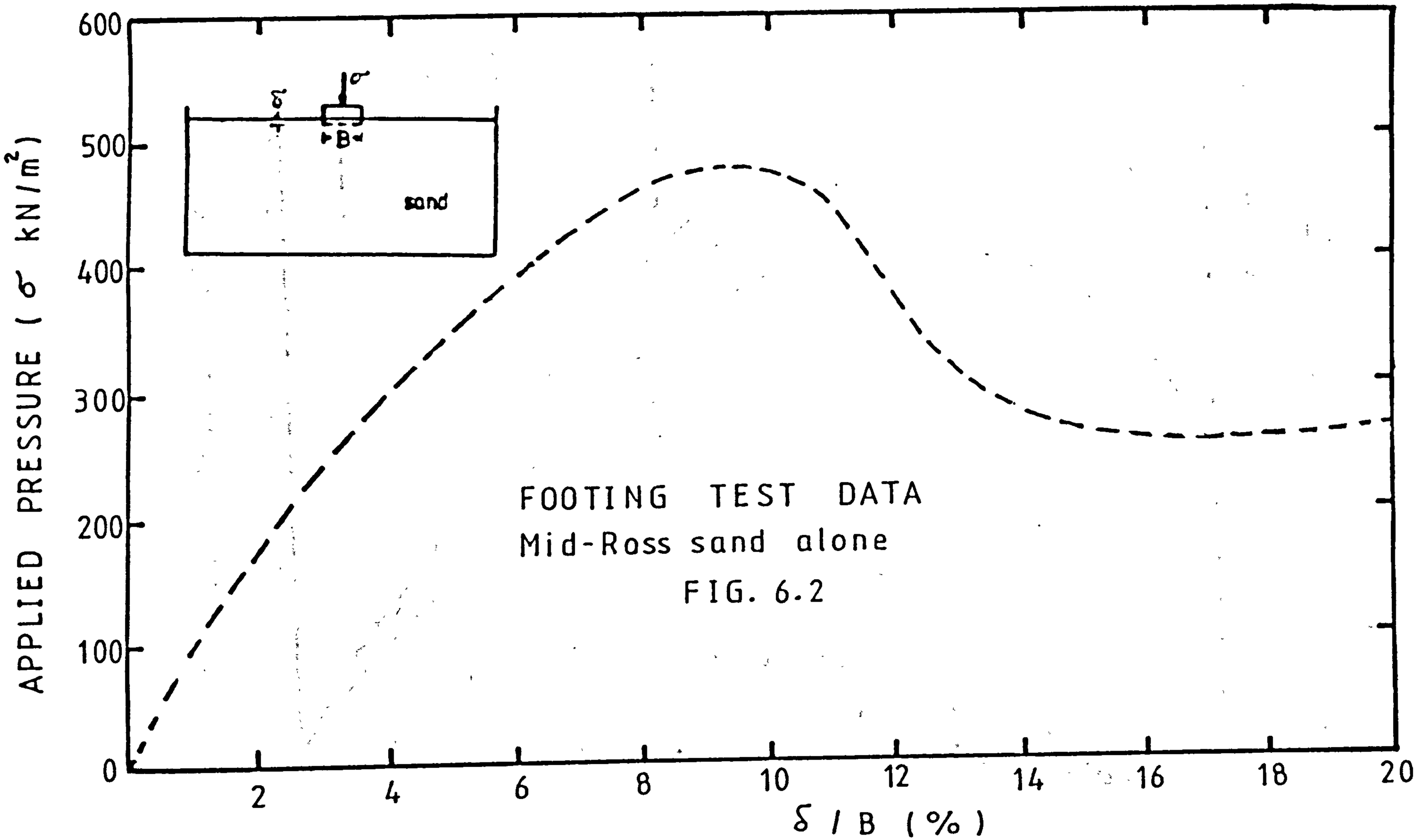

FOOTING TEST DATA
Mid-Ross sand alone
FIG. 6.2

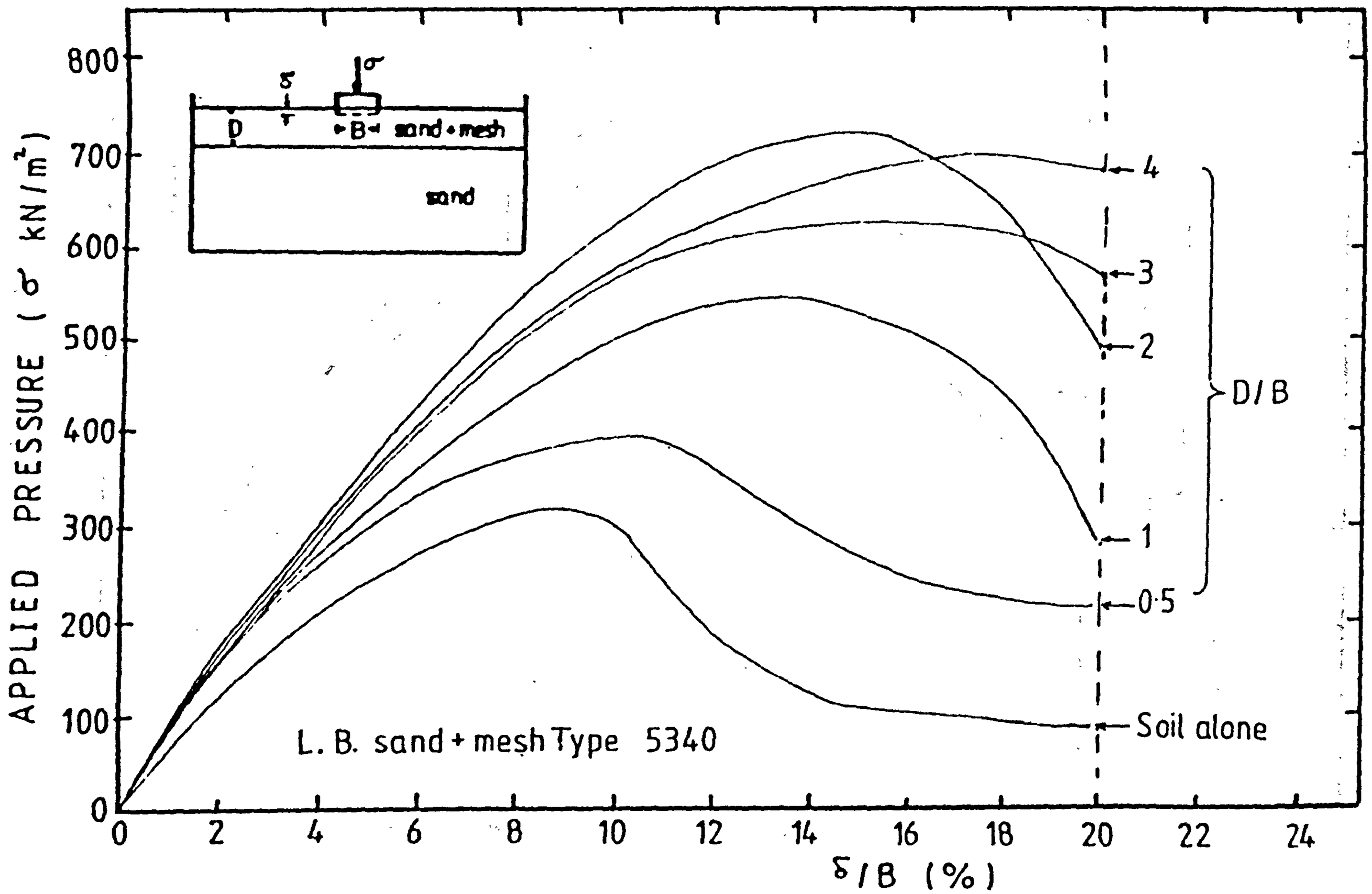

FIG. 6.3 Footing tests - effect of the depth of the stabilised layer on the load-settlement behaviour. Mesh element size 50 x 50 mm.

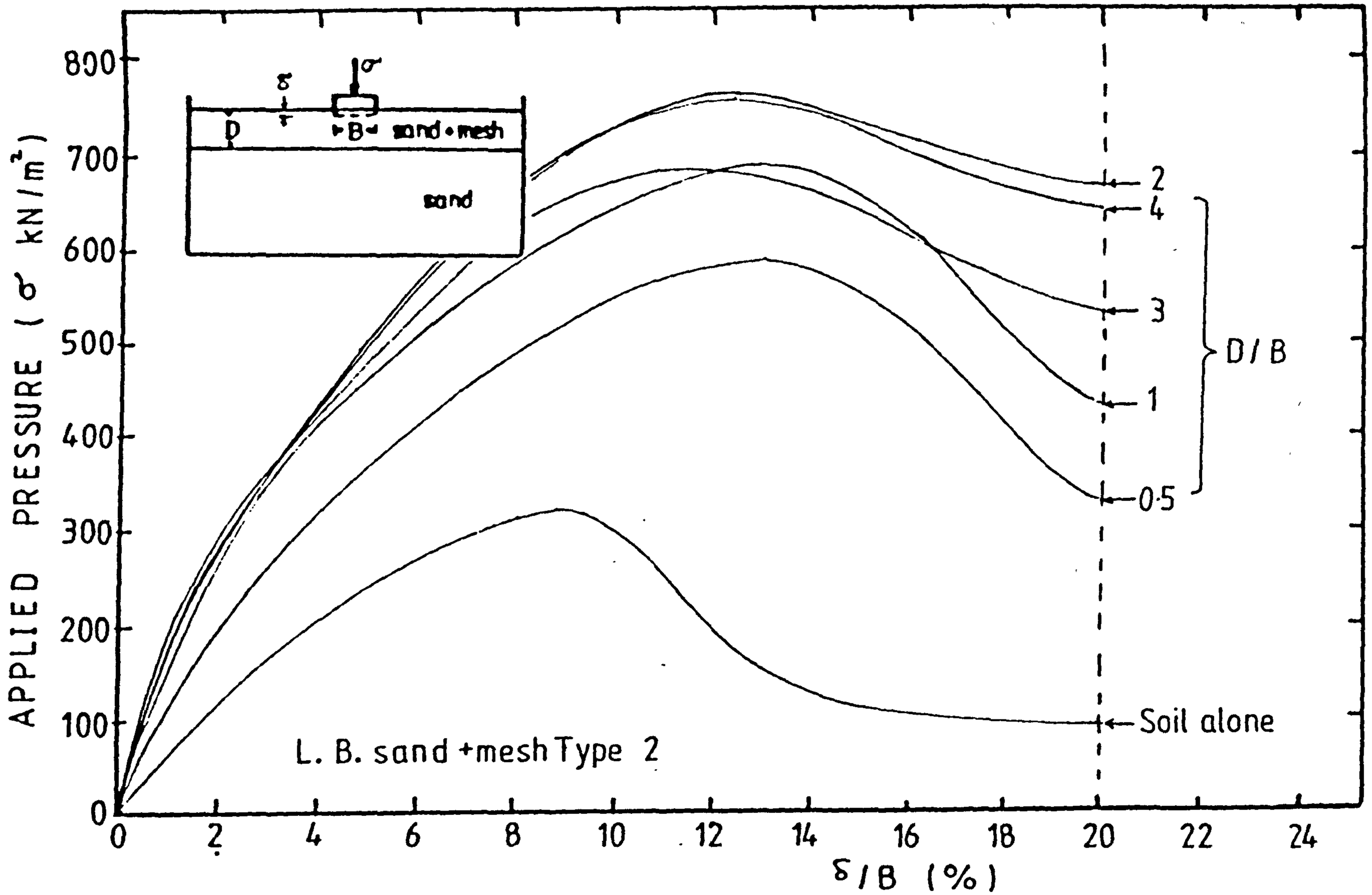

FIG. 6.4 Footing tests - effect of the depth of the stabilised layer on the load-settlement behaviour. Mesh element size 50 x 50 mm.

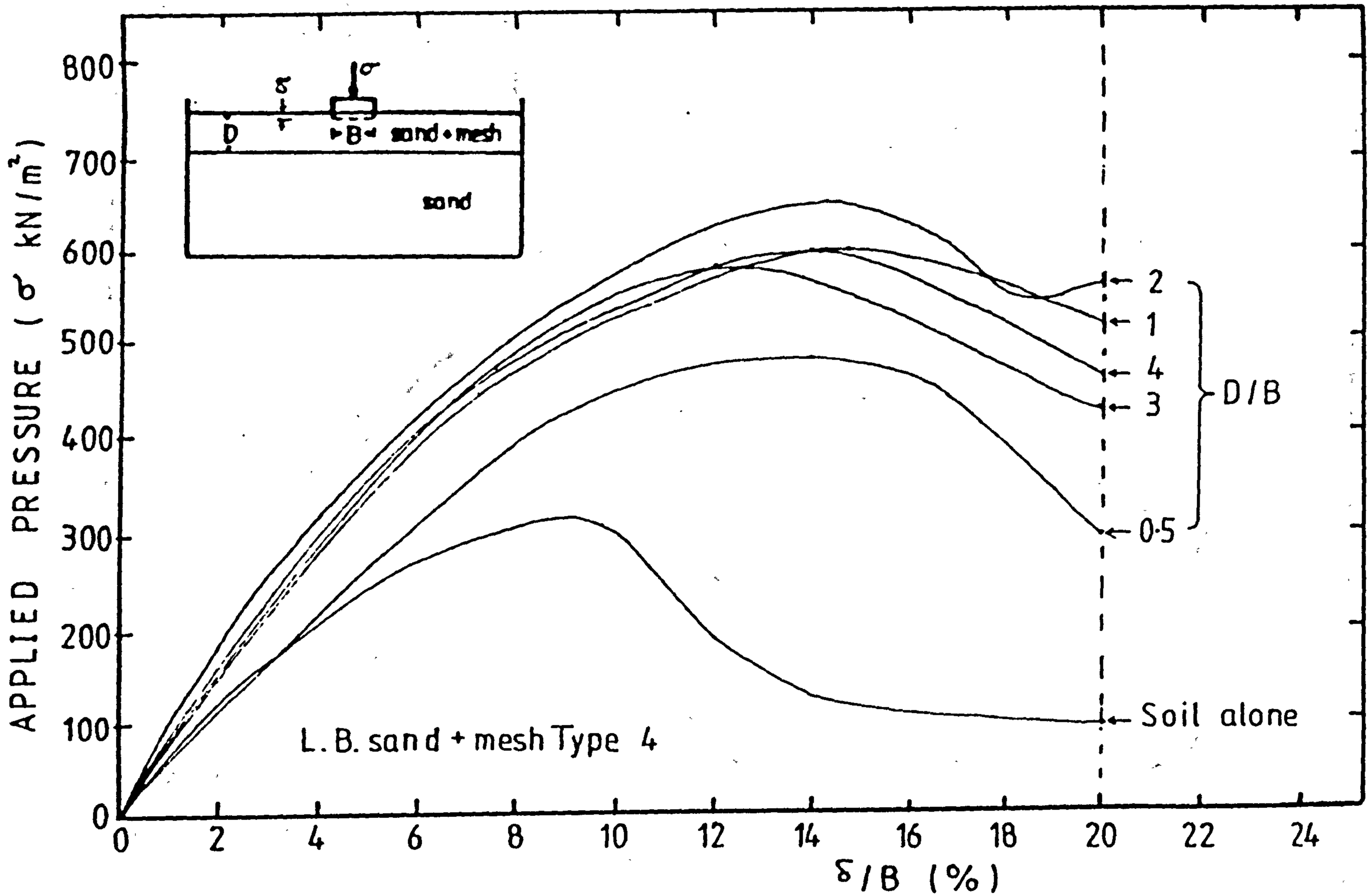

FIG. 6.5 Footing tests - effect of the depth of the stabilised layer on the load-settlement behaviour. Mesh element size 50 x 50 mm.

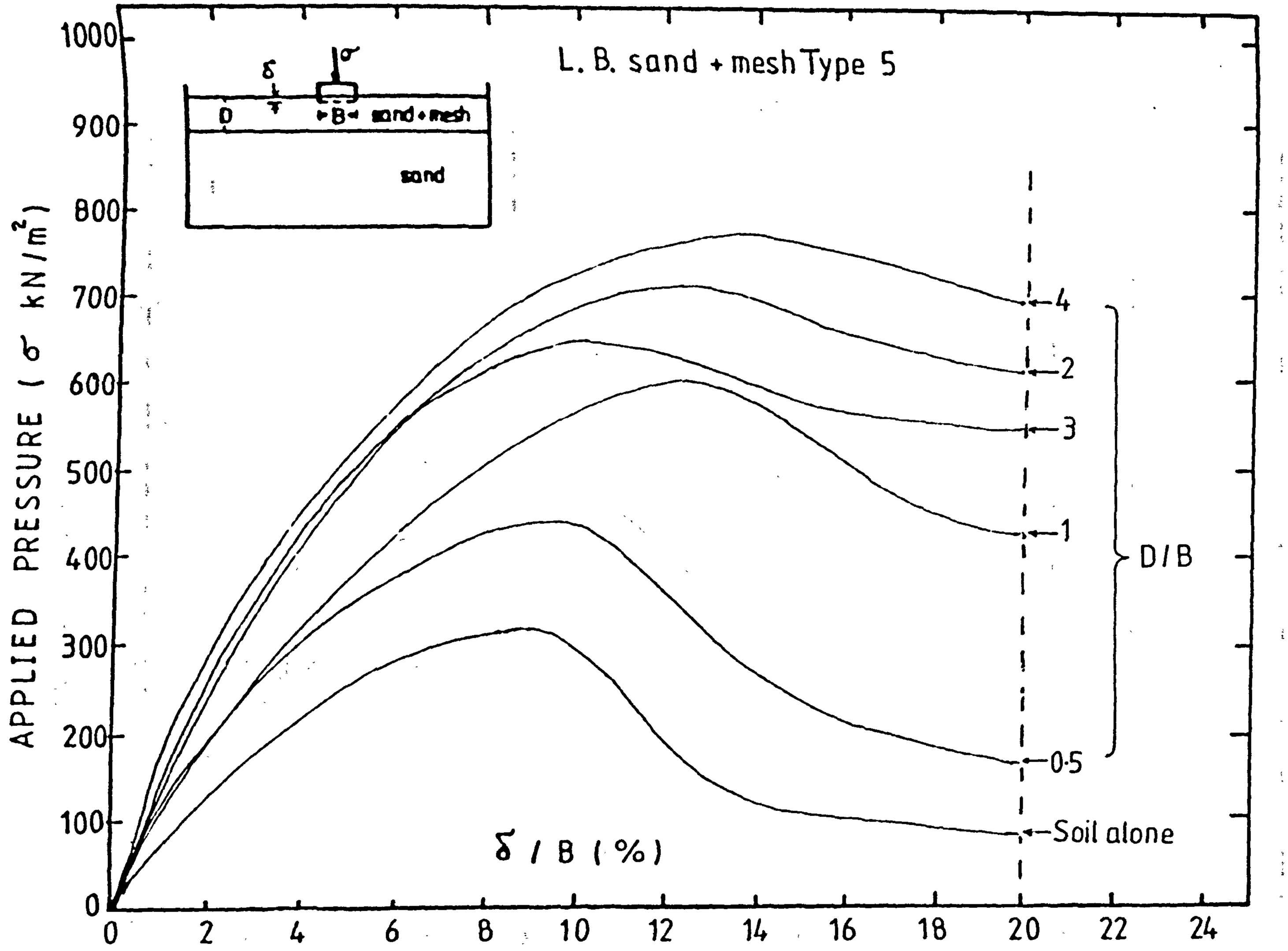

FIG. 6.6 Footing tests - effect of the depth of the stabilised layer on the load-settlement behaviour. Mesh element size 50 x 50 mm.

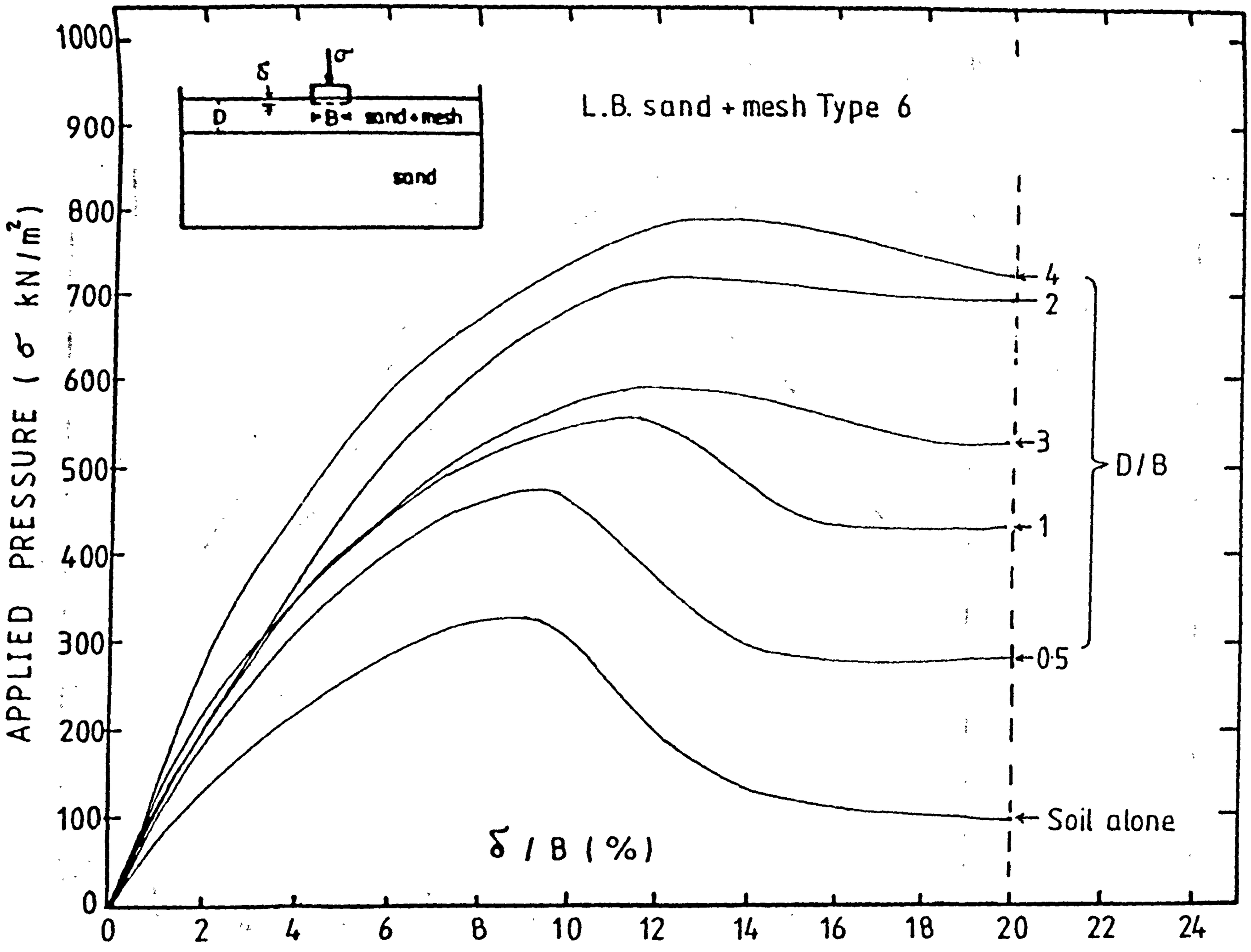

FIG. 6.7 Footing tests - effect of the depth of the stabilised layer on the load-settlement behaviour. Mesh element size 50 x 50 mm.

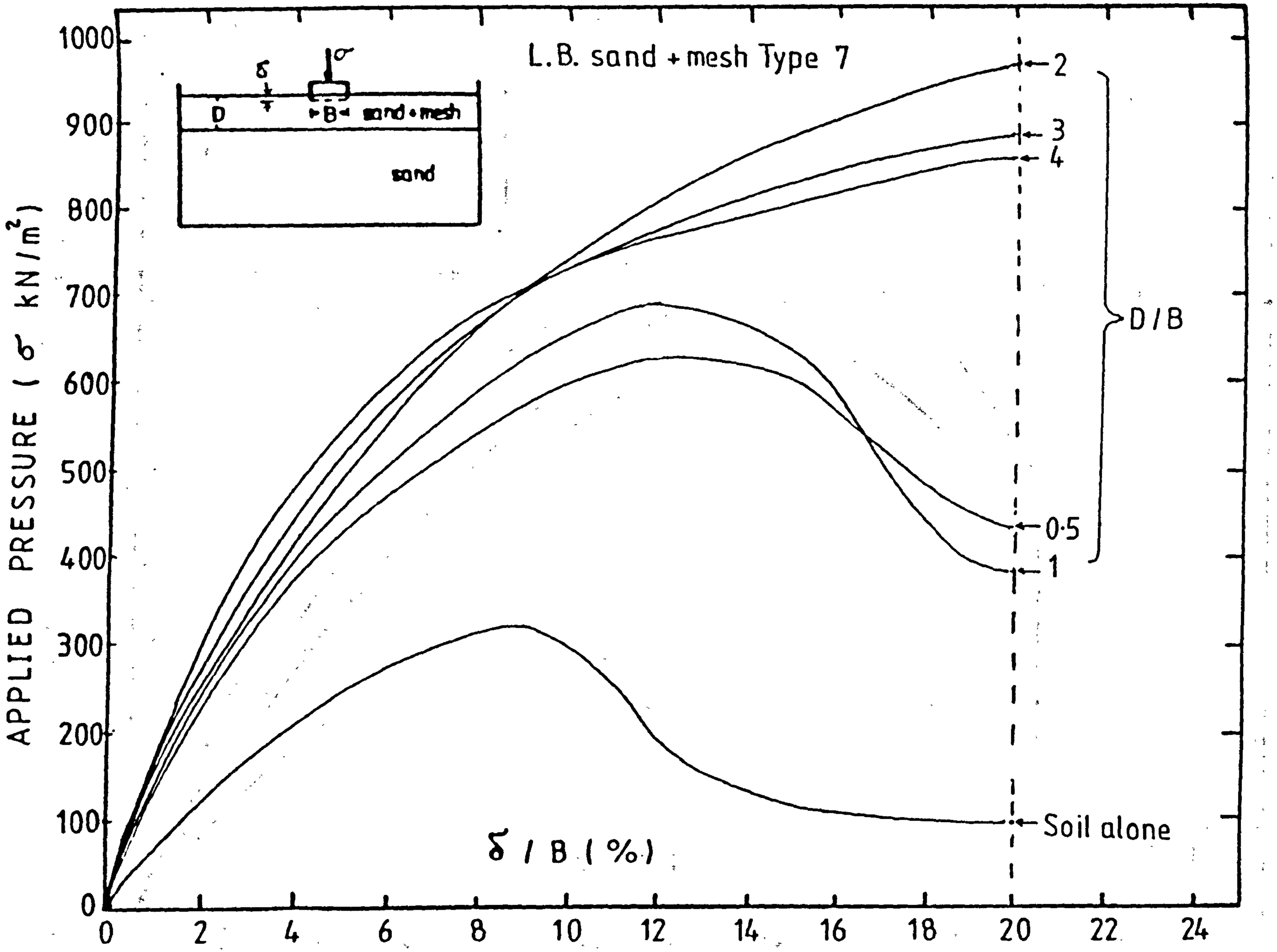

FIG. 6.8 Footing tests - effect of the depth of the stabilised layer on the load-settlement behaviour. Mesh element size 50 x 50 mm.

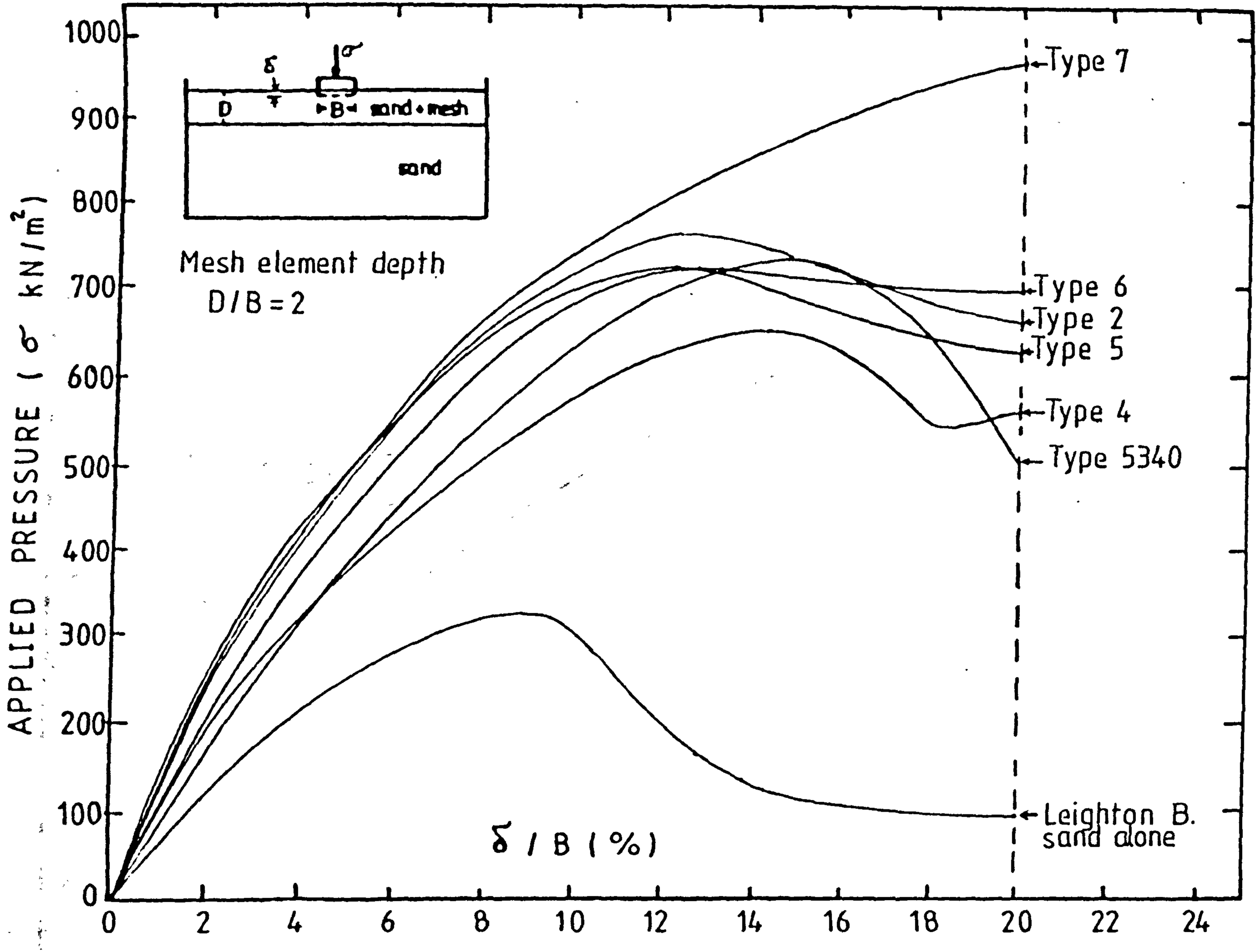

FIG. 6.9 Footing tests - effect of the depth of the stabilised layer on the load-settlement behaviour. Mesh element size 50 x 50 mm.

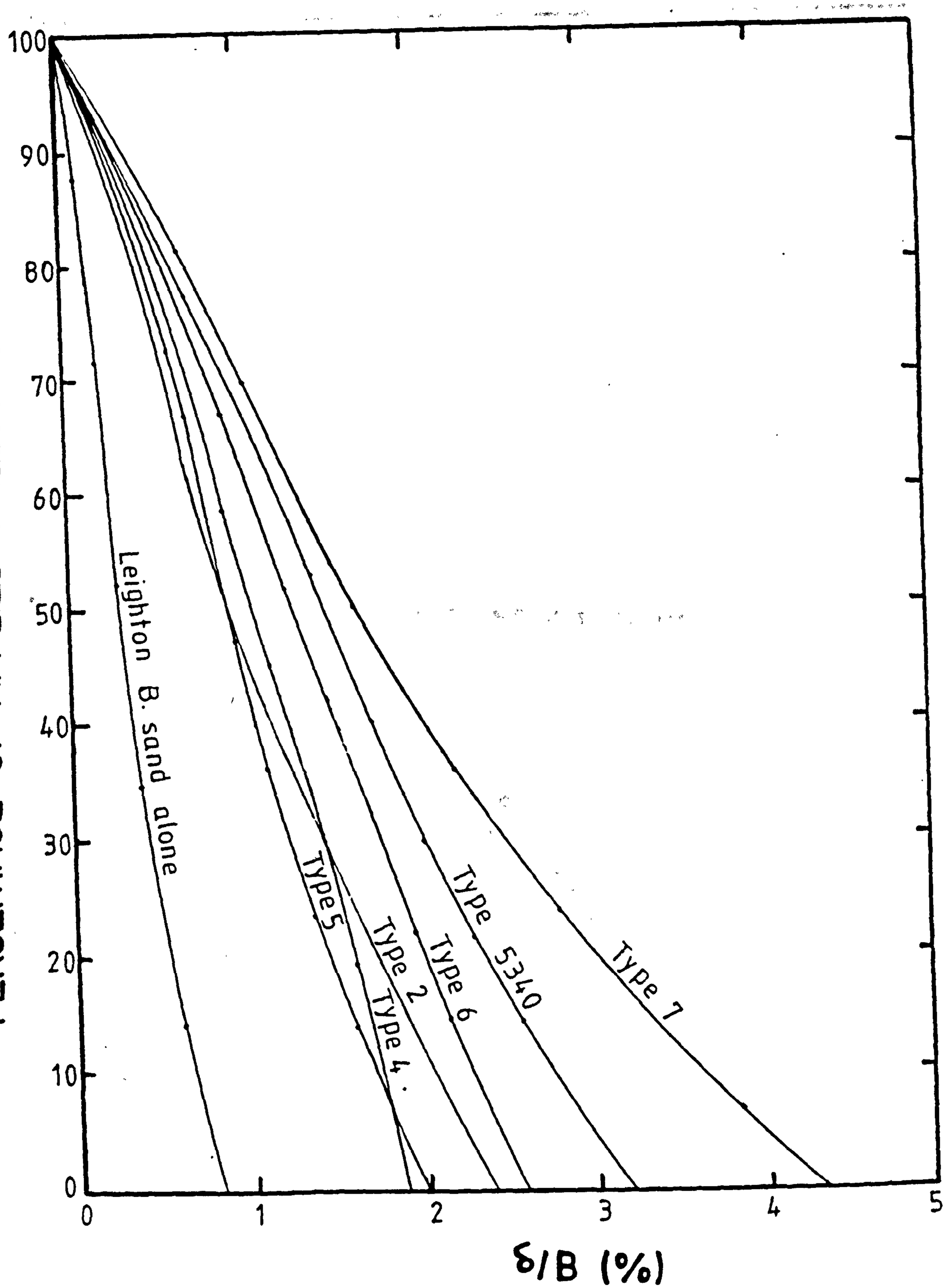

FIG. 6.10 Footing test - effect of mesh element on the unloading characteristics.

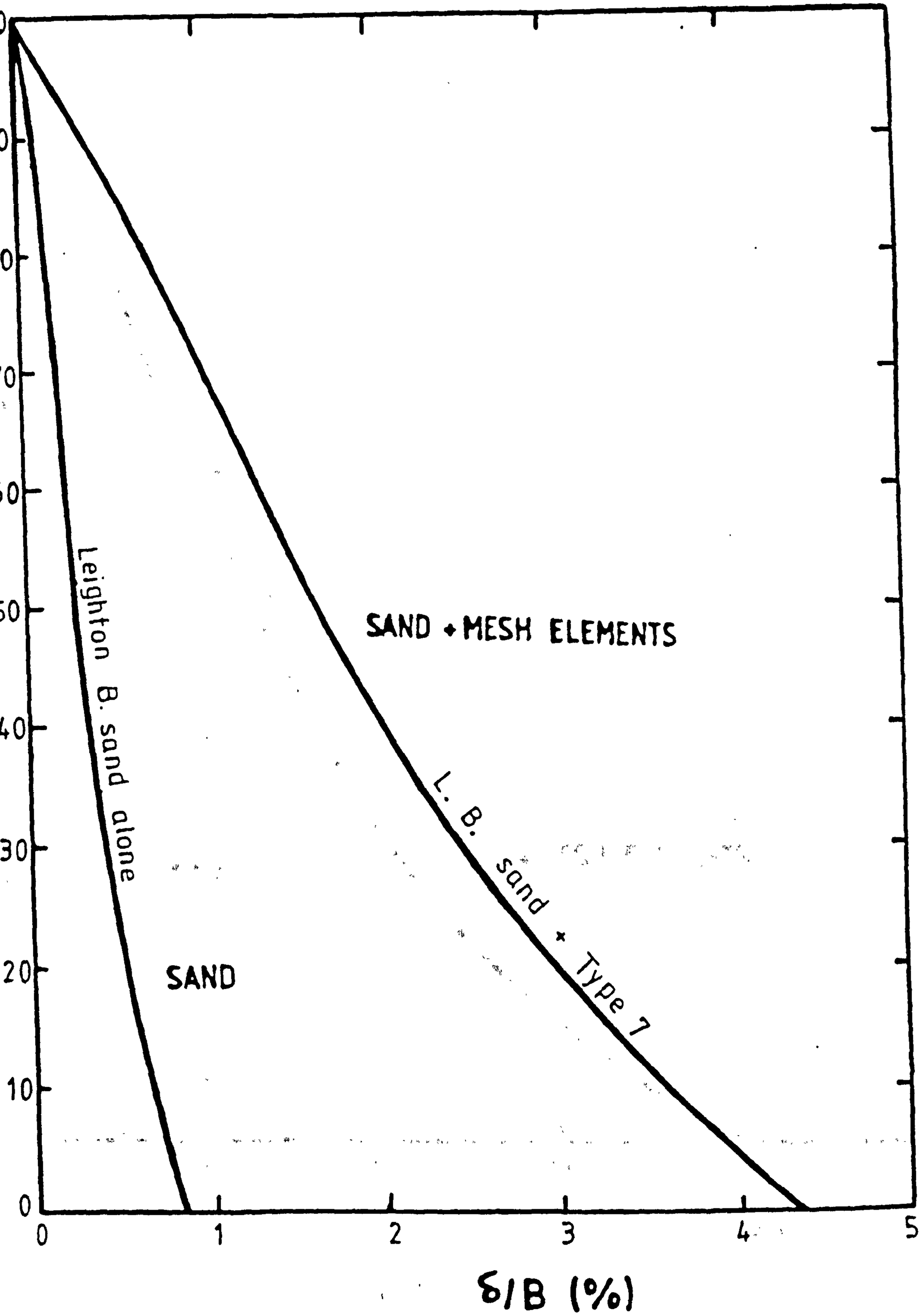

FIG. 6.11 Footing test - effect of mesh element on the unloading characteristics.

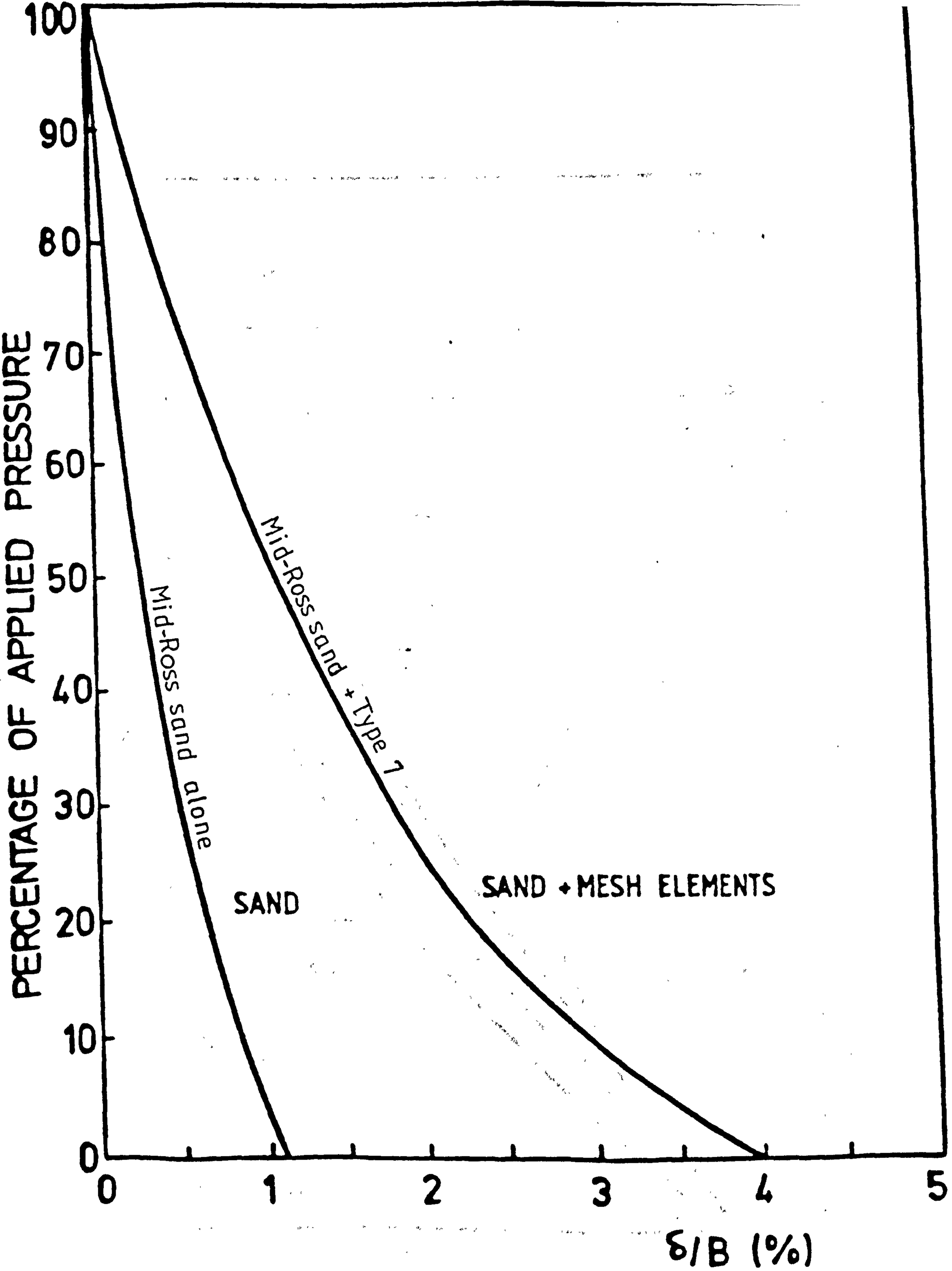

FIG. 6.12 Footing test - effect of mesh element on the unloading characteristics.

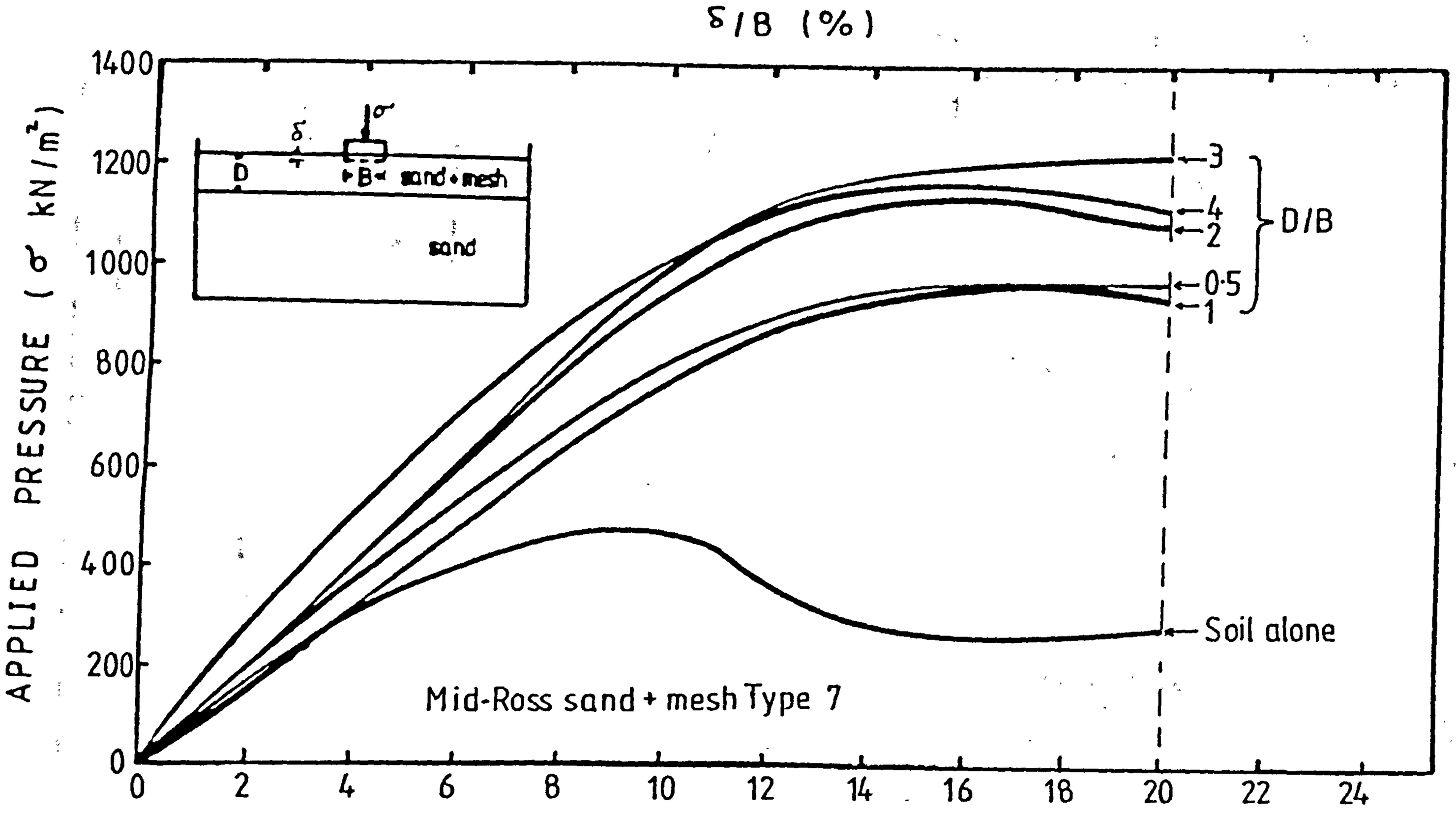

FIG. 6.13 Footing tests - effect of the depth of the stabilised layer on the load-settlement behaviour. Mesh element content 0.18%. Mesh size 50 x 50 mm.

FIG. 6.14 Footing tests - effect of the depth of the stabilised layer on the load-settlement behaviour. Mesh element size 50 x 50 mm.

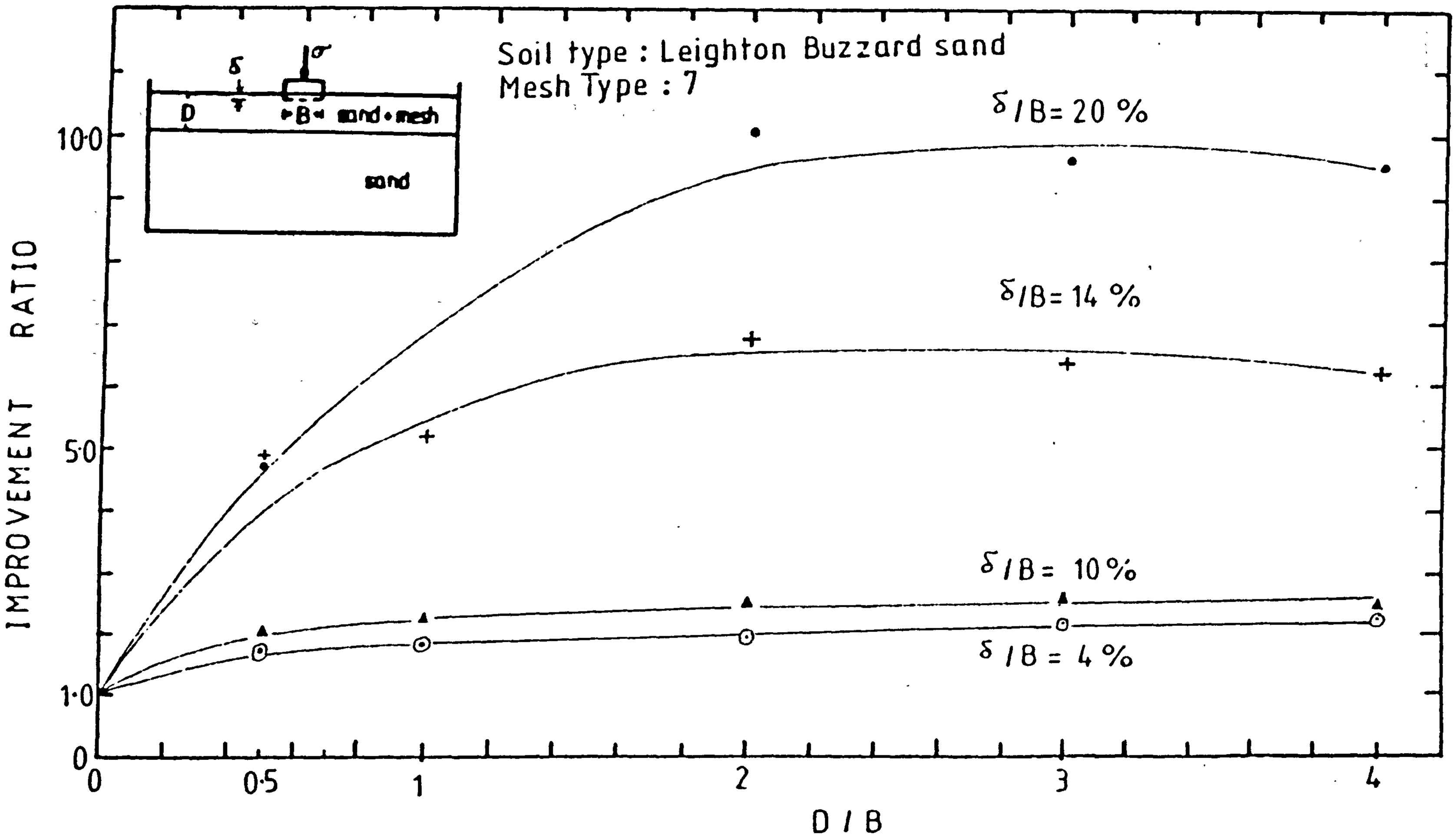

FIG. 6.15 Footing tests - effect of the depth of the stabilised layer on the load-settlement behaviour. Mesh element size 50 x 50 mm.

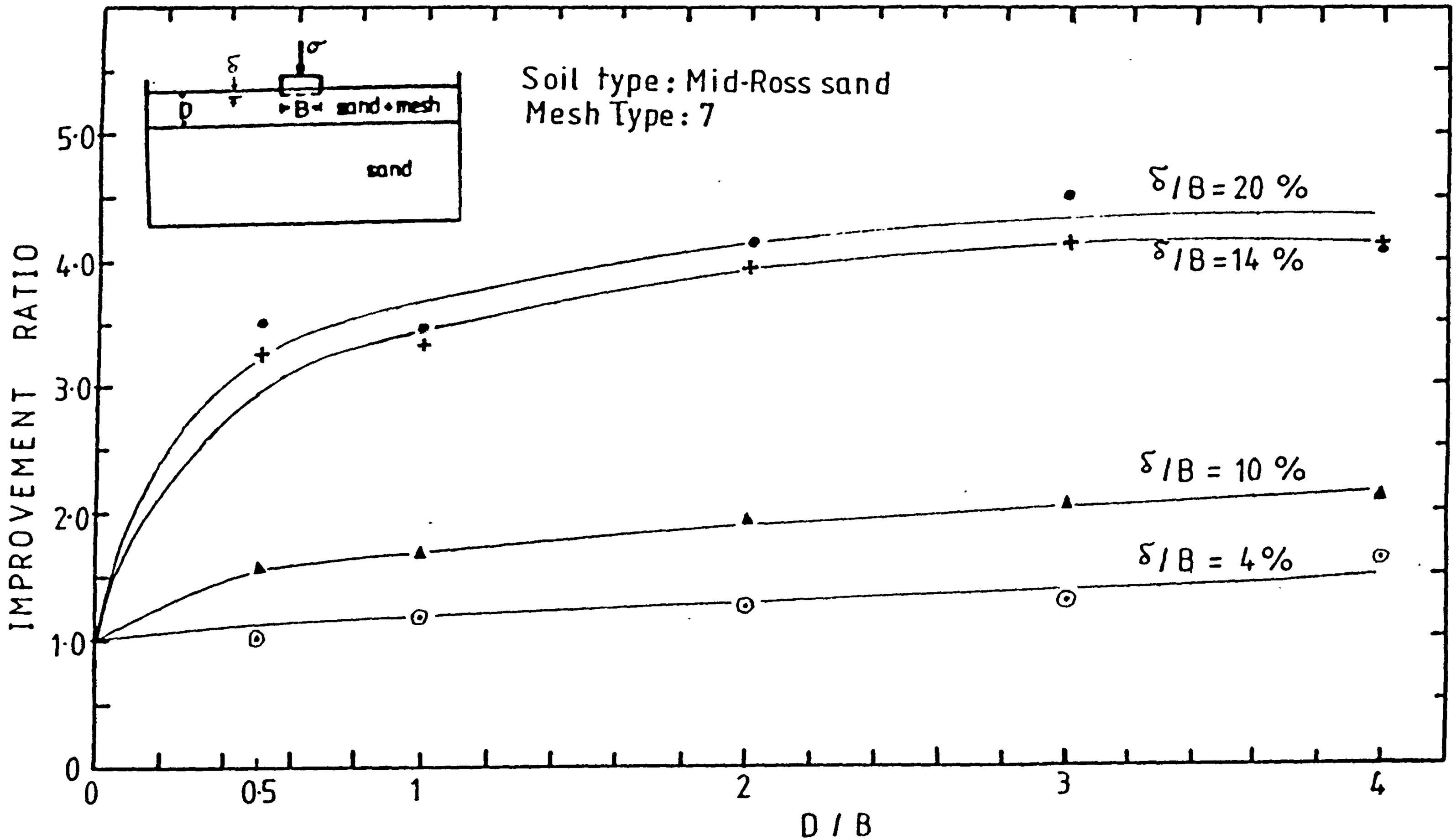

LIST

OF

TABLES

TABLE 3.1

MESH TYPE	Mass per unit area (gm/m^2)	Mesh Pitch Machine direction D_2 (mm)	Mesh Pitch Trans-verse machine direction D_1 (mm)	FILAMENT'S DIMENSIONS		
				HEIGHT h (mm)	WIDTH w (mm)	SHAPE w, h
5345	40.0	4.3	5.1	0.040	0.030	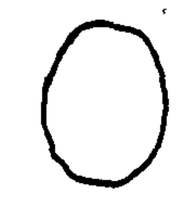
5340	18.5	6.2	7.2	0.022	0.021	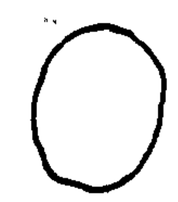
8630	15.4	3.3	3.5	0.010	0.009	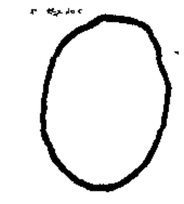
1	460.0	7.5	7.8	0.118	0.130	
2	128.0	17.8	4.7	0.03	0.06	
3	512.0	6.9	5.4	0.100	0.102	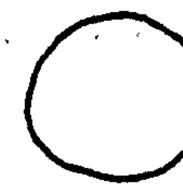
4	29.6	18.4	17.1	0.030	0.050	
5	41.0	19.6	17.3	0.05	0.100	
6	32.0	10.5	9.0	0.022	0.032	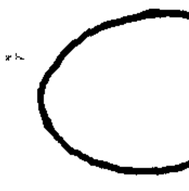
7	52.0	7.1	6.7	0.043	0.054	
10	40.0	10.0	10.0	0.060	0.039	
12	45.0	12.0	12.0	0.070	0.080	

TABLE 3.2

MESH TYPE	Mass per unit area (gm/m^2)	FLEXURAL Stiffness INDEX	Maximum average tensile strenght at 2%/min strain-rate (kN/m)
5345	40.0	5	2.78
5340	18.5	4	2.49
8630	15.4	1	1.30
1	460.0	65	5.71
2	126.0	12	3.32
3	512.0	40	6.04
4	29.6	4	3.09
5	41.0	9	4.31
6	32.0	7	2.51
7	52.0	10	3.36
10	40.0	10	3.45
12	45.0	9	3.76

TABLE 4.1

TEST PROGRAM OF COMPACTION & CBR TESTING

TYPE of SOIL	TYPE of Mesh Element	SIZE of Mesh Element (mm)	TYPE of Testing	RANGE OF TESTING	No of tests
Mid-Ross Sand	-	-	Compaction Tests	Variation of water content from 3.0% to 12.0%	34
Mid-Ross Sand	-	-	CBR Tests	Variation of CBR value with water content from 3.0% to 12.0%	34
Mid-Ross Sand	-	-	Compaction Tests	Estimation of an average Dry Density at 9.3% water content	10
Mid-Ross Sand	-	-	CBR Tests	Estimation of average CBR values at 9.3% water content	10
Mid-Ross Sand	5340	50x50 mm mm	Compaction Tests	Varying the percentage weight of the mesh-elements from 0.1% to 0.9% with respect to dry density of the soil	10
Mid-Ross Sand	5340	50x50 mm mm	CBR Tests	Establishing CBR values with respect to the mesh-element concentration from 0.1% to 0.9% weight	10

TABLE 4.1 (cont.)

TEST PROGRAM OF COMPACTION & CBR TESTING

TYPE of SOIL	TYPE of Mesh Element	SIZE of Mesh Element (mm)	TYPE of Testing	RANGE OF TESTING	No of tests
Mid-Ross Sand	8630	50x50 mm mm	Compaction Tests	Varying the percentage weight of the mesh-elements from 0.1% to 1.0% with respect to the dry density of the soil	14
Mid-Ross Sand	8630	50x50 mm mm	CBR Tests	Establishing CBR values with respect to the mesh-element concentration from 0.1% to 0.9% weight	14
Mid-Ross Sand	5345	50x50 mm	Compaction Tests	Varying the percentage weight of the mesh-elements from 0.1% to 0.9% with respect to the dry density of the soil	12
Mid-Ross Sand	5345	50x50 mm	CBR Tests	Establishing CBR values with respect to the mesh-element concentration from 0.1% to 0.9% weight	12
Mid-Ross	Type 1	50x50mm	Compaction Tests	Varying the percentage weight of mesh-elements from 0.1% to 0.6% with respect to the dry density of the soil	8

TABLE 4.1 (cont.)

TEST PROGRAM OF COMPACTION & CBR TESTING

TYPE of SOIL	TYPE of Mesh Element	SIZE of Mesh Element (mm)	TYPE of Testing	RANGE OF TESTING	No of tests
Mid-Ross Sand	Type 1	50x50 mm mm	CBR Tests	Establishing CBR values with respect to mesh-element concentration from 0.1% to 0.6%.	8
Mid-Ross Sand	Type 2	50x50 mm mm	Compaction Tests	Varying the percentage weight of the mesh-elements from 0.1% to 0.6% with respect to the dry density of the soil	6
Mid-Ross Sand	Type 2	50x50 mm mm	CBR Tests	Establishing CBR values with respect to this mesh element concentration from 0.1% to 0.6%	6
Mid-Ross Sand	Type 3	50x50 mm mm	Compaction Tests	Varying the percentage weight of the mesh-elements from 0.1% to 0.6% with respect to the dry density of the soil	6
Mid-Ross Sand	Type 3	50x50 mm mm	CBR Tests	Establishing CBR values with respect to this mesh element concentration from 0.1% to 0.6%	6

TABLE 4.1 (cont.)

TEST PROGRAM OF COMPACTION & CBR TESTING

TYPE of SOIL	TYPE of Mesh Element	SIZE of Mesh Element (mm)	TYPE of Testing	RANGE OF TESTING	No of tests
Mid-Ross Sand	Type 4	50x50 mm mm	Compaction Tests	Varying the percentage by dry soil weight of the mesh-elements from 0.1% to 0.6% with respect to the dry density of the soil	8
Mid-Ross Sand	Type 4	50x50 mm mm	CBR Tests	Establishing CBR values with respect to the mesh-element concentration from 0.1% to 0.6%	8
Mid-Ross Sand	Type 5	50x50 mm mm	Compaction Tests	Varying the percentage by dry soil weight of the mesh-elements from 0.1% to 0.6% with respect to the dry density of the soil	10
Mid-Ross Sand	Type 5	50x50 mm mm	CBR Tests	Establishing CBR values with respect to the mesh-element concentration from 0.1% to 0.6%	10
Mid-Ross Sand	Type 6	50x50mm mm	Compaction Tests	Varying the percentage by dry weight of the mesh-elements from 0.1% to 0.6% with respect to the dry density of the soil	10

TABLE 4.1 (cont.)

TEST PROGRAM OF COMPACTION & CBR TESTING

TYPE of SOIL	TYPE of Mesh Element	SIZE of Mesh Element (mm)	TYPE of Testing	RANGE OF TESTING	NO of tests
Mid-Ross Sand	Type 6	50x50 mm	CBR Tests	Establishing CBR values with respect to the mesh-element concentration from 0.1% to 0.6%	10
Mid-Ross Sand	Type 7	50x50 mm	Compaction Tests	Varying the percentage by dry weight of the mesh-elements from 0.1% to 0.6% with respect to the dry density of the soil	10
Mid Ross Sand	Type 7	50x50 mm	CBR Tests	Establishing CBR values with respect to the mesh-element concentration from 0.1% to 0.6%	10

TABLE 4.2

COMPACTION & C.B.R. TEST RESULTS

Mesh Type	Maximum CBR (bottom average between 0.1"/0.2" (%)	(%) ge of mesh required to reach max. CBR	Area/unit volume at max. CBR m^2/m^3	(%) ge of mesh required at 66 m^2/m^3	Corresponding max. CBR value at 66 m^2/m^3	Approximate Area/unit volume at an average 0·2(%) mesh content
5345	21·5	0·64	290	0·143	13·3	66
5340	12·5	0·35	310	0·069	6·9	66
8630	11·0	0·30	353	0·055	5·2	66
1	7·4	0·25	9·88	X	X	X
2	12·0	0·20	28·8	X	X	X Datum
3	8·5	0·175	6·30	X	X	X
4	24·0	0·40	252	0·103	7·7	66
5	16·1	0·52	231	0·146	6·2	66
6	11·5	0·46	260	0·115	6·2	66
7	16·6	0·52	158	0·180	8·1	66

TABLE 4.3

TEST PROGRAM OF COMPACTION & CBR TESTING

TYPE of SOIL	TYPE of Mesh Element	SIZE of Mesh Element (mm)	TYPE of Testing	RANGE OF TESTING	No of tests
Mid-Ross Sand	Type 7	50x100 mm	Compaction Tests	Varying the percentage by dry weight of these mesh-elements from 0.1% to 0.6% with respect to the dry density of the soil.	14
Mid-Ross Sand	Type 7	50x100 mm	CBR Tests	Establishing CBR values with respect to the mesh-element content from 0.1% to 0.6%.	14

TABLE 4.4

TEST PROGRAM OF COMPACTION & CBR TESTING

TYPE of SOIL	TYPE of Mesh Element	SIZE of Mesh Element (mm)	TYPE of Testing	RANGE OF TESTING	NO of tests
Leighton Buzzard Sand	-	-	Compaction Tests	Variation of water content from 8.0% to 0% establishing optimum moisture content and maximum dry density	12
Leighton Buzzard Sand	Type 7	50x50 mm	Compaction Tests	Varying the percentage by soil dry weight of mesh-elements from 0% to 0.6% with respect to the dry density of the soil.	14
Leighton Buzzard Sand	Type 7	50x 50. mm	CBR Tests	Establishing CBR values with respect to the mesh-element content from 0.1% to 0.6% at optimum water content.	14
Leighton Buzzard Sand	Type 7	50x100 mm	Compaction Tests	Varying the percentage by dry soil weight of mesh-elements from 0.1% to 0.6% with respect to the dry density of the soil.	8
Leighton Buzzard Sand	Type 7	50x100 mm	CBR Tests	Establishing CBR values with respect to the mesh-element content from 0.1% to 0.6%, at optimum water content.	8

TABLE 4.5

TEST PROGRAM OF COMPACTION & CBR TESTING

TYPE of SOIL	TYPE of Mesh Element	SIZE of Mesh Element (mm)	TYPE of Testing	RANGE OF TESTING	No of tests
West Highland Moraine	-	-	Compaction Tests	Variation of water content from 0% to 26%, establishing optimum water content and maximum dry density.	12
West Highland Moraine	Type 7	50x100 mm	Compaction Tests	Varying the percentage by dry soil weight of the mesh-elements from 0.1% to 0.3% with respect to the dry density of the soil.	10
West Highland Moraine	Type 7	50x100 mm	CBR Tests	Establishing CBR values with respect to the mesh-element content from 0.1% to 0.3% at optimum water content.	10

TABLE 4.6

Viscosity of water with respect to Temperature

TEMPERATURE (°C)	VISCOSITY (POISEUILLE)
0	1.7921 X 10 - 6
1	1.7313 X 10 - 6
2	1.6278 X 10 - 6
3	1.6191 X 10 - 6
4	1.5674 X 10 - 6
5	1.5188 X 10 - 6
6	1.4728 X 10 - 6
7	1.4284 X 10 - 6
8	1.3860 X 10 - 6
9	1.3462 X 10 - 6
10	1.3077 X 10 - 6
11	1.2713 X 10 - 6
12	1.2363 X 10 - 6
13	1.2028 X 10 - 6
14	1.1709 X 10 - 6
15	1.1404 X 10 - 6
16	1.1111 X 10 - 6
17	1.0828 X 10 - 6
18	1.0559 X 10 - 6
19	1.0299 X 10 - 6
20	1.0050 X 10 - 6
21	0.9810 X 10 - 6
22	0.9579 X 10 - 6
23	0.9358 X 10 - 6
24	0.9142 X 10 - 6
25	0.8937 X 10 - 6

NOTE : Poiseuille = kg s^{-1} m^{-1} = Nsm

TABLE 4.7

Coefficient of Permeability of Mid-Ross Sand Alone							
TEST NO	TEMP. (°C)	CONFIN. PRES-SURE (kN/m^2)	Δh (mm)	Δh/L	k (m/s) $\times 10^{-4}$	AVER. k (m/s) $\times 10^{-4}$	AVER. k $(m/s) \times 10^{-4}$ at 20 °C
1	19	0	192	1·71	2·75	2·64	2·70
2	19	0	152	1·36	2·86		
3	19	0	460	4·03	2·99		
4	19	0	379	3·38	2·59		
5	19	0	390	3·48	2·02		
6	19	25	277	2·76	2·59	2·52	2·58
7	19	25	365	3·59	2·45		
8	19	50	330	3·25	1·97	1·97	2·02
9	19	150	400	3·97	1·86		1·91
10	19	300	390	3·90	1·85	1·85	1·90

TABLE 4.8

Coefficient of Permeability of Mid-Ross Sand Mixed With Mesh Elements

TEST NO	TEMP. (°C)	CONFIN. PRES-SURE (kN/m^2)	Δh (mm)	$\Delta h/L$	k (m/s) $\times 10^{-4}$	AVER. k (m/s) $\times 10^{-4}$	AVER. k (m/s) $\times 10^{-4}$ at 20 °C
1	22·5	0	192	1·69	2·62	2·67	2·69
2	22·5	0	156	1·37	2·67		
3	22·5	0	475	4·18	2·67		
4	22·5	0	370	3·26	2·66		
5	21·5	0	370	3·26	2·75		
6	21·5	25	350	3·41	2·31	2·31	2·28
7	21·5	25	370	3·61	2·31		
8	21·0	50	405	3·95	2·25	2·25	2·19
9	21·0	150	400	3·95	2·17	2·17	2·11
10	21·0	300	391	3·88	2·09	2·09	2·04

TABLE 4.9

Coefficient of Permeability of West Highland Moraine Alone

TEMP. (°C)	CONFIN. PRES-SURE (kN/m^2)	AVER. k (m/s) $\times 10^{-6}$	AVER. k $(m/s) \times 10^{-6}$ at 20 °C
19.0	0	2.13	2.18
19.0	25	1.87	1.92
19.0	50	1.73	1.77

Coeff. of Perm. of West Highland Moraine Mixed With Mesh Elements

TEMP. (°C)	CONFIN. PRES-SURE (kN/m^2)	AVER. k (m/s) $\times 10^{-6}$	AVER. k $(m/s) \times 10^{-6}$ at 20 °C
18.0	0	2.38	2.48
19.0	25	1.69	1.74
19.0	50	1.52	1.56

TABLE 4.10

CLASSIFICATION OF SOIL ACCORDING TO PERMEABILITY

Degree of permeability	*Range of coefficient of permeability, k (m/s)*
High	Greater than 10^{-3}
Medium	10^{-3} - 10^{-5}
Low	10^{-4} - 10^{-7}
Very low	10^{-5} - 10^{-9}
Practically impermeable	Less than 10^{-9}

TABLE 5.1

TRIAXIAL TESTING PROGRAM

Rate of Strain (%)/min	Type of Soil	Type of Mesh Element	Size of Mesh Element (mm)	Mesh Element content (%) by weight	Mesh Element content (m^2/m^3)	Cell pressure (kN/m^2)	Number of Tests
0.05	M.R.sand	NONE	NONE	NONE	NONE	10	2
"	"	"	"	"	"	25	2
"	"	"	"	"	"	50	2
"	"	"	"	"	"	100	2
"	"	"	"	"	"	150	2
"	"	"	"	"	"	200	2
0.05	M.R.sand	NONE	NONE	NONE	NONE	300	2
0.05	M.R.sand	7	50x50	0.09	33	0	2
"	"	"	"	"	"	10	1
"	"	"	"	"	"	25	2
"	"	"	"	"	"	50	1
"	"	"	"	"	"	100	2
"	"	"	"	"	"	150	2
"	"	"	"	"	"	200	1
0.05	M.R.sand	7	50x50	0.09	33	300	1

TABLE 5.1 (cont.)

TRIAXIAL TESTING PROGRAM

Rate of Strain (%)/min	Type of Soil	Type of Mesh Element	Size of Mesh Element (mm)	Mesh Element content (%) by weight	Mesh Element content (m^2/m^3)	Cell pressure (kN/m^2)	Number of Tests
0.05	M.R.sand	7	50x50	0.18	66	0	2
"	"	"	"	"	"	10	1
"	"	"	"	"	"	25	2
"	"	"	"	"	"	50	1
"	"	"	"	"	"	100	1
"	"	"	"	"	"	150	2
"	"	"	"	"	"	200	1
0.05	M.R.sand	7	50x50	0.18	66	300	1
0.05	M.R.sand	7	50x50	0.24	90	0	2
"	"	"	"	"	"	10	1
"	"	"	"	"	"	25	2
"	"	"	"	"	"	50	1
"	"	"	"	"	"	100	1
"	"	"	"	"	"	150	2
"	"	"	"	"	"	200	1
0.05	M.R.sand	7	50x50	0.24	90	300	1

TABLE 5.1 (cont.)

TRIAXIAL TESTING PROGRAM

Rate of Strain (%)/min	Type of Soil	Type of Mesh Element	Size of Mesh Element (mm)	Mesh Element content (%) by weight	Mesh Element content (m^2/m^3)	Cell pressure (kN/m^2)	Number of Tests
0.05	L.B.sand	NONE	NONE	NONE	NONE	10	2
"	"	"	"	"	"	25	2
"	"	"	"	"	"	50	2
"	"	"	"	"	"	150	2
0.05	L.B.sand	NONE	NONE	NONE	NONE	300	2
0.05	L.B.sand	7	50x50	0.10	33	0	1
"	"	"	"	"	"	10	2
"	"	"	"	"	"	25	1
"	"	"	"	"	"	50	1
"	"	"	"	"	"	150	2
0.05	L.B.sand	7	50x50	0.10	33	300	1
0.05	L.B.sand	7	50x50	0.20	66	0	2
"	"	"	"	"	"	10	2
"	"	"	"	"	"	25	1
"	"	"	"	"	"	50	1
"	"	"	"	"	"	150	2
0.05	L.B.sand	7	50x50	0.20	66	300	1

TABLE 5.1 (cont.)

TRIAXIAL TESTING PROGRAM

Rate of Strain (%)/min	Type of Soil	Type of Mesh Element	Size of Mesh Element (mm)	Mesh Element content (%) by weight	Mesh Element content (m^2/m^3)	Cell pressure (kN/m^2)	Number of Tests
0.05	L.B.sand	7	50x50	0.27	90	0	2
"	"	"	"	"	"	10	1
"	"	"	"	"	"	25	2
"	"	"	"	"	"	50	1
"	"	"	"	"	"	150	2
0.05	L.B.sand	7	50x50	0.27	90	300	1

TABLE 5.2

SOIL TYPE : MID-ROSS SAND
MESH TYPE:7 , MESH SIZE : 50×50 mm
MESH CONTENT : 33 m^2/m^3

Cell Pressure (kN/m^2)	Deviator stress at Peak state of the soil alone (kN/m^2)	Deviator stress at Peak state of the composite material (kN/m^2)	Deviator stress at Residual state (15% axial strain) of the soil alone (kN/m^2)	Deviator stress at Residual state (15% axial strain) of the composite material (kN/m^2)	Performance Efficiency (η) at Peak state (%)	Performance Efficiency (η) at Residual state (%)
0	-	6	-	12	-	-
10	69	114	41	61	65.3	49.0
25	157	229	99	136	46.0	38.0
50	314	480	218	340	52.8	56.0
100	582	739	410	579	27.0	41.2
150	873	1010	649	783	16.0	20.6
200	1013	1298	752	1018	28.0	35.0
300	1446	1588	1104	1215	10.0	10.0

TABLE 5.3

SOIL TYPE : MID-ROSS SAND
MESH TYPE:7 , MESH SIZE:50×50 mm
MESH CONTENT: 66 m^2/m^3

Cell Pressure (kN/m^2)	Deviator stress at Peak state of the soil alone (kN/m^2)	Deviator stress at Peak state of the composite material (kN/m^2)	Deviator stress at Residual state (15% axial strain) of the soil alone (kN/m^2)	Deviator stress at Residual state (15% axial strain) of the composite material (kN/m^2)	Performance Efficiency (η) at Peak state (%)	Performance Efficiency (η) at Residual state (%)
0	-	39	-	34	-	-
10	69	182	41	130	164.0	217.0
25	157	285	99	222	81.5	124.2
50	314	503	218	347	60.2	59.2
100	582	751	410	597	29.0	45.6
150	873	1095	649	872	25.5	34.4
200	1013	1340	752	1058	32.2	40.6
300	1446	1740	1104	1378	20.3	25.0

TABLE 5.4

SOIL TYPE : MID-ROSS SAND
MESH TYPE:7 , MESH SIZE : 50×50 mm
MESH CONTENT : 90 m^2/m^3

Cell Pressure (kN/m^2)	Devictor stress at Peak state of the soil alone (kN/m^2)	Deviator stress at Peak state of the composite matericl (kN/m^2)	Deviator stress at Residual state (15% axial strain) of the soil alone (kN/m^2)	Deviator stress at Residual state (15% axial strain) of the composite material (kN/m^2)	Performance Efficiency (η) at Peak state (%)	Performance Efficiency (η) at Residual state (%)
0	-	71	-	29	-	-
10	69	243	41	160	252.2	290.3
25	157	440	99	365	180.3	268.7
50	314	640	218	485	104.0	122.5
100	582	835	410	673	43.5	64.2
150	873	1220	649	995	40.0	53.4
200	1013	1481	752	1238	46.0	64.6
300	1446	1831	1104	1610	27.0	46.0

TABLE 5.5

SOIL TYPE : LEIGHTON BUZZARD SAND
MESH TYPE:7 , MESH SIZE : 50×50 mm
MESH CONTENT : 33 m^2/m^3

Cell Pressure (kN/m^2)	Deviator stress at Peak state of the soil alone (kN/m^2)	Deviator stress at Peak state of the composite material (kN/m^3)	Deviator stress at Residual state (15% axial strain) of the soil alone (kN/m^2)	Deviator stress at Residual state (15% axial strain) of the composite material (kN/m^3)	Performance Efficiency (η) at Peak state (%)	Performance Efficiency (η) at Residual state (%)
0	-	5	-	5	-	-
10	62	105	37	63	69.4	70.3
25	139	217	86	153	56.2	78.0
50	273	427	193	334	56.4	73.0
150	697	786	566	642	13.0	14.0
300	1221	1420	1030	1233	16.2	19.7

TABLE 5.6

SOIL TYPE : LEIGHTON BUZZARD SAND
MESH TYPE:7 , MESH SIZE : 50×50 mm
MESH CONTENT : 66 m^2/m^3

Cell Pressure (kN/m^2)	Deviator stress at Peak state of the soil alone (kN/m^2)	Deviator stress at Peak state of the composite material (kN/m^2)	Deviator stress at Residual state (15% axial strain) of the soil alone (kN/m^2)	Deviator stress at Residual state (15% axial strain) of the composite material (kN/m^2)	Performance Efficiency (η) at Peak state (%)	Performance Efficiency (η) at Residual state (%)
0	-	33	-	93	-	-
10	62	191	37	159	208.0	330.0
25	139	310	86	251	123.0	192.0
50	273	505	193	413	85.0	114.0
150	697	1000	566	911	43.5	61.0
300	1221	1589	1030	1426	30.2	38.4

TABLE 5.7

SOIL TYPE : LEIGHTON BUZZARD SAND
MESH TYPE:7 , MESH SIZE : 50×50 mm
MESH CONTENT : 90 m^2/m^3

Cell Pressure (kN/m^2)	Deviator stress at Peak state of the soil alone (kN/m^2)	Deviator stress at Peak state of the composite material (kN/m^2)	Deviator stress at Residual state (15% axial strain) of the soil alone (kN/m^2)	Deviator stress at Residual state (15% axial strain) of the composite material (kN/m^2)	Performance Efficiency (η) at Peak state (%)	Performance Efficiency (η) at Residual state (%)
0	-	84	-	63	-	-
10	62	279	37	223	350.0	503.0
25	139	343	86	225	147.0	162.0
50	273	562	193	446	106.0	131.0
150	697	1193	566	1086	71.2	92.0
300	1221	1761	1030	1519	44.3	47.5

TABLE 5.8

TRIAXIAL TESTING PROGRAM

Rate of Strain (%)/min	Type of Soil	Type of Mesh Element	Size of Mesh Element (mm)	Mesh Element content (%) by weight	Mesh Element content (m^2/m^3)	Cell pressure (kN/m^2)	Number of Tests
0.05	M.R.sand	7	50x100	0.09	33	0	2
"	"	"	"	"	"	10	2
"	"	"	"	"	"	25	2
"	"	"	"	"	"	50	1
"	"	"	"	"	"	150	2
0.05	M.R.sand	7	50x100	0.09	33	300	1
0.05	M.R.sand	7	50x100	0.18	66	0	2
"	"	"	"	"	"	10	2
"	"	"	"	"	"	25	2
"	"	"	"	"	"	50	1
"	"	"	"	"	"	150	3
0.05	M.R.sand	7	50x100	0.18	66	300	1
0.05	M.R.sand	7	50x100	0.24	90	0	2
"	"	"	"	"	"	10	2
"	"	"	"	"	"	25	2
"	"	"	"	"	"	50	1
"	"	"	"	"	"	150	2
0.05	M.R.sand	7	50x100	0.24	90	300	1

TABLE 5.8 (cont.)

TRIAXIAL TESTING PROGRAM

Rate of Strain (%)/min	Type of Soil	Type of Mesh Element	Size of Mesh Element (mm)	Mesh Element content (%) by weight	Mesh Element content (m^2/m^3)	Cell pressure (kN/m^2)	Number of Tests
0.05	L.B.sand	7	50x100	0.10	33	0	1
"	"	"	"	"	"	10	2
"	"	"	"	"	"	25	1
"	"	"	"	"	"	50	2
"	"	"	"	"	"	150	1
0.05	L.B.sand	7	50x100	0.10	33	300	1
0.05	L.B.sand	7	50x100	0.20	66	0	2
"	"	"	"	"	"	10	2
"	"	"	"	"	"	25	1
"	"	"	"	"	"	50	1
"	"	"	"	"	"	150	2
0.05	L.B.sand	7	50x100	0.02	66	300	1
0.05	L.B.sand	7	50x100	0.27	90	0	1
"	"	"	"	"	"	10	2
"	"	"	"	"	"	25	1
"	"	"	"	"	"	50	1
"	"	"	"	"	"	150	2
0.05	L.B.sand	7	50x100	0.27	90	300	1

TABLE 5.9

SOIL TYPE : MID-ROSS SAND
MESH TYPE:7 , MESH SIZE : 50×100 mm
MESH CONTENT : 33 m^2/m^3

Cell Pressure (kN/m^2)	Deviator stress at Peak state of the soil alone (kN/m^2)	Deviator stress at Peak state of the composite material (kN/m^2)	Deviator stress at Residual state (15% axial strain) of the soil alone (kN/m^2)	Deviator stress at Residual state (15% axial strain) of the composite material (kN/m^2)	Performance Efficiency (η) at Peak state (%)	Performance Efficiency (η) at Residual state (%)
0	-	6	-	9	-	-
10	69	144	41	138	108.7	236.6
25	157	245	99	218	56.1	120.2
50	314	488	218	398	55.4	82.5
150	873	1008	649	825	15.5	27.1
300	1446	1640	1104	1374	13.4	24.4

TABLE 5.10

SOIL TYPE : MID-ROSS SAND
MESH TYPE:7 , MESH SIZE : 50×100mm
MESH CONTENT : 66 m^2/m^3

Cell Pressure (kN/m^2)	Deviator stress at Peak state of the soil alone (kN/m^2)	Deviator stress at Peak state of the composite material (kN/m^2)	Deviator stress at Residual state (15% axial strain) of the soil alone (kN/m^2)	Deviator stress at Residual state (15% axial strain) of the composite material (kN/m^2)	Performance Efficiency (η) at Peak state (%)	Performance Efficiency (η) at Residual state (%)
0	-	49	-	31	-	-
10	69	211	41	186	205.8	353.6
25	157	381	99	307	142.6	210.1
50	314	560	218	411	78.3	88.5
150	873	1139	649	1017	30.4	56.7
300	1446	1726	1104	1578	19.4	43.0

TABLE 5.11

SOIL TYPE : MID-ROSS SAND
MESH TYPE:7 , MESH SIZE : 50×100 mm
MESH CONTENT : 90 m^2/m^3

Cell Pressure (kN/m^2)	Deviator stress at Peak state of the soil alone (kN/m^2)	Deviator stress at Peak state of the composite material (kN/m^2)	Deviator stress at Residual state (15% axial strain) of the soil alone (kN/m^2)	Deviator stress at Residual state (15% axial strain) of the composite material (kN/m^2)	Performance Efficiency (η) at Peak state (%)	Performance Efficiency (η) at Residual state (%)
0	-	158	-	145	-	-
10	69	403	41	378	484.0	822.0
25	157	534	99	469	240.1	374.0
50	314	692	218	560	120.0	157.0
150	873	1275	649	1148	46.0	76.8
300	1446	1904	1104	1662	32.0	50.5

TABLE 5.12

SOIL TYPE : LEIGHTON BUZZARD SAND
MESH TYPE:7 , MESH SIZE : 50×100 mm
MESH CONTENT : 33 m^2/m^3

Cell Pressure (kN/m^2)	Deviator stress at Peak state of the soil alone (kN/m^2)	Deviator stress at Peak state of the composite material (kN/m^2)	Deviator stress at Residual state (15% axial strain) of the soil alone (kN/m^2)	Deviator stress at Residual state (15% axial strain) of the composite material (kN/m^2)	Performance Efficiency (η) at Peak state (%)	Performance Efficiency (η) at Residual state (%)
0	-	11	-	11	-	-
10	62	115	37	118	85.5	219.0
25	139	249	86	218	79.1	153.5
50	273	504	193	400	84.6	107.2
150	697	895	566	739	28.4	30.6
300	1221	1570	1030	1295	28.6	25.7

TABLE 5.13

SOIL TYPE : LEIGHTON BUZZARD SAND
MESH TYPE:7 , MESH SIZE : 50 × 100 mm
MESH CONTENT : 66 m^2/m^3

Cell Pressure (kN/m^2)	Deviator stress at Peak state of the soil alone (kN/m^2)	Deviator stress at Peak state of the composite material (kN/m^2)	Deviator stress at Residual state (15% axial strain) of the soil alone (kN/m^2)	Deviator stress at Residual state (15% axial strain) of the composite material (kN/m^2)	Performance Efficiency (η) at Peak state (%)	Performance Efficiency (η) at Residual state (%)
0	-	87	-	29	-	-
10	62	252	37	193	306.4	421.6
25	139	409	86	378	194.2	339.5
50	273	569	193	452	108.4	134.2
150	697	1070	566	914	53.5	61.5
300	1221	1639	1030	1437	34.3	44.4

TABLE 5.14

SOIL TYPE : LEIGHTON BUZZARD SAND
MESH TYPE:7 , MESH SIZE : 50 × 100 mm
MESH CONTENT : 90 m^2/m^3

Cell Pressure (kN/m^2)	Deviator stress at Peak state of the soil alone (kN/m^2)	Deviator stress at Peak state of the composite material (kN/m^2)	Deviator stress at Residual state (15% axial strain) of the soil alone (kN/m^2)	Deviator stress at Residual state (15% axial strain) of the composite material (kN/m^2)	Performance Efficiency (η) at Peak state (%)	Performance Efficiency (η) at Residual state (%)
0	-	164	-	101	-	-
10	62	360	37	336	480.6	808.1
25	139	514	86	460	270.0	435.0
50	273	621	193	580	127.4	200.5
150	697	1238	566	1164	77.6	105.6
300	1221	1808	1030	1709	48.1	66.0

TABLE 5.15

Strength Characteristics of Mid-Ross Sand

and Mid-Ross Sand + Mesh Elements (Type 7)

Mesh Elements Content % (m^2/m^3)	Stress State	Mid-Ross Sand ($c' = 0$) Φ°	Mid-Ross Sand + Mesh Elements								
			SINGLES (50 x 50 mm elements)			DOUBLES (50x 100 mm elements)			DISCS (155 mm diameter)		
			b (kN/m^2)	$(\Phi+\beta)^\circ$	β°	b (kN/m^2	$(\Phi+\beta)^\circ$	β°	b (kN/m^2)	$(\Phi+\beta)^\circ$	β°
0.09 (33)	Peak	46	23	46.7	+0.7	25	46.5	+0.5	-	-	-
	Residual	41	17	42.5	+1.5	28	43	+2.0			
0.18 (66)	Peak	46	32	46.7	+0.7	44	47.5	+1.5	70	46.5	+0.5
	Residual	41	25	43.5	+2.5	40	45	+4.0	62	44.00	+3.0
0.24 (90)	Peak	46	59	46.7	+0.7	73	47	+1.0	-	-	-
	Residual	41	44	45	+4.0	70	45	+4.0			

TABLE 5.16

Strength Characteristics of Leighton Buzzard Sand

and Leighton Buzzard Sand + Mesh Elements (Type 7)

Mesh Elements Content % (m^2/m^3)	STRESS STATE	LEIGHTON BUZZARD SAND ($c' = o$) $\Phi°$	LEIGHTON BUZZARD sand + Mesh Elements					
			50 x 50 mm elements			50 x 100 mm elements		
			b kN/m^2	$(\Phi+\beta)°$	$\beta°$	b kN/m^2	$(\Phi+\beta)°$	$\beta°$
0.10 (33)	PEAK	43.5	30	43.5	0	35	45.3	+1.8
	RESIDUAL	40.5	20	41.0	+0.5	48	41.5	+1.0
0.20 (66)	PEAK	43.5	40	45.2	+1.7	56	45.2	+1.7
	RESIDUAL	40.5	38	43.0	+2.5	53	43.3	+2.8
0.27 (90)	PEAK	43.5	52	46.0	+2.5	70	46.4	+2.9
	RESIDUAL	40.5	44	44.5	+4.0	67	45.5	+5.0

TABLE 5.17

TRIAXIAL TESTING PROGRAM

Rate of Strain (%)/min	Type of Soil	Type of Mesh Element	Size of Mesh Element	Mesh Element content (%) by weight	Mesh Element content (m^3/m^3)	Cell pressure (kN/m^2)	Number of Tests
0.05	M.R.sand	7	I3 Discs	0.I8	66	0	2
"	"	"	"	"	"	I0	2
"	"	"	"	"	"	25	2
"	"	"	"	"	"	50	2
"	"	"	"	"	"	I50	2
0.05	M.R.sand	7	I3 Discs	0.I8	66	300	2

TABLE 5.18

TRIAXIAL TESTING PROGRAM

Rate of Strain (%)/min	Type of Soil	Type of Mesh Element	Size of Mesh Element	Mesh Element content (%) by weight	Mesh Element content (m^3/m^3)	Cell pressure (kN/m^2)	Number of Tests
0.05	M.R.sand	NONE	NONE	NONE	NONE	I50	2
0.5	"	"	"	"	"	I50	2
2.0	M.R.sand	"	"	"	"	I50	2
0.05	M.R.sand	7	I3 Discs	0.I8	66	I50	2
0.5	"	7	I3 Discs	"	"	I50	2
2.0	M.R.sand	7	I3 Discs	0.I8	66	I50	2
0.005	M.R.sand	7	50xI00 mm	0.I8	66	I50	3
0.0I	"	"	"	"	"	"	I
0.05	"	"	"	"	"	"	3
0.5	"	"	"	"	"	"	2
2.0	M.R.sand	7	50xI00 mm	0.I8	66	I50	3
0.05	L.B.sand	NONE	NONE	NONE	NONE	I50	2
0.5	"	"	"	"	"	"	I
2.0	"	"	"	"	"	"	2
0.005	L.B.sand	7	50xI00 mm	0.20	66	I50	2
0.05	"	"	"	"	"	"	2
0.5	"	"	"	"	"	"	I
2.0	L.B.sand	7	50xI00	0.20	66	I50	2

TABLE 5.19

MID-ROSS SAND + 155mm DIAM. DISCS Type 7

Cell Pressure (kN/m^2)	Deviator stress at Peak state of the soil alone (kN/m^2)	Deviator stress at Peak state of the composite material (kN/m^2)	Deviator stress at Residual state (15% axial strain) of the soil alone (kN/m^2)	Deviator stress at Residual state (15% axial strain) of the composite material (kN/m^2)	Performance Efficiency (η) at Peak state (%)	Performance Efficiency (η) at Residual state (%)
0	-	215	-	220	-	-
10	69	254	41	252	268.1	514.6
25	157	483	99	432	207.6	336.4
50	314	561	218	490	79.0	125.0
150	873	1144	649	1010	31.0	56.0
300	1446	1918	1104	1581	32.6	43.2

TABLE 6.1

MODEL FOOTING TEST DATA

Soil and Type of mesh element mixture	D/B	Stress at peak kN/m^2	Stress at resid. kN/m^2	δ/B at peak (%)	Improv. ratio at peak	Improv. ratio at residual
L.B. sand alone	-	316	92	9.0	-	-
L.B. sand+Type 5340	0.5	400	217	10.6	1.26	2.36
"	1	546.5	281	13.5	1.73	3.06
"	2	732	485	15.0	2.31	5.26
"	3	626	574	15.5	1.98	6.24
L.B. sand+Type 5340	4	710	680	17.0	2.25	7.39
L.B. sand+Type 2	0.5	578	325	13.3	1.83	3.53
"	1	677	430	13.1	2.14	4,67
"	2	760	650	12.5	2.40	7.06
"	3	680	530	11.0	2.15	5.80
L.B. sand+Type 2	4	757	630	12.2	2.40	6.85
L.B. sand+Type 4	0.5	475	293	14.0	1.50	3.16
"	1	594	509	14.6	1.87	5.52
"	2	650	557	14.3	2.05	6.05
"	3	585	424	12.0	1.84	4.61
L.B. sand+Type 4	4	590	450	14.3	1.86	4.90

TABLE 6.1 (cont.)

MODEL FOOTING TEST DATA

Soil and Type of mesh element mixture	D/B	Stress at peak kN/m^2	Stress at resid. kN/m^2	δ/B at peak (%)	Improv. ratio at peak	Improv. ratio at residual
L.B. sand alone	-	316	92	9.0	-	-
L.B. sand+Type 5	0.5	448	172	9.6	1.42	1.87
"	1	594	509	14.6	1.87	4.73.
"	2	650	557	14.3	2.05	6.74
"	3	582	424	12.0	1.85	5.98
L.B. sand+Type 5	4	780	704	13.5	2.47	7.65
L.B. sand+Type 6	0.5	472	278	9.56	1.49	3.02
"	1	545	428	11.38	1.72	4.65
"	2	716	690	12.32	2.26	7.50
"	3	580	520	11.60	1.83	5.65
L.B. sand+Type 6	4	780	715	12.2	2.47	7.77
L.B. sand+Type 7	0.5	636	437	11.90	2.01	4.75
"	1	693	382	11.70	2.20	4.21
"	2	963	(963)	20.0	3.05	10.46
	3	888	(888)	20.0	2.81	9.65
L.B. sand +Type 7	4	853	(853)	20.0	2.70	9.27

TABLE 6.2

MODEL FOOTING TEST DATA

Soil and Type of mesh element mixture	D/B	Stress at peak kN/m^2	Stress at resid. kN/m^2	δ/B at peak (%)	Improv. ratio at peak	Improv. ratio at residual
Mid-Ross sand alone	-	470	270	9.5	-	-
M.R. sand + Type 7	0.5	950	(950)	20.0	2.02	3.52
"	1	960	930	17.0	2.04	3.44
"	2	1133.7	1062.1	16.0	2.41	3.93
"	3	1221	(1221)	20.0	2.60	4.52
M.R. sand + Type 7	4	1164.4	1104.2	15.3	2.48	4.09

LIST

OF

PLATES

PLATE 1

The tensile testing machine

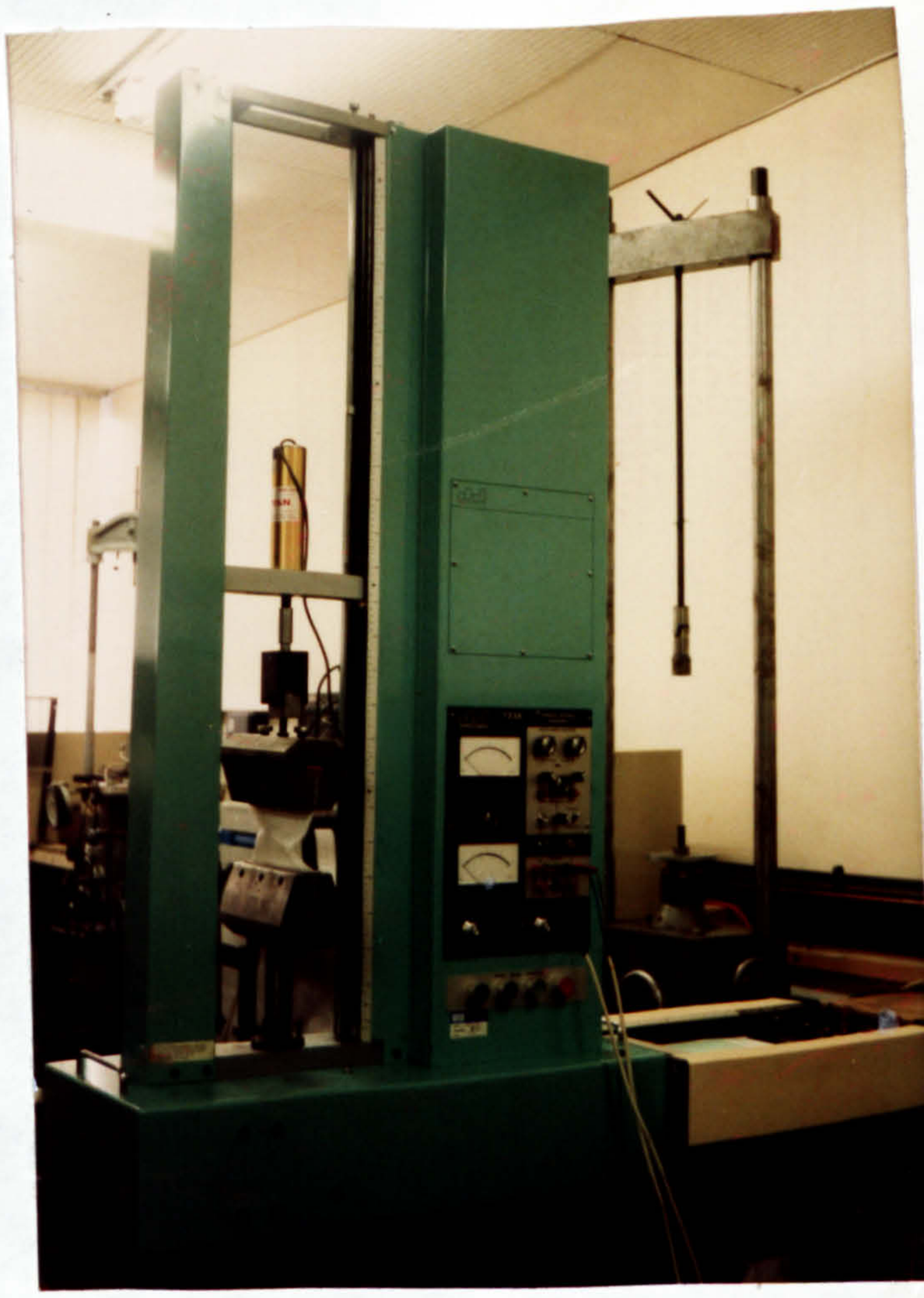

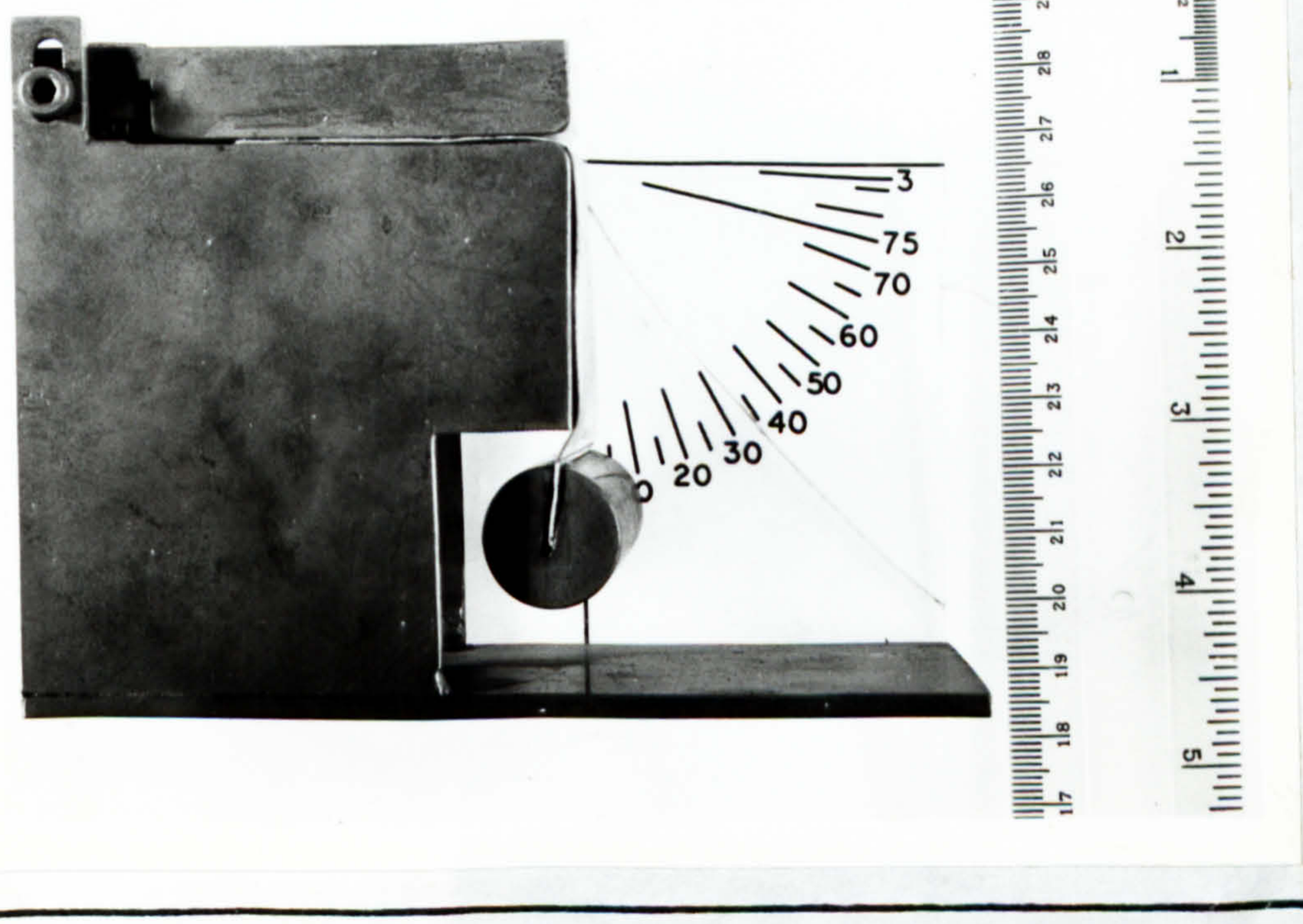

PLATE 2

The flexural stiffness Index testing apparatus

PLATE 3

The automatic Compaction machine

PLATE 4

The CBR apparatus

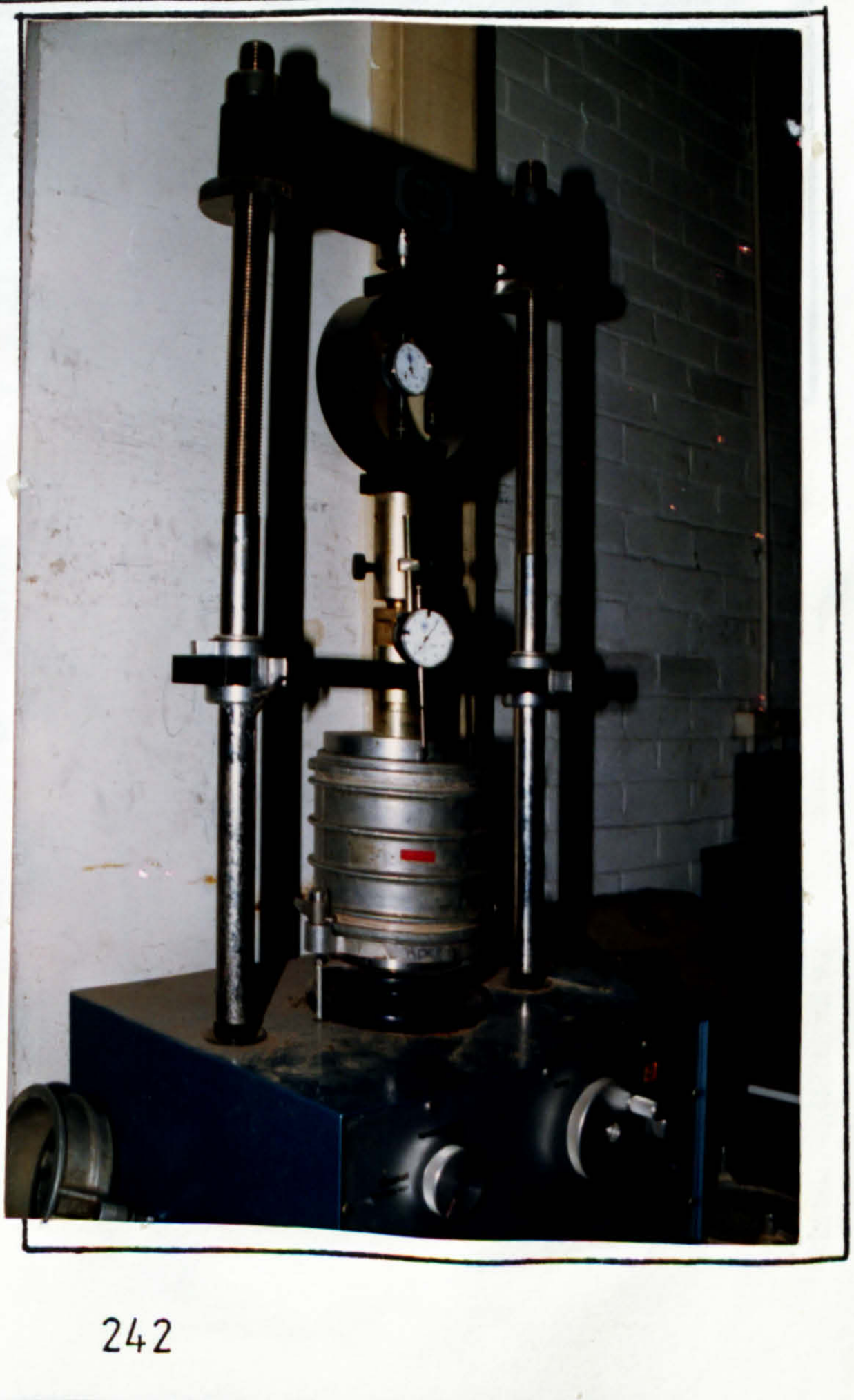

PLATE 5

Compaction of Mid-Ross sand mixed with Mesh elements in the CBR mould

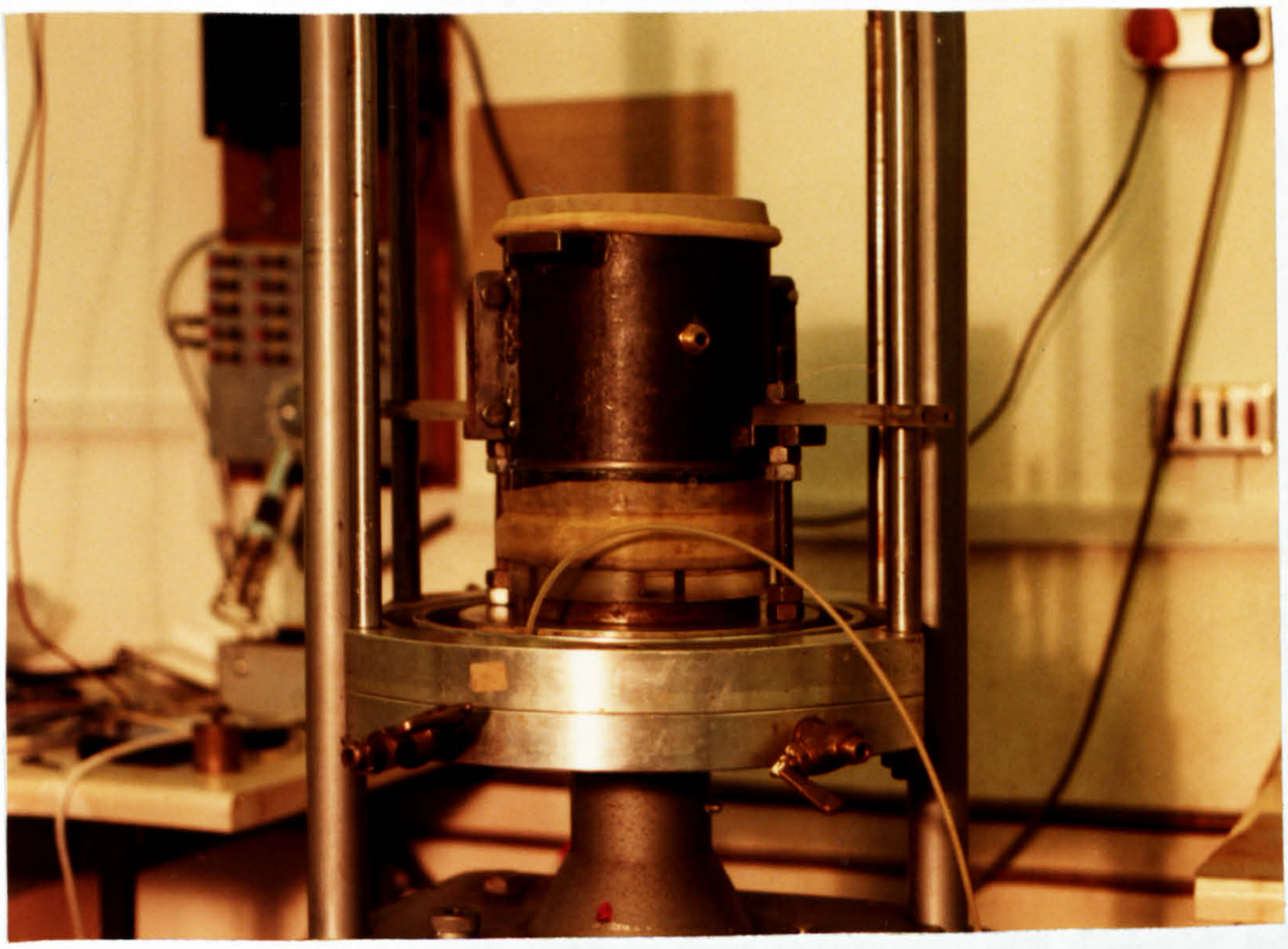

PLATE 6 The split-mould former in triaxial testing

PLATE 7 The triaxial testing apparatus

PLATE 8

Long term loading test apparatus

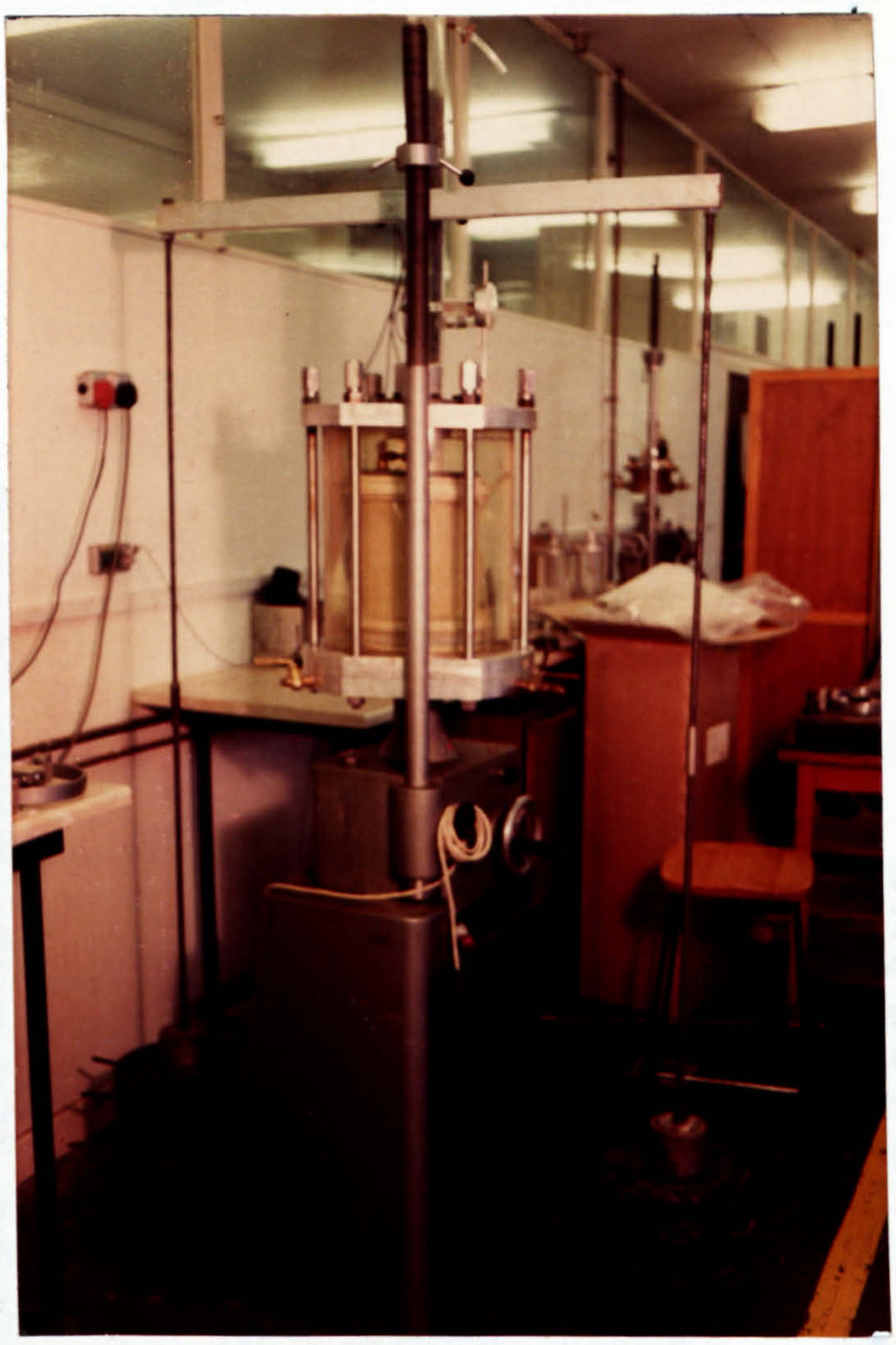

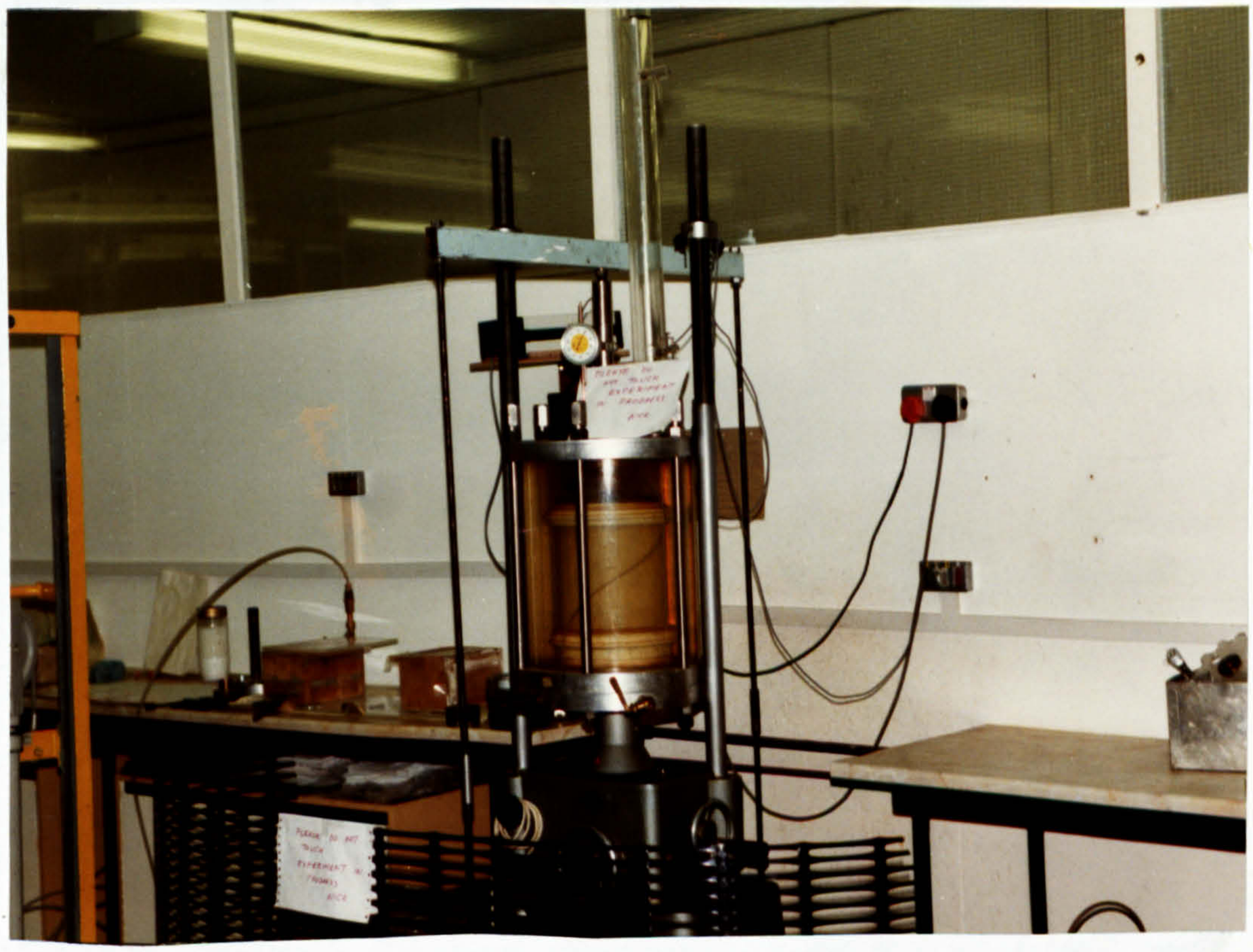

PLATE 9 Another view of the Long term loading test apparatus

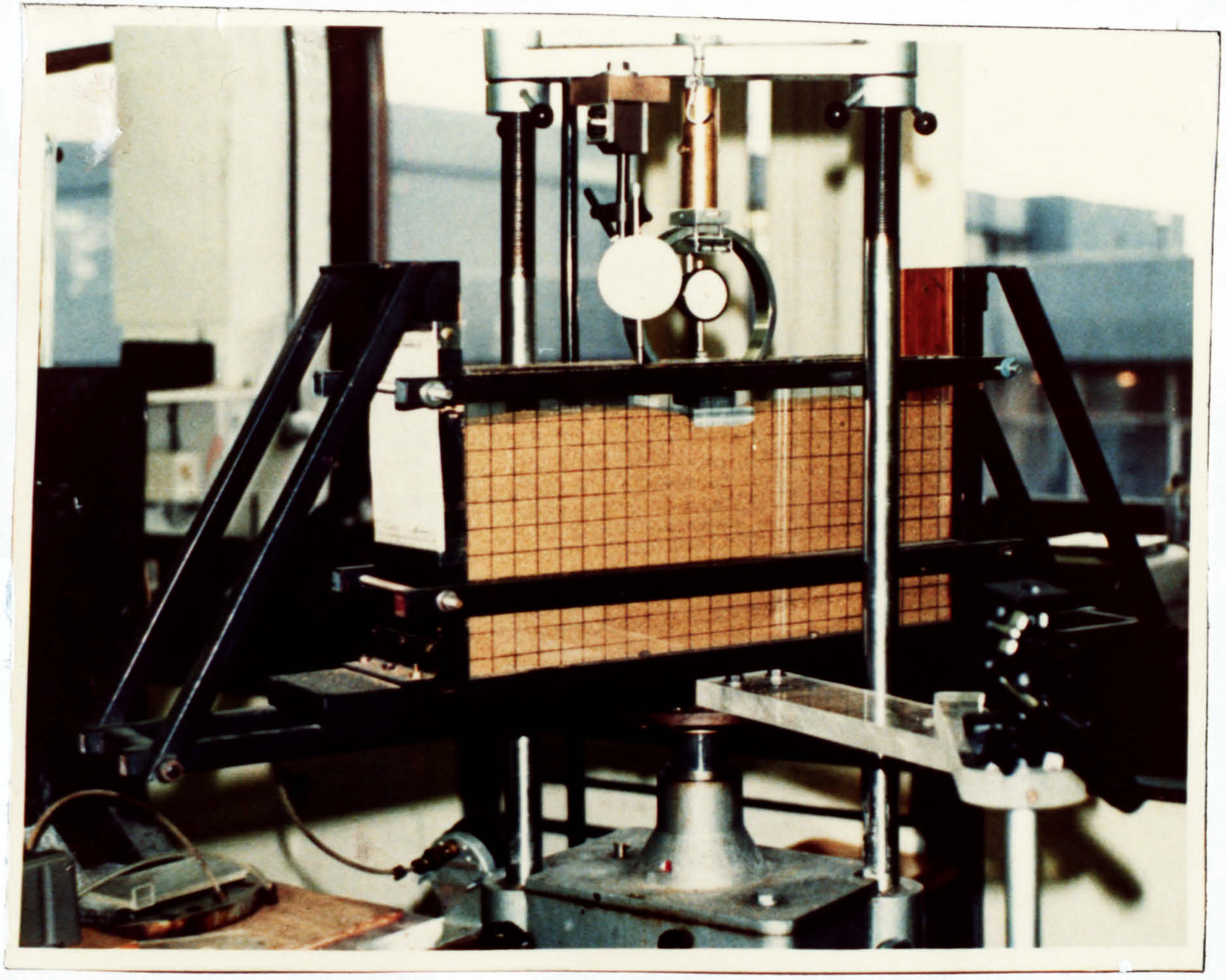

PLATE 10 The Model Footing apparatus

PLATE 11

The permeability testing apparatus

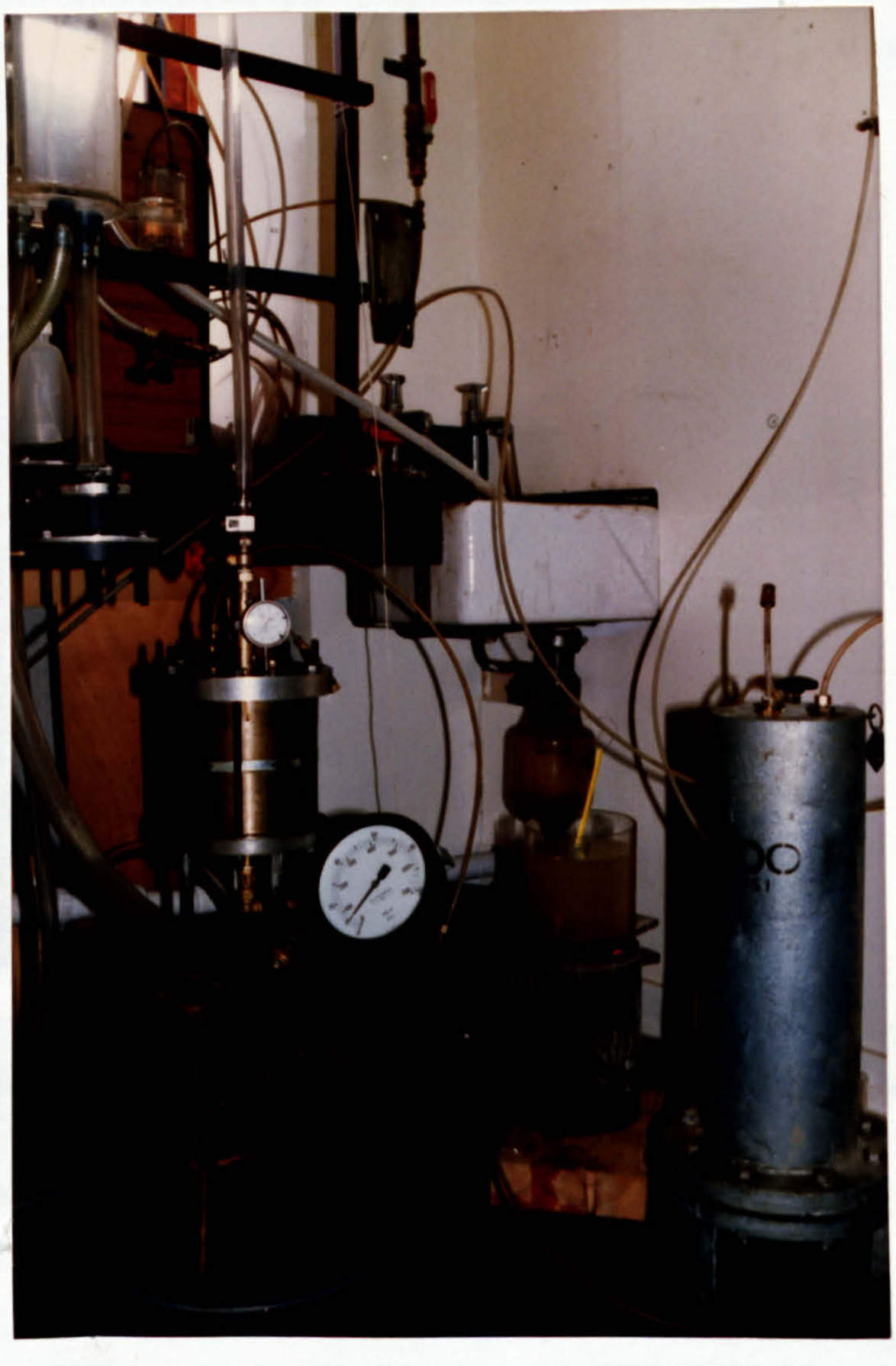

PLATE 12

Compaction of soil & mesh element mixture for permeability testing

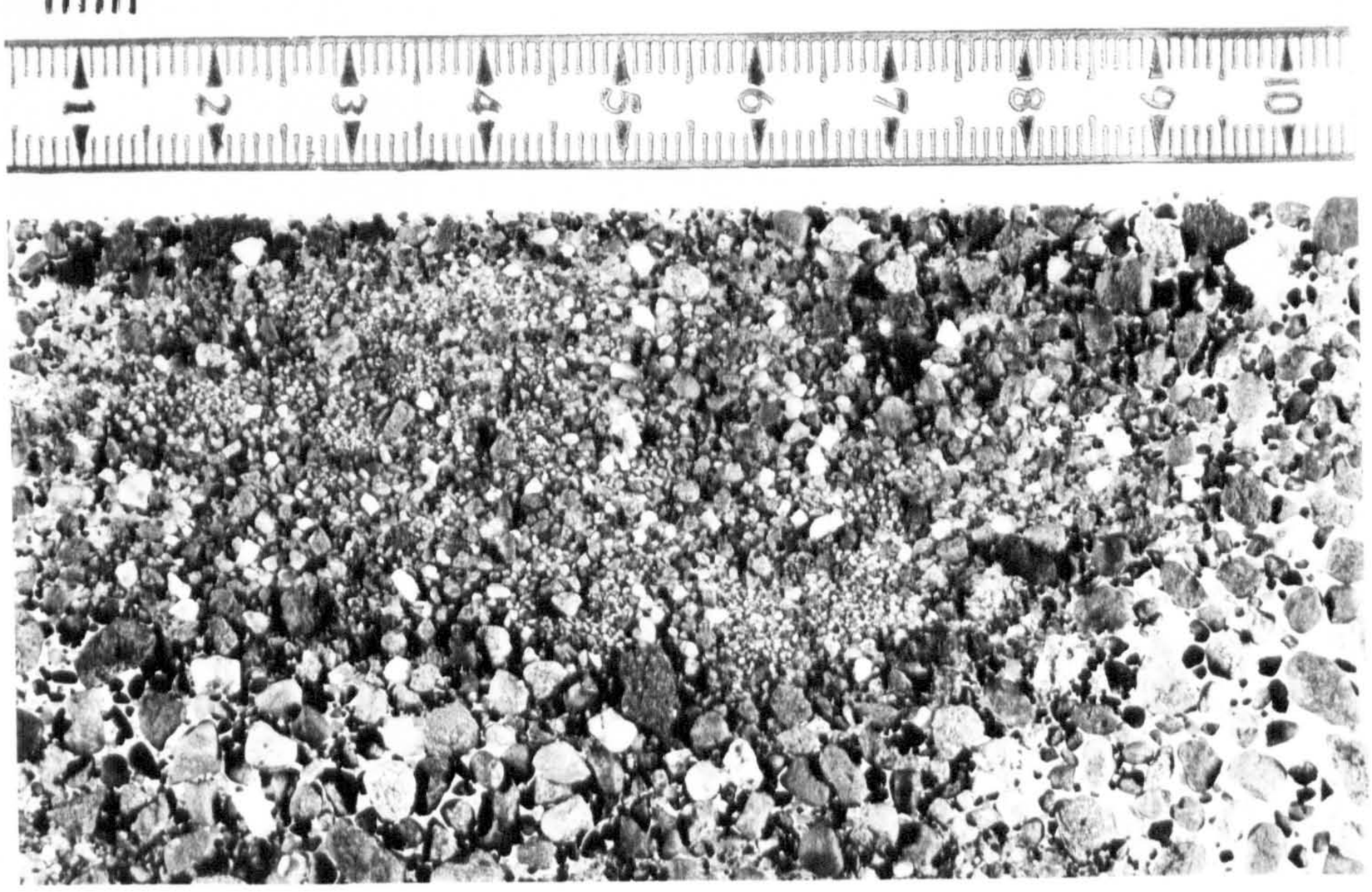

PLATE 13 MID-ROSS SAND

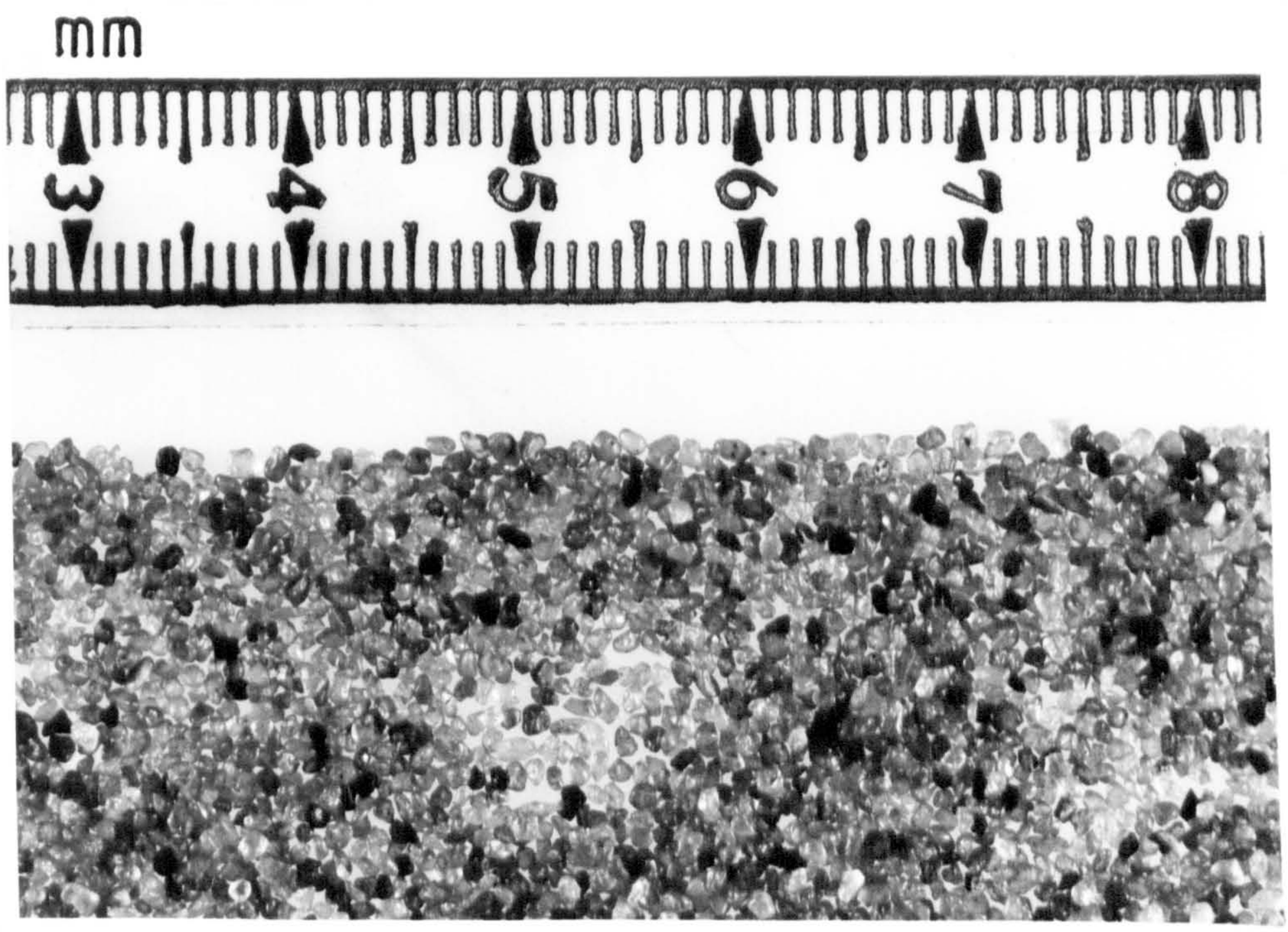

PLATE 14 LEIGHTON BUZZARD SAND

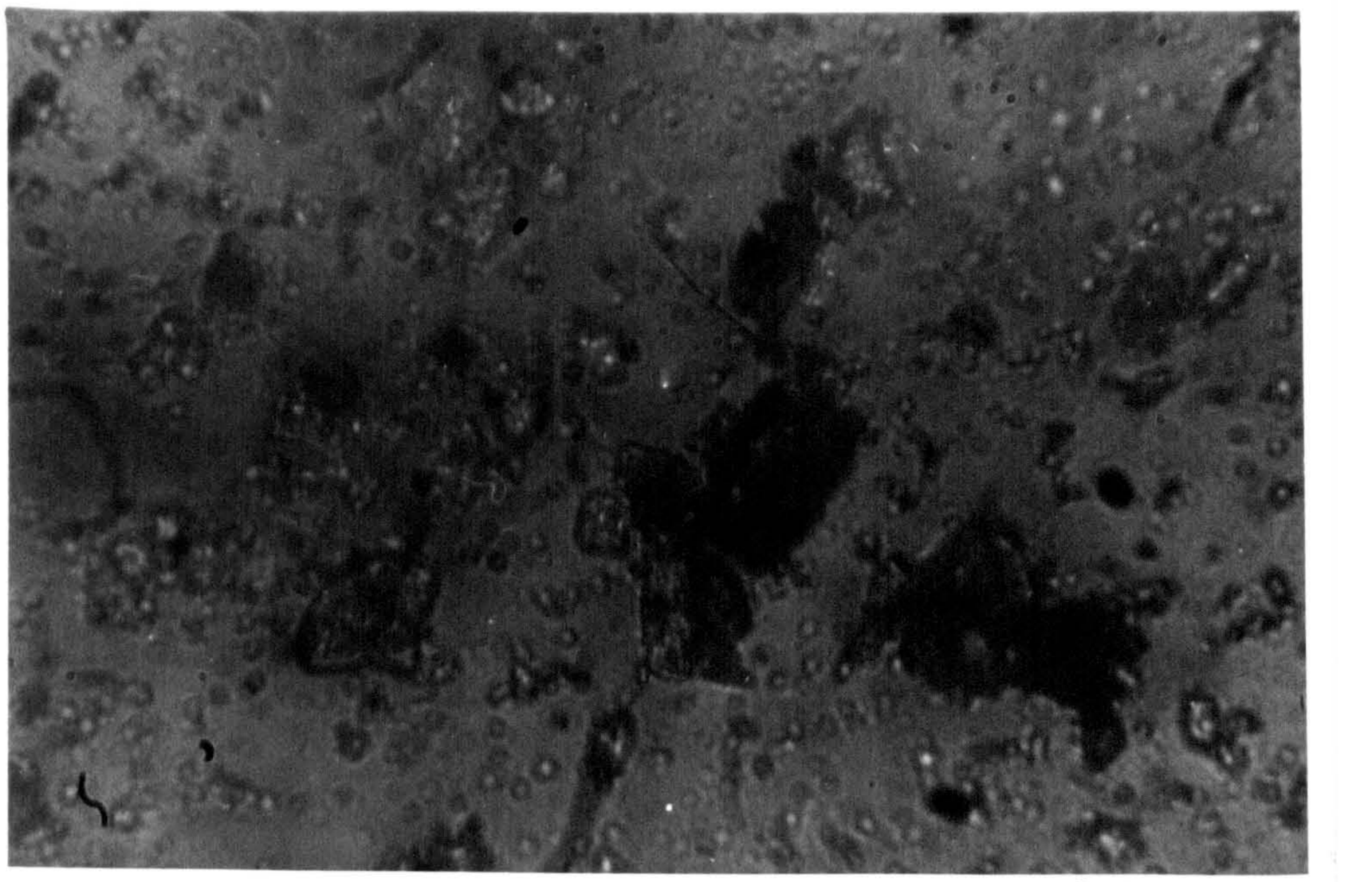

PLATE 15

WEST HIGHLAND MORAINE

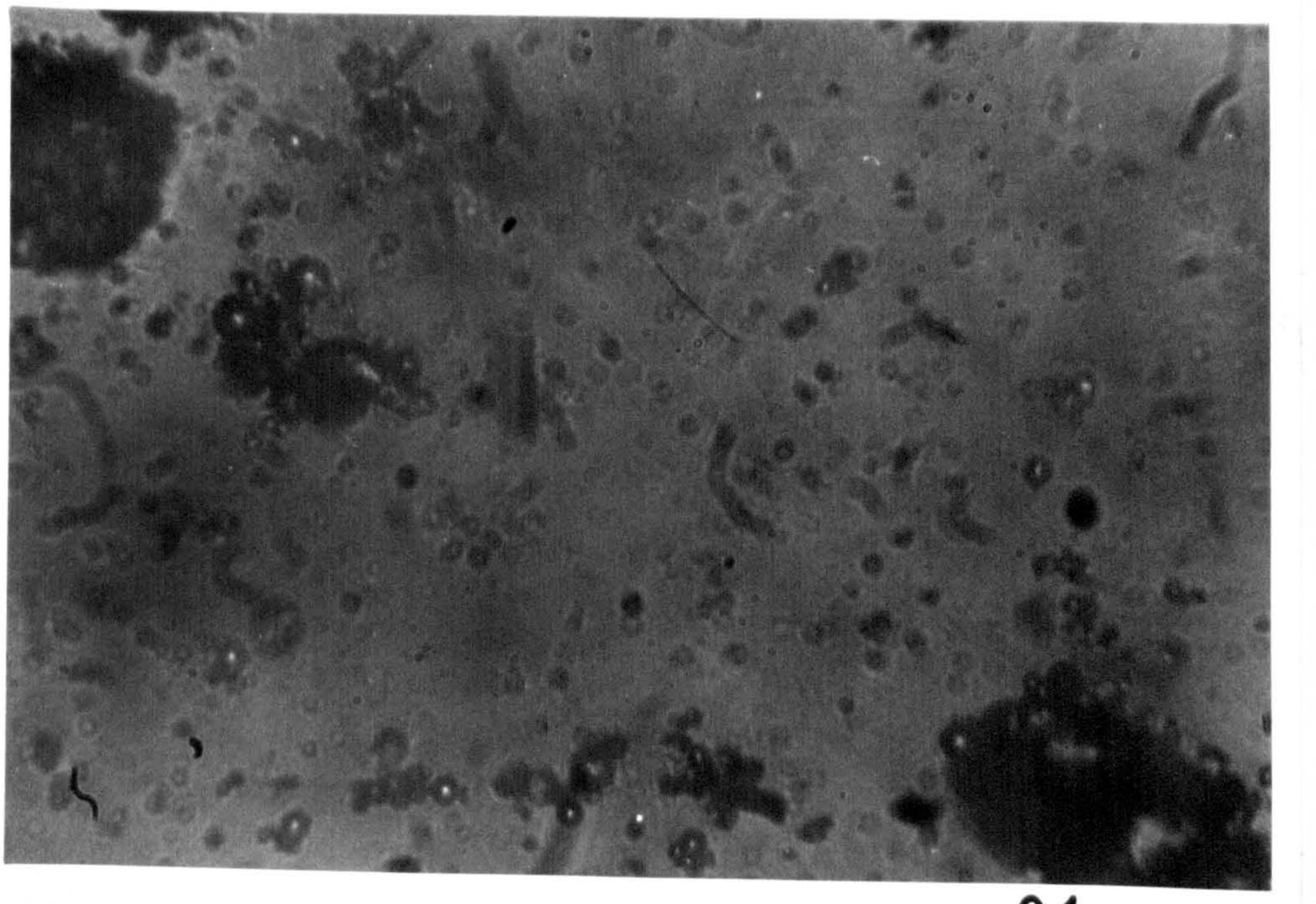

PLATE 16

PULVERISED FUEL ASH

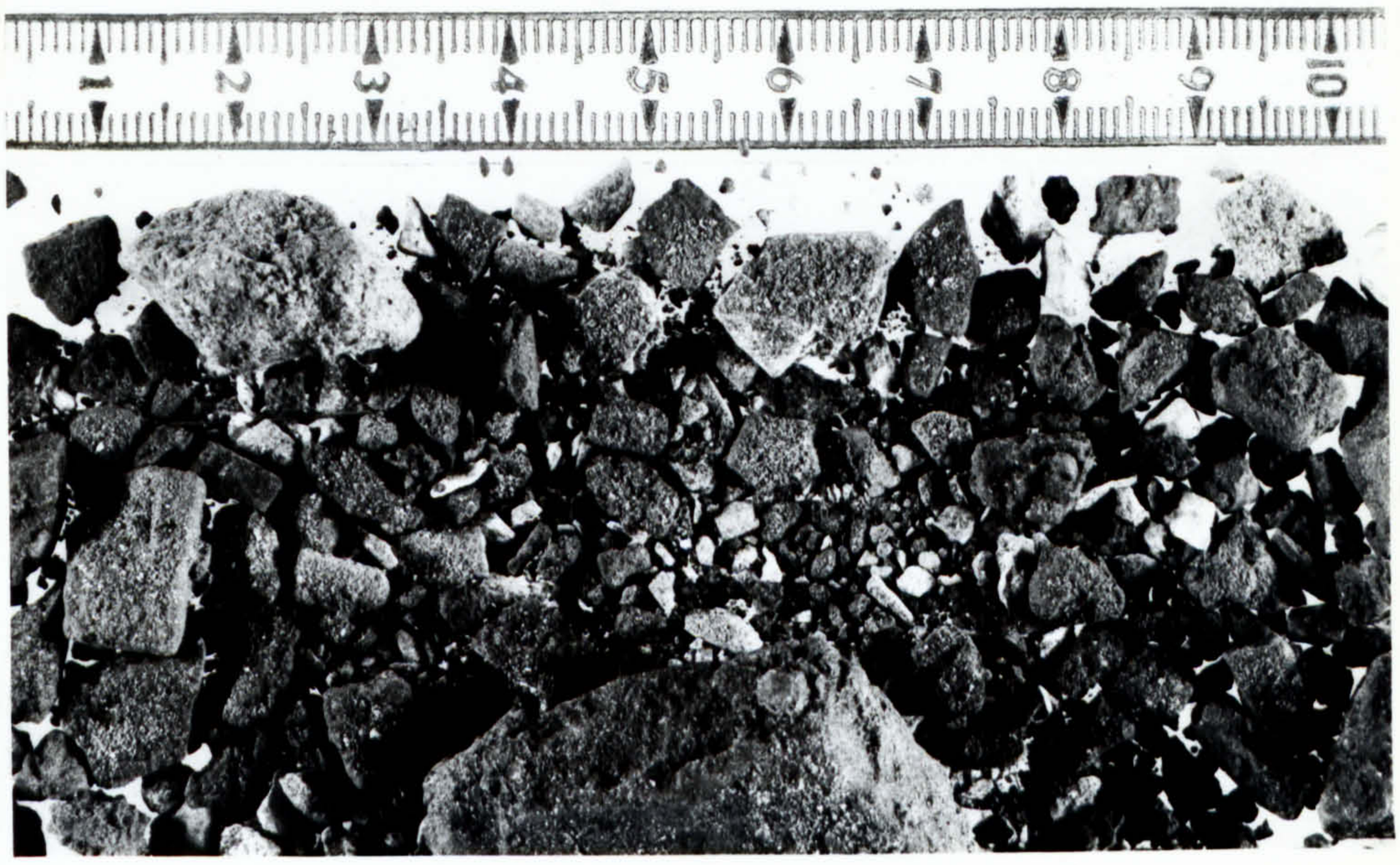

PLATE 17 COLLIERY SPOIL

PLATE 18 Types of Colliery spoil

PLATE 19 Compaction inside the triaxial split-mould

PLATE 20

A View of the Triaxial Specimen Kept "Upright" by Means of Vacuum Ready for Assembly.

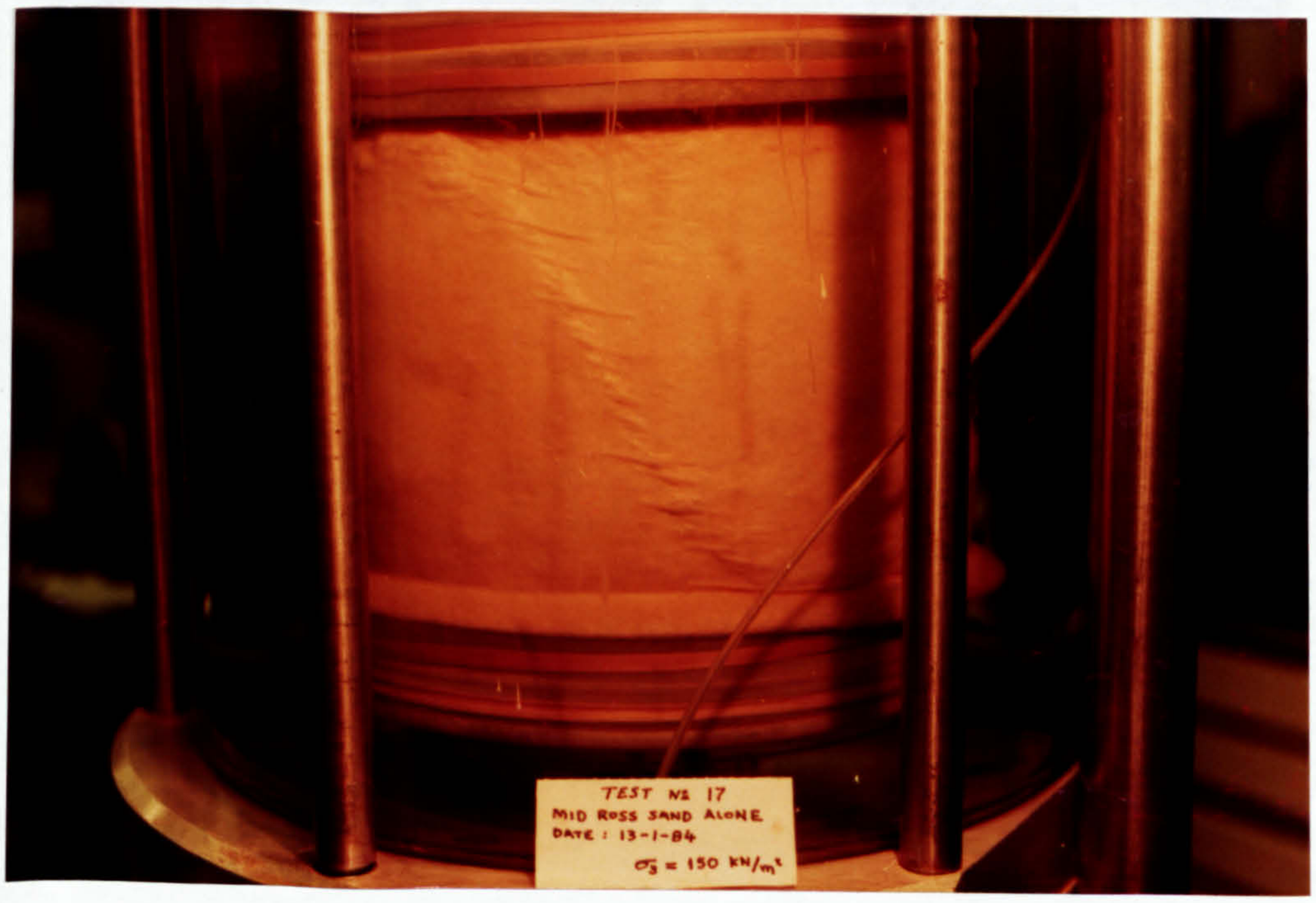

PLATE 21 The Deformed Triaxial Sample at Large Strains Consisting of Soil Alone

PLATE 22 The Deformed Triaxial Sample at Large Strains Consisting of Soil Mixed With Mesh Elements

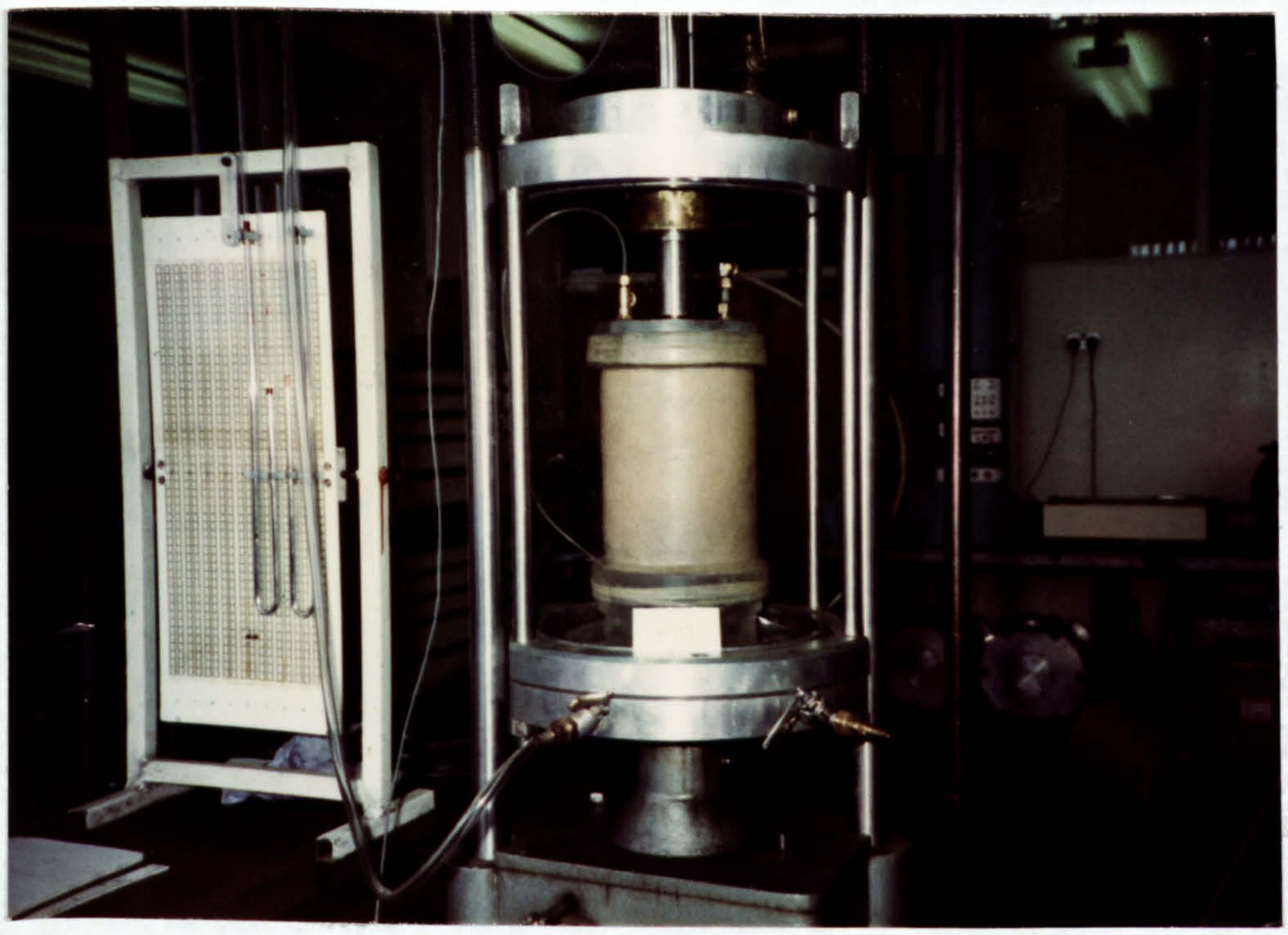

PLATE 23 Triaxial Testing at Low Cell Pressures Using Vacuum

PLATE 24 Triaxial Testing at High Cell Pressures Using Water Pressure

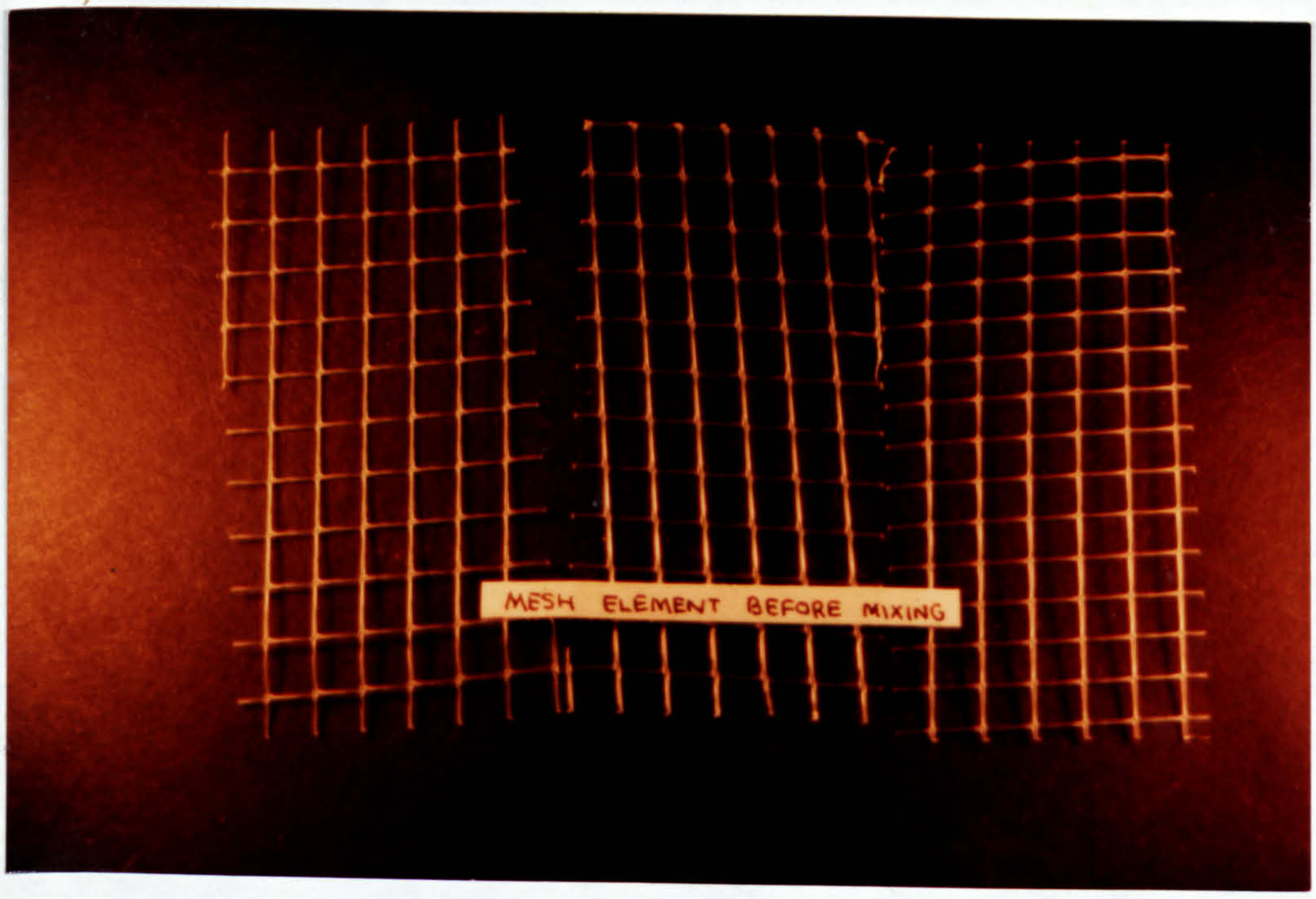

PLATE 25

The State of Mesh Elements Before Triaxial Testing

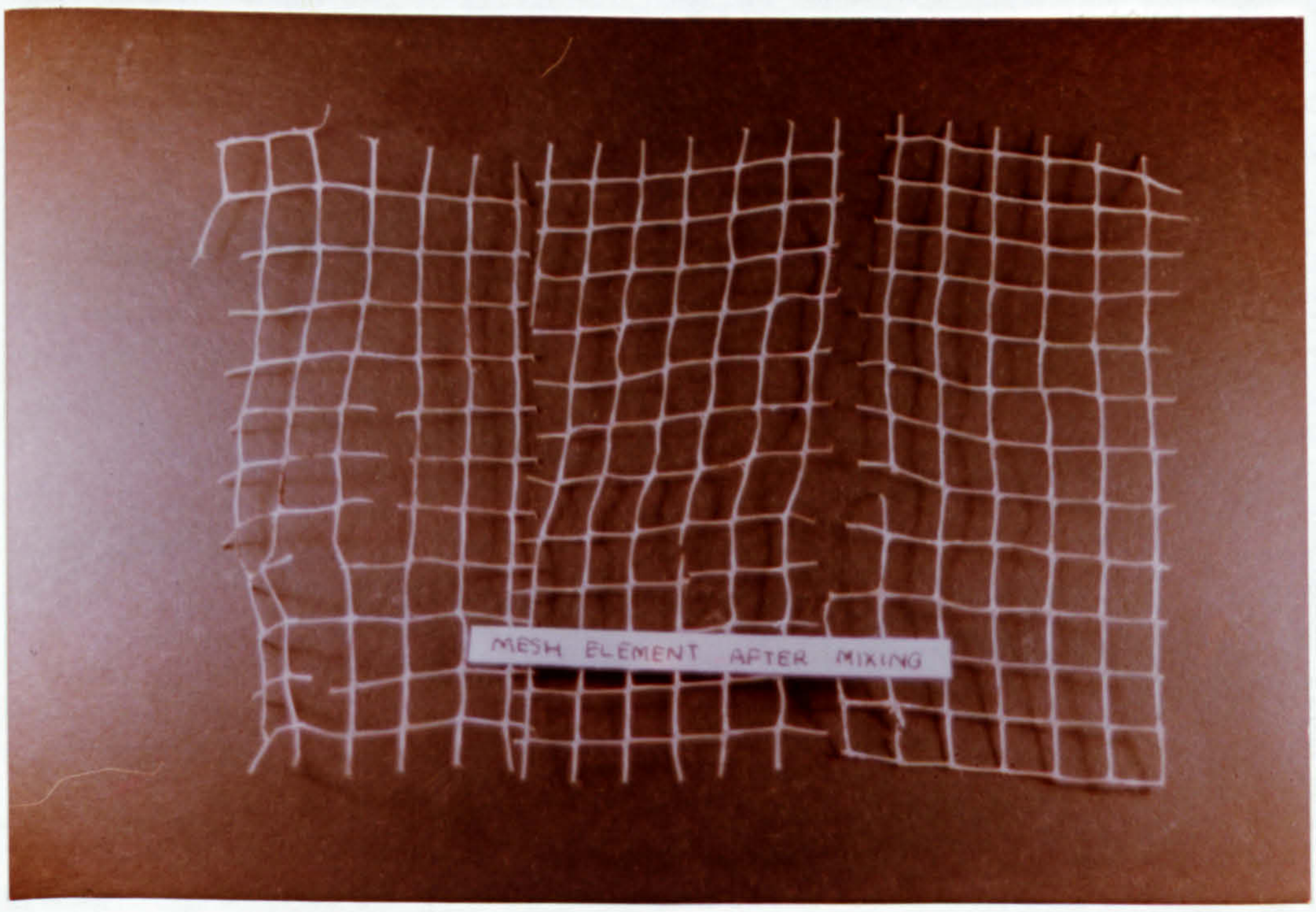

PLATE 26

The State of Some of the Mesh Elements After Triaxial Testing at Large Strains

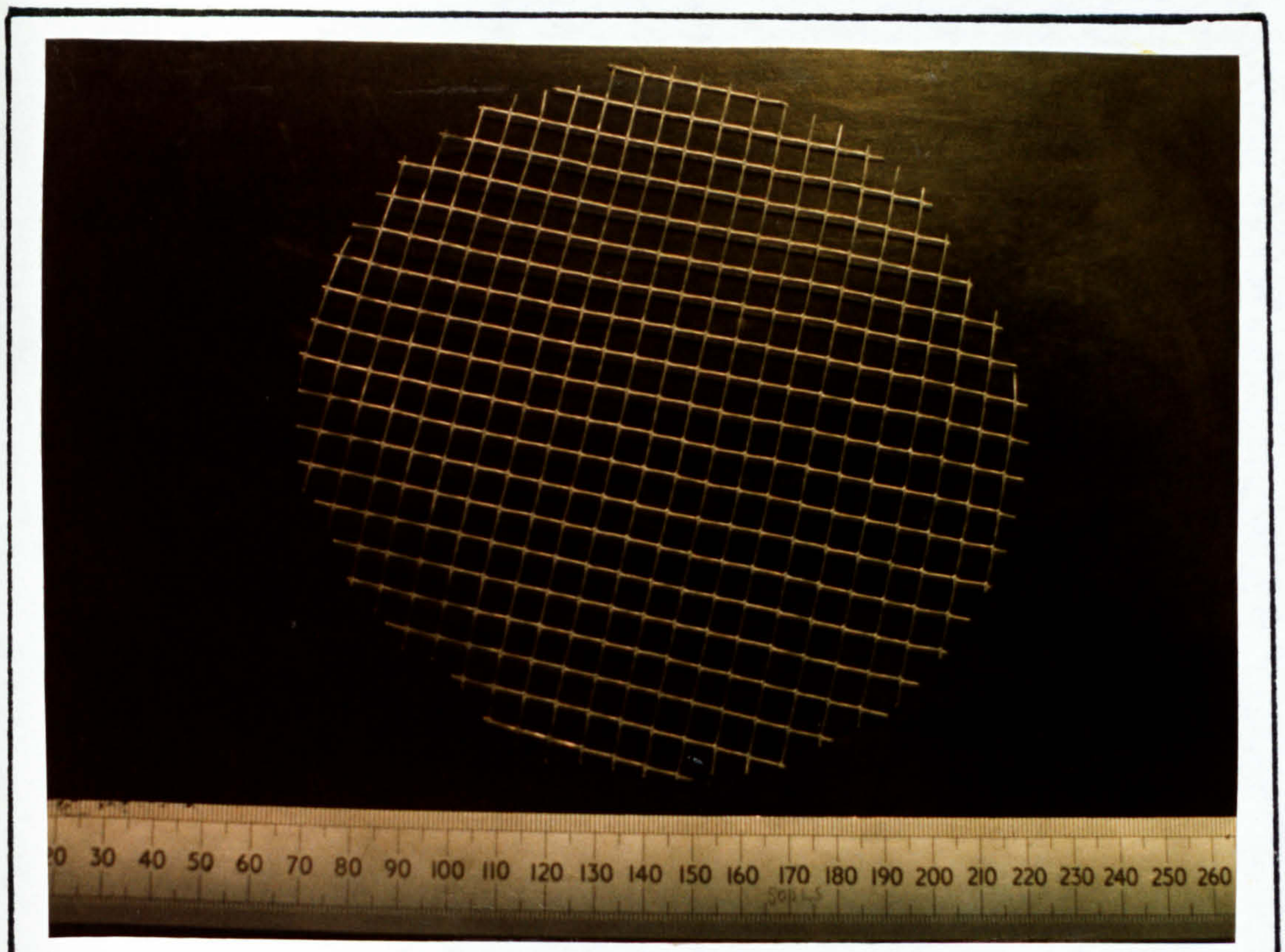

PLATE 27

The State of Mesh Type 7 Discs Before Triaxial Testing

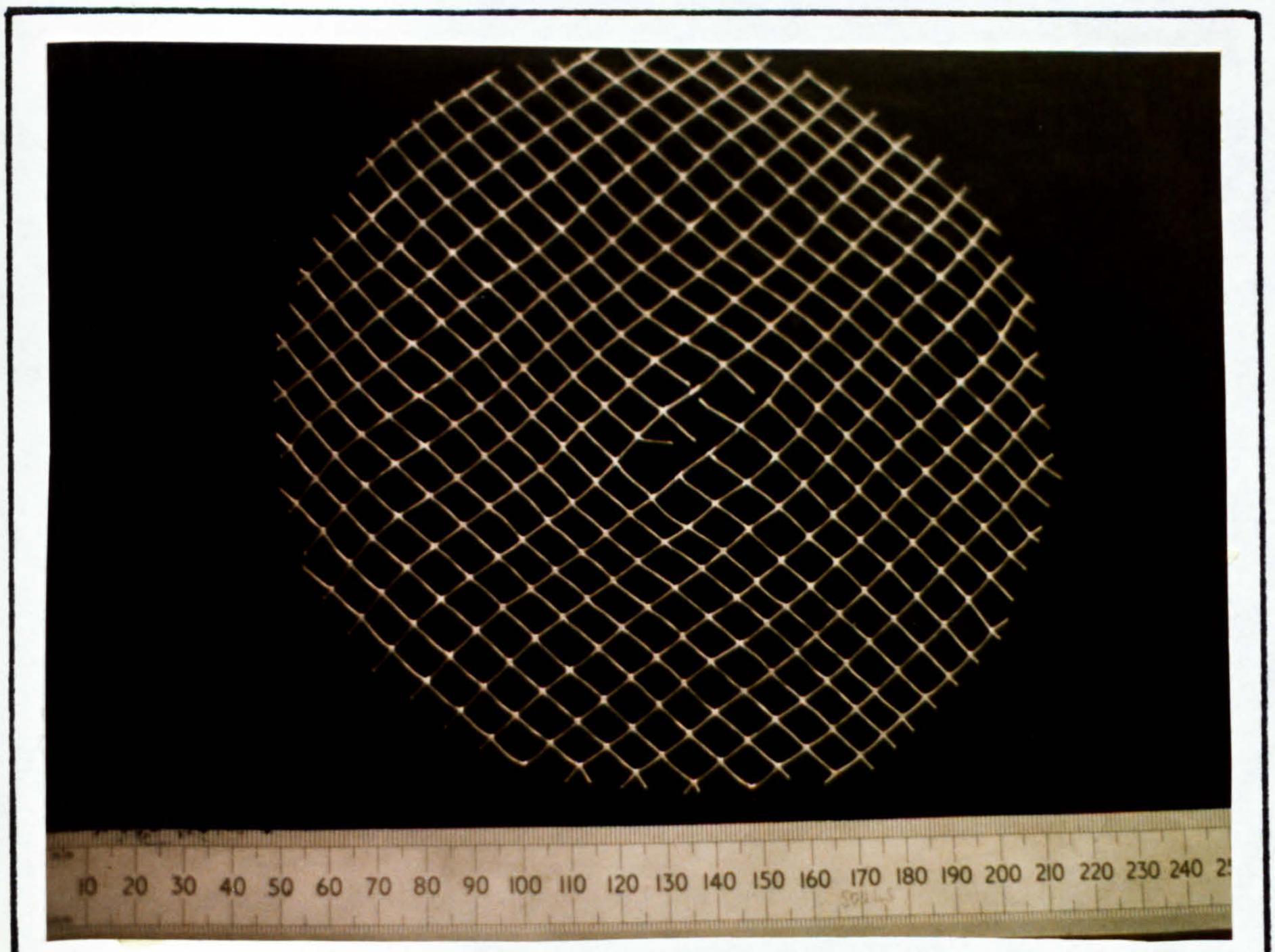

PLATE 28

The State of Some of the Mesh Type 7 Discs After Triaxial Tesing at Large Strains

PLATE 29

Triaxial Testing of Sand Mixed with Mesh Elements at 1% Axial Strain.

PLATE 30

Triaxial Testing of Sand Mixed with Mesh Elements at 11% Axial Strain.

LIST

OF

APPENDICES

APPENDIX A

PRINCIPLES of LOAD-CELL DESIGN & LOAD-CELL CALIBRATION

APPENDIX A

PRINCIPLES OF LOAD-CELL DESIGN AND LOAD-CELL CALIBRATION

BASIC EQUATION FOR DESIGNING A LOAD CELL

The basic principle of strain gauging is that when a strain gauge is cemented to a deforming test piece, both the specimen and the strain gauge will suffer the same amount of strain. If the strain gauge is subjected to a strain $\Delta l/l$, its electrical resistance, R, will be slightly changed to a value ΔR satisfying the following relationship:

$$\Delta R/R \propto \Delta l/l$$

i.e.
$$\Delta R/R = (G.F.)\ \Delta l/l \qquad -(A.1)$$

where G.F. is a constant termed the gauge factor.

For test pieces made of elastic materials the relationship between the stresses and strains is linear and is given by the following equation:

$$E = \text{stress} / \text{strain} = \sigma / (\Delta l / l) \qquad -(A2)$$

where E is Young's modulus for the tested material.

From equations (A.1) (A.2) the following expression can be derived :

$$\Delta R / R = (G.F.)\ \sigma / E \qquad -(A3)$$

Hence, by measuring the change in the gauge resistance, the stresses imposed on the test piece can be calculated.

Generally, the strains occurring in a piece of metal, within the elastic range, are very small. Accordingly, the change in the resistance will also be small. The measurement of such small resistance changes are made using a special circuit capable of measuring such small resistances. The Wheatstone bridge, which is composed of four resistances connected in the pattern shown in Figure A1, is one of the most convenient and accurate methods. As shown in the figure a D.C. current source with a constant input voltage, V_i, is applied across C.D. whereas a device to accurately

measure the output voltage, V_0, (e.g. high impedance voltmeter) is applied across AB. As the resistance of the voltmeter is extremely high compared to the resistance of any of the four arms forming the bridge the current passing through it is approximately equal to zero. Accordingly, the voltage across AD is given by (see Bransby, 1973):

$$V_{AD} = V_i \frac{R_1}{R_1+R_4} \qquad -(A.4)$$

and the voltage across BD is given by

$$V_{BD} = V_i \frac{R_2}{R_2+R_3} \qquad -(A.5)$$

The output voltage, V_0, between points A and B is calculated according to the following equation:

$$V_{AB} = V_{AD} - V_{BD} = V_i \frac{R_1R_3 - R_2R_4}{(R_1+R_4)(R_2+R_3)} \qquad -(A.6)$$

If the resistance of each strain gauge changes slightly so that R_1 becomes $R_1 + \Delta R_1$, R_2 becomes $R_2 + \Delta R_2$ and so on, and if all strain gauges have the same initial resistances, i.e. $R_1 = R_2 = R_3 = R_4 = R$, equation (A6) can be rewritten as follows:

$$V_o = V_i \frac{(R+\Delta R_1)(R+\Delta R_3) - (R+\Delta R_2)(R+\Delta R_4)}{[(R+\Delta R_1)+(R+\Delta R_4)][(R+\Delta R_2)+(R+\Delta R_3)]} \qquad -(A.7)$$

Ignoring terms of second order, equation (A.7) can be simplified to:

$$V_o = \frac{V_i}{4} \cdot \left(\frac{\Delta R_1 + \Delta R_3 - \Delta R_2 - \Delta R_4}{R} \right) \qquad -(A.8)$$

Accordingly, equation (A.8) will be reduced to:

$$V_o = V_i \cdot \frac{\Delta R}{4R} \qquad -(A.9)$$

Equation (A8) also indicates that if the changes in the resistance of the four strain gauges are of equal magnitudes, i.e. $\Delta R_1 = \Delta R_2 = \Delta R_3 = \Delta R_4 = \Delta R$, no change in the output voltage will be observed. Accordingly, it is

expected that any changes in the ambient temperature will not affect the load cell readings as the four gauges will be subjected to equal strains.

(i) Design of load cells

The load cells were designed to measure normal stresses only and no provisions were made to measure the shear stresses or the eccentricity of the normal stress. As the tests were performed with relatively smooth walls and the shear stresses acting on the wall were expected to be of relatively small magnitudes, it was considered sufficient to measure normal stresses only. Also, by using a large number of load cells the shape of the stress distribution could be accurately traced without the need for measuring the eccentricity in the normal force.

In designing the load cells, the following considerations were taken into account:

(1) The load cell reading should not be affected by any shear stresses acting on its face.

(2) The sresses in the load cell duc to the maximum expected loads should not exceed the elastic limit of the load cell material.

(3) The load cell should be sensitive to minor variations in stresses

(4) The deflection of the load cell under the expected loads should be a minimum since a movement of about 0.001 of the wall height may reduce the stresses from those corresponding to the at rest conditions to the active conditions (Wu, 1975).

(5) The load cell should be insensitive to ambient temperature changes.

EXAMPLE OF LOAD CELL DESIGN

From Figure A.2:

$$D_{nominal} = \frac{Do + Dj}{2} \qquad -(A.10)$$

where D_0 is the outer load cell diameter and D_i is the inner load cell diameter. $\sigma = \frac{\text{Normal Force}}{\text{Net Area}} = \frac{F}{\pi \cdot Dnom.t}$ $-(A.11)$

where t is the wall thickness of the load cell.

$$\varepsilon = \frac{\sigma}{E} \qquad -(A.12)$$

where E is Young's modulus of the material, ε is the axial strain and σ is the pressure capacity.

E for B. Copper = 1.24×10^8 kN/m^2 — (A.13)

$\Delta R = \varepsilon \times$ Gauge resistance x Gauge Factor

$\Delta R = \varepsilon \times R \times \lambda$ — (A.14)

where ;

$R = 120\Omega$ } specified by strain gauge manufacturers

$\lambda = 2.06$

Hence(A.14)becomes ;

$\Delta R = \varepsilon \times 120 \times 2.06$

Substituting (A.12) and (A.13) into (A.14) ,

$$\Delta R = \frac{120 \times 2{\cdot}06}{1{\cdot}24 \times 10^8} \cdot \sigma = \frac{199{\cdot}3}{10^8} \cdot \sigma \qquad -(A.15)$$

Assume the maximum axial piston forces to be about 3 tons (or 29.43 kN).

Then (A.1 1) becomes:

$$\sigma = \frac{29 \cdot 43}{\pi D_{nom.} t} = \frac{9 \cdot 37}{D_{nom.} t} \qquad -(A.16)$$

Substituting (A.16) into (A.15) becomes:

$$\Delta R = \frac{1 \cdot 86 \times 10^{-5}}{D_{nom.} t} \qquad -(A.17)$$

Similarly from equation A9:

$$V_{out} = V_{in} \cdot \frac{\Delta R}{4R} \qquad -(A.18)$$

For one strain gauge longitudinal and one transverse (see Figure A.3)

equation (A.18) becomes:

$$V_{out} = 2 \cdot 6\ V_{in} \cdot \frac{\Delta R}{4R} \qquad -(A.19)$$

If the provided D.C. power suppy is assumed to be 10 volts then

$$V_{out} = 26\, V_{in} \cdot \frac{\Delta R}{4R} \qquad -(A.20)$$

Substituting (A.17) into (A20) becomes,

$$V_{out} = \frac{0{\cdot}1007 \times 10^{-5}}{D_{nom.}\, t} \qquad -(A.21)$$

Assume t = 5 mm, (see Figure A.2)

Then D_{out} = 17.78 and D_{in} = 7.78 mm

Thus $D_{nominal}$ = 0.01278 m and t = 0.005 m.

Equation (A21) then becomes: 0.01638 Volts (or 16.38 mV say 16 mV increments). Thus the calibration factor will be;

$$29.43/_{16} = \underline{1.84\ kN/mV}$$

APPLICATION OF STRAIN GAUGES

The strain gauges used are 9.5 mm x 3.5 mm Showa foil strain gauges

with a guage factor of 2.06 and a nominal resistance of 120 ohms. These strain gauges are self-temperature compensated when used with aluminium alloys. A schematic diagram of a foil strain gauge is given in Figure A4.

After the body of the load cell was manufactured according to the required shape, it was heat treated by placing it in boiling water for 20 minutes to release the stresses induced in the manufacturing process. The load cell was left in the water to cool gradually. It was then removed and left in the air to dry. The strain gauges were glued to the surface of the load cell at the required positions using M-bond 200 adhesive according to the following procedure:*

(i) Dry lapping was achieved by using a fine grade '"wet-or-dry" emery paper to smoothen the surface and to remove any rust, oxides or dirt that might have been present on the surface of the metal.

(ii) Wet -lapping was then carried out by using the emery paper with a conditioner (M-Prep Conditioner A) to remove any grease on the

*M-Line Accessories-Instruction Bulletin B-127-2, March 1972.

surface. The conditoner was then removed by wiping with pieces of cotton wool untilthey were no longer discoloured indicating that the surface became clean. The conditioner was not allowed to dry by evaporation since this would leave a thin unwanted film between the adhesive, when applied, and the specimen surface.

(iii) A neutralizer (M-Prep. Neutralizer B), which is a weak detergent was applied to the surface and again wiped using cotton wool

(iv) Lay-out lines, to locate the positions of the strain gauges, were marked using a ball-point pen.

(v) The surface was scrubbed once more using the neutralizer and then wiped dry.

(vi) The gauge was removed from its envelope with tweezers and placed on a chemically cleaned glass plate with the bond side of the gauge down. A piece of cellophane tape was then placed on the gauge.

(vii) The gauge/tape assembly was placed in position over the layout lines. One end of the tape was then firmly pressed down to stick firmly to the specimen, while the other end was lifted slightly until the gauge was free from the specimen surface.

(viii) A very little amount of M-bond 200 catalyst was applied to the bond surface of the gauge to accelerate the hardening of the M-bond 200 adhesive.

(ix) One or two drops of the adhesive were applied on the surface of the specimen.

(x) The gauge was brought down over the alignment marks on the specimen and pressed with ones finger for a least one minule.

(xi) The cellophane tape was removed by peeling it slowly off the surface.

(xii) The lead wires of the gauge, (see Fig. A4), were insulated by sleeves to prevent any opened electric circuits if they come in contact with the load cell body. The end of the wires were then soldered to a terminal which was cemented near the gauge.

(xiii) Insulated wires were used in connecting the gauges together to form the electric circuit shown in Plate A.1.

(xiv) All the gauges and terminals were covered with a water proof coating to protect them from any moisture in the air.

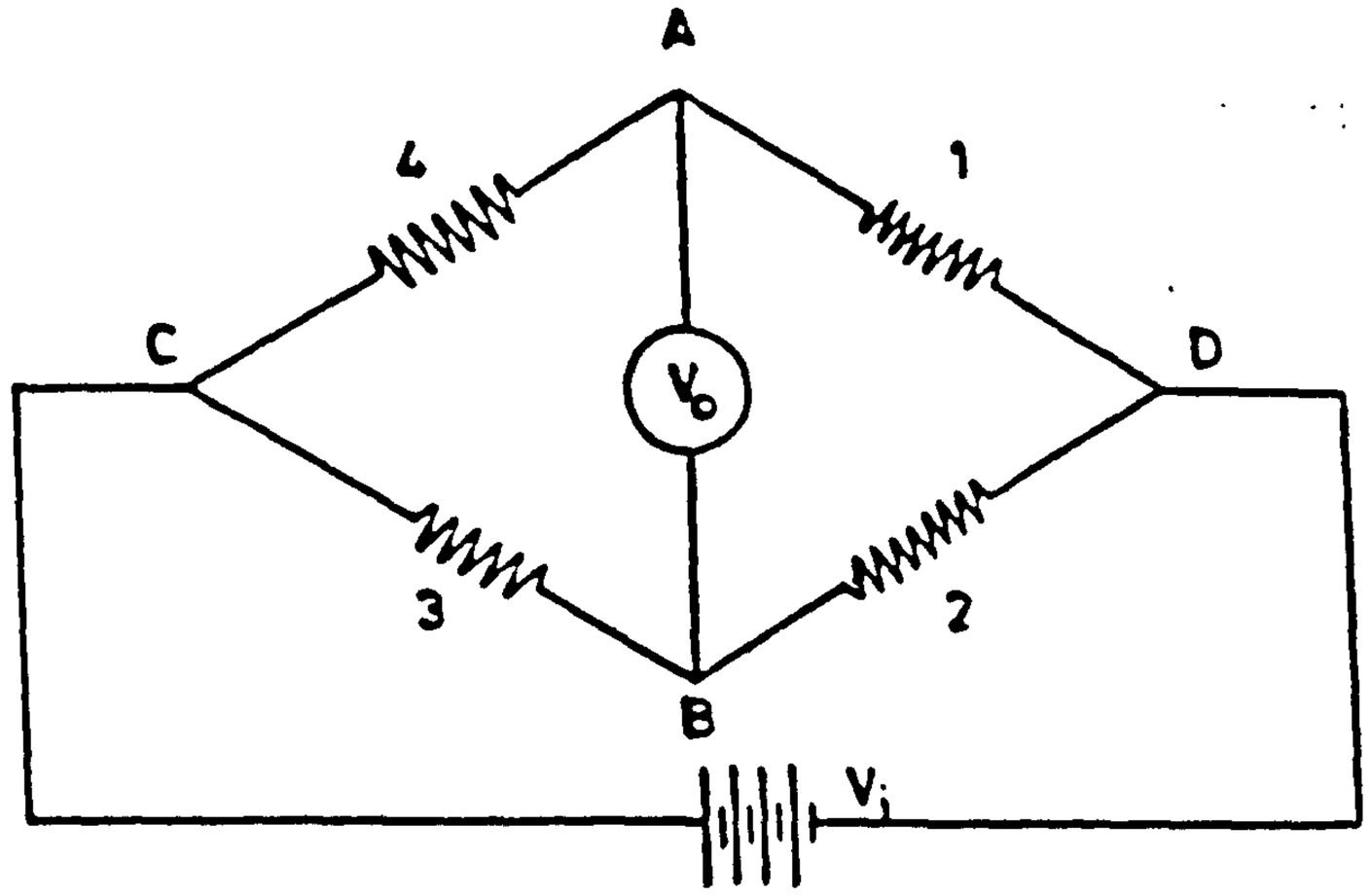

WHEATSTONE BRIDGE

FIG. A.1

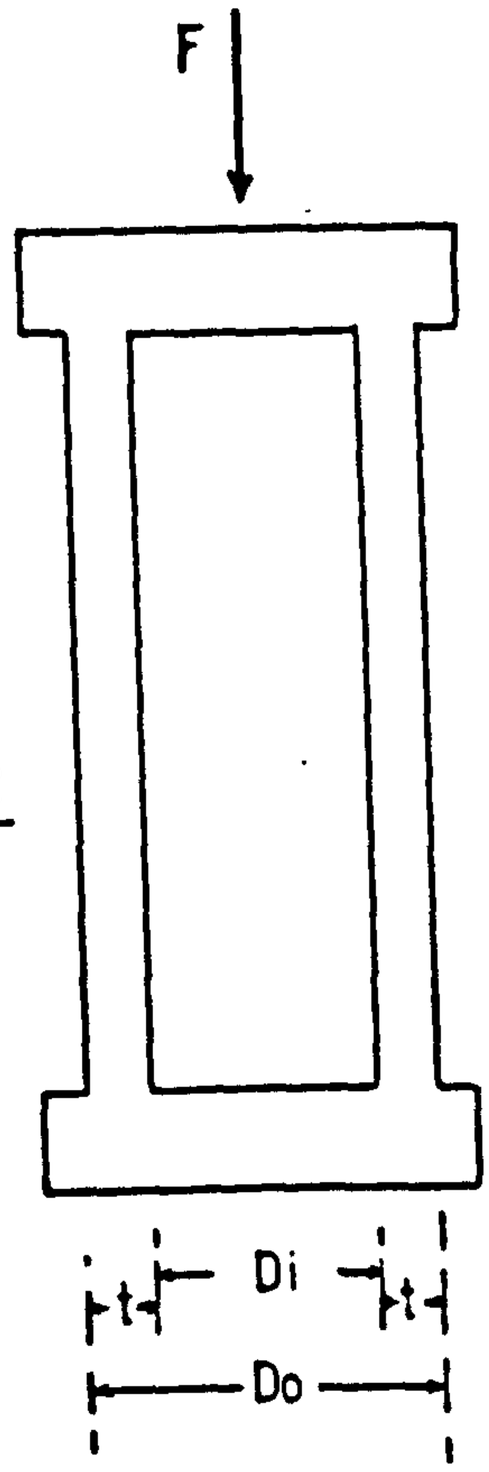

FIG. A.2

FIG. A.3

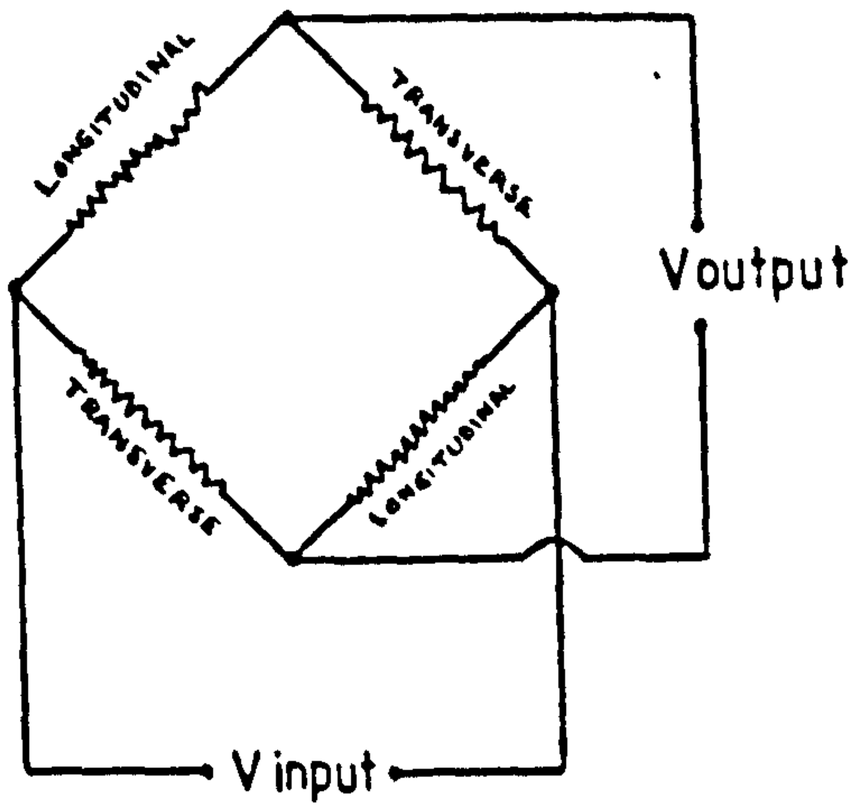

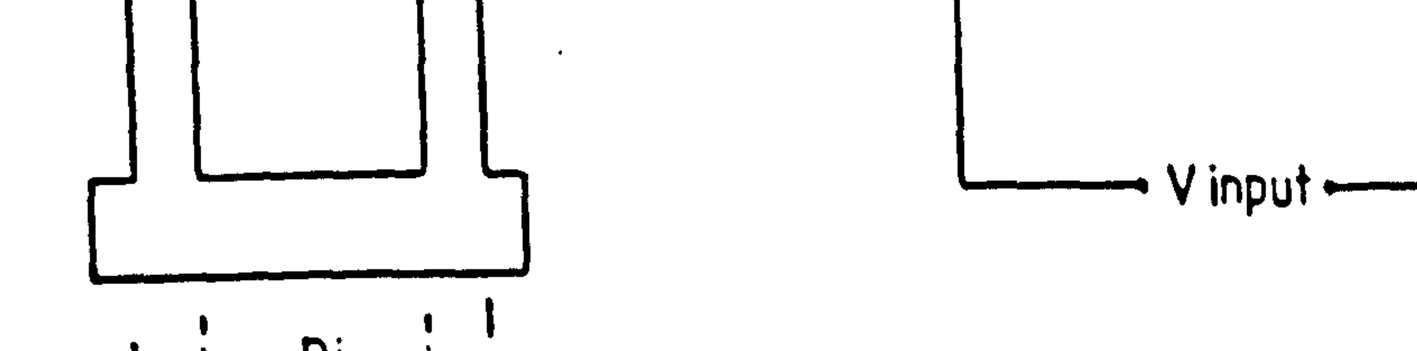

FIG. A.4 FOIL STRAIN GAUGE CONSTRUCTION

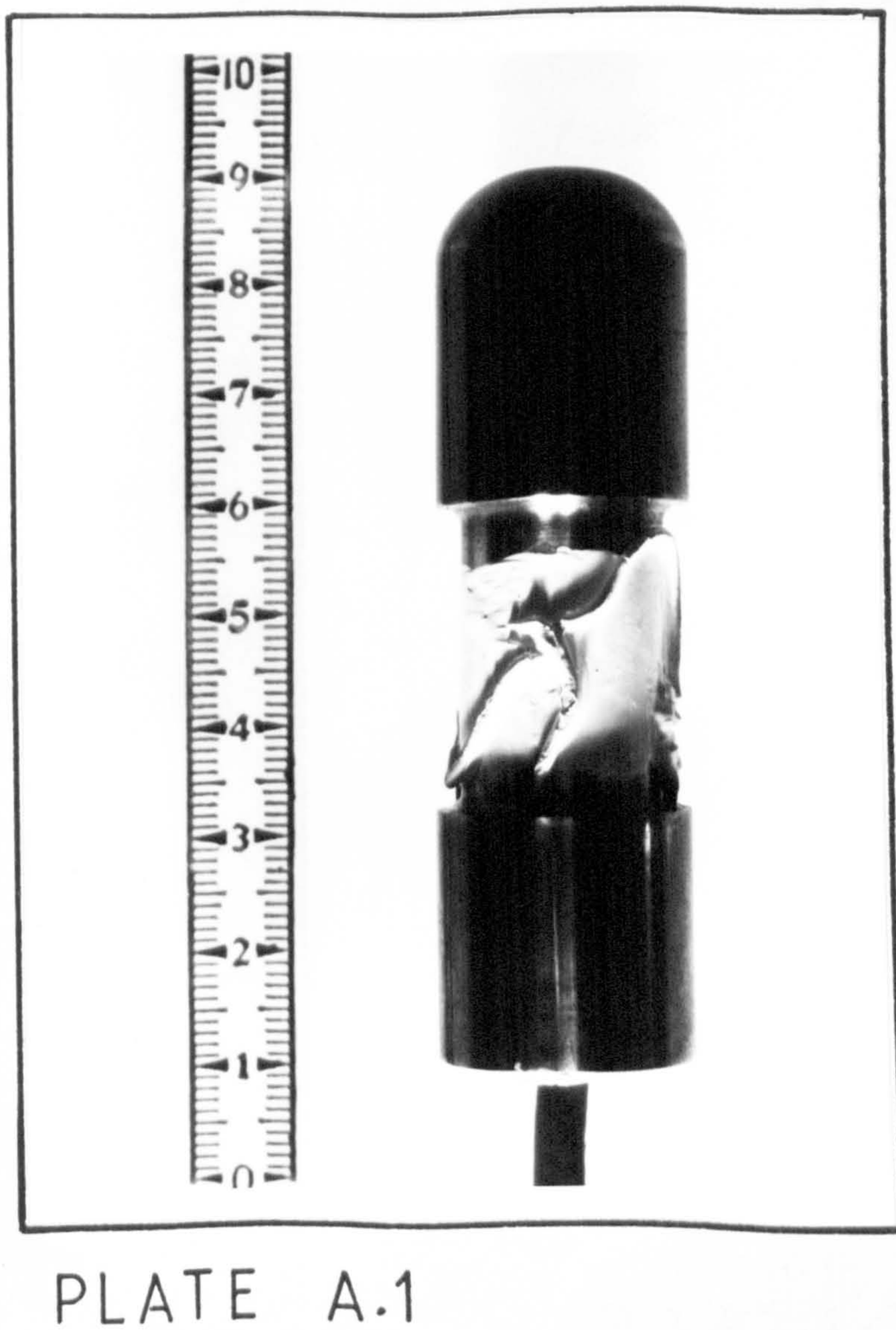

PLATE A.1

A typical Load-cell consisting of a metal strut with strain gauges attached on its web

APPENDIX B

COMPUTATION of TRIAXIAL TEST DATA

FIG. B.1

200mm x 155mm dia. TRIAXIAL TEST DATA	
SOIL TYPE	MID-ROSS SAND
MESH TYPE	NONE
MESH CONTENT	0.000 M^2/M^3 0.000 % dry weight

SLOPE - INTERCEPT RELATIONSHIP					
STRAIN %	0.5	1.0	2.0	3.0	4.0
M (deg)	58.58	69.77	74.36	76.95	78.41
N	109.1	74.35	161.0	174.1	165.4
ø (deg)	13.98	27.48	34.24	38.58	41.27
C (KN/M^2)	42.66	22.56	42.6	41.91	37.45

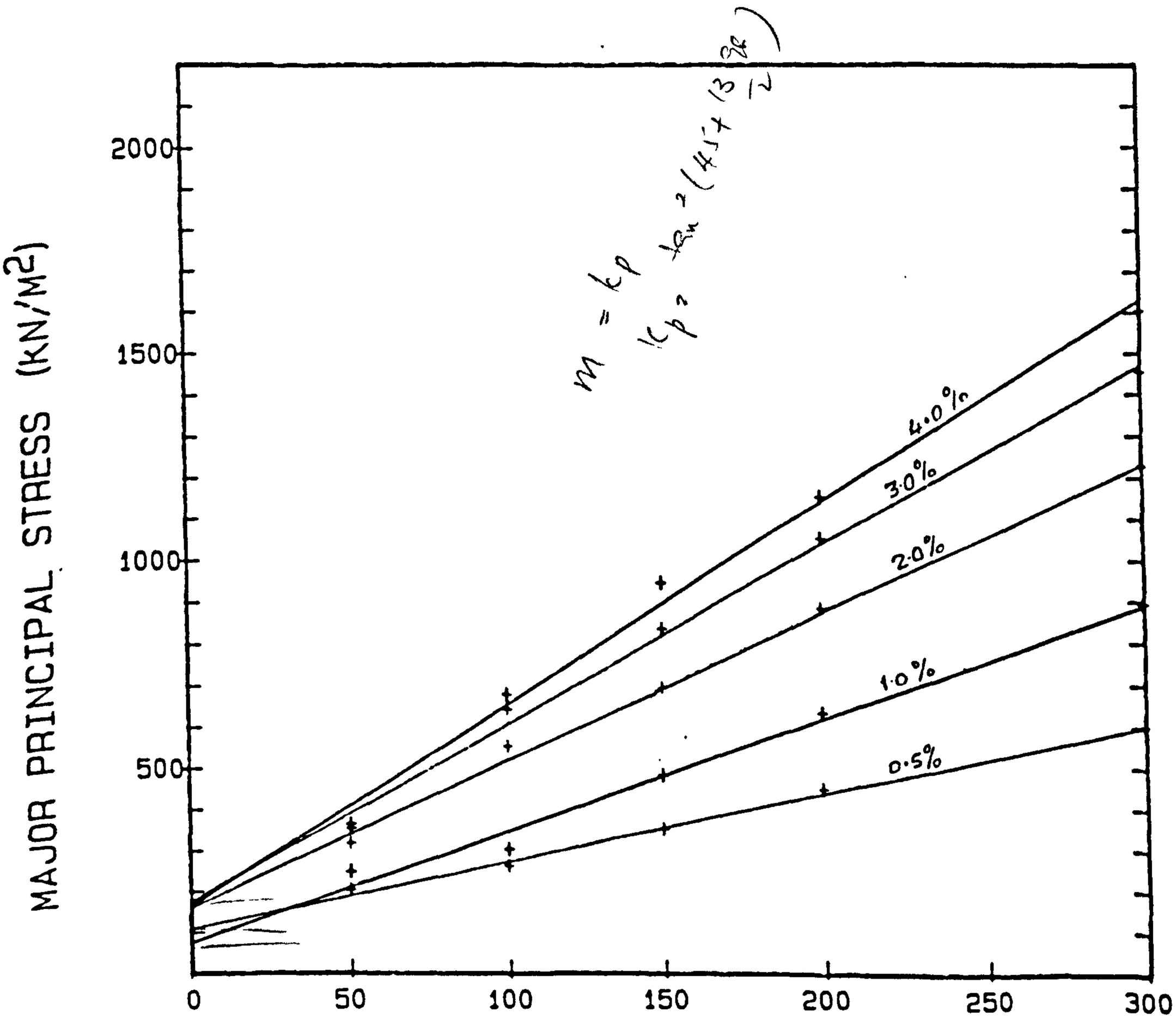

FIG. B.2

200mm x 155mm dia. TRIAXIAL TEST DATA	
SOIL TYPE	MID-ROSS SAND
MESH TYPE	NONE
MESH CONTENT	0.000 M^2/M^3 0.000 % dry weight

SLOPE - INTERCEPT RELATIONSHIP					
STRAIN %	5.0	6.0	7.0	8.0	9.0
M (deg)	79.15	79.66	79.94	80.07	79.95
N	152	115.5	70	18.91	-12.87
ø (deg)	42.72	43.74	44.33	44.6	44.35
C (KN/M^2)	33.26	24.67	14.73	3.95	-2.71

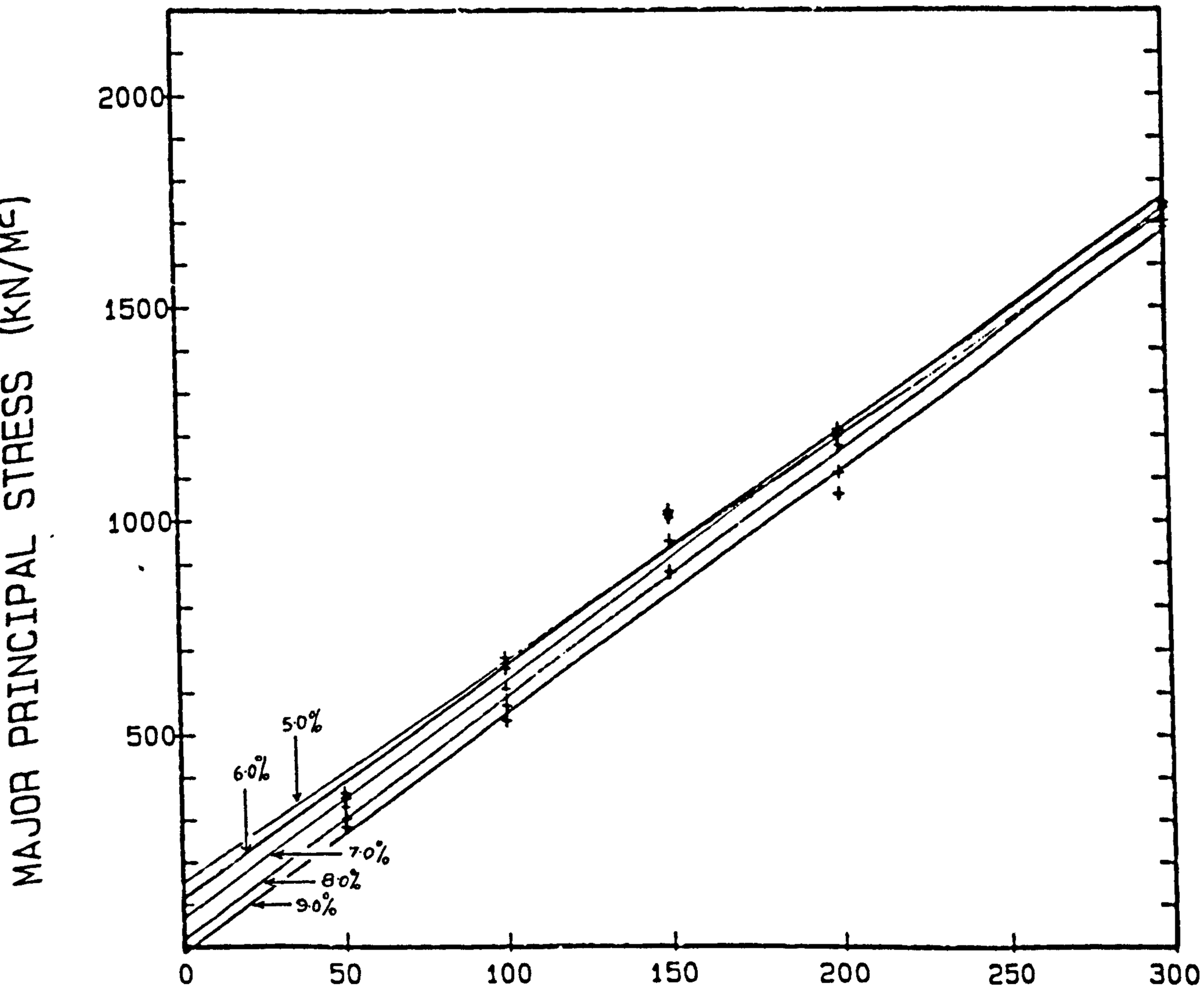

FIG. B.3

200mm x 155mm dia. TRIAXIAL TEST DATA	
SOIL TYPE	MID-ROSS SAND
MESH TYPE	NONE
MESH CONTENT	0.000 M^2/M^3 0.000 % dry weight

SLOPE - INTERCEPT RELATIONSHIP					
STRAIN %	10.	11.	12.	13.	14.
M (deg)	79.47	78.82	78.07	77.58	77.5
N	-6.9	21.59	51.1	67.27	67.59
ø (deg)	43.37	42.08	40.63	39.72	39.58
C (kN/M^2)	-1.49	4.79	11.74	15.78	15.9

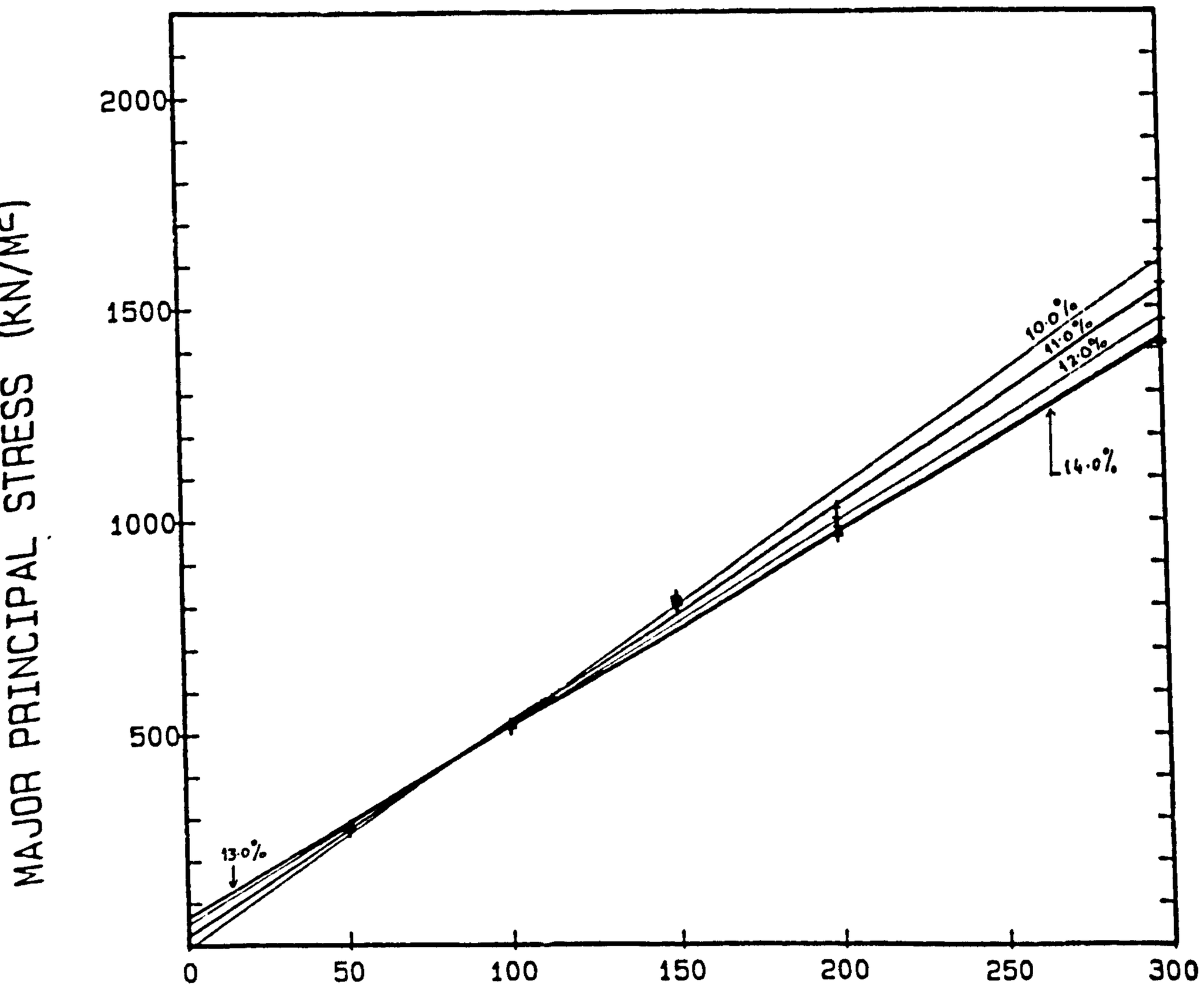

FIG. B.4

200mm x 155mm dia. TRIAXIAL TEST DATA	
SOIL TYPE	MID-ROSS SAND
MESH TYPE	NONE
MESH CONTENT	0.000 M^2/M^3 0.000 % dry weight

SLOPE - INTERCEPT RELATIONSHIP					
STRAIN %	15.				
M (deg)	77.47				
N	66.29				
ø (deg)	39.53				
C (KN/M^2)	15.62				

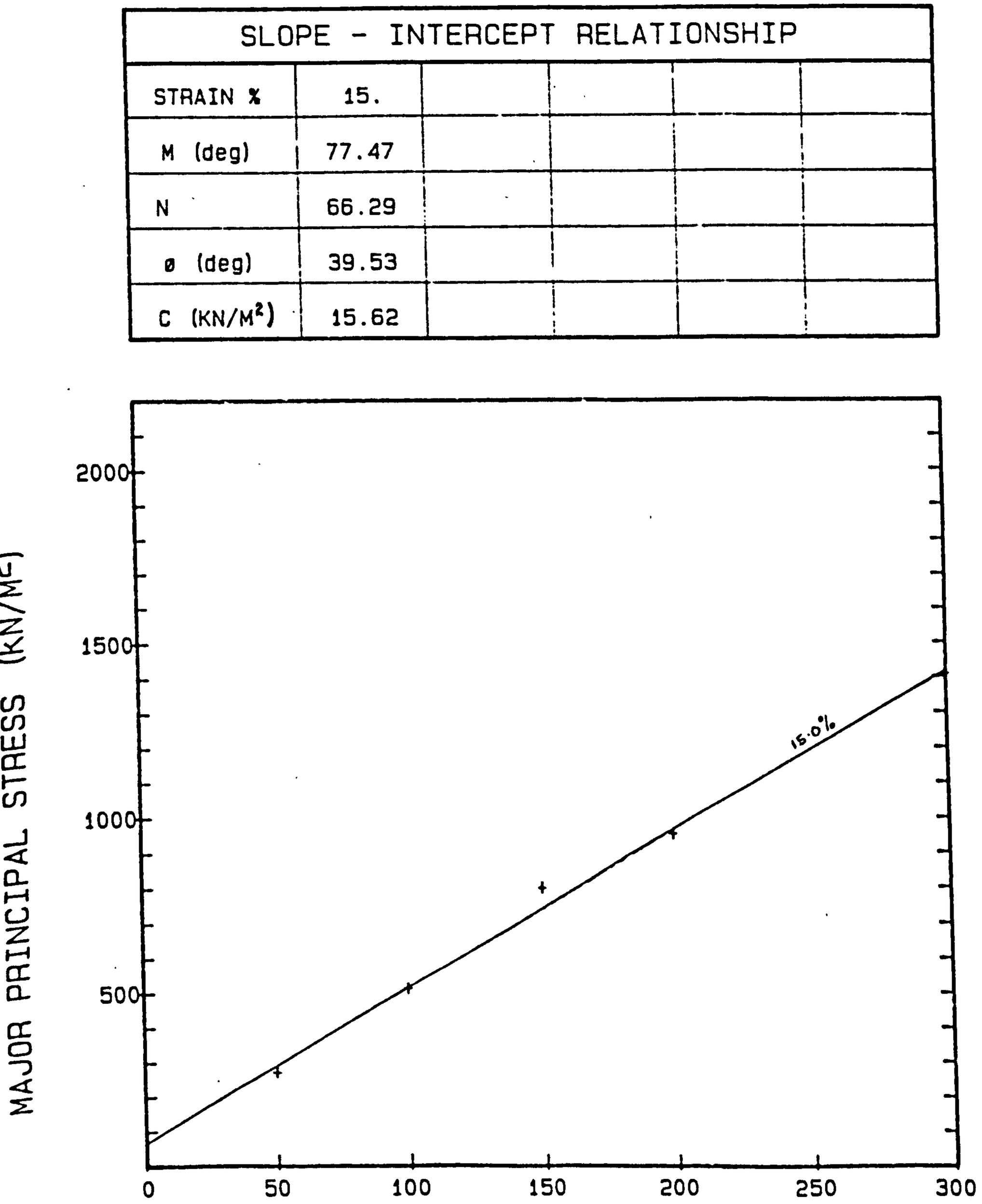

FIG. B.5

200mm x 155mm dia. TRIAXIAL TEST DATA	
SOIL TYPE	MID-ROSS SAND
MESH TYPE	NONE
MESH CONTENT	0.000 M^2/M^3 0.000 % dry weight

SLOPE - INTERCEPT RELATIONSHIP					
STRAIN %	PEAK	RESID.			
M (deg)	79.6	77.47			
N	133.0	66.29			
ø (deg)	43.63	39.53			
C (KN/M^2)	28.49	15.62			

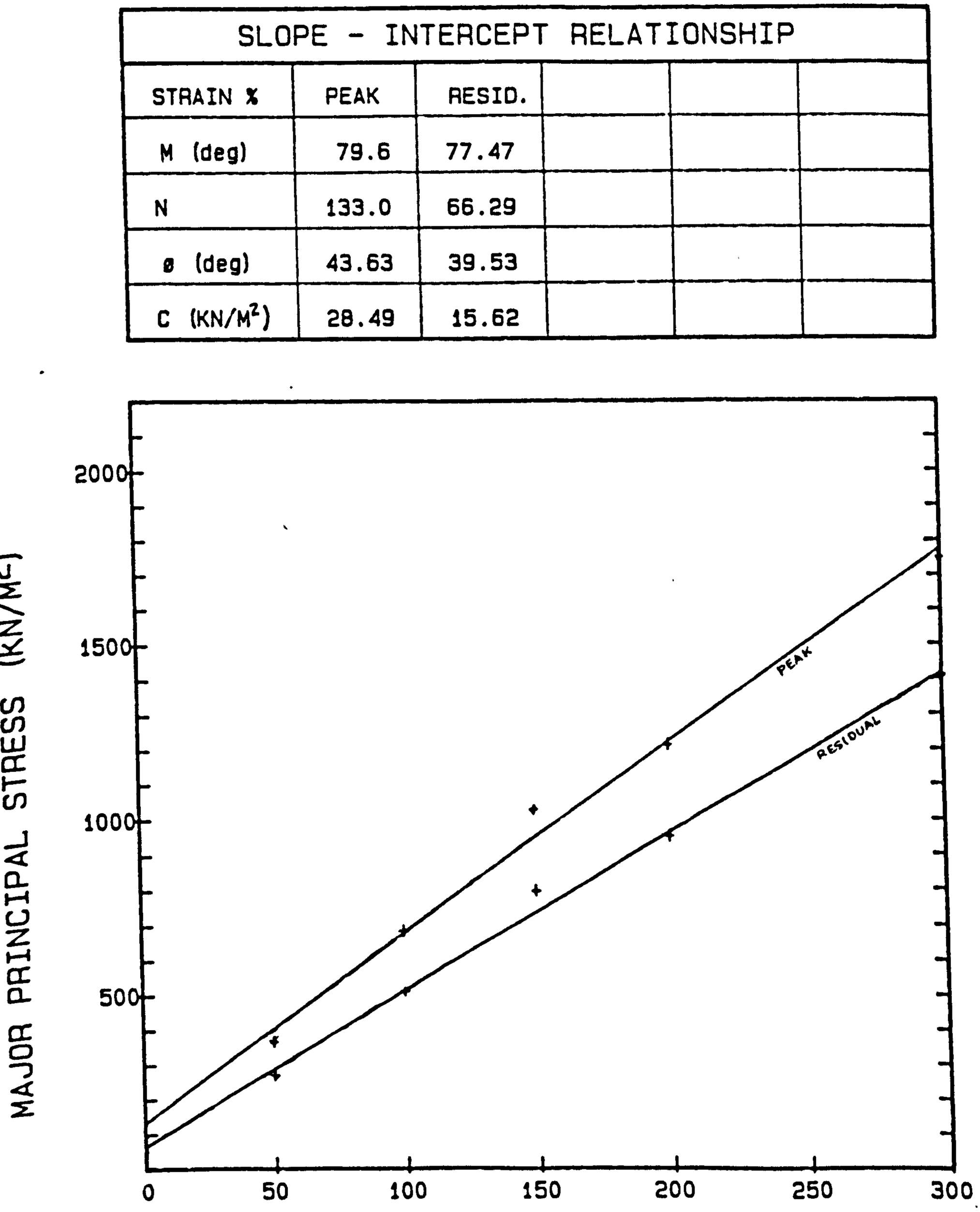

FIG. B.6

200mm x 155mm dia. TRIAXIAL TEST DATA	
SOIL TYPE	MID-ROSS SAND
MESH TYPE	7
MESH CONTENT	33.00 M^2/M^3 0.090 % dry weight

SLOPE - INTERCEPT RELATIONSHIP					
STRAIN %	0.5	1.0	2.0	3.0	4.0
M (deg)	59.13	68.32	74.71	76.76	78.23
N	124.3	165.4	241.4	296.7	318.5
S (deg)	14.58	25.54	34.3	38.24	40.93
I (KN/M^2)	48.05	52.13	63.11	71.97	72.68

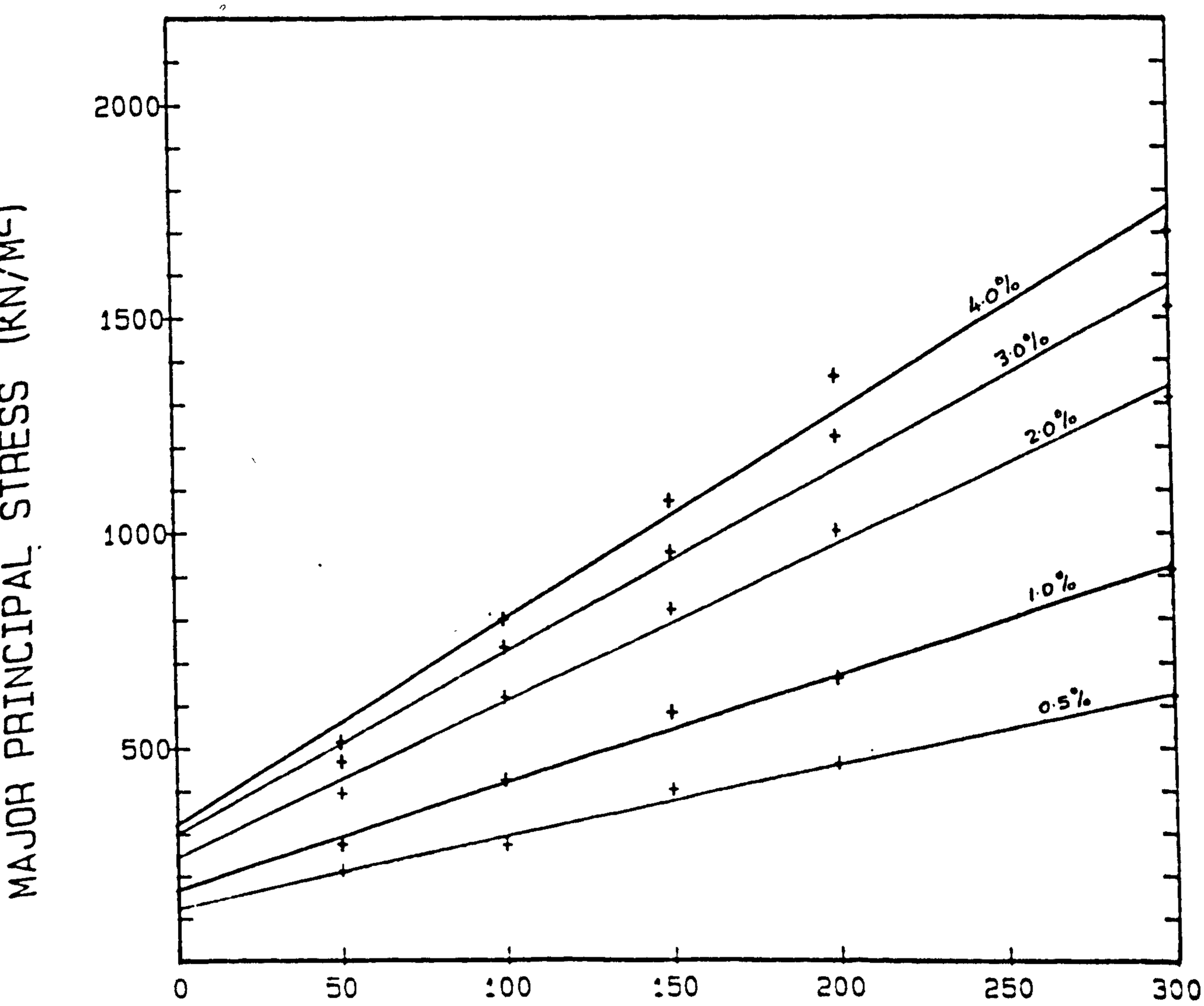

FIG. B.7

200mm x 155mm dia. TRIAXIAL TEST DATA	
SOIL TYPE	MID-ROSS SAND
MESH TYPE	7
MESH CONTENT	33.00 M^2/M^3 0.090 % dry weight

SLOPE - INTERCEPT RELATIONSHIP					
STRAIN %	5.0	6.0	7.0	8.0	9.0
M (deg)	78.96	79.69	80.25	80.35	80.11
N	329.6	285.0	212.1	160.7	137.2
S (deg)	42.33	43.81	44.98	45.18	44.68
I (KN/M^2)	72.8	60.76	43.34	33.14	28.64

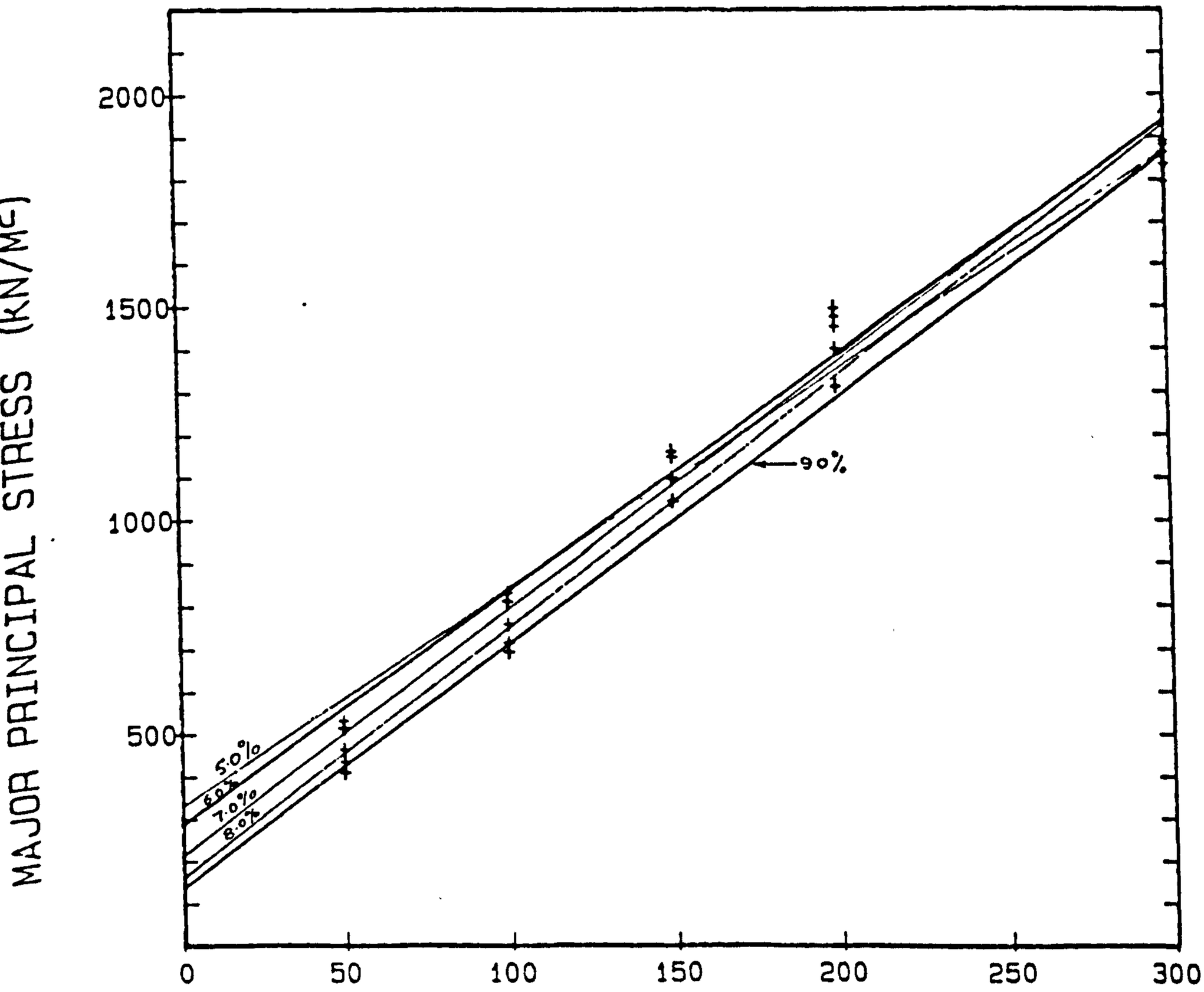

FIG. B.8

200mm x 155mm dia. TRIAXIAL TEST DATA	
SOIL TYPE	MID-ROSS SAND
MESH TYPE	7
MESH CONTENT	33.00 M^2/M^3 0.090 % dry weight

SLOPE - INTERCEPT RELATIONSHIP					
STRAIN %	10.	11.	12.	13.	14.
M (deg)	79.52	78.9	78.31	77.86	77.58
N	150.4	174.2	197.1	213.0	222.1
S (deg)	43.45	42.22	41.03	40.24	39.73
I (KN/M^2)	32.34	38.57	44.32	49.38	52.09

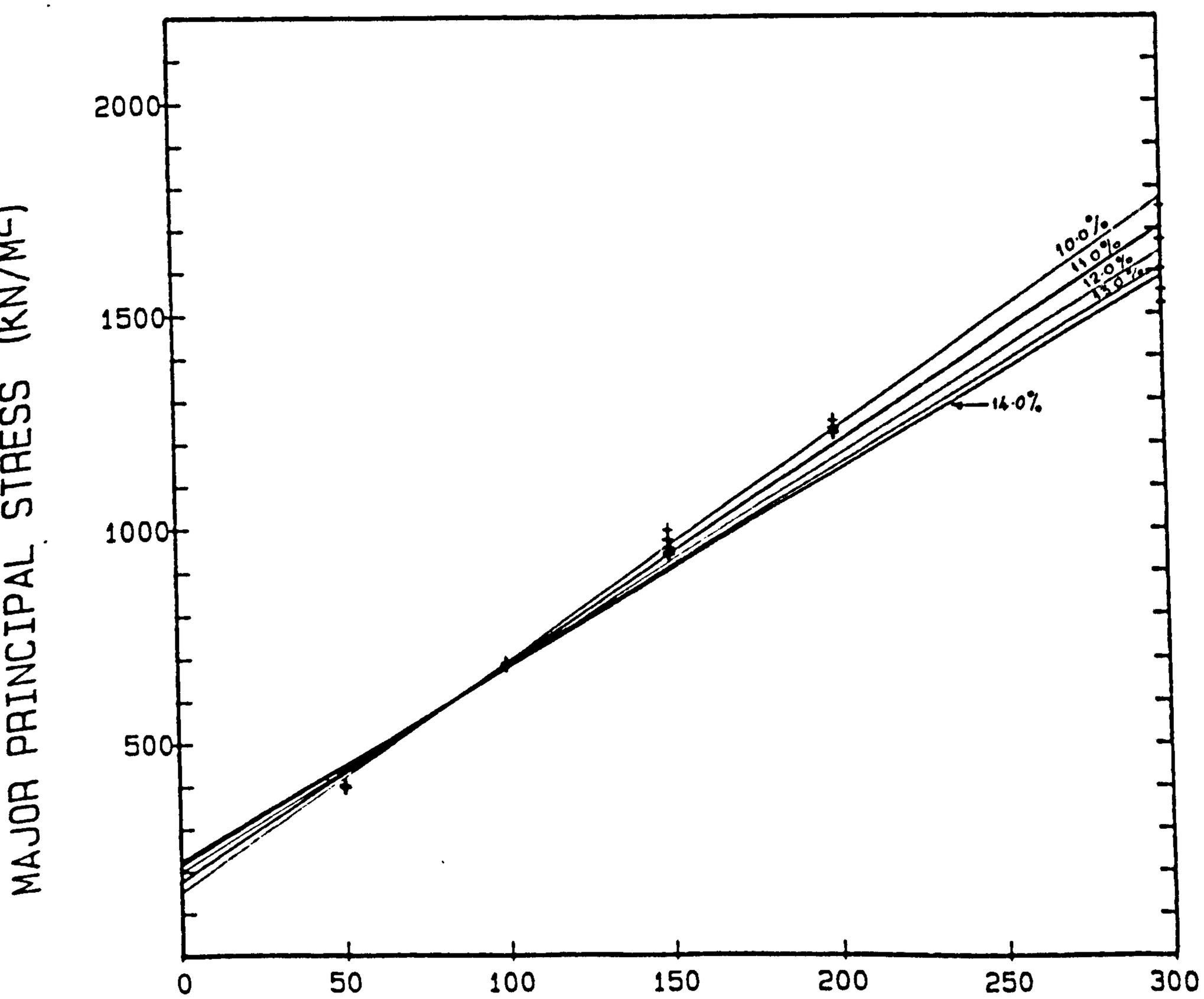

FIG. B.9

200mm x 155mm dia. TRIAXIAL TEST DATA	
SOIL TYPE	MID-ROSS SAND
MESH TYPE	7
MESH CONTENT	33.00 M^2/M^3 0.090 % dry weight

SLOPE - INTERCEPT RELATIONSHIP					
STRAIN %	15.				
M (deg)	77.56				
N	221.1				
S (deg)	39.69				
I (KN/M^2)	51.91				

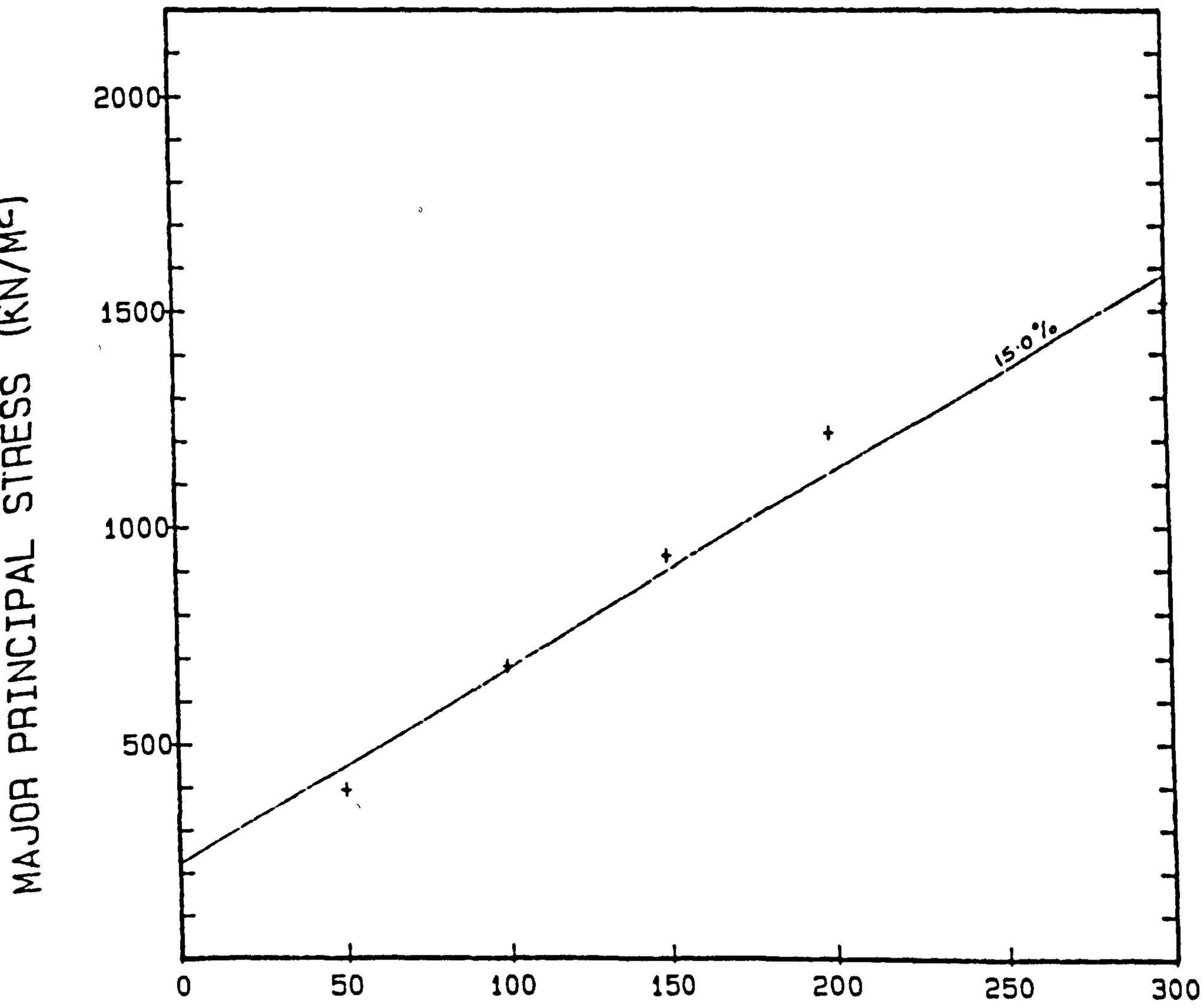

FIG. B.10

200mm x 155mm dia. TRIAXIAL TEST DATA	
SOIL TYPE	MID-ROSS SAND
MESH TYPE	7
MESH CONTENT	33.00 M^2/M^3 0.090 % dry weight

SLOPE - INTERCEPT RELATIONSHIP					
STRAIN %	PEAK	RESID.			
M (deg)	79.72	77.56			
N	300.1	221.1			
S (deg)	43.87	39.69			
I (KN/M^2)	63.89	51.91			

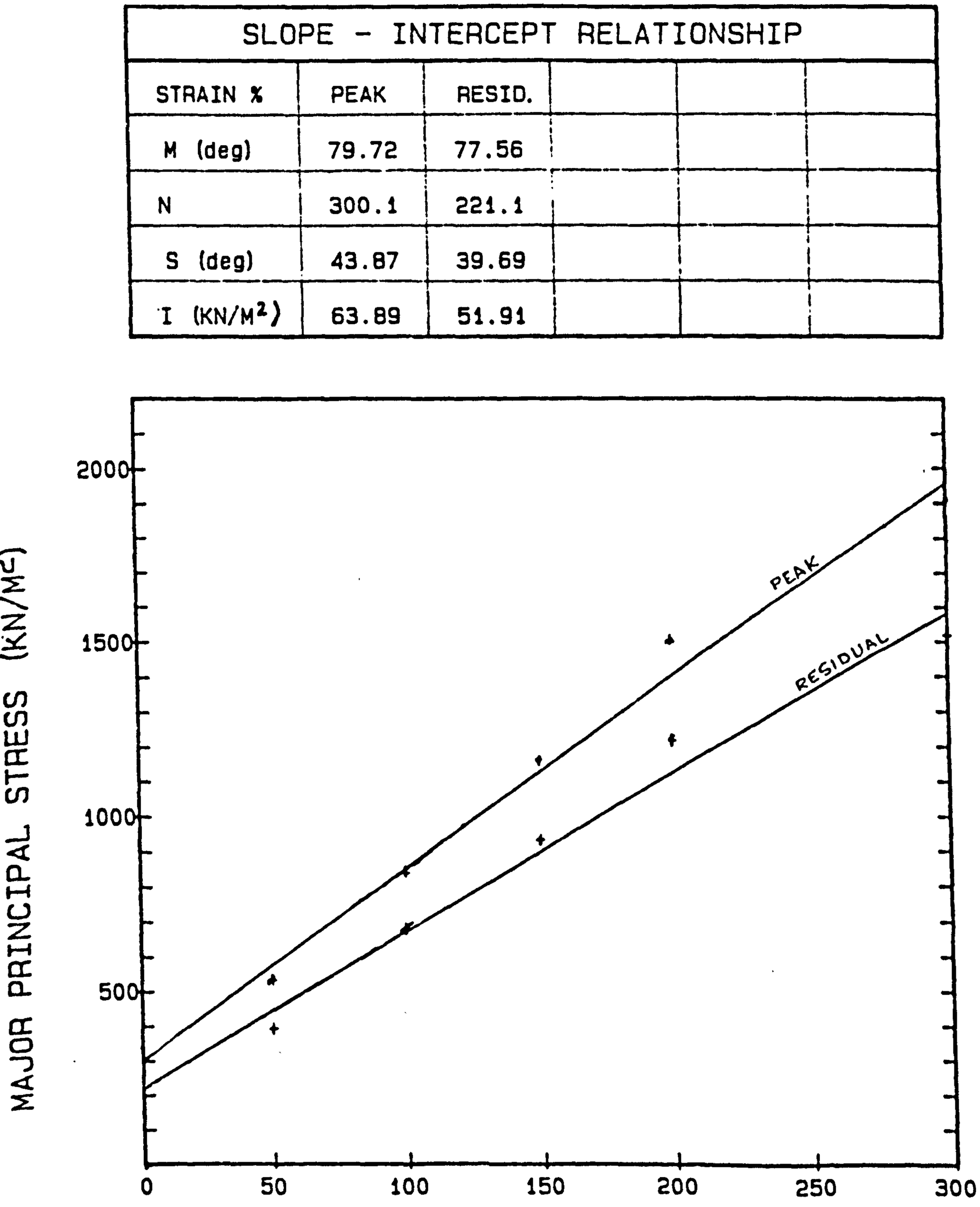

FIG. B.11

200mm x 155mm dia. TRIAXIAL TEST DATA	
SOIL TYPE	MID-ROSS SAND
MESH TYPE	7
MESH CONTENT	66.00 M^2/M^3 0.180 % dry weight

SLOPE - INTERCEPT RELATIONSHIP					
STRAIN %	0.5	1.0	2.0	3.0	4.0
M (deg)	61.69	68.65	75.23	77.37	78.84
N	118.9	176.4	241.0	301.1	318.0
S (deg)	17.45	25.97	35.64	39.35	42.11
I (KN/M^2)	43.63	55.16	61.89	71.25	70.61

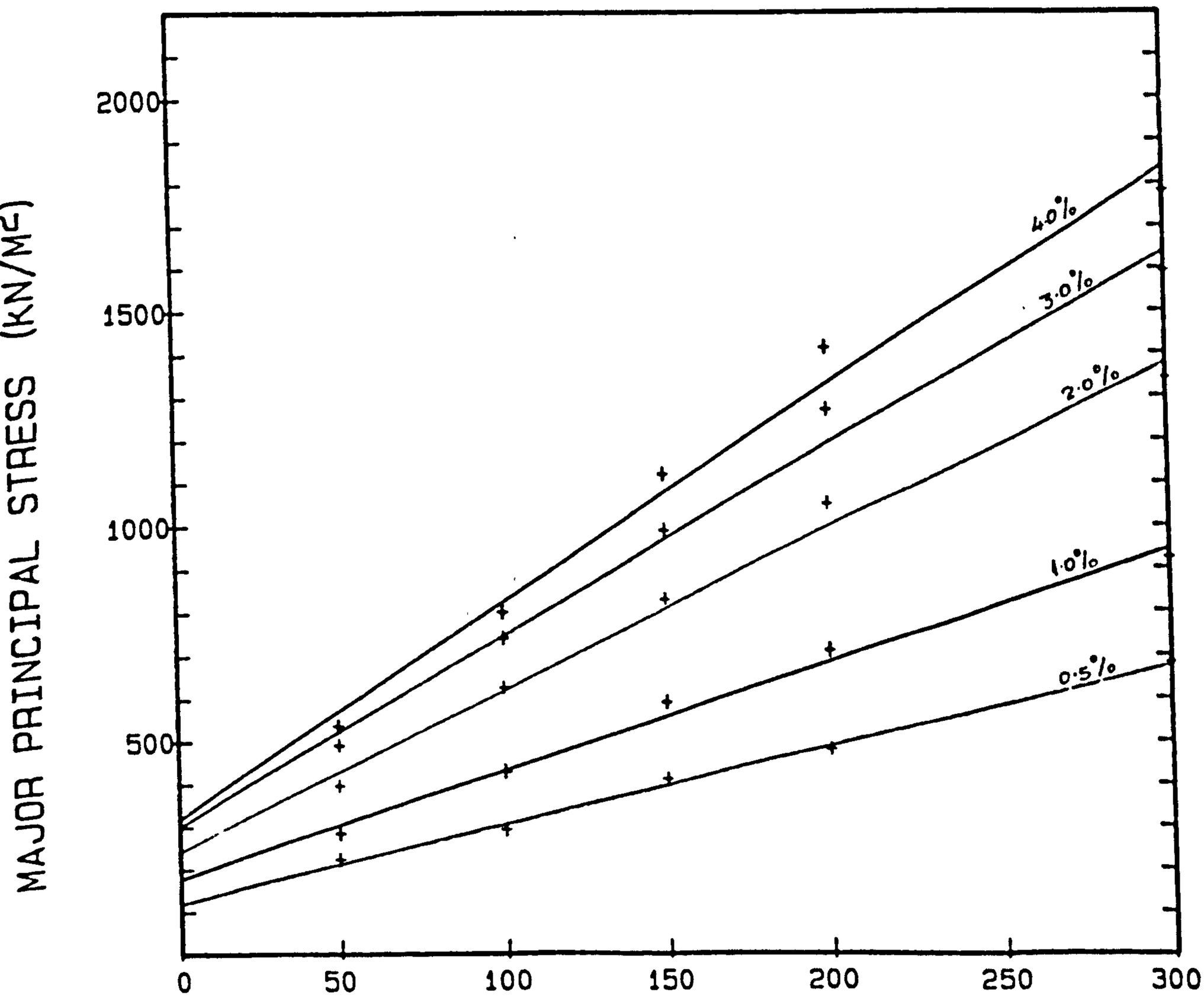

FIG. B.12

200mm x 155mm dia. TRIAXIAL TEST DATA	
SOIL TYPE	MID-ROSS SAND
MESH TYPE	7
MESH CONTENT	66.00 M^2/M^3 0.180 % dry weight

SLOPE - INTERCEPT RELATIONSHIP					
STRAIN %	5.0	6.0	7.0	8.0	9.0
M (deg)	79.75	80.5	60.91	81.02	80.88
N	322.2	272.2	213.7	163.3	128.6
S (deg)	43.93	45.52	46.4	46.66	46.35
I (KN/M^2)	68.51	55.66	42.75	32.45	25.75

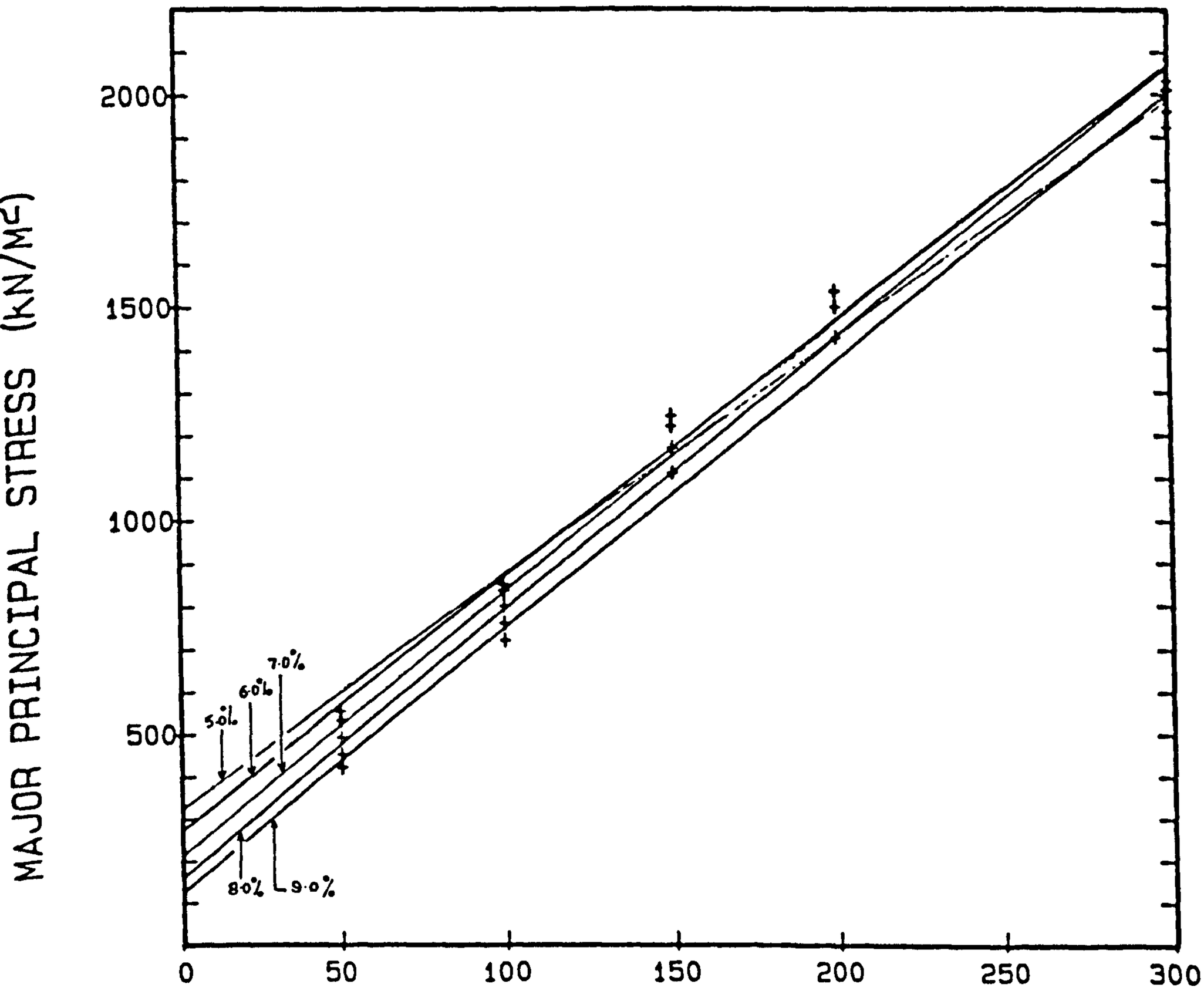

FIG. B.13

200mm x 155mm dia. TRIAXIAL TEST DATA	
SOIL TYPE	MID-ROSS SAND
MESH TYPE	7
MESH CONTENT	66.00 M^2/M^3 0.180 % dry weight

SLOPE - INTERCEPT RELATIONSHIP					
STRAIN %	10.	11.	12.	13.	14.
M (deg)	80.38	79.82	79.4	79.08	78.97
N	141.1	161.7	176.3	188.8	191.8
S (deg)	45.26	44.07	43.21	42.58	42.36
I $(KN/M)^2$	29.03	34.26	38.14	41.47	42.33

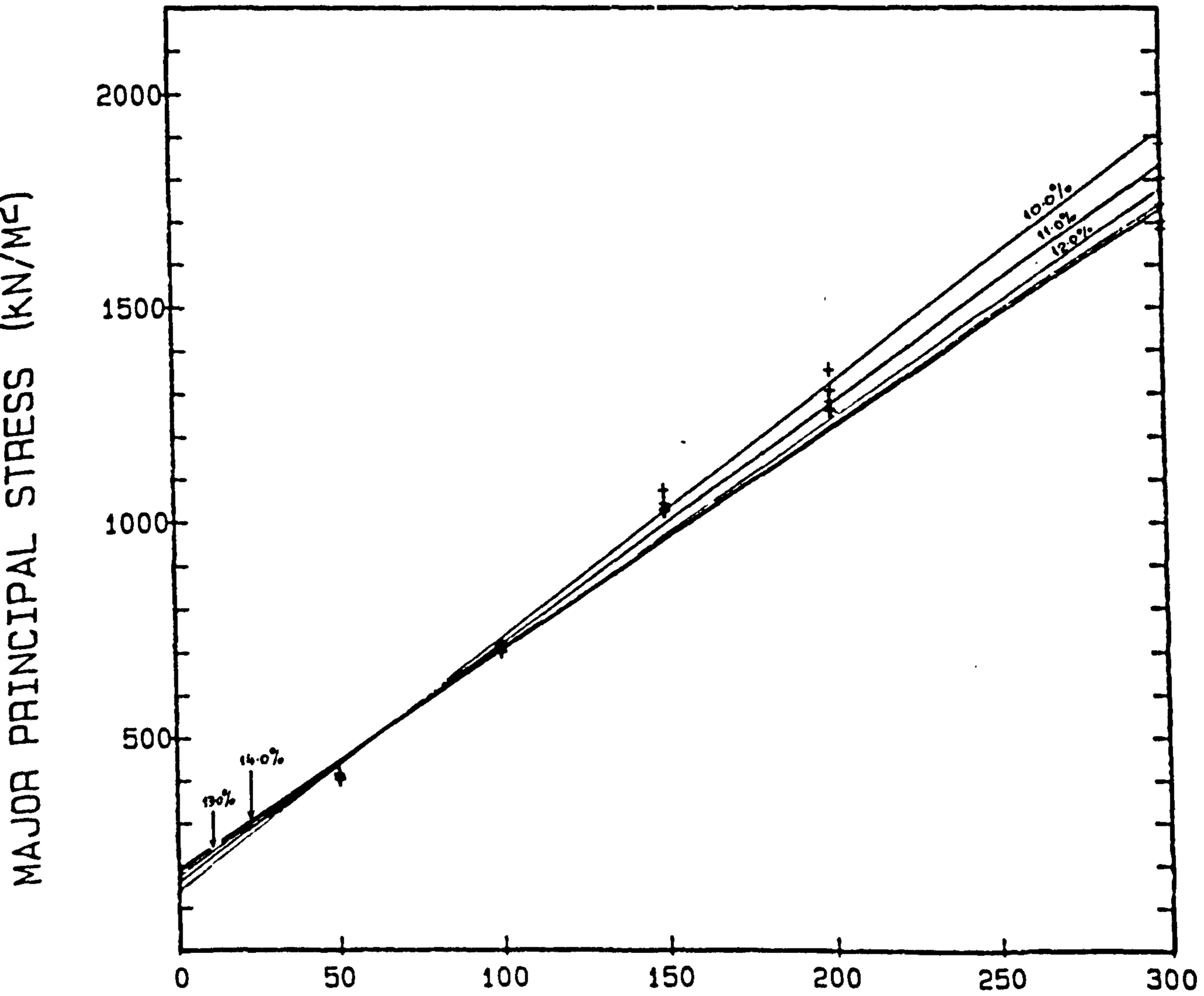

FIG. B.14

200mm x 155mm dia. TRIAXIAL TEST DATA	
SOIL TYPE	MID-ROSS SAND
MESH TYPE	7
MESH CONTENT	66.00 M^2/M^3 0.180 % dry weight

SLOPE - INTERCEPT RELATIONSHIP					
STRAIN %	15.				
M (deg)	78.95				
N	190.8				
S (deg)	42.32				
I (KN/M^2)	42.15				

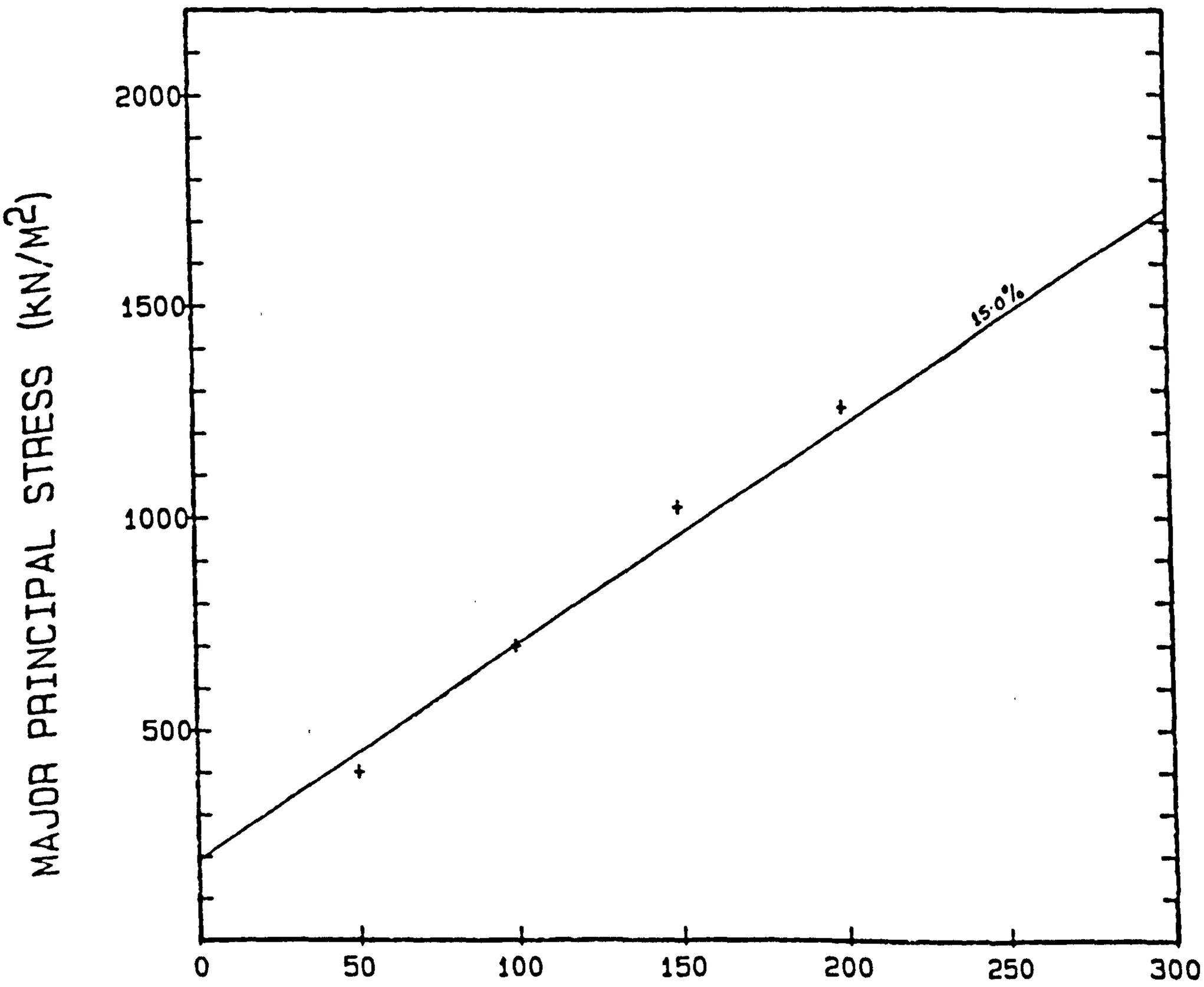

FIG. B.15

200mm x 155mm dia. TRIAXIAL TEST DATA	
SOIL TYPE	MID-ROSS SAND
MESH TYPE	7
MESH CONTENT	66.00 M^2/M^3 0.180 % dry weight

SLOPE - INTERCEPT RELATIONSHIP					
STRAIN %	PEAK	RESID.			
M (deg)	80.52	78.95			
N	285.3	190.8			
S (deg)	45.56	42.32			
I (KN/M^2)	58.27	42.15			

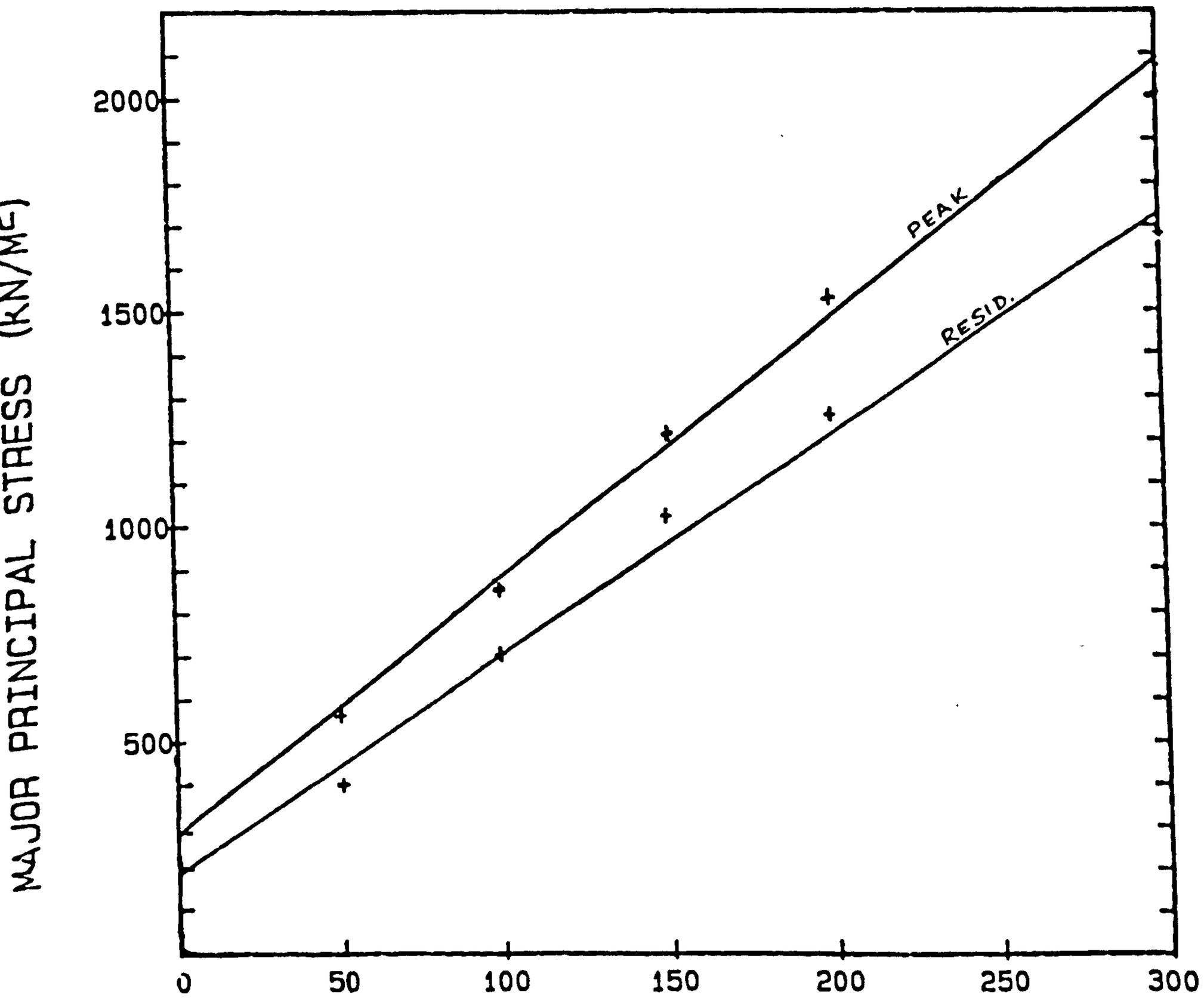

FIG. B.16

200mm x 155mm dia. TRIAXIAL TEST DATA	
SOIL TYPE	MID-ROSS SAND
MESH TYPE	7
MESH CONTENT	90.00 M^2/M^3 0.250 % dry weight

SLOPE - INTERCEPT RELATIONSHIP					
STRAIN %	0.5	1.0	2.0	3.0	4.0
M (deg)	63.09	68.15	74.89	77.75	78.99
N	116.7	234.8	320.1	376.1	423.5
S (deg)	19.06	25.32	35.09	40.04	42.39
I (KN/M^2)	41.59	74.35	83.15	87.62	93.39

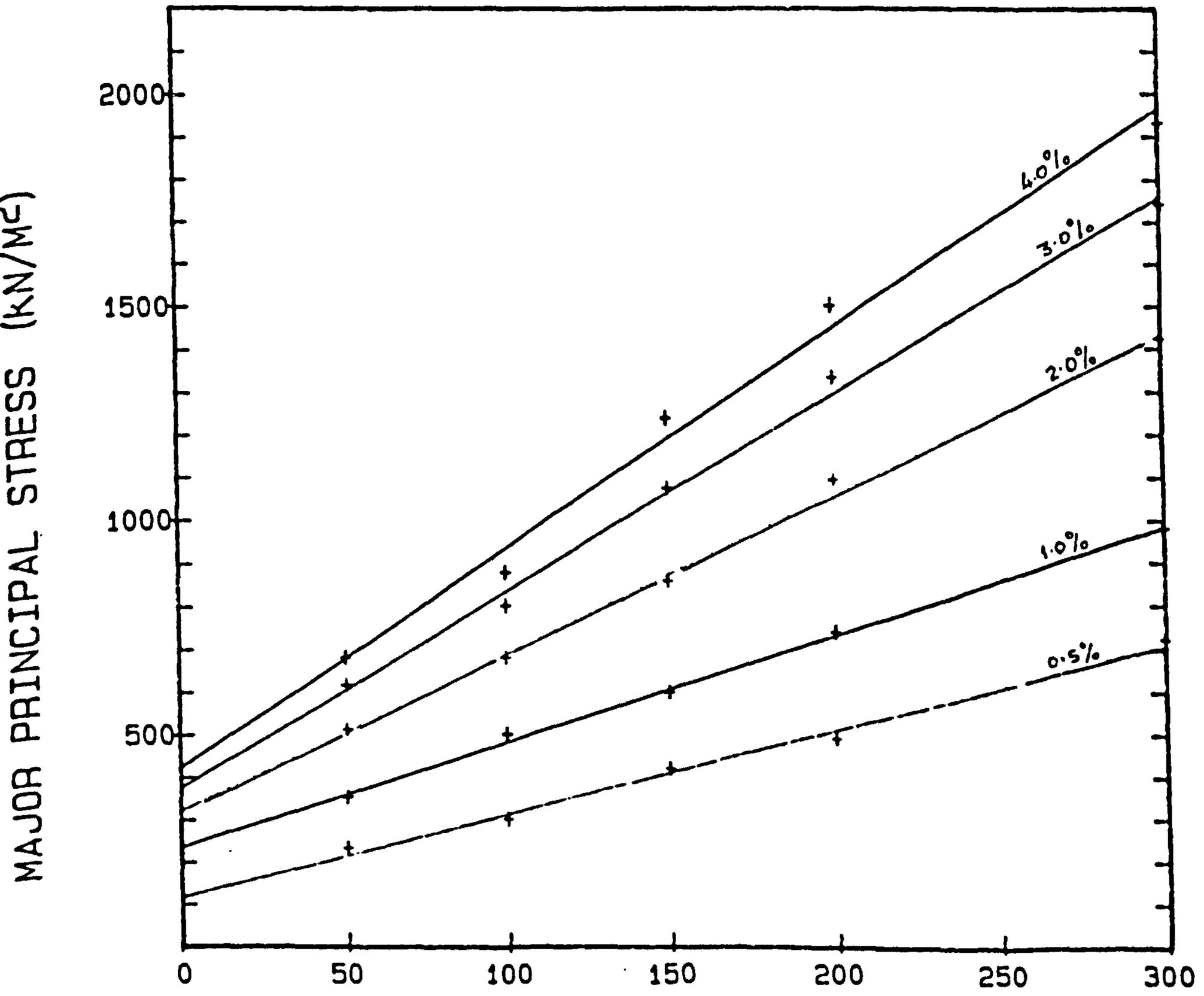

FIG. B.17

200mm x 155mm dia. TRIAXIAL TEST DATA	
SOIL TYPE	MID-ROSS SAND
MESH TYPE	7
MESH CONTENT	90.00 M^2/M^3 0.250 % dry weight

SLOPE - INTERCEPT RELATIONSHIP					
STRAIN %	5.0	6.0	7.0	8.0	9.0
M (deg)	79.82	80.49	80.9	81.05	80.85
N	430.7	390.5	327.7	274.3	252.8
S (deg)	44.07	45.49	46.39	46.71	46.28
I (KN/M^2)	91.25	79.9	65.55	54.41	50.71

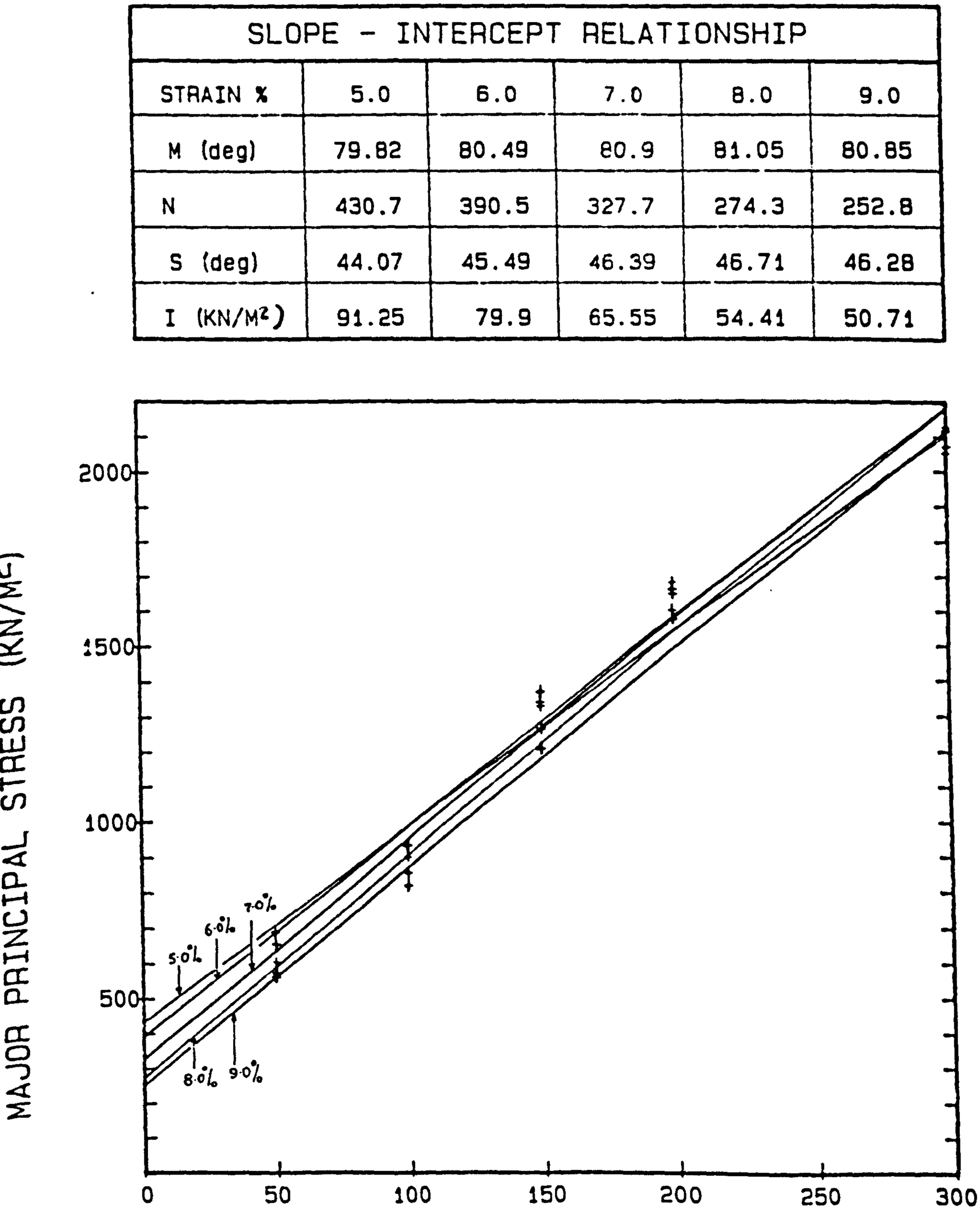

FIG. B.18

200mm x 155mm dia. TRIAXIAL TEST DATA	
SOIL TYPE	MID-ROSS SAND
MESH TYPE	7
MESH CONTENT	90.00 M^2/M^3 0.250 % dry weight

SLOPE - INTERCEPT RELATIONSHIP					
STRAIN %	10.	11.	12.	13.	14.
M (deg)	80.47	80.22	80.05	80.02	79.95
N	258.0	259.6	262.8	260.3	260.4
S (deg)	45.45	44.92	44.55	44.48	44.35
I (KN/M^2)	52.84	53.87	55.02	54.6	54.79

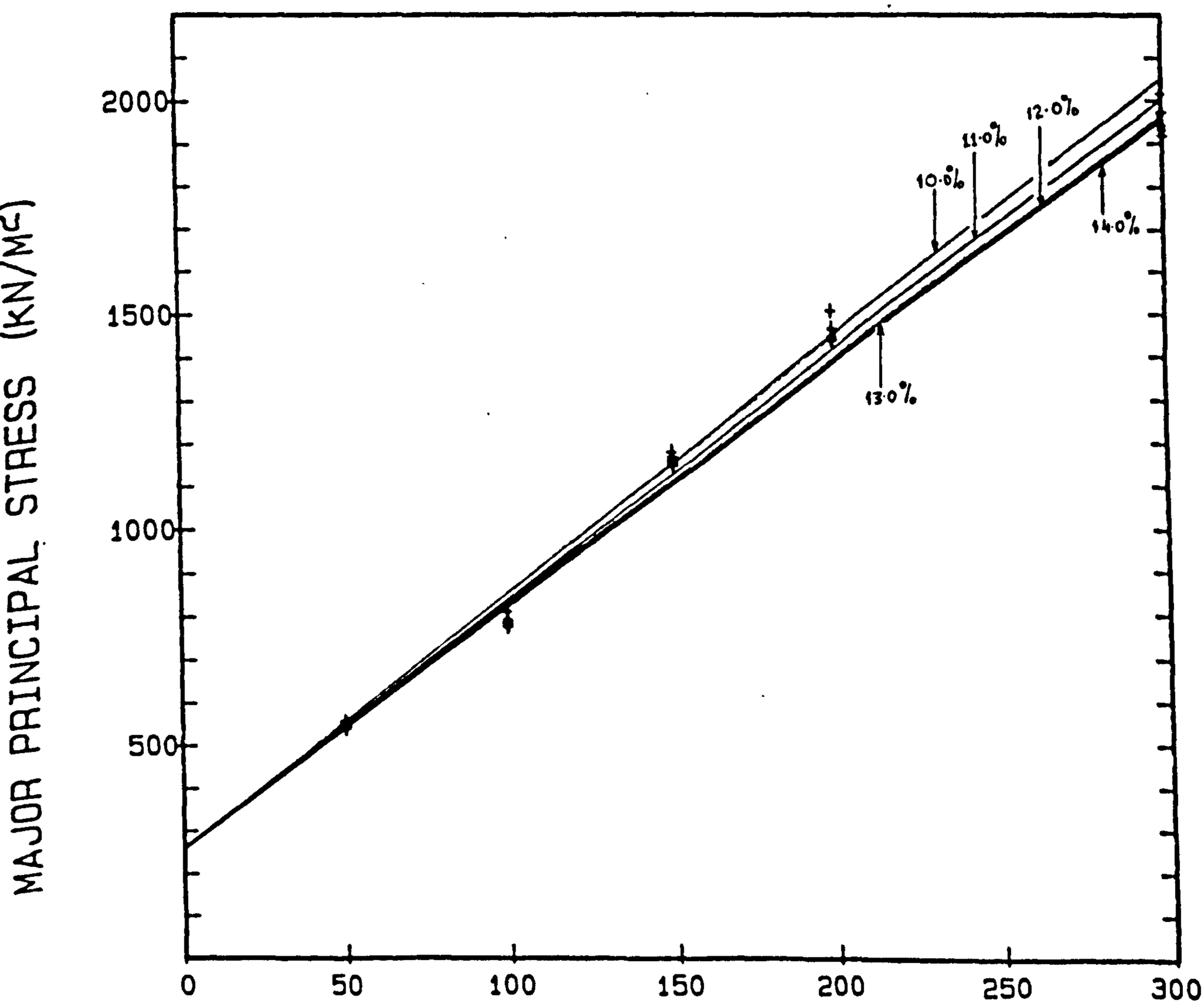

FIG. B.19

200mm x 155mm dia. TRIAXIAL TEST DATA	
SOIL TYPE	MID-ROSS SAND
MESH TYPE	7
MESH CONTENT	90.00 M^2/M^3 0.250 % dry weight

SLOPE - INTERCEPT RELATIONSHIP					
STRAIN %	15.				
M (deg)	79.92				
N	259.7				
S (deg)	44.28				
I (KN/M^2)	54.73				

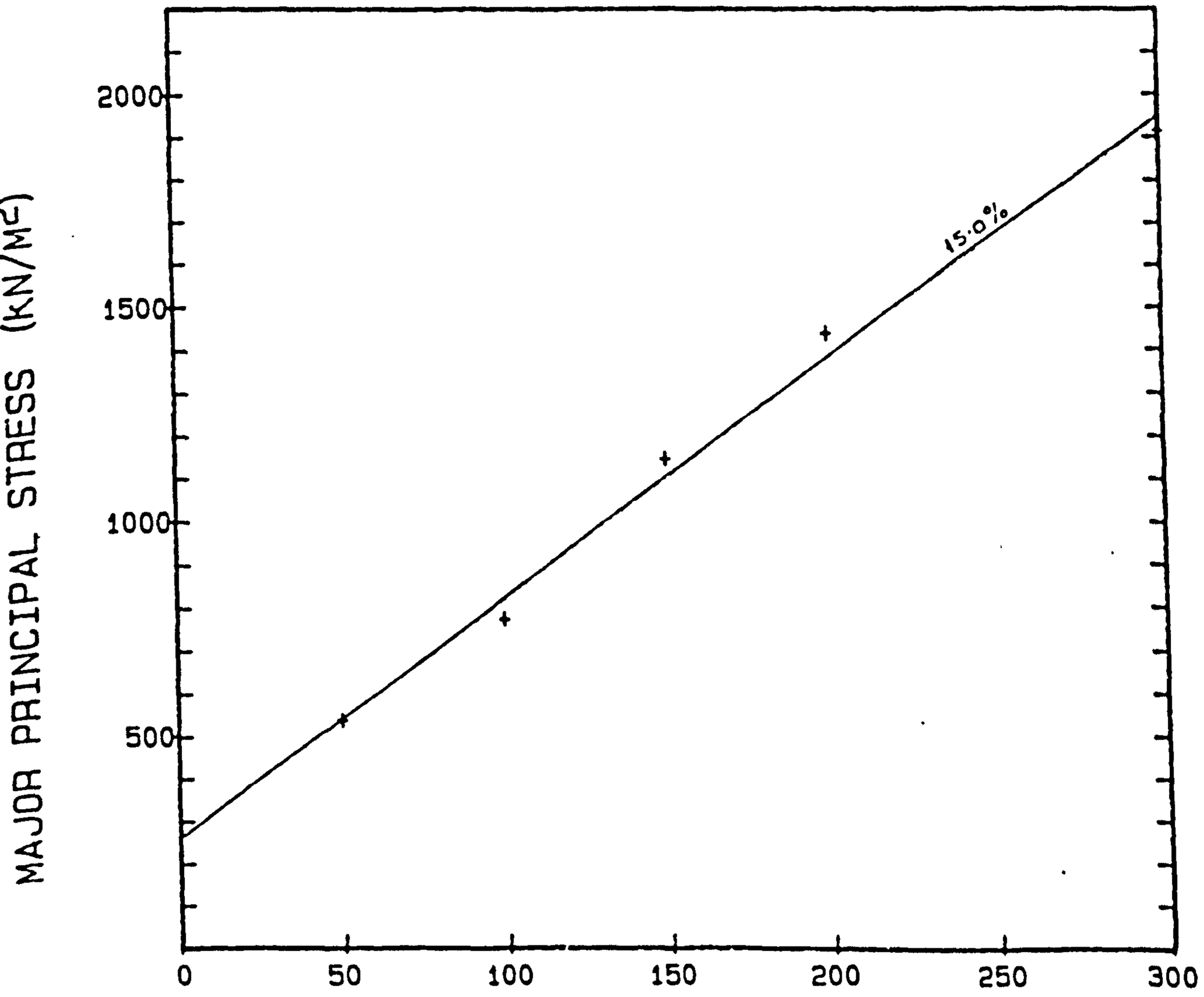

FIG. B.20

200mm x 155mm dia. TRIAXIAL TEST DATA	
SOIL TYPE	MID-ROSS SAND
MESH TYPE	7
MESH CONTENT	90.00 M^2/M^3 0.250 % dry weight

SLOPE - INTERCEPT RELATIONSHIP					
STRAIN %	PEAK	RESID.			
M (deg)	80.44	79.92			
N	410.5	259.7			
S (deg)	45.39	44.28			
I (KN/M^2)	84.2	54.73			

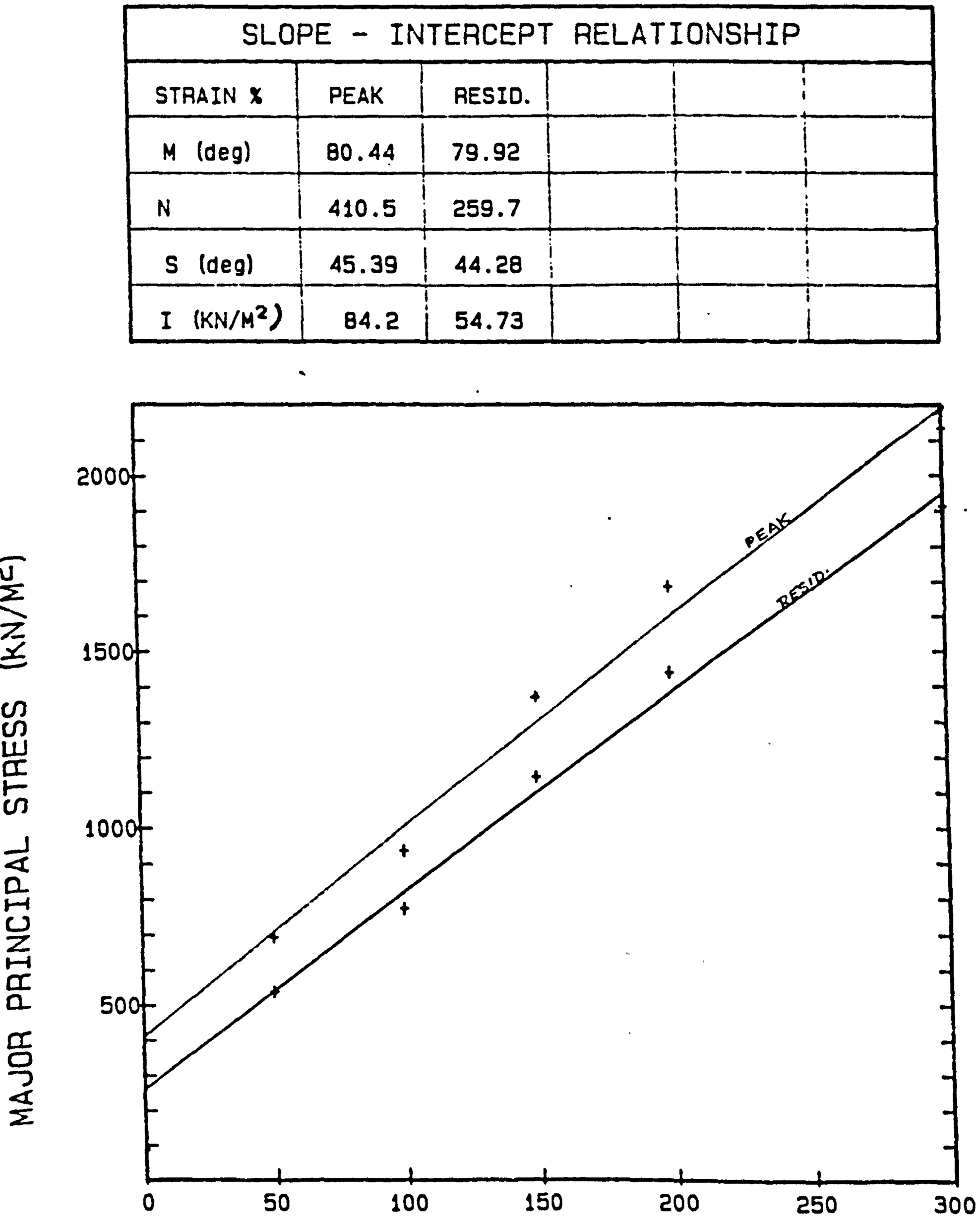

APPENDIX C

PRINCIPLES
of
PULL-OUT TESTING
TECHNIQE
&
SOME EXPERIMENTAL
RESULTS
of
TYPE 7, MESH

"PULL OUT" TESTING
(After Pradhan G.S. 1985)

1. General

In order to carry out pull-out (anchorage) tests on mesh, the apparatus described below was developed and used in this study, as shown in Plate C.1.

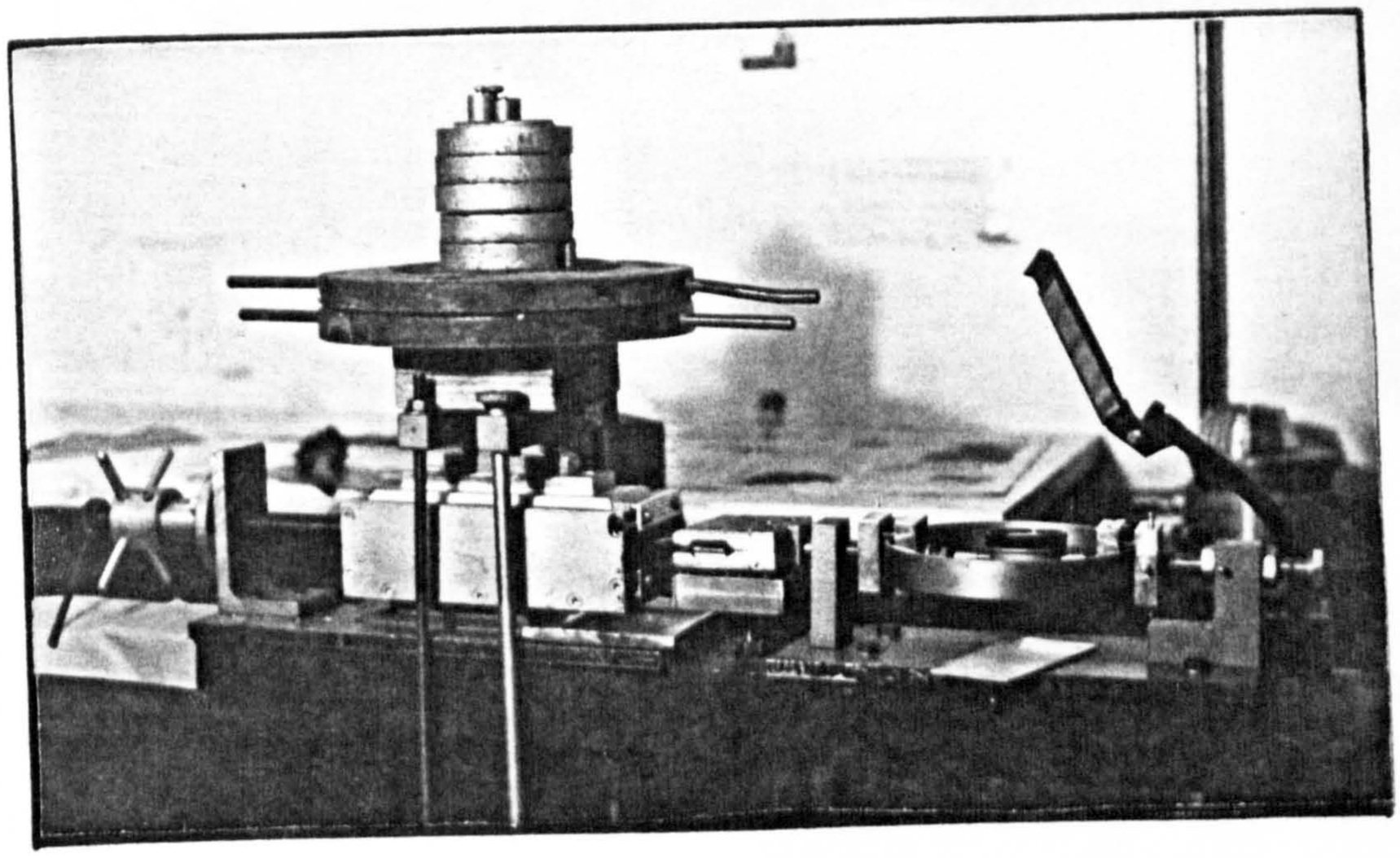

Plate C.1 General view of the pull-out apparatus.

2. Description of the Pull-out Test Apparatus:

Essentially the apparatus consists of the following parts:-

(i) Proving-ring with dial-gauge.
(ii) Mesh (specimen) clamping block.
(iii) Pull-out Box with its accessories.
(iv) Horizontal screw-jack with cross-pieces for applying pull-out force.

(i) The proving-ring is a standard steel ring with dial-gauge attached to it, Plate C.2. Application of load on the ring will change the shape of the ring. The

amount of change of shape of the ring will be recorded by

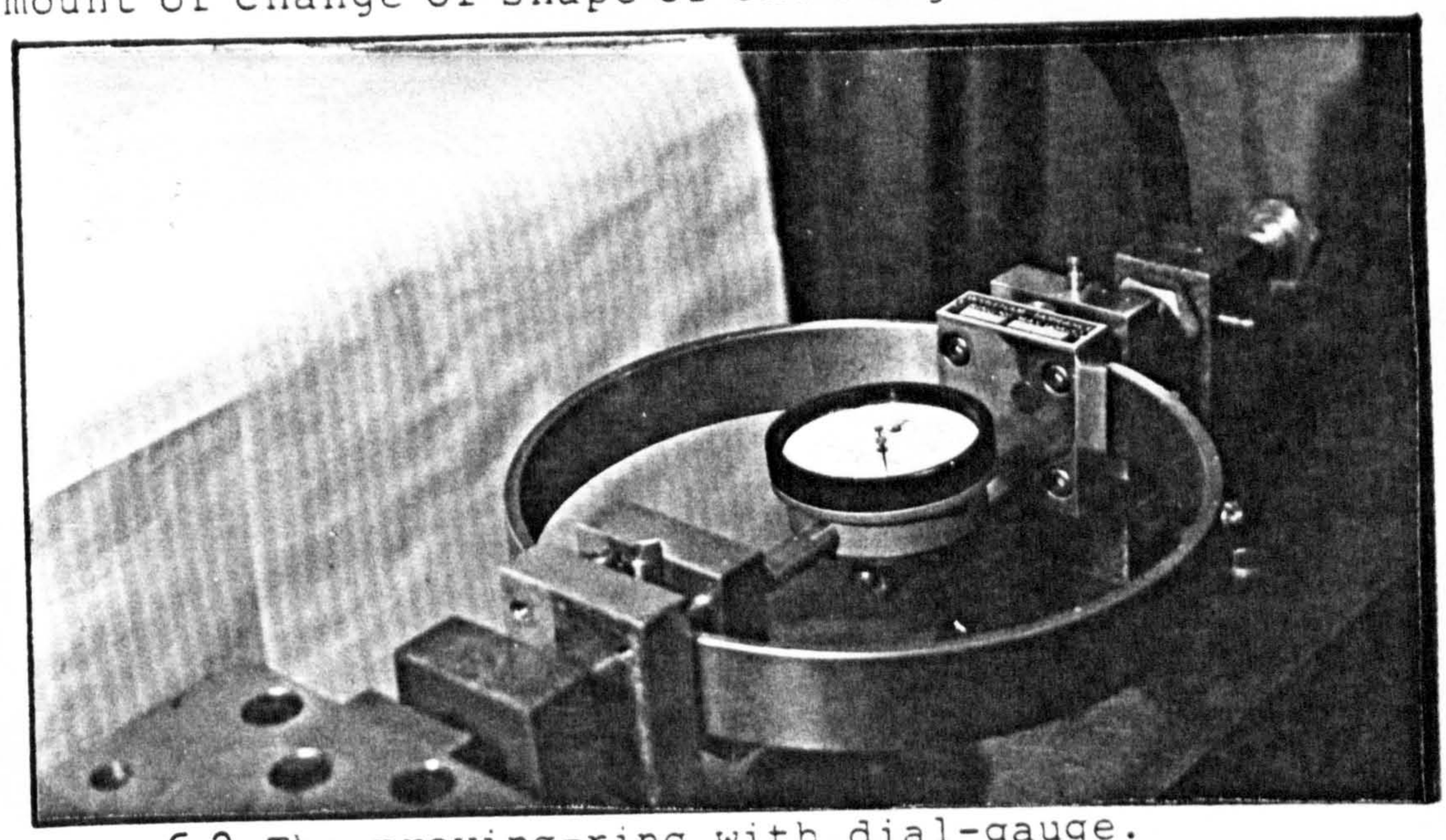

Plate C.2 The proving-ring with dial-gauge.

the dial-gauge. Thus the pull-out force can be calculated. The dial-gauge can record up to 0.002 mm distortion of the ring. The calibration chart is as shown in Fig. C.7.

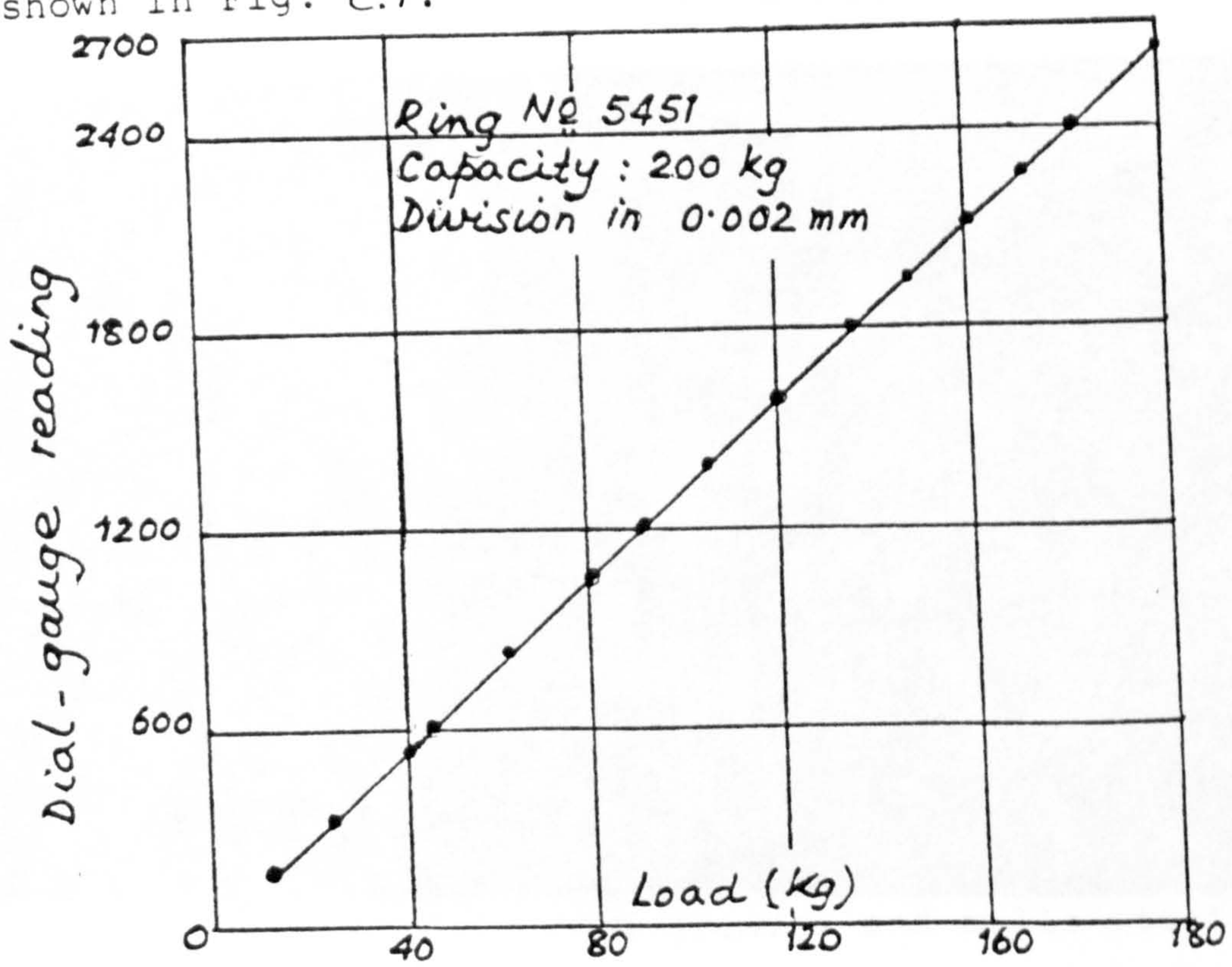

FIG. C.7 Proving-ring constant.

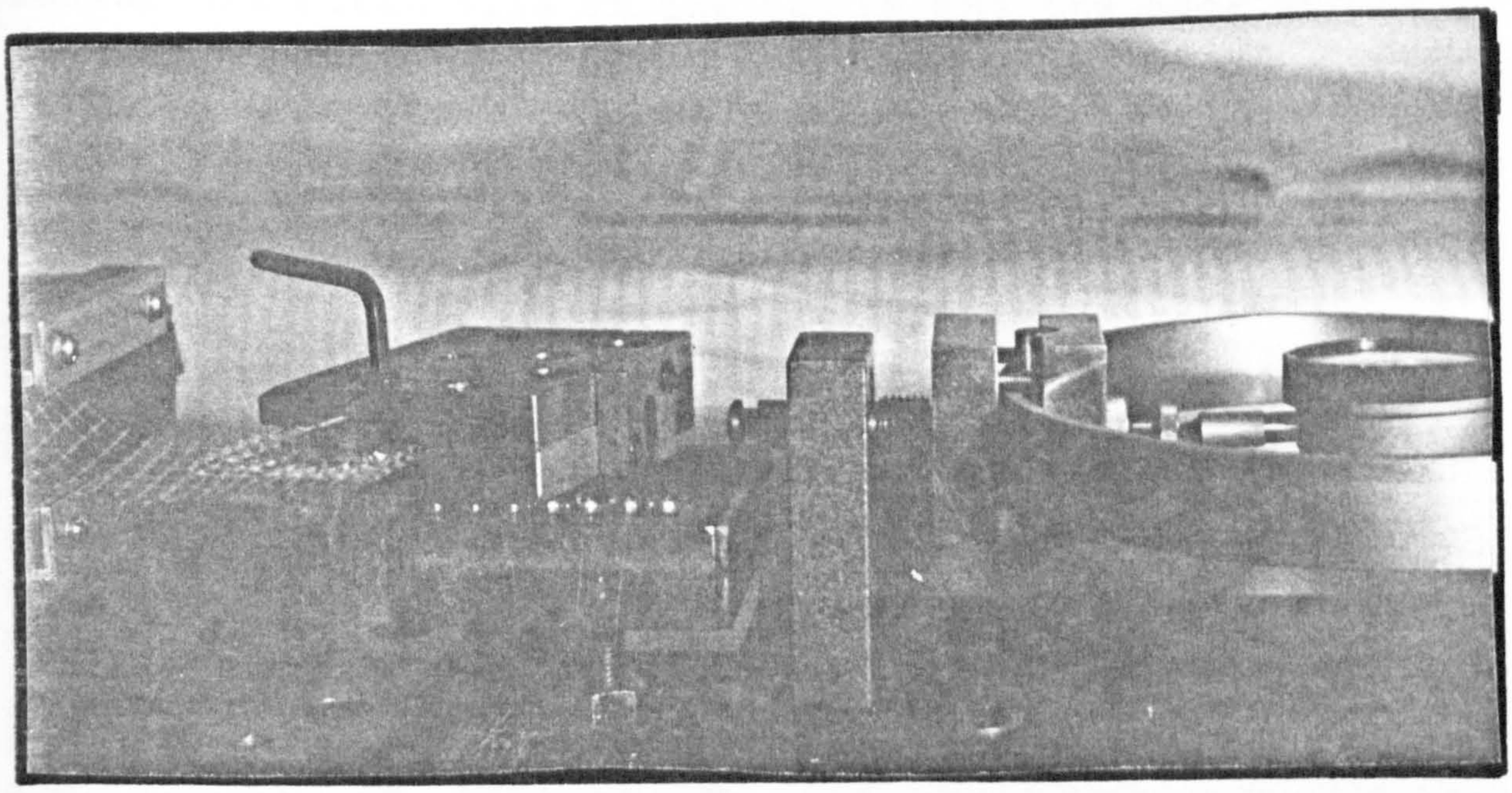

Plate C.3 Clamping block (Tensar - jaws block)

(ii) Mesh (specimen) clamping block is similar to Tensar-jaws block Plate C.3. The base plate is rigidly fixed to the main frame. It has two rows of parallel grooves containing six to seven balls in each groove Plate C. 4.

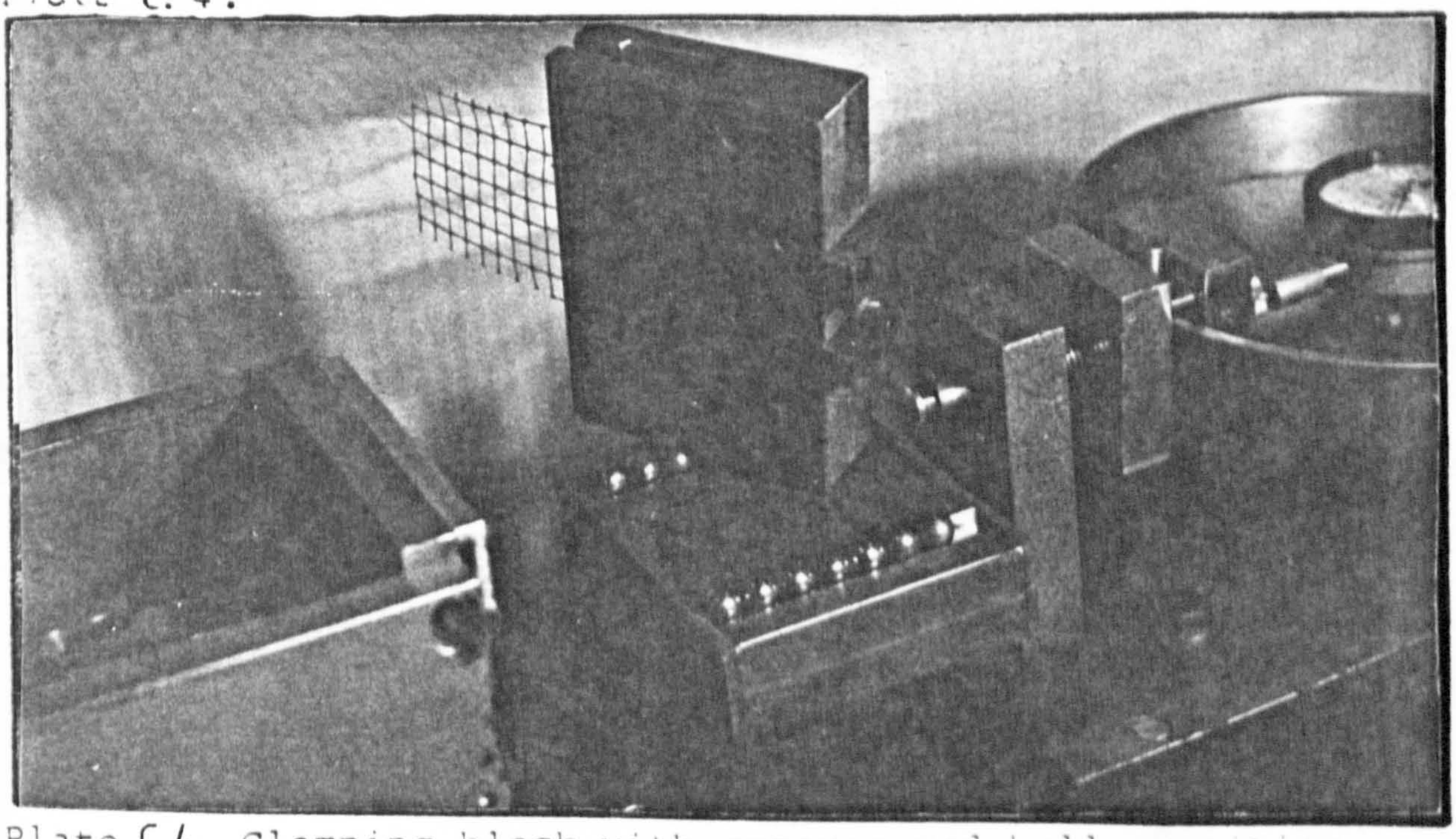

Plate C.4 Clamping block with grooves and balls position.

The grooves run longitudinally to the main frame. The

Tensar-jaw block sits on the balls and the back of the block attached to the proving-ring. Plate C. 5.

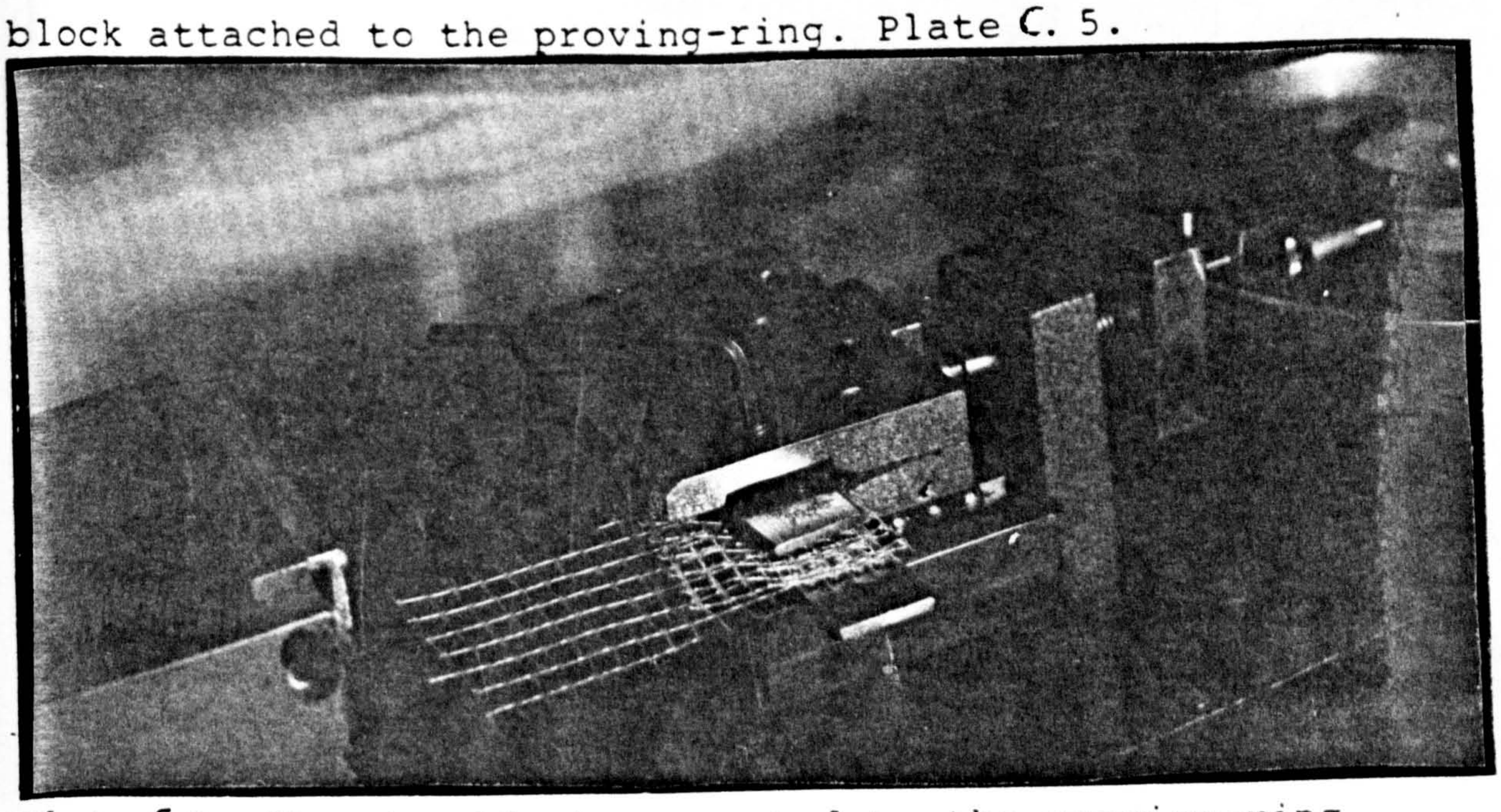

Plate C.5 Clamping block connected to the proving-ring.

The mesh is held inside the jaw by pressing two parallel thin plates with the help of three screws from the top of the block itself, Plate C.5.

(iii) The pull-out box is the main part of this apparatus. The inside dimensions of the box are 199 x 100 x 60 mm and it is made of 12 mm thick steel plates. The base of the box and the lower part of the cover are corrugated. Plate C.6. The cover exerts 1 kPa normal vertical pressure to the box and there are the provision for placing two hangers cn top of the cover which will exert load symmetrically to the pull-out box, Plate C.7.

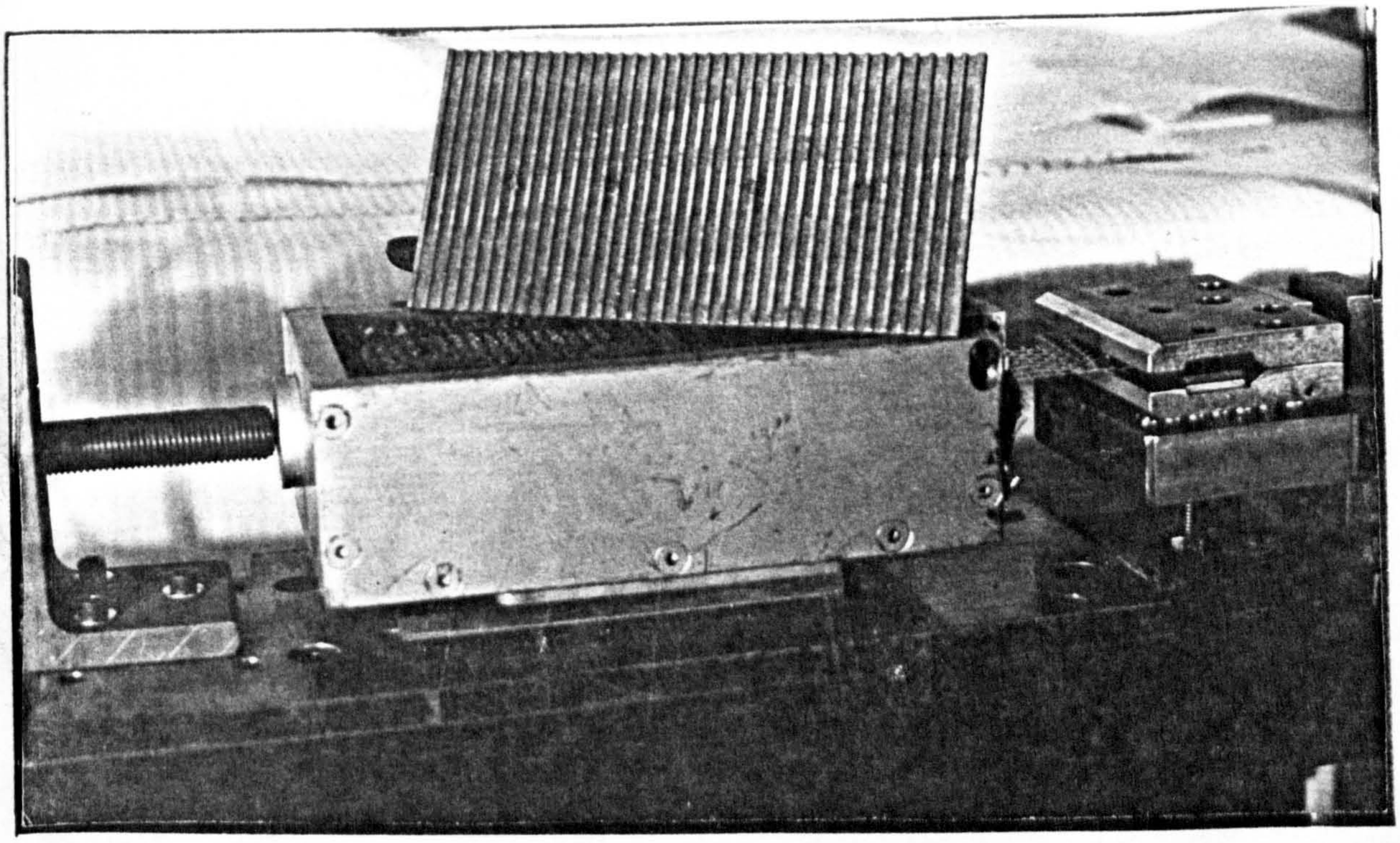

Plate C.6 Pull-out Box with cover.

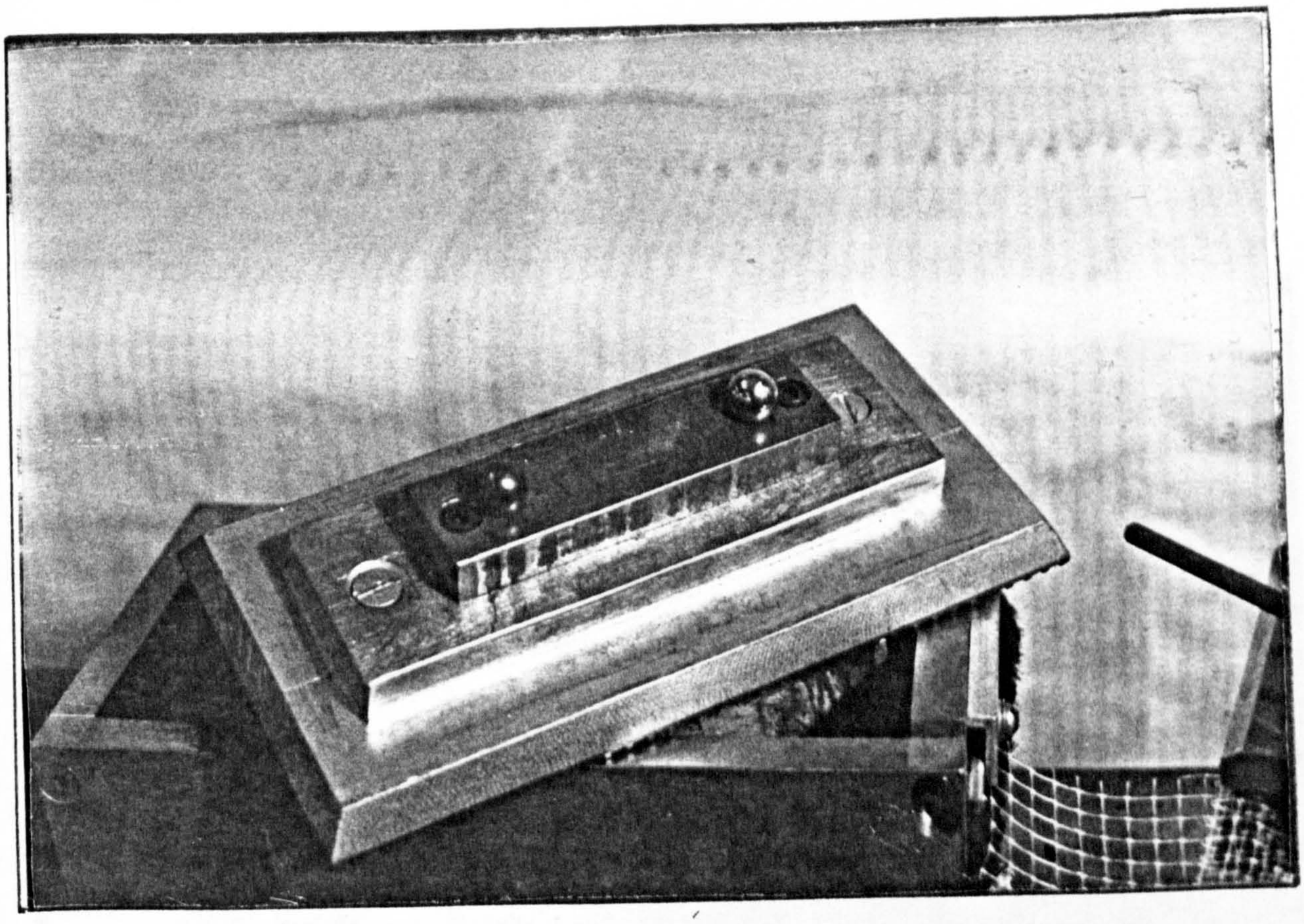

Plate C.7 Provision for hangers on top of cover.

To add additional weights, a wooden block is placed centrally on top of the two parallel horizontal bars of

the hangers. Weights are placed on top of the wocden block, Plate C.8.

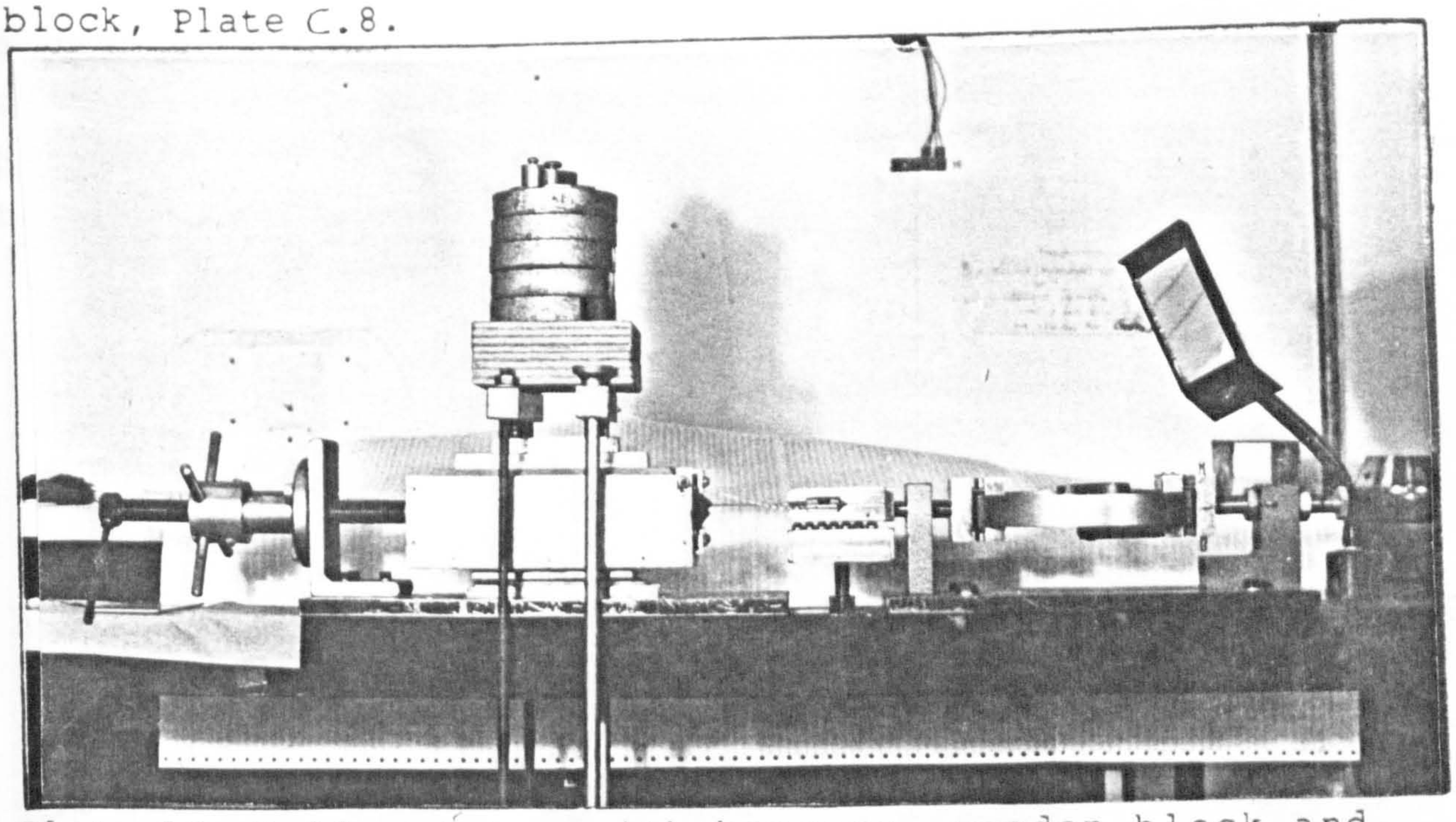

Plate C.8 Pull-out box with hangers, wooden block and weights.

The pull-out box sits on top of two rows of balls in a longitudinally placed parallel grooves, Plate C.9.

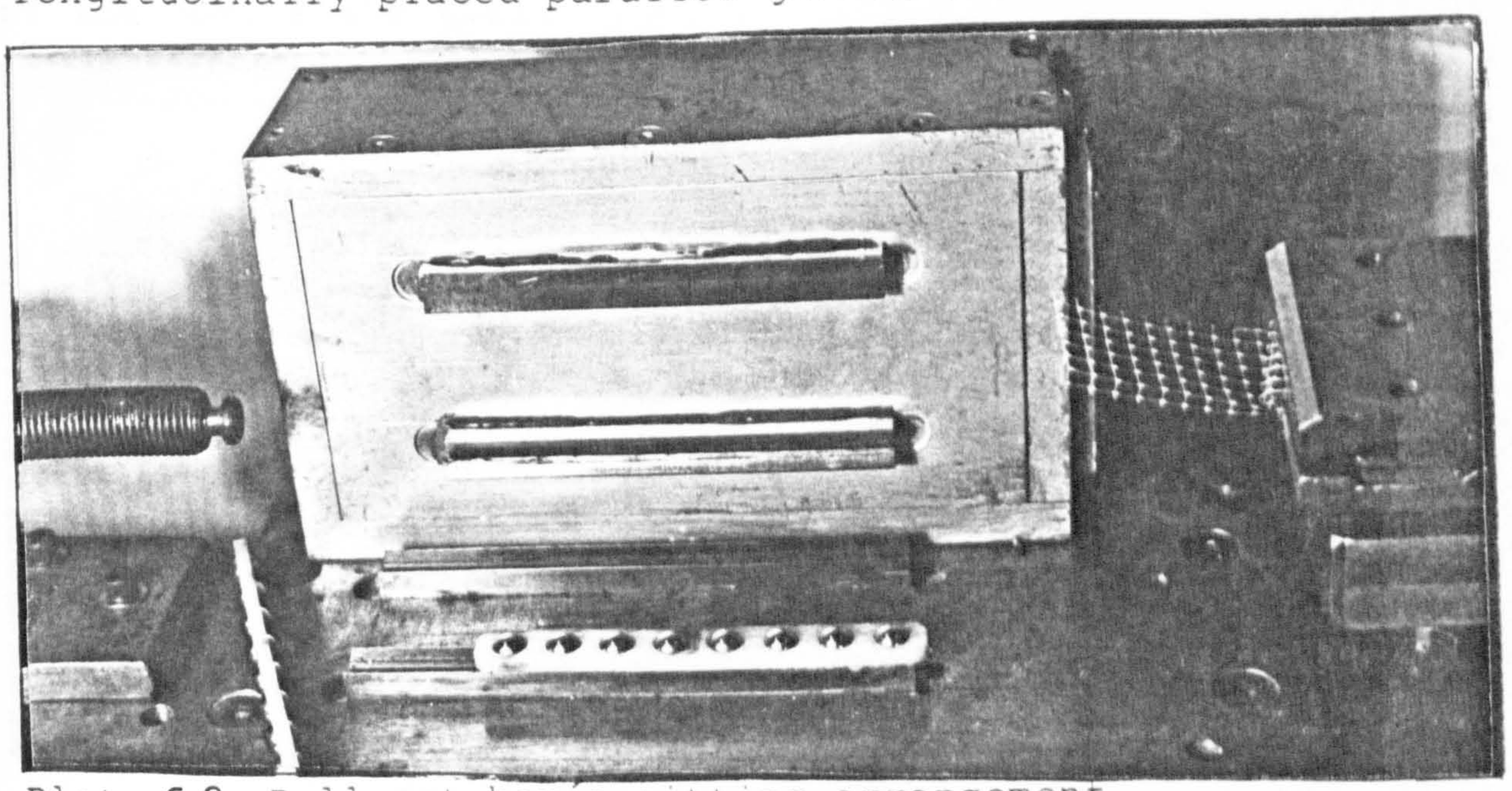

Plate C.9 Pull-out box s sitting arrangement.

There are two metal plates attached tc the bottom of the box and these come into contact with the balls. Of these

two plates, one has a plane smooth face and the other has a grooved face. The grooved plate when it comes into contact with the balls gets locked laterally and thus it prevents the sideways movement of the box, but it is free to move longitudinally, Plate C.10.

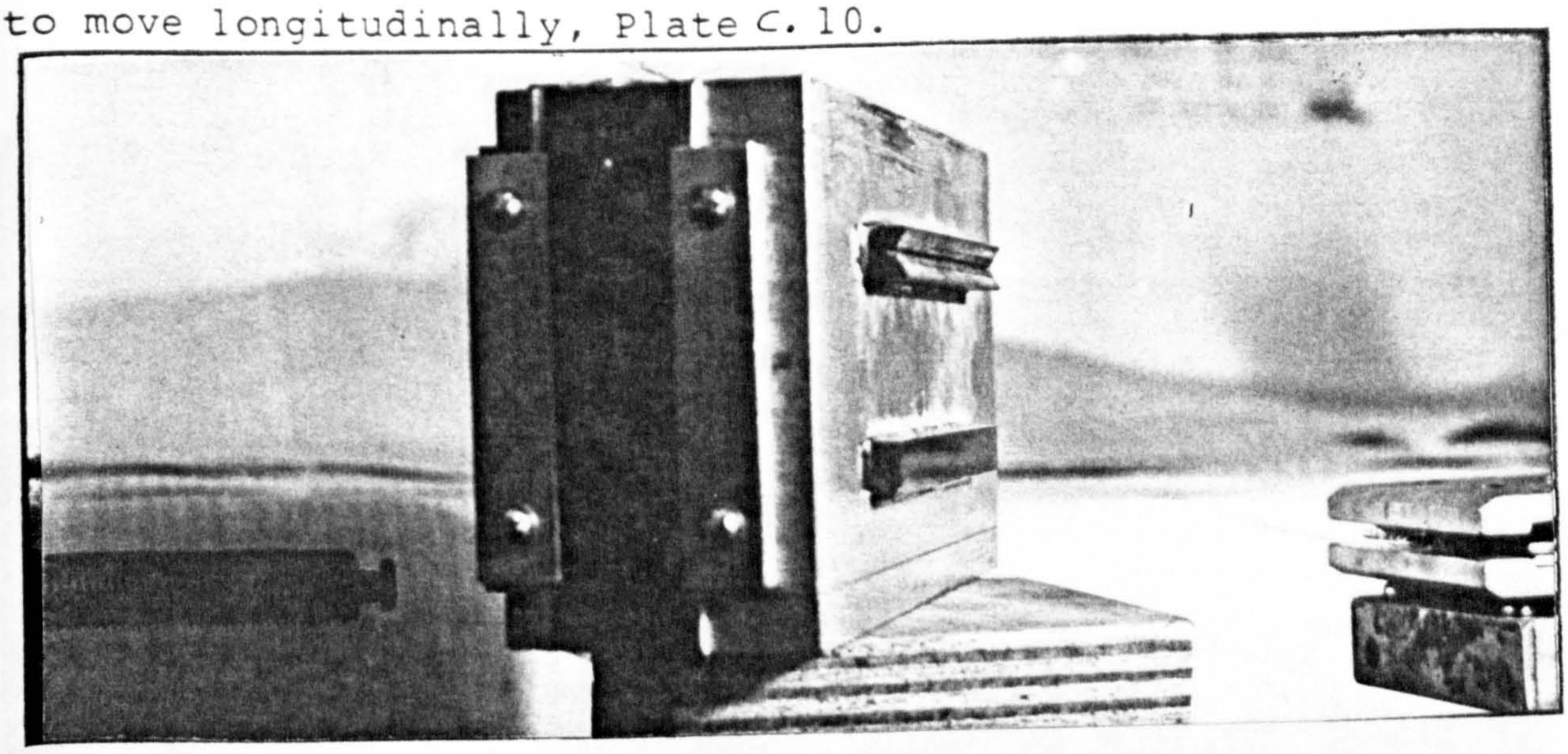

Plate C.10 Metal plates at the bottom of the box.

There is a thin horizontal slit opening to the full width of the box, Plate C.11.

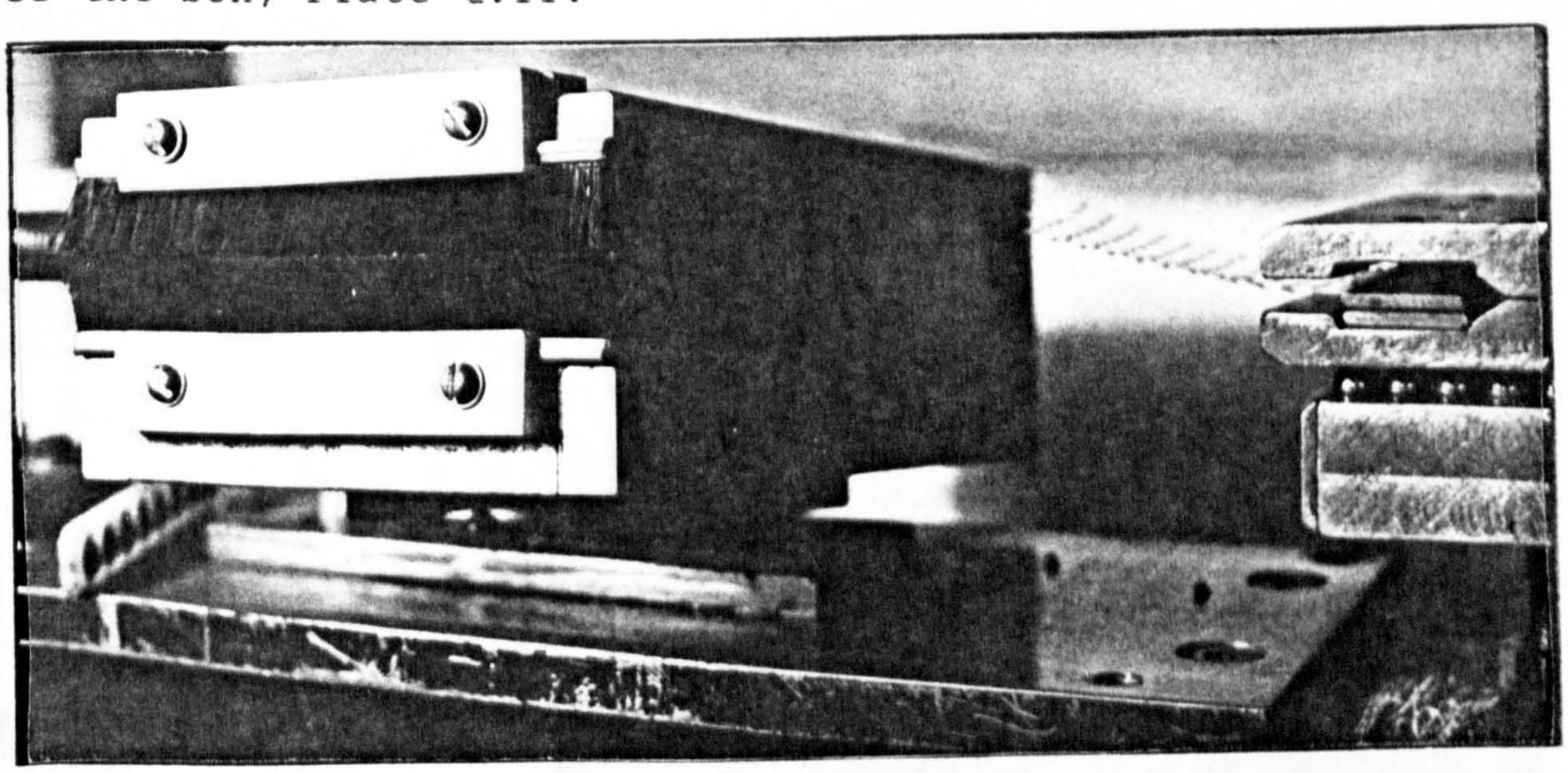

Plate C.11 Slit opening of the box.

The height of the slit opening in the box and the jaw of the Tensar clamping block are kept at the same level.

The mesh (specimen) is pushed through the slit opening intc the box after fixing the other end in the clamping block, Plate C.12. The slit opening is lined with a pair of brushes from outside just tc protect the spilling of

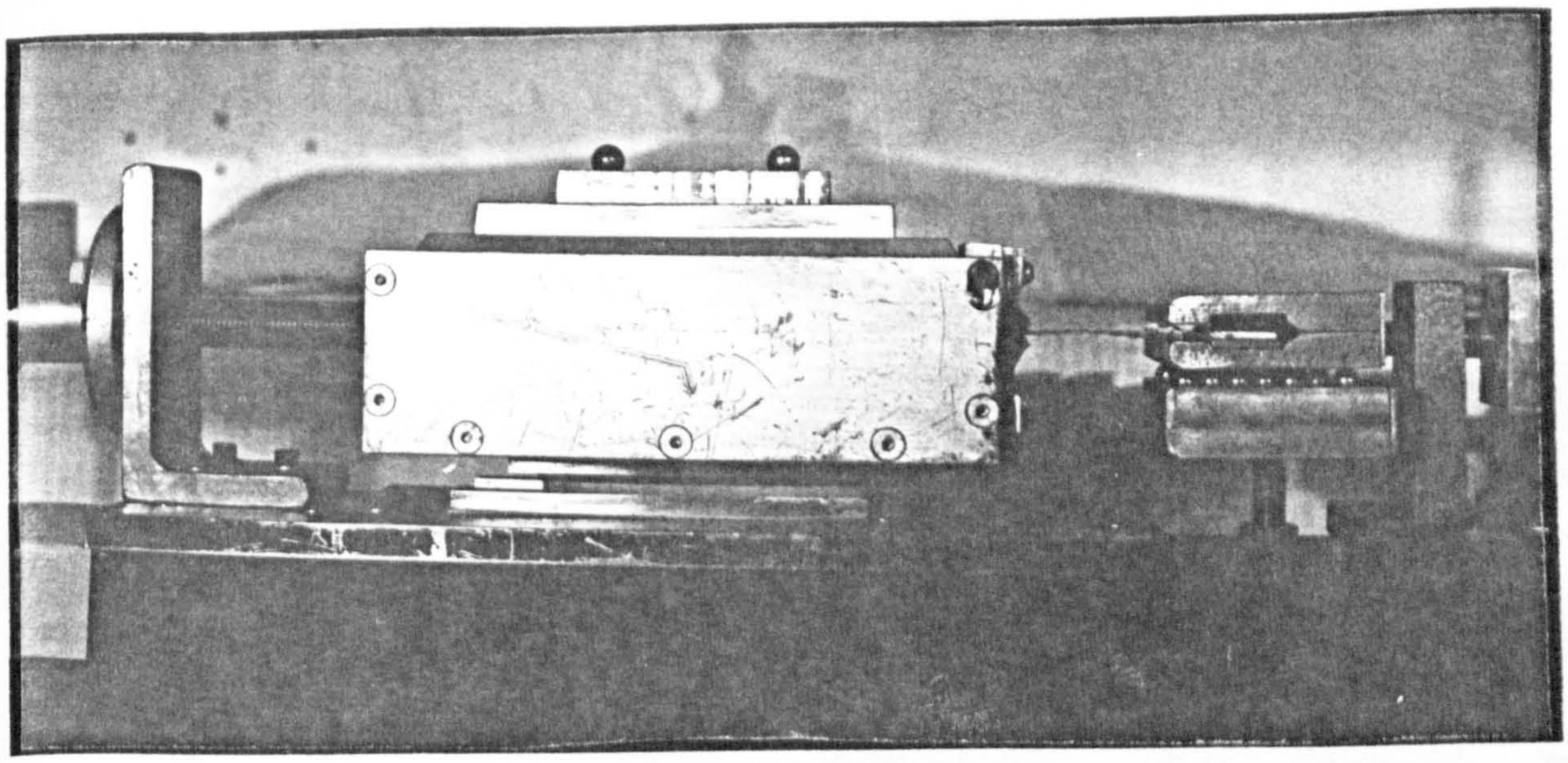

Plate C.12 Shows the height of slit opening and the clamping block.

sand through the openings, Plate C.11. The other end of the box is hocked with a strong threaded rod which forms part cf the moving part of the screw-jack, Plate C.13.

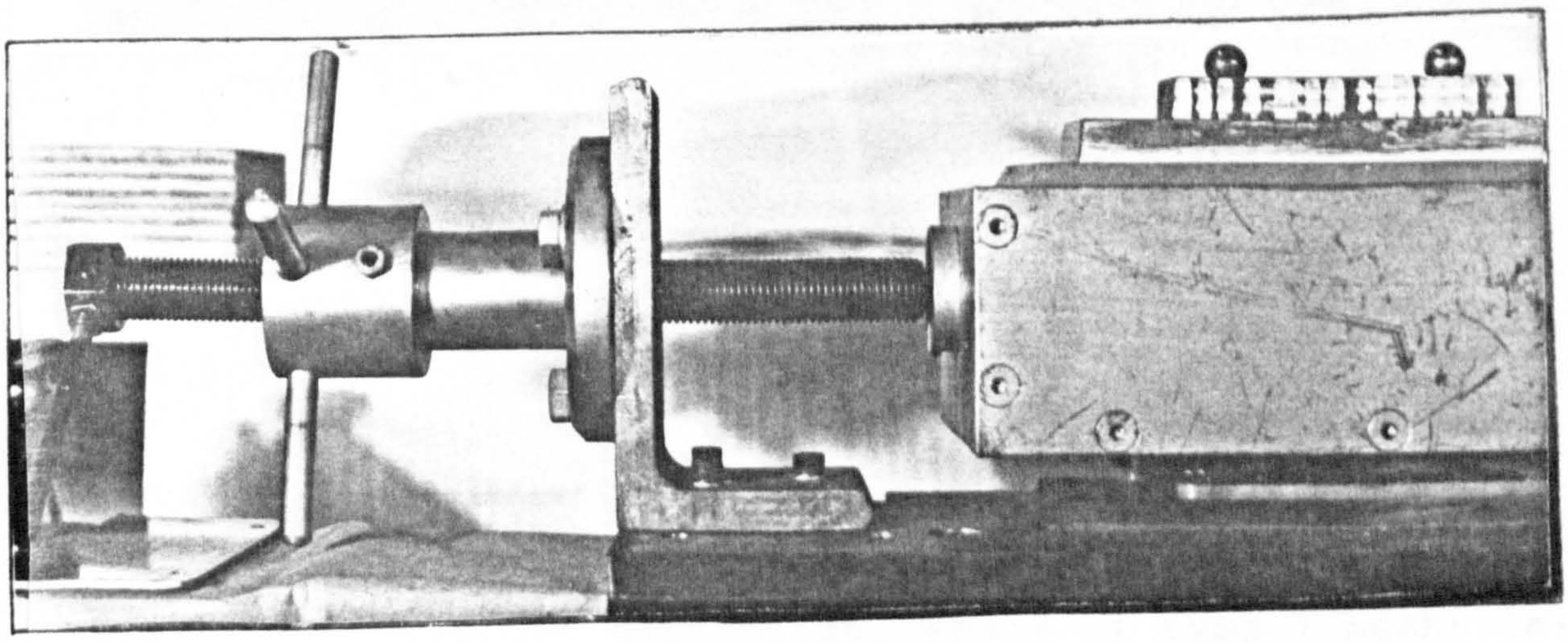

Plate C.13 Strong threaded rod connected tc the pull-out box.

(iv) The horizontally fixed screw jack is the main source of applying pulling force manually. There are four cross-pieces attached to it so that the screw jack can be operated by hand. The threaded rod passes through a rigid angle block attached to the main frame. The Pull-out box can be pulled or pushed back by simply operating the crew-jack, Plate C.14.

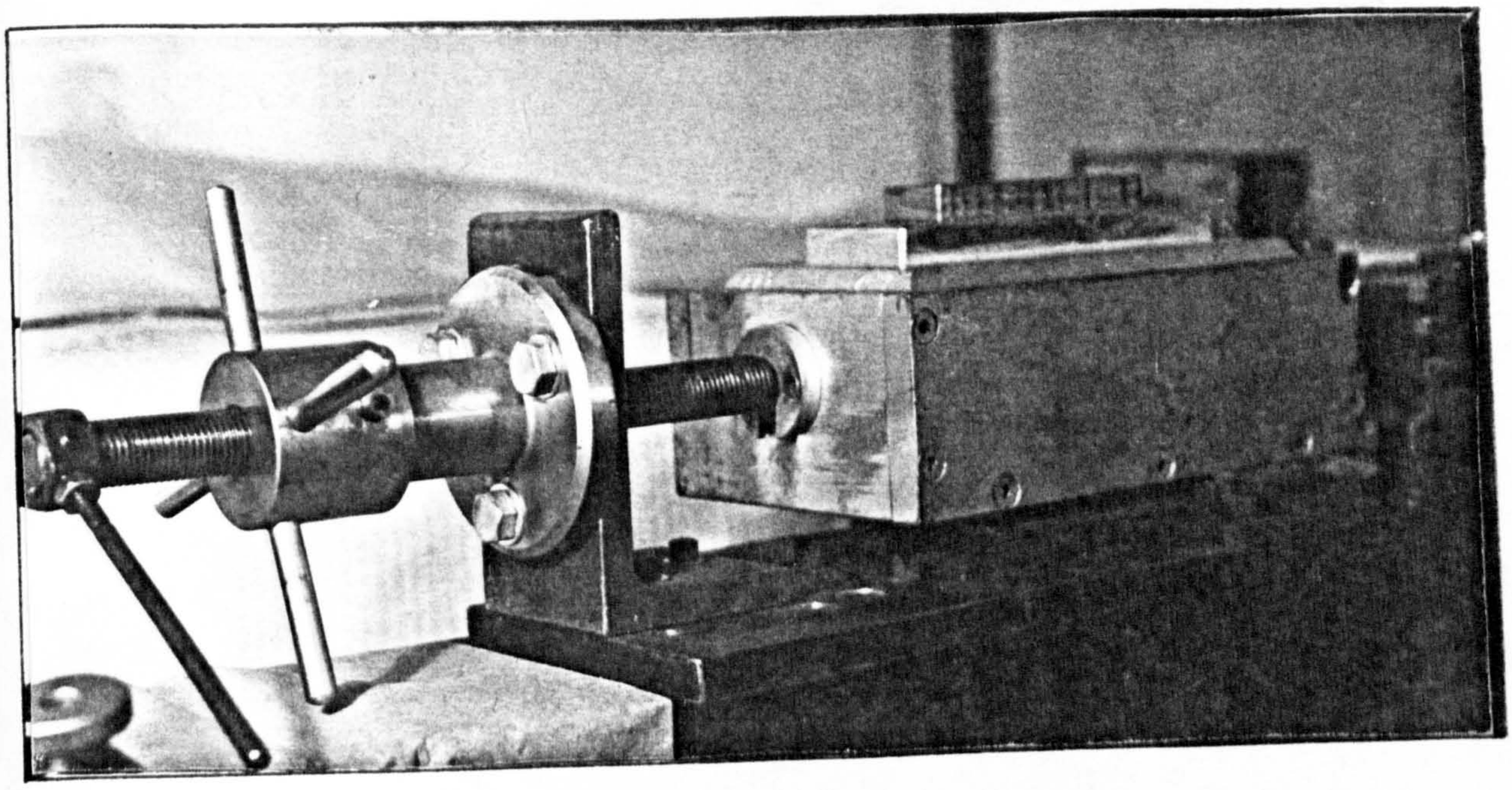

Plate C.14 Horizontal screw-jack's arrangement.

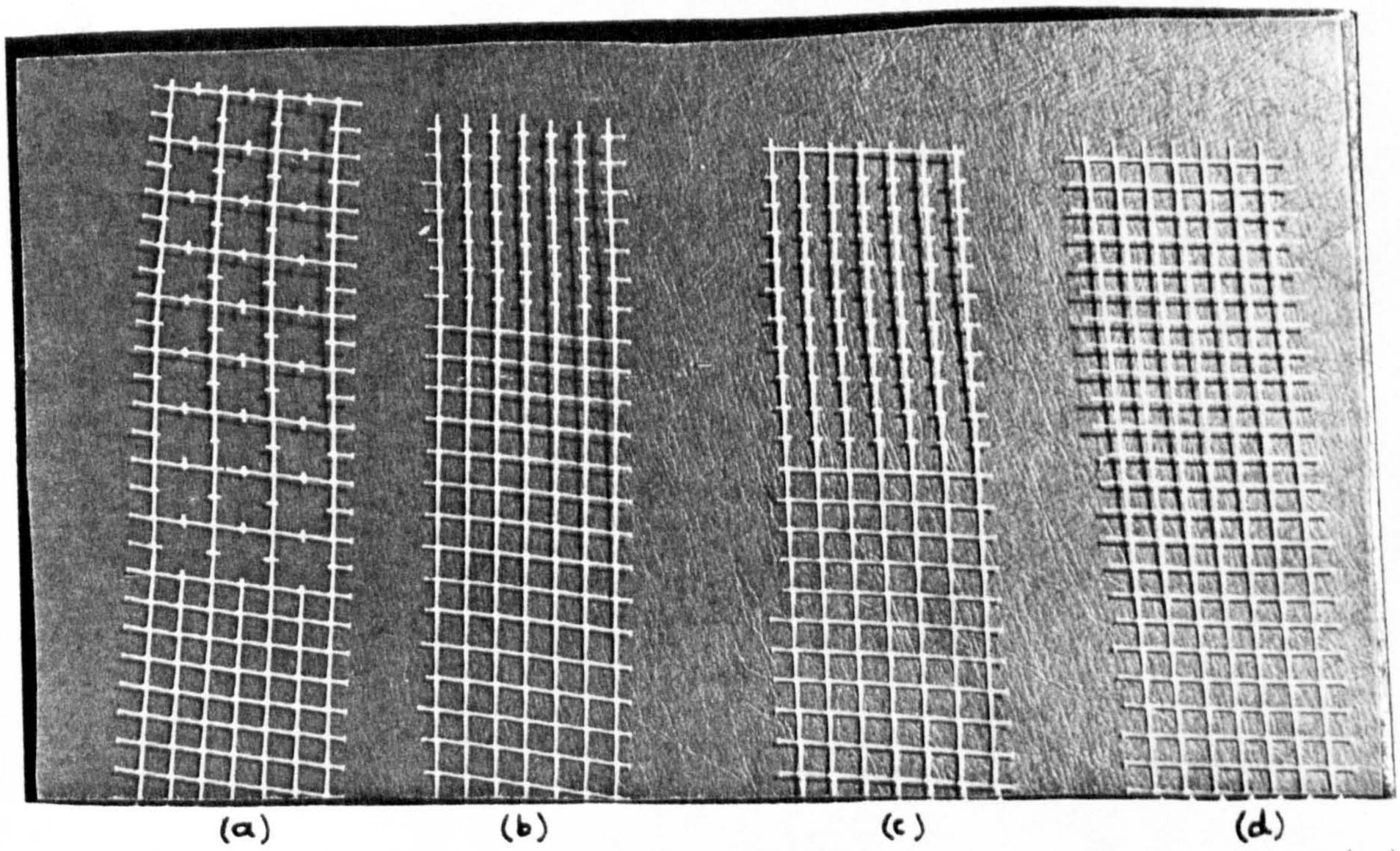

Plate C.15 Different geometrical shape of type 7 mesh: (a) Alternate cross and longitudinal ribs cut out (b) All cross ribs cut out (c) All cross-ribs cut out except for end rib (d) Full mesh.

Actual measurements were taken from the dial-gauge attached to the proving ring, Plate C.2. One reading was taken for a certain normal load applied to the particular embedded length of the mesh. Readings were divided into different groups according to the normal loads applied and of course when there was a change of mesh or sand.

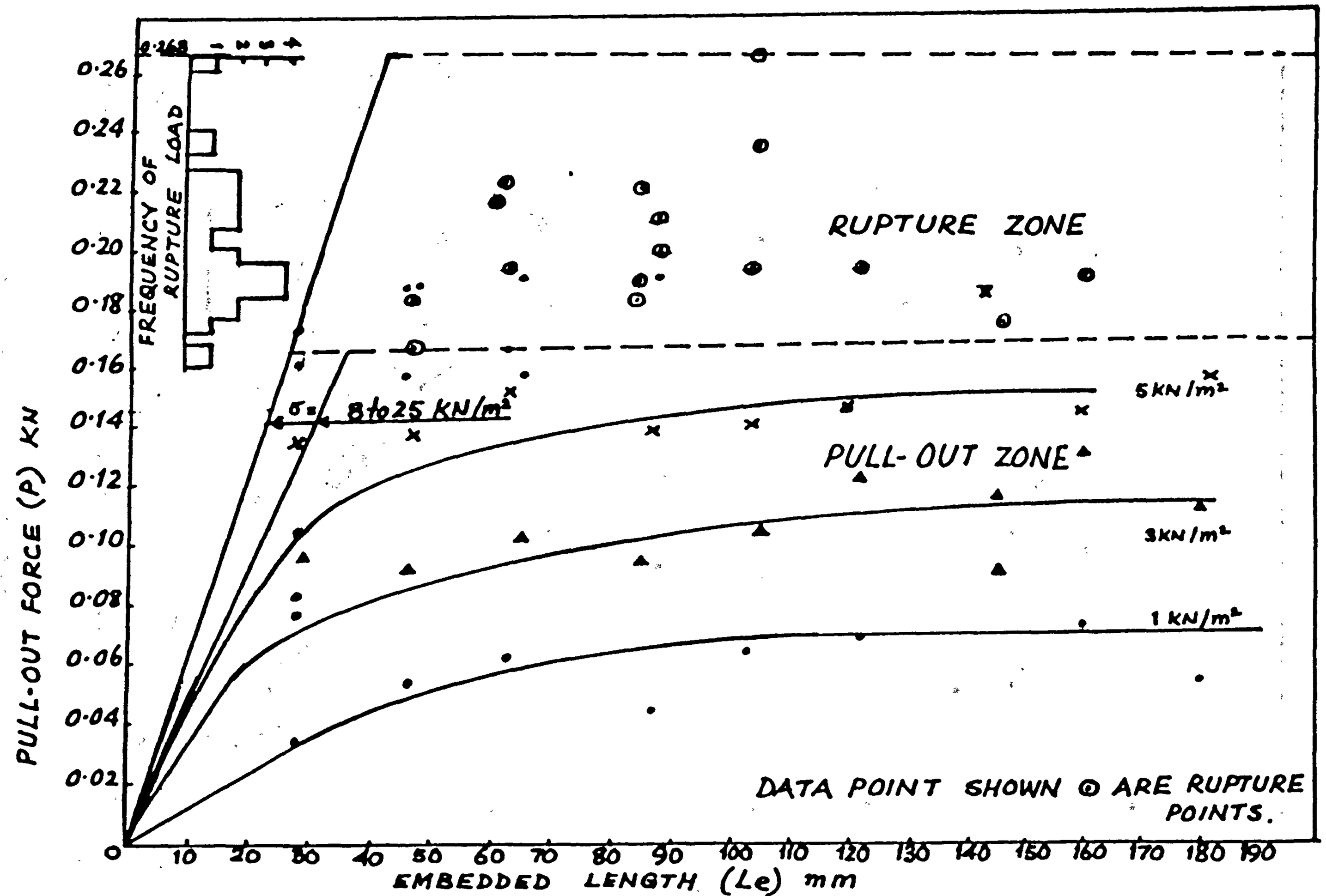

FIG: C.1 RELATION BETWEEN Le AND P FOR TYPE 7 MESH IN MID-ROSS SAND

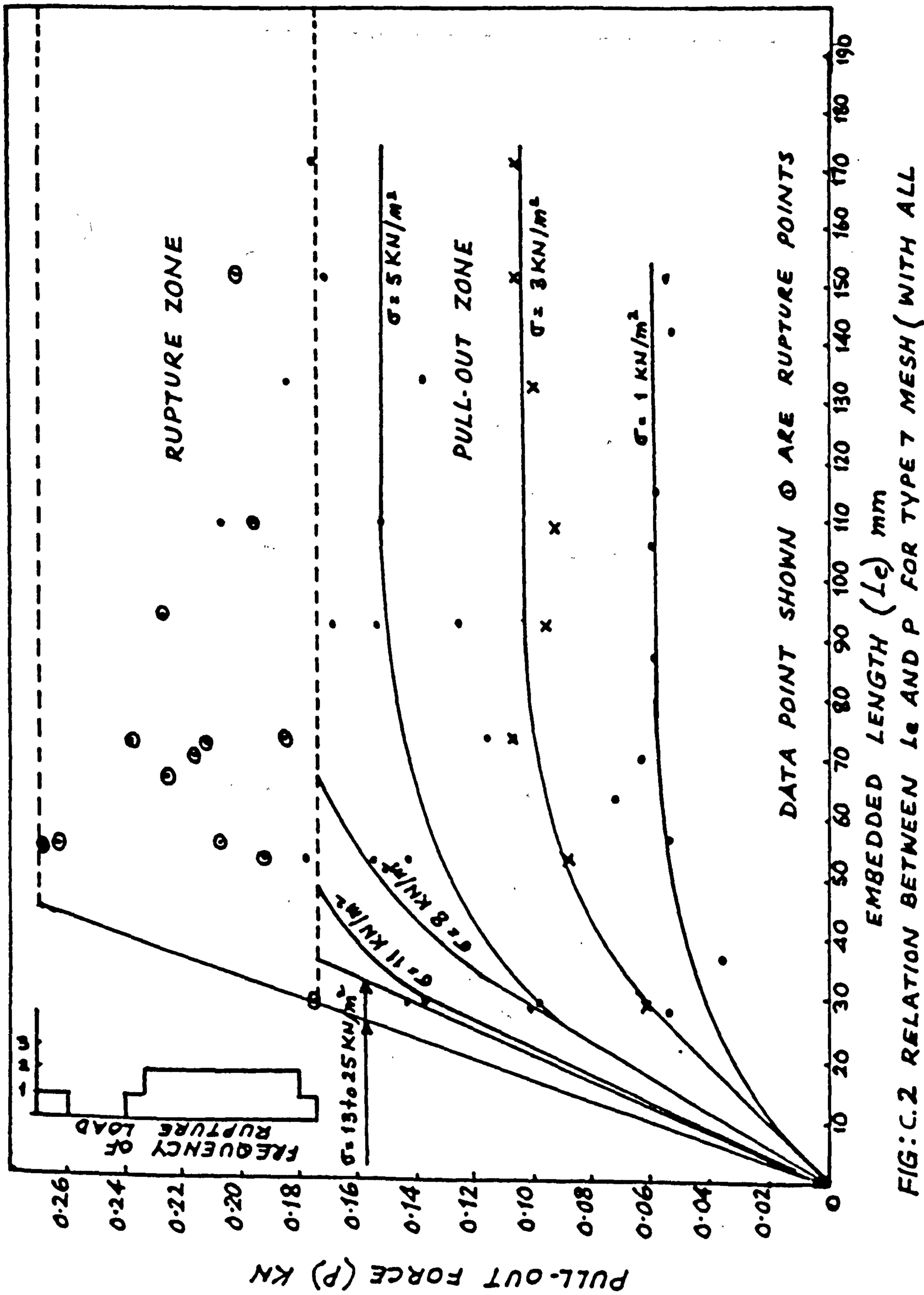

FIG: C.2 RELATION BETWEEN Le AND P

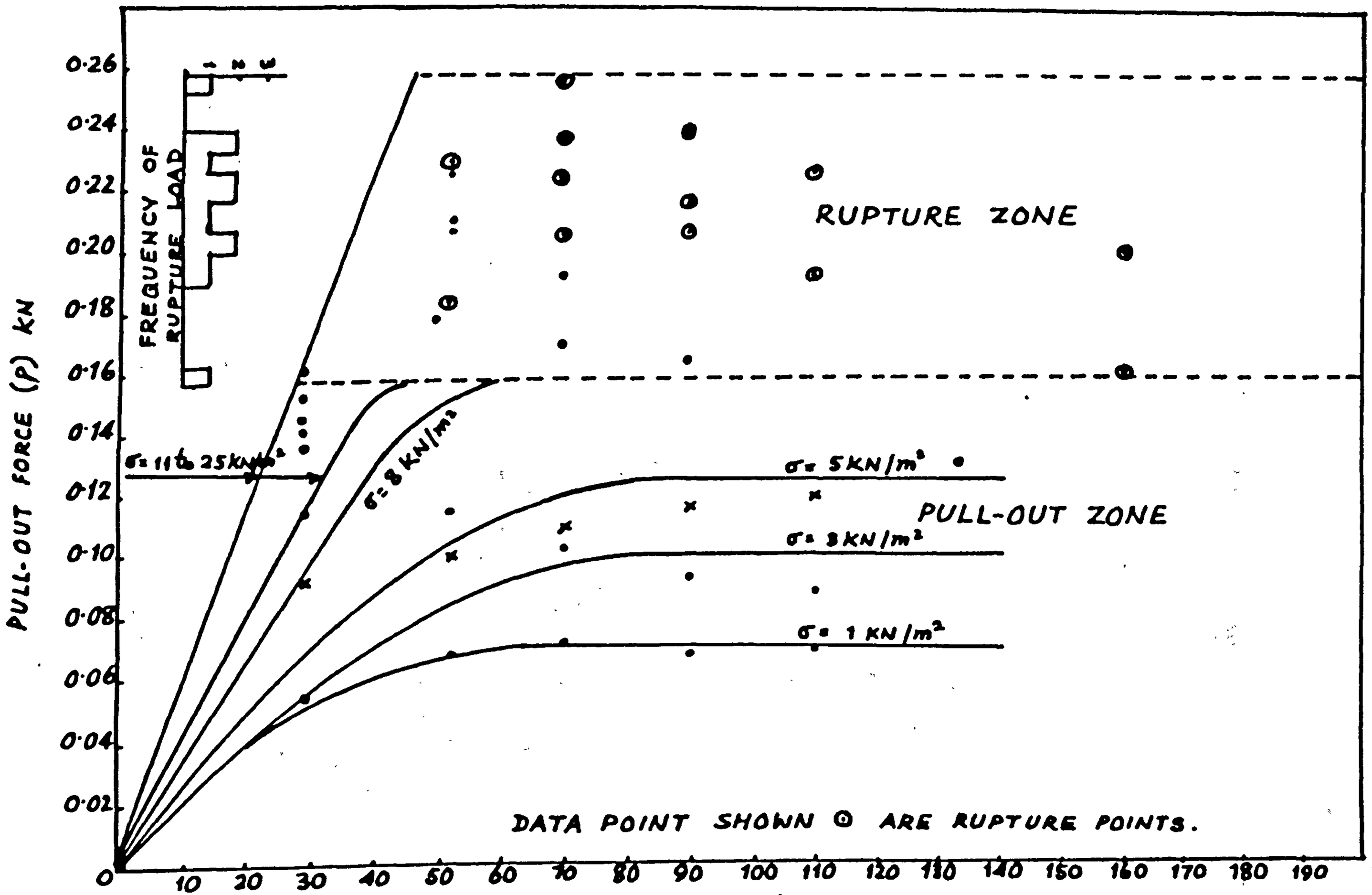

FIG: C.3 RELATION BETWEEN Le AND P FOR TYPE 7 MESH (WITH ALL CROSS RIBS CUT OUT) IN MID-ROSS SAND

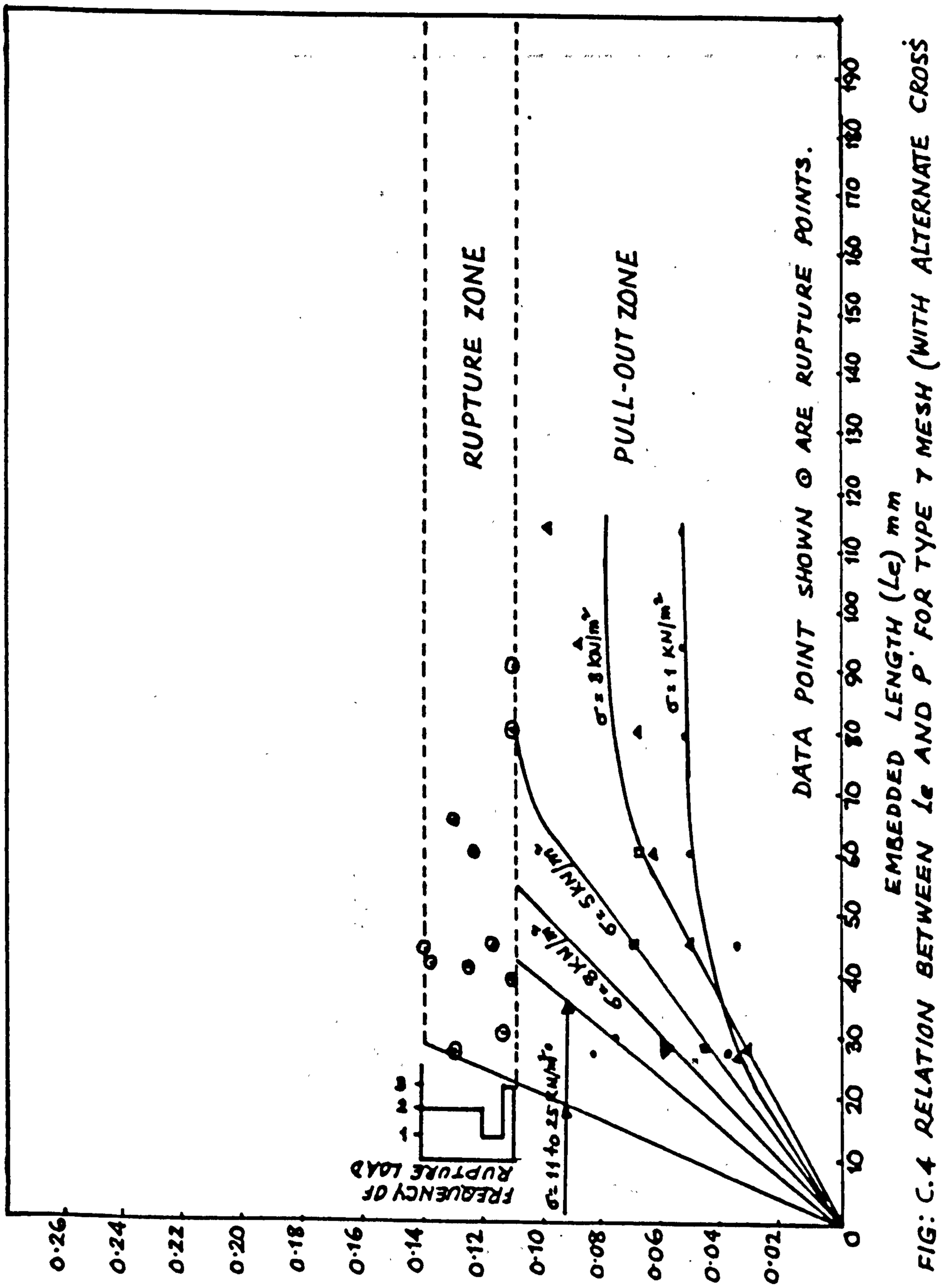

FIG: C.4 RELATION BETWEEN Le AND P' FOR TYPE 7 MESH (WITH ALTERNATE CROSS AND LONGITUDINAL RIBS CUT OUT)

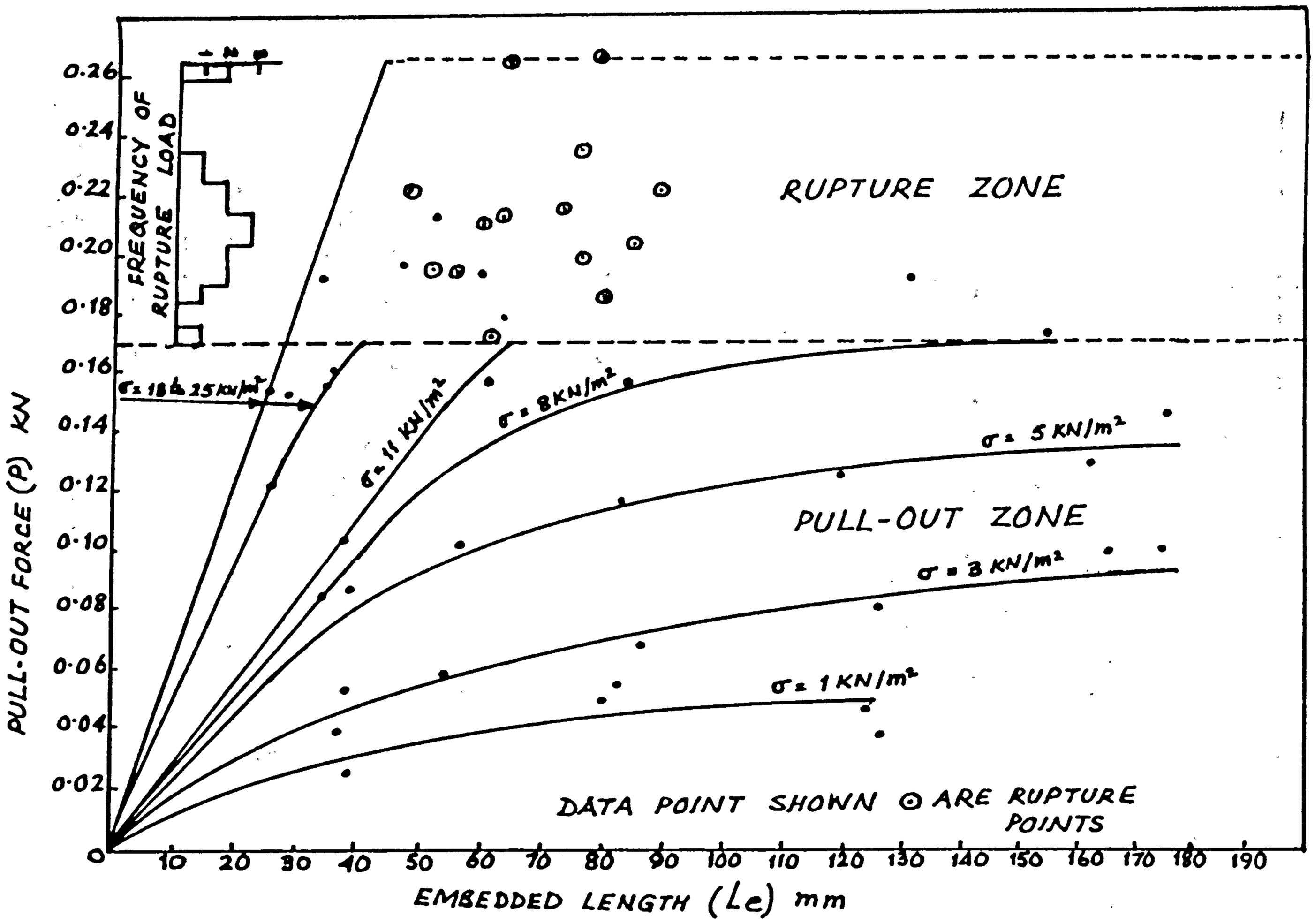

FIG: C.5 RELATION BETWEEN Le AND P FOR TYPE 7 MESH IN LEIGHTON-BUZZARD SAND

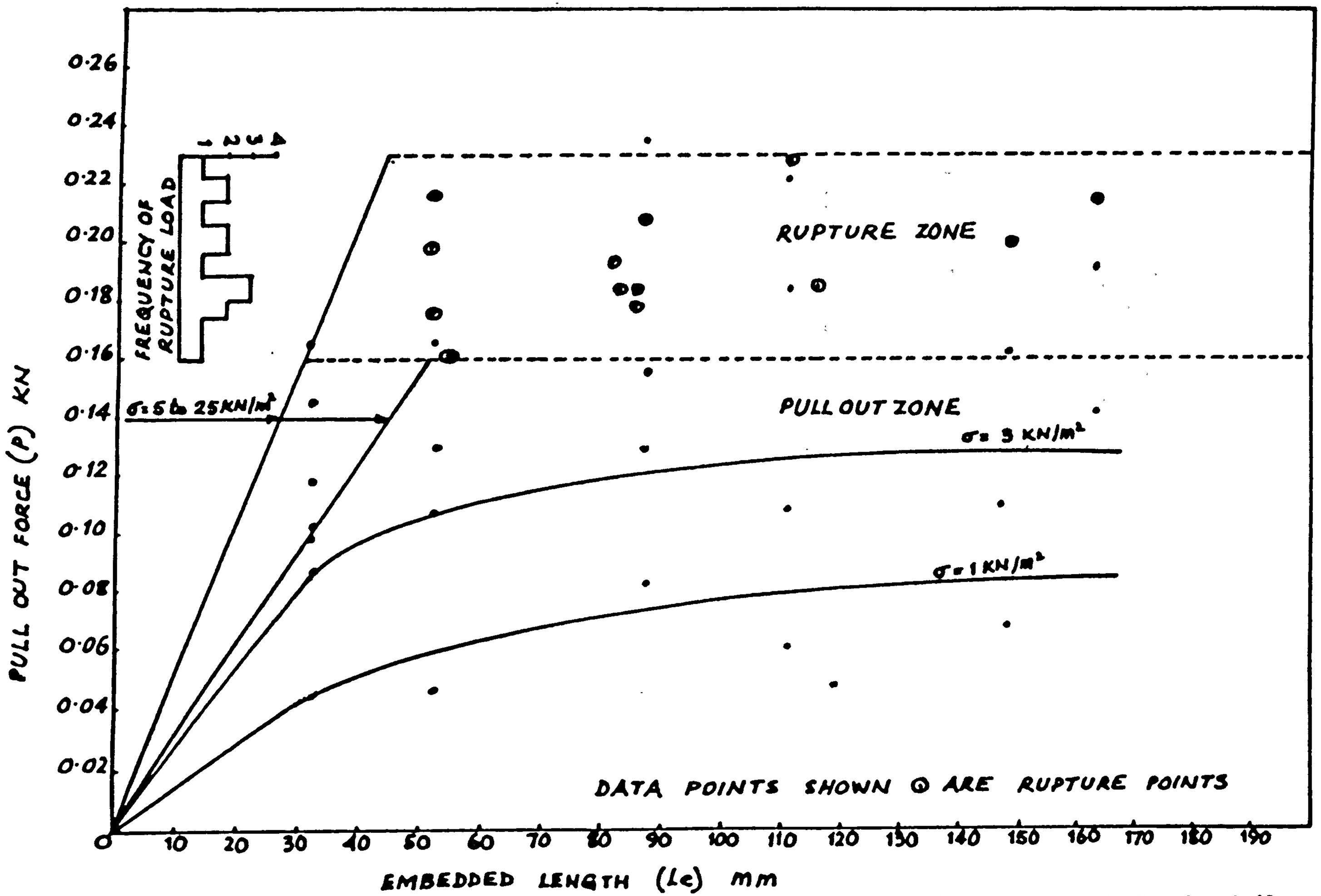

FIG: C.6 RELATION BETWEEN Le AND P FOR TYPE 10 MESH IN MID-ROSS SAND

APPENDIX D

CORRECTION STUDIES IN TRIAXIAL TESTING

APPENDIX D

CORRECTION STUDIES IN TRIAXIAL TESTING

(a) VOLUME CHANGE CORRECTION

All triaxial testing was carried out at fully drained and dry conditions. This whole work was a series of comparative tests between sand alone and sand mixed with mesh elements. In order to calculate the values of the deviator stresses at any particular axial strain, the piston force had to be divided by the cross sectional area of the triaxial sample at that strain. Thus referring to Figure D.1, a triaxial specimen at an axial strain ε_1 , having a cross sectional area A_1 and a piston force F_1, has a deviator stress:

$$(\sigma_1 - \sigma_3)_1 = \frac{F_1}{A_1}$$

or

$$(\sigma_1 - \sigma_3)_1 = \frac{F_1(L_o - \Delta l_1)}{(V_o \pm \Delta V_1)} \qquad -(D.1)$$

where:

L_0 : is the original sample height ,

Δl_1 : is the change in height at strain ε_1 ,

V_0 : is the original sample volume ,

ΔV_1 : is the change in volume at strain ε_1 .

Similarly at an axial strain ε_2, the deviator stress is :

$$(\sigma_1 - \sigma_3)_2 = \frac{F_2 (L_o - \Delta l_2)}{(V_o \pm \Delta V_2)} \qquad -(D.2)$$

where Δl_2 and ΔV_2 are the changes in sample height and volume respectively, at an axial strain ε_2 due to the piston force F_2.

From equations D.1 and D.2 it can be observed that the cross sectional area of the sample is a direct function of its original volume plus a change in volume (ΔV). This change in volume takes place during initial consolidation of the sample and during subsequent dilation (or shearing). For dry sand however, it is very difficult to monitor both of these. Additionally, the shape of triaxial specimens containing sand mixed with mesh elements (shown in Figure 5.71) and Plates 22 and 30) during testing, is irregular due to growths formed by sand/mesh agggregations that slip"sideways" during straining. Thus the analysis of the above equations that is based in pure geometry (from Figure D.1) is not fully valid and the determination of the average cross sectional area is rather complex. Thus in the

calculations of deviator stresses in triaxial testing, the initial volume has been assumed to be constant. As the testing of this work was of comparative nature, the error between deviator stresses for soil alone and the composite material calculated with this constant volume assumption, should be very small. A number of triaxial tests however were carried out on 38 mm ($1^{1}/2$ inch) fully saturated samples of sand alone and the change in volume ΔV during testing was assessed (see Figure D.4). From this figure it is apparent that a maximum error of about 5% is resulted between dry samples tested with constant volume assumption and triaxial samples tested measuring their volume change. Therefore the comparative error for the sand, or sand and mesh elements would be a fraction of this.

(b) MEMBRANE CORRECTION

The assumed restraints imposed on the specimen by the rubber membrane enclosing it, were taken into account and a correction study to the measured stresses was also made. A method of calculating this correction was developed by Henkel and Gilbert (1952) based on the properties of the rubber membrane. This method

gave results in substantial agreement of the measured values and was based in the following assumptions:

(1) that the membrane, when held against the sample by the cell pressure, was capable of taking compression;

(2) that the sample deforms as a right cylinder in the case of plastic failure. In the case of failure on a single shear plane, the behaviour of the rubber membrane is more complex than in the case of plastic failure. No satisfactory analysis has so far been possible but previous experimental evidence suggest that the correction increases slightly with cell pressure and, at the same same strain, may be considerably larger than for plastic failure.

Since the Poisson's ratio of rubber is almost exactly one-half, it follows that in undrained tests no hoop tension is induced in the membrane. The correction is therefore applied to the axial stress and not to the lateral pressure.

If $(\sigma_1 - \sigma_3)_m$ is the measured compression strength, then the actual compression strength $(\sigma_1 - \sigma_3)$ of the sample will be given by:

$$(\sigma_1 - \sigma_3) = (\sigma_1 - \sigma_3)_m - \frac{\pi.D.M.E}{a} \qquad -(D.3)$$

where a denotes the corrected area of the sample at an axial strain ε_1, D denotes the initial diameter of the sample and M denotes the compression modulus of the rubber membrane per unit width.

The correction σ_r, to the measured compression strength, due to the effect of the rubber membrane is therefore:

$$\sigma_r = \frac{\pi.D.M.\varepsilon}{a} = \frac{\pi.D.M.\varepsilon\ (1-\varepsilon)}{a_o} \qquad -(D.4)$$

where a_0 is the initial cross sectional area of the specimen.

The compression modulus M cannot be measured directly on a thin membrane but its value may reasonably be assumed to be similar to that measured in extension.

With the arrangement shown in figure D.3, a circumferential strip 1 in (or 25.4 mm wide) was used to find the extension modulus M. (Chalk on the contact face between the glass rods and the rubber served to reduce friction). The circumferential rubber strip was loaded gradually and its extension was measured against the applied loading. The average membrane thickness was in the order of about 0.028 mm.

The slope of the graph of $\frac{\text{load}}{2}$ versus strain (%) gave an extension Modulus of almost 4.55 kN/m/strain. Thus (D.4) becomes :

$$\sigma_r = 117.3\,\varepsilon\,(1-\varepsilon) \quad kN/m^2 \qquad -(D.5)$$

For the use of 2 membranes (D.5) becomes :

$$\sigma_r = 234.6\,\varepsilon\,(1-\varepsilon) \quad kN/m^2 \qquad -(D.6)$$

Theoretically when $\varepsilon = 0, \sigma_r = 0$

when $\varepsilon = 3.0\%$

then $\sigma_r \sim 6.8\ kN/m^2$

when $\varepsilon = 6.0\%$

then $\sigma_r \sim 13.2\ kN/m^2$

and when $\varepsilon = 15\%$ (assuming plastic failure)

$$\sigma_r \sim 30.0\ kN/m^2$$

The above calcualtions are based on the assumption that the failure is plastic.

If the failure however occurs at a single shear plane, then an actual correction of 4.15 kN/m^2 (0.6 $lb/sq.$ in.), or for 2 membranes, a total of 8.30 kN/m^2 could be applied because failure on a single shear plane usually occurs as a comparatively small strain and the actual correction at failure is generally of the same order as the 4.15 kN/m^2 applied to plastic failures at 15% strain. (Bishop and Henkel, 1962).

(c) CORRECTION STUDY DUE TO SHORTAGE IN CIRCUMFERENTIAL LENGTH OF THE NEW MEMBRANE

A correction factor had to be studied for the case of membranes having shorter circumferential length than the actual circumferential length of the triaxial specimen itself.

When rubber membranes were supplied new, their length was about 6 inches or 153 mm. Therefore they had to enclose a cylindrical soil sample which was exactly 155 mm according to the dimensions of the split mould. Thus the membrane length shortage applied a small radial pressure which was calculated (see Figure D.2) as follows:

$$L = \pi.D \qquad -(D.7)$$

Where D is the rubber membrane's original diameter

and L its circumferential length.

Assume Δl to be the shortage in circumferential length and ΔD a shortage in diameter.

Thus; $\pi(D + \Delta D) = L + \Delta l$ — (D.8)

Hence, $\pi.D + \pi.\Delta D = L + \Delta l$

and $\pi.\Delta D = \Delta l$ — (D.9)

Assuming the tensile strength of the rubber membrane (according to Figure D.2) to be σ_3, and the force induced due to shortage in length F, then;

$$\sigma_3 = \frac{F}{D} = \frac{M.\Delta l/L}{D} = \frac{M.\Delta l}{D.\pi.D} = \frac{M.\pi.\Delta D}{\pi.D^2}$$

Hence,

$$\sigma_3 = \frac{M}{D^2} \cdot \Delta D \qquad - (D.10)$$

Where M is the modulus of Elasticity of the rubber membrane, D is its original diameter and ΔD is its shortage in diameter.

(For equation (D.10) to be valid, an assumption has to be made that there will be no initial volume change in the specimen)

Substituting the previous numerical values in (D.10) for M and D;

$$\sigma_3 \simeq 2.0\ \Delta D \quad kN/m^2$$

If the shortening of the membrane is in the order of 1 to 2 mm, then σ_3 becomes a max of 4.0 kN/m^2, or 8.0 kN/m^2 for two membranes.

When the membrane is used twice, the circumferential length shortage-factor is eliminated because of the stretching of the membrane due to wash.

Thus an <u>initial</u> pressure of 0 to 8 kN/m^2 could be applied to the cell pressure as a correction factor, accordingly.

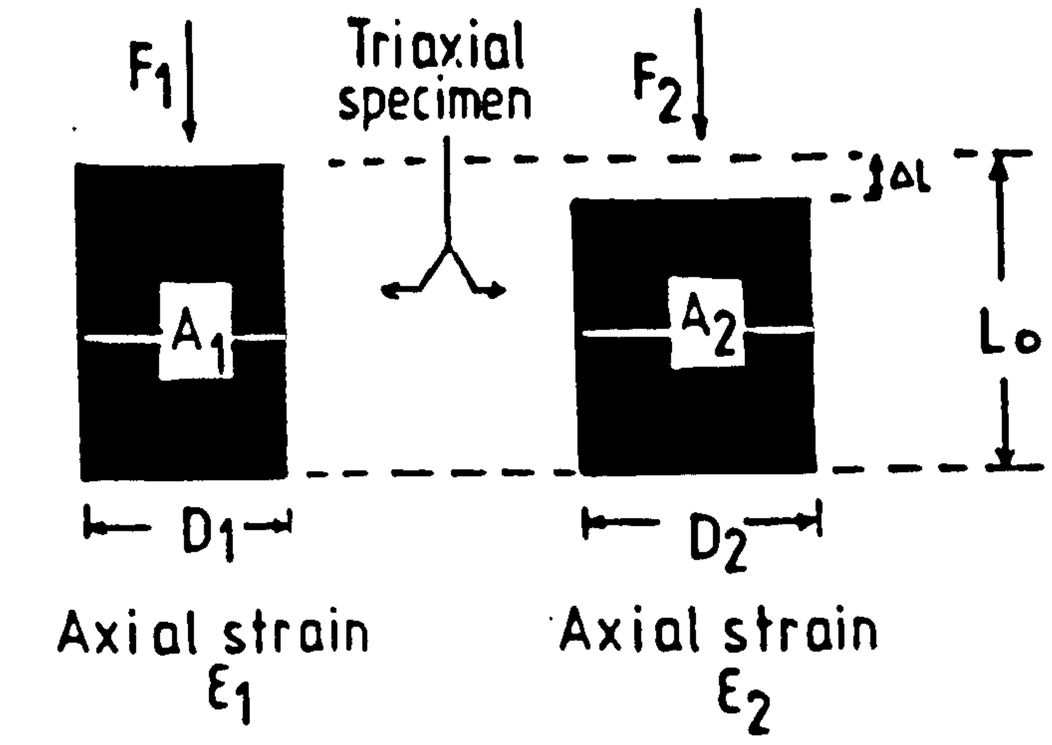

FIG. D.1

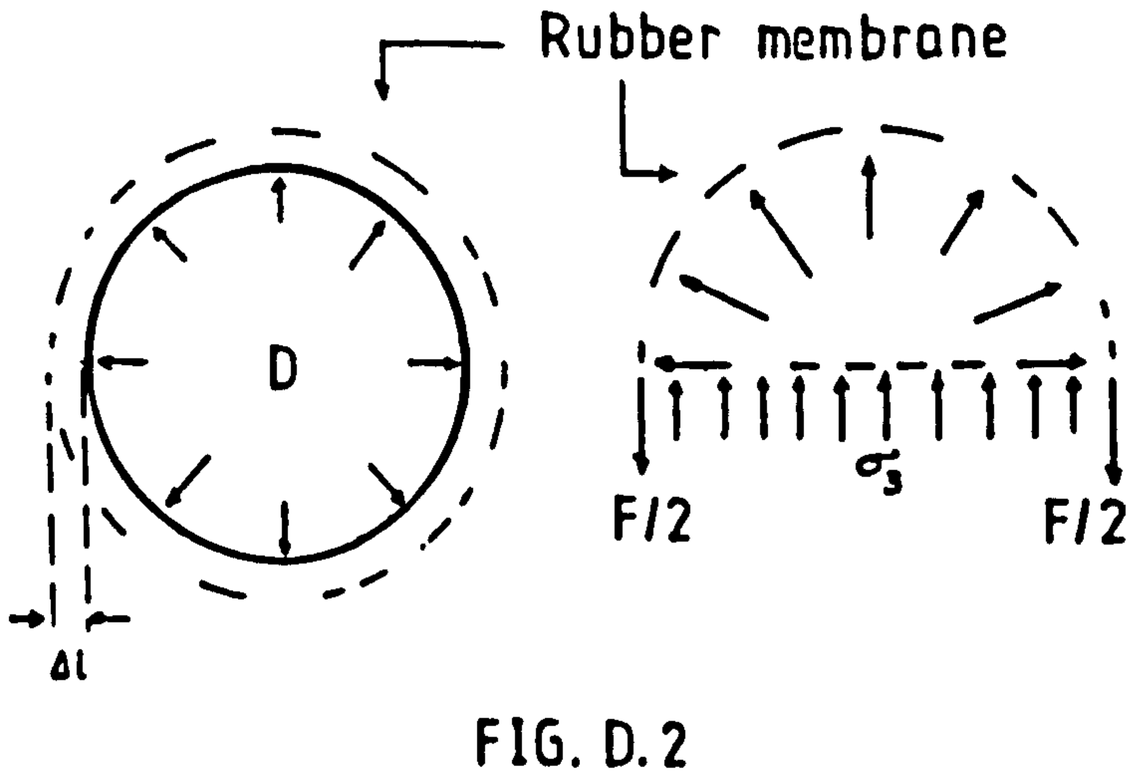

FIG. D.2

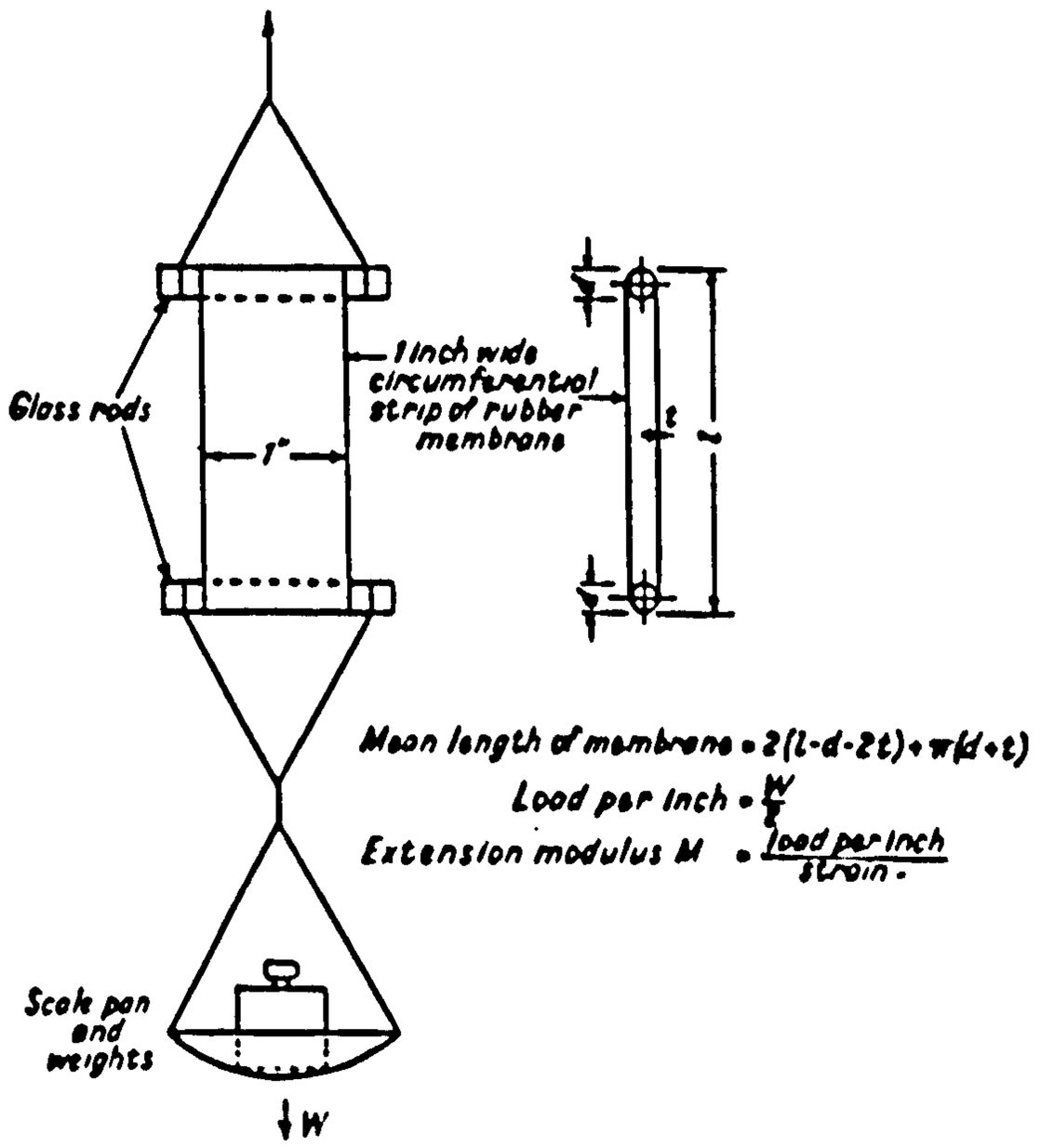

FIG. D.3 The apparatus for measuring the extension modulus of the rubber membrane (length measurement made with vernier telescope)

APPENDIX E

FULL SCALE TRIALS OF MESH ELEMENTS

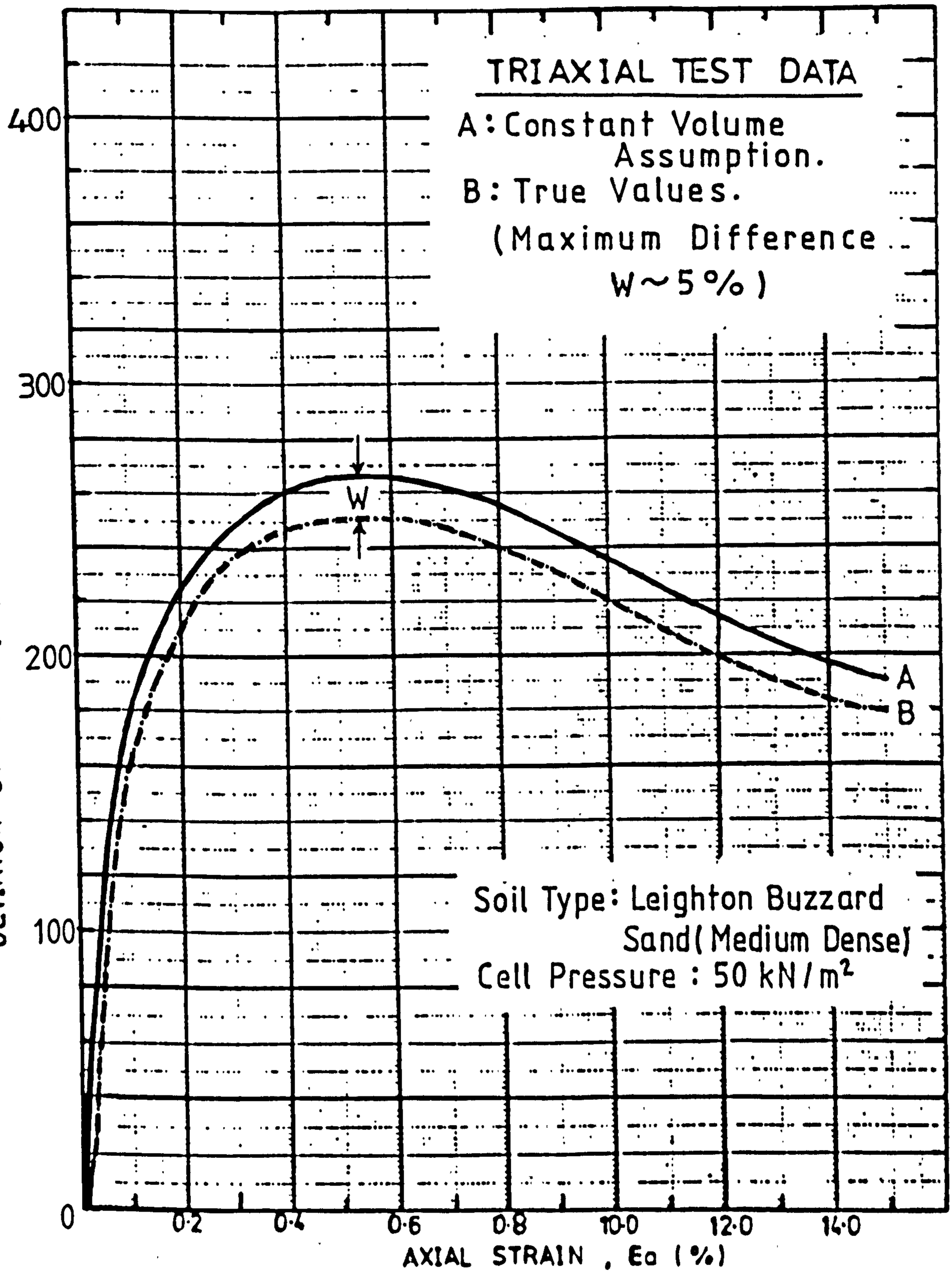

FIG. D.4 Comparison Between the True Values of the Deviator Stresses of Dry Sand Samples Tested Fully Drained in Triaxial, and the Ones Under Constant Volume Assumption.

APPENDIX E

FULL-SCALE TRIALS OF MESH ELEMENTS

1. INTRODUCTION

Extensive laboratory tests on a well-graded sand of fluvio-glacial origin (called 'Mid-Ross Sand') mixed with randomly distributed polymeric mesh elements have shown that the inclusion of mesh elements can substantially improve the shear strength properties of the composite material without altering its ductility or permeability (see Fig. E.1).

To take this work further, full-scale trials of the bearing capacity of fill containing mesh elements have been carried out at the Transport and Road Research Laboratory.

2. METHOD

The trials were carried out in one of the TRRL covered test bays, 17 m in length and 5 m wide with concrete side walls and a floor formed by the naturally occurring deposit (Bagshot Beds). The bay was divided up into 8 sections, as shown in Fig.

E.3, different materials being separted by plywood sheets. The materials used are described below.

2.1 Mesh elements

The mesh is manufactured from polypropylene using the Netlon extrusion process. It has a mass per unit are of about 52g/m^2. The maximum tensile strength of the mesh when tested as 200 mm x 100 mm specimens, at constant rate of strain of 2% per min and temperature of 20^{0}C was:-

Type 7 :	Machine direction	3.5kN/m
	Cross machine direction	3.8kN/m
Type 10:	Machine direction	4.3kN/m
	Cross machine direction	3.8 kN/m

Dimensions of mesh are:-

Type 7 : Filament thickness, machine direction

0.5 mm

Filament thickness, cross machine direction

0.48 mm

Filament openings

6.7 x 7.1 mm

Type 10: Filament thickness, machine direction

0.47 mm

Filament thickness, cross machine direction

0.45 mm

Filament openings

10 x 10 mm

2.2 Sand

The 'Mid-Ross sand' was obtained from the same source as for previous laboratory work. It had sub-angular particles ranging in size from 0.05 to 7 mm diameter with a coefficient of uniformity of 5. A preliminary grading curve* is given in Fig. E.2. The sand was delivered at a moisture content of 6%. Untreated sand was placed directly in the test bay and spread in 100 mm layers. Water was sprayed on to bring the moisture

content up to the 9% used in the laboratory work, and the sand compacted with 6 passes of a vibrating plate compactor (Benford VPC50). Sand containing mesh elements was mixed in half ton batches in a rotating paddle mixer with the required quantity of 'Type 7" mesh elements to give 66 m^2 of elements per m^3 of sand. Water was also added to bring the moisture content up to 9%. The sand was then placed and compacted in the same manner as the untreated sand.

Measurements with a Troxler nuclear gauge, using back-scatter mode gave :

	Untreated sand	Sand with mesh elements
Bulk density(Mg/m^3)	1.88	1.81*
Moisture content(%)	6.8	7.6*

The moisture content was confirmed with an oven drying test after completion of the trials (7.0%).

*Readings may have been affected by the presence of hydrogen in the polymer of the mesh elements

A volume of sand with mesh elements was excavated from beneath the sites of several bearing capacity tests. The sand and mesh elements were weighed. From the density of the sand, the proportion of mesh elements was calculated to be 36, 64 and 44 m^2/m^3. There is some uncertainty in this procedure because of the difficulty of counting elements at the edge of the hole.

2.3 Aggregate

The aggregate was a limestone aggregate from Somerset, intended as a 'Type 1' sub-base material (DTp Specification, Clause 803). This material had been used in previous trials with Tensar; a provisional grading is given in Fig. E.2. Shearbox testing on Type 1 aggregate gave a shear strength parameter of $\phi_{ult.} = 45^0$. The moisture content in this case was about 3%. The aggregate was treated similarly to the sand, except that each layer was compacted with 4 passes of a vibrating roller (Stothert and Pitt Vibroll D75), and an additional final compaction was given with four passes of a heavy vibrating plate (Whacker DPU 6760). One measurement only of the proportion of mesh element was made after the trials, which gave 83m^2/m^3.

2.4 Clay

The clay used was remoulded London Clay, of liquid limit 78 % and plastic limit 24% Cohesion;, measured, with a Pilcon shear vane was 25.1 kN/m^2 (40 tests, s.d. = 4.7 kN/m^2) for the clay and 36.4 kN/m^2 (8 tests, s.d. = 7.4 kN/m^2) for clay with mesh elements. The moisture content of clay alone was 39.6% (5 tests, s.d. 1.9%) and for the clay with mesh elements was 38.2% (5 test samples, s.d. 0.53%).

The untreated clay was placed in 200 mm layers, and compacted with 4-6 passes of a light roller (Vibrol D75 without vibration). The formation was too weak to permit heavier plant.

'Type 10' mesh elements were mixed into the clay with a rotavator, the clay being spread over an adjacent area. It was found necessary to reduce the proportion of elements to 38 m^2/m^3, as this was the maximum that could be dealt with by the rotavator.

3. TEST PROCEDURE

Kentledge for the bearing tests was applied through the moveable loading frame previously used for the Tensar trials; load was applied through a jack and load cell to either a 300 mm or a 100 mm diameter circular footing. The load cell calibration was checked in the laboratory against a second cell of known accuracy. Footing penetration was measured from two dial gauges on an independently mounted beam. In a few tests with the 100 mm plate, a surcharge of 19 kN/m^2 was applied through a loaded anulus of inner and outer diameters 105 mm and 300 mm resting on the formation around the plate.

For each test, an area was first levelled as far as possible without distrubing the mesh elements, and a thin layer of sand spread over it. The footing plate was then placed and carefully levelled. Care was also taken that the jack was mounted vertically. To carry out the test, a load increment was applied through the jack. The jack was then left 3 mins without any adjustment of load, and the penetration recorded (penetrations after 1 min were also recorded for some tests). After the trails had been completed, profiles across some of the tested areas were measured (Fig. E.4).

4. RESULTS

4.1 300 mm diameter plate on sand

Fig. E.5 shows peak pressures for the four sections with sand, and Fig. E.7 shows pressure/penetration relations obtained for the sand alone and sand with elements. There is little difference in peak pressure, and the only marked difference in behaviour is the large 'rebound' effect during unloading of the sand with mesh elements.

4.2 300 mm plate on aggregate

Fig. E.6 shows peak pressures for the four aggregate sections, and Fig. E.8 shows pressure/penetration curves for four of the tests carried out. Peak pressures on aggregate over clay with mesh elements are appreciably higher. In aggregate with mesh elements, peak pressures tend to occur at higher penetrations, and 'rebound' effects are more marked (Fig. E.9).

4.3 Comparison of 300 mm and 100 mm plates

To examine the possibility of a 'scale factor' (i.e. ratio of size of element to size of bearing plate), a few tests were carried out with a 100 mm plate on sand. The results are shown in Fig. E.10 and indicate that the mesh elements are no

more effective in improving bearing capacity for the smaller plate.

4.4 Effect of surcharge

The effect of a surcharge of 19 kN/m^2 on the bearing capacity of a 100 mm plate on sand is shown in Fig. E.11. There is an increase in bearing capacity both with and without elements, but the increase is far greater in sand with mesh elements (a four-fold increase). The pressure/penetration relation is also very different; with the elements, there is a further increase in pressure with penetration after the first peak is attained (Fig. E.12).

5. DISCUSSION

1. Without the use of a surcharge, there was little benefit in using mesh elements to increase the bearing capacity of either the sand or aggregate. In the case of the aggregate, the been aperture size of the elements may well have the inappropriate for such a coarse material. The elements may even have weakened the pavement after compaction. There may, however, be an improvement in performance at larger penetrations than those presently investigated. The 'rebound' effects suggest

that a more ductile material is formed. An additonal uncertainty is that the correct level of compaction for material containing mesh elements is not certain.

2. The benefits of the mesh elements in the sand did not improve with a smaller plate. This suggest that the size of the elements is not an important factor, at least in the range of 100 mm-300 mm diameter footings.

3. In the case of aggregate pavement on a clay subgrade, the use of mesh elements in the clay did appear to produce significant benefit. This requires further investigation; it must be confirmed that variability in moisture content or distribution of elements in the clay are not involved. The shear vane which was used is not an appropriate tool for clay containing mesh elements. It would be desirable to expose the subgrade for examination at a later date.

4. The tests with surcharge indicated that this is a very important factor; the few results available indicated

substantial benefits both in peak pressure, and at larger penetrations. This agrees with laboratory findings, that maximum benefit is obtained at a suitable level of confinement. Further tests should be carried out to confirm and enlarge on this aspect.

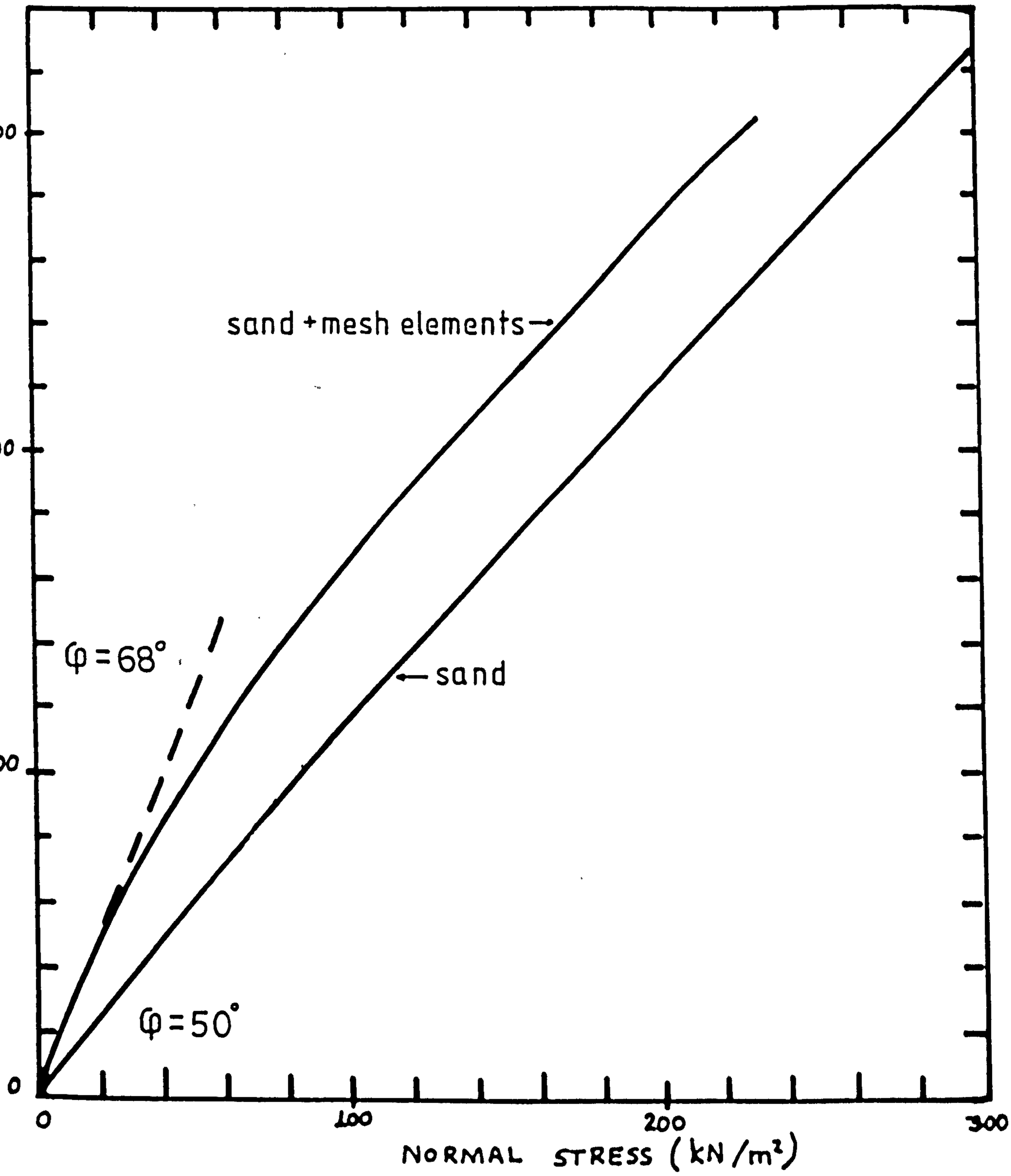

FIG. E.1 SHEAR STRENGTH PROPERTIES OF MID-ROSS SAND WITH MESH ELEMENTS (TRIAXIAL TESTS)

FIG. E.2

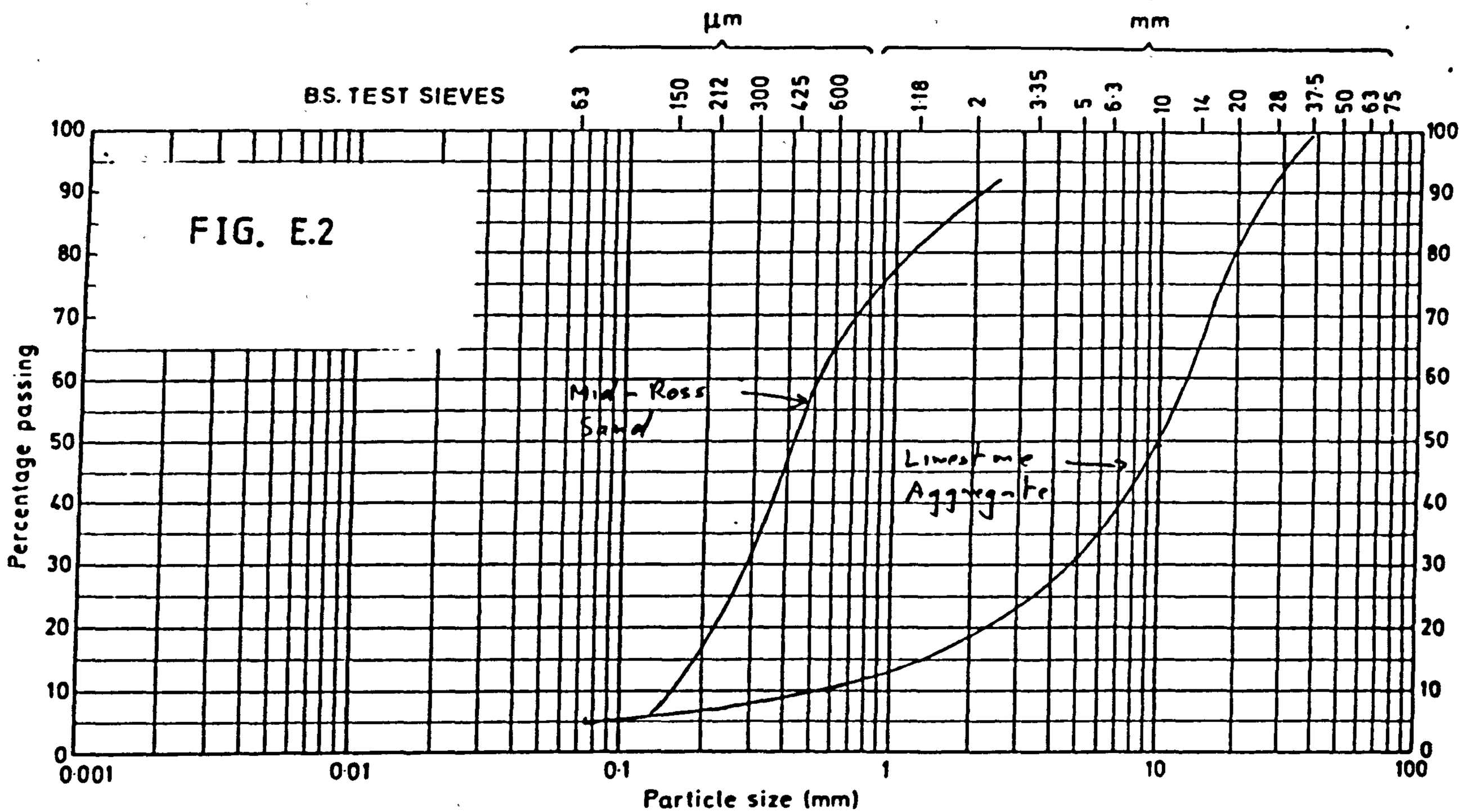

	FINE	MEDIUM	COARSE	FINE	MEDIUM	COARSE	FINE	MEDIUM	COARSE
CLAY	SILT			SAND			GRAVEL		

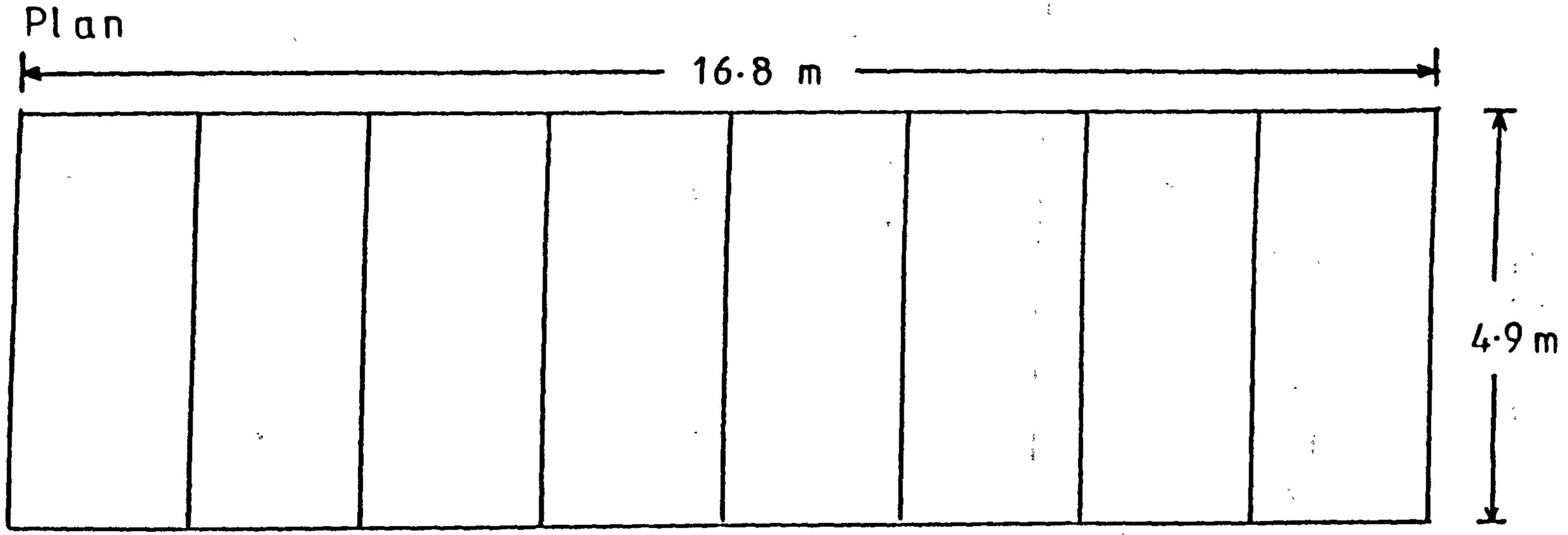

FIG. E.3
LAYOUT OF EXPERIMENTAL SECTIONS

TYPES OF FILL

1. CLAY
2. CLAY With MESH ELEMENTS
3. AGGREGATE
4. AGGREGATE With MESH ELEMENTS
5. SAND
6. SAND With MESH ELEMENTS

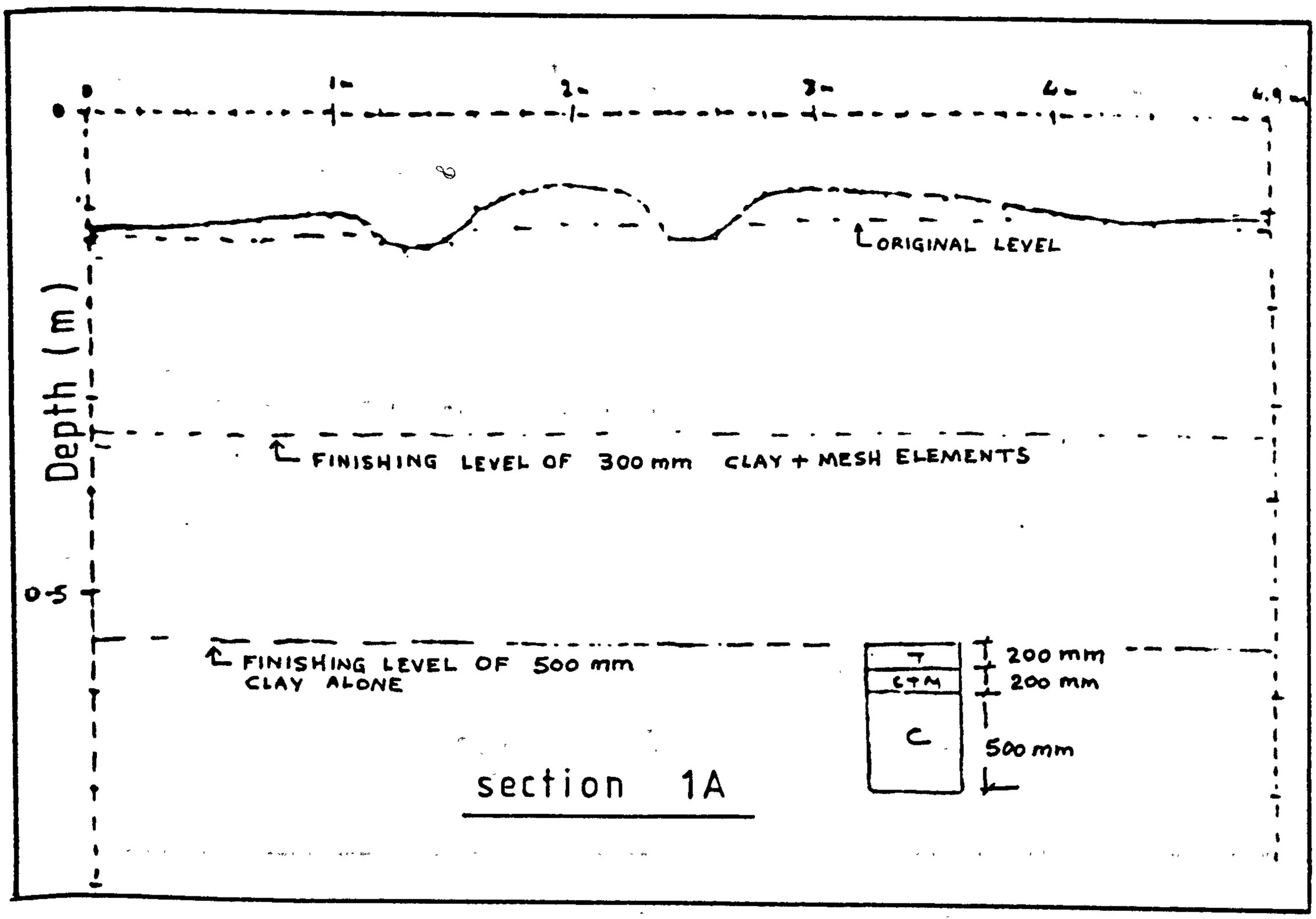

section 1A

FIG. E.4 PROFILES ACROSS TESTED AREAS OF AGGREGATE

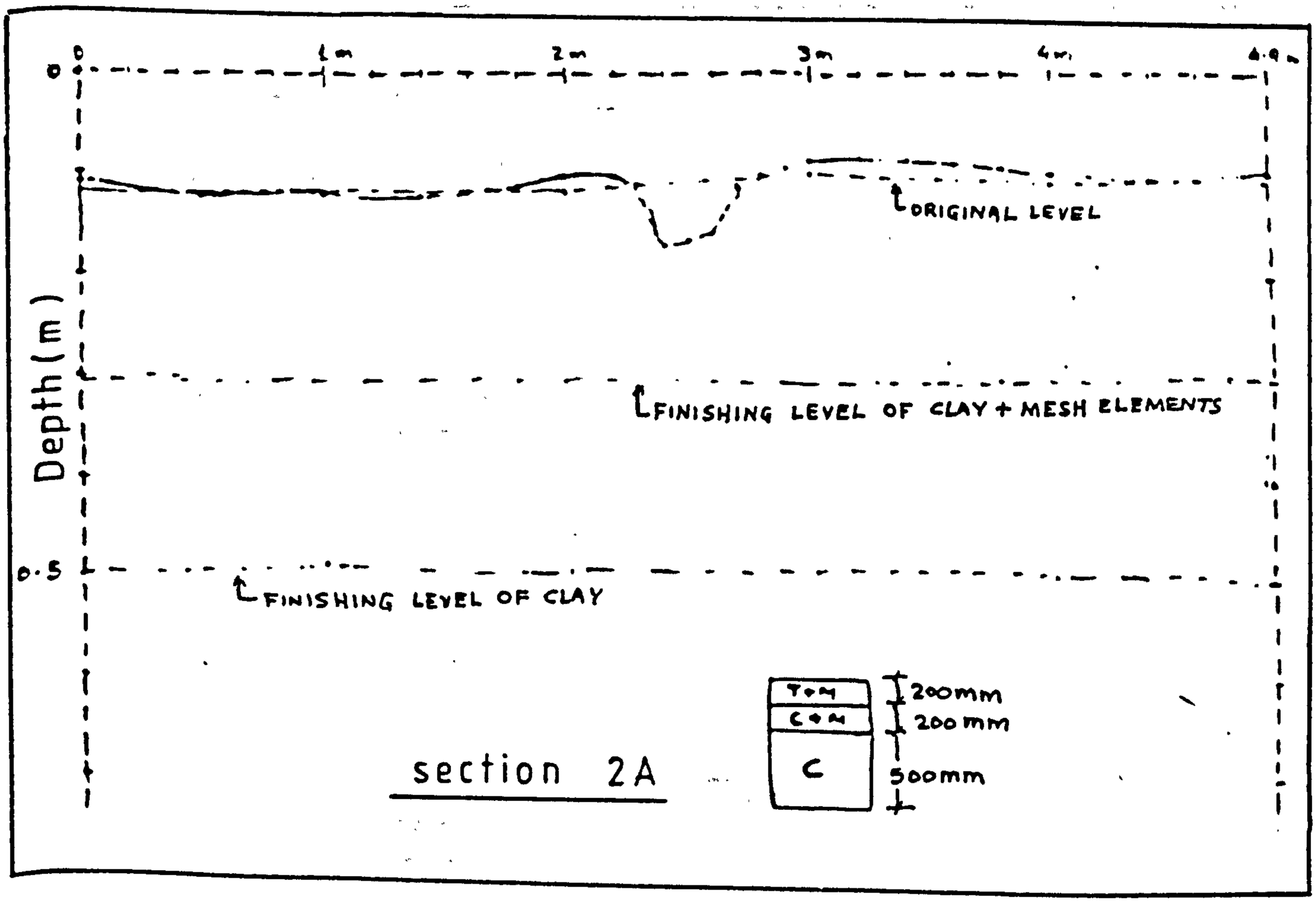

section 2A

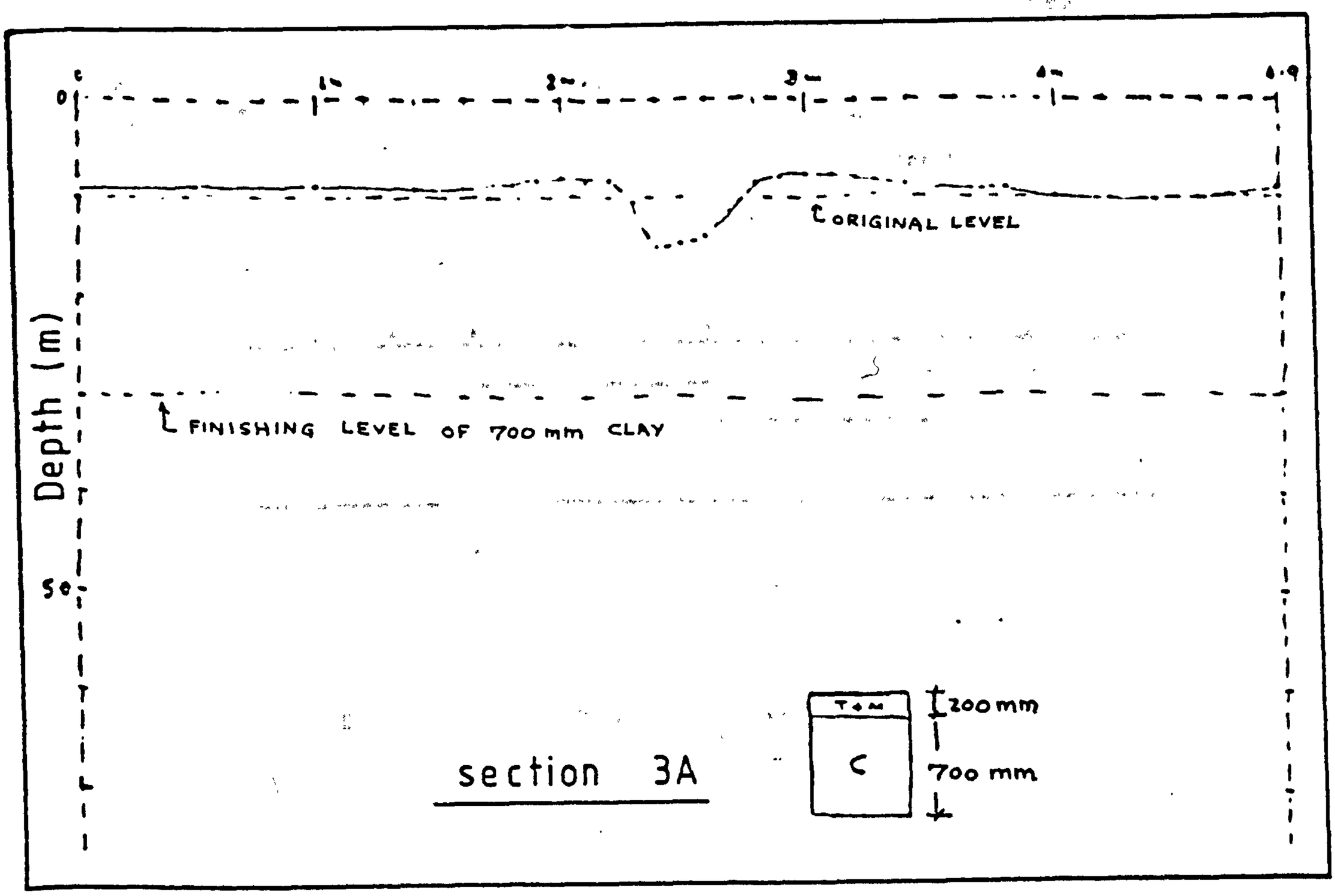

section 3A

section 4A

FIG.E.4 PROFILES ACROSS TESTED AREAS OF AGGREGATE (CONTINUED)

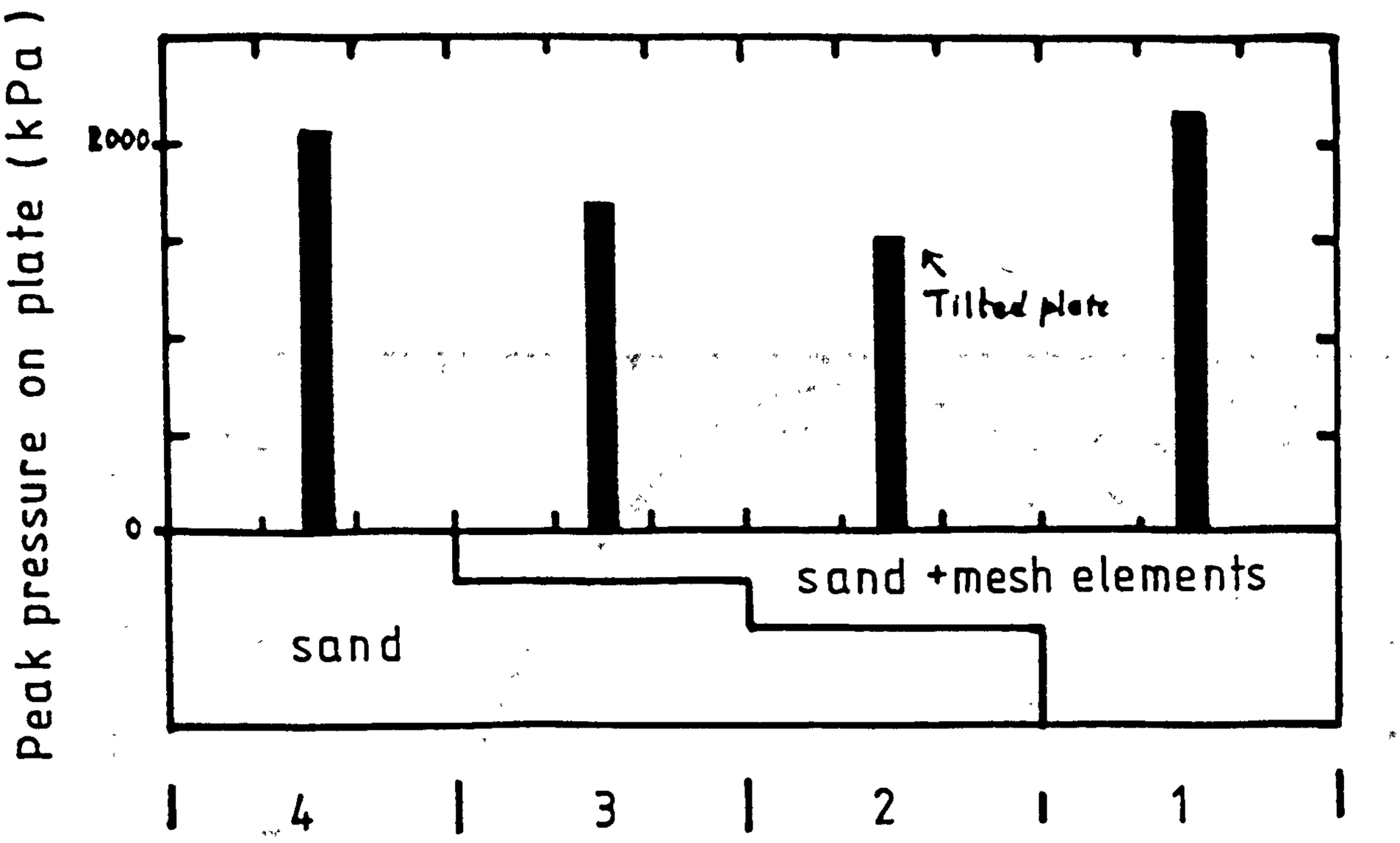

FIG. E.5 300 mm DIAM. PLATE ON SAND

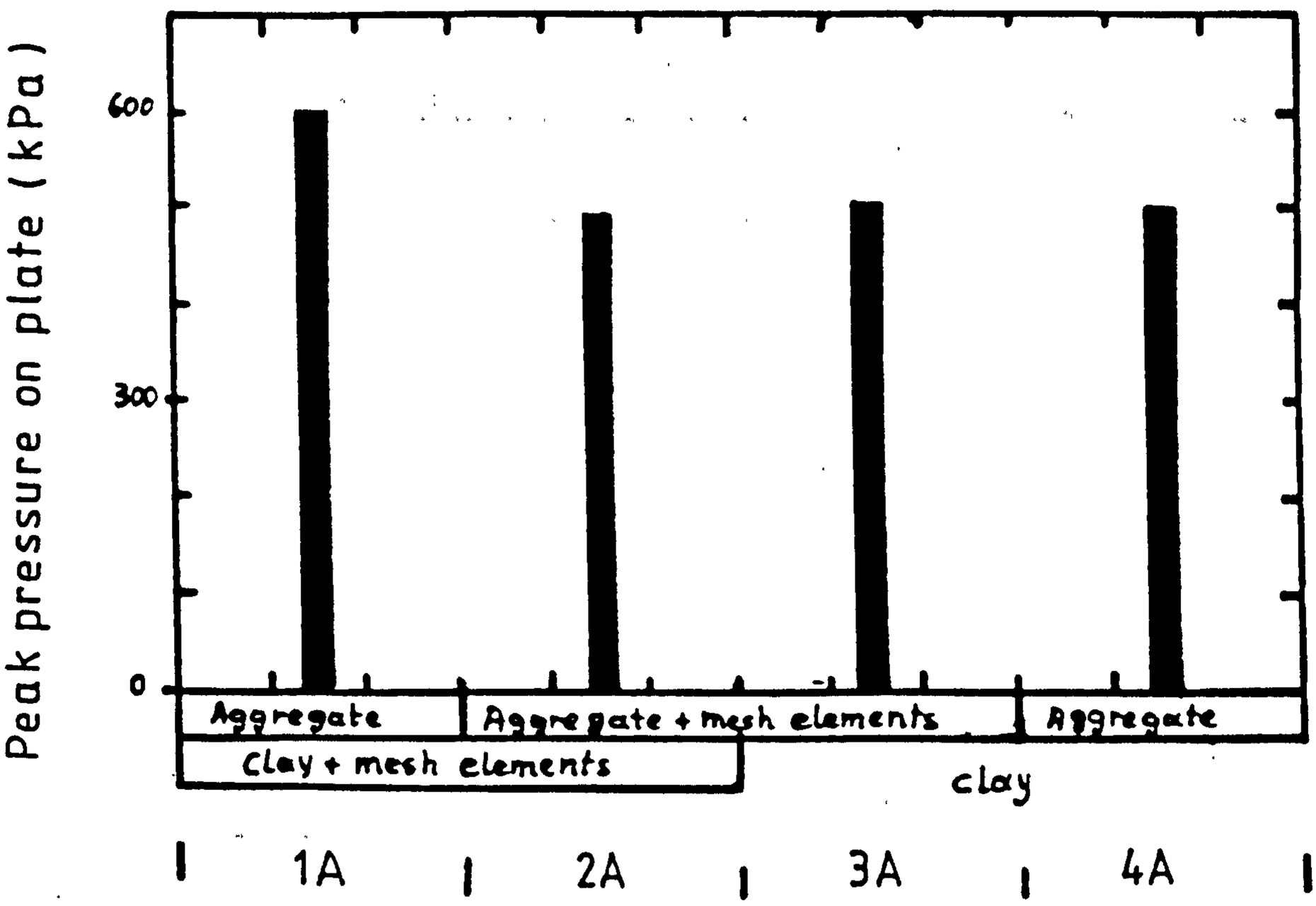

FIG. E.6 300 mm DIAM. PLATE ON AGGREGATE

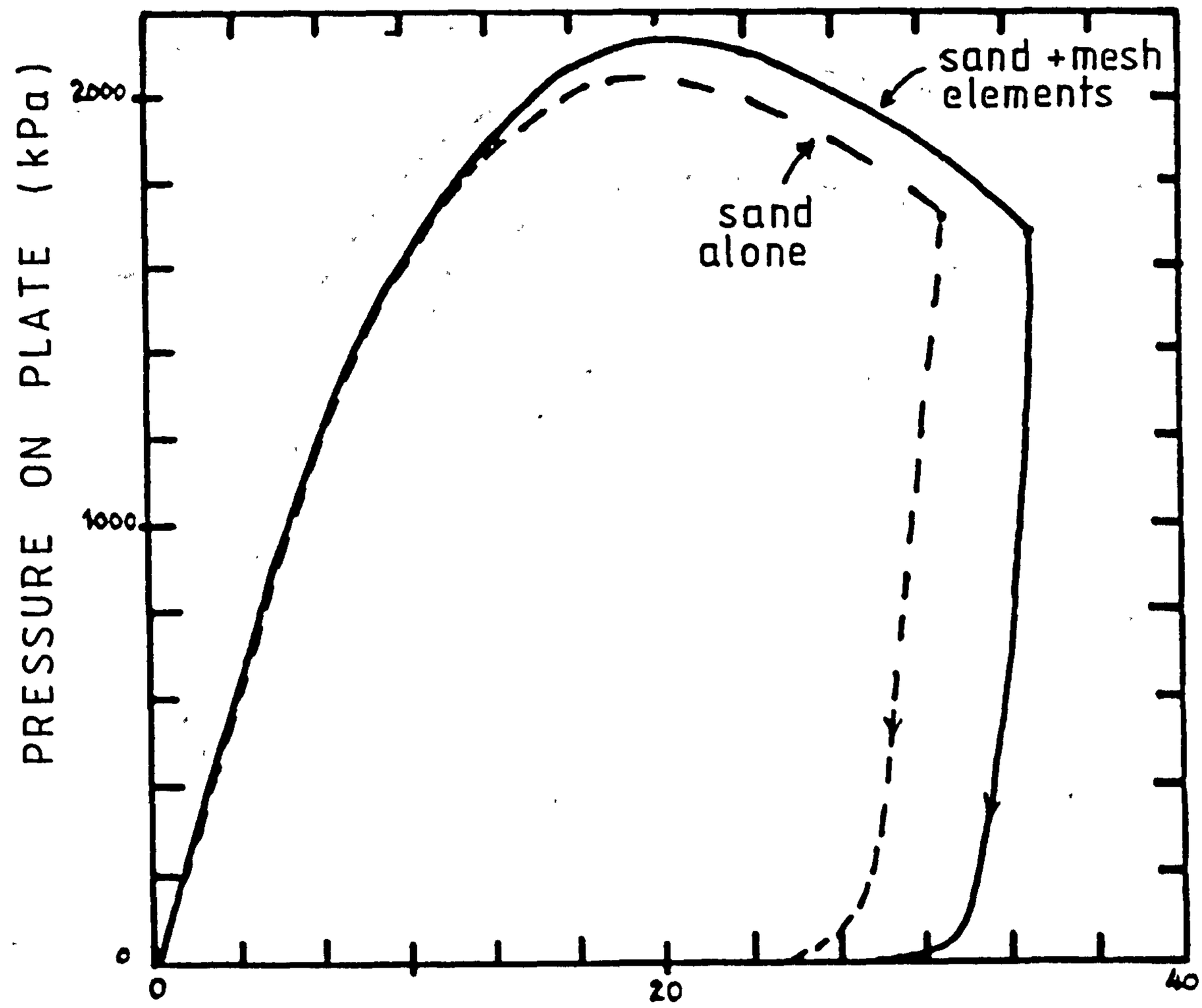

FIG. E.7 PRESSURE / PENETRATION RELATION, SAND
(300 mm DIAM. PLATE)

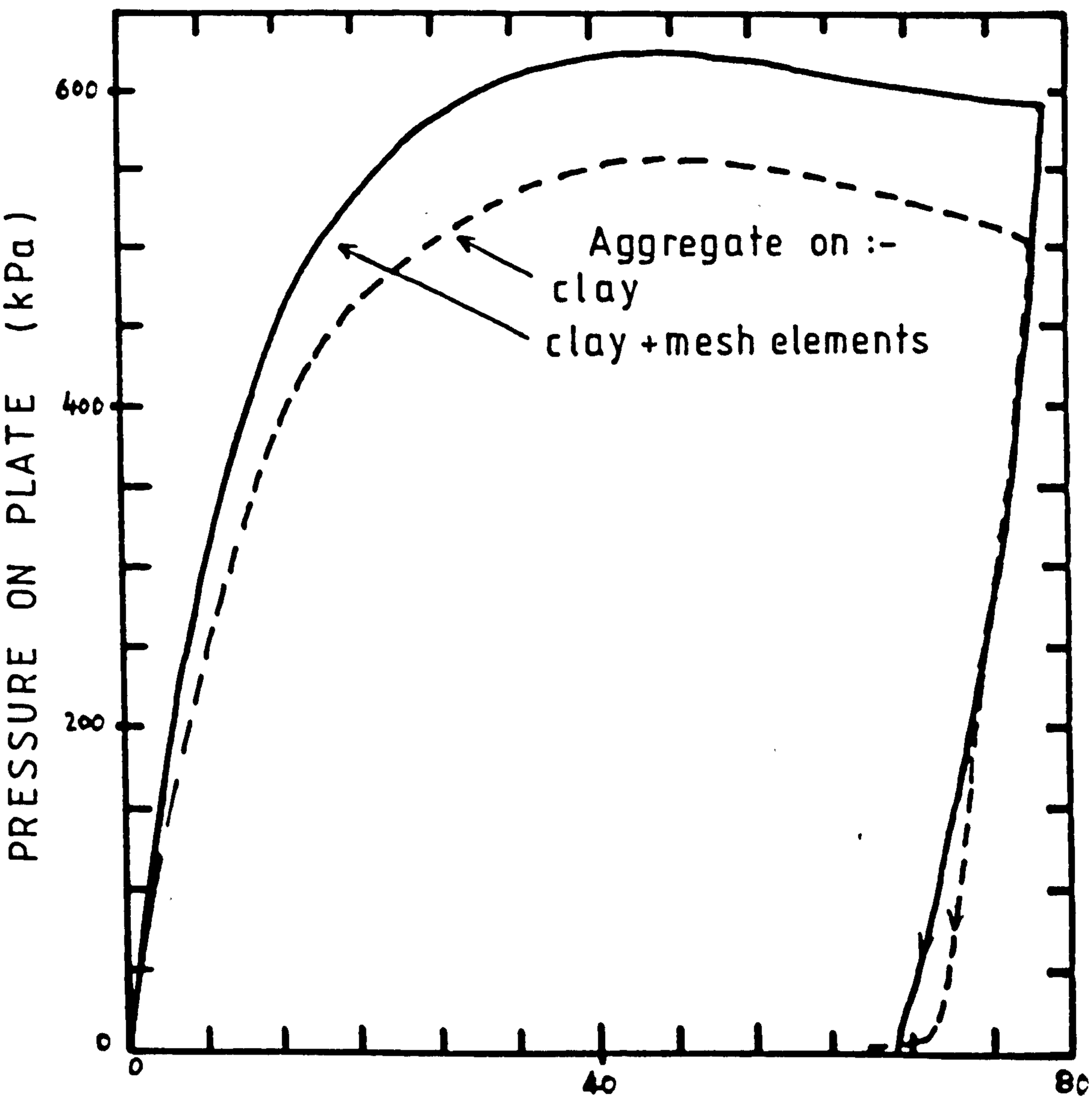

FIG. E.8

PRESSURE/PENETRATION RELATION, AGGREGATE
(300 mm DIAM. PLATE)

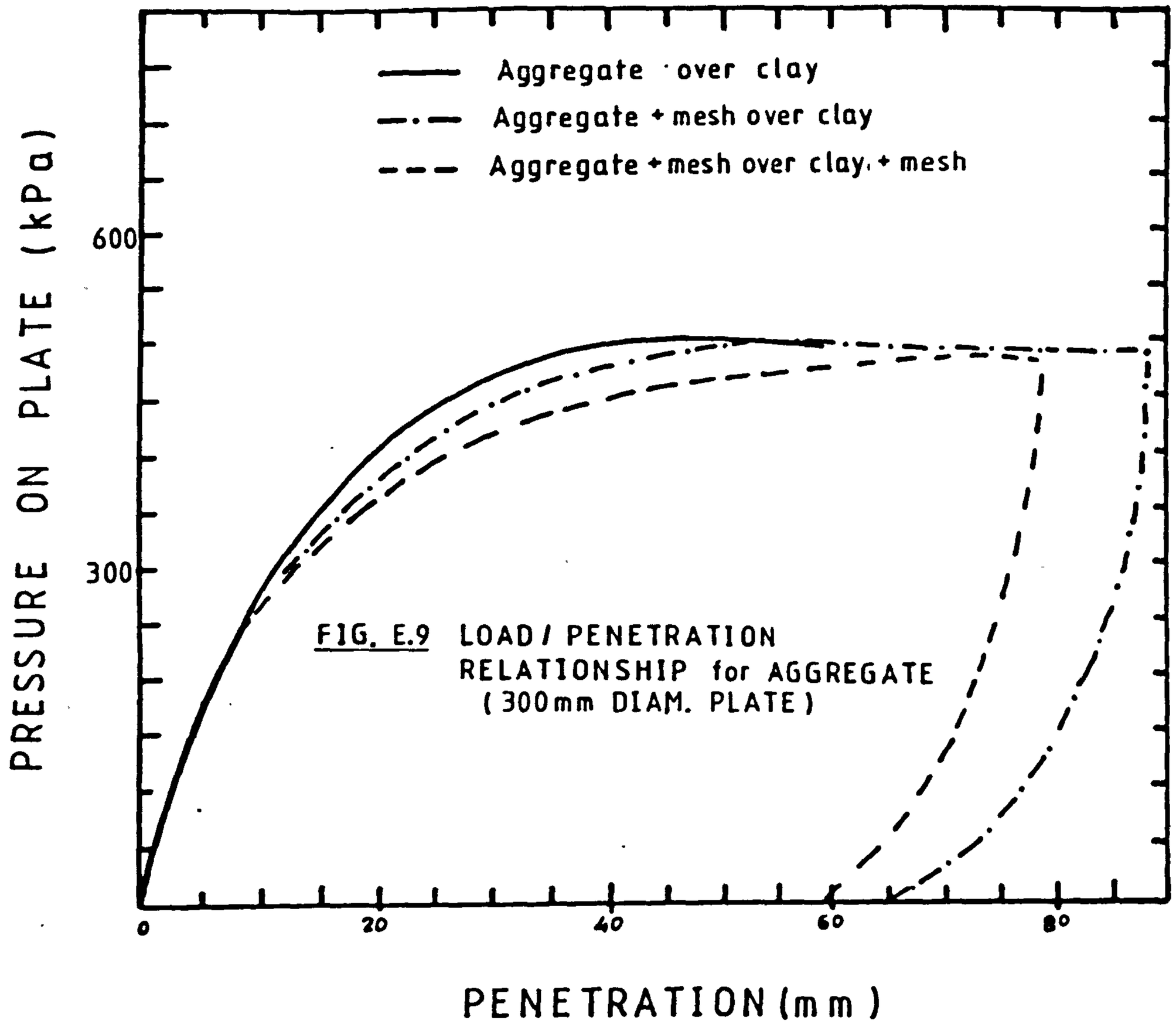

FIG. E.9 LOAD / PENETRATION RELATIONSHIP for AGGREGATE (300mm DIAM. PLATE)

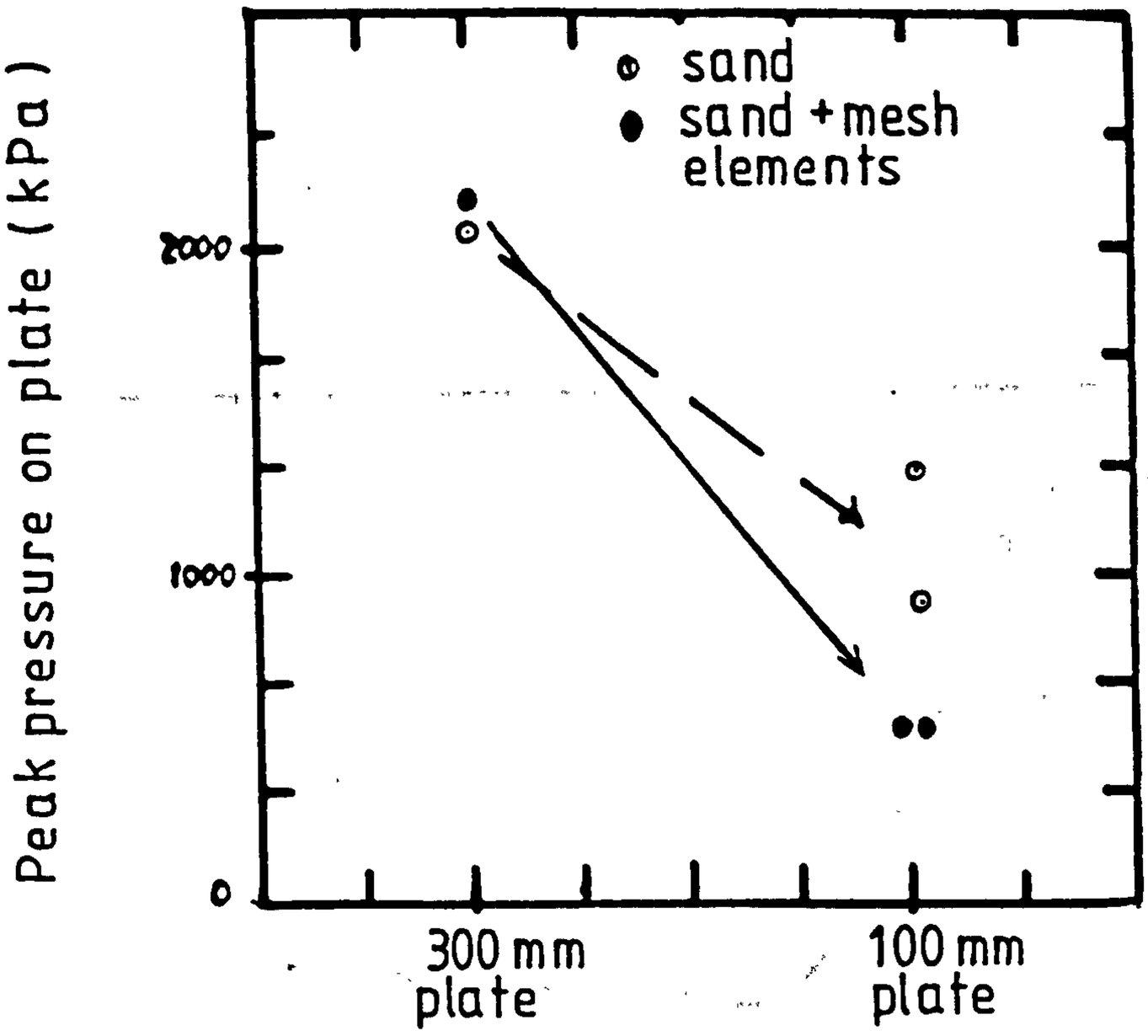

FIG. E.10 COMPARISON OF 300 mm AND 100 mm PLATES ON SAND

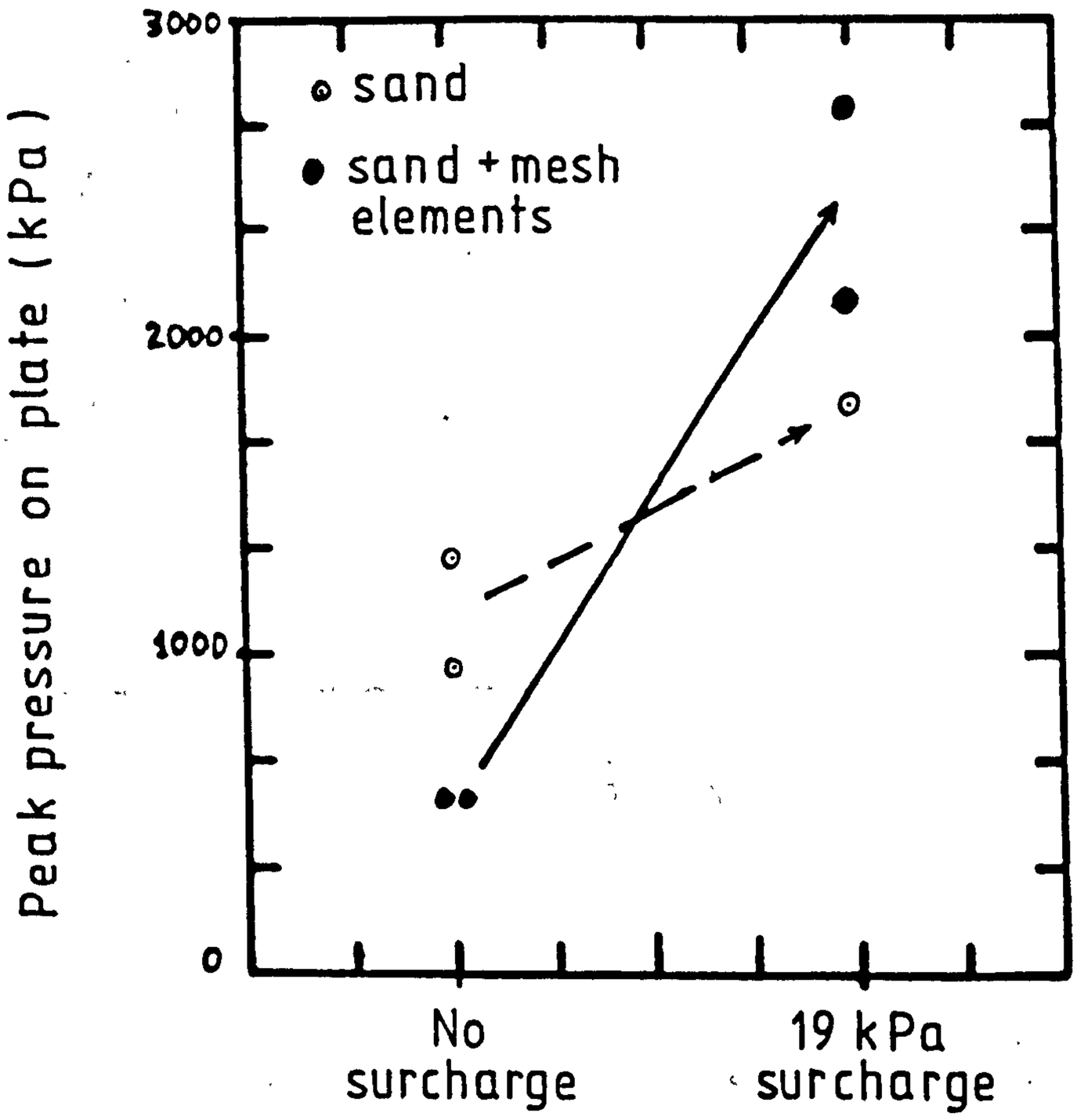

FIG. E.11 EFFECT OF SURCHARGE, 100 mm PLATES ON SAND

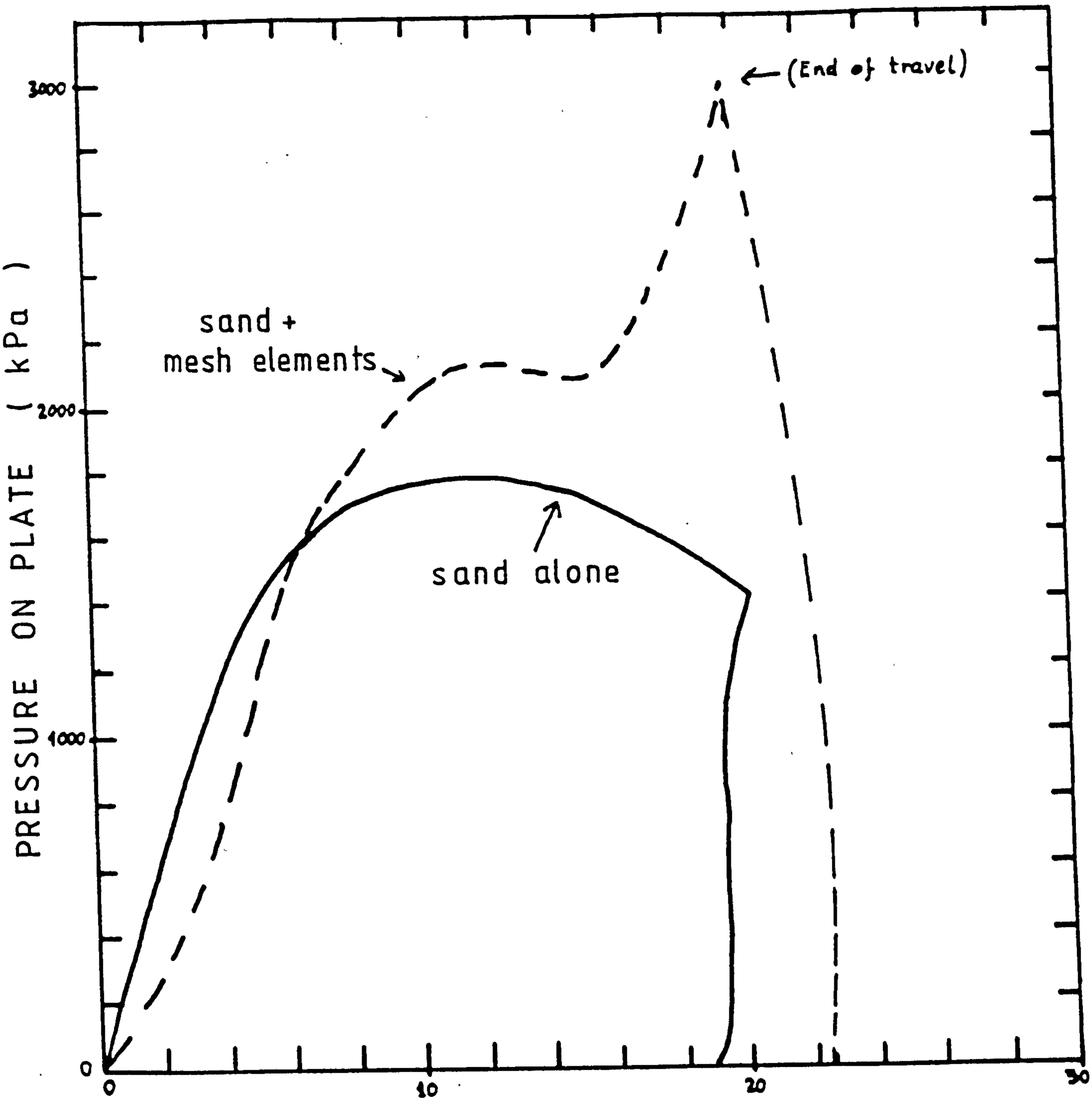

FIG. E.12 LOAD / PENETRATION RELATIONS, 100 mm PLATES WITH 19 kPa SURCHARGE ON SAND

LOAD-EXTENSION CURVES FOR TYPE 7 AND TYPE 10 MESH ELEMENTS

EXTENSION RATE 2% /MIN. (Netlon 1985)

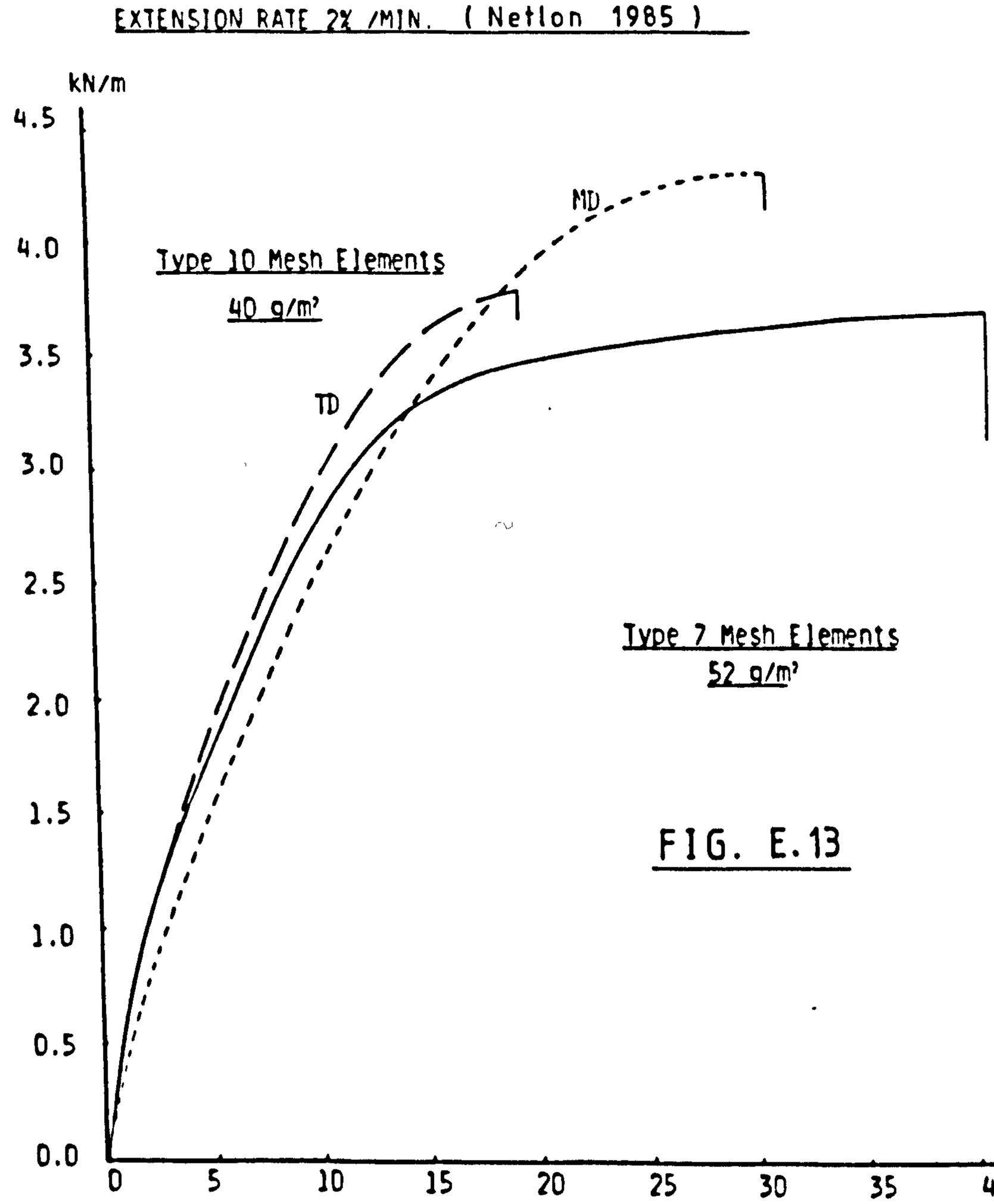

FIG. E.13

PLATE E.1 A View of the Batching and Mixing Plant

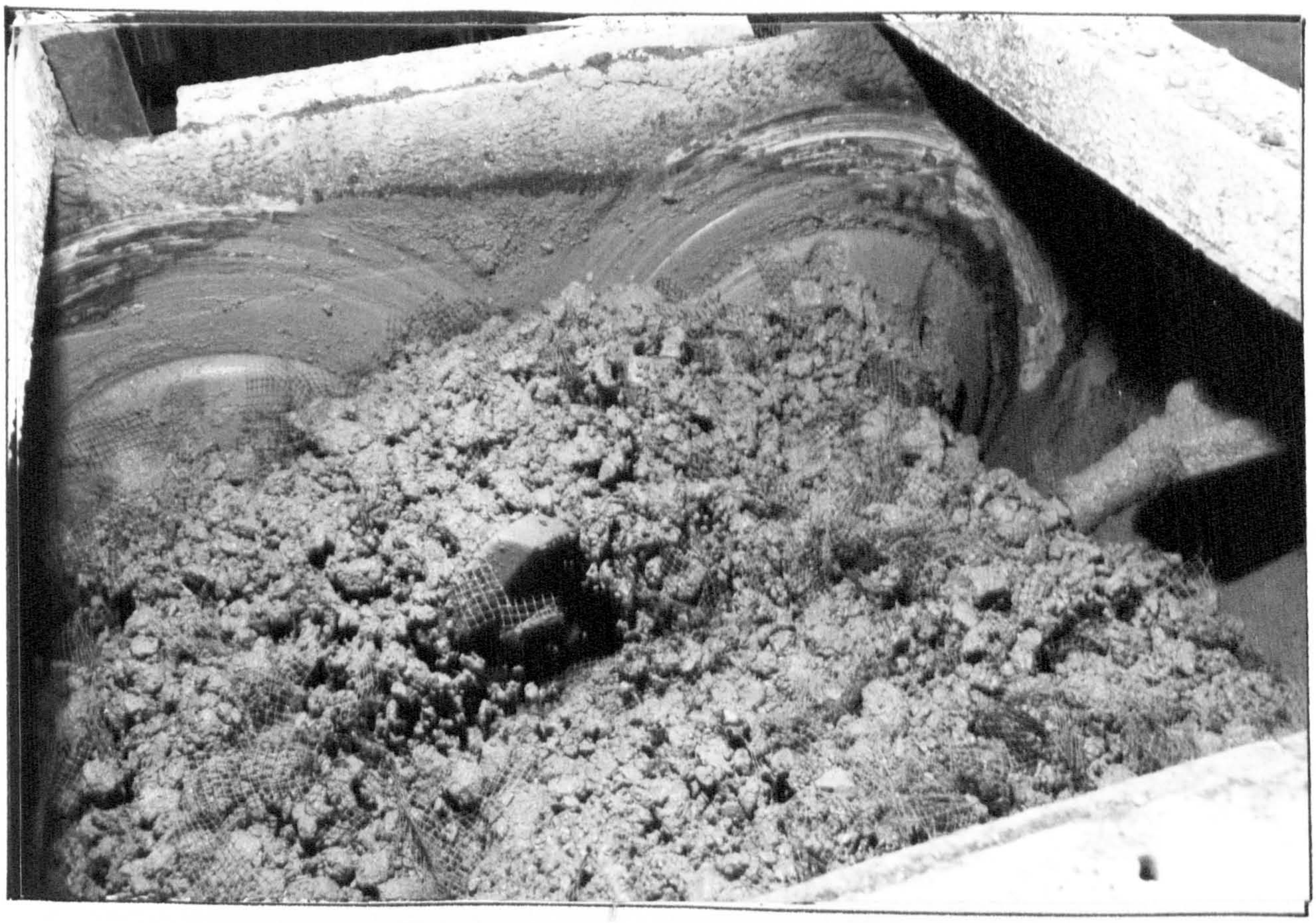

PLATE E.2 Mesh Elements and Aggregate are being Mixed in a Paddle Mixer

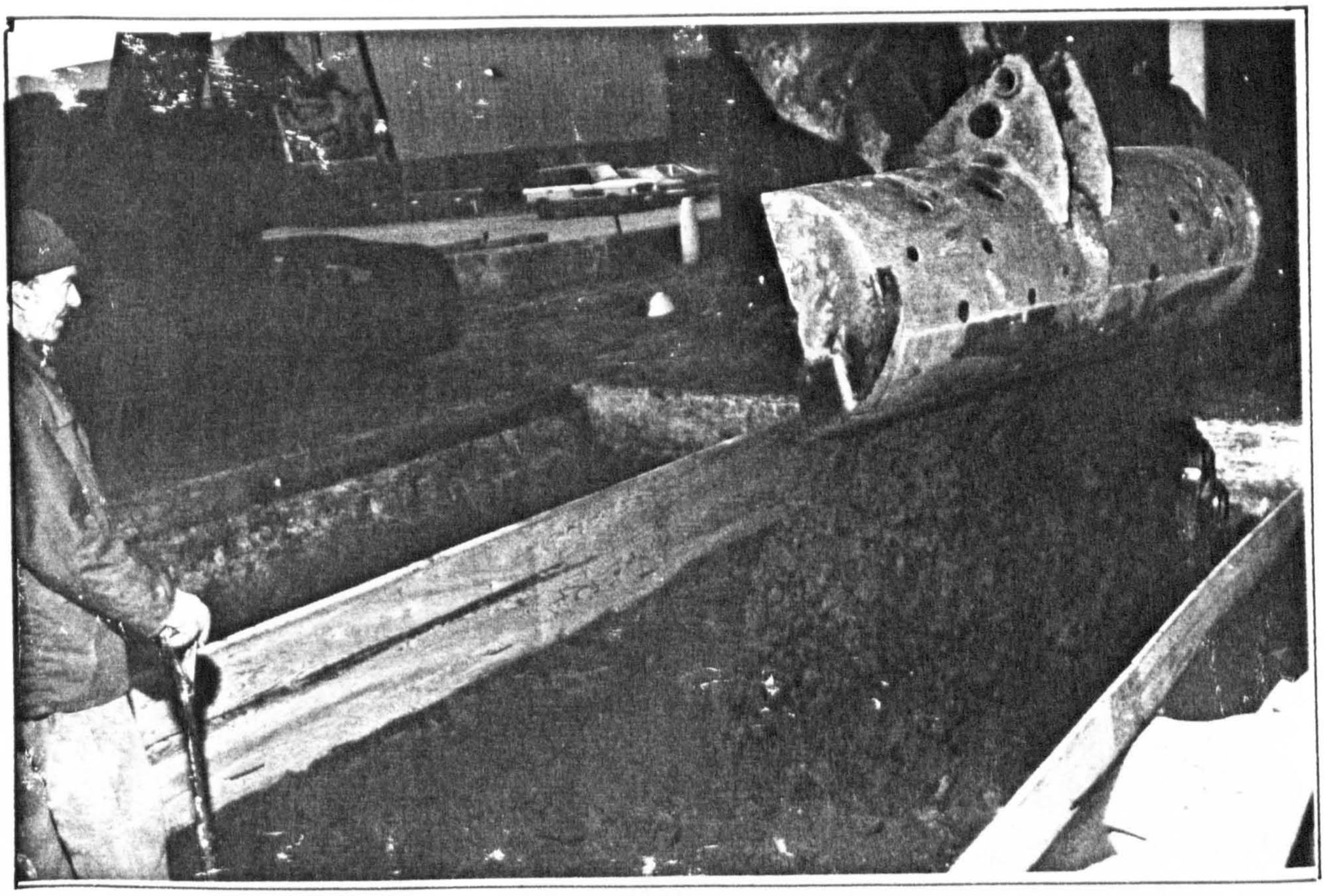

PLATE E.3 Placing of Sand Mixed with Mesh Elements into the Trial Pit

PLATE E.4 A View of Sand Mixed with Mesh Elements

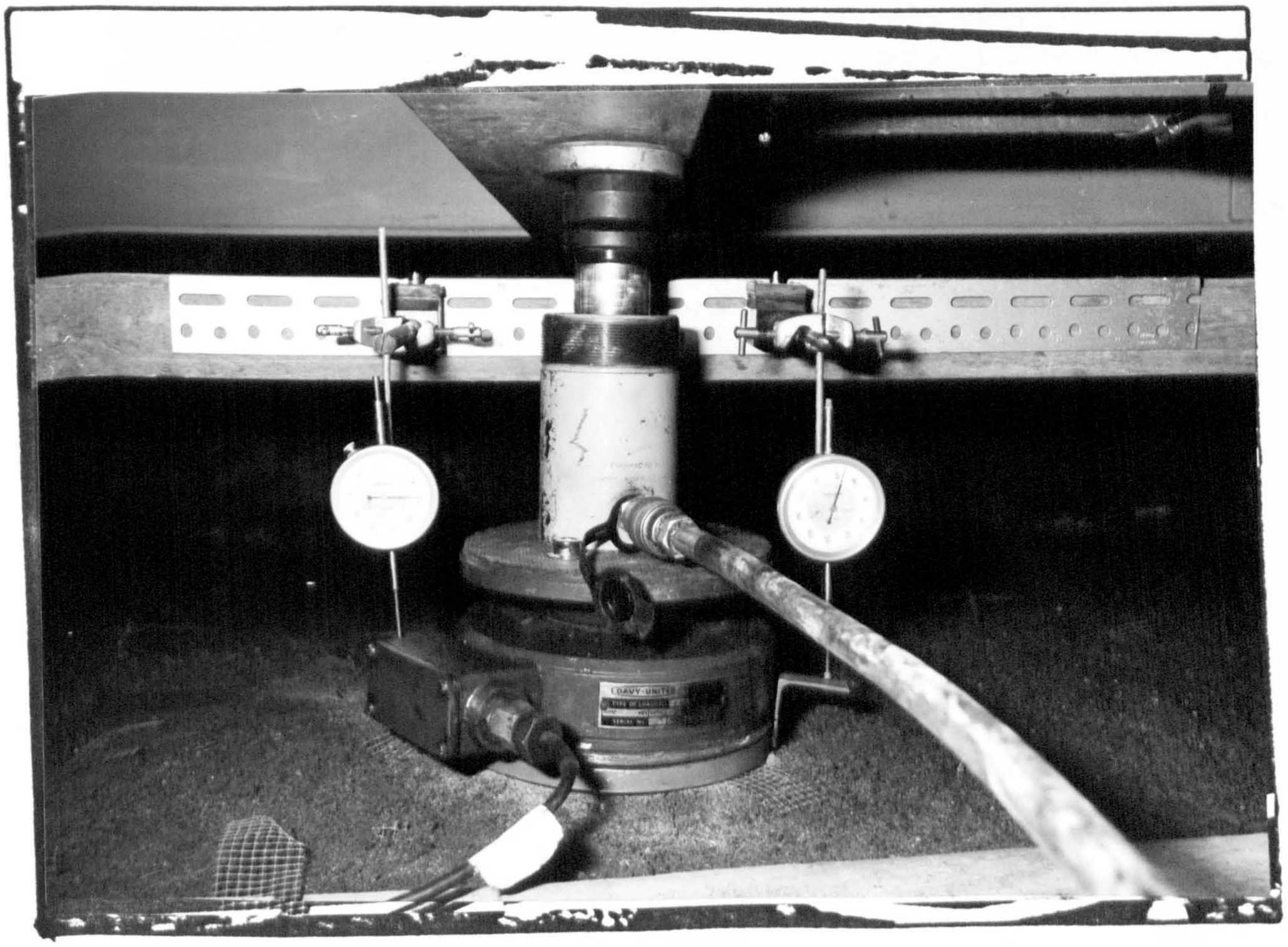

PLATE E.5 A View of Plate and Hydraulic Jack Under The Kentledge

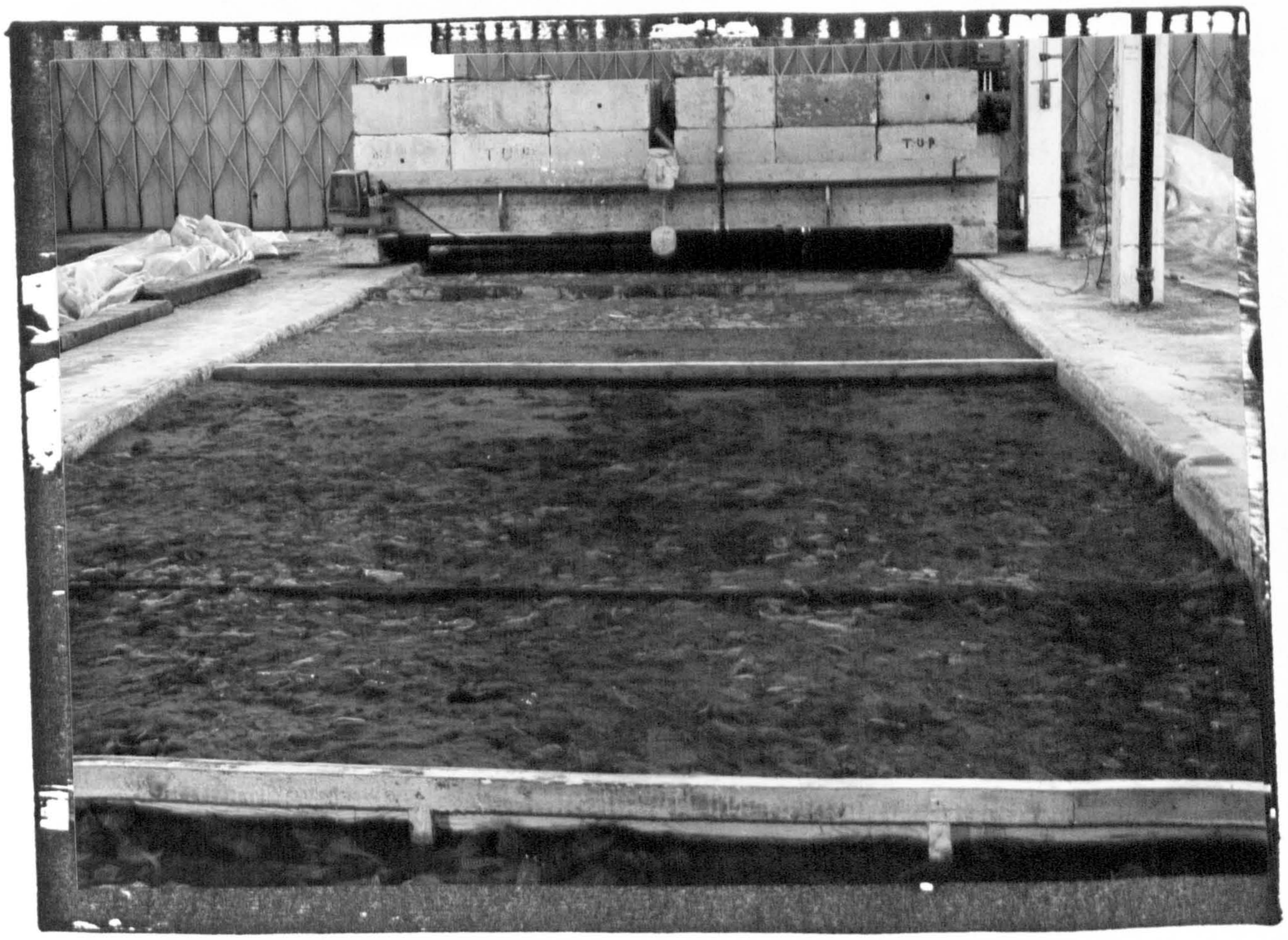

PLATE E.6 A View of the Moveable Bearing Frame

PLATE E.7 100 mm Diameter Hole After Plate-Load Bearing Tests of Sand

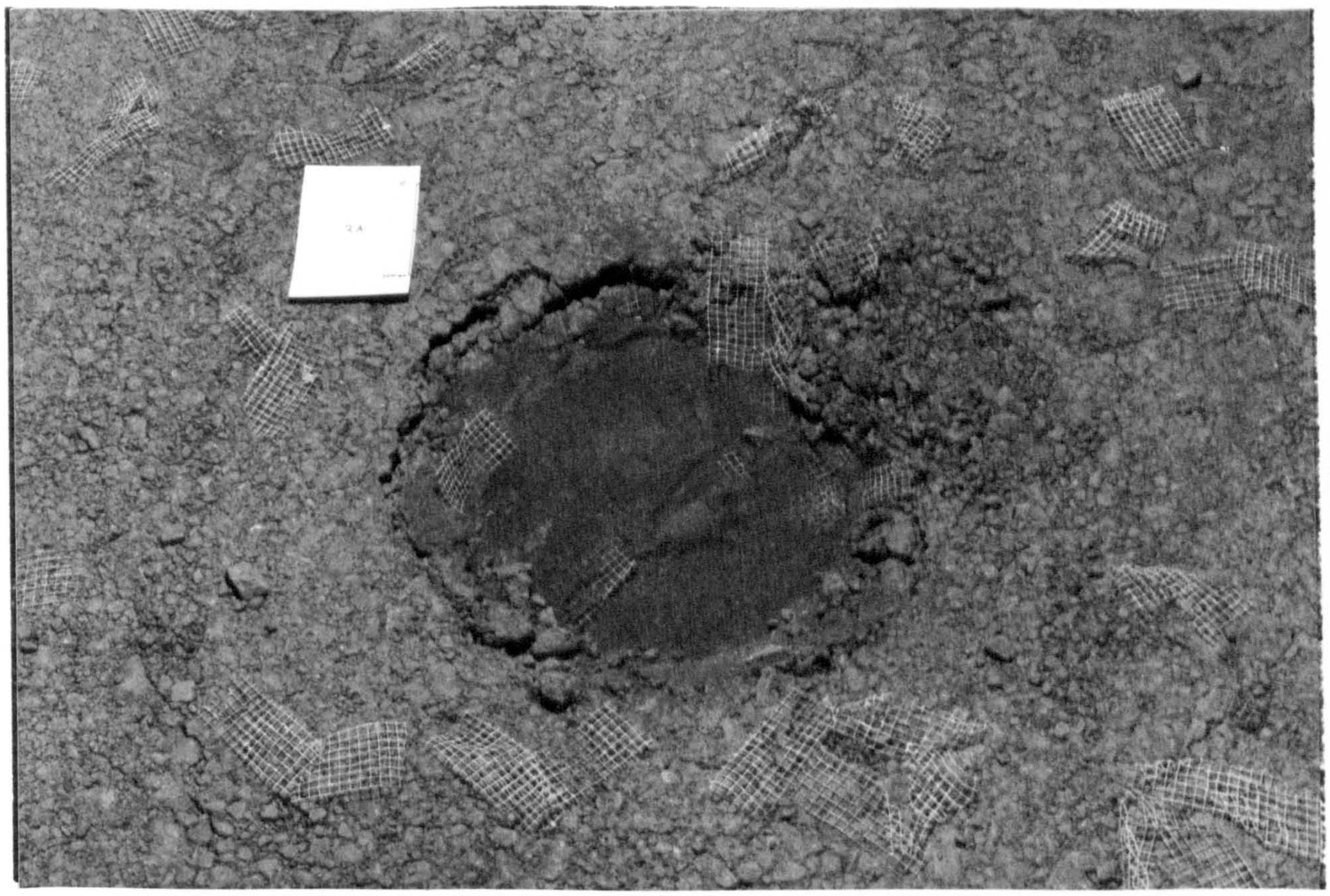

PLATE E.8 300 mm Diameter Hole After Plate-Load Bearing Tests on Aggregate

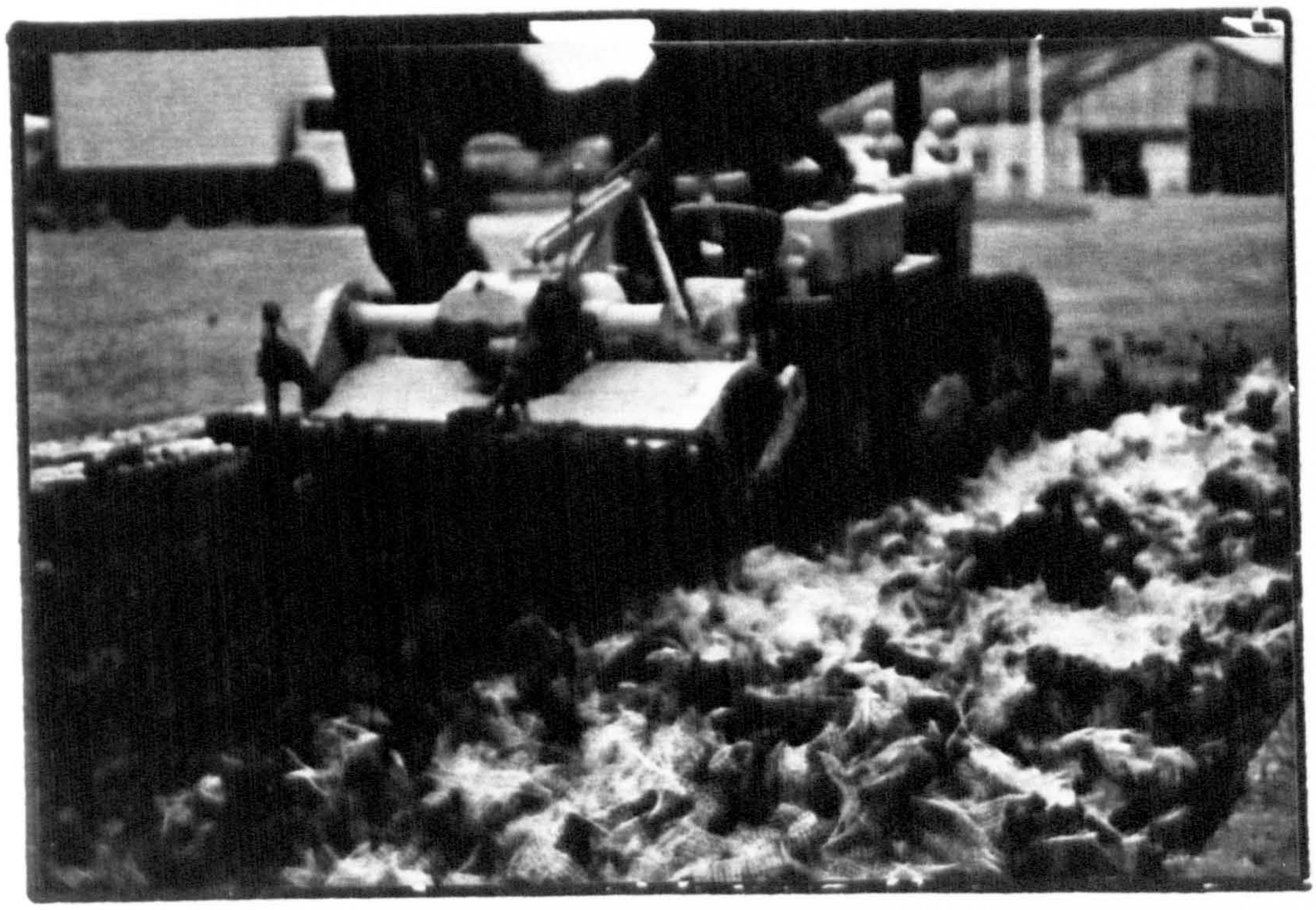

PLATE E.9 Mixing of Mesh Elements with Clay Using a Rotavator

PLATE E.10 Clay and Mesh Elements Before Rotavating

APPENDIX F

COMPARISON OF MESH TYPE 7 TO MESH TYPES 10 & 12

FIG. F.1

SOIL TYPE	MID-ROSS SAND
MESH SIZE	5 × 10 cm
MESH CONTENT	66 (m^2/m^3)

$\sigma_3 = 0\ kN/m^2$

200 mm × 155 mm diam. TRIAXIAL TEST DATA

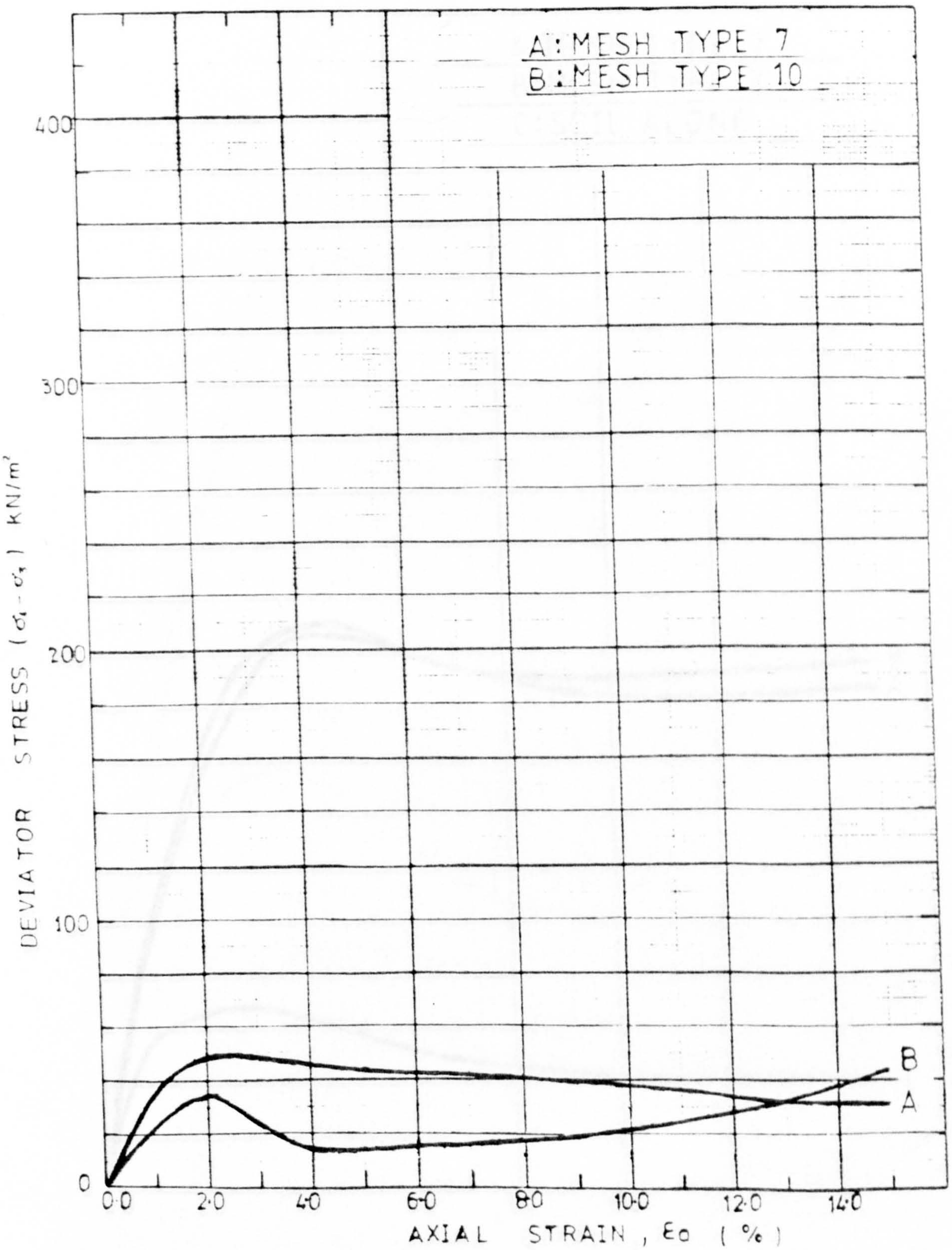

FIG. F.2

SOIL TYPE	MID-ROSS SAND
MESH SIZE	5 × 10 cm
MESH CONTENT	66 (m^2/m^3)

$\sigma_3 = 10\ kN/m^2$

200mm × 155mm diam. TRIAXIAL TEST DATA

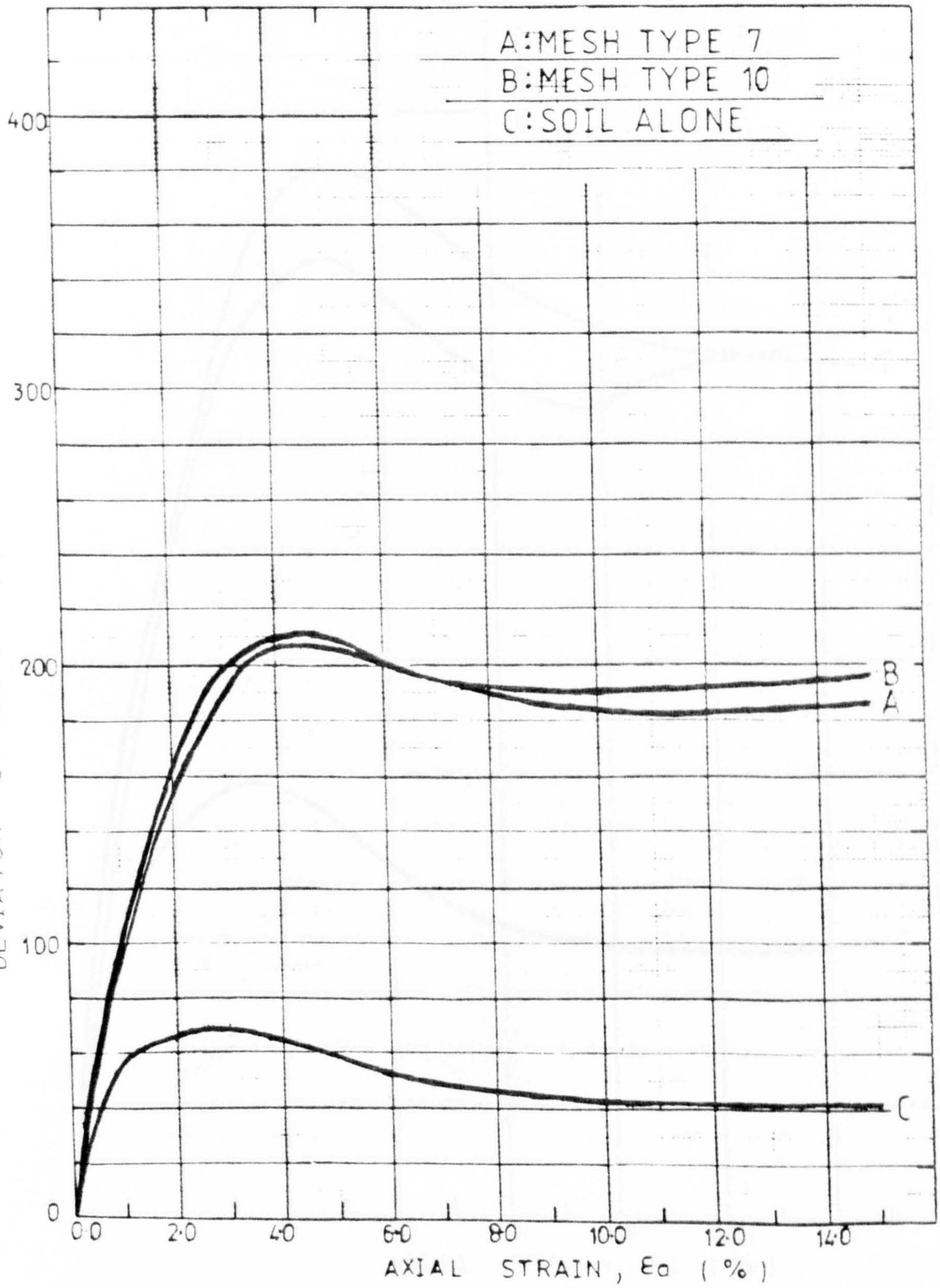

FIG. F.3

SOIL TYPE	MID-ROSS SAND
MESH SIZE	5 × 10 cm
MESH CONTENT	66 (m^2/m^3)

$\sigma_3 = 25\ kN/m^2$

200 mm × 155 mm diam. TRIAXIAL TEST DATA

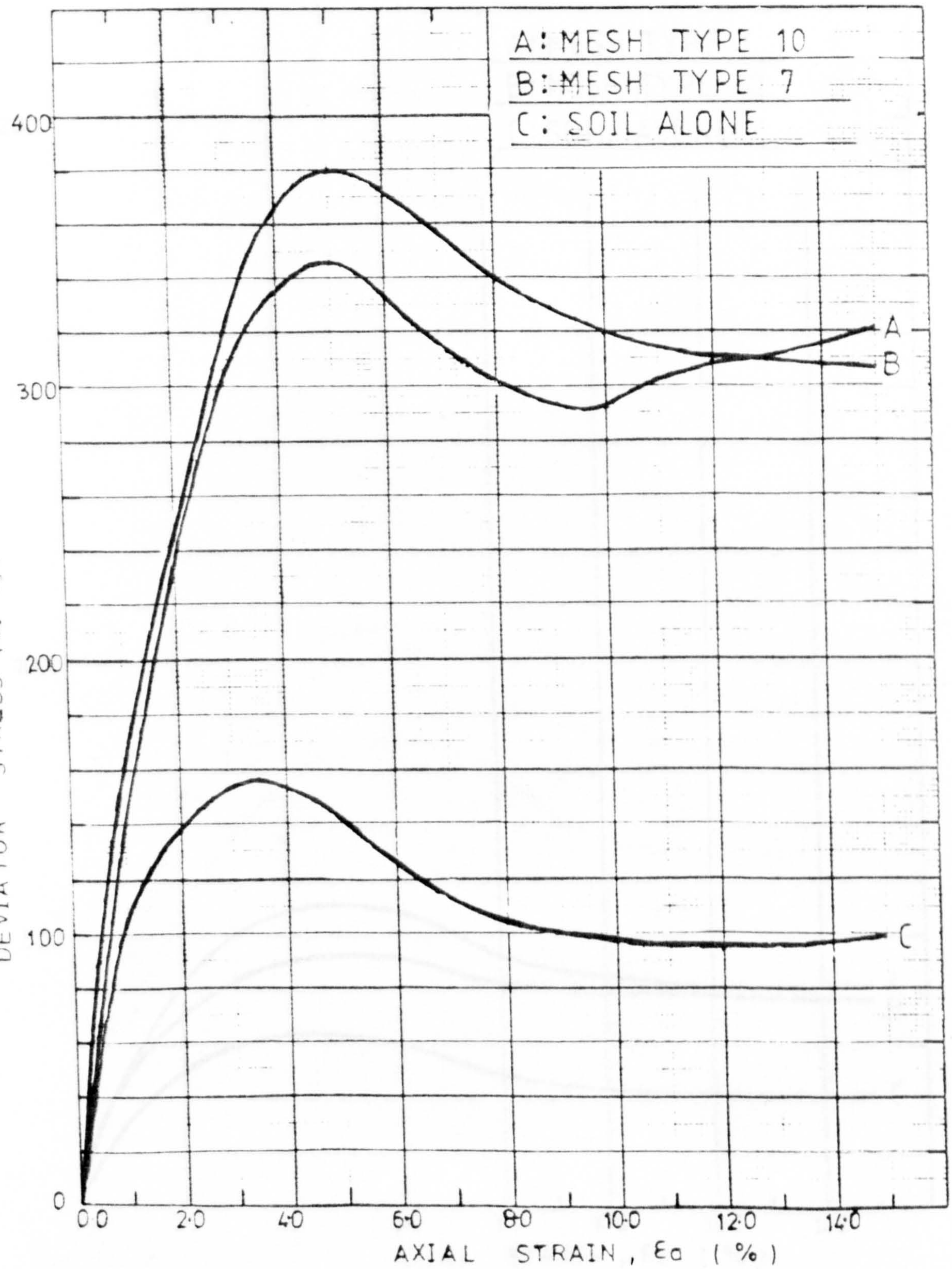

FIG. F.4

SOIL TYPE	MID-ROSS SAND
MESH SIZE	5×10 cm
MESH CONTENT	66 (m^2/m^3)

$\sigma_3 = 50\ kN/m^2$

200mm×155mm diam. TRIAXIAL TEST DATA

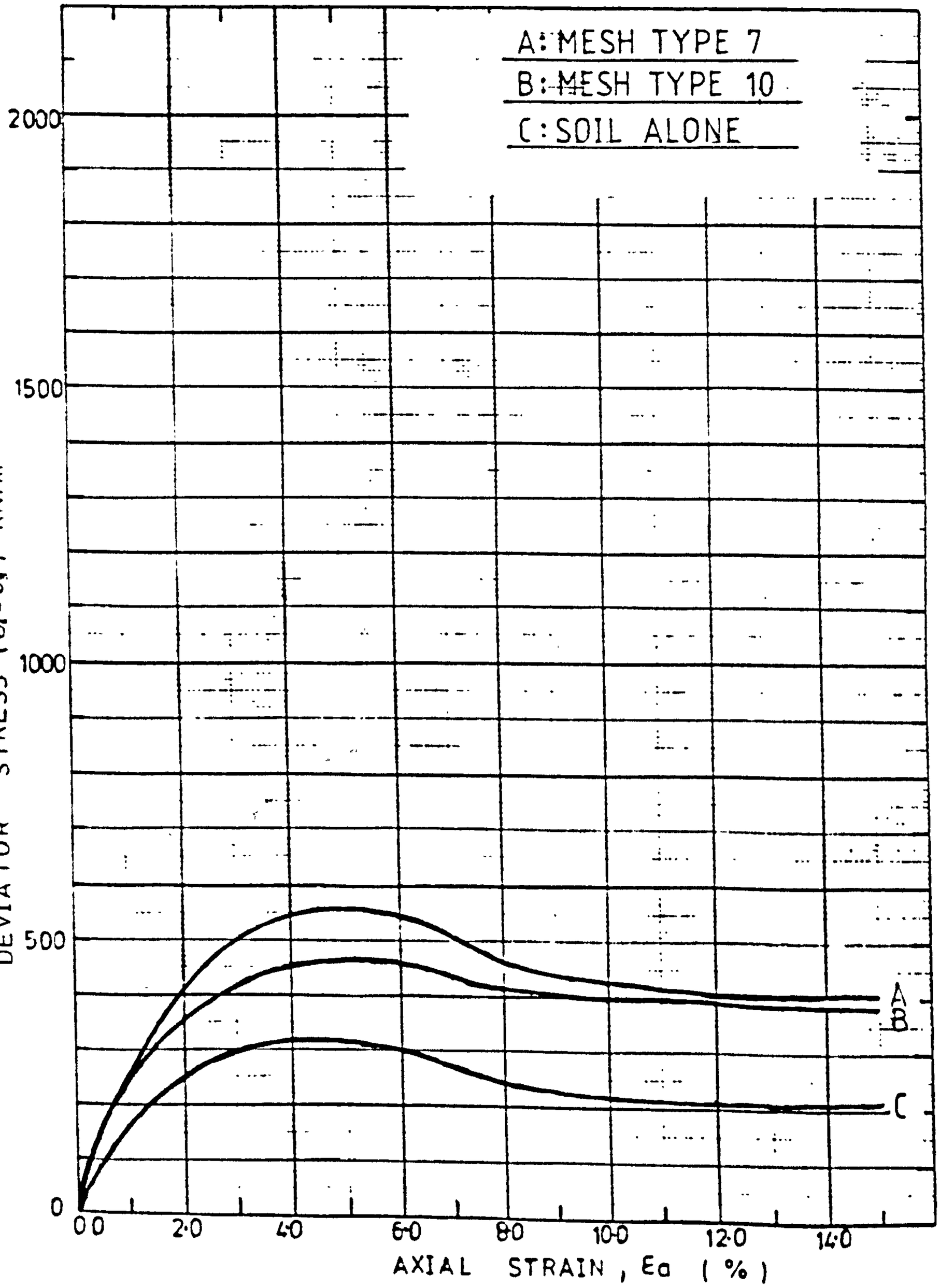

FIG. F.5

SOIL TYPE	MID-ROSS SAND
MESH SIZE	5 × 10 cm
MESH CONTENT	66 (m^2/m^3)

$\sigma_3 = 150\ kN/m^2$

200 mm × 155 mm diam. TRIAXIAL TEST DATA

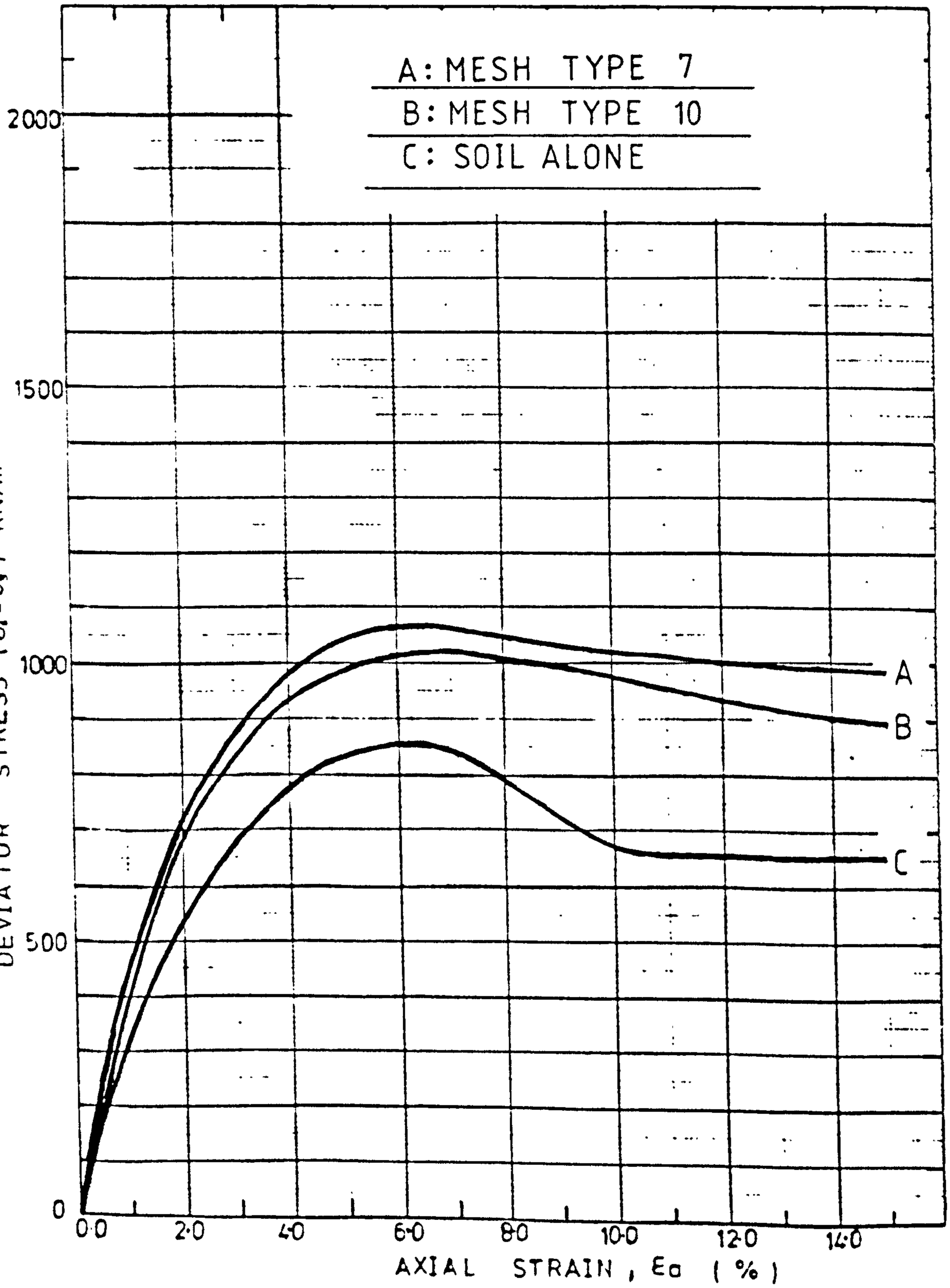

FIG. F.6

SOIL TYPE	MID-ROSS SAND
MESH SIZE	5×10 cm
MESH CONTENT	33 (m^2/m^3)

$\sigma_3 = 150^{kN/m^2}$

200mm × 155mm diam. TRIAXIAL TEST DATA

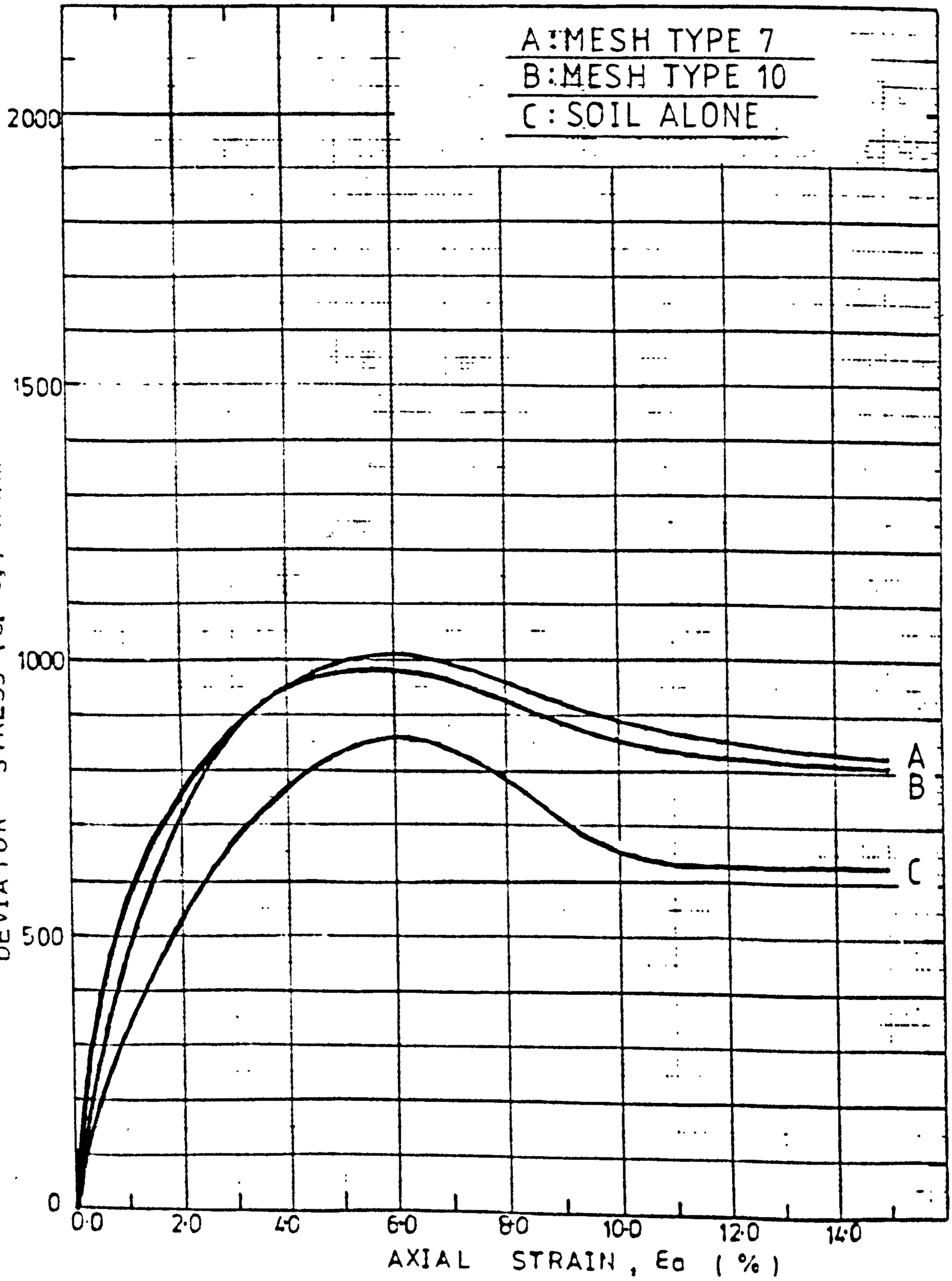

FIG. F.7

SOIL TYPE	MID-ROSS SAND
MESH SIZE	5×10 cm
MESH CONTENT	90 (m^2/m^3)

$\sigma_3 = 150\ kN/m^2$

200mm × 155mm diam. TRIAXIAL TEST DATA

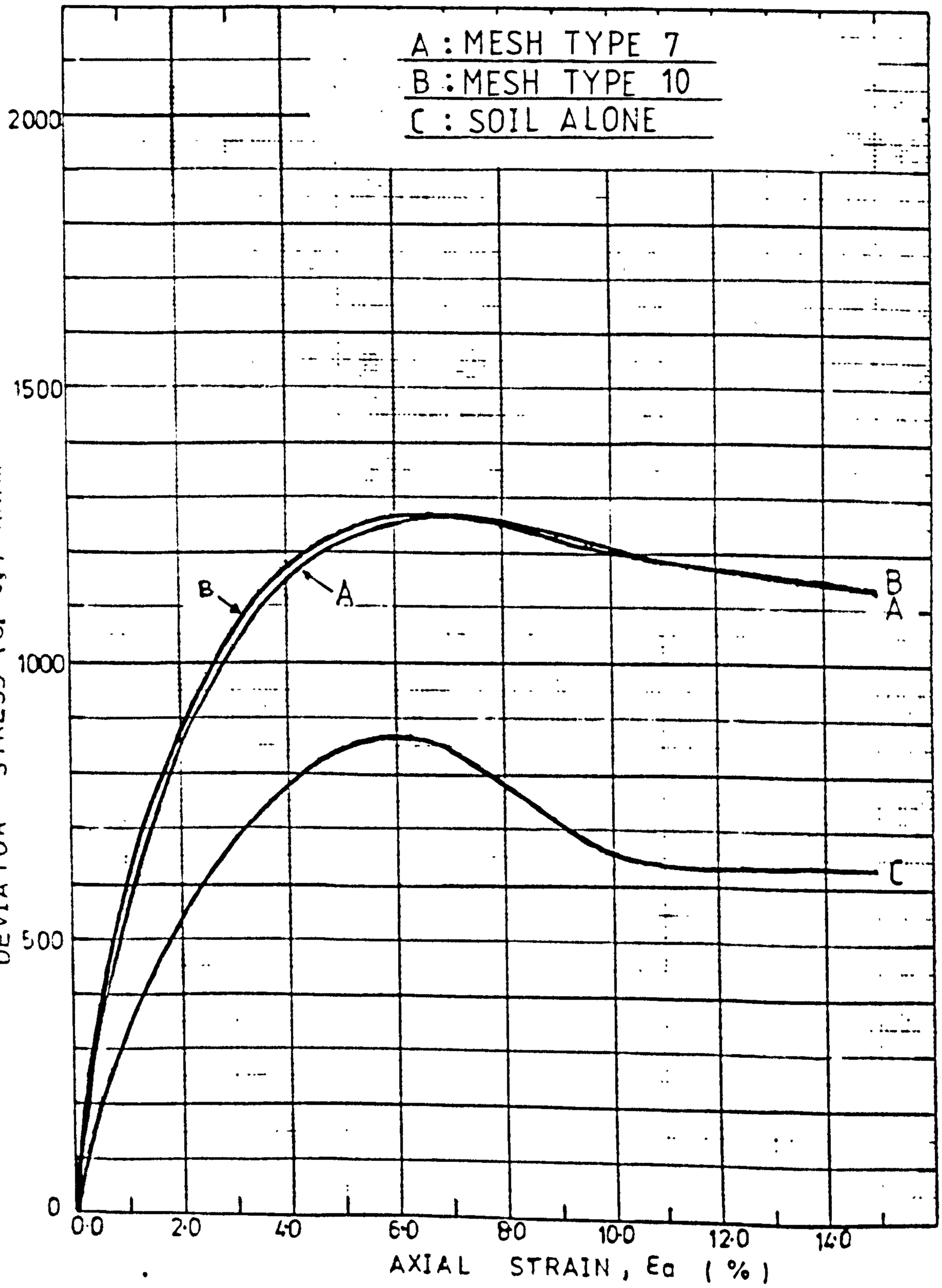

FIG. F.8

SOIL TYPE	MID-ROSS SAND
MESH SIZE	5×10 cm
MESH CONTENT	66 (m^2/m^3)

$\sigma_3 = 300\ kN/m^2$

200mm × 155mm diam. TRIAXIAL TEST DATA

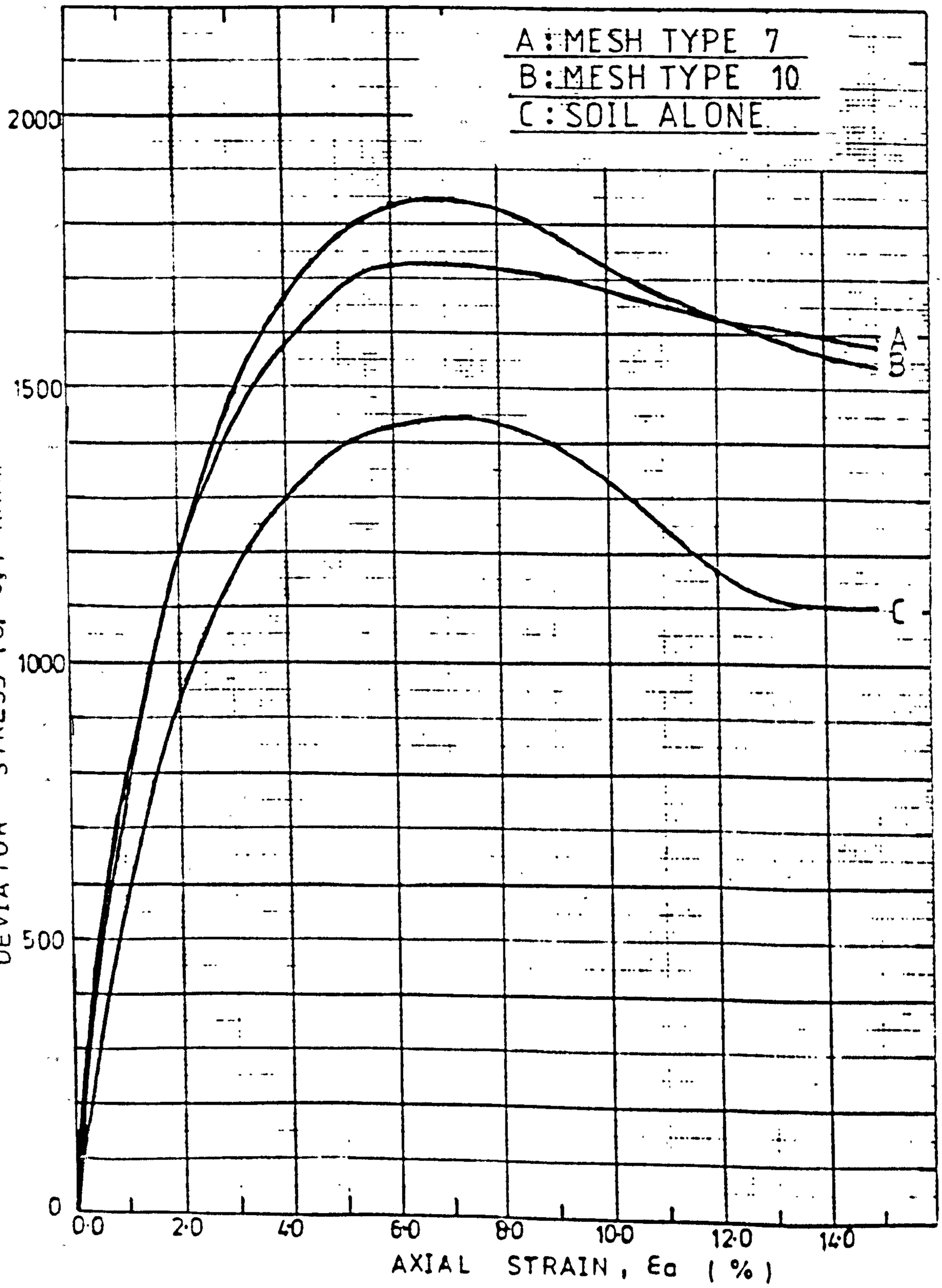

FIG. F.9

A. MID-ROSS SAND (ALONE)
B. MID-ROSS SAND + 66 m²/m³ MESH TYPE 7
C. MID-ROSS SAND + 66 m²/m³ MESH TYPE 12
D. MID-ROSS SAND + 84 m²/m³ MESH TYPE 12
E. MID-ROSS SAND + 66 m²/m³ MESH (STRIPS) 5×10 cm Type 12
F. MID-ROSS SAND + 84 m²/m³ MESH (STRIPS) 5×10 cm Type 12

200 mm × 155 mm diam. TRIAXIAL TEST DATA

σ_3 = 150 KN/m²

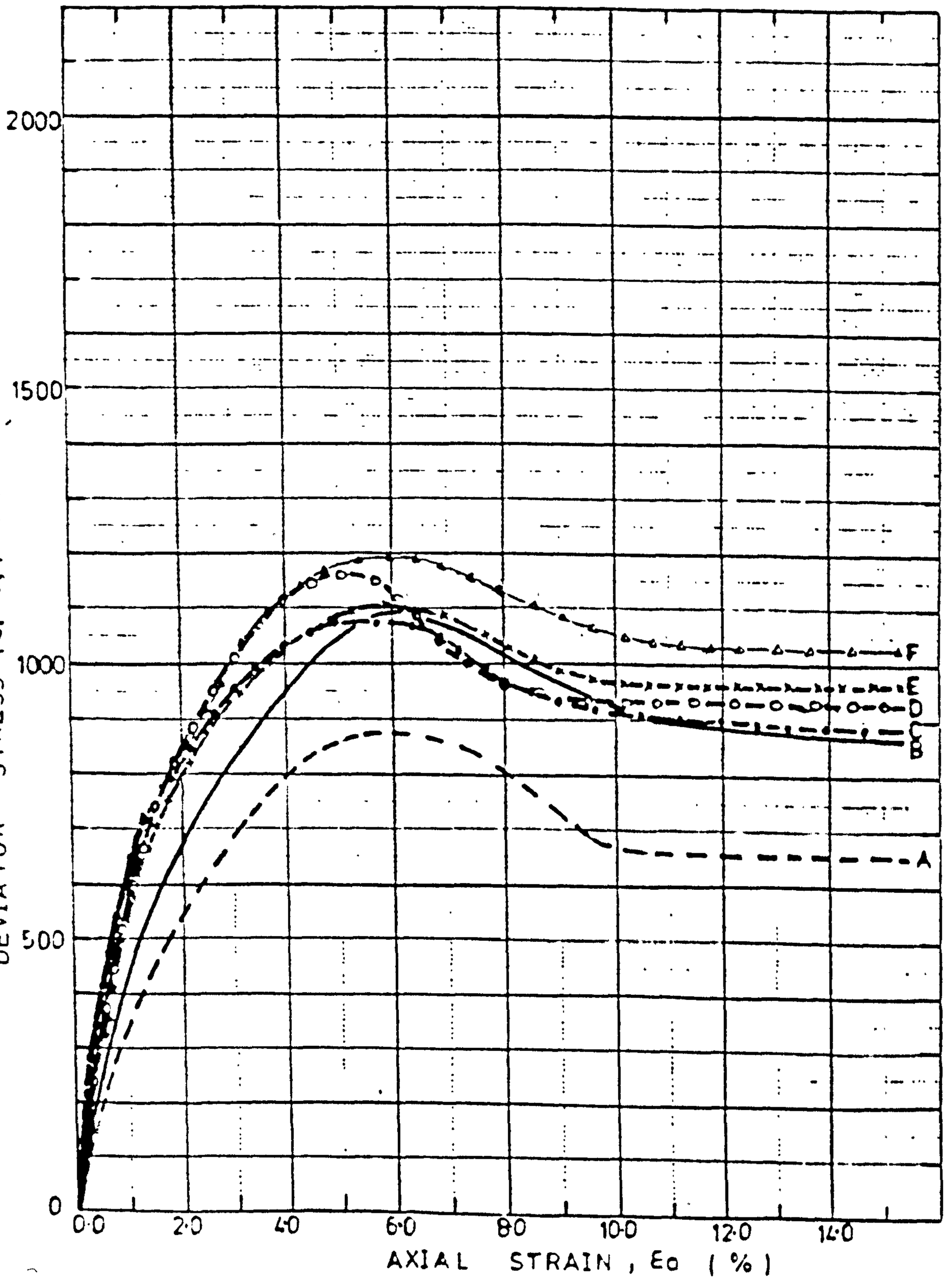

ANDRAWES*, K.Z., McGOWN*, A., MYTILIS*, N., MERCER°, F.B. and SWEETLAND°, D.B.
*Department of Civil Engineering, University of Strathclyde, U.K.
°Nellon Ltd, U.K.

THE USE OF MESH ELEMENTS TO ALTER THE STRESS-STRAIN BEHAVIOUR OF GRANULAR SOILS
L'EMPLOI DE PETITS BOUTS DE MAILLE POUR MODIFIER LA RESISTANCE A LA TRACTION DES SOLS GRANULAIRES
DIE VERWENDUNG VON MESH-ELEMENTEN ZUR AENDERUNG DER STRECKEN-SPANNUNG EIGENSCHAFTEN IN KORNIGE BODEN

Ein interessante neue Entwicklung in Geotextil-Ingenieurwesen ist die Verwendung von unorierten Verstaerkungen in kornige Boden zur Aenderung der Strecken-Spannung Eigenschaft des Bodens. Der Bericht beinhaltet die Verwendung von Mesh-Elementen, itire Anwendungen und Mischungs-Teckniken. Die Anwendburkeit von Laborunterschungen ist ebenfulls diskutiert und Weitergabe der gewonnene Test daten als Hilfemittel fuer die Ingenieure.

An exciting new development in the field of geotextile engineering is the use of randomly oriented tensile inclusions in granular soils in order to alter the stress-strain behaviour of the soils. The paper describes the use of discrete mesh elements, their applications and mixing techniques. The applicability of laboratory testing is discussed and the means of presenting the test data for the use of designers are suggested.

1. INTRODUCTION

A new development in the field of geotechnical engineering is the use of randomly oriented tensile inclusions in order to alter the stress-strain behaviour of granular soils. Various types of inclusions have been employed, such as textile fibres, metal or plastic rods and most recently mesh elements (Mercer et al, 1984 and McGown et al, 1985). The strengthening action of these mesh elements differs significantly from that of the other types of randomly oriented inclusions as the stress transfer mechanism between the soil particles and the mesh relies upon interlock and not simply surface friction, Fig. 1. The interlock occurs at two levels, with the ribs of individual mesh elements interlocking with groups of particles to form aggregations of particles and then adjecent aggregations interlocking to form a coherent matrix.

In order to achieve the maximum improvements using the minimum amount of mesh elements, the properties of the mesh must be carefully selected. Mercer et al (1984) described the important properties of the mesh required to optimise the interlock mechanism and since then extensive laboratory testing has been undertaken to identify the most efficient mesh element type for use in sandy silty materials. So far these investigations suggest that the mesh elements should have the properties given in Table 1.

Mercer et al (1984) and McGown et al (1984) have conducted laboratory C.B.R., triaxial and model footings tests to establish the improvements obtained by mixing mesh elements into granular soil. They reported rapid improvements in the measured strengths with the increase in the mesh element contents up to 0.4 to 0.5 per cent (by weight of dry soil). These were achieved without

ANDRAWES*, K.Z., McGOWN*, A., HYDARIS*, N., MERCER*, F.B. and SKEELAND*, D.B.
*Department of Civil Engineering, University of Strathclyde, U.K.
*Nelton Ltd, U.K.

THE USE OF MESH ELEMENTS TO ALTER THE STRESS-STRAIN BEHAVIOUR OF GRANULAR SOILS
L'EMPLOI DE PETITS BOUTS DE MAILLE POUR MODIFIER LA RESISTANCE A LA TRACTION DES SOILS GRANULAIRES
DIE VERWENDUNG VON MESH-ELEMENTEN ZUR AENDERUNG DER STRECKEN-SPANNUNG EIGENSCHAFTEN IN KORNIGE BODEN

reduction in the dry density of the soil or change in permeability of the mass, the latter being a significant advantage over alternative soil stabilisation techniques, such as lime, cement or bituminous stabilisation.

In practice, the amount of mesh elements employed could well be less than the maximu, being dependent on the level of improvement required in various applications and limited by the efficiency of on-site mixing techniques. So far field trials suggest that in a wide range of applications mesh contents of between 0.1 and 0.2 per cent will be required and that these can be efficiently mixed on-site using a number of different techniques.

In this paper, a number of the applications so far identified are presented and the suitability of a variety of on-site mixing techniques are considered. The applicability of various test methods is then discussed and the means of presenting test data for the use of designers are suggested.

2. APPLICATIONS FOR MESH ELEMENTS

A wide variety of end uses are envisaged for mesh elements mixed in granular soils with or without the addition of other stabilising agents such as lime, cement and bitumen. To date the field trials undertaken have been restricted to mesh element contents of 0.1 to 0.2 per cent in silty and sandy soils with no other stabilising agents involved. The types of applications are illustrated diagrmatically in Fig. 2.

3. METHODS OF MIXING

The method of mixing adopted must always ensure that the mesh elements are randomly oriented and uniformly distributed within the soil mass. Both the batching and in-situ mixing trials carried out so far, suggest that this canb e effectively and economically achieved by a variety of techniques. The selection of which technique to use on any particular site is dependent on the rate of production required. Table 2 indicates the production rates of a number of mixing techniques and some of the mixing trials are illustrated in Figs 3 to 5.

•The soil to be mixed in-situ should be near its optimum moisture content for maximum density. Soils wetter than optimum may be treated but with the addition of lime or cement. Soils drier than optimum should have water added prior to mixing mesh elements.

ANDRAWES*, K.Z., McGOWN*, A., MYTILIS*, N., MERCER*, F.B. and SKEELAND*, D.B.
*Department of Civil Engineering, University of Strathclyde, U.K.
*Netlon Ltd, U.K.

THE USE OF MESH ELEMENTS TO ALTER THE STRESS-STRAIN BEHAVIOUR OF GRANULAR SOILS
L'EMPLOI DE PETITS BOUTS DE MAILLE POUR MODIFIER LA RESISTANCE A LA TRACTION DES SOLS GRANULAIRES
DIE VERWENDUNG VON MESH-ELEMENTEN ZUR AENDERUNG DER STRECKEN-SPANNUNG EIGENSCHAFTEN IN KORNIGE BODEN

A. METHODS OF TESTING AND DATA PRESENTATION

On site, it will be necessary to check that the mixing technique has uniformly distributed the mesh elements within the soil. This can be simply achieved by taking arepresentative size sample and determining the per cent of mesh elements (by dry weight of soil) present in the sample. To measure the improvement in stress-strain properties attained by mixing in the mesh elements, it is suggested that plate bearing tests will provide the most effective means of in-situ testing in many situations. For pavements and similar applications, however, the in-situ C.B.R. test may prove to be suitable.

Normally for design purposes, laboratory testing will be undertaken. A requirement for this must be that the laboratory test specimen is representative of the in-situ soil-mesh element mixture. Care must therefore be taken to ensure that the mixing at laboratory scale ensures randomly oriented and uniformly distributed mesh elements. Also the test specimen sizes must be sufficiently large to allow the mesh elements to strain in the same manner as would occur in-situ. Further the mode of stressing should be as similar as possible to that in-situ.

Within the laboratory test programme at the University of Strathclyde, C.B.R., triaxial and model footing tests have been conducted. Of these the most useful has proven to be the triaxial testing carried out with monotonic or repeated loading. In both cases, it became apparent that the level of improvement was related to the strain levels induced within the soil. Thus it is suggested that measured improvements in the strength of soil by the inclusion of mesh elements should always be reported at equal strain conditions (with and without mesh elements). Figure 6 shows the Mohr envelopes for a fluvio-glacial silty sand with and without mesh elements at 1 and 15 per cent axial strains. Clearly the measured improvements vary with strain level and are different to those to be deduced from Fig. 7, which shows the Mohr envelopes for the more conventional peak stress (unequal strain condition). It is therefore suggested that for design purposes it would be most useful if test data were to be presented in terms of equal strain data.

From Figs. 6 and 7 it is also apparent that the Mohr envelope is non-linear, particularly at confining stress levels less than 50 kN/m^2. It is therefore recommended that this envelope be represented for design purposes as bi-linear envelope constructed in the manner shown in Fig. 8. The selection of 50 kN/m^2 as the "break" confining stress is based on a wide range of data obtained with different soils and the mesh element type with the properties described in Table 1, but this may not always be appropriate.

ANDRAWES*, K.Z., McGOWN*, A., HYTIRIS*, N., MERCER*, F.B. and SWEILAND*, D.B.
*Department of Civil Engineering, University of Strathclyde, U.K.
Netlon Ltd, U.K.

THE USE OF MESH ELEMENTS TO ALTER THE STRESS-STRAIN BEHAVIOUR OF GRANULAR SOILS
L'EMPLOI DE PETITS BOUTS DE MAILLE POUR MODIFIER LA RESISTANCE A LA TRACTION DES SOLS GRANULAIRES
DIE VERWENDUNG VON MESH-ELEMENTEN ZUR AENDERUNG DER STRECKEN-SPANNUNG EIGENSCHAFTEN IN KORNIGE BODEN

5. CONCLUSIONS

A wide variety of applications have been identified for the use of randomly oriented mesh elements mixed in granular soil. Mixing the mesh elements into granular soils can be effectively achieved using either batch or in-situ mixing. However, it is important to ensure that the mesh elements are randomly oriented within the soil mass.

As the level of improvement depends, among other factors, on the strain level induced in the soil, it is recommended that the measured strengths of the soil with and without mesh elements should be reported at equal strain conditions when using triaxial test data. Also due to the curvilinear nature of the Mohr's envelope a simplified bi-linear envelope is recommended to represent, for design purposes, the soil-mesh behaviour.

ACKNOWLEDGEMENTS

The work described in this paper has been carried out at the University of Strathclyde with the financial support of Netlon Ltd. It is based on fundamental reseearch conducted by F. Brian Mercer and patent applications have been filed in a large number of countries.

REFERENCES

Mercer, F.B., Andrawes, K.Z., McGown, A. and Hytiris, N. "A new method of soil stabilisation", Proc, Conf. on Polymer Grid Reinforcement, Thomas Telford, London, 1984, p. 244-249.

McGown, A., Andrawes, K.Z., Hytiris, N. and Mercer, F.B., "Soil strengthening using randomly distributed mesh elements", Proc. XI Int. Conf. S.M.F.E., Balkema, San Francisco, 1985, p. 1735 - 1738.

ANDRAWES*, K.Z., McGOWN*, A., MYTIRIS*, N., MERCER°, F.B. and SUTHERLAND°, D.B.
*Department of Civil Engineering, University of Strathclyde, U.K.
°Mellon Ltd, U.K.

THE USE OF MESH ELEMENTS TO ALTER THE STRESS-STRAIN BEHAVIOUR OF GRANULAR SOILS
L'EMPLOI DE PETITS BOUTS DE MAILLE POUR MODIFIOR LA RESISTANCE A LA TRACTION DES SOLS GRANULAIRES
DIE VERWENDUNG VON MESH-ELEMENTEN ZUR AENDERUNG DER STRECKEN-SPANNUNG EIGENSCHAFTEN IN KORNIGE BODEN

Table 1. Properties of the mesh elements

Rib/Mesh Properties	
Rib Dimensions:	0.6 x 0.4 mm
Mesh Opening Sizes:	10 x 10 mm
Polymer:	Polypropylene
Element Properties	
Element Dimensions:	100 x 50 mm
Mass per Unit Area:	45 g/m²
Tensile° Properties:	
Machine Direction	4.3 kN/m
Cross Machine Direction	3.8 kN/m

°Constant Rate of Strain Test at 2% strain/min at 20°C.

Table 2. Methods of mixing

METHOD	DESCRIPTION
Batch Mixing	
Manual techniques	Production rate < 2 m³/hr, batch volume 0.1 to 0.3 m³, Fig. 3
Small rotary drum (concrete) and Pan mixers	Production rate < 2 m³/hr, batch volume < 1 m³
Mobile truck (concrete) mixers	Production rate 2 to 40 m³/hr, batch volume 1 to 2 m³, Fig. 4
Continuous (Paddle/Pug Mill) mixers	Production rate > 40 m³/hr, suitable for large projects only
In-situ Mixing°	
Hand controlled (horticultural) rotavators	Production rate < 2 m³/hr, several passes may be required with effective depth of 100 to 200 mm
Tractor (agricultural) rotavator	Production rate 2 to 40 m³/hr, several passes may be required with effective depty of 150 to 300 mm
Bomag MPH 100 Recycler	Production rate < 40 m³/hr, single pass only may be required to mix to depths of 250 to 350 mm, Fig. 5.

ANDRAWES*, K.Z., McGOWN*, A., MYTILIS*, N., MERCER*, F.B. and SWEETLAND*, D.B.
*Department of Civil Engineering, University of Strathclyde, U.K.
*Nellon Ltd, U.K.

THE USE OF MESH ELEMENTS TO ALTER THE STRESS-STRAIN BEHAVIOUR OF GRANULAR SOILS
L'EMPLOI DE PETITS BOUTS DE MAILLE POUR MODIFIER LA RESISTANCE A LA TRACTION DES SOILS GRANULAIRES
DIE VERWENDUNG VON MESH-ELEMENTEN ZUR AENDERUNG DER STRECKEN-SPANNUNG EIGENSCHAFTEN IN KORNIGE BODEN

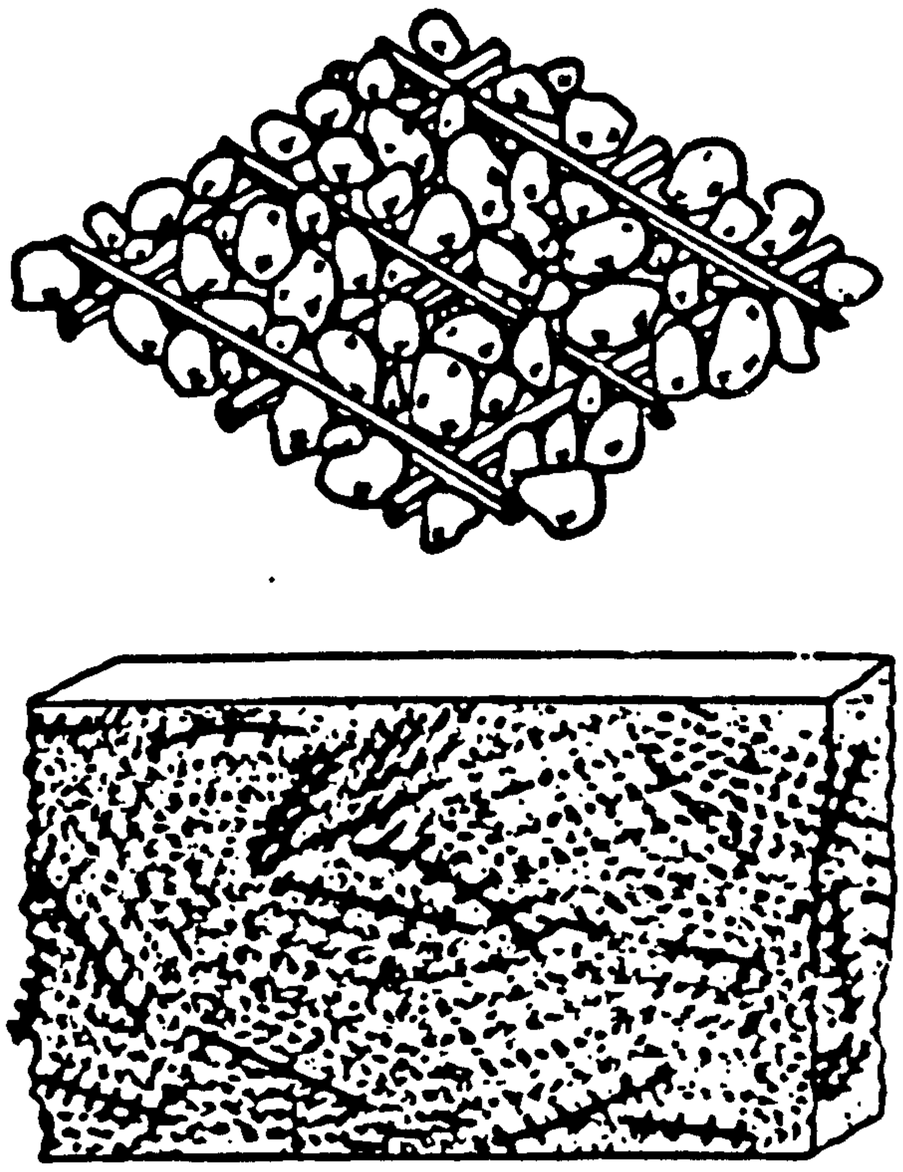

Fig. 1. The interlock mechanism for mesh elements.
(a) Interlock with groups of particles
(b) Interlock of adjacent aggregations.

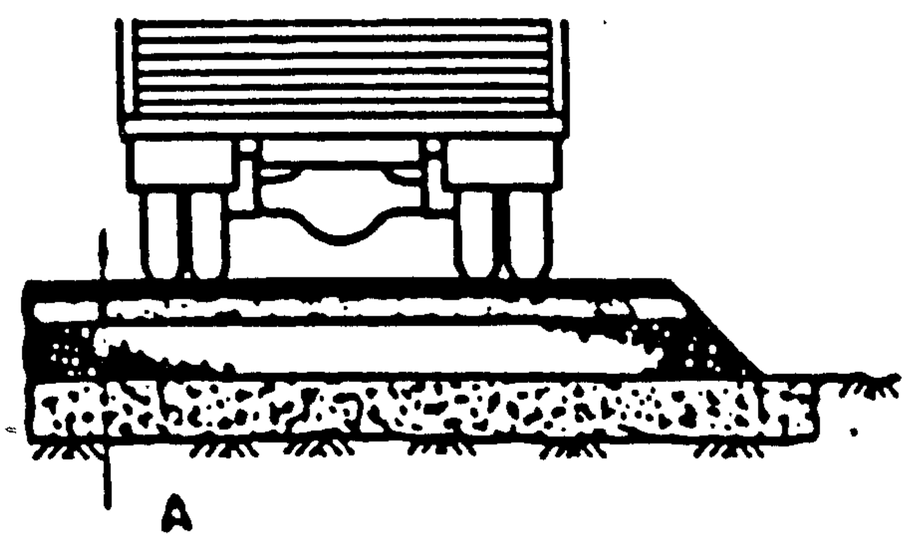

A. Permanent roads - subgrade

Fig. 2. APPLICATIONS FOR MESH ELEMENTS

ANDRAWES*, K.Z., McGOWN*, A., HYTIRIS*, N., MERCER*, F.B. and SKEITLAND*, D.B.
*Department of Civil Engineering, University of Strathclyde, U.K.
*Netlon Ltd, U.K.

THE USE OF MESH ELEMENTS TO ALTER THE STRESS-STRAIN BEHAVIOUR OF GRANULAR SOILS
L'EMPLOI DE PETITS BOUTS DE MAILLE POUR MODIFIER LA RESISTANCE A LA TRACTION DES SOILS GRANULAIRES
DIE VERWENDUNG VON MESH-ELEMENTEN ZUR AENDERUNG DER STRECKEN-SPANNUNG EIGENSCHAFTEN IN KORNIGE BODEN

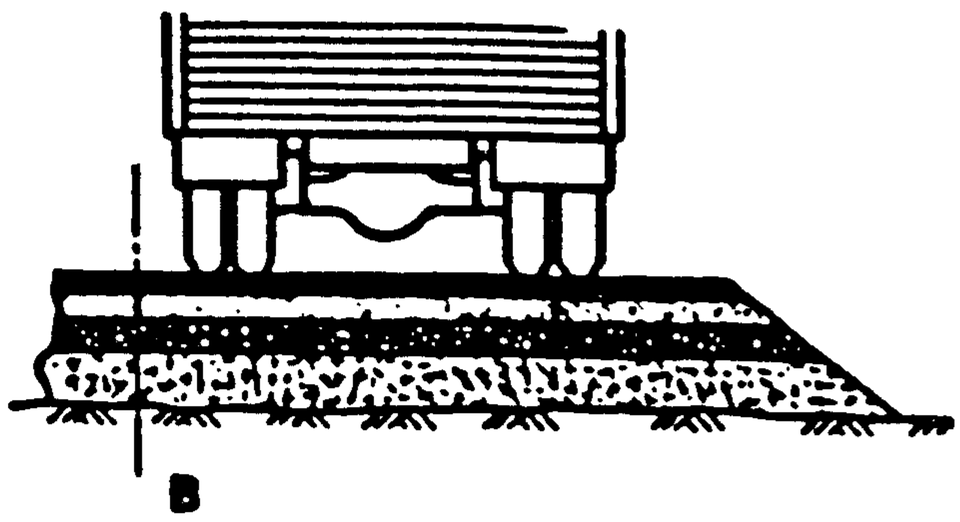

B. Permanent roads - capping layers

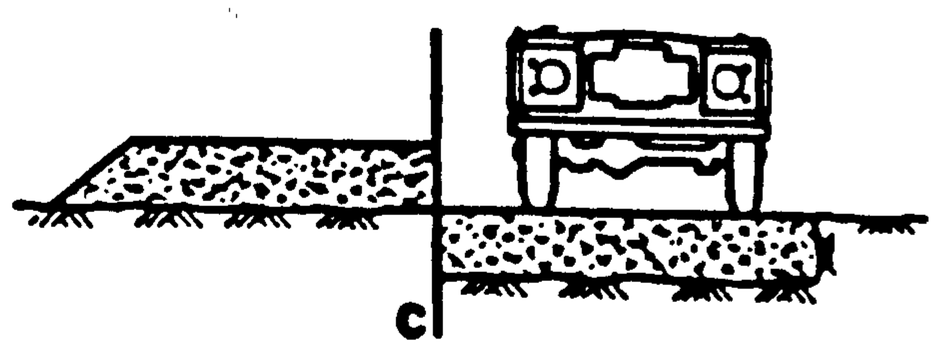

C. Unbound roads

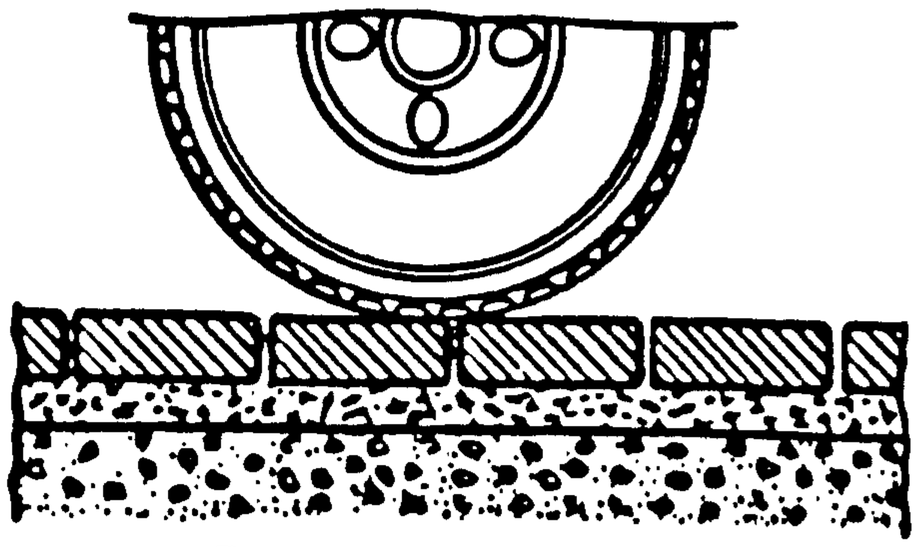

D. Concrete blocks and paved areas

E. Repairs to excavations in roads

Fig. 2. (contd.) APPLICATIONS FOR MESH ELEMENTS

ANDRAWES*, K.Z., McGOWN*, A., HYTIRIS*, N., MERCER*, F.B. and SWEETLAND*, D.B.
*Department of Civil Engineering, University of Strathclyde, U.K.
*Netlon Ltd, U.K.

THE USE OF MESH ELEMENTS TO ALTER THE STRESS-STRAIN BEHAVIOUR OF GRANULAR SOILS
L'EMPLOI DE PETITS BOUTS DE MAILLE POUR MODIFIER LA RESISTANCE A LA TRACTION DES SOLS GRANULAIRES
DIE VERWENDUNG VON MESH-ELEMENTEN ZUR AENDERUNG DER STRECKEN-SPANNUNG EIGENSCHAFTEN IN KORNIGE BODEN

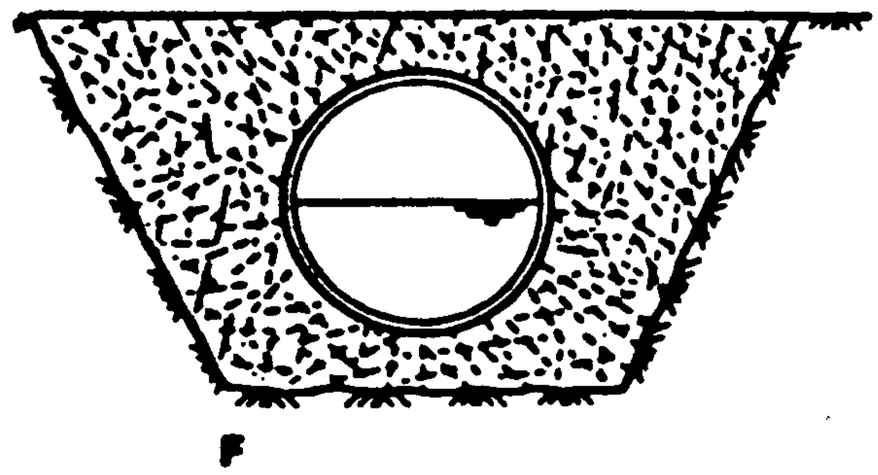

F

F. Bakcfill to pipe trenches

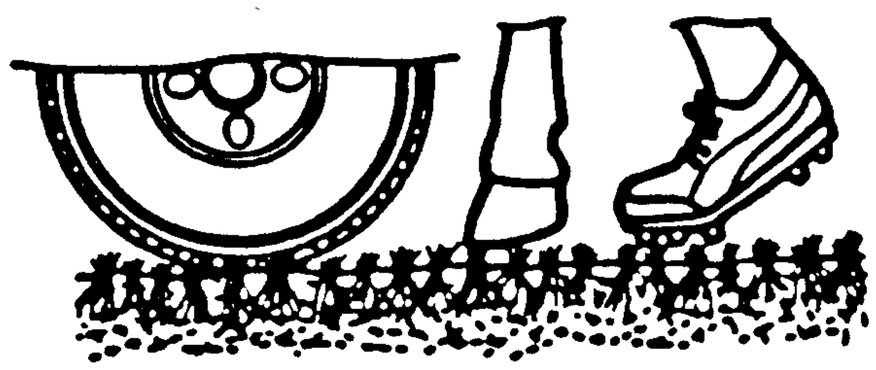

G

G. Sports turf and reinforced grass

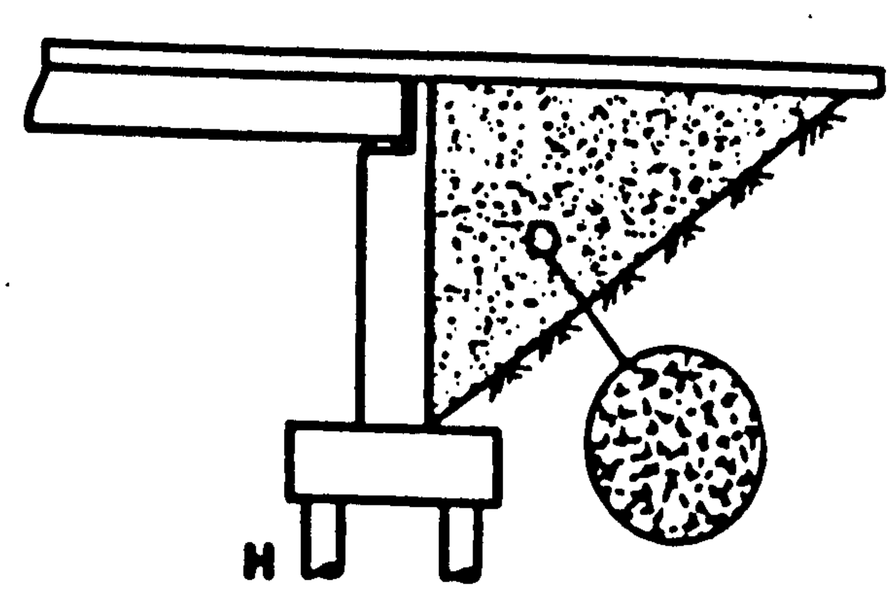

H

H. Backfill to bridge abutments

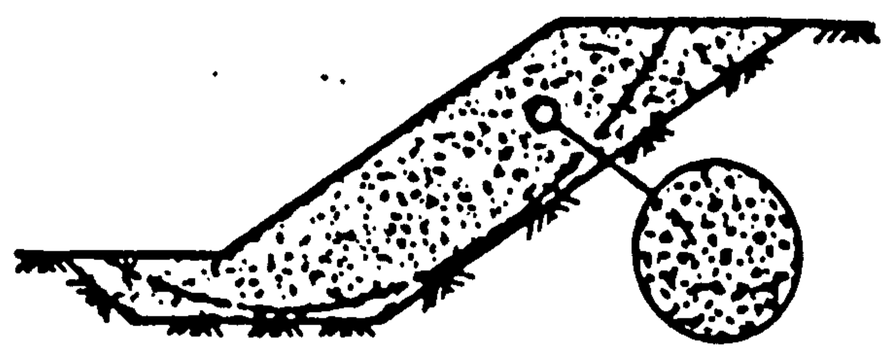

I

I. Slope failure repairs

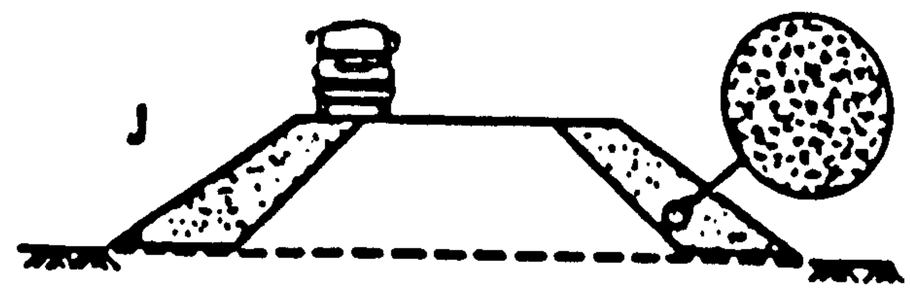

J

Fig. 2. (contd.) APPLICATIONS FOR MESH ELEMENTS

ANDRAWES*, K.Z., McGOWN*, A., WYLLRIS*, N., MERCER*, F.B. and SWEETLAND*, D.B.
*Department of Civil Engineering, University of Strathclyde, U.K.
*Netlon Ltd., U.K.

THE USE OF MESH ELEMENTS TO ALTER THE STRESS-STRAIN BEHAVIOUR OF GRANULAR SOILS
L'EMPLOI DE PETITS BOUTS DE MAILLE POUR MODIFIER LA RESISTANCE A LA TRACTION DES SOLS GRANULAIRES
DIE VERWENDUNG VON MESH-ELEMENTEN ZUR AENDERUNG DER STRECKEN-SPANNUNG EIGENSCHAFTEN IN KORNIGE BODEN

J. Reinforcing embankment slopes

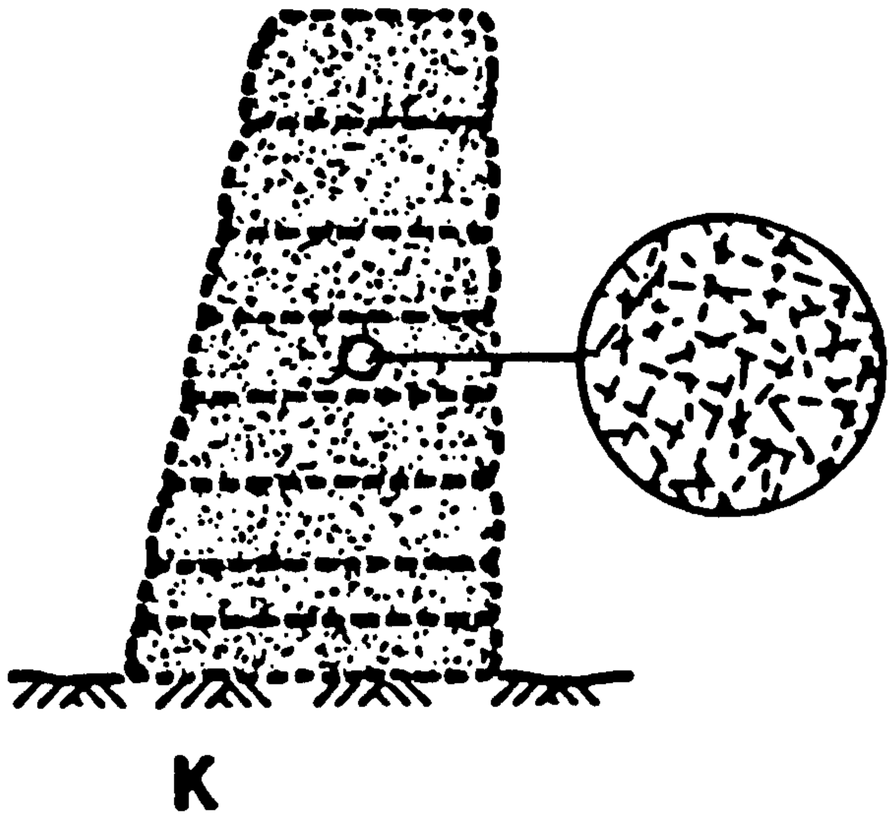

K. Crash and noise barriers

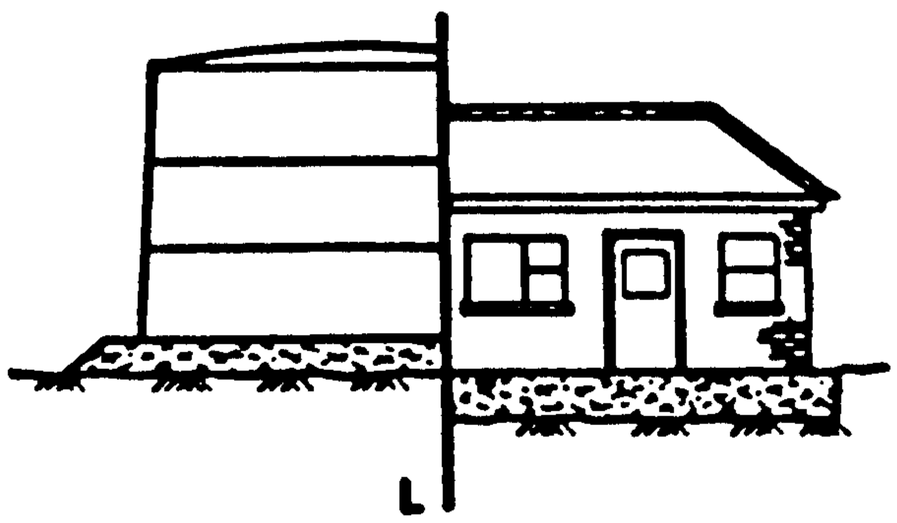

L. Shallow foundations

Fig. 2. (contd.) APPLICATIONS FOR MESH ELEMENTS

Fig. 3. Hand mixing

ANDRAWES*, K.Z., McGOWN*, A., MYTILIS*, N., MERCER°, F.B. and SWEETLAND°, D.B.
*Department of Civil Engineering, University of Strathclyde, U.K.
°Nellon Ltd., U.K.

THE USE OF MESH ELEMENTS TO ALTER THE STRESS-STRAIN BEHAVIOUR OF GRANULAR SOILS
L'EMPLOI DE PETITS BOUTS DE MAILLE POUR MODIFIOR LA RESISTANCE A LA TRACTION DES SOLS GRANULAIRES
DIE VERWENDUNG VON MESH-ELEMENTEN ZUR AENDERUNG DER STRECKEN-SPANNUNG EIGENSCHAFTEN IN KORNIGE BODEN

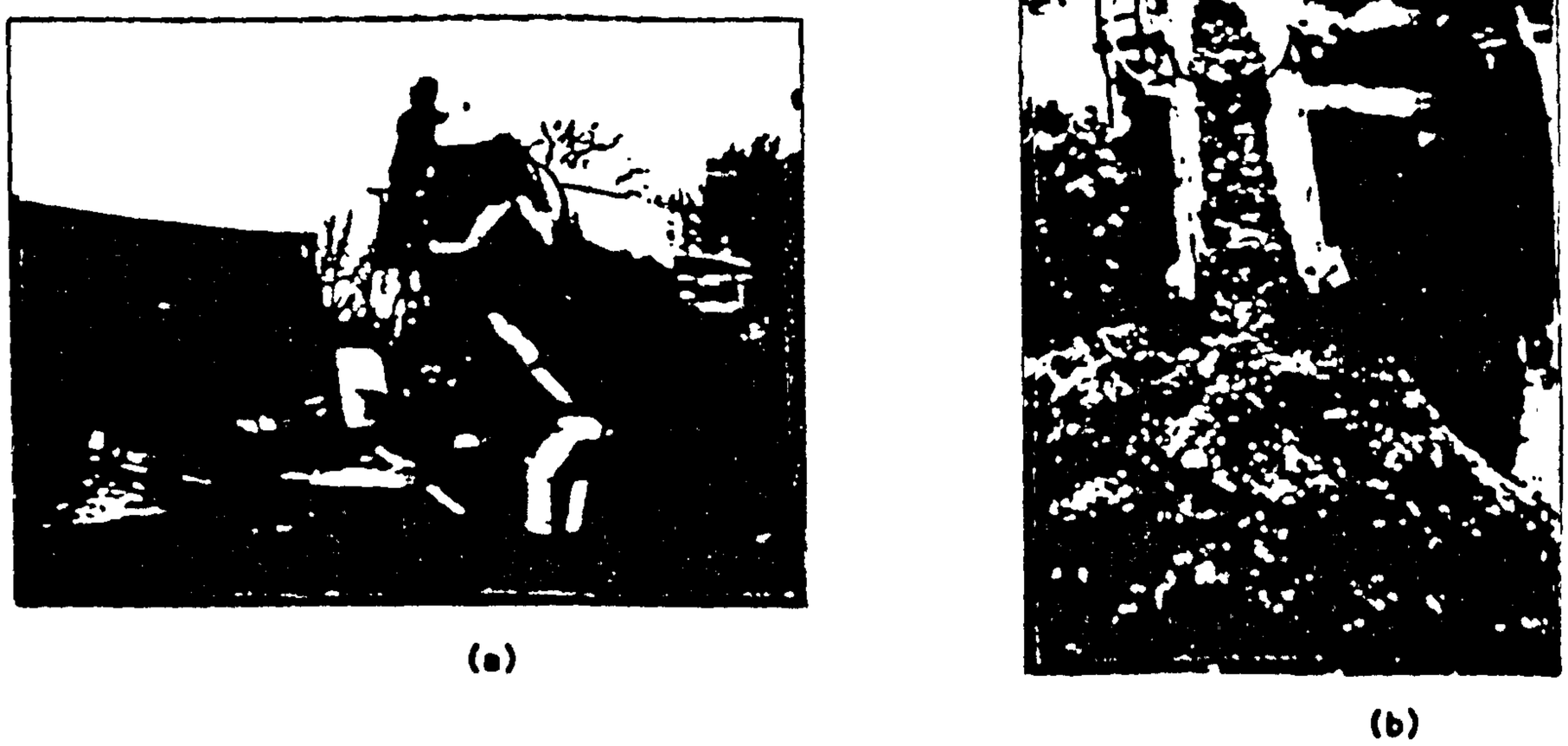

(a) (b)

Fig. 4. Mobile truck mixer
(a) Site delivery (b) Mixed materiels

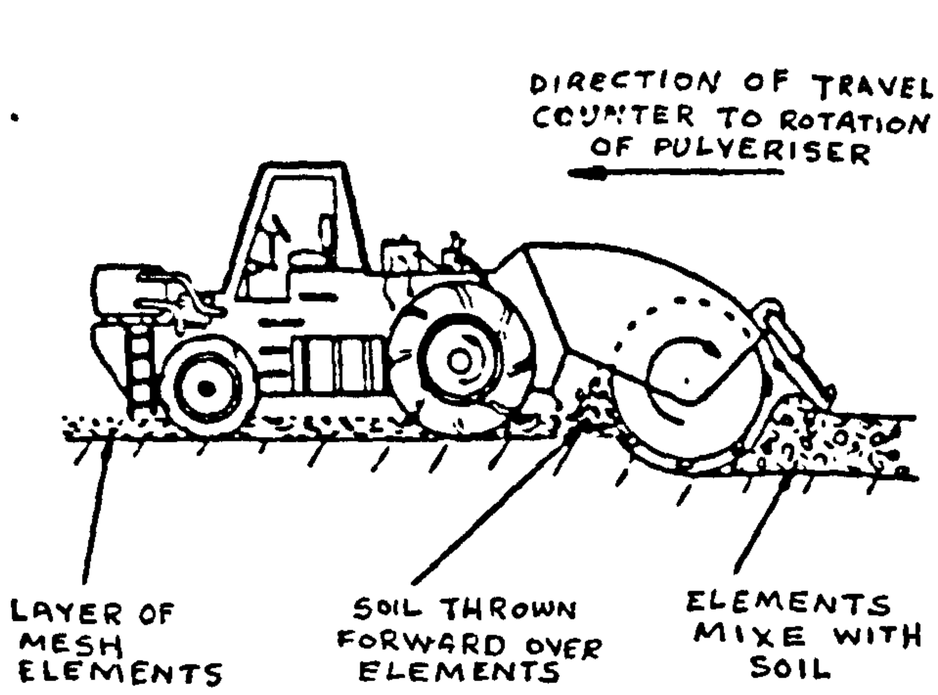

(a)

(b)

Fig. 5. Use of BOMAG RECYCLER
(a) Principle of operation (b) Machine in use

ANDRAWES*, K.Z., McGOWN*, A., MYTILIS*, N., MERCER*, F.B. and SKEETLAND*, D.B.
*Department of Civil Engineering, University of Strathclyde, U.K.
*Netlon Ltd., U.K.

THE USE OF MESH ELEMENTS TO ALTER THE STRESS-STRAIN BEHAVIOUR OF GRANULAR SOILS
L'EMPLOI DE PETITS BOUTS DE MAILLE POUR MODIFIER LA RESISTANCE A LA TRACTION DES SOLS GRANULAIRES
DIE VERWENDUNG VON MESH-ELEMENTEN ZUR AENDERUNG DER STRECKEN-SPANNUNG EIGENSCHAFTEN IN KORNIGE BODEN

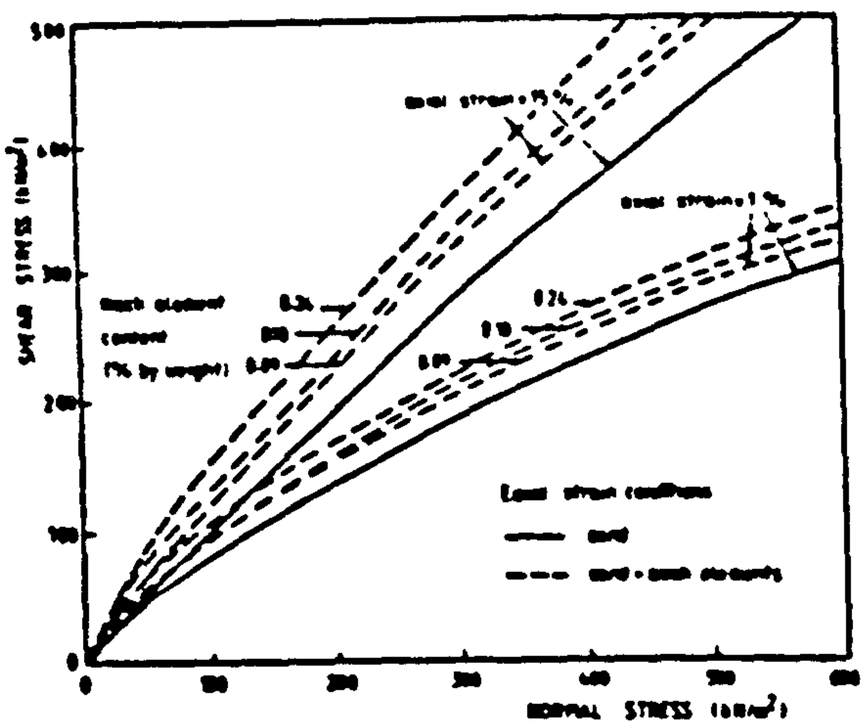

Fig. 6. Mohr envelopes at equal strains

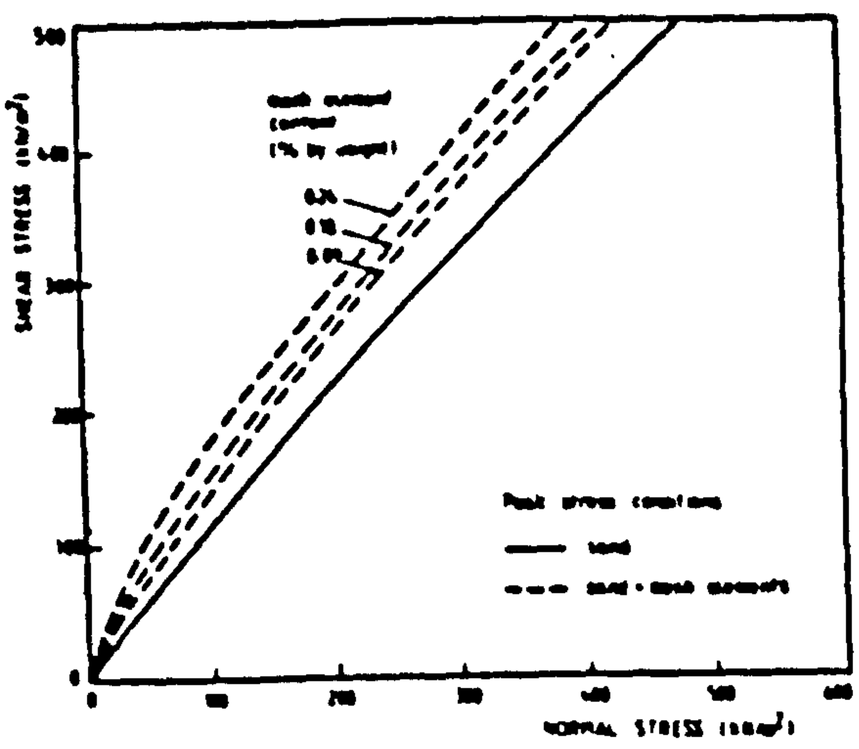

Fig. 7. Mohr envelopes at peak stress conditions

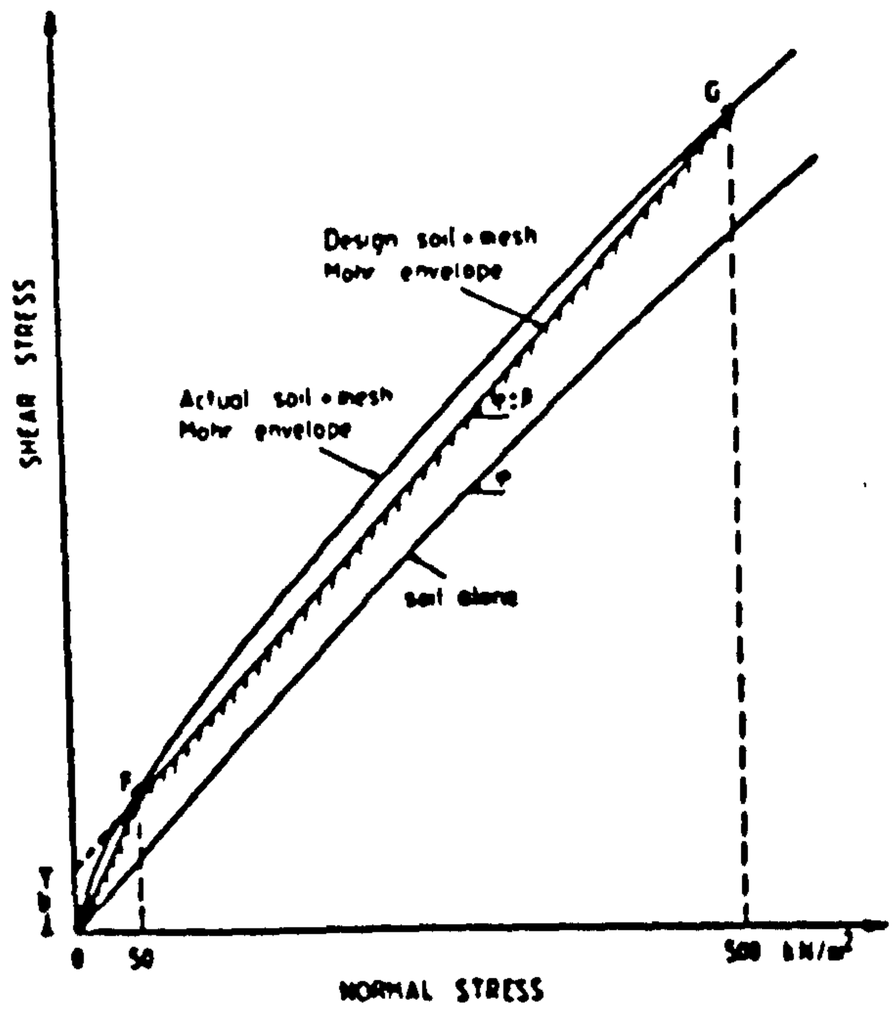

Fig. 8. Bi-linear representation of curved Mohr envelopes